CR-114642
AVAILABLE TO THE PUBLIC

Final Report

A Study of an Orbital Radar Mapping Mission to Venus

Volume III

Parametric Studies and Subsystem Comparisons

September 1973
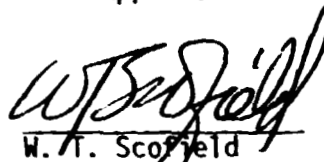
NASA CR-114642

A STUDY OF AN ORBITAL
RADAR MAPPING MISSION TO VENUS

FINAL REPORT

VOLUME III   PARAMETRIC STUDIES AND SUBSYSTEM COMPARISONS

September 1973

Approved

W. T. Scofield
Program Manager

D. B. Cross
Technical Director

Prepared Under Contract No. NAS2-7204 By
MARTIN MARIETTA AEROSPACE
DENVER DIVISION
Denver, Colorado 80201

for

NATIONAL AERONAUTICS AND SPACE ADMINISTRATION
AMES RESEARCH CENTER

FOREWORD

This report has been prepared in accordance with the require-
ments of Contract NAS2-7204 and under the direction of the NASA
Contract Monitor John S. MacKay. The data and conclusions are
the result of a nine month technical effort conducted for the
Ames Research Center by the Martin Marietta Aerospace, Denver
Division and the Environmental Research Institute of Michigan
(ERIM) as a subcontractor. The report is divided into the
following volumes:

>   Volume I   Summary
>
>   Volume II   Configuration Comparisons and
>   System Evaluations
>
>   Volume III   Parametric Studies and Suosystem Comparisons

The report is arranged so that Volume I provides a concise
overview of the study, Volume II provides an appreciation of the
major mission and system integration consideratiors as well as
cost and schedule implications and Volume III provides the
detailed supporting tradeoff studies down to the subsystem level.

ACKNOWLEDGEMENTS

We acknowledge the following individuals and companies for their contributions through making data available, reviewing the work accomplished, suggesting problem solutions and contributing to the establishment of science goals.

STUDY TEAM

The following individuals participated in this study and their efforts are greatly appreciated. The Environmental Research Institute of Michigan (ERIM) personnel are acknowledged for their able participation as a subcontractor.

Program Manager	W. T. Scofield
Technical Director	D. B. Cross
Technical Team	
Science Analysis	D. C. Wychgram Dr. B. C. Clark
Mission Analysis	S. K. Asnin T. W. Locke
Radar & Antenna System	F. A. Vandenberg Dr. R. Bayma, ERIM
Data Handling & Communication System	R. W. Stafford; Dr. R. Bayma, ERIM Dr. J. Zelenka, ERIM R. Larson, ERIM Dr. R. Lewis, ERIM Dr. P. McInnes, ERIM
Attitude Control System	F. D. Hauser R. S. Jackson
Spacecraft Systems Lead	O. O. Ohlsson
Power	A. A. Sorensen
Thermal	T. Buna
Design	N. M. Phillips
Mass Properties	W. D. VanArnam
Antenna Technology	W. Koppl Dr. K. F. Broderick

TABLE OF CONTENTS

PAGE

LIST OF FIGURES

LIST OF TABLES

I. Introduction

I. INTRODUCTION

The basic objective of this volume is best described by the SSD (Systems Studies Division) statement of work for this study which stated, "To perform a preliminary design of a Venus radar-mapping orbiter mission and spacecraft to identify and evaluate the important technological problems of producing such a spacecraft and obtaining and retrieving the necessary mapping data." In order to meet this objective the early part of the study, approximately the first half of the study effort, was devoted to the parametric analysis of each of the individual subsystems in order to evolve limiting criteria, develop boundary cases and to define limiting designs. The basic philosophy that permeated throughout the parametric analysis was to employ lightweight, minimum cost, low risk technology, off-the-shelf systems whenever possible.

In order to avoid any duplication of effort our initial approach was to draw extensively upon earlier Venus orbital radar mapping studies. Specifically, two earlier studies, one performed by SSD, entitled "A Preliminary Analysis of a Radar Mapping Mission to Venus" and one conducted by JPL, entitled "Planetary Imaging Radar Study," were instrumental in providing productive areas of investigation.

The parametric analysis produced several subsystem implementation alternatives, each of which satisfied the basic mission options. In order to evaluate how these choices compared and to determine which were the best selections it was necessary to integrate them into an overall spacecraft configuration to identify possible integration problems. The resulting spacecraft concepts then fell into two general classes of options, viz., shared and dedicated antenna options, which were carried over into the second half of the study in which these options were evaluated in more detail. Results of these studies are reported in Volume II.

It became apparent early in the parametric studies that a
Venus orbital radar mapper mission was much more interactive,
mission/system-wise, than most other unmanned planetary missions.
Accordingly, in conducting the mission design parametric studies
it was necessary to place additional emphasis on the mission
parameters which had significant impact on the general system
design studies. In this study, the necessary look at launch
energy and hyperbolic excess velocity at Venus arrival was taken
in ord r to establish the opportunities favorable for a Venus
orbiter mission during the 1980s. From a systems aspect this was
necessary in order to define launch vehicle requirements and to
evaluate primary orbiter propulsion system requirements. In addi-
tion, examination of the orientations of spacecraft, Sun, and the
planet during crucial trajectory phases was essential for the defi-
nition of the dependence or independence on mission year and tra-
jectory type of such parameters as communications range, solar
angles, occultation times, and orbit orientation possibilities.
Finally, the elements of the radar mapping design orbit corres-
ponding to size (eccentricity and periapsi altitude) and orienta-
tion (inclination and periapsis location) are perhaps the most
critical system design parameters. For this reason then, orbital
eccentricity was carried as a variable throughout the systems
studies. Results of the systems parametric analysis indicated
that orbit size and orientation interrelated with almost all of
the principal spacecraft systems and influenced significantly
the definition of orbit insertion propulsion requirements, weight
in orbit capability, apsidal shift penalty, approach navigation
accuracy and orbit determination, radar system design and mapping
strategy, occultations, telecommunications schedules and power
requirements and thermal design.

A description of the mission and system (down to the subsystem levels) parametric studies that were conducted together with a summary of study results and concerns are presented in subsequent sections of this volume.

II. Science Rationale

II. SCIENCE RATIONALE

INTRODUCTION

The exploration of Venus is the next logical step in man's
exploration of space. The Moor · Mars have received priority
because of their nearness and . ihood of sup ʋ ʼrting life
respectively. A primary intere   exploring Veʋus is geolʼgic.
Venus has many planetary characteristics which are similar to
Earth yet surface morphology is hidden from telescopic observation.
Venus has an estimated density which nearly equals Earth's, is very
similar in size, and is Earth's closest planetary neighbor. Knowl-
edge of Venusian geology will aid in understanding the origin and
evaluation of the solar system and Earth itself.

The exploratory mission under consideration is planned for the
mid to late 1980s time period. It is expected that basic questions
about the atmosphere, dynamic figure of reference, planetary dimen-
sions and shape, mass distribution, spherical harmonics and magnetic
field will be answered prior to the mappɛ.ʼ mission by precise orbit
tracking, fly-bys (Pioneer Venus and Venera) and analysis of Earth-
based observations. Therefore, optional sensors or techniques
which gather additional data on these features are suggested by
MMC as secondary considerations and are not a part of the study
contract.

Several scientific aspects of a Venus orbital mapper mission
have been considered in good detail by the Jet Propulsion Laboratory
in the publication "Planetary Imaging Radar Study" (Ref. II-i).
Therefore, these aspects are discussed only briefly i: this report.

Primary geologic information will be obtained from planet
surface morphology. Topographic data, which describes the shape,
distribution and relative height of surface features, will provide
the geologist with information on the heterogeneity of the crust,

geologic structure, stratigraphy, general rock type and construc-
tional/destructional surfac processes. Heterogeneity of the crust
would be suggested by variegat.j terrain and variations in topog-
raphy resulting from the interplay between various different lithol-
ogies and erosional processes. The establishment of the character
of the crust is important to understanding the origin of Venus and
possibly relating the crust of Venus with Earth's segregated con-
tinental and oceanic crustal materials. Structural information,
such as faults and folds, will suggest the degree of Venus.in
crustal mobility and allow the study of stress fields and plate
tectonics. Stratigraphy is most basic to understanding geologic
history and it may be possible to assign crude age relationships
to Venusian rock units based on their relative position. General
rock type identification or discrimination may be possible by
interpretation of erosion patterns, surface texture, and identifi-
cation of associated features such as calderas. The interplay
between constructional (mountain building) and destructional
(weathering and erosion) processes will reveal much about the geo-
logic environment and history of Venus.

Secondary geologic information can b obtained from surface
roughness. radiometic, polarization, and dielectric data. It is
important to note that these secondary surtace data are far less
important scientifically than topographic data.

Remote sensing techniques that use the visible and near inira-
red wavelengths of electromagnetic radiation (0.4 - 1.1), have
proved optimal for obtaining surface topographic data. Cameras,
scanners, and video instruments have been used with great success
to study Earth, the Moon, and Mars. The thick Venusian atmosphere
precludes the use of these systems. Side looking radar is the next
best remote sensing system for obtaining topographic data and, if
the proper frequency is selected, will be capable of penetrating

the Venusian atmosphere. The use of a synthetic aperture system
to minimize power and antenna requirements makes side looking
radar ideally suited for an orbital Venus mapping mission.

OBJECTIVES

The three overall objectives of the Venus Radar Mapper Mission
are necessarily interrelated.

Determine the Geologic History and Mode of Origin of Venus

This objective is directly related to the basic goal in explor-
ing the terrestial planets, of better understanding the origin and
evolution of Earth and the solar system. The primary means of
accomplishing this objective is to interpret topographic data and
compile a comprehensive geologic map.

Map the Major Topographic Features of Venus and Relate These to a Coordinate System

This map will be the data base for compiling and relating var-
ious surface and atmospheric data. The geologist will use these
basic data for global scale studies.

Provide Detailed Geologic and Terrain Analysis of Potential Landing Sites

Future mission planning for the exploration of Venus necessarily
includes the use of landers. A detailed geologic analysis would
increase the chances of collecting relevant geologic data and would
enable geologists to relate those data collected in situ by the
lander to a regional geologic framework. The high resolution needed
to accomplish this objective would allow the identification and
understanding of small-scale geologic features which can then be
related to t   t iled coverage. Detailed terrain analysis

would help insure a safe landing and can aid in lander design.
Since the resolution requirements for this objective surpass the
baseline requirements of the mission (approximately 100m), the
detailed lander site evaluation should be considered a secondary
objective.

ASSUMPTIONS

Several assumptions have been made while formulating the science
objectives and data requirements. These assumptions and clarifica-
tions are given below:

There Will Be Topography to Image on Venus

Most of the science return value of the mission depends on the
existence of topography and the manifestation of geology by geomor-
phology. Many radar system variables such as frequency, look angle,
and stereo overlap are specified based on this assumption. In
theory, the high Venusian surface temperature (estimated to be about
500 °C) would decrease the rigidity of the crust and its ability to
support loads which are not isostatic. Positive topographic features
that are not in isostatic equilibrium, such as volcanoes, would lit-
erally sink over short periods of geologic time. However, Earth-
based radar data indicate that the terrain is variegated. G.
Pettingill (Ref. II-2) of MIT states that these data suggest the
existence of mountain ranges with relief on the order of 2 km .

The Surface of Venus is at Least as Complex as the Martian Surface

This assumption strongly influences the resolution requirements
since more complex terrains require higher resolution in order to
understand surface phenomena. The complexity of a planet's terrain
seems to correlate with the size and mass of the globe and the amount
of atmosphere present. The moon, for instance, with no atmosphere
and small size and mass is less complex than Mars which has a thin

atmosphere and a size and mass comparable to Earth and Venus.
Depending somewhat on the dynamics of the Venusian lower atmosphere,
and also on the effect of decreased crustal rigidity, the Venusian
surface is probably quite complex requiring resolution on the order
of 100 meters.

The Venusian Atmosphere Is Reasonably Transparent to Longer Wavelength Radar

The data published by Muhleman (Ref. II-3) which are based on
Earth-based radar data, have been relied upon to help select radar
system frequency as it relates to atmospheric penetration. Muhleman's
data indicate that radar wavelengths smaller than about 5 cm are
largely attenuated whereas wavelengths greater than about 25 cm pene-
trate the atmosphere with relatively little loss.

There Is No Geologic Reason to Favor Any Particular Hemisphere, Latitude, or Longitude in Terms of Resolution or Coverage

It is important to cover at least one entire hemisphere (includ-
ing the pole) since variations in geologic processes may exist at
different latitudes just as they do on Earth and Mars. Earth-based
radar data show essentially equal amounts of variegated, high, and
low signal return areas for both northern and southern hemispheres.

Earth-based Radar Data Will Not Be An Adequate Basis for Interpreting The Geologic History of Venus

The best resolution obtainable with currently planned for equip-
ment is on the order of 1 km with very poor (50 km) resolution of
the polar regions. Resolution on the order of 0.1 km will be neces-
sary for a comprehensive geologic analysis.

DATA REQUIREMENTS

To insure that the mission science objectives are accomplished, each radar system variable has been considered in terms of science return impact. Following is a discussion of each system variable and how it affects the science return.

Resolution

The range of resolutions under consideration is limited by future Earth-based radar capability (about 1 km) on the coarse end and by possible atmospheric turbulence on the fine end. Inspection of Mariner 9 imagery (A-frame = 1000 m, B-frame = 100 m), ERTS (Earth Resource Technology Satellite) imagery (60-150 m), aerial photographs (0.5 m - 2 m), and side-looking radar (20 - 100 m) indicates that most regional geologic studies can be conducted with resolution on the order of 100 meters. Good topographic and geologic maps at a scale of about 1/1,000,000 can be constructed using 100 meter resolution imagery. The ERTS system is an excellent operating analogue to the proposed Venus Radar Mapper. This satellite orbits Earth in a near polar orbit at 912 km distance. The multispectral scanner telemeters (either real time or from tape storage) imagery with resolution that averages about 100 meters. An example of this imagery is shown in Figure II-1. ERTS imagery has proven valuable in topographic mapping (foreign countries), geologic structural studies, and gross lithologic discrimination and identification. Both the scale of the ERTS data format (1:1,000,000) and the 100 meter resolution are ideal for the global scale Earth resources survey. The baseline resolution of the Venus radar mapper should be on the order of 100 meters for maximum science return and reasonable data rates and data storage volume.

Finer resolution is desirable to identify and understand small scale geologic phenomena and to aid in lander site selection. A
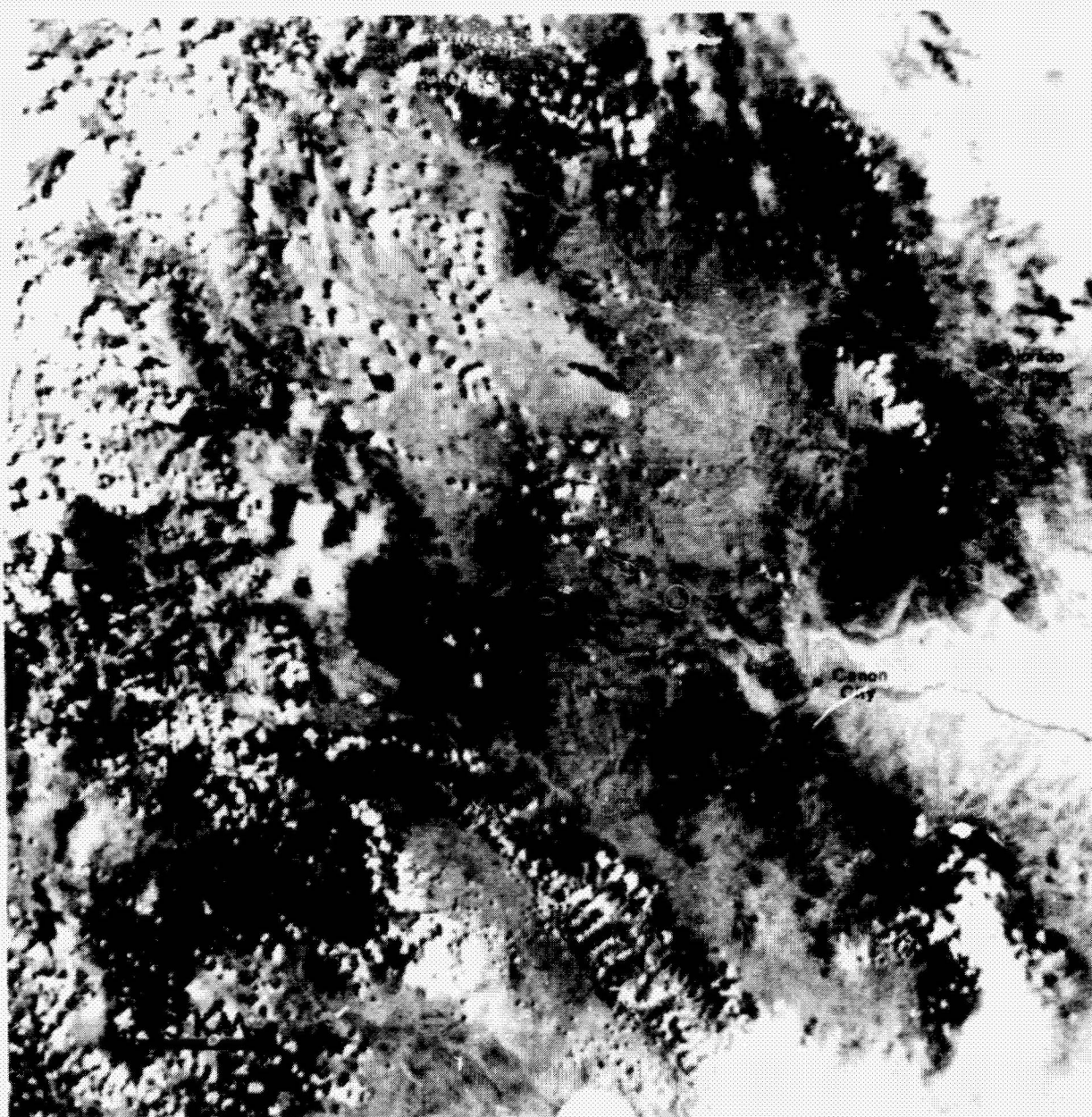
Figure II-1 ERTS-1 Satellite Imagery of South Central Colorado
Resolution is about 100 meters.

very small percentage of coverage (on the order of 2%) is all that
is needed if the areas of coverage are carefully selected by geol-
ogists based on future Earth-based radar data. Highly selective
coverage could be obtained in an extended mission by examining
previously obtained 100 meter resolution data. In the case of a
mission which lasts only the 243 days needed for Venus to rotate
beneath the spacecraft, it can be expected that some 100 meter cov-
erage would have to be sacrificed in order to handle the additional
data loads involved in getting higher resolution.

Stereo Coverage

Stereo coverage is considered to be of primary importance to
accomplishing the mission objectives. Experience with aerial photog-
raphy has clearly demonstrated the vast increase in the amount of
available information and increased geologic interpretability of
stereo viewing, as opposed to monocular viewing. The stereo model
provides precision quantitative information on relative heights and
surface slopes which will result in a much more accurate topographic
map. Fifty percent side-lap will provide 100% stereo coverage. It
is judged that high science return can be obtained with as little
as 15-20% side-lap which would provide good topographic control for
adjoining non-stereo coverage areas. Methods of using conjugate
(side-lap) SLAR imagery to create a stereo model are still being
developed and workable techniques are currently in use.

A discussion with J. J. Fenster of Westinghouse Earth Resource
Mapping Department indicates that stereo coverage is routinely
obtained for minerals exploration and land survey projects. A few
methods are being used which use either "opposite side" or "same
side" views of the target terrain (Figure II-2). Extreme stereo
parallax can be obtained by viewing the target terrain from opposite
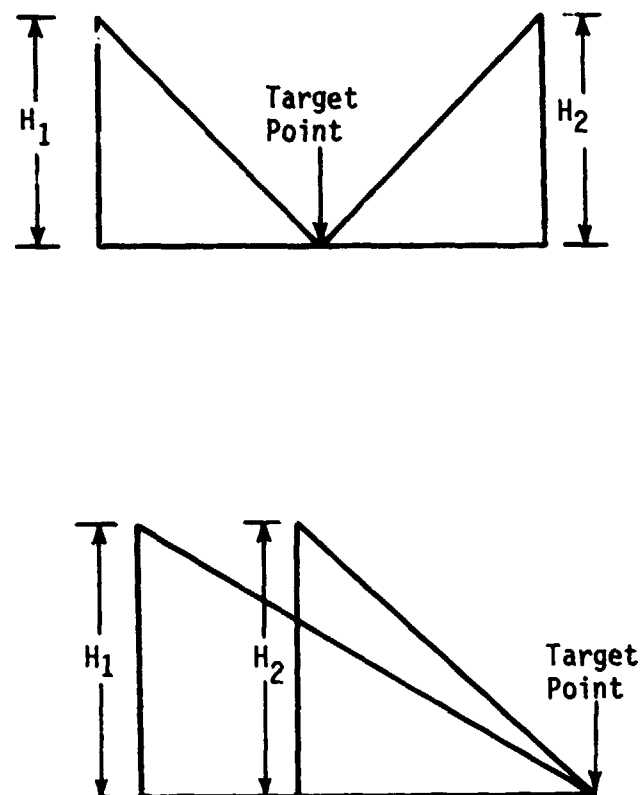
Figure II-2   Illustration of Opposite Side
and Same Side Viewing Geometry
for Obtaining Stereo Coverage

sides which is advantageous when a computer is used to construct a stereo model. The "opposite side" geometry is unsatisfactory for viewing by the human interpreter because of the resulting eye strain. Also, opposite side viewing is undesirable logistically for an orbital mission because additional spacecraft attitude changes would be required over the "same side" case. For these reasons, only the same side geometry is being considered as a means of obtaining stereo coverage.

One technique for obtaining stereo models from the same side geometry is the "AS-IIA Radar Program" developed by the Army at Fort Belvoir (Ref. II-4). The computer operating with the AS-IIA stereo-plotter has been programmed to electronically rectify the SLAR imagery into a corresponding aerial photo-like geometry for conjugate radar image presentation to the interpreter. The correction in geometry is so complete as to compensate for planet curvature in the range direction. A required data input for this technique is air station height so a radar altimeter would be required in orbital operation. Correlation between topographic maps compiled with stereo photography and stereo radar using the AS-IIA program is excellent except in areas of radar shadow.

Frequency

Selection of radar system frequency must take into account the wavelength dependent transmission characteristics of the Venusian atmosphere and the probability of topographic information loss at longer wavelengths. Inspection of 25-cm SLAR imagery suggests relatively high surface roughness information content but relatively low topographic information content, compared to typical 3-cm SLAR imagery. Unfortunately, there are few examples of longer wavelength SLAR imagery to evaluate for topographic information content and further study on this topic is needed.

Figure II-3 is reproduced from Radio Science, February 1970, "Interferometric investigations of the Atmosphere of Venus," by Duane O. Muhleman. This figure shows percent reflectivity as a function of wavelength. If the assumption is made that most of the fall-off in reflectivity is due to atmospheric attentuation (i.e., that surface reflectivity is not largely dependent on wavelength) then this graph is very helpful in selection of an appropriate radar frequency.

The "best-fit-curve" indicates that atmospheric transmission is only slightly wavelength-dependent at wavelengths longer than about 40 cm (15% reflectivity). The shortest wavelength tested was 3.8 cm which resulted in less than 1% reflectivity. The knee of the curve, where reflectivity is changing most rapidly with wavelength, is between 3.8 and 25 cm. Based on the data of Figure II-3 a 10 cm wavelength radar system (3.0 GHz, S-band) is recommended. While this is not the shortest possible wavelength which might be acceptable from an attenuation standpoint, it represents a considerable safety margin in assuring a strong signal return, being only four percentage points down from the maximum observed reflectivity of 15%.

Rectification

SLAR imagery has inherent geometrical distortions which can be removed by proper processing of the data. The most basic processing converts the raw data, known as slant range imagery, to ground range imagery by applying a hyperbolic correction factor. More complex rectifications, such as the AS-IIA program, can be applied for more complete corrections. A high order of rectification, in conjunction with precise knowledge of spacecraft location as a function of time, is needed to accurately locate topographic features with reference to a global coordinate system.
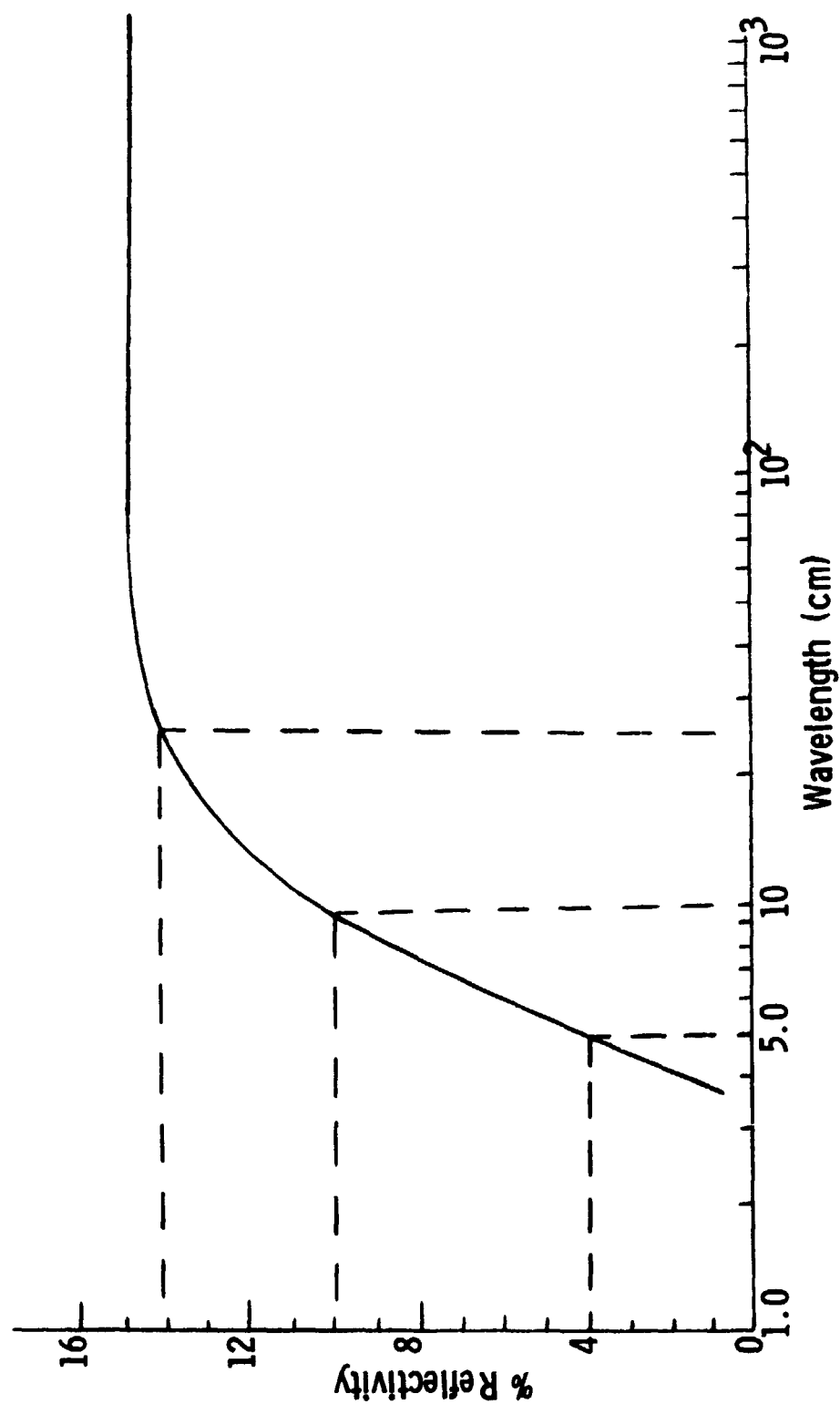
Figure II-3   The radar reflectivity spectrum of Venus. The solid line is the reflectivity obtained from a least-squares fit of an inverse-squared wavelength-dependent opacity law including the effects of the radar backscattering function. (Muhleman, 1970, Ref. II-3).

Coverage, Periapsis Latitude and Eccentricity

The science objectives are best realized by planet coverage of 80% or better needed to study global scale features and processes. Planet coverage between 80% and 50% are detrimental to global scale studies but provide a reasonable science return if at least one entire hemisphere is imaged. Coverage less than 50% is far below the baseline expectations of the mission.

Detailed and stereo coverage should be taken of all areas where variations in morphology, geologic structure, stratigraphy, and constructional/destructional geologic processes may exist. This will include several areas in the equatorial, temperate and polar regions. Ground-based radar maps indicate two markedly different types of terrain referred to as alpha and beta regions. One terrain type is thought to be smooth and lacking relief while the other terrain appear more variegated. About a dozen permanent "scattering anomalies" have also been noted although their precise nature has not been established. Several of these anomalies, and areas in both alpha and beta regions, should be examined with both high resolution and stereo coverage. Specific areas of interest cannot be selected until the ground based imagery has been examined in detail.

The equatorial periapsis geometry is illustrated in Figure II-4. It is apparent that as the orbiter leaves the vicinity of the equator the surface-to-orbiter distance (range) increases rapidly as a function of eccentricity. The following relationships indicate that the increased distance between the orbiter and the Venusian surface will result in poorer quality data (or lack of data) in the higher latitudes. (These points do not apply to a variable side-look angle mode of operation.)

> 1) As the range increases the power requirement increases and becomes the limiting factor on northward and southward coverage. Present planning indicates that at

eccentricities greater than 0.3, and using an
equatorial periapsis and a dual beamwidth system,
neither pole will be imaged.

2) Resolution in the range direction will be degraded
   when the orbiter is at maximum mapping altitude.

3) As range increases, the grazing angle increases.
   This results in a longer atmospheric path length
   with attendant increased signal attentuation and
   lower S/N ratio.

It seems reasonable to assume that at least small differences
in geologic processes and materials may exist in the equatorial
temperate, and polar regions due to heat budget variations and
weather conditions. The assumption that the northern and
southern hemispheres are similar is supported by Earth-based
radar data.

In view of these assumptions, it would be most advantageous
to examine at least one of the poles and all latitudinal zones
of at least one hemisphere closely. Clearly, this cannot be
accomplished with an equatorial periapsis unless eccentricities
less than about 0.3 are used or variable side look angle modes
are employed. However, if periapsis is moved to 45° north or
south latitude a more even distribution of higher quality data
exists in the polar, temperate and equatorial areas of one hemi-
sphere (see Figure II-5). A major disadvantage of a 45° peri-
apsis is considerable loss of coverage in the opposite hemisphere
(depending on eccentricity). Striped areas of Figures II-4, II-5,
and II-6 indicate unimaged areas.

A good trade-off is to locate periapsis as a function of the
eccentricity finally selected. Periapsis would then be located just
far enough from the equator to insure that one pole would be entirely
imaged. (See Figure II-6.) This would maximize global coverage and
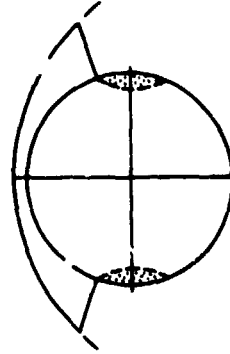
Figure II-4 Equatorial Periapsis, e = 0.5,
Dual Beamwidth Configuration
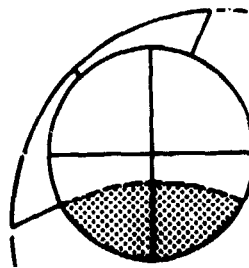
Figure II-5 Periapsis at 45° North Latitude, e = 0.5,
Dual Beamwidth Configuration
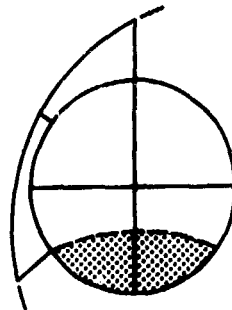
Figure II-6 Periapsis at 35° North Latitude, e = 0.5,
Dual Beamwidth Configuration

insure that at least one hemisphere would be totally imaged in good detail. Whether periapsis would be shifted toward northern or southern latitudes as a function of eccentricity will depend on mission year orbital considerations and examinations of future Earth-base radar imagery.

Orbital Eccentricity

The most desirable orbit for obtaining data of equitable quality and 100% coverage is circular. However, payload, propulsion, and stability requirements dictate using an elliptical orbit with eccentricities between 0.2 and 0.5. The following table shows the approximate relationship between eccentricity, location of periapsis (as per the trade-off previously discussed), percent resolution degradation (range direction) from periapsis to farthest mapping distance, and percent global coverage. Scientific goals are best accomplished with eccentricities of 0.3 and less or use of a variable side look angle configuration.

Table II-1   Relationship of Eccentricity and Periapsis Latitude to Resolution Degradation (between periapsis and maximum mapping range) and global coverage.   See Table III-3.

Eccentricity	Periapsis Latitude	% Resolution Degradation	% Global Coverage
0 (dual beamwidth)	0	0%	100%
0.3 (dual beamwidth)	±25	100%	82.2%
0.5 (dual beamwidth)	±35	100%	67.1%
0.5 (variable look angle)	0	400%	100%

Radar Look Angle - Grazing Angle

The topographic information contained in a side- looking radar
image is primarily due to 1) slope variation affecting intensity of
backscattering, 2) radar shadow on the far range side of topographic
features, and 3) stereo coverage producing a three dimensional model
of the terrain. Radar shadow is particularly important because it
lends a photograph-like quality to the image (appears similar to low
Sun-angle photography) and enhances topography. The amount of, or
existence of, radar shadow is a function of terrain slope and radar
look-angle/grazing angle. The terms radar "look angle" and "grazing
angle" define equal quantities when the altitude of the radar station
is near enough to the planet so that the target terrain is virtually
flat. This situation is depicted in Figure II-7 and is discussed
below. At very high altitudes, such as those encountered in the
planned Venus orbital mapper mission, planet curvature tends to
increase the grazing angle so that grazing angle is greater than
the radar side look angle. In terms of topographic shadowing and
layover distortion it is the grazing angle which is relevant to
the resultant imagery. Therefore, the term grazing angle is used
throughout this section.

Figure II-7 (Ref. II-5) shows the relationship between radar
grazing angle β and the amount of radar shadow enhancement for a
fixed back-facing slope angle (α) of 70°. In the example of Figure
II-7, no shadow occurs if the grazing angle is less than the slope
angle ($\beta<\alpha$), a grazing situation occurs if grazing angle equals
slope angle ($\beta = \alpha$), and shadowing occurs if the grazing angle is
greater than the slope angle ($\beta>\alpha$). The situation depicted in
Figure II-7 is for a slope which trends parallel to the flight line
of the radar platform. The effective slope angle decreases as the
slope trend intersects the flight line at increasing angles.

Experience has shown (Ref. II-6) that the optimum grazing angle
is dependent on the terrain being imaged. In areas of high relief
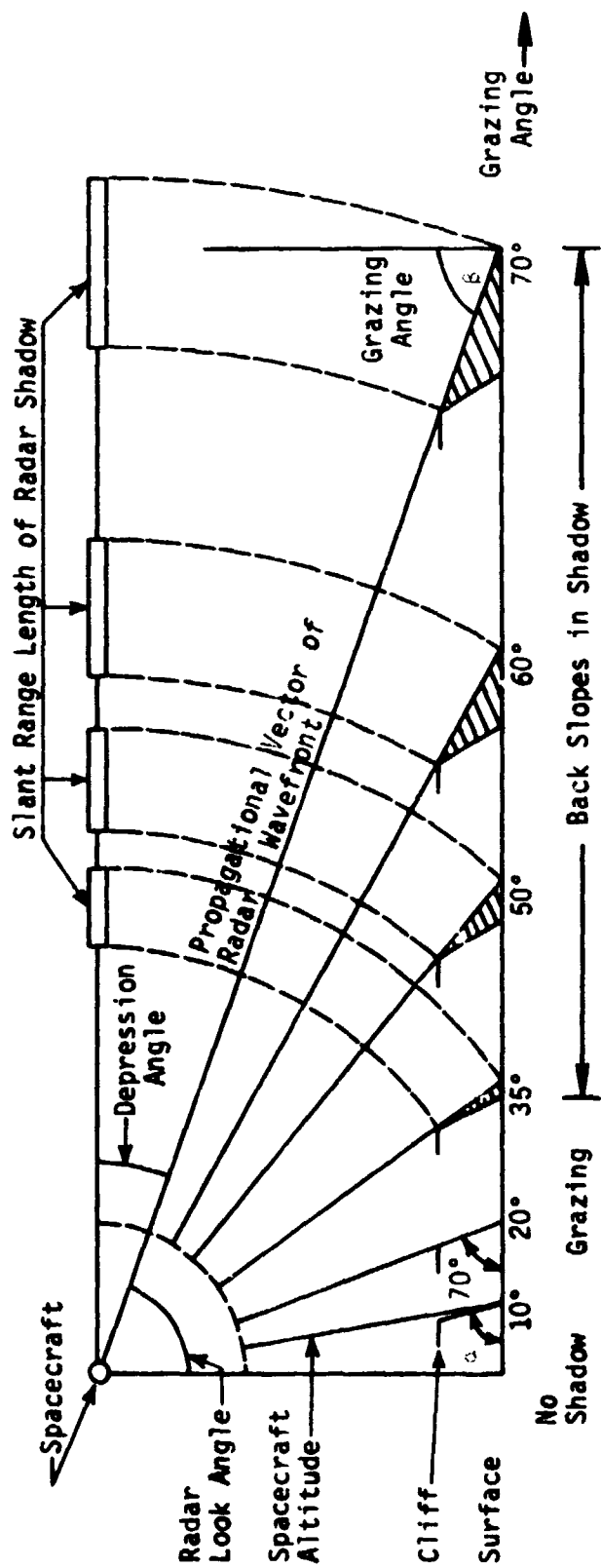
Figure II-7 Relationship of Radar Shadow (slant range length) with Grazing Angle β

and steep slopes, a relatively large grazing angle results in much
detail loss because the shadows cast by major topographic features
obscure smaller features. Conversely, when an area of low relief
and gentle slopes is imaged with small grazing angles, no shadow
enhancement is obtained. There are two possible solutions to the
problem of grazing angle selection for the Venus Radar Mapper mission.

The first solution requires a knowledge or prediction of the
slope angles that exist on the Venusian surface. There are little
factual data on the surface morphology of Venus, however, current
Earth-based radar data suggest the presence of mountains with 2 km
of relief. This information provides no knowledge of local slopes
because of the extremely coarse lateral resolution. Prediction of
surface slopes based on the high surface temperature and thick atmos-
phere of Venus can be made but are so speculative in nature that they
should not be considered as limiting factors on the radar system
design. It should be noted that speculation of this sort favors sub-
dued topography with gentle slopes. Current Earth-base radar data
are providing more detailed information on surface slopes, especially
in the equatorial regions.

The second solution eliminates guesswork or reliance on Earth-
based data. A method might be devised to adjust the look angle/graz-
ing angle while the spacecraft orbits Venus. One method would be to
examine the returned imagery during the non-mapping portion of the
orbit and then send a command to the spacecraft to adjust the grazing
angle to obtain maximum topographic enhancement. It is conceivable
that the radar system could be designed to automatically adjust the
grazing angle based on the percent of shadow area in the scene viewed.
A solution of this type could possibly create new problems in terms
of power and coverage.

There is a constraint placed on minimum grazing angles because
of radar layover. Radar layover occurs when the radar pulse strikes

a topographically high point before energy from the same pulse
strikes a topographically lower but closer point. The resultant
imagery shows the high point to be spacially closer to the nadir
point than the lower point which is actually closer. This distor-
tion produces a "chevron-like" pattern in areas of steep slopes
that virtually masks all topographic data. This effect is less
serious in areas of gentle slopes. The possibility of getting
radar layover at small grazing angles necessitates limiting grazing
angles to greater than about $20°$. Figure II-8 shows the effect of
grazing angle on layover distortion and shadow enhancement. The
image is calibrated in depression angle which is the complement of
grazing angle (flat planet model).

Auxiliary Instrumentation

Dual Polarization, Dual Frequency - Application of dual polari-
zation and dual frequency modes of operation for side looking radar
to geologic problems are in the very early stages of research. Dual
polarization has been used by several investigators but none have
reported an increase in or enhancement of topographic data. Rather,
they suspect that variations in the cross-polarized versus like-
polarized imagery are due to soil moisture content, surface rough-
ness, vegetation, and cultural feature characteristics. It is true
that the soil moisture, surface roughness and vegetation are often
indirectly controlled by the lithology, structure and hydrology of
an area but the occurrence of water and vegetation on Venus is
extremely unlikely. Some surface roughness data will be acquired
with the single polarization system.

Dual frequency has received less development than dual polari-
zation and very little geoscience experimentation has been accom-
plished. The primary advantages of dual frequency imaging are the
potential of obtaining more precise surface roughness data and dis-
crimination and identification of crop types. The use of a dual

Figure II-8 APQ-56 K-Band SLAR Imagery of North Central Colorado Calibrated in Radar Depression Angle. Note radar layover distortion at grazing angles smaller than about 20° (depression angle greater than 70°) and radar shadow enhancement at grazing angles greater than about 45°. Imagery was obtained through overcast conditions.

frequency radar system for a Venus orbital mapper would provide a measure of assurance that good data would be obtained at a longer wavelength if the atmosphere attenuated the shorter wavelength more than anticipated.

Radar Altimeter - Radar altimeter profiling would be a valuable capability to the mission science return. Data from this instrument is needed if a program such as the AS-IIA is to be applied to the imagery for stereo viewing. The topographic profile can be used to check and calibrate the relative height data provided by the imaging system. Additional science value can be obtained if a dual frequency altimeter is used. Proper selection of the two frequencies may allow the determination of relative surface pressures which, when compared to the topographic profile data, will allow the detection and study of mass concentrations.

Radiometer - A microwave radiometer, using the frequency, antenna and receiver of the imaging radar system, may provide useful secondary geologic information. Although it is unlikely that large variations in surface temperature will result from uneven insulation or rock thermal properties, it would be possible to study geothermal activity and the lower atmospheric lapse rate (calculated to be $8°C/km$).

Aerial Magnetometer - An aerial magnetometer could provide valuable data on the nature of the Venusian magnetic field, if the existence of a field is established by pre-mission fly-bys. Variations in direction, intensity and inclination may provide information on the core of Venus and the distribution of ferromagnetically rich rocks.

Dual Frequency Occultation - A dual frequency occultation experiment could be included on the mapper mission with minimum hardware modification. The X-band communication link and S-band imaging system equipment can be used to provide valuable information about the Venusian atmosphere and planet shape.

CONCLUSIONS AND RECOMMENDATIONS

The science objectives of the Venus orbital mapper mission can best be realized by obtaining Venusian surface topographic information. A synthetic aperture side-looking radar system is a practical means of collecting these topographic data. Radar system variables must be specified to optimize the topographic data return and yet be compatible with constraints placed on the system by the Venusian atmosphere and power, weight, data transmission rates and cost limitations.

A baseline imaging resolution of 100 meters can provide an excellent topographic map and allow geologists to interpret the basic geologic history and origin of Venus. A high resolution mode of operation would be valuable both to the geologist, enabling the identification and understanding of small scale geologic phenomena, and to the planners of surface lander missions. In order to obtain higher resolution coverage it is likely that small amounts of 100 meter resolution coverage would have to be sacrificed due to data rate limitations. If scientists are able to select the distribution of high resolution coverage, only a very limited amount of global coverage (on the order of 2%) is needed.

The use of orbital eccentricities greater than about 0.3 (with dual beamwidth configurations) may result in less than 100% global coverage and variation in the quality (resolution) of the imagery. In order to maintain coverage of at least one entire hemisphere, and yet maximize global coverage, periapsis latitude should be located north or south of the equator just far enough to cover one polar region with resolution not coarser than about 200 meters. This strategy will insure that high quality data will be obtained of equatorial, temperate and polar latitudes. A variable side-look

angle configuration would allow pole-to-pole coverage with an equa-
torial periapsis. Present knowledge (Earth-based radar imagery)
suggest no geologic reason to prefer coverage of either the northern
or southern hemisphere so mission year orbital considerations may
determine the most advantageous periapsis hemisphere.

Stereo coverage is important to the science objectives of the
mission and may be obtained by viewing the target area from the same
side on subsequent orbital passes. Several techniques are being
developed to correct SLAR imagery for stereo viewing such as the
Army's AS-IIA radar program. Fifteen to twenty percent side lap
will provide sufficient stereo coverage to satisfy the science
requirements. More study of particular stereo processing techniques
is needed.

An imaging radar system frequency of 3.0 GHz (10 cm, S-band)
is recommended. This frequency offers a good compromise between
atmospheric penetration and ability to obtain topographic data.
There is some ambiguity as to whether there is inherent loss of
topographic information when using longer wavelengths. This prob-
lem should be reconsidered as more longer wavelength imagery becomes
available for evaluation.

Radar look-angle/grazing angle has important consequence on the
quality and amount of topographic data content of the resultant
imagery. The optimum grazing angle is inversely proportional to
local surface slopes and provides some shadow enhancement of topog-
raphic features. Without a knowledge of Venusian surface slopes to
base selection of grazing angle on, a real time variable system which
operates either automatically or on command from Earth is desirable.
A constraint of about 20° is placed on minimum grazing angle because
of radar layover distortion near the nadir line of the spacecraft.

Radar altimeter profiling is considered the most valuable auxil-
iary instrumentation and may be necessary for correcting the stereo

imagery for interpretive viewing. A dual frequency altimeter would offer the additional ability to measure relative surface pressure and allow the study of mass concentrations.

Dual polarization and dual frequency modes of operation of the imaging system appear to offer little to accomplishing the mission science objectives. Additional secondary geologic information, mainly surface roughness data, may be gathered with these techniques. It is recommended that both dual polarization and dual frequency be considered as optional auxiliary instrumentation.

Limited microwave radiometry, using the imaging system hardware, is a virtually "free" experiment that may provide valuable information about geothermal activity and lower atmosphere lapse rates. If pre-mission fly-bys indicate the existence of a Venusian magnetic field a magnetometer on board the orbiter could measure variations in direction, intensity, and inclination of the field to provide information on the Venusian core and distribution of ferromagnetically rich rocks. Dual frequency occultation experiments would require minimum modification of hardware and can provide information about the atmosphere and the shape of Venus.

REFERENCES AND BIBLIOGRAPHY

II-1   *Planetary Imaging Radar Study*. JPL Report 701-145, 6 Vols., June 1972.

II-2   G. Pettengill: *Use of Earth-based Radar for Planetary Observation*. Lecture presented at the AIAA Local Section Meeting, March 29, 1973.

II-3   D. O. Muhleman: "1970, Interferometric Investigations of the Atmosphere of Venus. *Radio Science*, February 1970.

II-4   F. R. Norvelle: "1972, AS-IIA Radar Program." *Photogrammetric Engineering*, Vol. XXXVIII, No. 1, p 77-82.

II-5   A. J. Lewis, W. P. Waite: "Radar Shadow Frequency." *Photogrammetric Engineering*, Vol. 19, No. 2, p 189-196, 1973.

II-6   D. C. Wychgram: *Geologic Remote Sensing Study of the Hayden Pass-Orient Mine Area, Northern Sangre de Cristo Mountains, Colorado*. Colorado School of Mines Remote Sensing Report 72-3, April 1972.

II-7   W. P. Waite and H. C. MacDonald: "Vegetation Penetration with K-Band Imaging Radars." *IEEE Transactions on Geoscience Electronics*, Vol. GE-9, pp 147-155, July 1971.

II-8   R. K. Moore and G. C. Thomann: "Imaging Radars for Geoscience Use." *IEEE Transactions on Geoscience Electronics,* Vol. GE-9, pp 155-164, July 1971.

II-9   J. W. Rouse Jr., H. C. MacDonald and W. P. Waite: "Geoscience Applications of Radar Sensors." *IEEE Transactions on Geo - science Electronics*, Vol. GE-7, pp 2-19, January 1969.

II-10   "Side-Looking Radar Plays Key Role." *Aviation Week and Space Technology*, July 17, 1972.

II-11   D. J. Lewinski and R. D. Hays: *Side Looking Radar for Venus Orbiter*. Brown Engineering Technical Note AST-254, December 1967.

II-12   *Remote Sensor Systems for Unmanned Planetary Missions*. NAR Report SD70-361-1, September 1970.

II-13   G. G. Schaber and W. E. Brown, Jr.: *25 cm Wavelength Radar Images of Northern Arizona: A Geologic Evaluation.* U. S. Geological Survey Research, pp B175-B181, 1972.

II-14   M. I. Skolnik: *Introduction to Radar Systems.* McGraw Hill, 1962.

II-15   *Orbital Imagery for Planetary Exploration.* IITRI Report, 5 Vols., 1969-1970 (Contract No. NAS2-4494).

II-16   R. K. Brandenberg and D. J. Spadoni: *Preliminary Radar Systems Analysis for Venus Orbiter Missions.* IITRI Report M-32, November 1971 (Contract No. NASw-2144).

II-17   J. S. MacKay, et al: *A Preliminary Analysis of a Radar Mapping Mission to Venus.* Draft, ACMD, Moffett Field, California, October 11, 1972.

II-18   L. F. Dellwig, R. K. Moore: "The Geological Value of Simultaneously Produced Like- and Cross-Polarized Radar Imagery." *J. of Geophysical Research.* Vol. 77, pp 3597-3601, July 15, 1966.

II-19   D. G. Rea, N. Hetherington, R. Mifflin: "Calculations of the Effect of Roughness in Microwave Emissivity with Application to the Moon and Venus." *J. of Geophysical Research,* Vol. 73, pp 7009-7017, November 1968.

II-20   M. A. Slade and I. I. Shapiro: "Interpretation of Radar and Radio Observations of Venus." *J. of Geological Research,* Vol. 75, pp 3301-3317.

II-21   L. F. Dellwig: *Pluses and Minuses of Radar in Geological Exploration.* Earth Resources Aircraft Program Status Review, Vol. I, NASA, 1968.

II-22   J. P. Hennes, and C. V. Fulmer: *Identifying Relevant Scientific Goals in Planetary Exploration.* AIAA Paper 70-1244, AIAA 7th Annual Meeting and Technical Display, October 19-22, 1970.

II-23   D. B. Campbell, R. B. Dyce, R. P. Ingalls, G. H. Pettengill and I. I. Shapiro: "Venus: Topography Revealed by Radar Data." *Science,* Vol. 175, 4 February 1972.

II-24   H. D. Greyber: *Some Hasty Comments on the Science Objectives for a Venus Mapping Mission.* Martin Marietta Corporation Advanced Viking Science Note 84, 24 January 1972.

II-25   H. D. Greyber: *Science Requirements for a Venus Mapping Mission.* Martin Marietta Corporation Advanced Viking Science Note 88, 29 February 1972.

II-26   Anon: "Lifting Venus' Veil." *Time,* September 25, 1972.

II-27   Space Science Board: *Venus, Strategy for Exploration.* National Academy of Sciences Report, June 1970.

II-28   T. M. Don- hue: "Planetary Exploration: Accomplishments and Goals." *Reviews of Geophysics and Space Physics,* Vol. 9, No. 2, May 1971.

II-29   R. J. Mackis, Jr., et al: *Scientific Questions for the Exploration of the Terrestrial Planets and Jupiter.* A Progress report of the Advanced Planetary Mission Technology Program, NASA JPL Tech Memo 33-410, October 1, 1968.

II-30   M. B. McElroy: "Venus - A Mystery Still to Unfold." *Astronautics and Aeronautics,* January 1971.

II-31   R. D. Bourke and J. G. Beerer: "Mariner Mission to Venus and Mercury in 1973." *Astronautics and Aeronautics,* January 1971.

II-32   M. H. Carr, ed.: *Interagency Report: Astrogeology 19 Strategy for the Geologic Exploration of the Planets.* NASA Contract W-129650, 1969.

II-33   Request for Proposal 2-18270 (HK-66) for *A Study of an Orbital Radar Mapping Mission to Venus.* NASA Ames Research Center, April 24, 1972.

III. Mission Analysis

III. MISSION ANALYSIS

INTRODUCTION AND ASSUMPTIONS

Relevant Mission Design Parameters

Mission design, as it relates to either a preliminary search for or definition of lunar or interplanetary trajectories, must treat those key parameters which are nearly universal for all mission analyses, and those which derive from the specific objectives of a particular mission concept. In this study, the necessary look at launch energy and hyperbolic excess velocity at Venus arrival has been taken in order to establish the opportunities favorable for a Venus orbiter mission during the 1980s. In addition, examination of the orientations of spacecraft, Sun, and planets during crucial trajectory phases has been essential for visibility into the dependence or independence on mission year and trajectory type of such parameters as communications range, solar angles, occultation times, and orbit orientation possibilities. Finally, the elements of the radar mapping design orbit corresponding to size (eccentricity and periapsis altitude) and orientation (inclination and periapsis location) are perhaps the most crucial parameters. These interrelate with the principal spacecraft systems and influence/are influenced by orbit insertion propulsion requirements, weight in orbit capability, apsidal shift penalty, approach navigation accuracy and orbit determination radar system design and mapping strategy, occultations, telecommunications schedules and power requirements, and thermal design. The mission analysis section of this volume incorporates each of these relationships into a parametric study, and indicates the relevant trades.

Rationale for Mission/Orbit Selection

Mission opportunities in the 1980s have been searched with the general assumption of optimizing inserted weight in orbit for 1) a 20-day launch window, 2) impulsive coplanar insertion into an eccentricity orbit with 400 km periapsis, 3) a "rubber" propellant load and useful weight, and 4) Viking 2-tank inert weights. The assumed launch vehicle is Titan IIIE/Centaur, and where indicated, the capability of a Shuttle/Centaur is included. For all opportunities both Type I and II trajectories have been examined, but unless the performance of both types is found comparable, only the more favorable trajectory mode is treated in detail. Isolation of promising periods for Earth-Venus transfers during the decade has drawn in large part from the performance contours of Reference III-1. Figures III-1 and III-2 illustrate a typical set of launch energy (C_3) and arrival hyperbolic excess velocity (Vhp) curves for the 1984 opportunity, derived from the reference. Launch azimuth restrictions for departure from the Cape Kennedy facility are assumed to be between 44° and 114°. This constraint is not violated for the range of Venus mission opportunities considered if coast times of 1 hour can be achieved for Centaur by the 1980s.

Behind the design of the mapping orbit lies the overall objective of a complete Venusian surface profile map at resolutions approaching 100 meters. This commands an orbit inclination near polar (90°) to gain access to all latitudes, a reasonably low periapsis altitude to achieve the desired resolution, and an orbiter mission lifetime of about 240 days with an eccentric orbit (or 120 days with a circular orbit) to map all longitudes. A periapsis altitude of 400 km has been selected as a nominal target value--this combines the expected minimum altitude necessary to avoid slipping into the Venus atmosphere (300km) with an expected 3-sigma altitude dispersion (74 km) from navigation error sources. Location of periapsis with respect
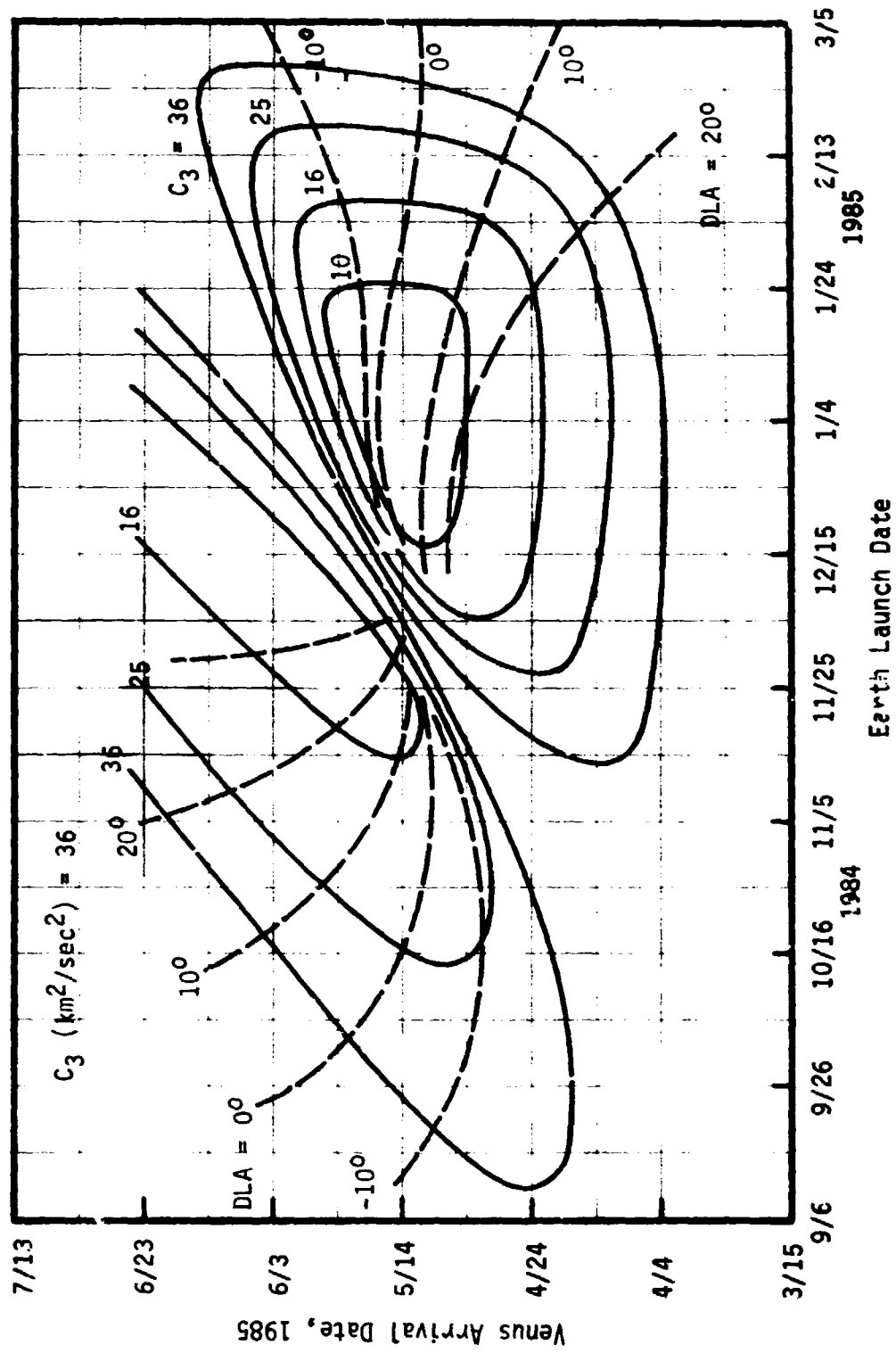
Figure III-1 Launch Energy Profile for 1984-85 Opportunity
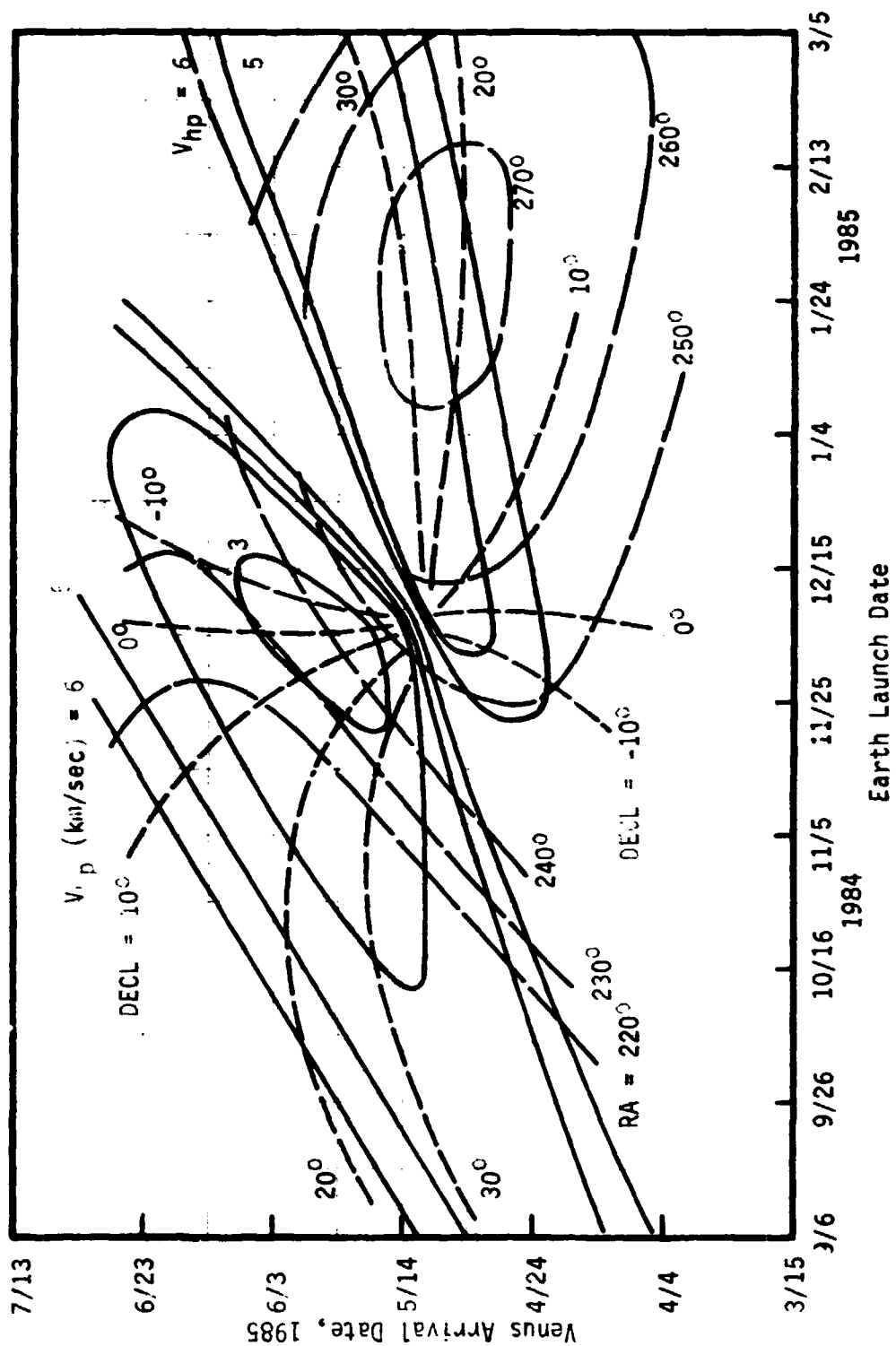
Figure III-2 V_{hp} Profile for 1984-85 Opportunity

to the planet equator becomes a function of the particular radar
system and mapping strategy considered. All other orbit parameters
and trajectory characteristics are allowed to play against specific
spacecraft requirements in the parametrics that follow.

It should be noted that the convention used in this study for
directions with respect to the Venus surface corresponds to a Venus
orbit plane system, which locates North in the direction of North
ecliptic and preserves a common sense of direction among all bodies
considered. Due to the planet's reverse spin, its equatorial coor-
dinate system is actually reversed North to South. The Venus orbit
plane system is illustrated in Figure III-3.

Structure of the Parametric Study

The nature of the approach to mission design for the radar mapper
was such that, although an initial structure was defined early for
the general direction of the parametrics, the structure was expanded
upon as required to include additional emphasis on mission parameters
which became significant as the general design evolved.

Initially, the parametrics were grouped into three categories to
facilitate understanding of the whole. Assigned to one category were
those studies which were clearly dependent upon mission year and tra-
jectory type. Included here were definitions of launch energy and
arrival velocity, nominal orbit insertion orientations for coplanar
transfer, and trajectory geometry. A second category included studies
relatively independent of mission year, such as assessment of orbit
stability for varying orbit size and orientation, analysis of surface
coverage potential for various orbits, and definition of orbit trims
and attitude maneuvers. A third category grouped together studies
which could not a priori be assigned to either of the first two
groupings. Included here were occultation characteristics, periapsis
shift requirements, and certain features of orbit stability. Areas
which required considerable expansion from the preliminary structure,
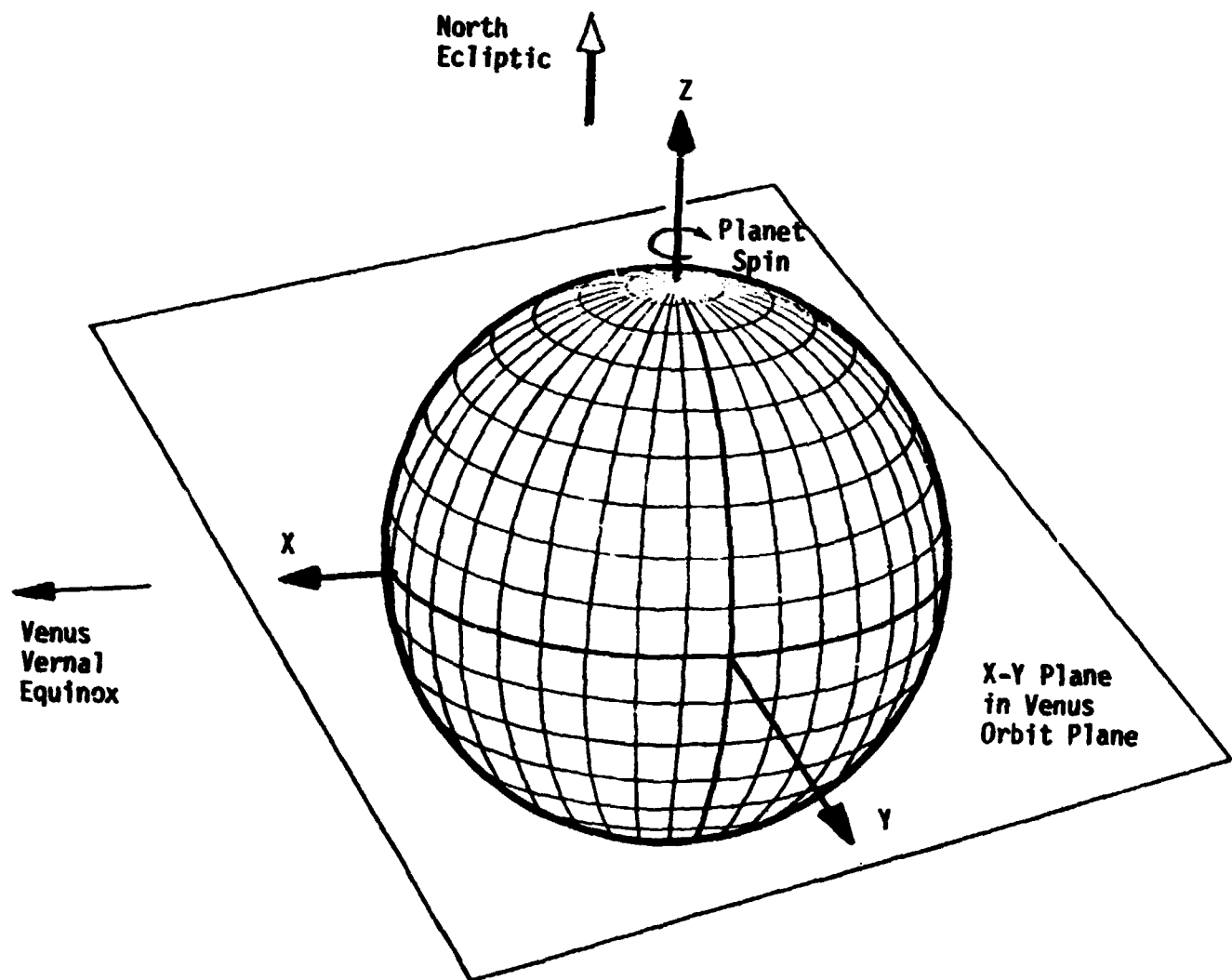
Figure III-3 Venus Orbit Plane Coordinate System

due to their critical impact on systems design, were finite burn loss effects on insertion ΔV, reassessment of weight in orbit capabilities for a variety of insertion propulsion systems, and determination of overlap coverage for various radar systems and mapping strategies.

PARAMETRIC STUDIES

Mission Performance

Mission performance assessment has been directed in large part toward definition of the performance capability for the considered Venus opportunities of the 1980s. The view has been one of isolating areas of maximum weight in orbit potential based on the assumptions of 1) Titan IIIE/Centaur, 2) Viking orbit insertion propulsion, 3) a "rubber" propellant load, and 4) optimizing for coplanar insertion into an orbit of moderate eccentricity ($e = 0.3$). For all mission years both Type I and II trajectories were investigated, but only where performance was found comparable have both types been included in the detailed description. To complete the view, the performance of a Shuttle/Centaur launch system has been included in the study.

Listed in Table III-1 are the performance parameters and trajectory characteristics for a 20-day launch windows for each opportunity, optimized under the assumptions described above. The table presents weight in orbit, C_3, trip times, transfer angles, Vhp, and other related parameters, all for the start, midpoint, and end of each window.

Of primary importance to the parametric analysis is the profile of performance as the desired orbit eccentricity varies. This situation is summarized in Figures III-4 and III-5, where the curves represent worst day conditions for each 20-day opportunity. It is this profile which becomes a key trade in sizing the reference orbit. With the preliminary assumption of an arbitrary desired in-orbit

Table III-1 Trajectory Characteristics For All Mission Years

Mission	Window Day	Launch Date	Arrival Date	Trip Time (days)	Transfer Angle (deg)	C_3 (km²/sec²)	V_{hp} (km/sec)	Useful Weight in Orbit for e = 0.3 (kg)
1983 I	1	06-02-83	10-15-83	135	162	11.00	3.08	1352
	10	06-11-83	1C-26-83	137	171	8.49	2.92	1463
	20	06-21-83	10-23-83	124	15?	10.65	3.14	1365
1983 II	1	05-21-83	11-02-83	165	?2	6.40	3.55	1380
	10	05-30-83	11-02-83	156	194	6.32	3.36	1427
	20	06-09-83	11-03-83	147	186	10.10	3.09	1376
1984 I	1	12-09-84	05-12-85	154	178	12.96	3.34	1233
	10	12-18-84	05-12-85	145	169	9.25	3.95	1213
	20	12-28-84	05-13-85	136	161	7.98	4.16	1191
1984 II	1	11-21-84	05-21-85	181	211	14.67	3.12	1264
	10	11-30-84	05-22-85	173	203	13.06	2.91	1342
	20	12-10-84	05-27-85	168	201	13.10	2.72	1304
1986 I	1	08-20-86	12-15-86	117	140	8.92	4.91	987
	10	08-29-86	12-18-86	111	136	10.71	4.69	1008
	20	09-08-86	12-21-86	104	132	14.61	4.46	987
1988 I	1	04-02-88	07-26-88	115	138	15.10	4.72	914
	10	04-11-88	07-30-88	110	136	18.14	4.26	959
	20	04-21-88	08-03-88	104	132	24.18	3.89	919
1989 I	1	11-10-89	03-05-90	115	144	15.50	3.65	1140
	10	11-19-89	03-10-90	111	143	16.93	3.20	1197
	20	11-29-89	03-17-90	108	145	20.86	3.55	1140

Figure III-5 Weight in Orbit Capability,

Titan-Shuttle Comparison
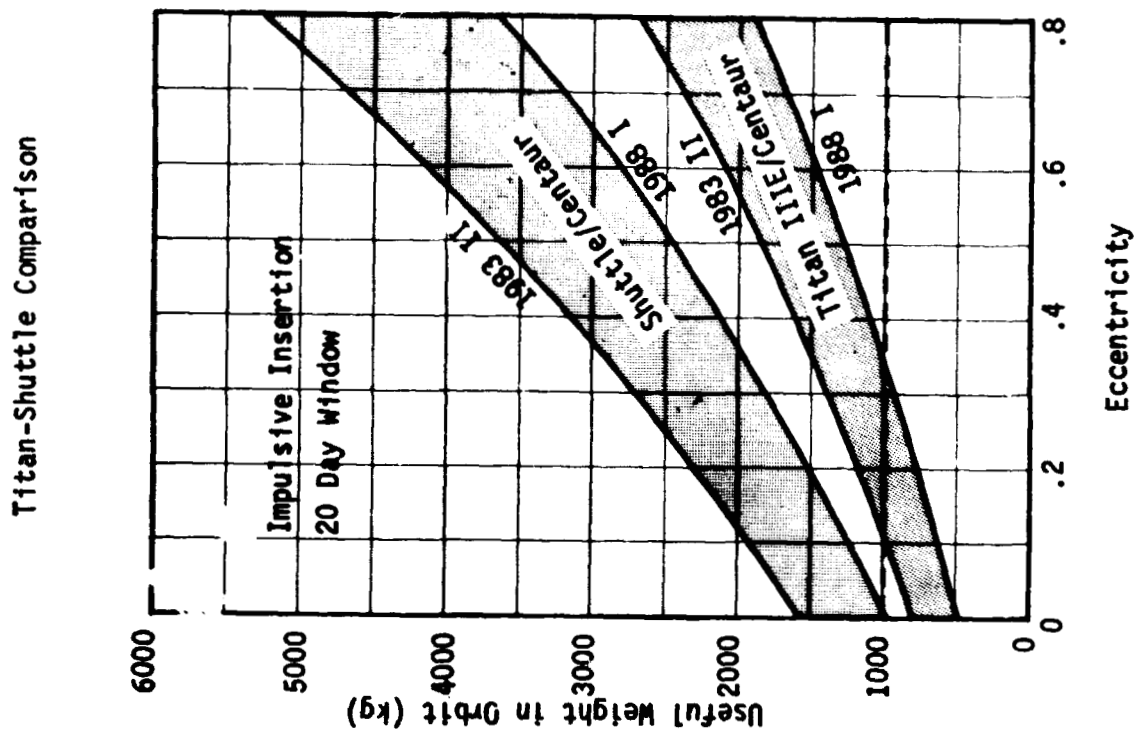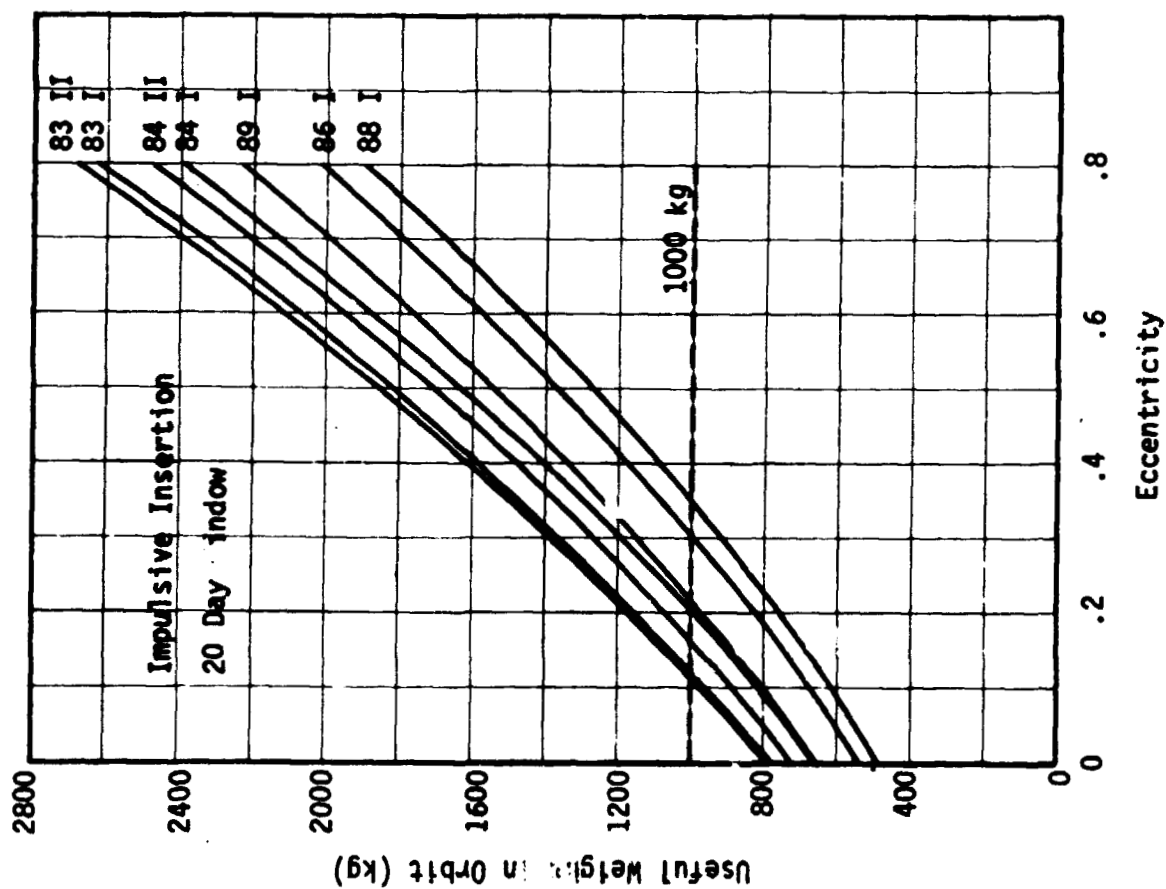
Figure III-4 Weight in Orbit Capability, Impulsive Insertion

weight of 1000 kg, the curves can be related to mission feasibility.
For all opportunities to be viable, with sufficient margin to account
for normal systems growth and more realistic assessments of orbit
insertion ΔV, orbit eccentricity must be 0.5 or greater. As eccentri-
cities lower than 0.5 are considered, mission years become lost in
the order 1988, 1986, and 1989 with decreasing eccentricity. An
eccentricity of 0.2 represents probably the least eccentric orbit that
could be realized for any of the mission years. Again, these conclu-
sions rest on the set of assumptions detailed previously, and are
indicative of trends and potential limiting criteria.

As the parametrics progressed into other areas related to per-
formance capability, the payload profile became modified to incor-
porate the refinements. Specifically, the analyses discussed in the
following subsections concerns a more sophisticated and complete
treatment of orbit insertion requirements and an allowance for a 20°
apsidal shift to place periapsis on the equator in any mission year.
These considerations strongly influenced the design of the insertion
propulsion system and ultimately led to the treatment of a 3-engine
inadequate for orbit eccentricities of 0.5 or less given the qualify-
teristics, were in turn incorporated into the capability profile,
and the curves of Figures III-6 and III-7 illustrate the more real-
istic picture with inclusion of higher inert weight values, and ΔV
adjustments and losses. Details of these adjustments are discussed
in the following subsection. It is sufficient to note here that in
this more realistic view the 1986 and 1988 opportunities would be
inadequate for orbit eccentricities of .5 or less given the qualify-
ing assumption of a 1000 kg payload.

Optimization for a 20-day launch window was considered most rep-
resentative of interplanetary mission philosophy. Over a shorter
design window, such as 10 days, performance improves as the less
favorable "tails" of the weight in orbit curve are truncated.

Figure III-7 Weight in Orbit Capability,
Titan-Shuttle Comparison
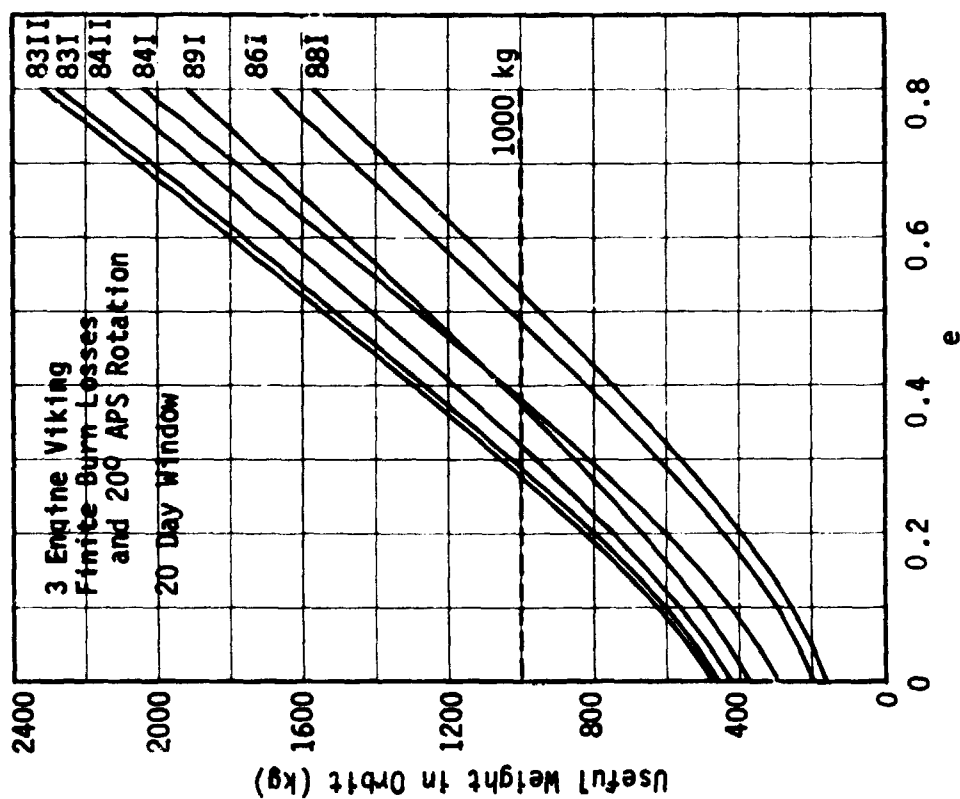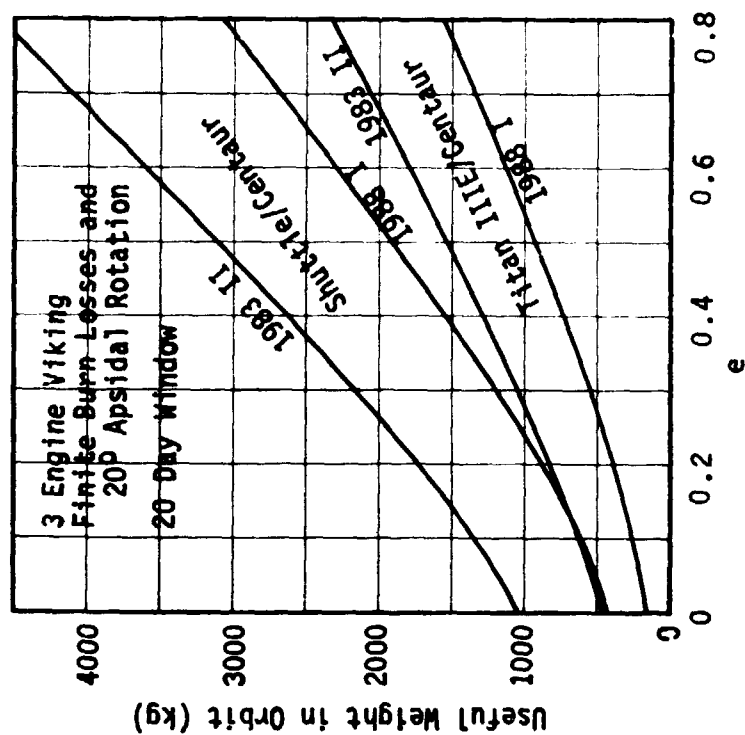
Figure III-6 Weight in Orbit Capability, 3-Engine Viking Propulsion

Additionally, a narrower range of apsidal rotation requirements can
be treated, which tends to eliminate the more extreme cases for these
missions. The opposite is true of a longer window. If a 30-day
window were to be designed, the problem of the performance "tails"
and extremes for apsidal shift would be aggravated, with a corres-
ponding loss of in-orbit weight capability.

Finally, the value of Shuttle/Centaur as a launch alternative
can be derived from Figure III-7. Its potential capability for
delivering a payload to Venus is about twice that of Titan IIIE/
Centaur, and this opens the possibility of a dual spacecraft mission.
With two spacecraft in Venus orbit a variety of options is made avail-
able. First, the two vehicles could be targeted separately to con-
centrate mapping coverage over each hemisphere, north and south, with
each orbiter's periapsis located at opposing mid-latitudes. This
would ensure 100% surface coverage from pole to pole, with reduced
apsidal shift requirements. Probably a more attractive option would
involve a time-staggered insertion sequence for the two spacecraft,
placing them into identical, but lagging, orbits. With this concept,
the leading orbiter could map in the nominal resolution mode gaining
the desired complete, overlapping surface profile. The second space-
craft in its trailing orbit, phased to allow digestion of the area
coverage map, could then be a high resolution mapper, concentrating
on real or near real-time-selected features of interest. A third
option would simply be the idea of redundant vehicles assigned the
same basic mission, serving as a mutual backup system. This summa-
rizes a few of the more promising alternatives for a Space Shuttle/
dual spacecraft mission design.

Orbit Insertion Requirements

As indicated previously, the initial performance evaluation
treated a simplified orbit insertion in order to set the picture for
the in-depth study. Early design work on location of periapsis,

which will be discussed in detail in the subsection on orbit orien-
tation possibilities, indicated that some provision be made for the
inclusion of apsidal shift capability during orbit insertion. In
brief this arises from the desire to relocate periapsis for eccentric
orbits either to the equator, or other specified latitude, by shift-
ing the nominal location gained by coplanar, optimal insertion. A
20° shift has been selected as sufficient to provide enough capa-
bility to achieve a periapsis at most considered latitudes for most
missions. In addition, the large burn times and areas associated
with the resulting insertion maneuvers indicated that finite burn
'osses needed consideration for a complete assessment of insertion
requirements.

The detailed analysis has considered the effects of inserting the
delivered payload at Venus into orbits of varying eccentricity. Pro-
pellant load and payload weight in orbit were dependent parameters,
as was the resulting ΔV. A pre-insertion weight of 4000 kg was ini-
tially assumed as nominal, based on the Titan IIIE/Centaur capability to
deliver that weight to Venus for most mission years. Burns were con-
sidered to be at fixed attitude. Orbit eccentricity was a primary
independent variable, along with Vhp magnitude at Venus. For the
missions considered, Vhp ranged from 3 to 5 km/sec.

These assumptions yielded a conservative evaluation of the bounding
values of finite burn loss, and the degree of conservatism will be ad-
dressed later. Given the thrust level (2.669 N) and mass flow (-.95162
kg/sec) typical of a 2-engine Viking class insertion propulsion system,
the burn times and arcs for insertion into even the relatively "loose"
orbit of 0.5 eccentricity were found to produce unacceptable losses. The
ΔV penalties assessed orbit insertion ranged between 400 and 700 m/sec
for the appropriate Vhp range, with losses of far greater magnitude
for less eccentric orbits. The dashed line of Figure III-8 represents
the losses and apsidal shift penalty with two engines and .5 eccentri-
city.
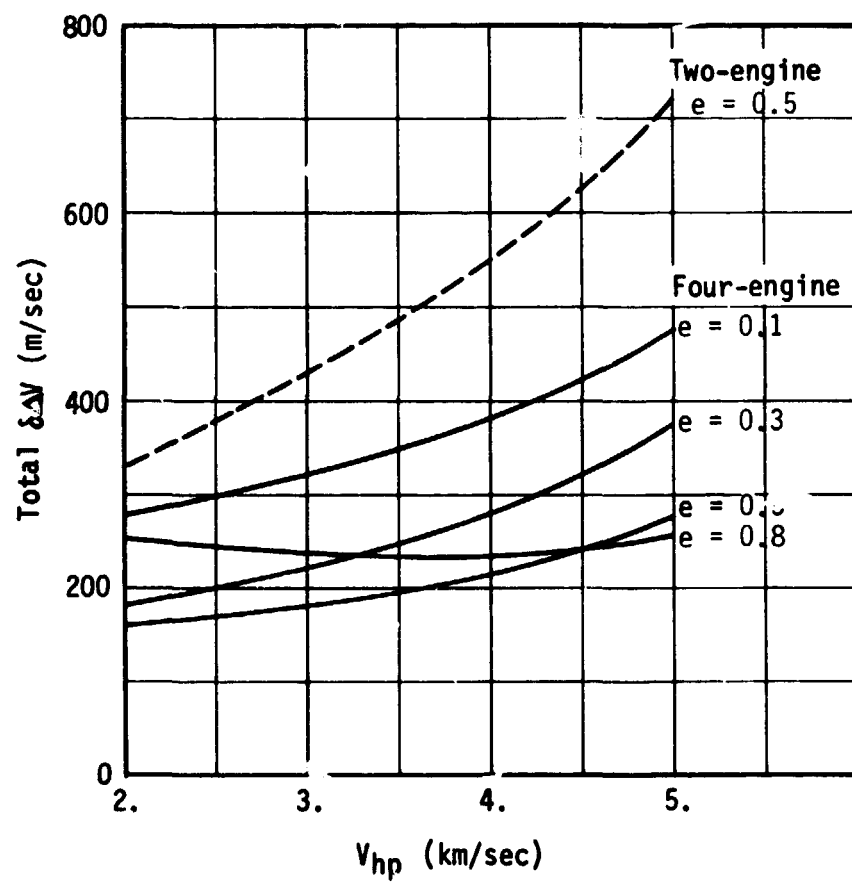
Figure III-8 Finite Burn Loss and Apsidal Shift for 2 and 4 Engines

Due to the severity of finite burn loss, a 4-engine system was
evaluated, with net thrust level thereby doubled. Predictably,
losses were reduced to more reasonable levels, in some cases reduced
by more than 60%. In Figure III-8 the family of curves for the 4-
engine configuration presents the burn loss/apsidal shift require-
ments for varying e and Vhp. System studies intervened at this point
and indicated that from an operational view, growth to a 3-engine sys-
tem would be far superior to anything larger. Losses associated with
that system were then examined, and found to be nearer the 4-engine
figures than they were to the 2-engine case, and of a manageable
nature. Loss levels for the 3-engine system are illustrated by
Figures III-9 and III-10. All curves include the allowance, or
penalty, of the 20° apsidal shift. These ΔV penalties underlie the
modification of performance presented in Figures III-6 and III-7 of
the preceding subsection.

In assessing the quantitative nature of finite burn loss charac-
teristics for various propulsion thrust levels, considering different
orbit sizes and pre-insertion weights, a convenient parameter for
measuring these losses is the pre-insertion thrust to weight ratio
(T/W). With T/W as the principal independent parameter, a family of
curves has been developed, Figure III-11, which relates the amount
of finite burn loss to the impulsive ΔV requirement and removes the
previous conservatism. This set of curves can then be used to evaluate
each mission opportunity in terms of defining reasonable thrust levels
for a variety of desired orbit sizes. The impulsive ΔV requirements for
each opportunity, with adjustment made for a 20° apsidal shift, are shown
in Figure III-12 varying with orbit eccentricity. Here the highest Vhp
of each launch window has been selected for worst case analysis.

Figure III-11 includes curves for impulsive ΔV equal to 1800,
2400, 3000, and 3800 m/sec, which roughly correspond to the range
appropriate to the Venus orbiter missions considering eccentricities

Figure III-10 Finite Burn Loss and Apsidal Shift

for 3 Engines, Versus Eccentricity

Figure III-9 Finite Burn Loss and Apsidal Shift

for 3 Engines, Versus V_{hp}
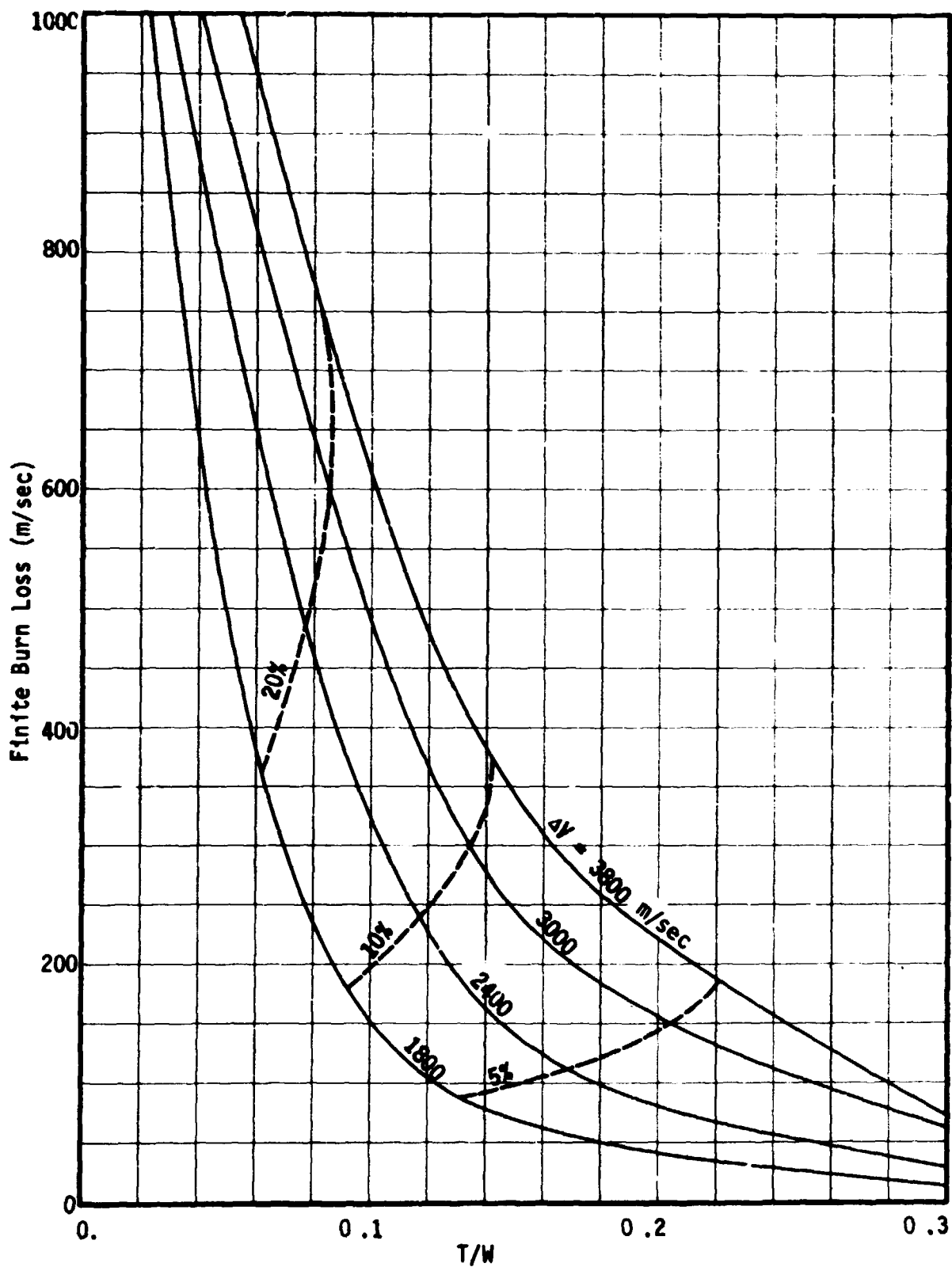
Figure III-11 Finite Burn Loss Versus Initial T/W and Impulsiv· ΔV
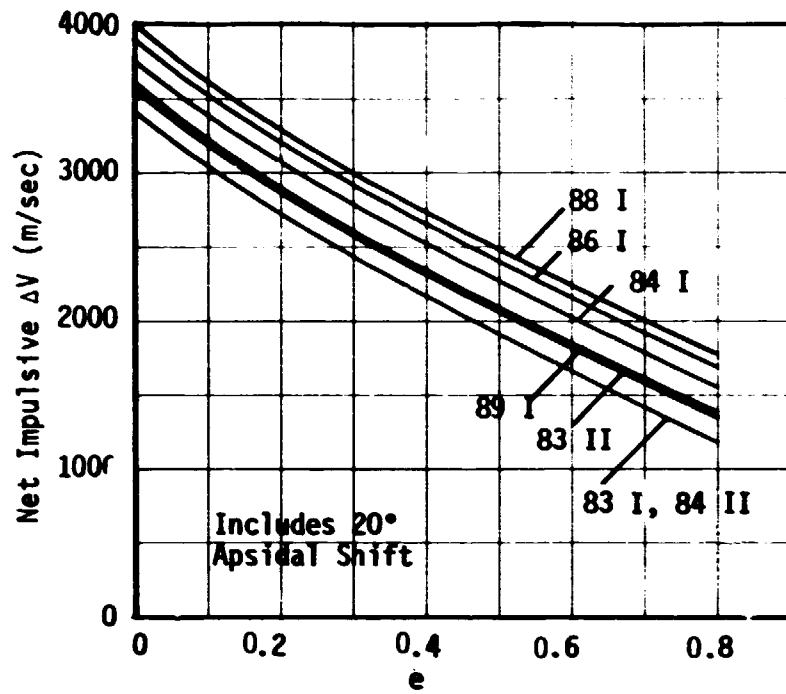
Figure III-12 Impulsive ΔV (Including 20° Apsidal Shift) For All Missions
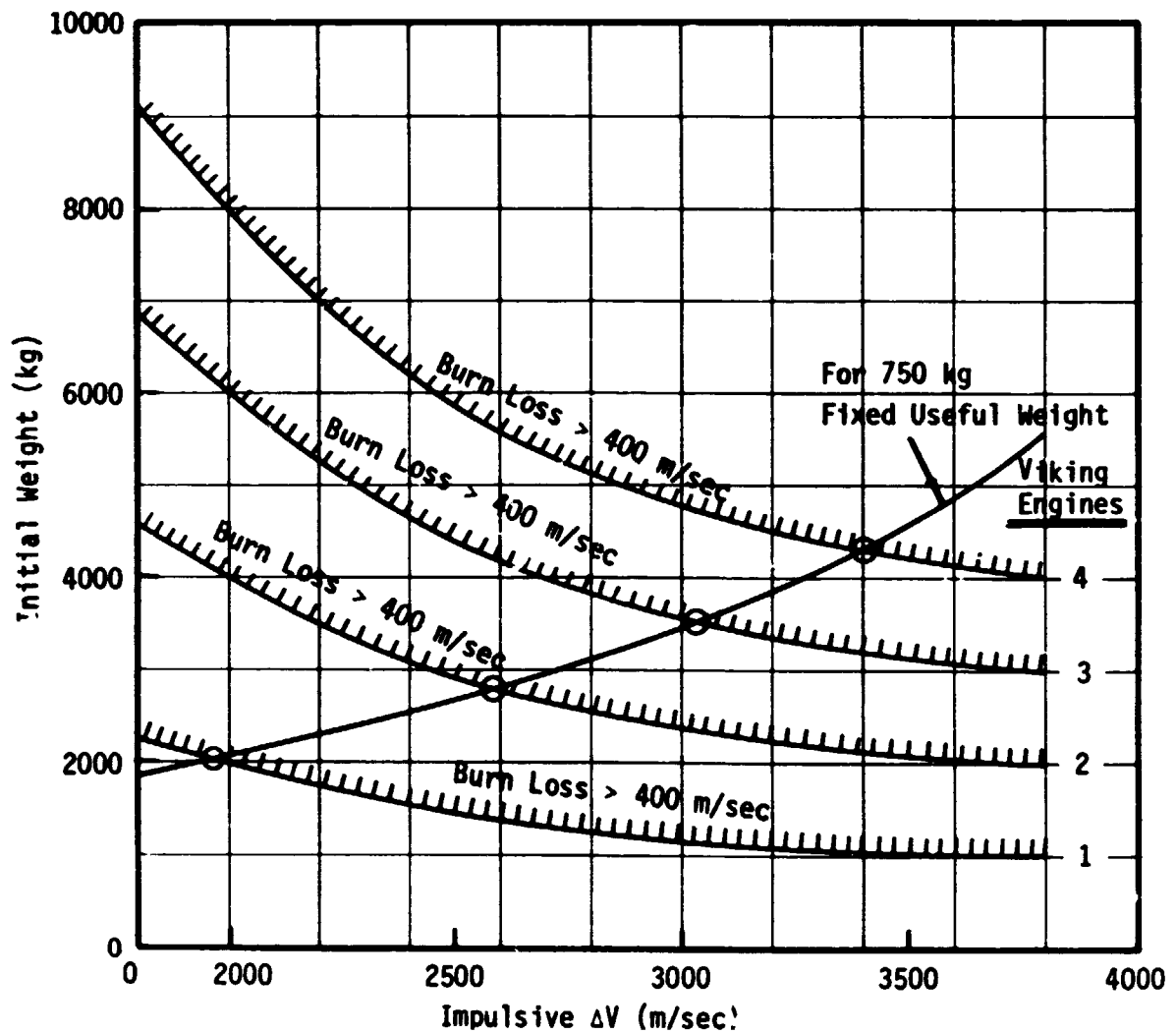
Figure III-13 Initial Weight Requirements for Fixed Useful Weight (750 kg) and Varying Thrust Levels

from 0 to 0.8. The dashed lines portray curves of burn loss as a
constant percentage of impulsive ΔV. To establish some criterion
for determining the thrust level (number of Viking class insertion
engines) adequate for a given ΔV requirement and initial weight, an
arbitrary limit on burn loss magnitude has been assumed. A fixed
magnitude limit is probably a more reasonable constraint than a fixed
percentage of impulsive ΔV, since with the fixed percentage higher
losses would be allowed where higher basic ΔV levels already exist.
On this premise, a burn loss limit of 400 m/sec has been selected.
Also, at this point the losses are increasing rapidly for small
variations in T/W.

From this limit, a minimum T/W can be defined for the various ΔV
levels, and as thrust is equated to the 1, 2, 3 and 4-engine combina-
tions, maximum initial weight limits are established for each config-
uration. This picture is illustrated in Figure III-13, where the
"switchover points" are related to ΔV and initial weight. On the
same plot can be superimposed a curve which represents the initial
weight required to achieve some fixed, desired payload weight in
orbit, also varying with ΔV level. Based on detailed systems' assess-
ments of weight-in-orbit req ements, a nominal payload of 750 kg
has been considered in this ysis. These assumptions then lead
to the definition of the maximum initial weight to achieve the desired
payload in orbit appropriate to each engine combination, as finite
burn loss is kept under 400 m/sec. The critical points are circled
in Figure III-13. An additional constraint of total burn time limits
the one engine use to the single burn ΔVs associated with the 750 kg
useful weight and 2000 kg initial weight.

From the philosophy detailed above, all mission years can be re-
examined, not on the basis of simple payload capability, but instead
with the view of defining required insertion propulsion system char-
acteristics for gaining a realistic desired payload (of 750 kg).
Figure III-14 then represents an alternative picture of performance
for the Venus radar mapper missions. Here the curves are of pre-
insertion weight requirements for the mission years and are functions
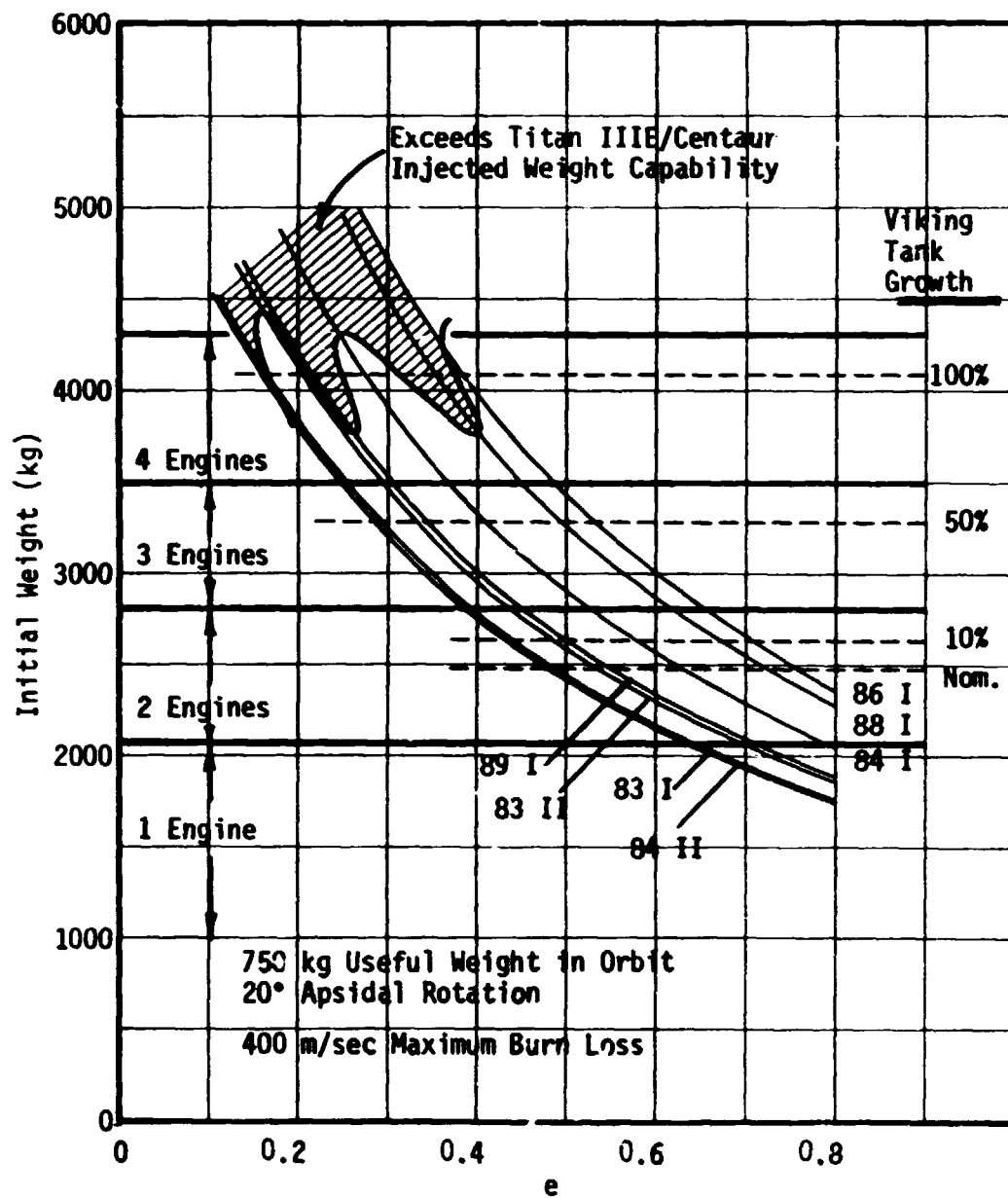
Figure III-14 Mission Year Performance: ^re-Insertion Weight Requirements

for 750 kg Useful Weight with Varying Eccentricity

of arrival Vhp, desired orbit eccentricity, and the assumed 750 kg
payload in orbit. These initial weight requirements in turn serve to
define the required propulsion system. In the figure engine level
"switchover points" are indicated, along with propellant load expressed
as a percentage of nominal Viking propellant tank capacity. Propel-
lant load is directly related to initial weight when payload weight
is fixed, and is also a function of the propellant inert weight algo-
rithm assumed -- here,

$$\text{PROPELLANT INERTS} = 130 \text{ kg} + 0.135 * \text{PROPELLANT LOAD} \quad \text{(III-1)}$$

The cross-hatched region indicates limits to pre-insertion weight
which derive from the capability of Titan IIIE/Centaur, based on the
launch energy (C_3) associated with each mission.

For an orbit of 0.5 eccentricity all mission years can achieve
the desired inserted payload with an insertion propulsion system of 3
engines, and with propellant requirements ranging from a nominal
Viking tankage situation in 1983 and 1984 to a 60% growth in 1986.
With an eccentricity of 0.3, given the same range of propulsion con-
figuration and stretch, missions in 1986 and 1988 would be unattain-
able from launch energy limits, while the 1984 Type I trajectory
would need 4 engines. For orbit eccentricity below 0.2, nearly all
years require a higher performance insertion system and much larger
propellant allocations with Titan IIIE/Centaur as the launch vehicle.

Current indications point to the 3-engine configuration as work-
able, and although a 60% growth in the nominal Viking tankage is
significant, the primary conclusion to be drawn from this analysis
is the attractiveness of the 0.5 orbit for our reference mapping orbit
design. Under the section Spacecraft Systems, Volume III, the supe-
riority of the 3-engine configuration, against either the 2 or 4
engine systems, is discussed in terms of its value as the simplest
mechanization growth alternative for standard Viking insertion pro-
pulsion.

Encounter Geometries

Examination of the planet/trajectory geometries at Venus encounter was essential to the development of what degree orbit design could be divorced from dependency on mission year. The determination of those parameters which were significantly variable with mission opportunity would indicate the range of options and situations which the analysis would have to treat.

In Figure III-15 are illustrated typical orientations with respect to Venus of the Earth, Sun, Vhp vector, and subperiapsis locus for all considered mission years. Specific angles are tabulated in Table III-2. Of immediate note is a general similarity of arrival geometry for all cases in the plane of the ecliptic. The Vhp vector is generally directed opposite the Earth vector, implying orbit insertion out of Earth view for all cases. In addition, the orientation of the Earth vector with respect to the Sun is nearly constant, ranging only between 90° and 110° East of the Sun for all missions. The recurrence of this same basic geometry in the ecliptic has implications of similarity for occultation characteristics, orbit stabil .y, power profiles, communications schedules and thermal load, and supports a general independence of these parameters from launch year and trajectory type.

The only significant variations of the arrival picture involve the Vhp vector. Specifically, both the magnitude and declination of Vhp exhibit substantial variation and mission dependency. Vhp magnitude varies from values under 3 km/sec for 1983 and 1984 missions, to a maximum near 5 km/sec for 1986, as shown by Figure III-16. This condition has a strong, direct influence on orbit insertion ΔV requirements, since as hyperbolic excess velocity at arrival increases, more energy must be removed from the trajectory to transfer into orbit. Vhp declination also varies considerably, ranging from -40° (South) for 1986 to +40° (North) in 1988. The declination range is

South Polar View

North Polar View

1983 I

1986 I

1989 I

1984 II

1988 I
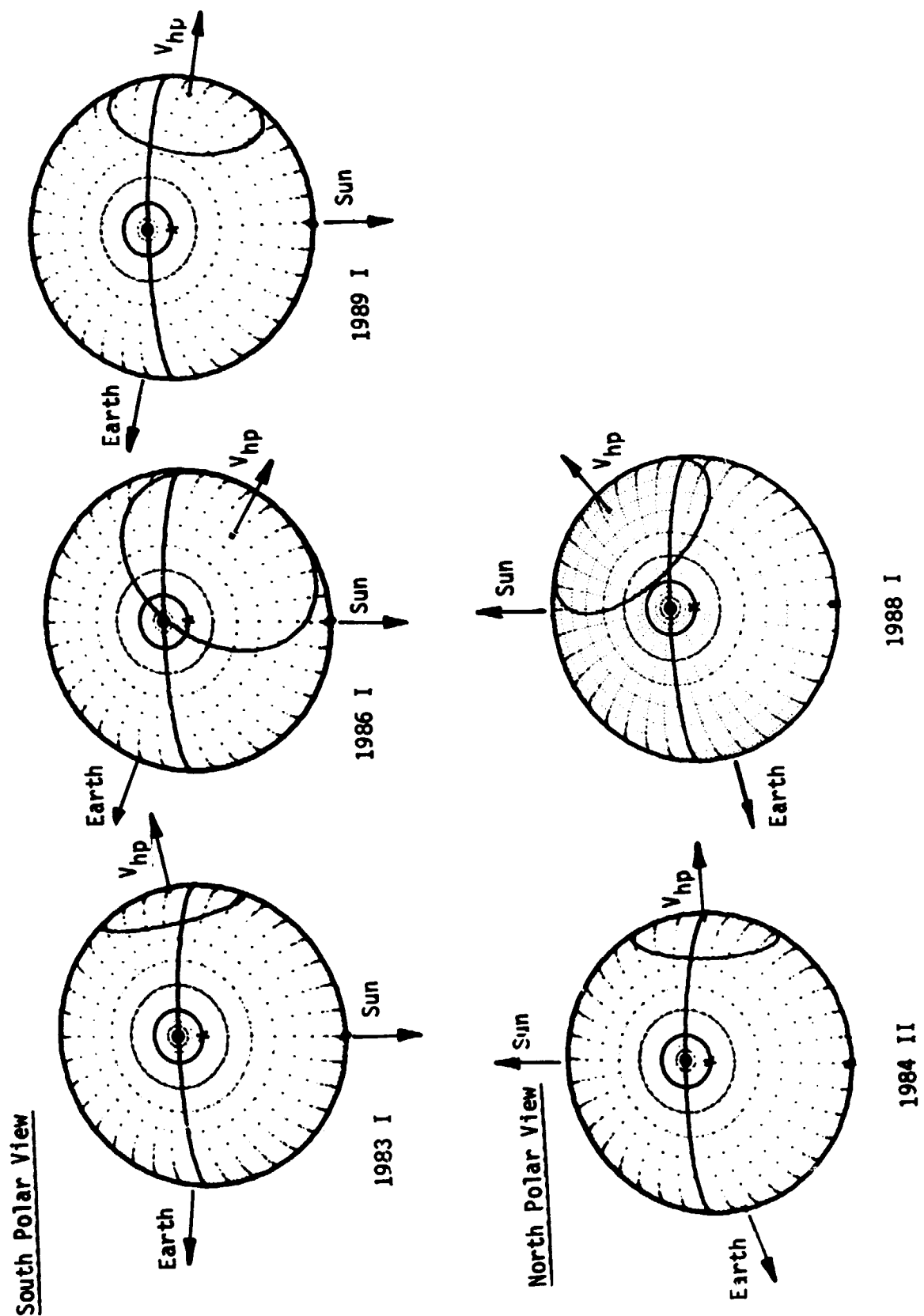
Figure III-15 Typical Venus Encounter Geometries

Table III-2 Trajectory Arrival and V_{hp} Characteristics For All Mission Years

Mission	Window Day	Arrival Date	Sun-Spacecraft-Earth Angle (deg)	V_{hp} Declination* (deg)	V_{hp} Right Ascension* (deg)
1983 I	1	10-15-83	104	14	293
	10	10-26-83	95	-13	263
	20	10-23-83	97	-22	271
1983 II	1	11-02-83	91	-30	241
	10	11-02-83	91	-26	244
	20	11-03-83	90	5	244
1984 I	1	05-12-85	115	4	309
	10	05-12-85	115	29	315
	20	05-13-85	114	32	317
1984 II	1	05-21-85	107	26	269
	10	05-22-85	106	18	275
	20	05-27-85	102	-3	269
1986 I	1	12-15-86	114	-42	318
	10	12-18-86	111	-43	312
	20	12-21-86	108	-43	303
1988 I	1	07-26-88	110	39	318
	10	07-30-88	106	38	307
	20	08-03-88	103	34	293
1989 I	1	03-05-90	108	-31	305
	10	03-10-90	104	-24	290
	20	03-17-90	99	-13	268

* Venus orbit plane system, Sun referenced.
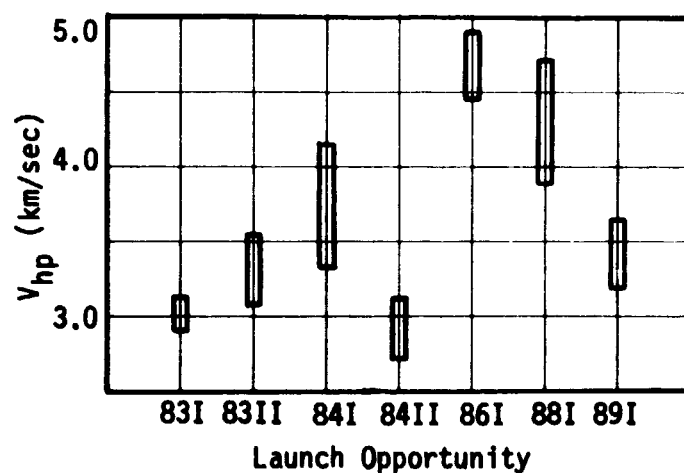
Figure III-16 V_{hp} Magnitude Range for All Mission Years
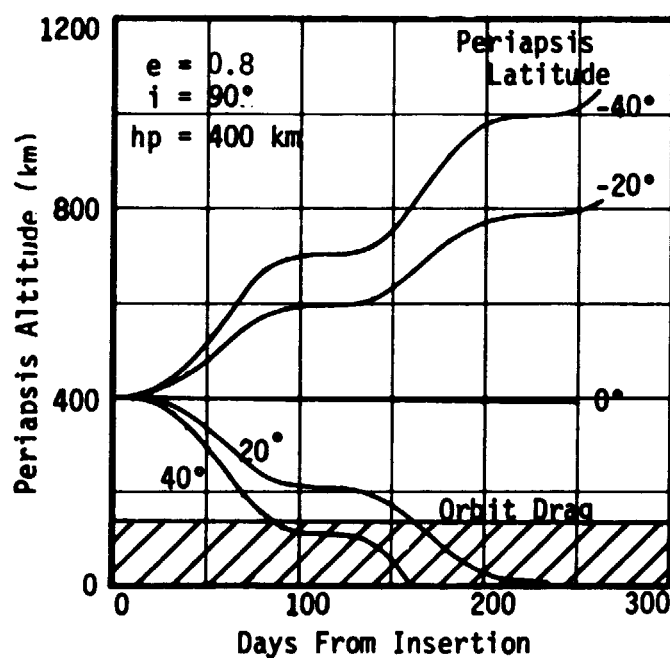
Figure III-17
Polar Orbit Stability
for 0.8 Eccentricity
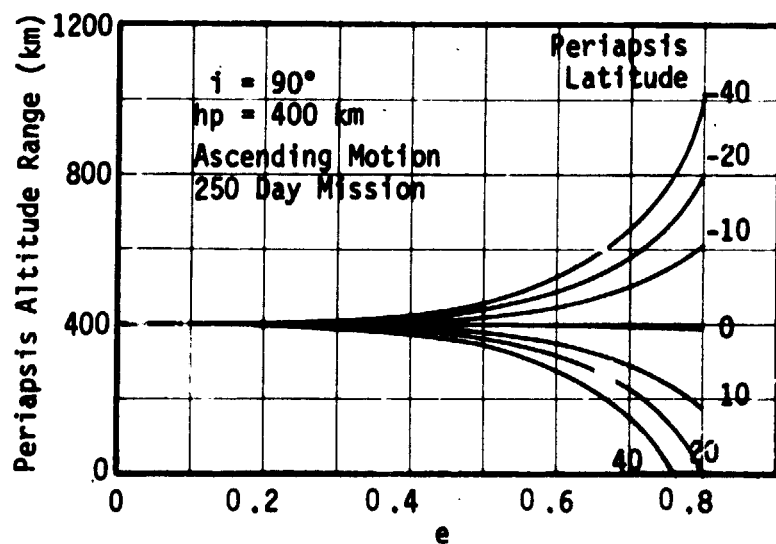
Figure III-18
Polar Orbit Stability
for Varying Eccentricity

an important determinant of the locus of possible orbit orientations and periapsis locations, and will be addressed in detail in a later subsection. In brief, it allows for polar orbits a nominal placement of periapsis at almost any latitude when the entire set of opportunities during the 1980s is considered.

Orbit Stability

As a result of the indication that orbit stability might be relatively independent of mission opportunity due to encounter geometry similarity, that hypothesis was first tested by computer analysis using the "lifetime" program (ref. III-2) and found to be valid. Detailed analysis of orbit stability then proceeded in the direction of determining practical limits to orbit size (eccentricity) given the set of orbit inclinations (90° ± 15°) and periapsis locations (0°± 40°) deemed appropriate to the orbiting mapper.

Assumptions relevant to this analysis involve the influence of various perturbative terms on the life of a Venus orbiter. Gravity harmonics which can be estimated for Venus based on the little knowledge available, as the J2 term for oblateness, appear to be insignificant. Higher order harmonics remain unknown. The existence of mascons would be only speculative, certainly unmodelable. Given this situation and the proximity of Venus to the Sun, the dominant influence on orbit stability is assumed to be from solar perturbations on the orbit.

The stability analysis that follows has concentrated on the characteristics of polar orbits, of both descending and ascending node motion near periapsis. Since a side-looking radar system would require some off-polar inclination bias to view the actual pole of the planet, inclinations up to ±15° off true polar were examined to determine whether their stability characteristics were sufficiently close to 90° inclination to allow the simplifying polar orbit assumption to be made for the parametric analysis. Differences in

periapsis altitude variation over the 240 day mission lifetime were found to be on the order of only 5 km for orbits of 0.5 eccentricity with inclination between 90° ±15°, so the data presented can be assumed to hold for all reasonable mapping orbits considered.

The type of instability which can exist for a polar orbit is illustrated most clearly by Figure III-17. This does represent a rather extreme case, for a very high eccentricity of 0.8, but shows the crucial influence of periapsis location in latitude. This case corresponds to periapsis near the orbit ascending node. If periapsis is located on or near the planet equator (again in the Venus orbit plane system) variation in periapsis altitude is minimal over the life of the mission. As periapsis is located much off the equator, however, the altitude variation becomes significant. A location at only 20°S causes the initial periapsis altitude of 400 km to grow to 800 km in 250 days, while a location at 20°N results in entry into the sensible Venus atmosphere only 140 days after insertion, with impact soon following. Locations further removed from the equator tend to aggravate the variation, although the amount of the increased variation is not as large at the higher latitudes, as seen by the differences between the 40° and 20° curves of Figure III-17. If periapsis were near the descending node of the orbit, the curves would reverse for positive and negative latitudes. That is, with ascending node motion about periapsis, as is the case in these figures, a Northern periapsis causes altitude decay. With descending node motion about periapsis, the same northern location would cause periapsis growth at about the same rate. To summarize this effect, periapsis altitude in polar orbit decays for a northern periapsis when nearest the ascending node, and for a southern periapsis when nearest the descending node. To avoid altitude decay then, ascending node missions should seek a southern periapsis, and descending node missions a northern periapsis.

Of primary interest to the mission parametric trades is the effect of eccentricity on this polar orbit stability picture. Figure III-17 illustrated an extreme situation for 0.8 eccentricity. In Figure III-18 the maximum variation in periapsis altitude is shown varying with eccentricity, with periapsis latitude a field parameter, again considering ascending node motion about periapsis. From this view, orbit stability becomes much less of a problem if eccentricity can be kept below about 0.6. At an eccentricity of 0.5 the variation is no more than 50 to 60 km even with periapsis at $\pm 40°$, and this would require two orbit trims of 5 m/sec each to hold within a 10 km deadband around the nominal 400 km altitude. For eccentricities of 0.4 or less the variation becomes negligible for the orbital mapper, and orbit trims could no doubt be ignored for these orbit sizes.

To summarize, an eccentricity of 0.6 for a polar orbit mission represents a probable upper limit for manageable orbit stability characteristics. Lesser eccentricities yield increasingly more stable orbits, while orbit eccentricities above 0.6 tend to become unstable exponentially. At these higher eccentricities the location of periapsis off the equator determines the degree of instability.

Orbit Orientation Possibilities

For each arrival date and Vhp vector, of each launch/arrival date set, for all considered missions, there exists a set of orbit inclination-periapsis latitude combinations which can be achieved under the assumption of nominal coplanar transfer into orbit. The set is derived from rotation of the Vhp vector 360° about the planet in the "aim plane" when the trajectory is targeted to specific arrival conditions. The resulting curve of periapsis location is referred to as subperiapsis locus. When plotted against the corresponding orbit inclination, football shaped curves are obtained which illustrate orbit orientation possibilities. Figure III-19 shows these possi-

bilities for a 1983 Type I mission where each football represents orbit orientation loci for the appropriate launch/arrival date set at the beginning, midpoint, and end of a 20-day launch window defined for the mission.

From Figure III-19 it can be observed that if only polar orbits are considered (i = 90°), there exists a double-valued periapsis latitude solution for nominal insertion, corresponding to northern and southern locations, and these solutions can shift considerably over the launch window. This shift is directly the result of variations in Vhp vector declination already discussed. Northern periapsis locations correspond in all considered cases to periapsis near the orbit descending node, with southern solutions corresponding to an ascending node periapsis. Referring back to the preceding section on orbit stability, the situation yields for all cases the desirable feature of periapsis growth rather than decay.

In Figure III-20 are illustrated the periapsis latitude solutions for polar orbits, for each mission opportunity, as these solutions vary over the launch window appropriate for each mission. The curves indicate first of all that in considering the set of all Venus opportunities during the 1980s, periapsis could be placed almost anywhere over the Venusian surface, from near the South Pole in 1986 to the North Pole in 1988, with points in between for other years. The second bit of information which can be derived from the figure is the amount of apsidal rotation which may be requir. o place periapsis at some specified latitude for each opportuni', One product of this view is a criteria based on insertion propulsion limits, for selecting the orbital sense (motion) at periapsis, either ascending or descending. To illustrate, if periapsis were designed for an equatorial location in 1984 (Type I), the optimal choice would be ascending node motion, since this would nominally bring periapsis between 8° to 20° of the equator. Descending orbit motion would

Figure III-19 Orbit Orientation Possibilities for a 1983 Type I Mission
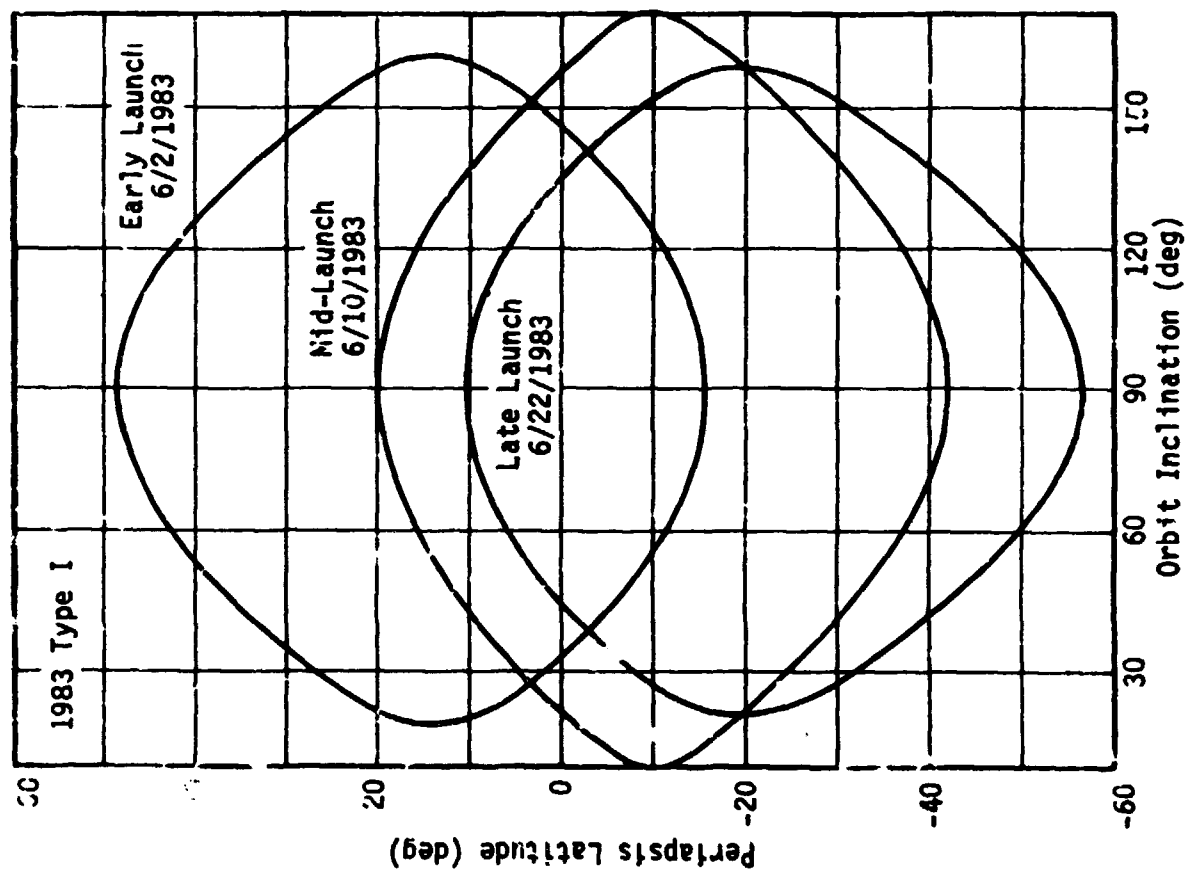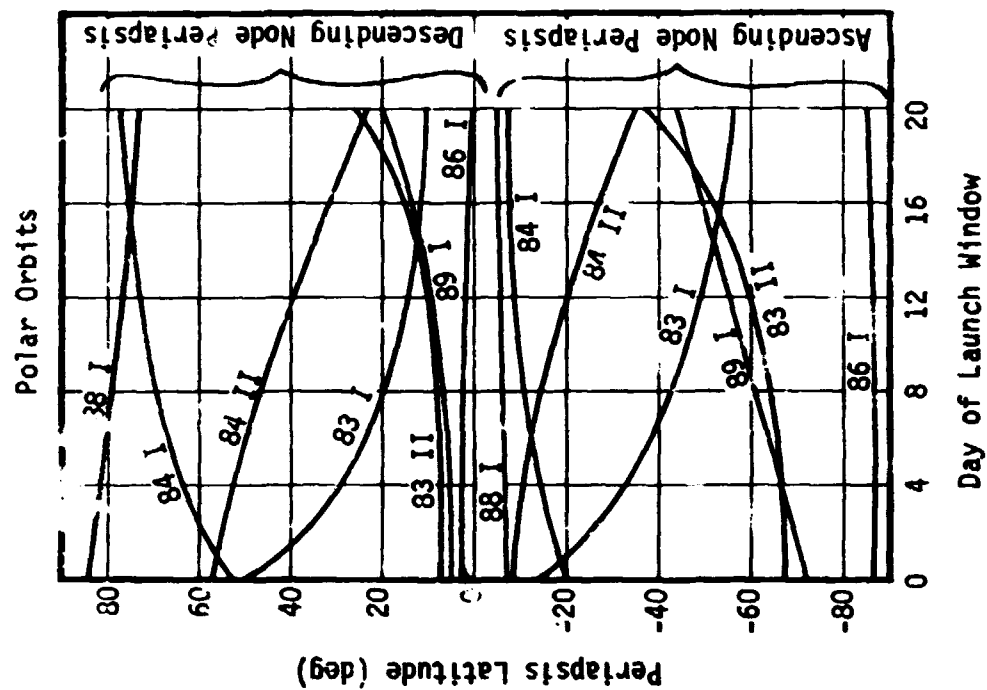
Figure III-20 Nominal Periapsis Latitudes for Polar Orbits, All Missions

place periapsis at latitudes ranging from 50° to 75° north, requiring an unacceptably large apsidal shift maneuver to relocate periapsis. If the nominal design were actually for an equatorial periapsis, missions in 1984 and 1988 would prefer ascending motion at periapsis, while descending motion would be appropriate in 1983, 1986, and 1989. Of course, for periapsis locations at other specified latitudes each mission would have to be assessed individually, with the aid of the curves of Figure III-20, to determine the most efficient node which gains the desired location with least apsidal shift.

For much of the mission analysis study, specifically for the assessment of performance characteristics, a nominal shift capability of 20° has been selected. This is chosen as a mean value which allows access to most of the desirable latitude regions for most of the mission opportunities, yet is not an unmanageable shift from an orbit insertion view. The amount of this shift provides a $\pm 20°$, or 40°, spread around the nominal periapsis location for polar orbits, so where periapsis is not constrained to a particular hemisphere, a high degree of flexibility in periapsis latitude placement usually exists. Exceptions do occur for the 1986 and 1988 opportunities, where the double-valued periapsis solution falls near a pole, and near the equator. For these cases an apsidal shift limit of 20° leaves inaccessible the regions at mid-latitudes (around 45°).

The effect of launch window size on these shift requirements can also be determined from Figure III-20. With 20-day windows, the extremes of nominal periapsis latitude must be considered, as best illustrated by the 1983 Type I mission. For this case the latitude possibilities vary between 50° and 10° in the north, and 15° to 55° in the south. Obviously, if the considered window were reduced to 10 days, for example, the extremes are truncated and the latitude variation diminished. The reverse situation arises with longer launch windows.

In summary, the curves of Figure III-20 serve to indicate areas most access ble for periapsis location with each mission, and the degree of apsidal shift needed to locate periapsis somewhere other than its nominal latitude. Illustrated in Figure III-21 is a typical orientation for a polar mapping orbit, with 0.5 eccentricity. In this case periapsis has been shifted off the subperiapsis locus for placement over the equator, with radar map· ω, $\pm 90°$.

Surface Coverage Potential

Surface coverage is primarily a function of the particular radar system considered, and its limitations. As has been previously addressed, access to 100% of the Venus surface is readily available through the design of polar or near-polar orbits, in combination with a mission life of at least 243 days to allow one complete rotation of the planet under the mapping orbit. Since the circular orbit is not the most economical solution to the problem of increased range due to the associated high insertion propulsion requirements, the eccentric orbit influence on radar mapping strategy and surface coverage limitations must be considered. Radar mapping limits arise from the increased range, hence increased power and ambiguity problems, as true anomaly increases in an eccentric orbit. Essentially these limits show themselves for a fixed side-look angle radar in bounds on the spread of true anomaly through which the radar sy. em c in operate, and this spread decreases with increased eccentricity as radar range versus true anomaly increases with eccentricity.

Where radar mapping is limited to a true anomaly spread less than $\pm 90°$, two alternative strategies are available which determine the desired location of periapsis. If a balanced treatment of both hemispheres is to be obtained, the mapping swath should be centered around the equator and periapsis would be located there. If instead it is more desirable to map at least one pole, as indicated by the science analysis, periapsis must be offset sufficiently to allow

III-33
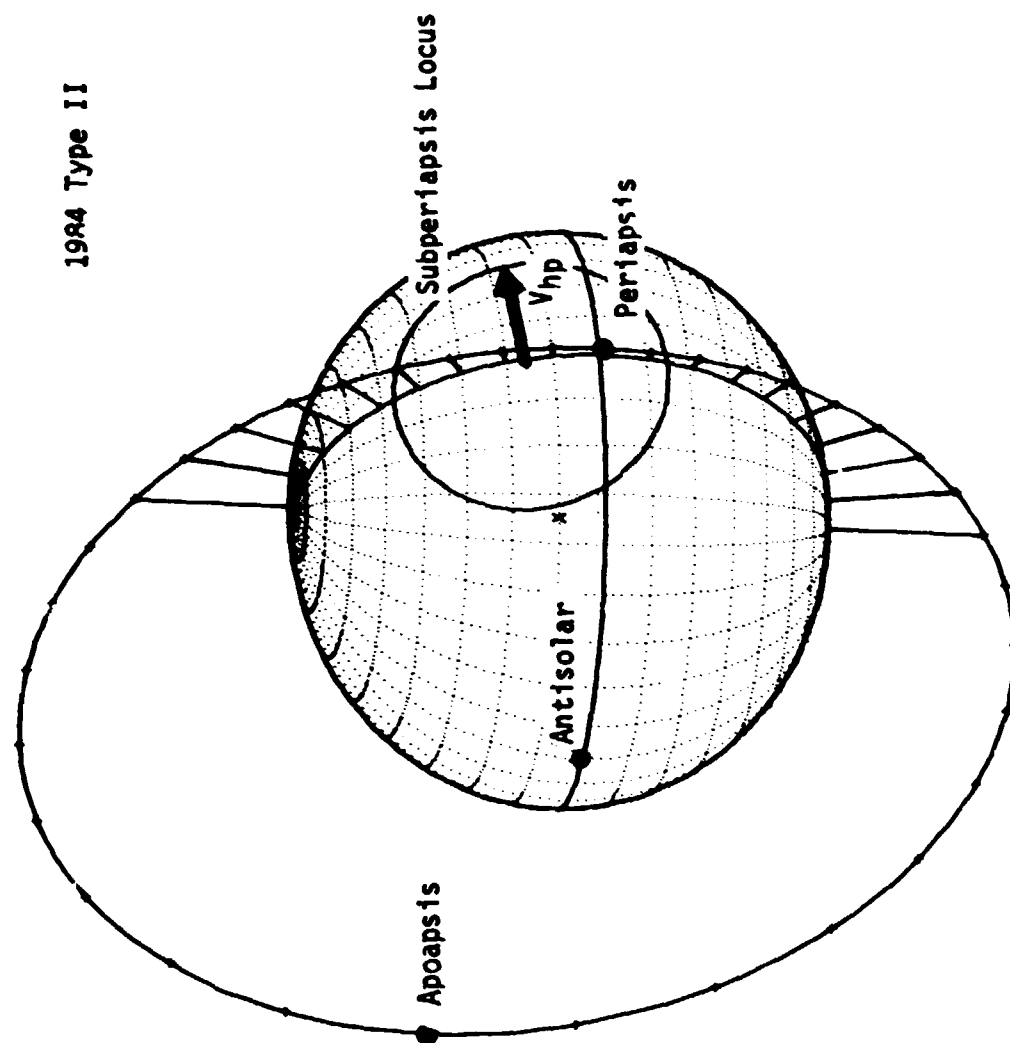
Figure III-21 Typical Mapping Orbit Orientation, 0.5 Eccentricity

1984 Type II

Subperiapsis Locus

V_{hp}

Periapsis

Antisolar

Apoapsis

extension of the swath up to polar latitudes. For example, given a true anomaly limit of ±60°, a balanced treatment would correspond to periapsis of the equator, mapping ±60° in latitude. The polar treatment would require locating periapsis at a latitude of 30° with mapping latitudes then ranging -30° to 90°.

These two strategies yield somewhat different potentials for the amount of surface actually mapped. The resulting coverage potentials for various mapping limits and strategies are summarized in Table III-3, with percentages of total planet coverage listed for each. For contiguous and overlapping coverage from subsequent mapping passes the radar must be designed to the appropriate beamwidth that achieves the specified overlap. This design is a function of orbit spacing (orbit size) and mapping frequency for each orbit considered, and is treated in de.._ii in a major section devoted to radar and antenna systems design in Volume III.

Table III-3 Surface Coverage Potential
(Fixed Side Look Angle)

Mapping True Anomaly Range	Equatorial Balance		Polar Coverage	
	Latitudes	% Surface	Latitudes	% Surface
±90°	-90° to 90°	100.0	-90° to 90'	100.0
±75°	-75° to 75°	96.6	-60° to 90°	93.3
±65°	-65° to 65°	90.6	-40° to 90°	82.2
±55°	-55° to 55°	82.0	-20° to 90°	67.1

Occultation Characteristics

Occultation histories in polar orbit have been generated to facilitate those system trades which are closely related to Sun and Earth shadow times. These system design trades include definition of mission timelines, power profiles, thermal load assessment, and the definition of schedules for communications and data handling.

Figures III-22, 23, and 24 illustrate characteristic occultations for orbits 0, 0.3, and 0.5 eccentricity with periapsis located at the equator and at an altitude of 400 km. As was indicated by the examination of encounter geometry, orbit insertion at periapsis occurs out of Earth view. Soon after insertion periapsis begins a period of occultation from the Sun. For the radar mapping, illumination of the surface under periapsis does not have the same relevance as it would for photographic or television mapping, but solar occultation does have an influence on thermal and power profiles. Midway into the orbiter mission apoapsis passes through Earth shadow, and 30 days later, through the Sun shadow. This period represents maximum per orbit occultations with which the spacecraft must contend. The duration of these maximum occultations is presented in Figure III-25 for varying eccentricity, shown as total hours occulted per orbit and % of orbit period. As indicated by the two curves, although the occultation time per orbit increases with increased eccentricity, the percent of the orbit period spent in occultation actually decreases, representing a net decrease in total occultation time over the mission duration.

Figure III-26 illustrates how the occultation picture varies when periapsis is located off the equator--in this case, at -35 for a 0.5 eccentricity. The effect of off-equatorial periapsis location is that of increasing the duration of near-periapsis occultation. This situation is summarized by Figure III-27 where maximum periapsis and apoapsis occultation times are shown varying with both eccentricity and periapsis latitude. The more significant effect is from eccentricity but periapsis latitude becomes significant at the higher eccentricities.

As suggested by encounter geometry similarity, the occultations were found to be relatively independent of mission opportunity. It was observed that over the set of all 1980s opportunities, the
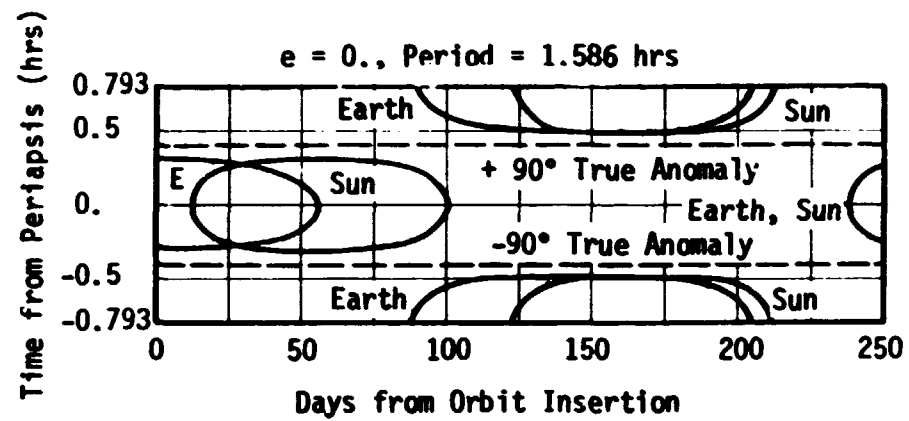
Figure III-22 Occultation History for 400 km Circular Orbit, Periapsis at Equator
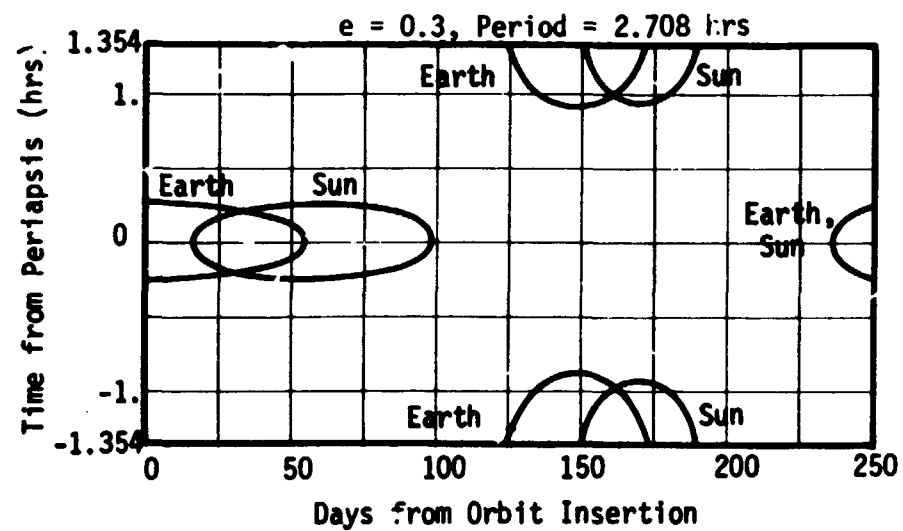
Figure III-23 Occultation History for 0.3 Eccentricity, Periapsis at Equator
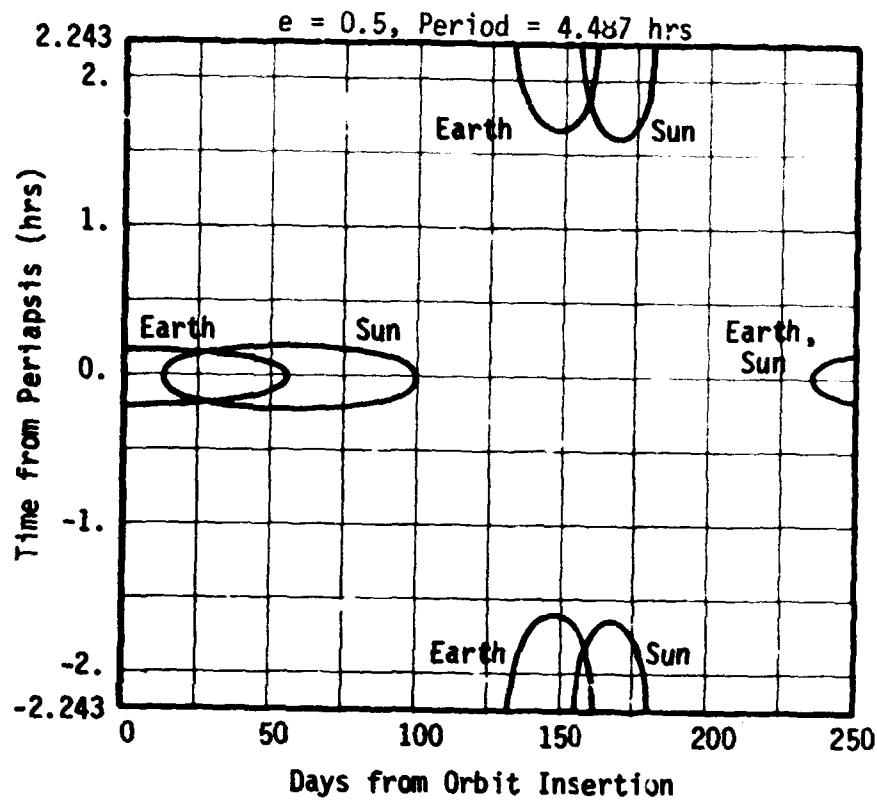
Figure III-24 Occultation History for 0.5 Eccentricity, Periapsis at Equator
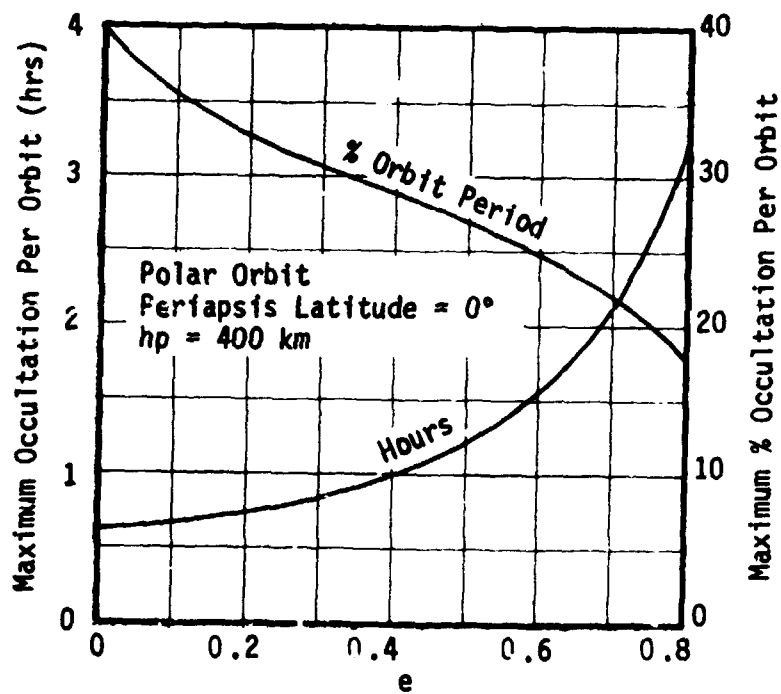
Figure III-25 Maximum Occultation Periods for Varying Eccentricity
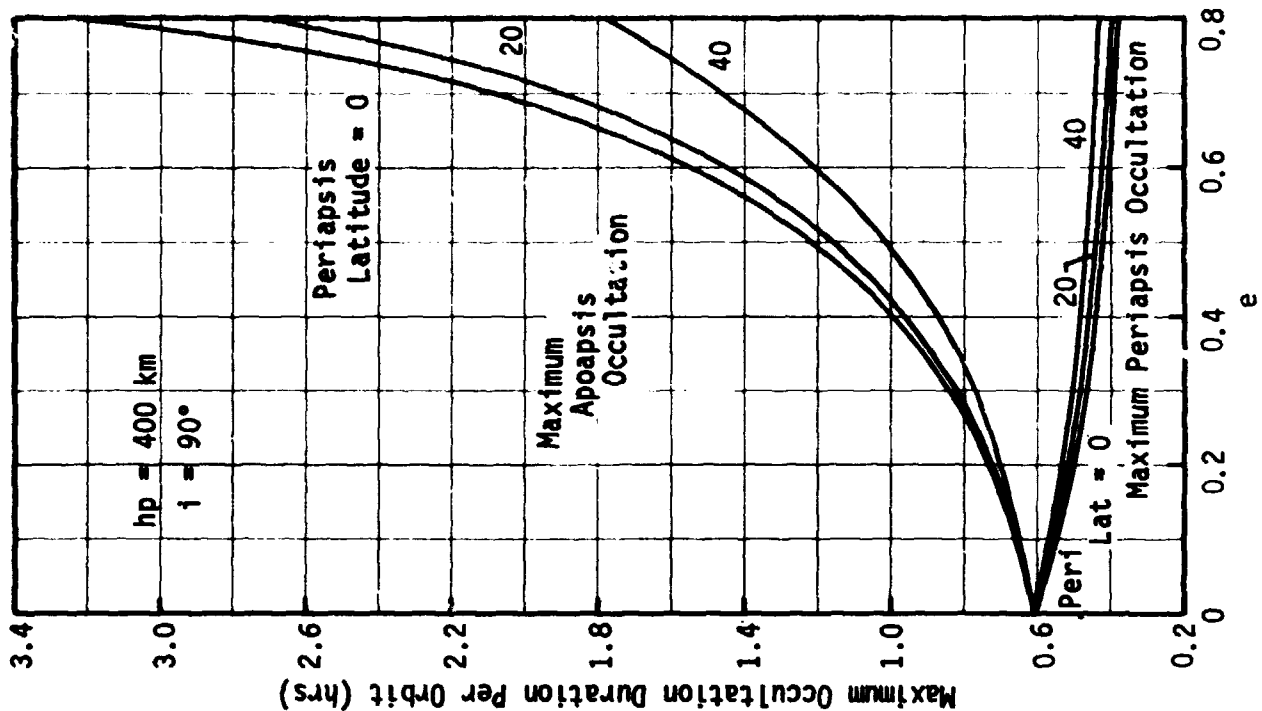
Figure III-27 Effect of Off-Equatorial Periapsis on Maximum Occultation Periods
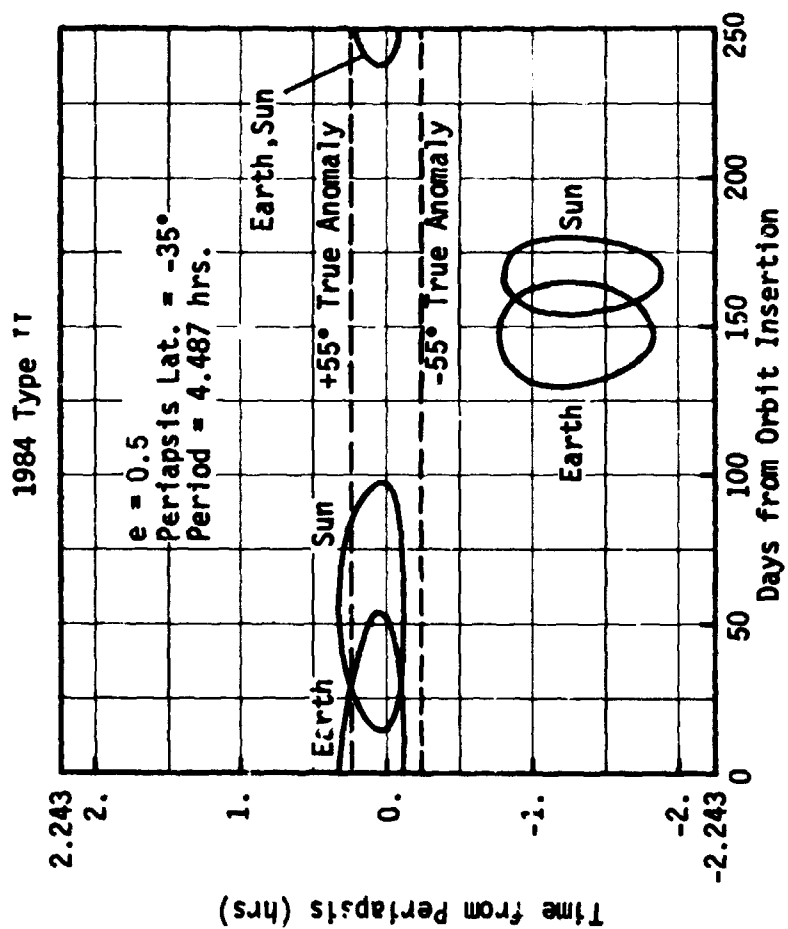
Figure III-26 Occultation History for 0.5 Eccentricity Periapsis at -35°

timing of the overall occultation pattern might shift by ±30 days
with respect to orbit insertion, but the relationship of particular
occultations with one another remained unchanged. In all cases, the
243-day mission duration necessitated passage through both periods
of maximum periapsis and apoapsis occultation. Hence, the impact of
occultation times can be reduced only by shortening the mission
duration.

Navigation and Orbit Determination

The missions to Venus in the 1980s have been examined to deter-
mine navigation characteristics associated with their interplanetary
cruise phases and to assess the accuracy with which orbit determina-
tion can define the resultant orbit about the planet. Midcourse ΔV
requirements have been evaluated for two of the missions considered
representative of the entire set--a Type II trajectory in 1984, and
a Type I trajectory in 1988. For each mission an Encke integrated
trajectory, targeted to the desired arrival conditions, has been
generated to allow the statistical definition of midcourse ΔV and
trajectory dispersions. Both evaluations considered a somewhat pessi-
mistic assumption of navigation error levels existent in the 1980s.
Neither Quasi-Very-Long-Baseline Interferometry (QVLBI) tracking
processing, nor charged particle calibration capability, have been
assumed. Hence, equivalent station location errors are sized at
4.5 m for spin radius, 4.25 m for Z-height, and 5.0 m for longitude,
all one-sigma values. Execution errors for the midcourse corrections
correspond to 0.25% proportionality, 25 mm/sec resolution, and 0.5
pointing error. Errors in the Venus ephemeris have also been con-
sidered, and assumed to be 20 km spherical in position.

For each mission two midcourse corrections are adequate. The
first is executed 5 days after launch to remove injection errors.
A second is executed 10 days prior to Venus arrival to remove those
trajectory errors which grow from the execution of the initial mid-

course, and its effect is that of fine-tuning the trajectory to
achieve the desired encounter conditions. Table III-4 presents the
resulting statistical ΔV magnitude (mean + 3 sigma) for both missions,
along with the resulting B-plane dispersions mapped to encounter.

Table III-4 Statistical Midcourse ΔV and Encounter Errors

Mission	M/C 1 (m/sec)	M/C 2 (m/sec)	Total ΔV (m/sec)	One-Sigma Encounter Errors		
				σRp (km)	σW (deg)	σi (deg)
1984 II	28.54	8.00	36.54	38	0.51	0.18
1988 I	26.53	3.47	30.00	112	0.42	0.64

The results of the analysis indicate that 1) midcourse ΔV require-
ments are about the size anticipated and of a manageable nature, 2)
neither errors in periapsis location (σW) or inclination (σi) are
significant, and 3) dispersions in the radius of closest approach
(σRp) may be somewhat larger than expected. Considering the 3-sigma
radius error for 1988 Type I yields a potential dispersion of 336 km,
which would not be acceptable when targeting nominally to an altitude
of 400 km.

Two techniques exist which can rectify the problem of radius
error. The first involves incorporation of charged particle cali-
bration into the navigation process. This would necessitate inclu-
sion of both X-band and S-band capability on-board the spacecraft,
but would reduce encounter dispersions to about half the quoted
levels. A second alternative would be biasing the trajectory aim-
point at Venus sufficiently to ensure that encounter radius would
fall beyond any point which might lead to rapid altitude decay.
This technique implies insertion ? an altitude greater than the
desired 400 km for nominal orbit periapsis, and s such necessitates
some provision for a small orbit trim maneuver to be executed soon
after insertion to bring periapsis back down to the desired altitude.

The technique has been successfully used for most of the Lunar
Orbiter missions of the late 1960s and has proven feasibility.
Additional study is indicated to determine the most appropriate
scheme for our missions.

The considered mapping orbits have been evaluated to assess
the degree to which nominal orbit determination can define position
and velocity of the spacecraft in its orbit. Orbit sizes corres-
ponding to e = 0, 0.3, and 0.5 have been studied and the in-orbit
uncertainties associated with each, after 24 hours of tracking, are
listed in Table III-5. The results indicate that although the cir-
cular orbit does exhibit a somewhat higher level of uncertainty than
the eccentric orbits, in σ_{RAD} and σ_{VEL}, the difference is minimal.
One-sigma errors range from 25 m to 17 m in radius (altitude) for
all orbits, with velocity uncertainty between 8 and 3 m/sec as eccen-
tricity increases to 0.5. None of the observed error magnitudes sug-
gests any impairment of the basic mapping capability, and all are of
a manageable nature.

Table III-5 Orbit Determination Accuracy, In-Orbit Errors

e	σ_{RAD}	σ_{POS} (RMS)	σ_{VEL} (RMS)
0	25 m	2.14 km	8.18 m/sec
0.3	20 m	2.54 km	5.63 m/sec
0.5	17 m	1.60 km	2.81 m/sec

EVOLUTION OF LIMITING CRITERIA

Orbit Orientation

For the radar mapper mission design to yield access to the entire
planet, from pole to pole, an orbit inclination very near polar is
essential. No compelling reasons have been disclosed by this study
which would prohibit this design. Location of periapsis in latitude
was, however, found to be limited for each opportunity to a range
determined by the Vhp declination range unique to the launch/arrival
dates of the associated launch window. Since unlimited capability
for apsidal shift cannot be assumed, periapsis latitude is therefore
subject to propulsion system limits, and so has been constrained to
a maximum shift of $\pm20°$ from its nominal location on the subperi-
apsis locus. Still, given the doubled-valued nature of the subperi-
apsis locus for polar orbit inclination, in combination with a 20°
apsidal shift, most reasonable design latitudes can be reached (or
nearly reached) if the location desired is not restricted to a
specific hemisphere (north or south). A consequence of this situa-
tion is that where a particular hemisphere _is_ specified, the orbital
motion at periapsis is also specified--ascending motion to gain a
southern periapsis, descending motion to gain a northern periapsis.
As will be addressed in the next section, high periapsis latitude
locations do impose limits of their own on orbit size when consid-
ering highly eccentric orbits, and serve to produce instabilities
in periapsis altitude.

Limiting criteria specifically deriving from or related to orbit
orientation, then, can be summarized as 1) a mission year dependent
restriction on the periapsis latitudes which can be achieved, 2) a
potential determinant of apsidal shift requirements, 3) a determinant
of orbit motion at periapsis when the hemisphere of periapsis lati-
tude is specified, and 4) a restriction deriving from orbit stability
for orbits of higher eccentricities.

Orbit Eccentricity

Eccentricity of the mapping orbit has been considered a principal mission parametric and is involved in almost all of the mission trades. Its primary role as a limiting criterion to mission design involves establishing upper and lower bounds on the range of orbit sizes that can reasonably be consdered.

A lower bound is formed by the consideration of various performance system characteristics for the Venus missions. If only the injected weight capability of Titan IIIE/Centaur were of concern, the lower limit to orbit size would range from around e = 0.2 in 1983 and 1984, to e = 0.4 in 1988, for periapsis altitude equal to 400 km. But when the consideration of holding to realistic growth of existing Viking orbit insertion propulsion is involved, allowing up to a 3-engine configuration and 60% increase in tank size, the lower bound then ranges between 0.3 and 0.5 eccentricity over the same range of mission years.

The upper bound on orbit size has been established by considering orbit instabilities. It was found that for eccentricities greater than about 0.6, periapsis variation becomes unmanageable when coupled with periapsis locations at latitudes much removed from the equator. Since it will not always be possible, or desirable to achieve an equatorial periapsis, the eccentricity of 0.6 effectively becomes the upper bound for polar orbits.

Indirectly as a limiting criterion, eccentricity also has implications for the design of the radar mapping system, mapping strategy, power profiles, and communications scheduling. But here it is a case of tailoring these designs to achieve the optimal mapping performance given the orbit spacing, radar range, and power requirements associated with the particular orbit size.

Where higher performance launch and orbit insertion systems become feasible alternatives, such as Shuttle/Centaur and space stor-

ables, the value of eccentricity as a criterion for setting the lower limit to orbit size is diminished, and the design of a circular mapping orbit becomes very attractive. If achievable and cost effective, the circular orbit does serve to simplify the mapping process, ease power requirements, and halve the required orbiter mission duration to 120 days.

CONCLUSIONS AND RECOMMENDATIONS

Areas of Concern and Future Work Emphasis

On balance, nothing prohibitive of the basic Venus orbital mapper concept has been disclosed by the mission analysis portion of this feasibility study. There do exist a few areas of concern which correspond to the directions in which future work should be concentrated.

First, the problem of orbit insertion, given the relatively long duration burns for the Vhp range at Venus arrival, has given rise to high levels of finite burn loss. The situation has been alleviated in this study by the incorporation of a multiple-engine propulsion system, based on the performance of single Viking class orbit insertion units in simultaneous operation. This solution is operationally adequate, yet does require additional weight allocation for the extra hardware. Alternatives to the simple increased propulsion system performance would lead to 1) the evaluation of a more optimally programmed attitude burn to counter gravity losses, and 2) the study of a phased insertion sequence with multiple burns designed to minimize finite burn loss effects. The added complexity of both options might be weighed against the multiple-engine concept in efficiency of burn loss reduction.

Secondly, the problem of closest approach radius errors at Venus encounter must be addressed in greater detail. Estimates of these dispersions show them to be of an unacceptable level for some of

the considered opportunities. Options which need to be evaluated
here include the use of aimpoint bias, which implies provision for
a necessary orbit trim following insertion to adjust periapsis, or
the inclusion of charged particle calibration in the navigation pro-
cess. The degree of dispersion improvement for each option must be
determined quantitatively.

A third area which deserves attention is the continued gather-
ing of data from all available sources to define as well as possible
significant Venus gravity harmonics which might affect the stability
of an orbiter. Additionally, room exists for fine-tuning the orbit
design to yield the optimal mission from specific system considera-
tions--specific side-look-angle programs, data handling schedules,
and power acquisition cycles. The design parametrics of this study
have been dir cted toward consideration of a broad range of systems,
to serve as a foundation for evaluating overall mission/systems inter-
actions. These parametrics point the way to a preferred design for
whatever system concept is ultimately selected.

Recommended Design

The reference orbit design upon which the preferred spacecraft
configuration rests is characterized by a polar (or near-polar) in-
clination, a 400 km periapsis altitude, eccentricity of 0.5, with
periapsis near the equator. Inclination may easily be offset up to
$\pm15^{\circ}$ from true polar to gain coverage of the poles without affecting
other characteristics of the orbit. The 0.5 eccentricity allows orbit
insertion with a 2 or 3 engine Viking propulsion system in 1983, 1984
and 1989 keeping under a 10% growth in the nominal Viking propellant
tanks. In 1986 and 1988 three engines are still adequate, but pro-
pellant tank growth may require up to a 60% increase. Location of
periapsis at the equator assumes the existence of a radar system
which is capable of mapping $\pm90^{\circ}$ in true anomaly, and that location
can be achieved for all mission years with an apsidal shift under

20°. During the 243-day lifetime of the orbiter mission, the orbit
passes through periods of full occultation at periapsis and apoapsis,
of both Earth and Sun, for maximum occultation times of 1.2 hours
out of the 4.487 orbit period. Orbit motion at periapsis, ascending
or descending, is a function of mission year. Orbit trim require-
ments for this design orbit are minimal.

REFERENCES AND BIBLIOGRAPHY

III-1 J. S. MacKay, et al: *A Preliminary Analysis of a Radar Mapping Mission to Venus.* Ames Research Center, 11 October 1972.

III-2 C. M. Vairin: *General Perturbations Computer Program.* Study Task 2.1.1 B5, Martin Marietta Aerospace, June 1970.

III-3 S. K. Asnin: *Standard Venus Constants.* Venus Mapper Technical Note 3, Martin Marietta Aerospace, 7 September 1972.

III-4 S. K. Asnin: *Request for Preliminary Mission Analysis Data.* Venus Mapper Technical Note 4, Martin Marietta Aerospace, 7 September 1972.

III-5 S. K. Asnin: *Preliminary Sample Mission Definition.* Venus Mapper Technical Note 5, Martin Marietta Aerospace, 14 September 1972.

III-6 S. K. Asnin: *Standard Coordinate Systems - Mission Analysis.* Venus Mapper Technical Note 12, Martin Marietta Aerospace, 30 October 1972.

III-7 D. B. Cross: *Limiting Altitude Considerations.* Venus Mapper Technical Note 17, Martin Marietta Aerospace, 4 December 1972.

III-8 S. K. Asnin: *Orbit Characteristics for the 1984 Type II Mission - Considering e = 0, .2, and .5.* Venus Mapper Technical Note 18, Martin Marietta Aerospace, 8 December 1972.

III-9 T. W. Locke: *Propulsion Alternatives for Venus Mapper Mission in 1983.* Venus Mapper Technical Note 20, Martin Marietta Aerospace, 30 January 1973.

III-10 S. K. Asnin: *Major Event Timeline for 1984 Type II Mission/ .5 Eccentricity Reference Orbit.* Venus Mapper Technical Note 40, Martin Marietta Aerospace, 26 February 1973.

III-11 S. K. Asnin: *Updated Mission Philosophy and Occultation Characteristics for Second Phase, Considering e = 0, .3, and .5.* Venus Mapper Technical Note 41, Martin Marietta Aerospace, 26 February 1973.

III-12   S. K. Asnin: *Major Events Timeline for 1984 Type II Mission/
         Configurations 1 (400 km circular) and 2 (.3 eccentricity).*
         Venus Mapper Technical Note 48, Martin Marietta Aerospace,
         27 February 1973.

III-13   S. K. Asnin: *Program DSNHIST, for DSN Mission Requirements
         and the Relationship of Communication Windows with DSN
         View Periods.*   Venus Mapper Technical Note 50, Martin
         Marietta Aerospace, 8 March 1973.

III-14   S. K. Asnin: *DSN Requirements for Reference Venus Mapper
         Missions Using the Program DSNHIST.* Venus Mapper Technical
         Note 54, Martin Marietta Aerospace, 26 March 1973.

IV. Radar and Antenna Systems

IV. RADAR AND ANTENNA SYSTEM

INTRODUCTION AND ASSUMPTIONS

The radar subsystem is the primary science instrument for this
mission and must generate a high resolution topographic map of the
surface. The study groundrules on the resolution are to map at
least 80 percent of the surface at 1 km resolution and 20 percent
of the surface at 100 m resolution or better. A design philosophy
of mapping as much of the surface as possible at 100 m resolution
is used in this study because it is felt that this kind of reso-
lution can be obtained with today's technology. In addition to
this capability, a fine resolution of 33 meters would be available
on command to give ultra high resolution pictures of interesting
topographic features. The fine resolution capability may be data
limited to narrower swath width and short mapping times.

Initially in this study, it was decided that certain desired
characteristics would be needed in a Venus mapping spacecraft
(S/C). These desired characteristics are expressed as design
goals shown below:

         Utilize continuous inertial reference.

         Antenna designs that can be articulated.

         Point spacecraft at some near inertial point.

         Complete surface mapping.

         Use existing spacecraft.

         Use the highest radar operating frequency.

         Meet launch vehicle packaging constraints.

         Science requirements at minimum cost.

These desired characteristics will be described in detail in the
following paragraphs.

A continuous inertial reference would be desirous so that good
pointing information would be available at all times. Because
very accurate pointing is required for mapping and communication
phases, a very accurate reference system is needed. It was deter-
mined early in this study the kind of system used by the Mariner
class of vehicle should be adequate to do the Venus mapping mission.
This type of system utilizes a Sun sensor system and a Canopus sen-
sor to orient the vehicle to this reference and uses strapped down
rate gyro system to keep track of this reference when either of
the sensors are occulted. When the Sun sensor system is occulted,
the vehicle is controlled by pitch and yaw rate gyros; when the
Canopus sensor is occulted, the vehicle is controlled with the
roll rate gyros. Since occultation from the Sun or Canopus is
never more than one hour and the gyro drift rate is one-half de-
gree per hour, vehicle pointing knowledge should be one-half de-
gree plus alignment mounting errors about each plane. The vehicle
will limit cycle about this pointing direction. Pointing capa-
bility will be described in the attitude control section.

Antennas that can be articulated would be a desired charac-
teristic because the spacecraft can be inertially or nearly in-
ertially pointed. For example, in Volume II configuration A is
a Sun pointing spacecraft and the C-configuration is an inertially
oriented spacecraft that is controlled to point the spacecraft
roll axis perpendicular to the orbital plane. Articulated an-
tennas eliminate the need for spacecraft maneuver, which are
expensive in terms of the ACS propellant required.

As much of the surface should be mapped as possible for the
developmental dollar. The maximum surface area that can be mapped
is constrained by the radar subsystem power needed, PRF constraints
and spacecraft data subsystem data transmission capability to Earth.
The data that has to be transmitted to Earth is a function of the
resolution needed and total mapping area required.

IV-3

Existing spacecraft or modification of existing spacecraft were implemented wherever possible in the final designs to save developmental costs. Initially the spin stabilized and the three axis stabilized systems were compared, where the 3-axis system seemed to be the easiest to implement with the least development risk. A feasibility study would be needed to determine whether a synthetic aperture could be processed from the radar data obtained from a spinning vehicle. Either the antenna has to be mechanically or electronically despun or mapping epicycles would have to be processed to generate a pseudo synthetic aperture. On the other hand, it was determined early in the study that a three-axis system about the size of the Mariner or the Viking Orbiter spacecraft would be needed to do a Venus mapping mission. This type of system takes full advantage of using existing equipment and should be the cheapest to implement. For these reasons, the three-axis system was developed into the final designs.

The highest operating frequency was used to get the maximum topographic return. A S-band frequency with a wavelength of 10 cm was chosen for the baseline designs using a single frequency because this frequency would not suffer large atmospheric losses and would minimize the subsurface return.

The spacecraft has to be packaged within the dynamic envelope of the launch vehicle. This usually means that the antennas and the solar panels have to fold up and be constrained to meet the launch loads. In addition to folding, sometimes the antennas have to be deployable to meet packaging constraints.

The last design goal is obvious, maximum science return is desired for minimum cost.

Figure IV-1 shows the side looking radar geometry needed to map Venus. The vehicle is in an orbit perpendicular to this figure and points its radar antenna boresight out at a 30 degree
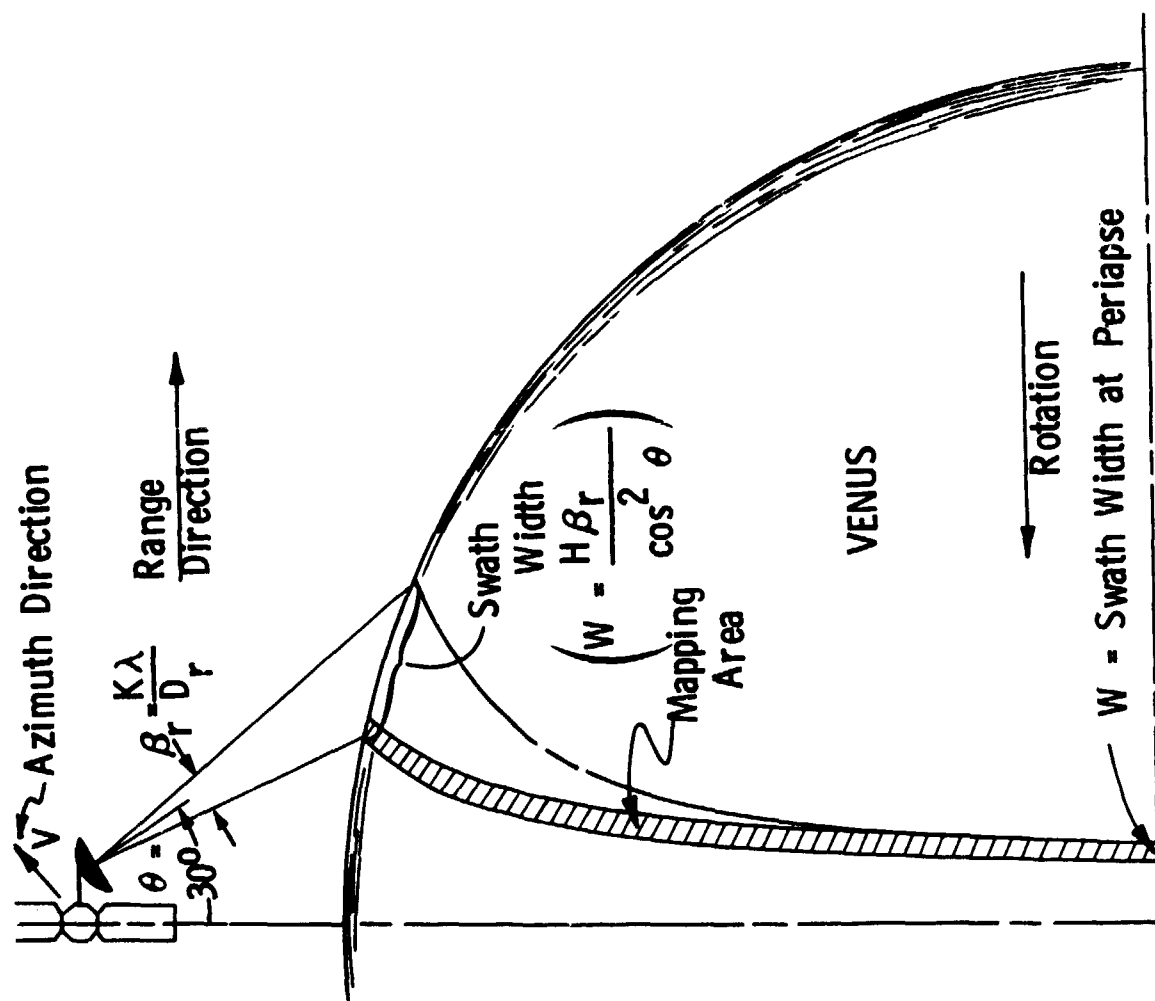
Figure IV-1 Mapping Area and Swath Width

side look angle (θ) when a constant side look angle is used. The
range direction is perpendicular to the orbital plane and the azi-
muth direction is parallel to the orbital plane as shown on the
figure. The range beamwidth (β_r) of the antenna illuminates a
swath width (W), that is a function of altitude. When circular
orbits are used, a constant swath width is generated throughout
the mapping phase, which is generally the same as the mapping
width that is processed. The planet rotates under the spacecraft
to give th mapping coverage desired.

When elliptical orbits are used, the illuminated swath width
is sized at periapsis to give the desired coverage. The illumi-
nated swath width increases many times to that at periapsis due
to altitude changes, which creates range ambiguity constraint
problems for the radar subsystem designer because he has to guar-
antee that range ambiguities will not degrade the mapping quality
for the widest swath width. This means a very low PRF must be
selected which forces the subsystem designer to very large an-
tennas in the azimuth direction that cannot be articulated.

We will show how the range ambiguity problems in elliptical
orbits can be solved so elliptical orbits can be used for mapping
like circular orbits without paying the propulsion cost of getting
into that orbit.

PARAMETRIC STUDIES

This section describes some of the parametric studies that
were necessary to define the final designs. The parametric
studies are independent efforts and can stand alone. All but the
first four of these studies were conducted by ERIM--Environmental
Research Institute of Michigan--which was formerly the Willow Run
Laboratories at the University of Michigan. The following para-
metric studies were conducted:

IV-6

1) Antenna sizing;

2) Range ambiguity constraint problem;

3) Antenna subsystem design;

4) Radar subsystem design;

5) Power requirements;

6) Ambiguity spectrum of synthetic aperture;

7) Radar system augmentation;

8) Reduction of antenna size;

9) Range and azimuth ambiguity elimination for elliptical orbits;

10) Range and azimuth aperture dimensions for elliptical orbits;

11) Attitude control and radar system stability.

These parametric studies are independent and self-contained studies that can stand alone.

Antenna Sizing

Figure IV-2 shows how constraints limit the size of the radar antenna that can be used in a synthetic aperture side looking radar. The type of synthetic aperture (focused, unfocused, or partially focused) that is used depends only on how the radar data are processed and will be discussed in the Data Handling and Communications section. A partially focused synthetic aperture is suggested for this mission.

The maximum size antenna that can be used in the range direction is determined by the beamwidth needed to illuminate the swath width at periapsis. This is the smallest beamwidth that can be used to get the coverage necessary. The maximum size in the range direction is generally used in elliptical orbits to reduce the power required and relieve the range ambiguity constraint. It is easier to guarantee that the contribution due to range ambiguities will be small if the largest possible antenna size is used in the range direction.

Range Direction

Azimuth Direction

Size That Can Be Articulated

Planar Array Antenna

Sized by Luminated Swath Width at Periapse

Area Constraints At All Altitudes

Enough Area: To Have Adequate Power

To Meet Range Ambiguity Constraint

To Meet Doppler Ambiguity Constraint

$$\frac{2V}{D_a} \leq PRF \leq \frac{C}{2W\sin\theta}$$
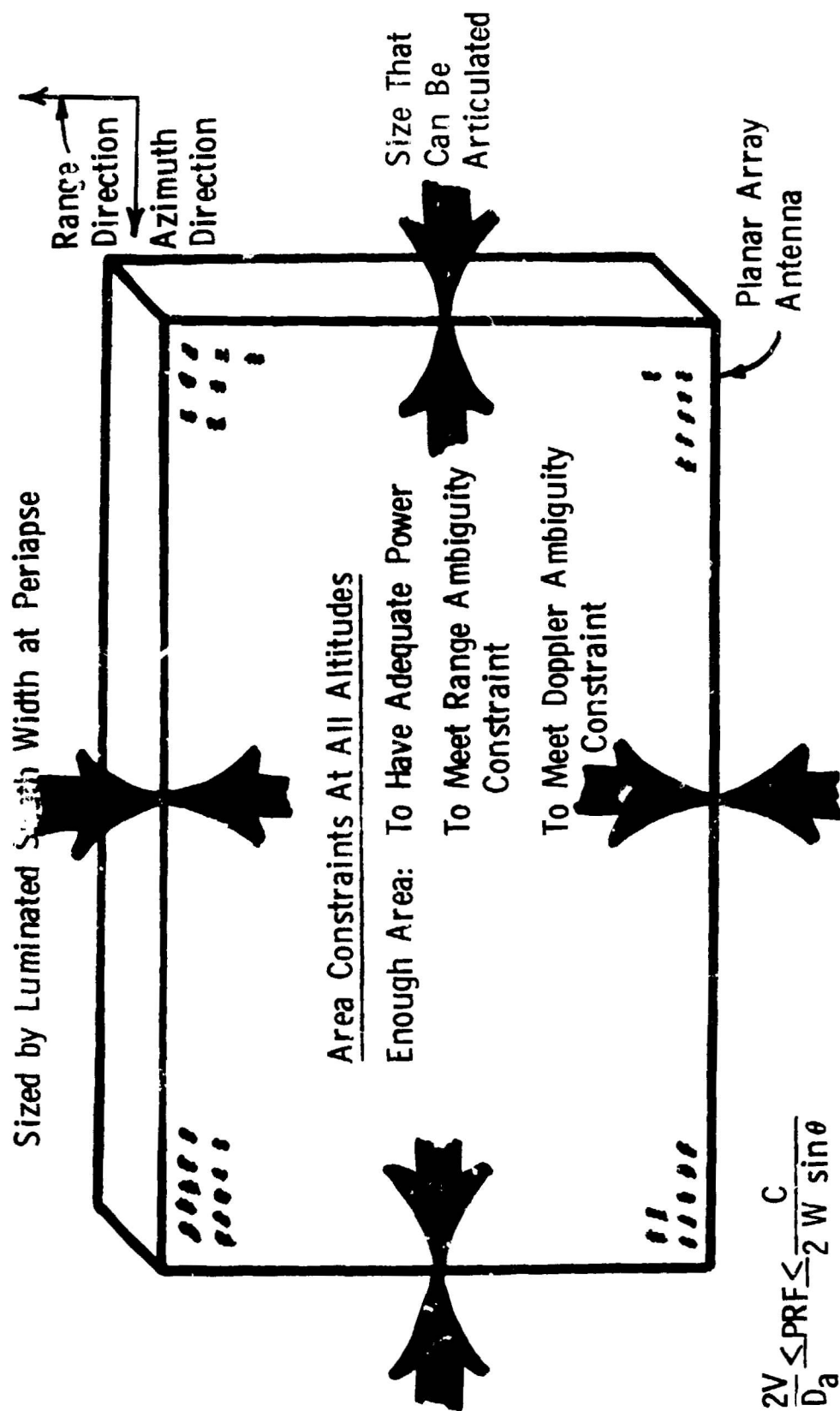
Figure IV-2 Antenna Sizing Constraints

In the azimuth direction, the size of antenna is limited by the size that can be articulated. The antenna has to be so big in this direction, so there is adequate power and the doppler ambiguity constraint can be met, which guarantees the contribution due to doppler ambiguities will be small. The upper and lower PRF constraints are shown in Figure IV-2 by the inequality in the lower left hand corner. The upper PRF constraint ($C/2W\sin\theta$) guarantees that the range ambiguities content will be small and the lower PRF constraint ($2V/D_a$) guarantees the content of doppler ambiguities will be small.

The doppler velocities generated by linear motion of an antenna past fixed surface targets can be expressed by the following equation:

$$f_D = \frac{2V_R}{\lambda} = \frac{2V\sin\alpha}{\lambda} \simeq \frac{2V\alpha}{\lambda} \tag{IV-1}$$

where f_D = doppler frequency (hz)

V_R = radial velocity of spacecraft (m/sec)

λ = radar frequency wavelength (m)

V = spacecraft velocity (m/sec)

α = target angle (rad)

Because the beamwidth is generally a small angle, the target angle is small and the small angle approximation can be used. It can be proven that the target angle is equal to the azimuth beamwidth (β_a) when the maximum change in the doppler frequency (Δf_D) over the beam is required.

$$\Delta f_D = \frac{2V\beta_a}{\lambda} \simeq \frac{2V}{D_a} \tag{IV-2}$$

where $\beta_a = \frac{K\lambda}{D_a} \simeq \frac{\lambda}{D_a}$ \tag{IV-3}

K = proportionality constant

D_a = azimuth dimension of antenna

β_a = azimuth beamwidth of antenna

In order to measure the sampling frequency unambiguously, two
samples per cycle are needed as stated by the well known sampling
theorem. In a sample data system such as a pulse radar, the
sampling theorem imposes a restriction on the minimum PRF that
can be used:

$$PRF \leq \frac{4V}{D_a} \simeq \frac{2MV}{D_a} \qquad \text{(IV-4)}$$

In actual practice, since all the doppler bandwidth is not used in
a partially focused synthetic aperture, M may have a value of
either 1 or 2 depending on the type of data processing used.

In the range direction, the time available to map unambiguously
is equal to the interpulse period (T), but since the pulse must
travel to the target and back, the maximum unambiguous range is
given by:

$$R_{max} = \tfrac{1}{2}CT = \frac{C}{2(PRF)} \qquad \text{(IV-5)}$$

where   C = speed of light (m/sec)

   T = interpulse period (sec)

   PRF = pulse repitition frequency (PPS)

In order to guarantee that there will be adequate time available
for mapping unambiguously in the range direction, the following
constraint must be satisfied.

$$PRF \geq \frac{C}{2R_{max}} = \frac{C}{2Ws\,in\theta} \qquad \text{(IV-6)}$$

where   W = illuminated swath width (m)

   θ = side look angle

These PRF constraints can be used to derive an area constraint as
shown below:

$$\frac{2V}{D_a} \leq PRF \leq \frac{C}{2Ws\,in\theta} = \frac{Ccos^2\theta}{2H\beta_r s\,in\theta} \qquad \text{(IV-7)}$$

where $W = \dfrac{H\beta_r}{cos^2\theta}$ & $\beta_r = \dfrac{K_r\lambda}{D_r} = \dfrac{1.2\lambda}{D_r}$

hence $\quad \dfrac{2V}{D_a} \le PRF \le \dfrac{C\ D_r\ \cos^2\theta}{2HK_r\lambda\sin\theta}$ (IV-8)

and $\quad \dfrac{4VHK_r\lambda\sin\theta}{C\ \cos^2\theta} \le \dfrac{2HK_r\lambda\sin\theta PRF}{C\ \cos^2\theta} \le D_r D_a$ (IV-9)

$\therefore\ D_r D_a \ge \dfrac{4.8VH\lambda\sin\theta}{C\ \cos^2\theta}$ (IV-10)

This is the "so called" area constraint that is a combination of the upper and lower PRF constraints.

Figure IV-3 shows the various antenna constraints for the selected S-band frequency for various mapping strategies, i.e., for some eccentricity (e = 0.5) and mapping every third orbit (N = 3). The vertical lines represent range constraints. The swath width needed to map the planet with the desired overlap can be determined by calculating how much the planet moves under the spacecraft during the communication and mapping phases. The antenna must be this big or smaller to illuminate the desired mapping swath width. The curved lines represent area constraint curves for each orbital eccentricity. Larger azimuth dimensions are required for the higher orbital eccentricities. Swath widths greater than 36 km are needed generally to have time to get the data back to Earth with reasonable sized communication antennas. The parabolic design or the antenna with equal dimensions in both directions are also indicated on this figure. As shown on the figure, long narrow antennas have to be used at this frequency.

The mapping constraints are shown for a C-band frequency (λ = 5 cm) in Figure IV-4. The area constraint for favored orbital eccentricity is shown; if this figure is used for other orbits, there will be additional conservation in the final designs. If a C-band frequency is used, very narrow impractical antennas must be used with a proportional loss of antenna gain. The antenna with a rectangular aperture can be used at this frequency only for very narrow swath widths.

Figure IV-3 Mapping Constraints (λ = 10 cm)
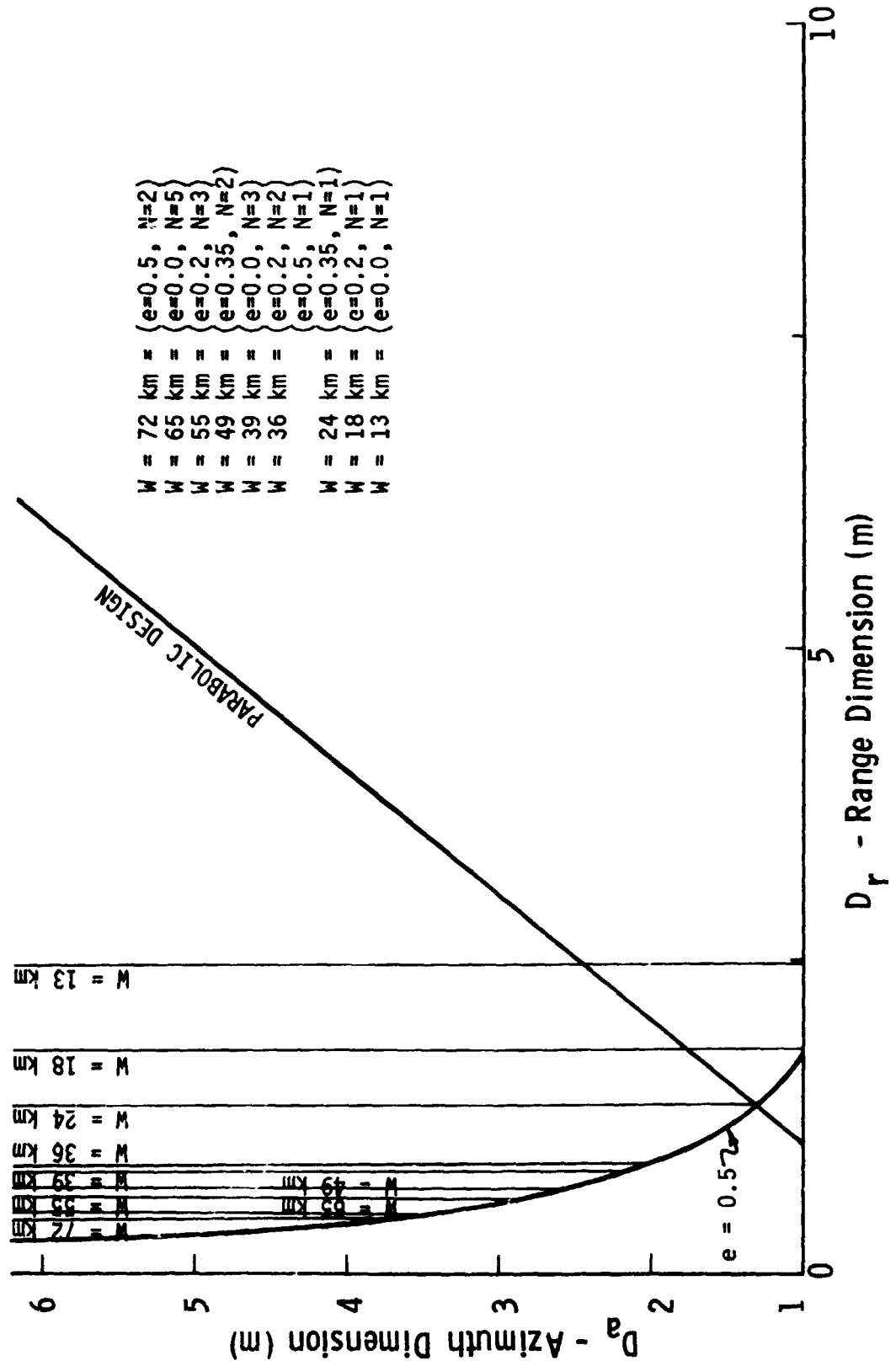
Figure IV-4 Mapping Constraints (λ = 5 cm)

The mapping constraints using L-band (20 cm wavelength) radar
is shown in Figure IV-5. The rectangular apertures can now be
used to map reasonable swath widths. Smaller azimuth dimensioned
antennas can be used for this frequency. This frequency has less
atmospheric loss and a more reasonable shape antenna can be used,
but an S-band operating frequency was used in the favored designs
to maximize the topographic return and minimize the return from
subsurface features. An L-band frequency could probably be used,
but the engineering risk is higher in terms of getting the most
topographic information about the surface which looks like a
clutter target. It is a good idea to use the highest operating
frequency possible to reduce these engineering risks unless ground
truth data is available. In a dual frequency mapping radar, this
frequency would be a good selection for a second frequency. The
altimeter could also use this frequency to increase the science
return in terms of sounding the surface and giving an altitude
profile. Figure IV-6 shows the mapping constraints for an L-band
frequency (λ = 40 cm). Antennas with square or circular apertures
can be used for this frequency to map very wide swath widths. How-
ever, it is felt that this frequency is too low to get good topo-
graphic information.

Using an S-band frequency (λ = 10 cm) and mapping every orbit,
a 36 km swath width is needed to get 20 percent overlap at peri-
apsis. Using Figure IV-3, an antenna range dimension of 1.75
meters will meet the range constraint, when a constant side look
angle of 30 degrees is used. Antenna range dimensions of 1.0,
1.45, and 1.75 can be selected for the orbits with the eccentrici-
ties of 0.0, 0.3, and 0.5, where swath widths of 65, 44, and 36 km
respectively are required to get the desired overlap.
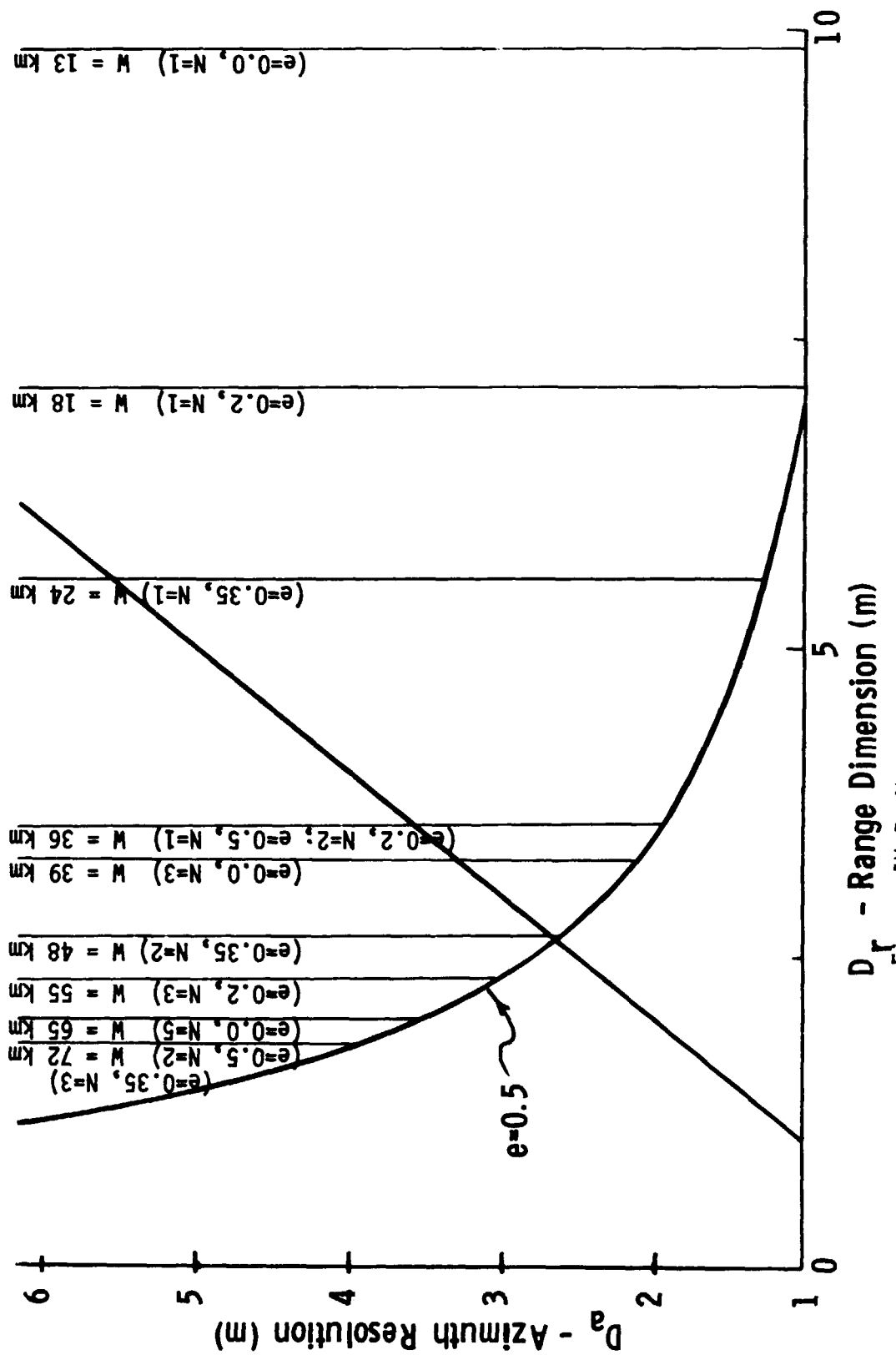
Figure IV-5 Mapping Constraints (λ = 20 cm)
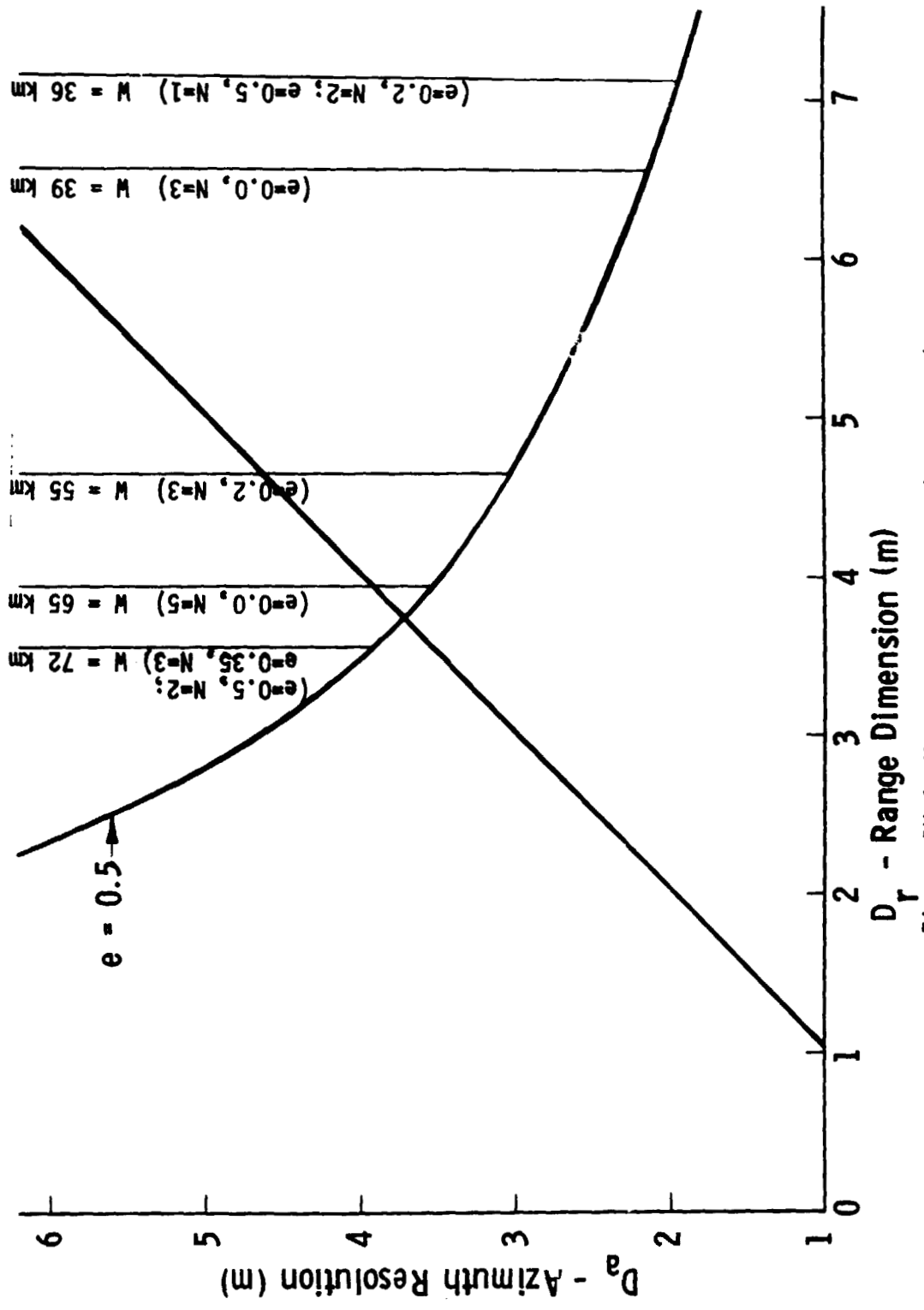
Figure IV-6 Mapping Constraints (λ = 40 cm)

Range Ambiguity Constraint Problem

Figure IV-7 shows how the PRF constraint changes as a function of mapping position for the 0.5 eccentric orbit. The 0.5 orbit is favored because a Viking Orbiter spacecraft with present propulsion capability can be used to map Venus. This figure shows how the lower PRF constraint $(2V/D_a)$ varies as a function of mapping position for an antenna with an azimuth dimension of 3.66 m. The upper PRF constraint $(C/2Wsin\theta)$ for a single beamwidth antenna $(\beta_r = 67.5$ mrad) sized at periapsis, when periapsis is over the equator, decr. .ses with altitude. As shown on this figure, mapping to ±30 degrees can be achieved before the range ambiguities become a problem if a single beamwidth antenna is used. Range gating, which has been considered an acceptable solution to the ambiguity problem, was eliminated in the parametric studies discussed later in this volume.

The obvious solution is to use a multi-beam width antenna to increase the mapping capability. The simplest solution is to utilize a dual beamwidth antenna, which is also shown in this last figure. This scheme uses a wide beamwidth antenna (67.5 mrad), which will illuminate the swath width at periapse. This beamwidth is used for mapping the lower latitudes (up to 24 degrees true anomaly), then the antenna beamwidth is changed to a narrower band-width for the higher latitudes. An antenna with one-half the beamwidth (33.75 mrad) is used for the latitudes above 24 degrees. Using a dual beamwidth antenna, increased mapping coverage is achieved before range ambiguities become a problem. As you can see in this figure, mapping to ±55 degrees can be achieved before the upper PRF constraint is violated. Normally, if the standard Viking Orbiter spacecraft is used with two existing solar panels with 80 square feet of area, the mapping is also constrained by power to ±60 degrees true anomaly. The mapping coverage could
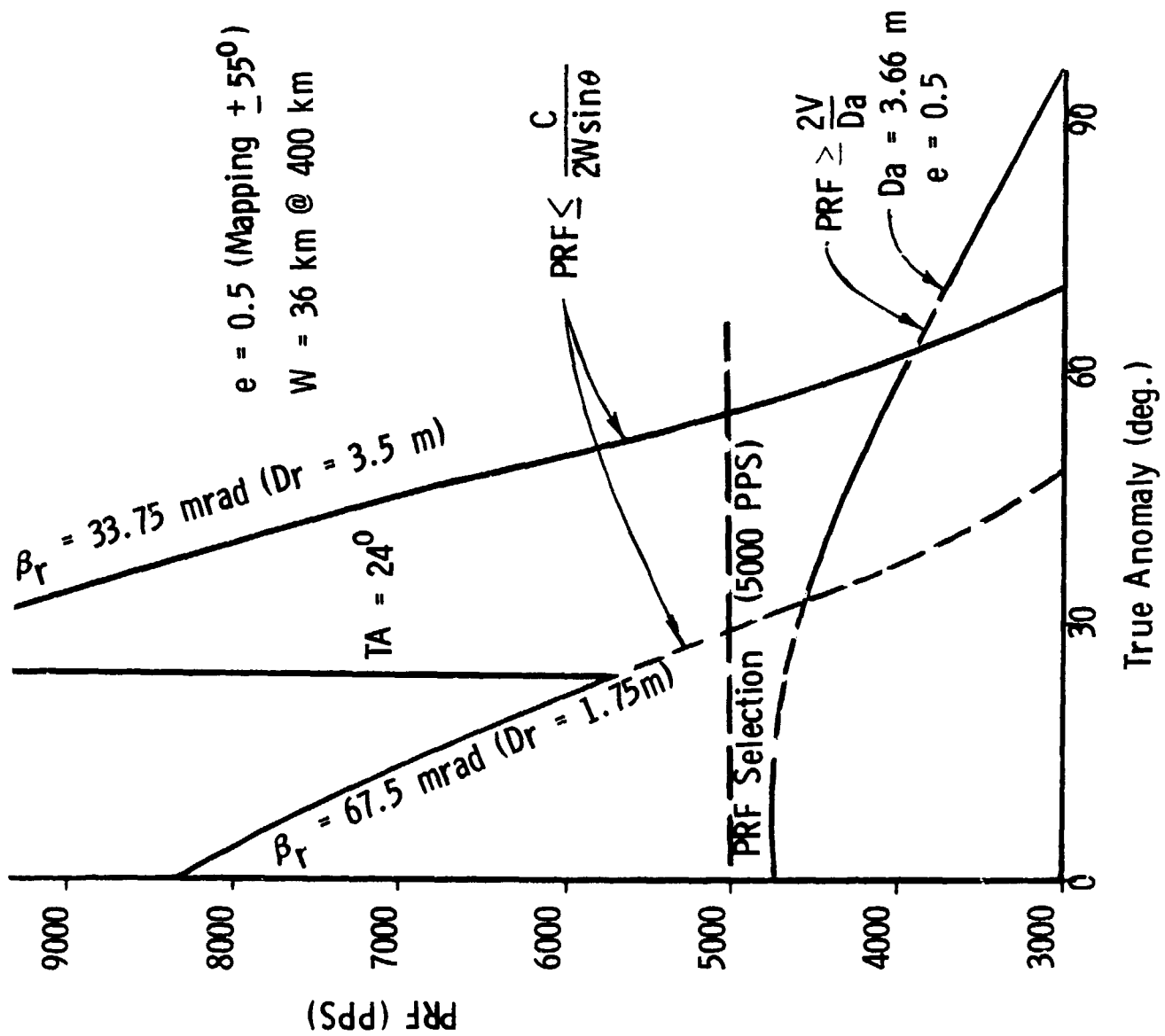
Figure IV-7   Dual Beamwidth Antenna PRF Constraints (Periapsis at Equator)

not be increased much by using a multi-beamwidth antenna, because
power would constrain the mapping for reasonable sized antennas.
Planet coverage of 82 percent of the surface is achieved when the
spacecraft maps between ± 60 degrees true anomaly. From the figure,
a constant PRF of 5000 PPS can be selected for either the single
or the dual antenna beamwidth case. A variable PRF can easily be
implemented so the selection should not be constrained to select-
ing a constant PRF. There are advantages to selecting a variable
PRF. A variable PRF of $2V/D_a$ (lower PRF constraint) is often a
good selection because constant spacial pulses are generated which
simplifies the processing of the radar data. An antenna with an
azimuth dimension of 3.66 m (12 ft) is required for the preferred
mapping stra-egy ($e = 0.5$, $N = 1$).

Figure IV-8 shows how the PRF constraints vary as a function
of latitude when periapsis is placed at -35 degrees latitude so
that the south pole can be mapped. One of our science ground-
rules is to always map one of the polar regions. The wide beam-
width antenna is used from -56 degrees to +5 degrees latitude.
The lower PRF constraint using a 4.1 m antenna is shown for the
0.5 orbit. If a variable PRF is used to give constant spacial
pulses, the size shown on the figure can be used. If a constant
PRF is used then a bigger antenna will be needed in the azimuth
direction.

A dual beamwidth antenna can be implemented by using multiple
feeds when using reflector type antennas or by switching in extra
elements when a planar array is used. A set of feeds or a shaped
feed designed to illuminate the center portion of the reflector
can be used to get the wide beamwidth. An additional feed can be
used to illuminate the whole aperture when a narrow beamwidth
antenna is needed. The beamwidth is changed then by switching
between the different feeds. When a planar array is used, extra
elements are switched in to narrow the beamwidth.
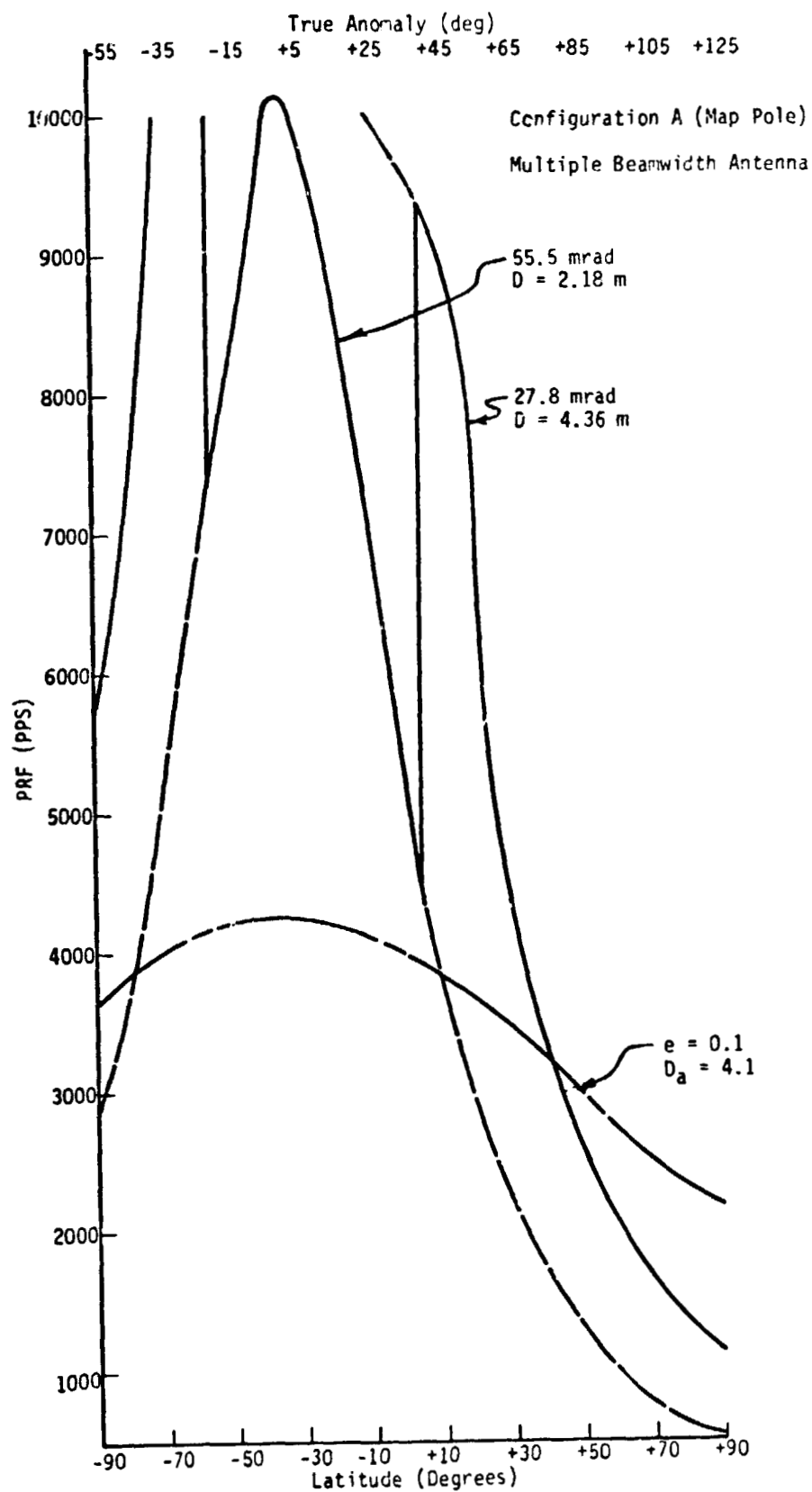
Figure IV-8   Dual Beamwidth PRF Constraints
(Periapsis at -35° Latitude)

The dual beamwidth antenna would be more expensive to develop than a single feed antenna. In addition to this, the feeds would have to be designed for two frequencies when the antenna is shared to do both the mapping and communicatir... Antenna blockage due to multiple feeds will affect the anten   ttern; custom designs have to be developed so the side lobe   ·ls are small enough.

The dual beamwidth antenna is one way to solve the range ambiguity problem, but varying the side look angle is another way to solve the problem. This solution is favored because complete planet mapping can be achieved with little or no additional complexity.

The upper PRF constraint for a single beamwidth antenna and a constant side look angle of 30 degrees a.e shown again in Figure IV-9 for an orbit with an eccentricity of 0.5. This curve is shown for comparison purposes only. If a variable side look angle is used where the grazing angle varies from 50 degrees at periapsis to 12 degrees at the mapping extremities as shown in Figure IV-9, a constant upper PRF constraint is obtained. The grazing angle is the angle between the surface normal in the middle of the illuminated area and the antenna boresight line. The factor in the upper PRF inequality that is a function of grazing angle compensates for the 1/H term to give essentially a constant upper PRF constraint as shown below:

$$\text{PRF} \leq \left(\frac{C}{2W\sin\theta}\right) = \left(\frac{C\,D_r}{2K\,\lambda}\right)\left(\frac{\cos^2\theta}{\sin\psi}\right)\left(\frac{1}{H}\right) \qquad \text{(IV-11)}$$

where C = speed of light

D_r = range dimension of the antenna

K = range proportionality constant = 1.2

λ = radar operating wavelength

θ = side look angle

ψ = grazing angle

H = spacecraft altitude

Constant Side Look Angle (30°)
$\beta_r = 67.5$ mrad ($D_r = 1.75$ m)

Upper PRF Constraint

$$PRF \leq \frac{C}{2\,W\,\sin\theta}$$

$$PRF \leq \left(\frac{CD_r}{2K}\right)\left(\frac{\cos^2\theta}{\sin\psi}\right)\left(\frac{1}{H}\right)$$

Programmed Side Look Angle

PRF Selection

Lower PRF Constraint

Grazing Angle

Grazing Angle (deg)

True Anomaly (deg)

PRF (PPS)
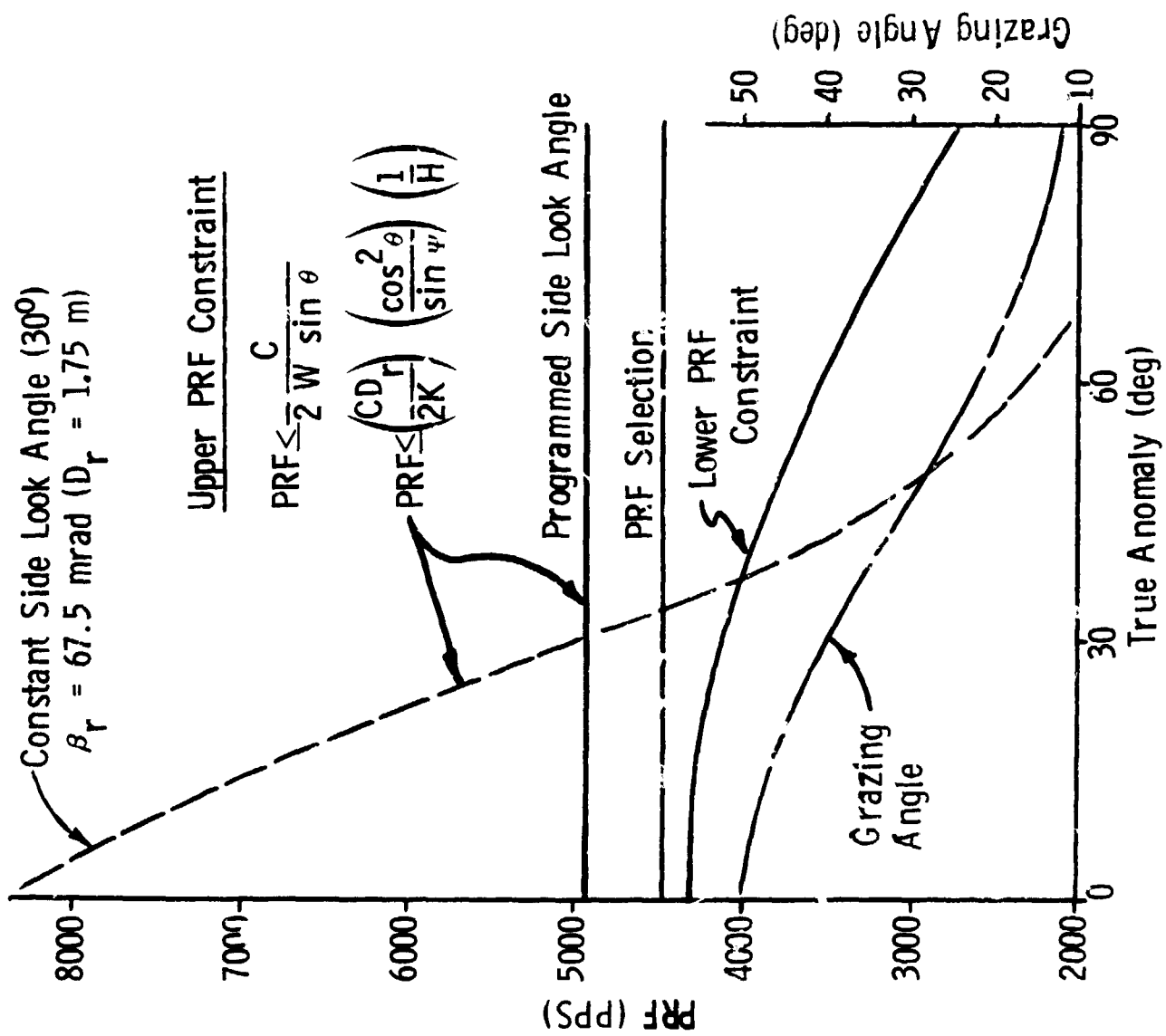
Figure IV-9   PRF Constraints for VSL Angle

The upper PRF constraint is now a well behaved function, where a variable or constant PRF can be selected easily.

This scheme should be easy to implement by stepping the antenna slowly from 12 degrees at the mapping extremity to 50 degrees at periapsis and then back to 12 degrees. The antenna elevation control system which controls the side look angle, can be commanded by a simple subroutine in the control computer. The antenna side look angle is controlled to give the required programmed grazing angle. This subroutine which controls the side look angle can be a relatively simple polynomial in altitude or time. A polynomial in altitude would be preferable because an altitude algorithm would be more accurate as the altitude from the radar altimeter could be used. The variable side look angle can be used on any of the favored configurations that were mentioned.

The variable side look angle helps also in terms of the maximum power required. The power required is also a function of side look angle as shown below:

$$P = \left(\frac{16\pi}{C}\right)\left(\frac{\sin \psi}{\cos^3\theta}\right)\left[\frac{H^3 \lambda V K T L B (S/N)}{A^2 \sigma_o}\right] \tag{IV-12}$$

where C = speed of light

ψ = grazing angle

θ = side look angle

H = spacecraft altitude

λ = radar operating wavelength

V = spacecraft velocity

K = Boltzman's constant

T = absolute temperature

L = microwave losses

B = radar ster bandwidth

(S/N) = signal-to-noise ratio

A = aperture area

σ_o = normalized radar cross section

Using a variable side look angle, a radar power of 333 watts can be
used for complete surface mapping (mapping to maximum altitude of
3600 km) for an orbit with an eccentricity of 0.5 where 600 watts are
required using a constant side look angle of 30 degrees and mapping
to ±55 degrees latitude (maximum altitude of 1500 km). There is
some concern whether this kind of power gain can be achieved with
a variable side look angle since clutter type targets are being
mapped at low grazing angles where the return has a large specular
component. Probably a higher power requirement will be needed to
guarantee good imaging and reduce the mission risk. A degraded
image is produced by an underpowered mapping radar similar to that
demonstrated in the lunar sounding done on Apollo 17. To guaran-
tee imaging quality for minimum power require ents, additional
studies should be conducted on clutter type targets at low side
look angles.

If a clutterlock system is used to point the radar antenna,
the antenna is normally pointed along the zero doppler (ZD) line.
At periapsis, the antenna is pointed essentially in the radial
direction using the clutterlock system. As the radial velocity
increases with altitude, the zero doppler line deviates greatly
from the radial direction. The antenna has higher squint angles
at the higher true anomalies. The antenna is pointed forward or
aft and out to the side, when operated in the squint mode. The
change of the zero doppler direction as a function of true anomaly
is discussed in the mission analysis section of this volume. The
grazing angle, which is the angle between a vector normal to the
planet surface and the zero doppler look angle line, would have a
26.6 degree grazing angle at 90 degrees true anomaly and a 12 de-
gree side look angle.

The variable side look angle scheme can be mechanized in many
ways, but only two of the more promising ways will be considered
here. An electronic offset system or a constant squint

mode system can be used to mechanize a variable side look angle
type of technique. The electronic clutterlock system is programmed
to always look radially and the side look angle is programmed to
get the grazing angle profile shown for the VSL case. The con-
stant squint angle system is described below.

In order to implement a variable side look angle type of
scheme, an antenna with a constant side look angle can be used in
a squint mode. A 26.6 degree forward squint angle can be used dur-
ing the first half of the mapping phase and then a 26.6 degree rear
squint angle can be used in the other half of the mapping phase to
implement the type of scheme described in a variable side look
angle section. The antenna control system points the antenna down
the radial direction at the start of the mapping phase and then
the clutterlock system will lock on the side lobe that is nearest
to this direction. The first half of the mapping phase from -90
degrees to 0 degrees latitude, if periapsis is at the equator,
will have a forward squint angle as shown in Figure IV-10. At
the equator the antenna is rotated backward to have the same rear
squint angle. This maneuver will take about a minute assuming
the antenna can be maneuvered at one degree per second. About a
900 km overlap area is achieved at the equator by using this
scheme. The rear squint angle is used throughout the last half of
the mapping phase. The antenna boresight direction is indicated
by arrows on this figure and the zero doppler direction is also
shown. This technique will implement a variable side look angle
scheme by using an antenna with a fixed side look angle. Complete
surface mapping can be obtained with about the same amount of
power required as was needed for the variable side look angle case.

Figure IV-11 shows PRF constraints for the squint mode implemen-
tation using a 10 degree side look angle in a 0.5 orbit. The
grazing angle is shown as a function of latitude. The grazing
angle profile is not quite as optimum a case as the VSL case,
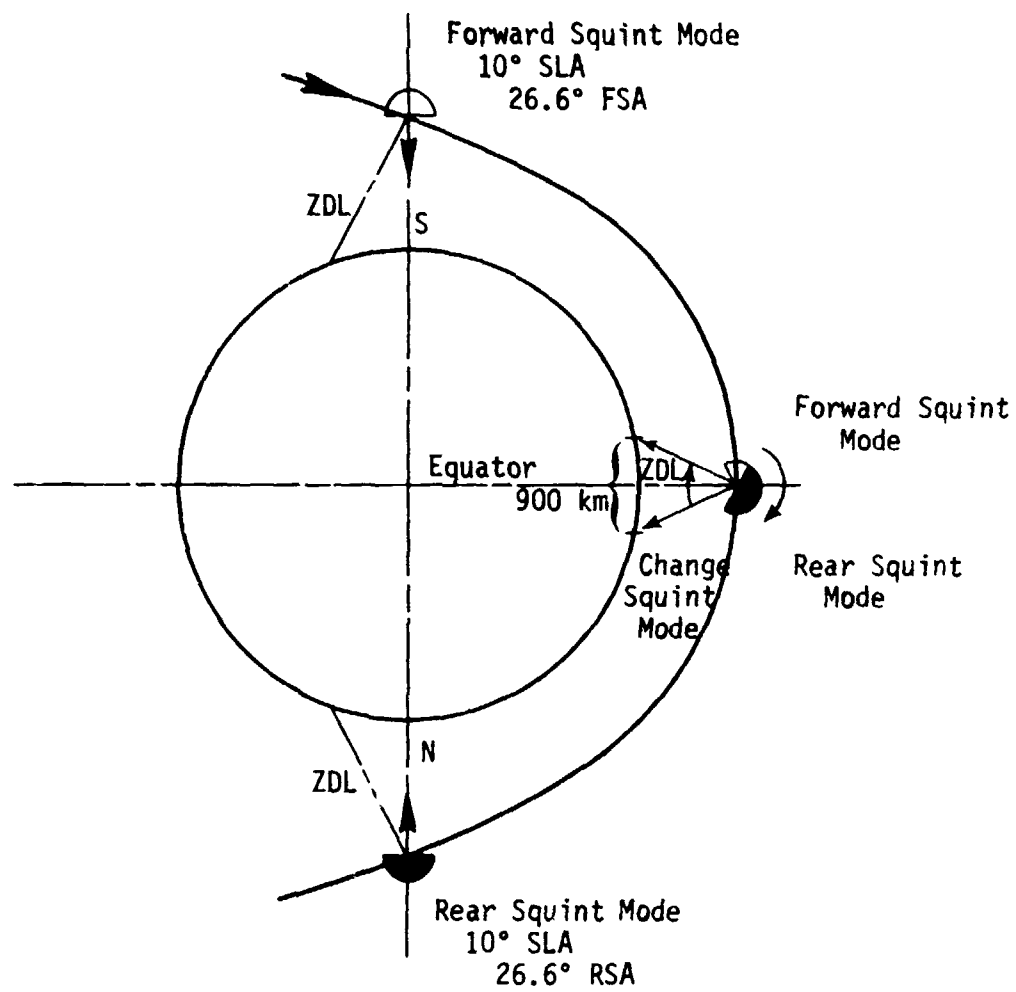
Figure IV-10 Antenna Maneuvering for Squint Mode Implementation
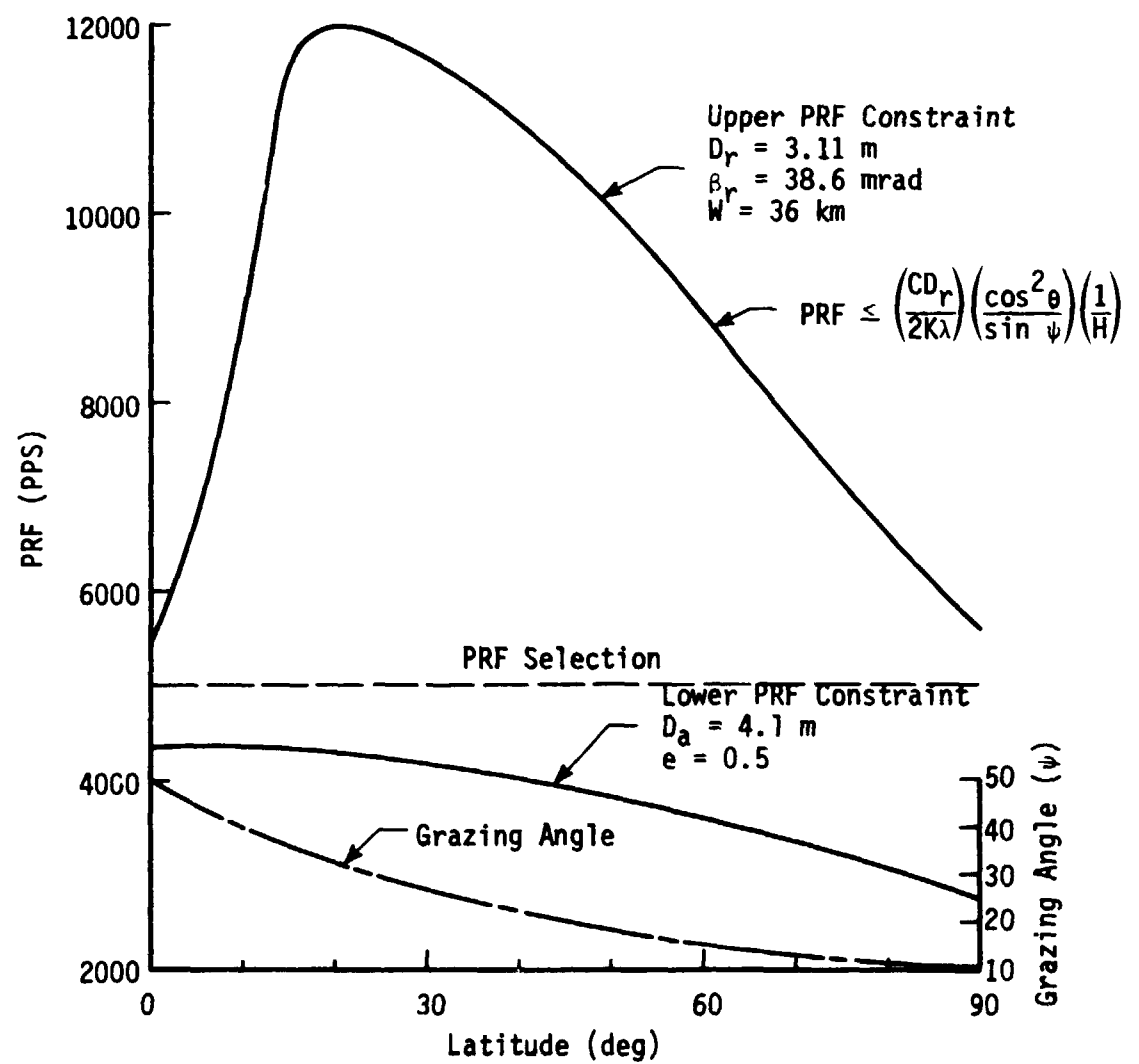
Figure IV-11 Squint Mode Implementation (Constant SLA = 10°)

because lower grazing angles are obtained at the higher latitudes.
The upper PRF constraint for the grazing angle profile is also
shown and is not constant as in the VSL angle case. A constant
PRF of 5000 PPS can be used if an antenna with an azimuth dimen-
sion of 4.1 meters is used for the 0.5 orbit.

Using a constant side look angle of 10 degrees and using the
change in direction of the zero doppler direction, a variable side
look angle type of scheme can be used. The clutterlock system
controls the one gimbal needed to implement this system on the C-
configuration and controls the antenna to be approximately 26.6
degrees from the zero doppler direction. The clutterlock system
uses the side lobe closest to this direction to control the an-
tenna.

Antenna Subsystem Design

Two configurations have been considered for the antenna, a
reflector and an antenna array. The major advantage of a reflector
configuration lies in its simplicity and relatively low weight,
while its principal disadvantage is lack of precise control over
the vertical antenna pattern. In the design of reflectors, pattern
control can be obtained by varying the primary source pattern, the
reflector shape, or both. The extent of control is limited, how-
ever, with respect to that needed to produce the types of aperture
distribution desired in a synthetic aperture imaging radar. For
this application it is desirable to approximate a "pulse-shaped"
vertical beam with side lobes at least 10 db down and preferably
as much as 20 db down. Theoretically, this ideal "pulse-shaped"
pattern corresponds to a sin x/x aperture distribution function
to plus or minus infinity. A practical approximation to this is
to truncate the function symmetrically. The computed pattern
which results from this procedure is then given by the following
expression:

$$\text{Si}\left\{\pi\left(n + D/\lambda\ \sin\theta\right)\right\} + \text{Si}\left\{\pi\left(n - D/\lambda\ \sin\theta\right)\right\} \qquad \text{(IV-13)}$$

where   n = multiple of π at point of truncation

θ = angle from broadside

D/λ = aperture size in wavelengths

The expression for the aperture efficiency is given by:

$$\eta = \frac{1}{n\pi}\ \frac{[\text{Si}\ (n\pi)]^2}{\text{Si}\ (2n\pi) - \dfrac{\sin^2\ (n\pi)}{n\pi}} \qquad \text{(IV-14)}$$

These expressions are for continuous aperture distributions.
Typically a sin x/x distribution truncated at $\pm1.5\pi$ will have an
aperture efficiency of 37.1%. To obtain appropriate control over
the aperture illumination of a reflector one can vary the shape
and dimensions of the primary radiator, or the reflector contour.
Nevertheless, it is very difficult to realize the zero crossings
from primary radiators of convenient dimensions at S-band. They
could be forced by introducing discontinuities in the reflector,
such as strips spaced approximately one-quarter wavelength above
the surface. This achieves phase reversal but does not provide
the desired amplitude taper in the region of the zero crossings.
It also complicates the design of erectable and unfoldable reflec-
tors in space applications. The reflector tolerances required for
reflector antennas are shown in Figure IV-12, which gives the maxi-
mum permissible surface tolerance for 20 and 30 db side lobes for
two illumination tapers based on a perfect reference surface. It
is evident that at S-band the reflector surface contour must be
held to an accuracy of better than 0.4 to 0.6 cm (0.97 to 1.63 in.)
if the 20 db side lobe level requirements are to be satisfied.
Actually only 10 db side lobe level requirements are needed to im-
plement the Venus mapping radar in this study. Only a portion of
the doppler bandwidth is used since a partially focused synthetic
aperture is implemented. For 10 db side lobe levels, the reflec-
tor surface tolerances must be held within about one-tenth of a
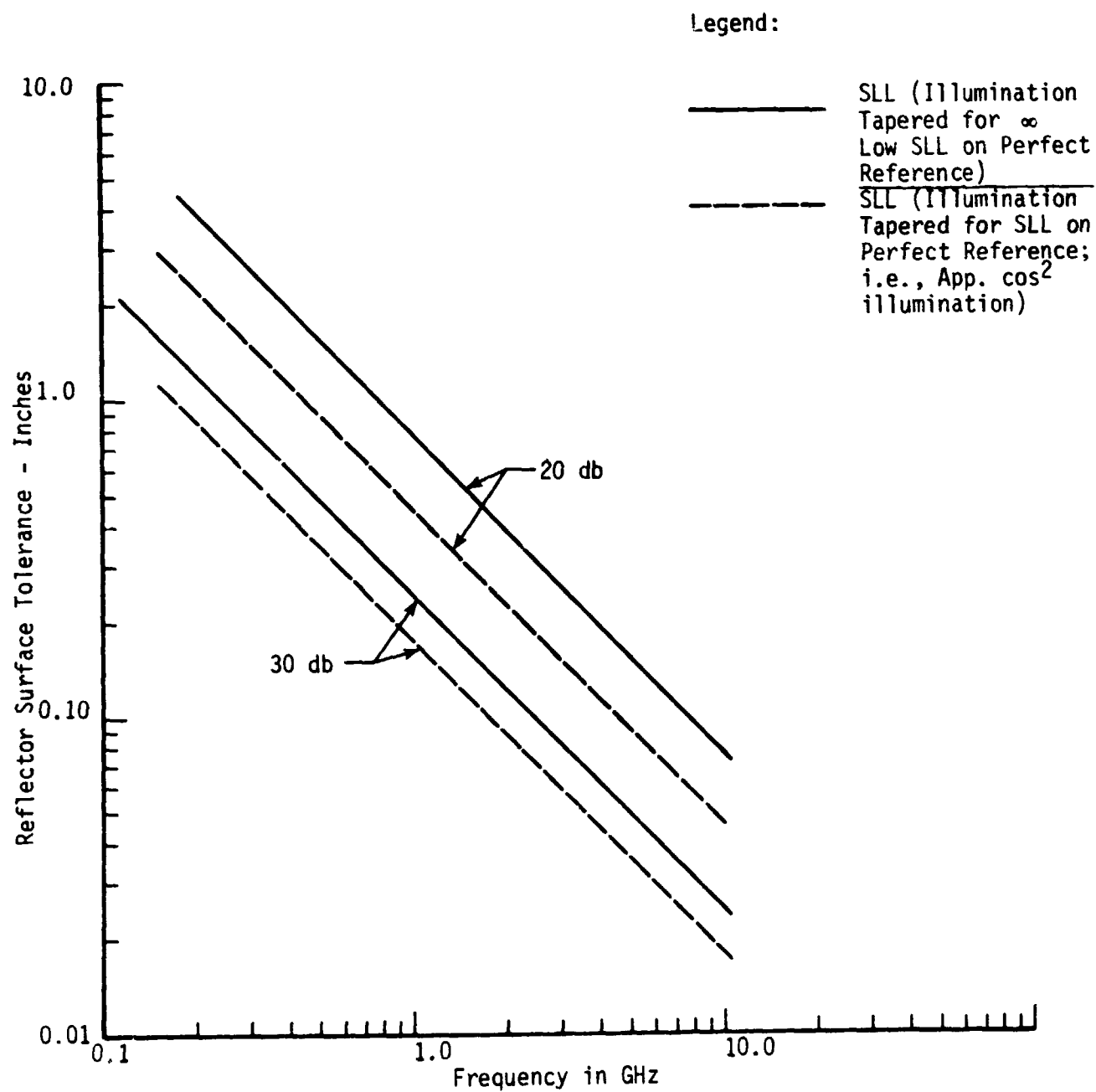
Figure IV-12   Reflector Surface Tolerance vs Frequency

wavelength ($\lambda/10$). This is the maximum permissible tolerance and would include errors due to deflections and deformations as well as thermally induced surface errors. For space applications an erectable or unfoldable dish would be required. The maximum gain achievable from such configurations is limited by the mechanical distortions inherent with such structures. There are many implementations of spaceborne dish antennas which can be considered for both symmetrical and unsymmetrical antenna configurations. These concepts are briefly described below with some references to achievable tolerances wherever this data is available.

Radial Rib Parabolic Reflector (Figure IV-13) - This concept was implemented for a 2.44 m (8 ft) symmetrical dish but can also be applied to unsymmetrical structures. Models have been constructed in several configurations using spring-loaded hinges, leaf spring continuous surface, spring wire cable, and various type beam formations. Most of the manufacturing and assembly surface tolerance deviations can be corrected by individual joint adjustments. Thermal deflections in the space environment are unknown at this time. This concept is also called the vertebrae beam ground plane concept and can be equally applied to phased arrays. Acceleration deflections will be a function of how many ribs are used and the type and size of beam construction. The beams can be tapered. The cable tension rigidizes the vertebra and also affects the deflection. It would appear from the above that this type of configuration will not meet the tolerance requirements of the reflector antenna as set forth in the previous paragraph.

Continuous Vertebra Beam Slab (Figure IV-14) - This concept is similar to the vertebra beam ground plane, except that the structural members are longitudinally continuous. Again manufacturing tolerances can be compensated for by local hinge and surface adjustment devices; 1.27 cm (0.5 in.) r.m.s. surface deviations can

Mesh: Wire or metallized Dacron

Grommet (Typ) Prevents Buckling.

Tapered Pin Dowel (Typ) Strengthens for ground test.

Actuator

Rib ~ 18 places

Wire Helix/
Expandable disc
on hod

Mesh

Rib - Al. formed "ω"
tape... tapered from root to i.p.~ 84 to 12.

Size: 30.5 m

Weight: 1918 kg structure

Shape: Parabolic, adaptable to round plane

Surface: 5.1 cm r.m.s.

Packaging: 10:1 maximum diameter

Deployment: Controlled Spring Ribs

Figure IV-13 Radial Rib Parabolic Reflector

Figure IV-14 Continuous Vertebra Beam Slab

MYLAR SURFACE WITH DOUBLE SPIRAL ELEMENTS
(ALTERNATE: QUADRAFILAR HELIXES, NO RES. BOX)

ALUM. FORMED
RESONANT BOXES

CABLE DRUM
(5 PLACES)

DRIVE MOTOR

DOUBLE SPIRAL ELEMENTS

TRANSPARENT
METALLIZED
MESH

STAINLESS STEEL
TENSION CABLE
(5 PLACES)

Size: 2.4 to 6.1 m square
Weight: 136 kg
Shape: Square and Flat (curve possible)
Surface: 1.3 cm r.m.s.
Packaging: 7:1
Deployment: Gearhead Motor/
            Tension Cable

be expected from this antenna for aperture sizes of 3.05 m (10 ft) to 6.1 m (20 ft) square. Hence, this approach is unlikely to meet the side lobe level specifications for a 3.5 m x 3.6 m synthetic aperture radar antenna utilizing a reflector configuration.

Hinged Beam Panel (Figure IV-15) - This principle was utilized in the manufacture of two 2.44 m (8 ft) parabolic reflector antennas. One had twelve angle ribs, while the other had 24 channel ribs actuated by a gearhead motor to tension the cables. Both antennas used silver metallized dacron mesh surface. Each joint is adjustable and surface mesh ties can also be adjusted to yield extremely close tolerances. Thermal effects of this configuration are expected to be small due to the structural aluminum sizes and design flexibility to minimize deflections. These advantages are, however, more than offset by the extremely large weight of this configuration. Even then, it is still questionable whether the surface tolerances could be met with this configuration.

Tension Panel Reflector (Figure IV-16) - This concept consists of a multiple structural framework which supports a light film work of some type in tension. It has been modeled into a .915 m (3 ft) square section by Aerospace Corporation, El Segundo, California, using a single framework with spring-actuated extendable arms. It was also designed into a six-rib hexagonal shape, spring-actuated, and hydraulically dampened. These designs used two flat surfaces, one as a reflector, one with a single spiral element surface. GDC used a similar principle for small triangular panels for a parabolic reflector. Except for thermal distrotion and arm and mesh strength, for acceleration loads, this concept is attractive. There are many extendable structures that offer potential panel support. These include the tubular scissor truss, the triangular tri-pan (extendable triangular pantograph), the extendable bridge (dual extendable pantograph forming a truss), and an extendable four-sided spider supported pantograph. All of
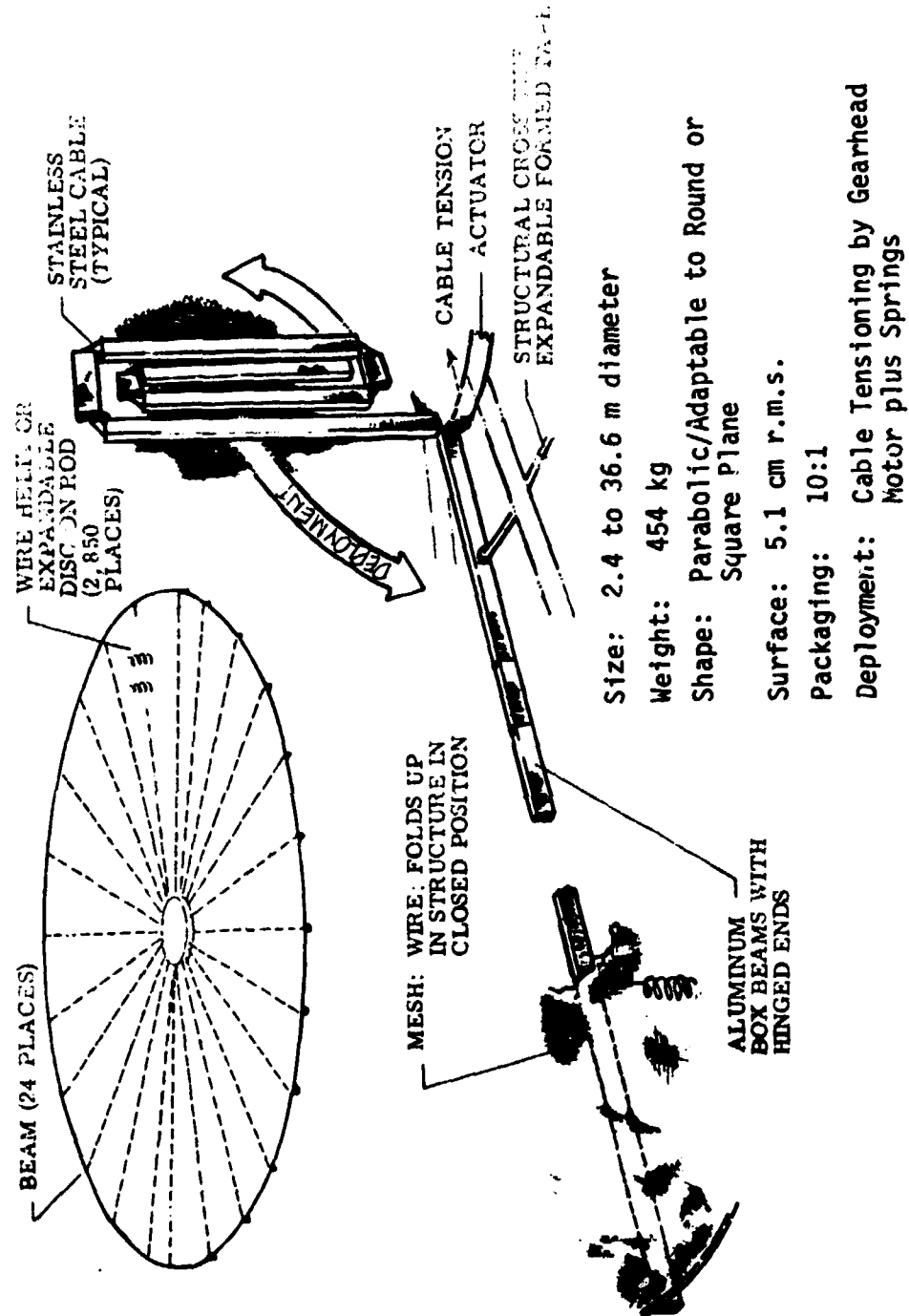
Figure IV-15 Hinged Beam Panel

BEAM (24 PLACES)

WIRE HELIX OR EXPANDABLE DISC ON ROD (2,850 PLACES)

STAINLESS STEEL CABLE (TYPICAL)

MESH: WIRE: FOLDS UP IN STRUCTURE IN CLOSED POSITION

ALUMINUM BOX BEAMS WITH HINGED ENDS

DEPLOYMENT

CABLE TENSION ACTUATOR

STRUCTURAL CROSS TIE EXPANDABLE FORMED BAR.

Size: 2.4 to 36.6 m diameter

Weight: 454 kg

Shape: Parabolic/Adaptable to Round or Square Plane

Surface: 5.1 cm r.m.s.

Packaging: 10:1

Deployment: Cable Tensioning by Gearhead Motor plus Springs

WIRE HELIX OR EXPANDABLE
DISC ON ROD

ACTUATOR

WIRE OR METALLIZED
DACRON (FOLDABLE)

ALTERNATE
CONFIGURATION

TENSION
DEVICE
(4 PLACES)

TUBULAR
SCISSOR TRUSS ...
SIMILAR TO
SURVEYOR SURFACE
SAMPLER

ACTUATOR

Size: 2.4 to 30.5 m

Weight: 454 kg

Shape: Square (hexagonal, octagonal, etc.)
Double/Single Skin

Surface: 7.3 cm r.m.s.

Packaging: 18:1

Deployment: Springs and Gearhead Motor

Figure IV-16 Tension Panel Reflector

these are extremely heavy, and would, therefore, not be suited
for space applications. For extremely light weir' . beams the STEM
principle could be considered and would have def_nite advantages
in a zero "g" environment. This design can be used and will meet
the $\lambda/10$ specifications.

Swirlabola Hinged Segment Assembly (Figure IV-17) - This con-
cept was developed by Goodyear Aircraft Corporation, who have
built a number of reflectors using this principle. Its open-to-
closed ratio is very low d·.e to the fact that the tubular struc-
tural members wrap around the central hub. This means that the
open size can be only approximately 2.8 times the spacecraft di-
ameter. By providing surface adjustments to overcome manufacturing
tolerances and designing deep, open, swirling ribs to minimize ac-
celeration and thermal deflections, it is possible to hold surface
tolerances to better than 0.46 cm (3/16 in.) r.m.s. for a 6.1 m
(20 ft) square aperture. Deployment is effected by spring loading
the hinges and sclenoid or explosive released latches. Fifteen to
twenty ribs would probably provide adequate mesh support for a
6.1 m (20 ft) reflector. The weight of this assembly would appear
to be reasonable and the approach merits further consideration,
if only for its superior surface accuracy properties.

Mesh Petaline Structures (Figure IV-18) - Petaline refers to
devices which open like petals. Many types have been developed
such as interconnected petals (hinged longitudinally). hybrid
petals (petal and mesh), individual petals (sunflower hinged),
double hinged petals, etc. Both Goodyear Aircraft Corp., and TRW
Systems, Inc., have done considerable work on these configurations.
Goodyear has developed a 9.15 m (30 ft) diameter petal reflector
antenna with interconnected petals which are all hinged. Each
petal is permanently attached to its two adjacent petals, and the
antenna forms a continuous surface when open. Such antennas are
generally limited in diameter to approximately twice their furled

HELIX, DISC OR ROD OR QUADRAFILAR HELIX

MESH: **WIRE OR METALLIZED FABRIC**

POSSIBLE BEAM CONFIGURATIONS

ACTUATOR

ALUM. TUBE

ACTUATOR

ALUM. TAPERED CHANNEL

d_H

$2.8 d_H$

DEPLOYMENT

HELIX IN CLOSED POSITION
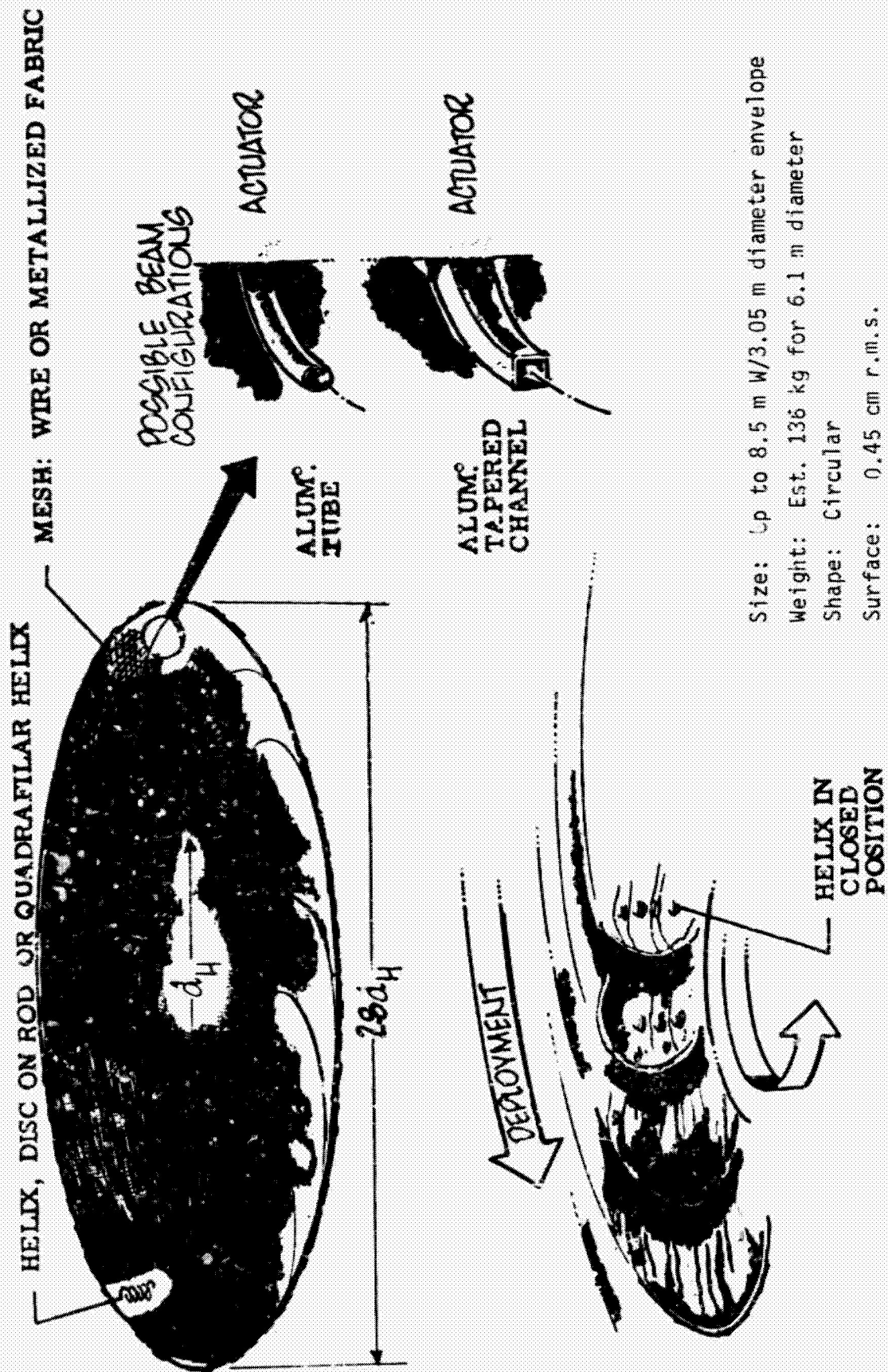
Size: Up to 8.5 m W/3.05 m diameter envelope

Weight: Est. 136 kg for 6.1 m diameter

Shape: Circular

Surface: 0.45 cm r.m.s.

Packaging: 2. 8:1

Deployment: Springs or Gearhead Motor/
             Levers

Figure IV-17 "Swirlabola" Hinged Segment Assembly

WIRE HELIX
EXPANDABLE
DISC ON ROD
QUADRAPILAR
HELIX

WIRE OR METALLIZED
DACRON/MYLAR

RIB (24 PLACES)
ALUM.

HINGE
(TYP.)

Size: Up to 12.2 m dia. from
3.06 m dia. x 6.1 m Package

Weight: Est. 182 kg for 9.2 m dia.

Shape: Round

Surface: 0.685 cm r.m.s. (GDA)

Packaging: 4:1

Deployment: Springs or Gearhead
Motor/Levers

INTERCONNECTED PET-
ALS (GOODYEAR)

STAR PETALINE   MESH PETALINE
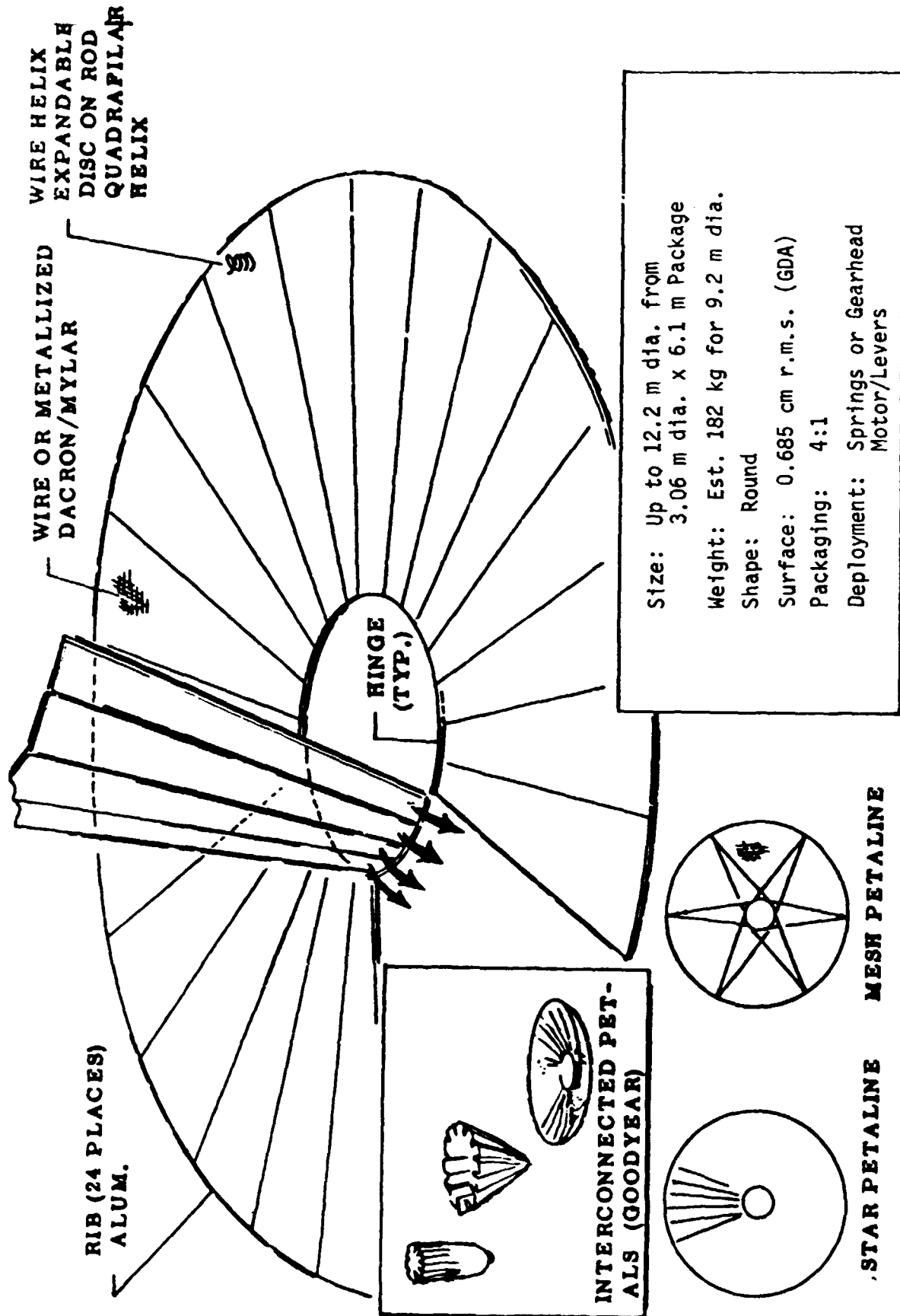
Figure IV-18   Petaline Types

IV-39

length. Surface tolerances of 0.68 m (0.27 in.) r.m.s. can be
achieved for parabolic type reflectors in the 6.1 m (20 ft) di-
ameter region and the weight appears reasonable. This approach is
best suited for round reflectors, but certainly merits further
consideration for the synthetic aperture radar antenna.

Expandable Truss Space Frame Structures (Figure IV-19) - This
concept has been developed by Convair, GDA for reflector type space
vehicle antennas. The truss concept offers potential to very
large antenna sizes (up to 152 m) using double truss networks,
and can be implemented for any smaller sizes. It has the advan-
tages of inherent rigidity, openness to thermal effects, good
packaging, and self-expansion capability. Its major disadvantages
are high weight and poor reliability due to the numerous compon-
ents, hinges, and joints making up this assembly. Also, control
of uniform deployment could present a problem unless damping was
built in. Surface tolerances of 0.79 cm (0.31 in.) r.m.s. can be
achieved for structures up to 30.5 m (100 ft) in diameter. The
approach does not appear too attractive because of the very high
weight of this antenna.

Flex-Rib Reflector (Figure IV-20) - This concept has been de-
veloped by Lockheed, Missiles and Space Division, again for re-
flector type antennas. They have built a 1.8 m x 2.74 m (6 ft x
9 ft) rectangular antenna with a parabolic contour which was
covered with metalized fabric reflecting surface. The furled
size was 14 cm x 46 cm (5.6 in. x 18 in.) diameter, giving a
good expansion ratio. This ratio could be increased for larger
antennas where beam depth would increase but rib thickness would
not be increased linearly. The concept is simple and very re-
liable, and for its size is relatively light weight. Surface
tolerances are still not good enough to meet the side lobe speci-
fications, but should be comparable with some of the above con-
figurations.

Wire Helix on Expandable disc on hat (typ)

Fully Deployed

Mesh: Wire or Metallized Dacron

Al. or Beryllium Tubing (typ) Perforated to lighten

Size: 2.4 to 46 m (to 152 m w/Double Truss, GDA)

Weight: 1640 kg for 46 m diameter

Shape: Hexagonal

Surface: 0.79 cm r.m.s. for 46 m dia. (GDA)

Packaging: 7:1 (14:1 w/Double Truss)

Deployment: Spring Joints to 30.6 m, EVA assist above 30.6

Partially Deployed

Packaged

TRUSS DETAIL Partially Deployed

Figure IV-19 Expandable Truss Space Frame

WIRE HELIX, EXPANDABLE DISC
ON ROD, OR QUADRAFILAR HELIX

RIB (TYPICAL) 24 PLACES

MESH: WIRE OR METALLIZED DACRON

MESH

RIB: ALUM. OR
BeCu (TYPICAL)
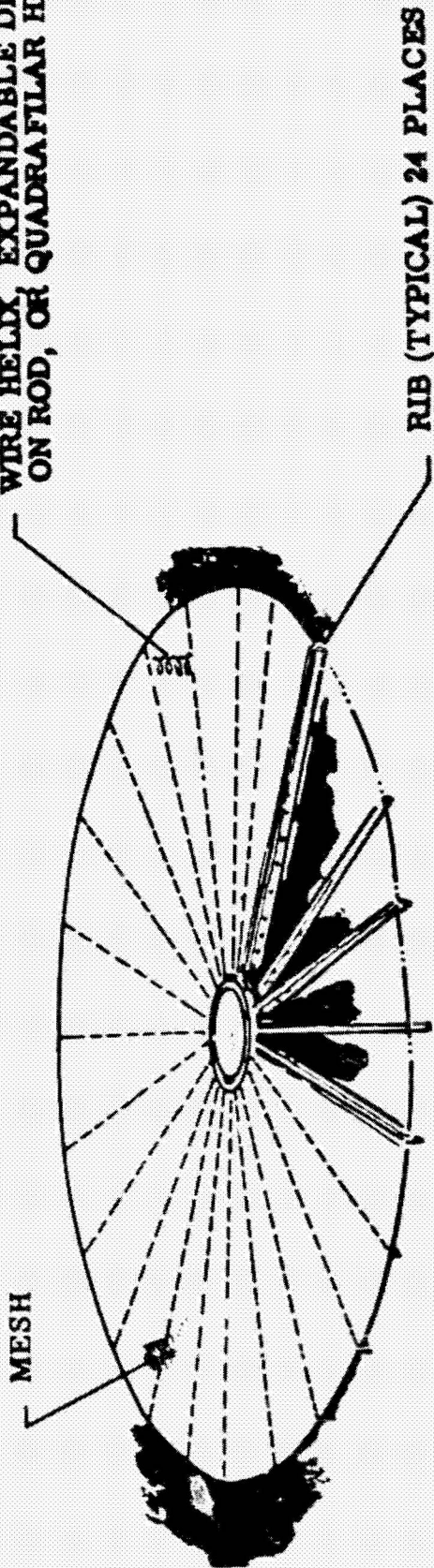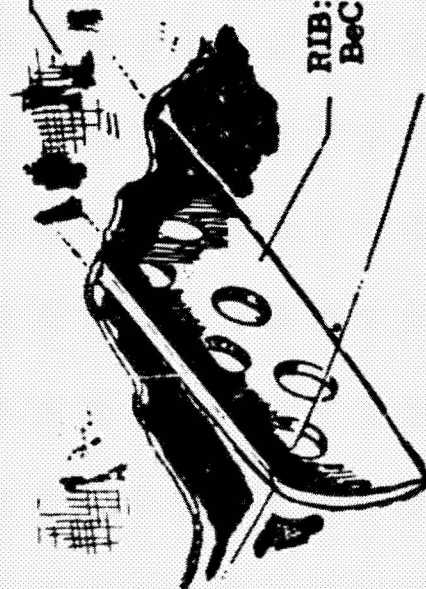
RIB DETAIL

Size: 2.4 to 36.6 m dia.
Weight: 91 kg for 3.06 m dia.
Shape: Square, Rectangular, Round
Surface: 5.1 cm r.m.s./3.06 m
Packaging: 6:1 or greater
Deployment: Spring Ribs

Figure IV-20 Flex-Rib Reflector

Special Deployable Reflector - A new concept has been developed
by Radiation, Inc., Melbourne Florida, which provides an r.m.s.
surface accuracy of 0.076 cm (0.030 in.) for a deployable, 3.66 m
(12 ft) diameter parabolic reflector. No data is currently avail-
able on this reflector, and it is suggested that all pertinent
technical data be obtained on this approach since it is the one
of the concepts that would meet the surface accuracy requirements
for the side looking radar antenna.

Tne various configurations discussed above illustrate some of
the problems associated with reflector antennas when applied to
the synthetic aperture radar problem. In addition, positioning of
the feed system introduces another tough mechanical problem. The
characteristics of all but one of these erectable and unfurlable
reflector antennas are summarized in Table IV-1. The maximum gain
achievable from various space vehicle reflector antennas has been
plotted in Figure IV-21 as a function of frequency for both rigid
and erectable reflectors, giving both current state-of-the-art
data and expected capabilities in the 1980-85 era. The gain fig-
ures are based on normal parabolic reflector antenna illuminations
(-11 db edge taper) and, therefore, do not reflect the low side
lobe requirements required for side looking radar applications.
The steeper illumination tapers required will decrease the overall
antenna gain by about 2 db under those given in Figure IV-21.
This would also require a larger, more complex feed system and,
further, suggest the use of offset feeds to prevent aperture block-
age which could also cause an increase in the side lobe level.

A phased array can also be employed as the radar antenna and
it would appear to have some significant advantages. In the S-
band region of the microwave spectrum various types of array ele-
ments can be considered in the design of the array. These are:
dipoles, discpoles, disc-on-rod, shunt slots, helices, planar
spirals, conical spirals, open-waveguide, and small horns.

IV-43

Table IV-1 Characteristics of Erectable and Unfurlable Reflector Antennas

Type	Size	Shape	Weight (kg/m²)	Surface	Packaging	Deployment
Radial Rib	6.1 m² 20 ft²	square or rectangular	1.47-2.44	2.54 cm rms	7:1 on dia. 1:1 on length	gearhead motor/ cable tension
Continuous Vertebra Beam Slab	6.1 m² 20 ft²	square and flat, curved	2.44-3.67	1.77 cm rms	7:1	gearhead motor/ cable tension
Hinged Beam Panel	up to 30.5 m diameter	square or round curved	2.44-4.4	2.5 - 5.0 cm rms	10:1	gearhead motor plus springs/ cable tension
Tension Panel Reflector	up to 30.5 m square	square or hexagonal	2.44-4.9	7.6 cm rms	18:1	springs and gearhead motor
Swirlabola Hinged Assembly	6.1 m dia.	circular	3.9 -5.87	0.46 cm rms	2.8:1	spring or gearhead motor/ levers
Mesh Petaline Structures	up to 12.2 m diameter	circular	1.96-2.94	0.69 cm rms	4:1	springs or gearhead motor/ levers
Expandable Truss Space Frame	up to 46 m diameter	hexagonal	0.98-1.96	0.79 cm rms	7:1 (14:1 with double truss)	spring joints to 30.6 m
Flex-Rib Reflector	2.44 m to 36.6 m dia.	square, rectangular, circular	0.98-1.96	5.1 cm rms/ 30.6 m dia.	6:1 or greater	30.6 m spring ribs
Special Deployable Reflector	3.66 m dia.	circular	N/A	0.076 cm rms	N/A	N/A
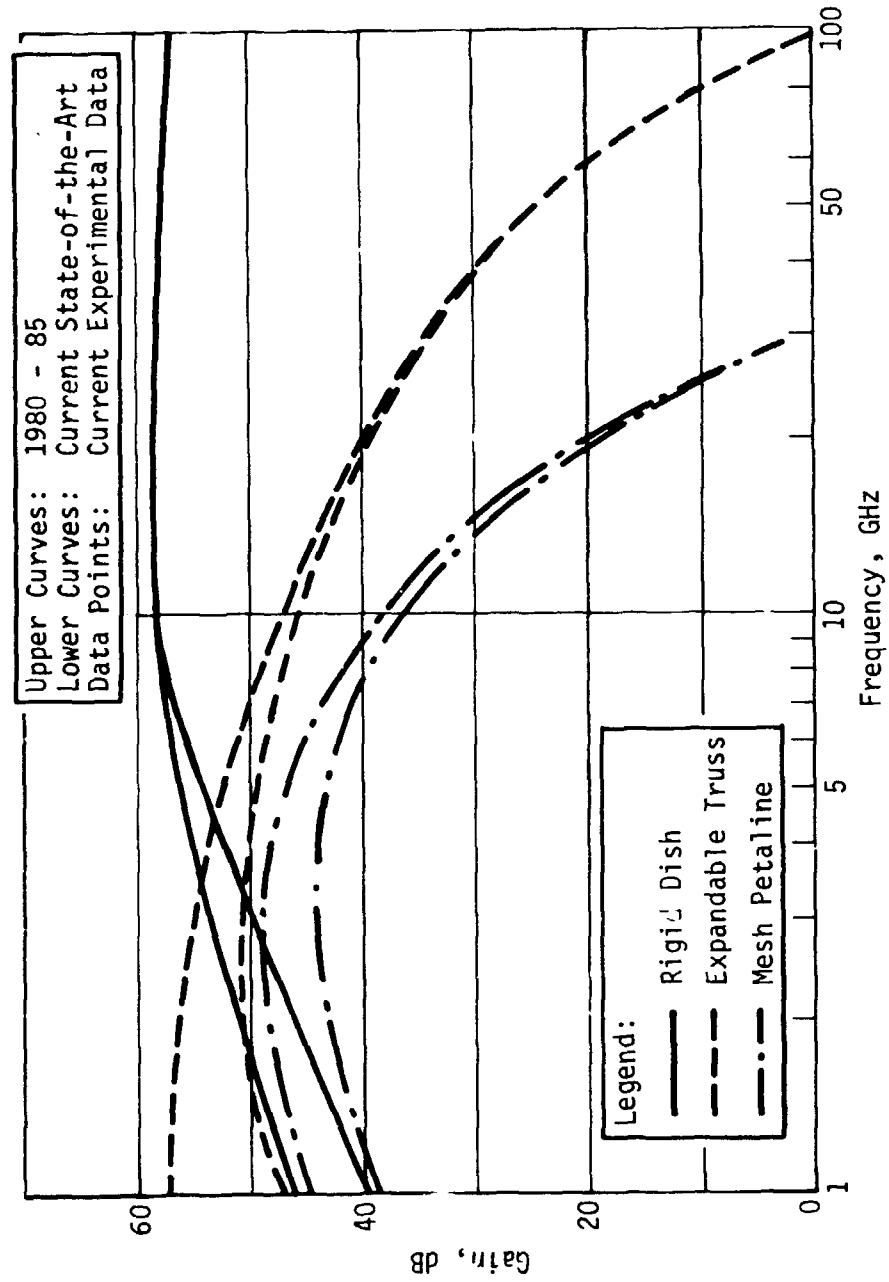
Figure IV-21 Maximum Achievable Gain for Spaceborne Dish Antennas

Since no scanning is required, selection is based mainly on physical and geometrical factors. To obtain a pulse-shaped vertical antenna pattern with narrow horizontal beamwidth and low side lobes, three types of arrays were considered:

1) Horizontal non-resonant array with vertical feeders.
2) Vertical non-resonant array with horizontal feeders.
3) Array of vertical arrays of resonant elements.

Of these, the vertical array of resonant elements would appear to have the best chance of meeting the beamwidth and side lobe requirements. This approach can be implemented by feeding each of the vertical resonant arrays from a separate solid state transceiver module, or by subdividing the antenna into a convenient number of subarrays which are interconnected by a true time-delay feed network. The latter network is required in order to avoid transit time effects and loss in antenna gain. A reasonable subdividion of the overall aperture would entail 8 subarrays consisting of 8 vertical resonant arrays, which can again be interconnected by true time delay feed networks. For packaging and ease of deployment, flush-mounted array elements are preferred. This would suggest the use of resonant slots elements with either a waveguide or strip line feed system. It is well known that shunt slots offer the advantage of very low mutual coupling and this type of element is therefore recommended for the antenna array. The typical 7.63 x 3.82 cm (3 x 1½ in.) S-band waveguide system was considered, but in order to reduce the weight of the array, the height of the waveguide can be reduced depending only on power and impedance requirements. For peak power levels of 1 kw (166 watts average), each vertical array would be required to carry only 65 w peak (10 watts average) power, which is easily achieved with 1.27 cm (½ in.) high waveguide which would have an impedance of about 100 ohms. Furthermore, if the waveguide does not form part of the supporting structure, it is feasible to

reduce the wall thickness to effect a further reduction in weight. If structural strength is required of the waveguide, then the waveguide walls could be of honeycomb construction yielding high strength with low weight. The inner surface would have a conductive coating to assure low losjes. Such a configuration could be made to fold up for packaging of the antenna. Alternately, stripline transmission lines could be used with resonant slot elements, where again the ground plane spacing is reduced to affect a minimum weight configuration. This reduces the amount of teflon required for the dielectric insulator between the center strip and the two ground planes. Foamdiele·trics could also be considered to further reduce the weight of the antenna. Deployment schemes considered are similar to those discussed for the reflector antennas, and include the following:

1) Vertebra Beam Ground Plane (Figure IV-22)
2) Continuous Vertebra Beam Slab (Figure IV-14)
3) Accordion Panel (Figure IV-23)
4) Biaxial Dual Tape Array (Figure IV-24)
5) Self-Forming Sandwich Panel (Figure IV-25)
6) Radiation Inc. Deployment System

The first two were described previously. The accordion panel concept was developed by Fairchild Hiller Corp., Space Systems Division, for the solar arrays of the Pegasus Satellite. It is of interest here if the subarray approach is employed, since each panel would then consist of a 3.5 m x .457 m (11.5 ft x 1.5 ft) subarray. Since the size is limited to the envelope length available in the spacecraft, there may be some problems with the long dimension. The deployment scheme is simple and reliable, although close tolerances are required at the hinge joints. Deployment is by means of spring and gearhead motor and the 8:1 packaging ratio is easily obtained. Array aperture tolerances of about 1.9 cm (0.75 in.) r.m.s. are achievable in the horizontal

WIRE HELIX (TYPICAL) ALTERNATE CONFIGURATION: EXPANDABLE DISC ON ROD OR QUADRAFILAR HELIX

10.2 cm dia. x 63.5 cm (Open)
10.2 cm dia. x 7.6 cm (Closed)

CABLE DRUM (TYPICAL) (5 PLACES)

DRIVE MOTOR

POSSIBLE BEAM CONSTRUCTIONS (ALUM. EXTRUSION OR FORMED)

MESH: WIRE METALLIZED DACRON OR MYLAR FILM

STAINLESS STEEL TENSION CABLES

Size: 2.4 to 6.1 m square
Shape: Square or Rectangular only
Weight: 91 kg
Surface: 2.5 cm r.m.s.
Packaging: 7:1 on dia., 1:1 on length
Deployment: Gearhead Motor/Cable Tension

Figure IV-22 Vertebra Beam Ground Plane

ELEMENT: WIRE HELIX OR EXPANDABLE
DISC ON ROD
ALTERNATE: DOUBLE SPIRAL/
RES. BOX

MYLAR OR METAL FACE

MOTOR AND
DEPLOYMENT SPRINGS

PARTIALLY
DEPLOYED
POSITION

FULLY CLOSED
POSITION

SCISSORS
LINKAGE
(TYP.)

FULLY
DEPLOYED
POSITION

ALUM. BOX
TUBE (TYP.)

Size: 2.4 x 6.1 m (Pegasus = 3.06 x 30.6)
Weight: Est. 136 kg for 6.1 m

Shape: Square
Surface: Est. 2.54 cm r.m.s.

Packaging: Up to 10:1
Deployment: Springs and Gearhead Motor

Figure IV-23 Accordian Panel

WIRE HELIX, EXPANDABLE DISC ON ROD, OR QUADRAFILAR HELIX MESH

MESH: METALLIZED GROUND PLANE NETTING

FURLED POSITION

BEAM (TYPICAL) ALUM. OR BERYLLIUM COPPER (BeCu) TAPE

EXTENDED ELEMENT

BEAM

ANTENNA ELEMENT LEAD

SECTION A·A

A

A

Size: 2.4 to 30.6 m

Weight: 682 kg

Shape: Square

Surface: 5.1 cm r.m.s.

Packaging: 15:1 Radially, 5:1 Axially

Deployment: Gearhead Motor

Figure IV-24 Biaxial Dual Tape

ELEMENT:
WIRE HELIX
OR
EXPANDABLE
DISC ON ROD
(ALTERNATE: QUADRAFILAR
HELIX)

CLOSED
CONFIGURATION

HEAVY GAGE
METAL FOIL

PLASTIC (EXPANDS
WITH HEAT)

LIGHT GAGE METAL FOIL

Size: 2.4 to 6.1 m square
Weight: 68 kg
Shape: Square (circular/hexagonal possible)
Surface: Est. 5.1 cm r.m.s. in 6.1 m
Packaging: 10:1 on dia., 1:1 on length)
Deployment: Gas/Thermal Setting Plastic
           (408°K) - Heating Coils
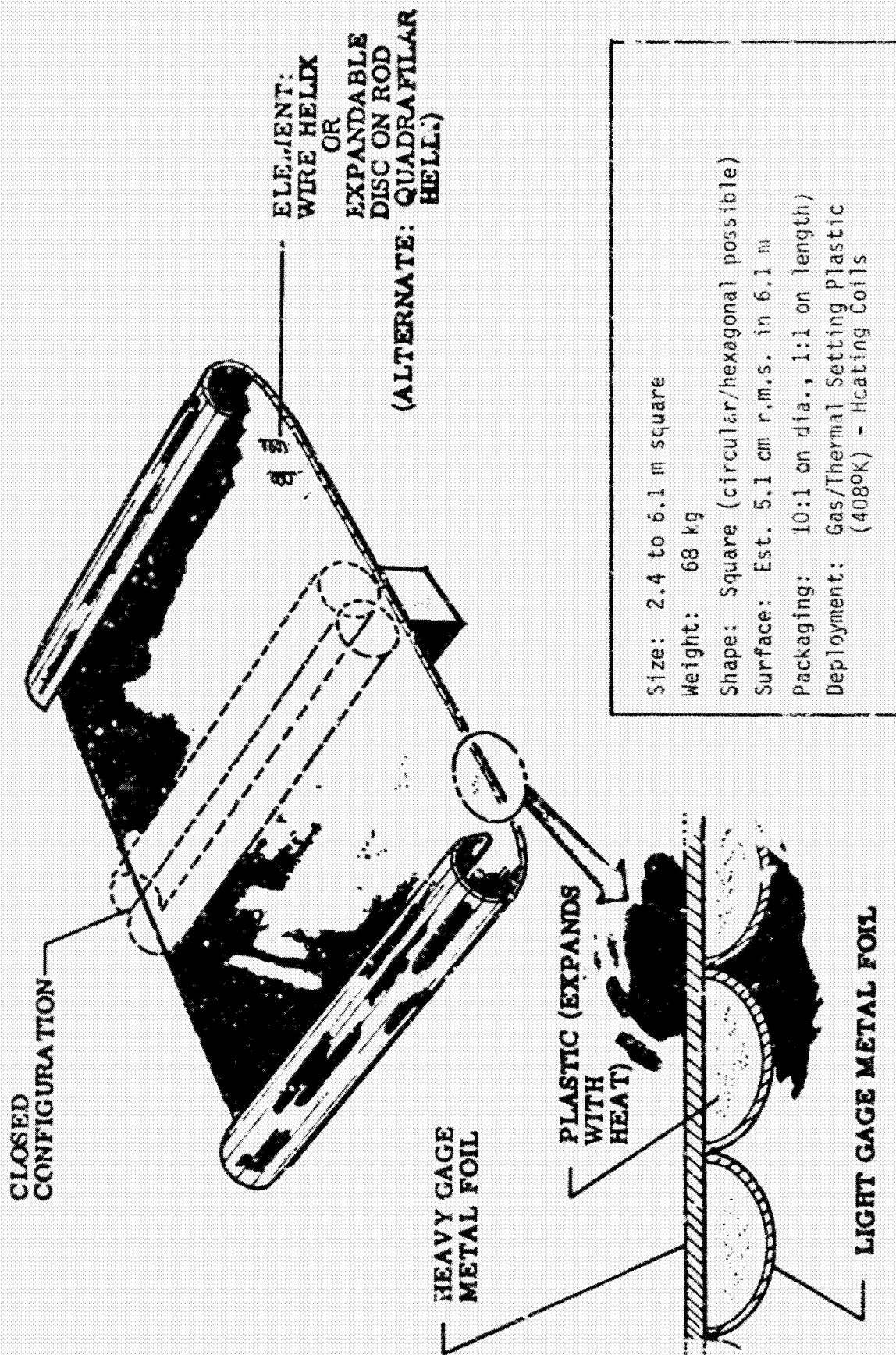
Figure IV-25 Self-Forming Sandwich Panel

plane, while in the vertical plane the r.m.s. surface error is expected to be considerably better (< 0.38 cm). This would allow the necessary control over the side lobe level of the vertical pattern of the array which is required in a synthetic aperture radar antenna. The biaxial dual tape array deploys tape in a flat arrangement so that the antenna can be unrolled from two spools and the spocls themselves can be telescoped axially. Although complex and fairly heavy, this scheme would require a design using a flexible dielectric for the vertical arrays such as are commonly available in printed circuit work. The concept provides two-directional deployment from a roll type package and would thus allow vertical deployment of the antenna with the transmitters and feed systems contained within the rolls. Packaging ratios of 15:1 radially and 5:1 axially can be achieved with deployment by a gearhead motor. In this scheme array aperture tolerances of about 1.28 - 1.9 cm (0.5 - 0.75 in.) r.m.s. are achievable in both planes which is inferior to other schemes discussed previously. The self-forming sandwich panel concept is also of interest since it, too, provides the capability to expand on one axis either in one direction or both. It appears simple and effective, and has a reasonable weight (< 1.96 kg/m^2). However, the foaming and setup characteristics to produce consistent, reliable surfaces with very small surface deviations are unknown. It is, therefore, not expected that surface tolerances of better than 2.54 cm (1 in.) r.m.s. for a 3.66 m (12 ft) square aperture could be achieved with this approach unless considerably more development work is carried out. Also, thermal deflections in space could be severe because of its surface area and material differences.

The radiation Inc. concept for a deployable dish could probably be modified to allow its use for erectable array configurations. However, too little is known about the design details of this

approach at this time to arrive at definite conclusions regarding its application to the array to allow accurate performance predictions.

Radar Subsystem Design

The major tradeoffs which must be considered in the choice between vacuum tubes and solid state devices are peak power, duty cycle, and reliability. In general, tubes will exhibit peak to average power characteristics several orders of magnitude greater than semiconductors which is primarily due to the difference in thermal time constants. For tubes this time constant is of the order of a few seconds compared to a few hundred sec for semiconductor devices. In Figure IV-26 the peak to average power ratio is plotted as a function of pulse length for both vacuum tubes and semiconductor devices. The advantages of the vacuum tube are quite apparent. Nevertheless, it is important to consider solid state trans ters because of their increased reliability. This is achieved both by the increased reliability of the solid state device and by distributing the transmitter modules over a large phased array which reduces the required output power of each module. Furthermore, by using separate transceiver modules for each array element or for each vertical array of the overall planar array, the failure of any one module in the array will not appreciably affect the performance of the radar. This further increases the reliability of the overall system. At S-band, a consideration of solid state sources must include the following devices as potential r.f. transmitters:

1) SRD/varactor frequency multiplier chains;
2) Transistor oscillators and amplifiers;
3) Pulsed Gunn oscillators;
4) Trapatt oscillators and amplifiers;
5) LSA oscillators.
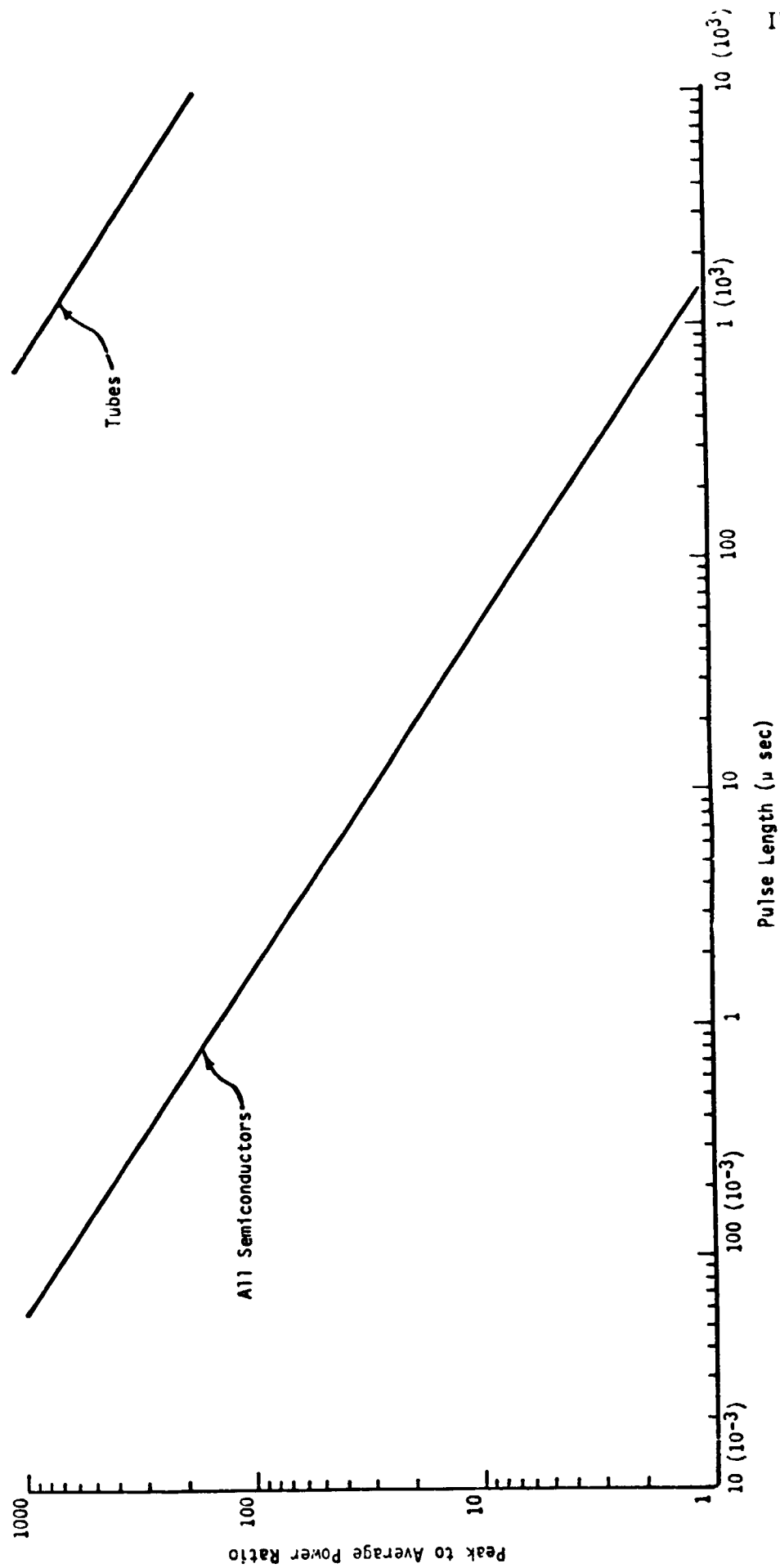
Figure IV-26   Comparison of Pulsed Performance of Tubes and Solid State Devices

In like vein, various vacuum tube types should be considered
for the synthetic aperture imaging radar including both conven-
tional types and some of the more recently developed printed cir-
cuit configurations. The following tube type transmitters were,
therefore, investigated:

1) Backward wave CFA;

2) Forward wave CFA;

3) Printed circuit forward wave CFA;

4) Conventional PM-TWT amplifier;

5) Printed circuit TWT amplifier;

6) Electron beam semiconductor amplifier;

7) Bonded grid triode.

Typical RF pulse tube parameters are shown in Table IV-3.
The conventional backward wave CFA and forward wave CFA provide
very high peak power levels which are not required for this appli-
cation. The radar peak power requirements at S-band are 1 kw with
an average power of 166 w. Hence the tubes of most interest would
be the TWT amplifier, the PC/forward wave CFA, and the bonded grid
triode. The latter has been implemented recently at L-band, but
should also be feasible in the S-band region of the microwave
spectrum. A brief discussion of these tube types is given below:

CFA Tubes - Crossed field amplifiers have seen extended use
in the last few years and a considerable amount of development
work has been accomplished on these devices. Conventional CFAs
are best suited for high power applications. For the synthetic
aperture radar transmitter the printed circuit CFA is of interest
even though it is still in the developmental stage. It is small,
light, and reliable and has measured efficiency of 40% at S-band.
Gain of 13 db, however, is low compared to saturated gain figures
available with traveling wave tube amplifiers. This means that
higher gain preamplifiers would be required to drive the CFA. For
this application average powers of 8 watts should be available to

drive the CFA, which is not an unreasonable requirement with current state-of-the-art techniques.

Traveling Wave Tube Amplifiers - Many TWT amplifiers have been developed which will meet the power requirements of the synthetic aperture radar. Two of these are shown in columns 5 and 6 of Table IV-2. The first of these provides a peak power output of 2 kw with a gain of 30 db and an efficiency of 30%. The second TWT shown is a high power pulse amplifier developed by Hughes which provides either 1 kw peak of 200 w/cw over the 2-4 GHz band at a duty cycle of 5%. Typical dimensions are 44.5 cm x 6.35 cm (17.5 in. x 2.5 in.) diameter and the tube weight is 4.55 kg (10 lbs). Again, for future space applications such as the synthetic aperture radar, the printed circuit TWT should be of utmost interest because of its increased reliability and comparable performance. This tube is currently under development by Varian and already has provided power outputs of 2 kw peak at S-band with an efficiency of 25%. It is expected that in the 1980-85 era printed circuit TWTs will be available with power outputs of 4-5 kw providing 35 db gain with an efficiency of 30% or better.

Another possible power amplifier is a hybrid tube-semiconductor device generally called an EBS amplifier (electron beam semiconductor amplifier). This device combines an electron gun modulation system, semiconductor target, and output coupling network within a vacuum envelope. It eliminates the need for focusing magnets as in PPM-TWTs. It offers gains in excess of 40 db and requires much lower beam current than conventional TWTs. Thus, it is considerably smaller, lighter, and operates at efficiencies of over 65%. Watkins-Johnson has obtained 400 w peak power at 100 MHz from an EBS pulse amplifier with a duty cycle of a few tenths of one percent. This device is still in the research stage, but it is felt that power levels of up to 1 kw are possible at 2 GHz using a lumped element target device. Further-

Table IV-2 RF Pulse Tube Parameters

Tube Class	CFA				TWT					EBS*		TRIODE		
Tube Type	BW/CFA	FW/CFA	PC FW/CFA	1980-85 FW/CFA	PM/TWT #1	PM/TWT #2	1980-85 PM/TWT	PC/TWT	1980-85 PC/TWT	Current EBS	1980-85 EBS	Bonded-Grid Triode	Bonded-Grid Triode	1980-85 Bonded-Grid Triode
Waveband	S	S	S	S	S	S	S	S	S	P	S	L	S	S
Peak Power-KW	750	150	2	3	2	1(pulse) 0.2(CW)	3	2	4	0.4	1	5	2	3
Duty Cycle-%	6	4	6	6	6	5	6	6	6	0.5	5	10	8	8
Average Power-W	45 (10³)	6(10³)	120	180	120	50	180	120	240	2	50	500	160	240
Bandwidth-%	15	20	20	20	20	100	20	20	20	20	20	20	20	20
Gain-DB	10	13	13	15	30	30	35	30	35	40	40	15	15	18
Modulation	Cathode	RF key	RF key	RF key	Grid	Grid	Grid	Grid	Grid	Electron Gun	Electron Gun	Grid	Grid	Grid
Operating Voltage-KV	25-35	20	5	4.5	6	7.8	7	6	5.5	N/A	N/A	1.5	2.0	1.8
Efficiency-%	50	35	40	45	30	30	35	25	30	63	65	60	45	50
Cost (Large Quan.)	10K	10K	0.2K	0.5K	0.25K	0.5K	1K	0.15K	0.3K	N/A	N/A	0.2K	0.5K	1K

*Currently under military development by Watkins-Johnson.

more with this technique Class B amplifier operation is possible
with r.f. sine wave efficiencies up to 65% and video pulse effici-
encies of 85%. Watkins-Johnson is trying to improve target life
reliability by using junction passivation techniques and shielding
critical portions of the diode from direct electron bombardment.
They are also considering a distributed element target where the
meander line is distributed in a dimension perpendicular to the
electron flow, rather than parallel to it. It is felt that be-
cause of its small size, lightweight, and high efficiency this
device must be seriously considered for the synthetic array appli-
cation since it is expected that by 1980-85 acceptable, space-
qualified hardware should be available.

Triodes - Another device which has just recently received re-
newed attention in the vacuum tube field is the triode amplifier.
General Electric Co. has developed a bonded grid amplifier at L-
band which is capable of 5 kw peak power output at a duty cycle
of 10% with an efficiency of 60%. It is felt that by 1980-85 S-
band tubes should be available with 3-5 kw of peak pulse power and
efficiencies of 50%. GE has developed a very effective emission
control unit for these tubes. It would, therefore, appear that
the bonded grid triode should also receive serious consideration
for the synthetic array radar, particularly since it should pro-
vide highly reliable performance in space applications.

Solid State Sources - The solid state sources that must be
considered as candidates for radar transmitters are listed in
Table IV-3. In comparing transistor, bulk, and avalanche power
sources it is important to remember that transistors cannot be
operated at their full average power ratings due to system duty
cycle constraints. A derating factor of 5 to 10 is often necessary
depending on the permissible transmitter duty cycle. Bulk and
avalanche sources generate substantially higher peak than average
power, so no such derating is necessary. A brief description of

Table IV-3 RF Solid State Source Parameters

Solid State Source	Transistor	Transistor	Transistor	Trapatt	Trapatt	Trapatt	Pulsed Gunn	Pulsed Gunn	Pulsed Gunn	Pulsed Gunn	LSA	LSA	LSA
Transmitter Type	Trans. Osc.	Trans. Amp.	1980-85 Transistor Amp.	Trapatt Diode Osc.	Class C Trapatt Amp.	1980-85 Trapatt Osc.	Pulsed Trapatt Osc.	Pulsed Gunn Osc.	Pulsed Gunn Osc.	1980-85 Gunn Osc.	LSA Diode Osc.	LSA Diode Osc.	1980-85 LSA Osc.
Wave-band	S (2.3GHz)	S	S	S (2GHz)	S (3.4-3.6GHz)	S (2GHz)	S (2GHz)	S (3GHz)	S (3GHz)	S (3GHz)	S (2GHz)	S (4GHz)	S (2GHz)
Peak Power-W	20	30W(2GHz) 10W(4GHz)	100W(2GHz) 30W(4GHz)	100	10	250	5	4.5	30	50	500	250	700
Duty Cycle-%	10	10	10	1.0	N/A	1.0	1.0	1.0	1.0	1.0	0.1	0.1	0.1
Average Power-MW	300	N/A	N/A	1000	N/A	2500	50	45	300	500	500	250	700
Band-width-%	10	10	10	N/A	10	N/A	5	10	10	10	N/A	N/A	N/A
Gain-DB	Osc.	23	25	Osc.	6	Osc.	Osc.	Osc.	Osc.	Osc.	Osc.	Osc.	Osc.
Operating Voltage-V	28	28	28	80	80V 4-6A	80	38V 3A	45V 2.5A	45V 3.5A	50V 3.5A	400V	400V	500V
Efficiency-%		50(2GHz) 30(4GHz)	60(2GHz) 40(4GHz)	25	20	35	0.45	0.40	1.5	2.8	10	8	15

(Note: the Pulsed Gunn group is captioned "Pulsed Transit Time Oscillators.")

the semiconductor sources shown in Table IV-3 is given below:

Transistor Oscillators and Amplifiers - Although transistor performance advances seem to have levelled out, the transistor amplifier still forms the basis of most solid state radar transceiver modules. Current state-of-the-art in power transistors is shown in column 1 and column 2 of Table IV-3. Thus, the best power transistors are capable of about 10-30 w peak power at S-band with efficiencies in the 30%-50% range. In the 1980-85 era it is expected that peak pulse powers of 100 watts should be achievable. It is common practice to parallel transistors in solid state circuits so that considerably higher power levels can be achieved even after derating the transistors. Typical pulse power amplifier performance is indicated in column 2 with expected 1980-85 performance in column 3. Transistors can also be operated as amplifier-multipliers and oscillator-multipliers to produce power output at frequencies well above their maximum fundamental frequency. The performance of these circuits is shown in Figure IV-26 and discussed more fully in a later section.

Trapatt Oscillators and Amplifiers - The current status of Trapatt oscillators and amplifiers is shown in columns 4 and 5 of Table IV-3. These units show higher peak power performance than transistors, and when operated in multiple chip configurations, both peak and average power can be increased considerably. A crude estimate of multiple chip capability can be obtained by multiplying the single device peak power capability (Table IV-3) by the number of chips. The major drawback of Trapatt oscillators is their low duty cycle, although progress is being made in increasing both the duty cycle and maximum frequency of operation of these devices. Trapatt oscillators exhibit very high efficiencies with actually measured values of up to 50% at S-band. Wideband Trapatt amplifiers have been developed with pulsed power as a saturated amplifier having a small dynamic range and an efficiency

of about 20%. Projected 1980-85 capability for Trapatt oscillators is shown in column 6 of Table IV-3.

Pulsed Gunn Oscillators - Pulsed Gunn diodes have been used at S-band with maximum peak power outputs in the 30 watt region and dc-r.f. efficiencies of 1.5%-2%. These devices are thermally limited, that is, the ratio of peak to average power is very large. It is expected that by 1980-85, further development work should improve the efficiency of these devices to possibly 10 to 15%, which by comparison with other solid state oscillators would still be very low. Recently ITT-Gilfillan has utilized bulk-diode oscillators in a solid state radar operating in the 3.1-3.7 GHz region. Each transmit-receive module contains a 10 w peak power source, modulator, duplexer, T-R switch, phase shifter, logic circuits, and provisions for polarization diversity. Improvements contemplated by ITT include the development of bulk-effect sources that will emit 1 kw at 1 percent duty cycle. For the synthetic array application pulsed Gunn diodes would not appear to be competitive with other solid state sources due to their inherently low efficiencies.

LSA Oscillators - The LSA diode is capable of producing peak powers materially higher than the pulsed Gunn or Trapatt diodes. The average and peak power output of an LSA transmitter increases with decreasing temperature. This is due both to the increase in applied voltage at lower temperatures and to the increase in efficiency at lower temperatures. Among solid state power sources it provides not only the highest peak power but also very rugged, high reliability performance. Its major drawbacks are the very low duty cycles associated with these devices. This is illustrated in columns 11 and 12 of Table IV-3 which shows the performance of two LSA transmitters at S-band. Thus, despite the high peak power levels, average power levels are generally less than 1 w at S-band, and overall efficiencies rarely exceed

8-10%. These efficiency figures include losses in the diode, modulator, power supply, and frequency stabilization circuitry. It is expected that by 1980-85 efficiencies of 15% may be achievable and peak powers of 700 w-1 kw should be readily available in the 2-4 GHz region. Nevertheless, for the synthetic array application the low average powers and comparatively low efficiencies would appear to place this device at a distinct disadvantage.

The peak power performance of microwave semiconductor devices is summarized in Figure IV-27 which shows the peak power output available from transistor, Trapatt, pulsed Gunn, and ISA transmitters as a function of frequency. Transistor frequency multiplier performance is also shown in this chart, although additional data on frequency multiplier chains is given in the next section.

Solid State Modules and Frequency Multiplier Chains - Step recovery diodes have been widely used for efficient high order frequency multiplication in solid state microwave circuits. These devices facilitate the use of low-frequency driver amplifiers in solid state modules and thus provide a stable source of energy at the carrier frequency. Table IV-4 lists the characteristics of various multiplier chains capable of providing r.f. power outputs of 5 mw to 2 watts at S-band. For the synthetic array application the total average power required is 166 watts which would be subdivided among the eight principal subarrays. Since each subarray contains 6 to 8 vertical arrays, it is feasible to consider a separate solid state module feeding each vertical array. This would require an average power output per module of about 3 watts. The multiplier chain shown in the fourth column of Table IV-4 uses a step recovery diode to deliver an output of 2 watts at 2.7 GHz from an input of 5 watts at 450 MHz. The driver amplifier uses a 2N5016 transistor in the output stage and the r.f. output of the multiplier chain can be controlled by varying the dc input
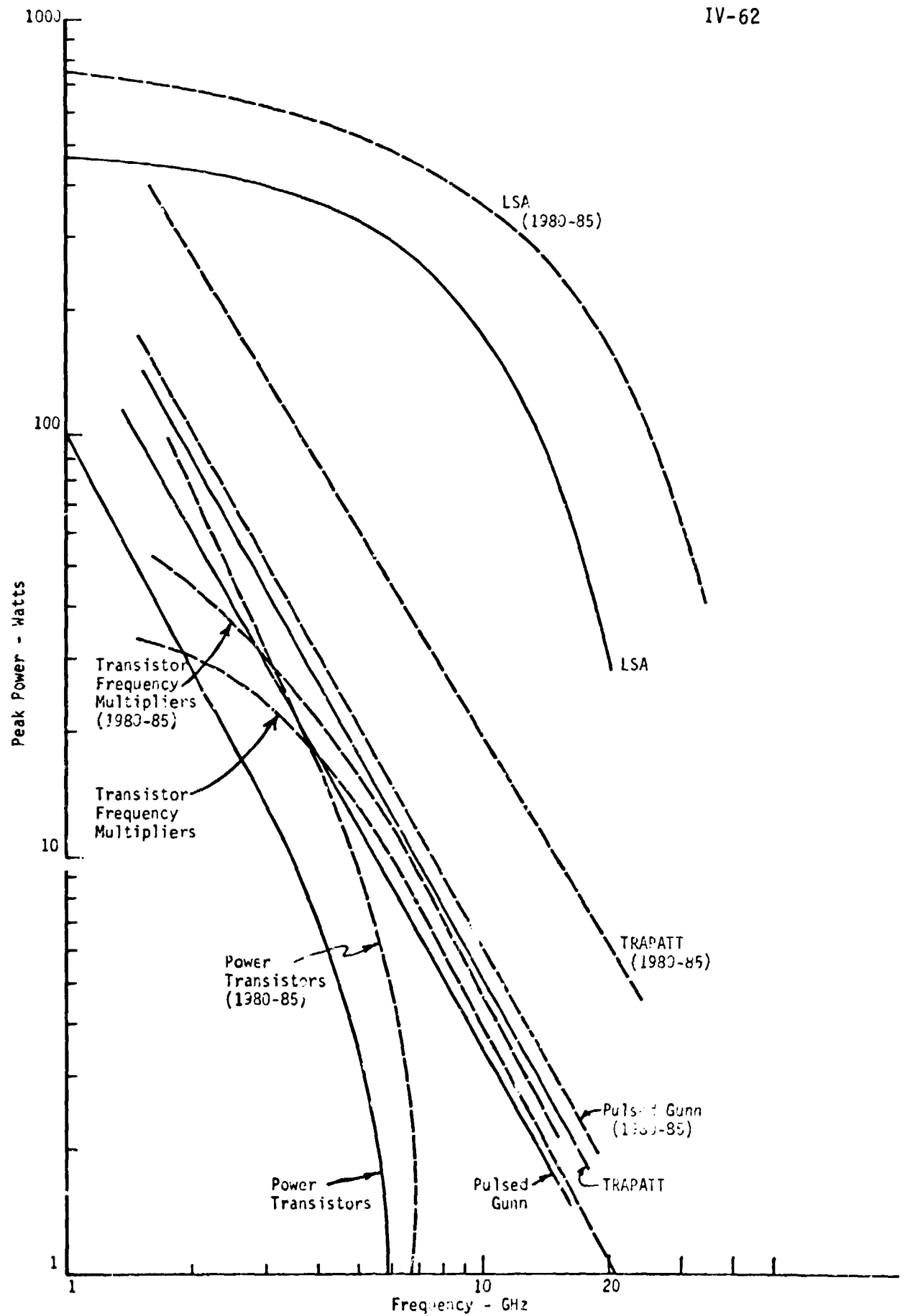
Figure IV-27 Peak Power Performance

Table IV-4 RF Solid State Multiplier Chains and Modules

Solid State Source / Device	Transistor Oscillator-Varactor Multiplier — Step Recovery Diode/Varactor						Solid State Modules — MERA Module (TI)	CW Module (RCA)	Phase Control Module (Teledyne-Ryan)
Waveband	S (3.4-4.2 GHz)	S (2.3-3.6 GHz)	S (2.5-3 GHz)	S (2.7 GHz)	S* (2.23 GHz)	1980-85 Mult.	X (9 GHz)	S (3 GHz)	C (5.74 GHz)
Power Output -MW	250	250	1000	2000	4	3000	0.7 w (pulse)	12 w	0.30 w (pulse)
Input Frequency GHz	0.30 GHz	0.50 GHz	1.5 GHz	0.45 GHz (5 w)	0.223 GHz (20 mw)	0.45 GHz (8 w)	2.25 GHz (2.25 w)	1.5 GHz (.1 w)	0.711 GHz
Multi-plication	x4 x3	x2 x3	x6	x6	x10	x6	x4	x2	x8
Input Volts -V	27	60	28	24	N/A	30	Other Data:	Other Data:	Other Data:
Input Current -MA	600	300	300	700	N/A	900			
Spurious Output -DB	-30	-40	-30	-50	-30	-50			
Cost (Large Quan)	N/A	1K	N/A	N/A	N/A	1K			

MERA Module (TI) — Other Data:
1) Receiver Gain -14.2 DB
2) Noise Figure -11.9 DB
3) 500 MHz IF Frequency

CW Module (RCA) — Other Data:
1) 1.5 GHz Preamp RF Bandwidth -12%
2)
3) Doubler Efficiency - 53%

Phase Control Module (Teledyne-Ryan) — Other Data:
1) Change in Bias Current from 0.4 to 0.8 MA. Causes 360° Change in Phase.
2) 360° Phase Change Causes ± 0.5 DB Amplitude Variations.

*With phase control.

IV-63

to the driver output stage. Typical performance data for this
multiplier are shown in the table below:

2N5016 D.C. Input	2N5016 Power Output (watts)	Multiplier Output (watts)	Multiplier Efficiency (%)
12V-0.45A	1.8	0.65	37
18V-0.60A	3.4	1.4	41
24V-0.70A	5.0	2.0	40
3CV-0.90A*	8.0*	3.0*	38*
*Projected 1980-1985 capability.			

Thus, it would appear that an average power of 3 watts per
module is not an unreasonable expectation for the 1980-85 era.
The multiplier chain shown in the fifth column of Table IV-4
uses a step recovery diode as both a multiplier and a phase shift-
er by controlling the bias applied to the diode. A linear phase
shift as a function of bias current may be obtained by proper
design of the bias network so that the multiplier chain can be
used to control the phase of a radiating element of a solid state
array. Thus, once the aperture illumination of the antenna has
been specified to produce the desired vertical pattern, it is
feasible to design a solid state array consisting of one trans-
ceiver module per element where control of the phase and ampli-
tude of each element is easily accomplished by the bias control
network and the d.c. input to the output stage of the driver am-
plifier. Be steering of the array could also be accomplished by
shifting the phase of the signal received or transmitted by the
antenna element. In the receive mode of the radar the phase
shifting multiplier chain can be used as a local oscillator in
each receiving module. Here a change in the phase of the local
oscillator signal will produce a corresponding phase shift in the

intermediate frequency which is equivalent to shifting the phase of the received signal.

The frequency multiplier chains listed in Table IV-4 utilize a single varactor for performing the multiplication process. If higher power levels are required, substantial improvements in the power handling capabilities of varactor multipliers can be achieved by the following techniques:

1) Use of circuits when the r.f. power is divided between two or more varactors.

2) Use of multiple junction varactor diodes.

3) Use of series stacked varactor diodes.

The current state-of-the-art in multiple varactor multiplier chains is about 8 watts output at 2.7 GHz at a conversion efficiency of 55%. This multiplier utilized 4 varactors to achieve a 3 times multiplication from 900 MHz. Still higher output powers can be achieved by using transistor drivers containing several transistors in parallel followed by parallel chains of varactor multipliers. With this arrangement 20 watts output has been achieved at 2.7 GHz which now opens up the feasibility of using a transistor driven multiplier chain for driving a complete subarray of the synthetic array radar.

Three types of solid state modules are listed in Table IV-4. The performance of the phase control module is shown in the last column for a C-band solid state radar. For an S-band radar the ten times multiplier shown in the fifth column of Table IV-4 could be employed with pulse output powers of 1 watt per module. Higher output levels can be obtained by increasing the output of the low-frequency driver amplifier, and it would appear that a solid state radar using this approach can be mechanized for the synthetic array application. The MERA solid state modules have been successfully employed in various radar configurations. This module includes a transmitter, receiver, and two phase shifters,

including logic. The transmitter input is at S-band and the
output is 0.7 w pulsed signal at X-band. The S-band pulsed power
amplifier consists of five transistor stages providing a minimum
gain of 23 db at 2.25 GHz and is operated in saturation for best
efficiency and phase performance. An S-band, 2 stage preampli-
fier providing 11 db gain is also included, so that the r.f.
module can be driven with a 2 mw signal at 2.25 GHz which is
easily obtained with simple low-output multiplier chains. This
type of module without the S-X multiplier, could be adapted to
the synthetic array application by employing one module for each
vertical array, which would require pulse power outputs of about
20 watts. Thus, a ten-fold increase in the pulse power output
would be required which can be readily achieved by state-of-the-
art redesigns of the transmitter portion of the module. Current
power transistor development work in the 1.7-2.3 GHz and 2.6-3.2
GHz ranges indicates that pulse power levels of 1^5 to 30 watts
are easily achievable and modules utilizing this technology should
be available by the end of 1973. The other module listed in Table
IV-4 is a CW solid state module which has a 12 w output at 3 GHz
and utilizes a 1.5 GHz driver. Its main features are the high
conversion efficiency achieved by the frequency doubler ($\eta = 53\%$)
and the small amount of input power required to drive the 1.5 GHz
preamplifier. These techniques are equally applicable to pulse
modules and indicate that by paralleling high power transistors
it should be possible to achieve the required pulse power outputs
to drive the subarrays.

In comparing vacuum tube transmitters with solid state devices,
the reliability of the transmitter in extended space operations
must be seriously considered. Normally, to preclude catastrophic
failure of the radar system, transmitter redundancy would be re-
quired if vacuum tubes are employed. With solid state transmitters
inherent redundancy can be achieved by distributing the transmitter

power among many transmitter-receiver modules, which guarantees
that failure of a few modules will not greatly impair the per-
formance of the radar system. Further inherent redundancy can be
achieved by paralleling transistors in the transmitter modules,
which would again guarantee against catastrophic failure of a
module. Despite these advantages it is not easy to make a relia-
bility comparison between vacuum tubes and solid state devices
unless the two devices can be interchanged on a one-for-one basis
without performance differences. If one considers all factors
such as size, weight, cost, and reliability in such an analysis,
then the table below is a rough indication of the relative merits
of the different transmitters in a phased array radar system.

Application	Tube		Solid State	
	Grid	Beam	Transistor	Diode
CW (0.5-2 GHz)	Avg.	Avg.	Good	Poor
High Duty Pulse (0.5-2 GHz)	Good	Good	Good	Poor
Low Duty Pulse (0.5-2 GHz)	Exc.	Good	Poor	Poor
CW (2-8 GHz)	Avg.	od	Good	Avg.
High Duty Pulse (2-8 GHz)	Avg.	Exc.	Avg.	Avg.
Low Duty Pulse (2-8 GHz)	Exc.	Good	Poor	Good

It is to be emphasized that the ratings in this table do not take
into account the inherent reliability advantages of solid state
devices enumerated above, and, therefore, should only be used in
comparing the various devices on a one-for-one basis.

Radar Receiver Front Ends - A considerable amount of progress
has been made in the development of low-noise front ends for radar
receivers. Broadband solid state amplifiers have been steadily
improving in noise figure, output power and gain, largely through
improved bipolar devices and microwave field effect transistors

as well as the employment of cooled and uncolled parametric am-
plifiers. A summary of the performance of various front ends is
given in Table IV-5. It is of interest that for the synthetic
array application a simple front end would be desirable in order
to maintain receiver module simplicity and reliability. Thus,
either MESFET or bipolar transistor amplifiers would appear to be
a natural choice for a low-noise front end at S-band.

Table IV-5 Low-Noise Receiver Front Ends - Current State-of-the-Art

Type of Front End	2 GHz		4 GHz	
	Noise Figure	Noise Temp.	Noise Figure	Noise Temp.
Image SSB Mixer (F_{IF} = 1.5 DB)	5.54 DB	$750^{O}K$	5.76 DB	$800^{O}K$
TWT Amplifier	4.88 DB	$600^{O}K$	5.54 DB	$750^{O}K$
Std. Ge TDA	4.62 DB	$550^{O}K$	5.10 DB	$650^{O}K$
Best GaSb TDA	3.76 DB	$400^{O}K$	4.24 DB	$480^{O}K$
Best Mixer (F_{IF} = 1.5 DB)	3.10 DB	$300^{O}K$	3.46 DB	$350^{O}K$
Std. Trans. Amp.	3.56 DB	$370^{O}K$	5.24 DB	$680^{O}K$
Best FET Amp.	1.92 DB	$160^{O}K$	2.19 DB	$190^{O}K$
Best Trans. Amp.	2.10 DB	$180^{O}K$	2.78 DB	$260^{O}K$
Non-Degenerate Paramp.	0.92 DB	$68^{O}K$	1.40 DB	$110^{O}K$
Degenerate Paramp.	0.70 DB	$50^{O}K$	1.00 DB	$75^{O}K$
Non-Degenerate Paramp. (Cooled)	0.23 DB	$15^{O}K$	0.27 DB	$18^{O}K$
Degenerate Paramp. (Cooled)	0.18 DB	$12^{O}K$	0.21 DB	$14^{O}K$
Traveling Wave Maser	0.06 DB	$4^{O}K$	0.09 DB	$6^{O}K$

Power Requirements

Most of the literature on synthetic aperture radar (SAR) theo-
ry deals with imaging isolated point target fields. This theory
shows that for ideal point targets, the resulting doppler histories
can be compressed (i.e., match filtered) with a data processor.
The signal-to-noise ratio at the processor output is increased
over its input value by approximately the along-track time-bandwidth
product, that is, the time to generate the synthetic aperture times
the doppler bandwidth generated. The above type of performance
assumes perfect pulse to pulse coherence (negligible phase errors
while generating a synthetic aperture). If pulse modulation is
used the output signal-to-noise is also increased by the range
time-bandwidth product if matched processing techniques are util-
ized. If all the SAR data is not coherently processed then the
resulting output signal-to-noise ratio is reduced by the ratio of
the two-dimensional bandwidth associated with the data to the
bandwidth incorporated in the processor.

When clutter maps of extended surface are of interest, the
point target theory of SAR systems does not directly apply.
Clutter is measured as an r.m.s. value; and except for magnifi-
cation, it is the same in all planes of the processor (i.e., at
the input, Fourier transform, and output planes). To eliminate
much of the confusion associated with designing SAR systems for
ground mapping use, let us now consider transmitted power require-
ments.

According to the radar range equation the received peak power
is given by

$$P_r = \frac{P_t \, G \, A}{(4\pi R^2)^2} \, \sigma \qquad (IV-15)$$

where P_t is the peak power transmitted

G is the antenna gain

A is the effective collecting aperture

R is the one-way range to the target

σ is the radar cross-section

Now for an extended rough surface the cross-section is

$$\sigma = \sigma_o \, a \qquad\qquad\qquad\qquad \text{(IV-16)}$$

where σ_o is the cross-section density and $\underline{a}$ is the area which is illuminated. But the illuminated area is

$$a = (C_r \rho_r \csc \theta) \, (\gamma \frac{\lambda}{D_R} R) \qquad\qquad \text{(IV-17)}$$

where ρ_R is the range resolution

C_r is the range compression factor

θ is the antenna pointing angle measured from the orbital plane

λ is the transmitted wavelength

D_R is the effective length of the antenna aperture (along-track dimension)

and γ is the illumination factor of the antenna in the along-track dimension.

The radar range can be expressed in terms of the operational altitude as

$$R = H \sec \theta \qquad\qquad\qquad\qquad \text{(IV-18)}$$

The relationship between antenna gain and effective area is

$$G = \frac{4\pi}{\lambda^2} \, A \qquad\qquad\qquad\qquad \text{(IV-19)}$$

Substituting equations (IV-16)-(IV-19) into (IV-15) yields

$$P_r = \frac{P_t \, A^2 \, \sigma_o \, \gamma \, C_R \, \rho_r \, \cos^3 \theta}{4\pi \, H^3 \, \lambda \, D_r \, \sin \theta} \qquad\qquad \text{(IV-20)}$$

The equivalent noise at the input of the receiver is

$$P_n = kT \, F \, B \qquad\qquad\qquad\qquad \text{(IV-21)}$$

where $k = 1.38 \times 10^{-23}$ joules is Boltzmann's constant.

T is the absolute temperature

F is the receiver noise figure and atmospheric losses

and B is the transmitted range bandwidth

Before taking doppler processing into account the signal-to-noise ratio, according to equations (IV-20) and (IV-21) is

$$\frac{S}{N} = \frac{P_r}{P_n} = \frac{P_t A^2 \sigma_o \gamma C_r \rho_r \cos^3 \theta}{4\pi H^3 \lambda D_r kTFB \sin \theta} \qquad \text{(IV-22)}$$

The average transmitted power is given by

$$P_{ave} = P_t \tau \, (PRF) \qquad \text{(IV-23)}$$

where τ is the transmitted pulse length.

Now to a good approximation we have

$$C_r \rho_r = \frac{c\tau}{2} \qquad \text{(IV-24)}$$

where c is the speed of light in free space.

Substituting equation (IV-24) into (IV-22) and then simplifying the result by using (IV-23) yields

$$\frac{S}{N} = \frac{P_{ave} A^2 \sigma_o \gamma c \cos^3 \theta}{8\pi H^3 \lambda D_r kTFB \, (PRF) \sin \theta} \qquad \text{(IV-25)}$$

For a SAR system operating unambiguously, a data processor can increase the above signal-to-noise ratio by the ratio of the PRF to the recorded doppler bandwidth, that is

$$\left(\frac{S}{N}\right) \text{out} = \frac{S}{N} \frac{(PRF)}{f_d} \qquad \text{(IV-26)}$$

This is true since filtering down to the doppler bandwidth discriminates against the system noise but not clutter energy. However, additional filtering reduces the clutter (signal) and receiver noise equally. The doppler bandwidth is approximately

$$f_d = \gamma \frac{2V}{D_r} \qquad \text{(IV-27)}$$

IV-72

where V is the speed of the radar with respect to the target field.

Combining equations (IV-25)-(IV-27), we obtain the desired result

$$\left(\frac{S}{N}\right)\text{out} = \frac{P_{ave} A^2 \sigma_o c \cos^3 \theta}{16\pi H^3 \gamma V kTFB \sin \theta} \qquad \text{(IV-28)}$$

Solving the above expression for average transmitted power yields

$$P_{ave} = \frac{16\pi H^3 \lambda V kTFB \sin \theta}{A^2 \sigma_o c \cos^3 \theta} \left(\frac{S}{N}\right) \text{out} \qquad \text{(IV-29)}$$

The above equation for average transmitted power required to map surface clutter is expressed in such a form that is essentially invariant to the processor implementation. It does not depend upon the processed range and along-track bandwidth, the presence of phase errors, or the utilization of mixed integration. The above expression will now be evaluated for illustrative purposes.

The parameters for a dual beamwidth system at e = 0.5 are:

λ = 0.1 m (S-band)

σ_o = 0.06

F = 14.8 (11.7 db)

H = 1481 km

V = 8.692 x 10^3 m/sec

θ = 30°

B = 3 x 10^6 Hz (i.e., ground range resolution = 100 m)

kT = 1.38 x 10^{-20} joules (T = 10^{3}°K)

A = 12.80 m^2 = 3.50 m x 3.66 m

$\left(\frac{S}{N}\right)$out = 10

Substituting the above values into equation (IV-29) yields

P_{ave} = 166 watts

Ambiguity Spectrum of Synthetic Aperture Radar

It can be shown that the azimuthal complex signal modulation received by a Synthetic Aperture Radar (SAR) from a point scatterer is determined in amplitude by the geometry of the system and by the far-field two-way pattern in range. For a system operating with a periodic pulse modulation which functions near the ambiguous limit, aliases will occur which overlap into the passband of the matched filter. These aliases can be separated into those occurring in azimuth and those occurring in range; the result is a two-dimensional unambiguous response degraded by an effective clutter level due to the overlapping aliases.

Figure IV-28 shows the two-way antenna illumination pattern in the range direction. The range swath width occupies the central portion of the two-way antenna range pattern and the range ambiguities fold in about the unambiguous range swath $(\frac{C}{2PRF})$, which is determined by the PRF.

The radiation pattern in one plane of a rectangular aperture can be written in the form $G = F(\pi X)$.

$$\text{where} \quad X_r = \frac{D_r \sin\xi}{\lambda} \tag{IV-30}$$

D_r = range aperture dimension

ξ = angle from the antenna boresight

λ = wavelength

The radiation pattern in the azimuth direction can be written in a more convenient form.

$$X = \frac{f_D}{2V/D_a} = \frac{f_D}{B} \tag{IV-31}$$

where f_D is the doppler frequency

V is the antenna velocity

$B = \frac{2V}{D_a}$ is termed the doppler bandwidth of the system.

In the range direction, X is defined by equation IV-30 and the unambiguous swath $= \frac{C \sec \psi}{2PRF}$ as shown in Figure IV-28, where ψ is the grazing angle. The range swath (W) is approximately equal to $2R\xi \csc\psi$ and the angle to the edge of the unambiguous range swath is given by $\xi_u = \frac{C(\text{Tan}\psi)}{4R(PRF)}$.

From equation IV-30 and the angle to the edge of the unambiguous range swath, the range criterion $(S_r = 2X_r = \frac{2D_r}{\lambda} \sin \frac{C(\text{Tan}\psi)}{4R(PRF)}$ can be defined.

Ambiguity levels for three values of S_r (range criterias) and three values of PRF/B have been computed and are plotted in Figures IV-30 through IV-43. These figures are displayed in a similar fashion to Figure IV-29 except the values on the abscessa are normalized with respect to the bandwidth (B). The ambiguity levels for each value of $\frac{f_D}{B}$ (X) have been summed to give a resultant level relative to the unambiguous response at both the center of the range swath and at the edge. The response has been calculated for uniform and cosine amplitude illumination of the aperture with uniform phase distribution in each case. The values of S_r (range criteria) and PRF/B(X) correspond to the 6 db, 16 db, and 26 db beamwidths of the two-way antenna pattern.

Relative levels of the unambiguous return for a zero doppler frequency are given in Tables IV-6 and IV-7. It has been assumed that the range swath is illuminated by a 6 db beamwidth of the two-way pattern. These tables show that the ambiguity levels for $S_r = 0.885$ and 1.186 (6 db beamwidth) are less than 20 db down at mid range and approximately equal to the unambiguous response at far range. For $S_r = 1.356$ and 1.856 (16 db beamwidth) the ambiguity levels are acceptable for cosine illumination ($>$ 20 db down) but are too high in the case of uniform illumination. Consequently some illumination taper is desirable if the unambiguous doppler bandwidth is between the 16 db levels of the two-way pattern.

Table IV-6 Ambiguity Levels for Zero Doppler Frequency With
Uniform Antenna Illumination

Azimuth Beamwidth PRF/B	Range Beamwidth (db)					
	Mid-Range			Far-Range		
	6	16	26	6	16	26
6	26.6	22.5	24.2	-0.12	21.6	21.0
16	23.2	20.9	21.9	-0.16	17.6	17.4
26	25.4	22.0	23.5	-0.13	20.1	19.7

Table IV-7 Ambiguity Levels for Zero Doppler Frequency With
Cosine Antenna Illumination

Azimuth Beamwidth PRF/B	Range Beamwidth (db)					
	Mid-Range			Far-Range		
	6	16	26	6	16	26
6	24.3	24.9	25.0	7.3	18.9	19.0
16	32.4	42.6	43.2	7.6	34.4	37.2
26	32.8	50.4	58.1	7.6	37.4	52.2
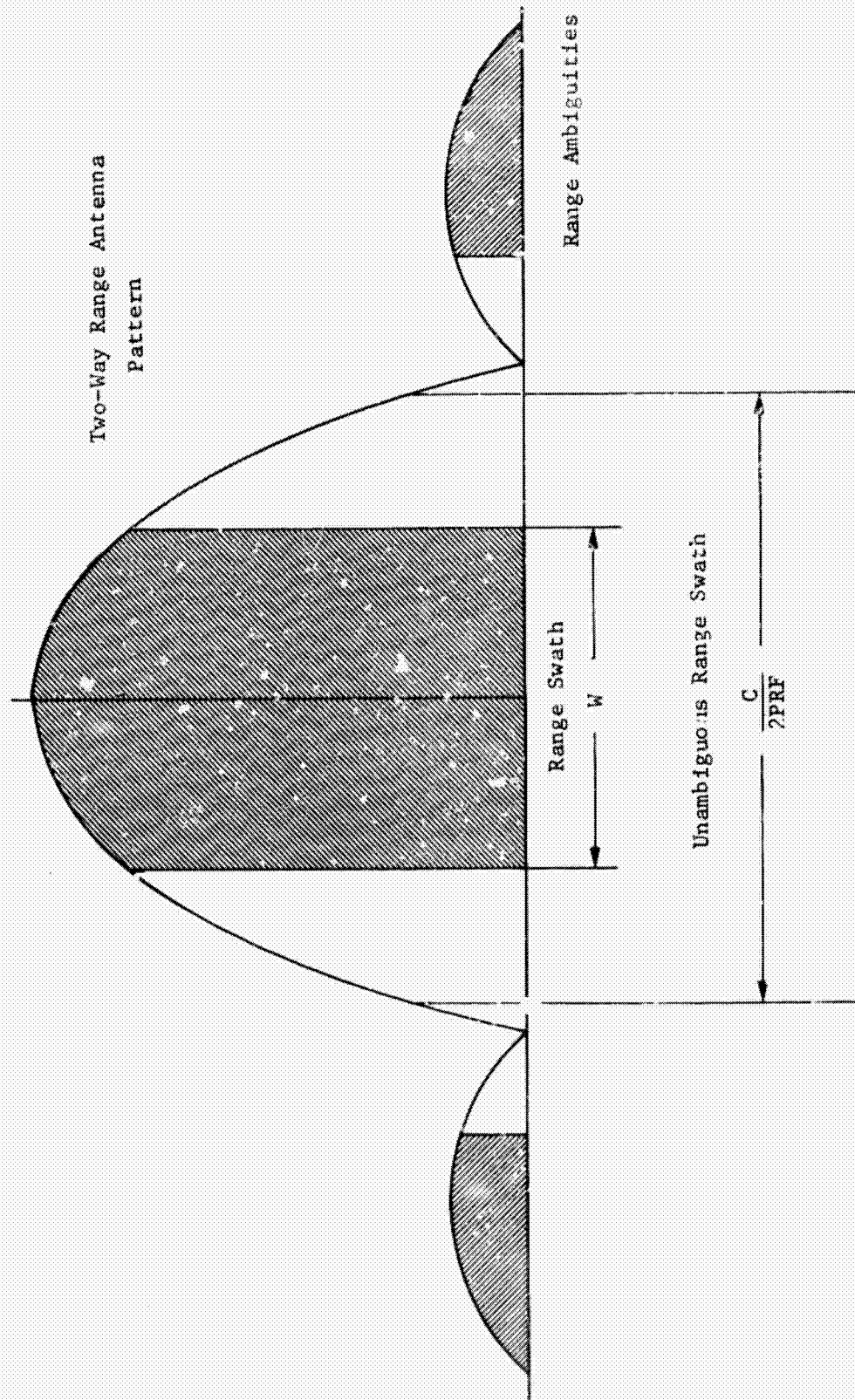
Figure IV-28 Range Channel Ambiguities
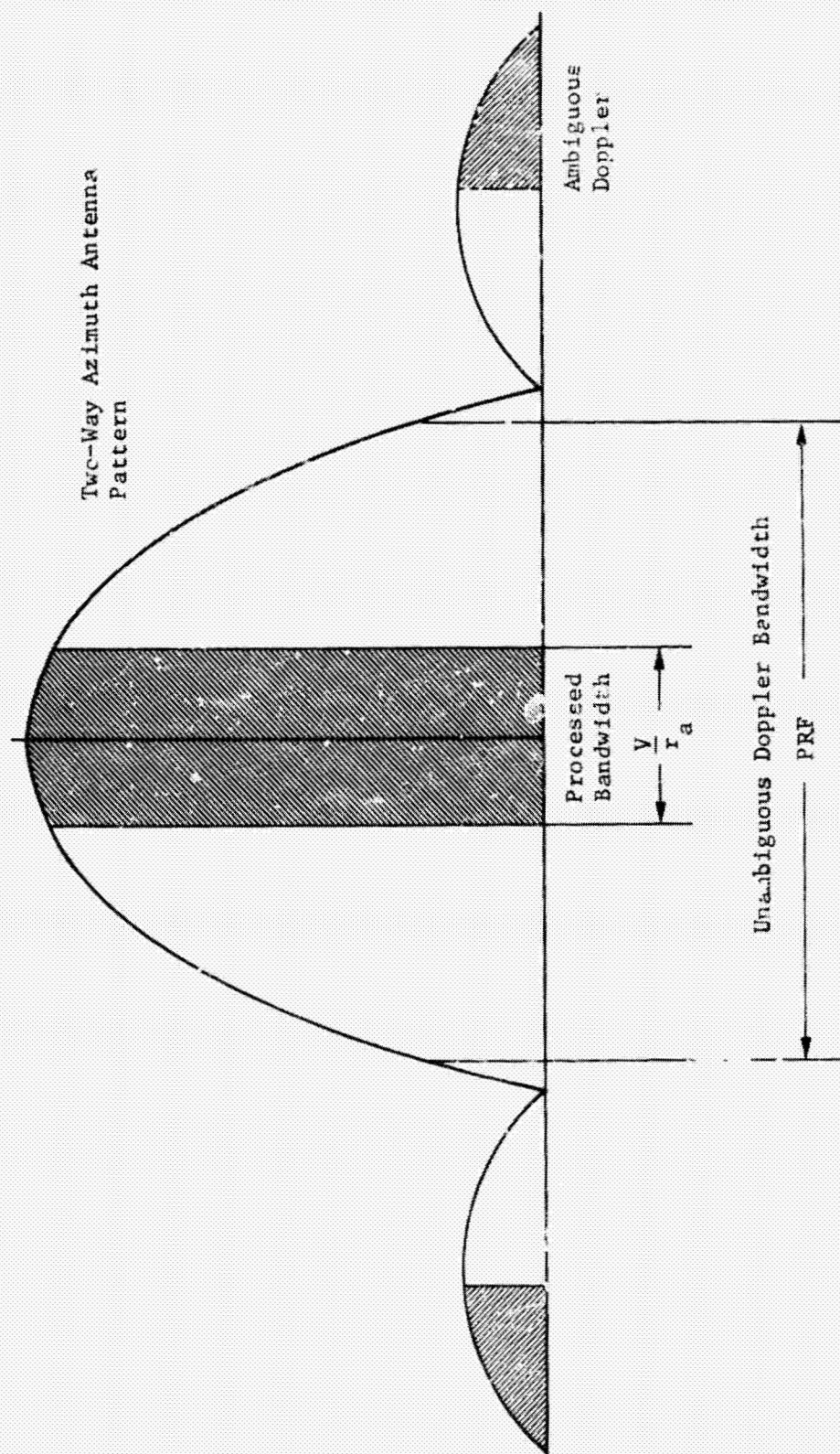
Figure IV-29 Azimuth Channel Ambiguities
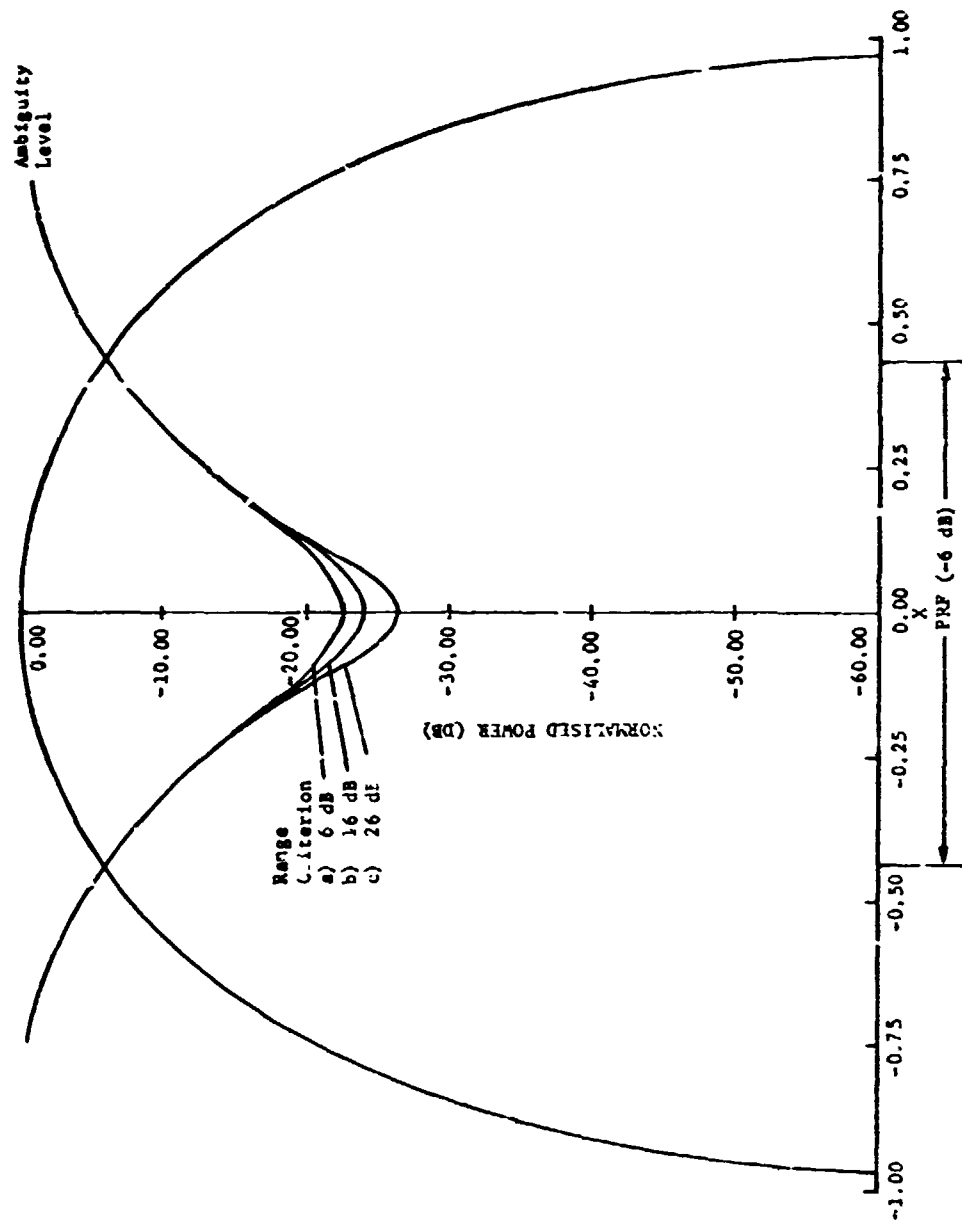
Figure IV-30 Azimuth Channel Ambiguities - Uniform Illuminated Antenna (Mid-Range)
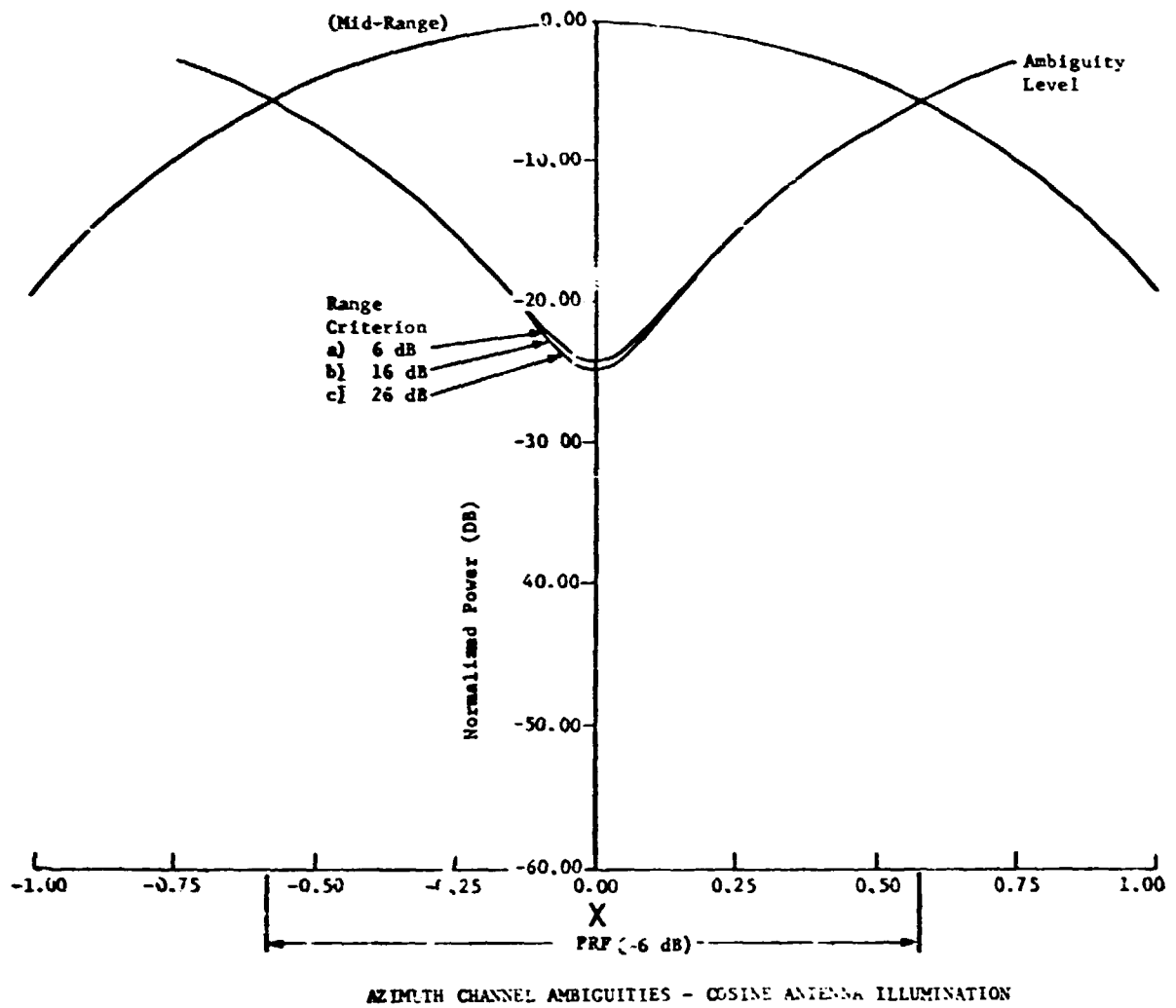
Figure IV-31 Azimuth Channel Ambiguities - Cosine Antenna Illumination (Mid-Range)
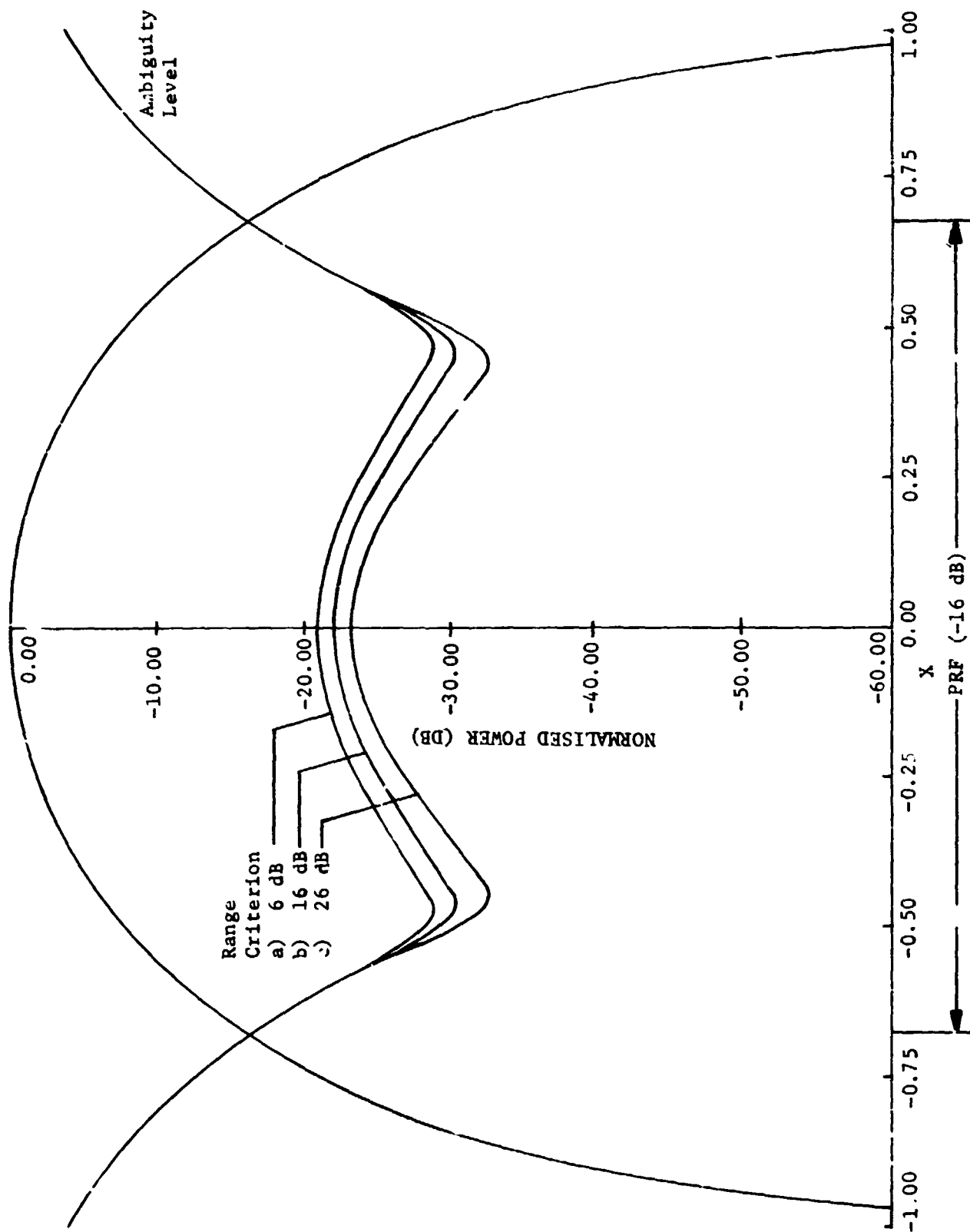
Figure IV-32 Azimuth Channel Ambiguities – Uniformly Illuminated Antenna (Mid-Range)
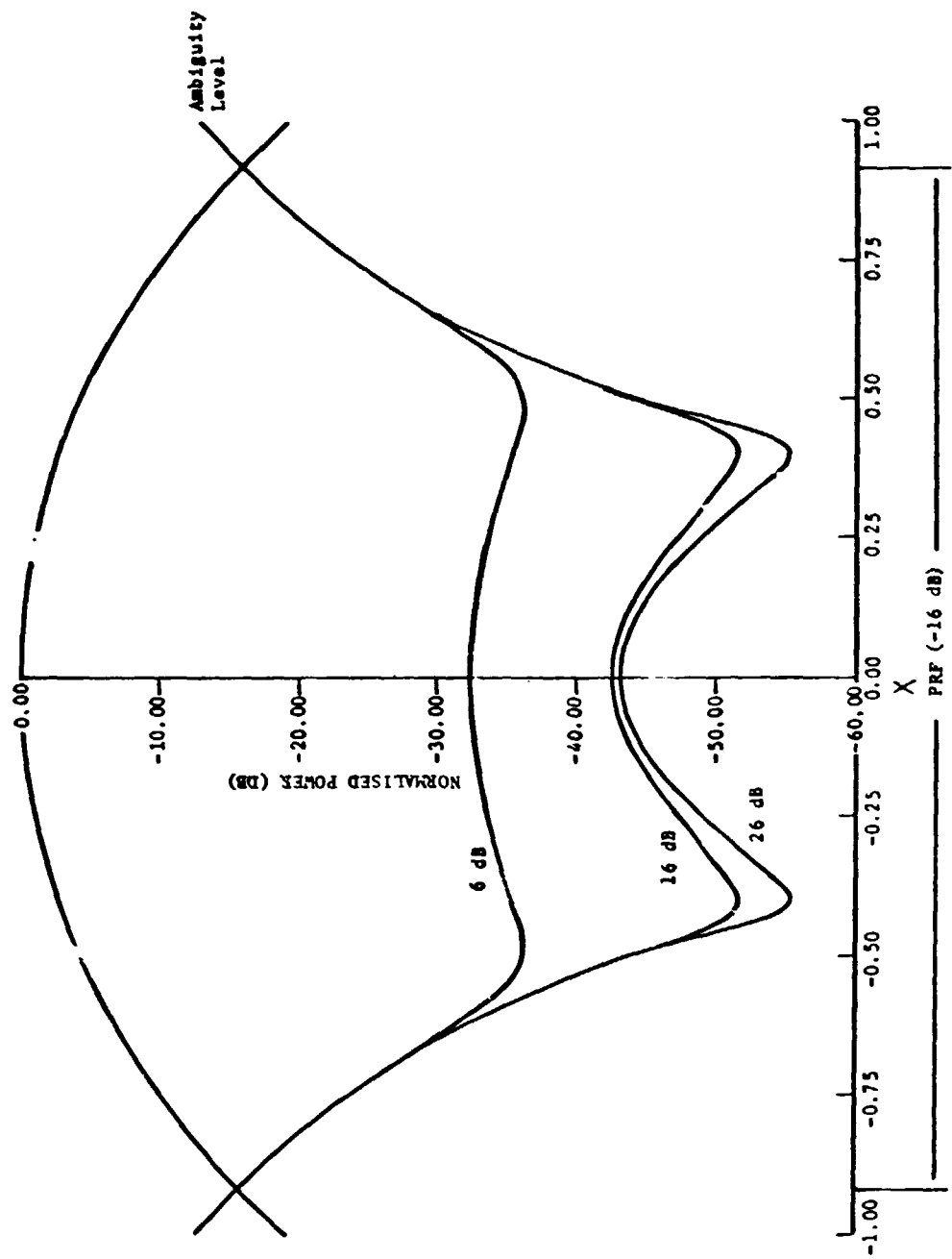
Figure IV-33 Azimuth Channel Ambiguities - Cosine Antenna Illumination (Mid-Range)
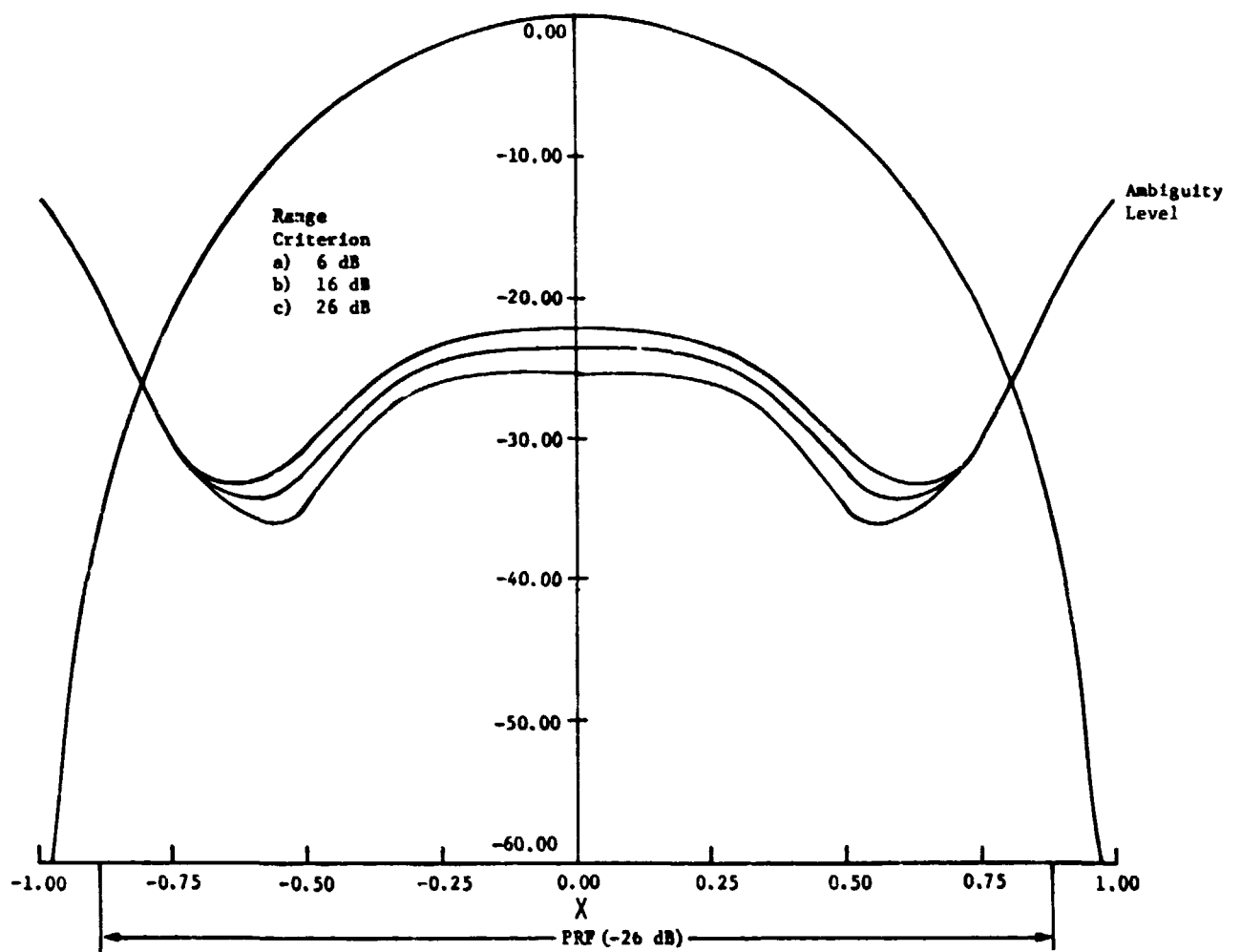
Figure IV-34 Azimuth Channel Ambiguities - Uniformly Illuminated Antenna (Mid-Range)
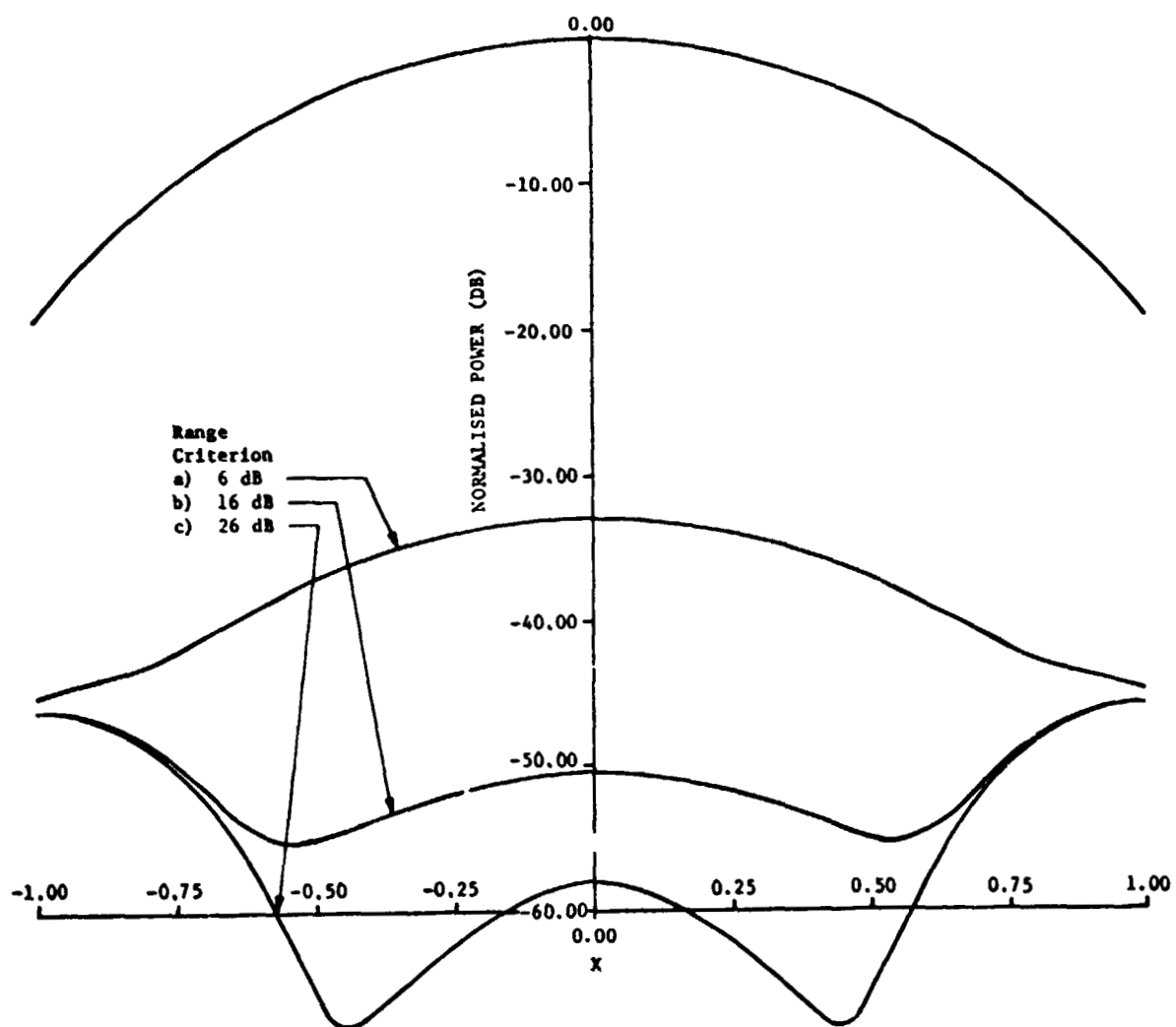
PRF from -1.43 to +1.43   (-26 dB points)

Figure IV-35 Azimuth Channel Ambiguities - Cosine Antenna Illumination (Mid-Range)
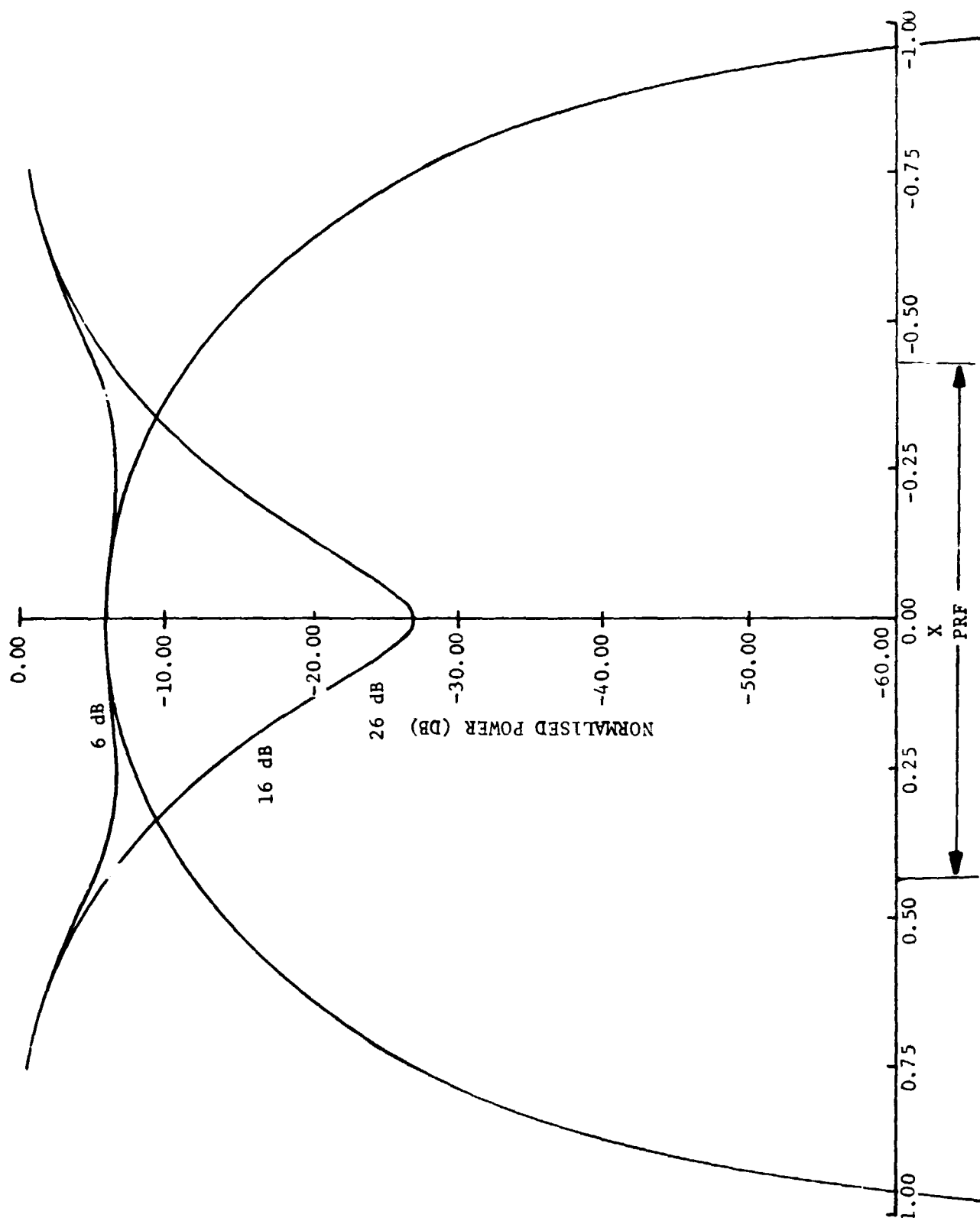
Figure IV-36 Azimuth Channel Ambiguities - Uniform Illumination (Far Range)

IV-85
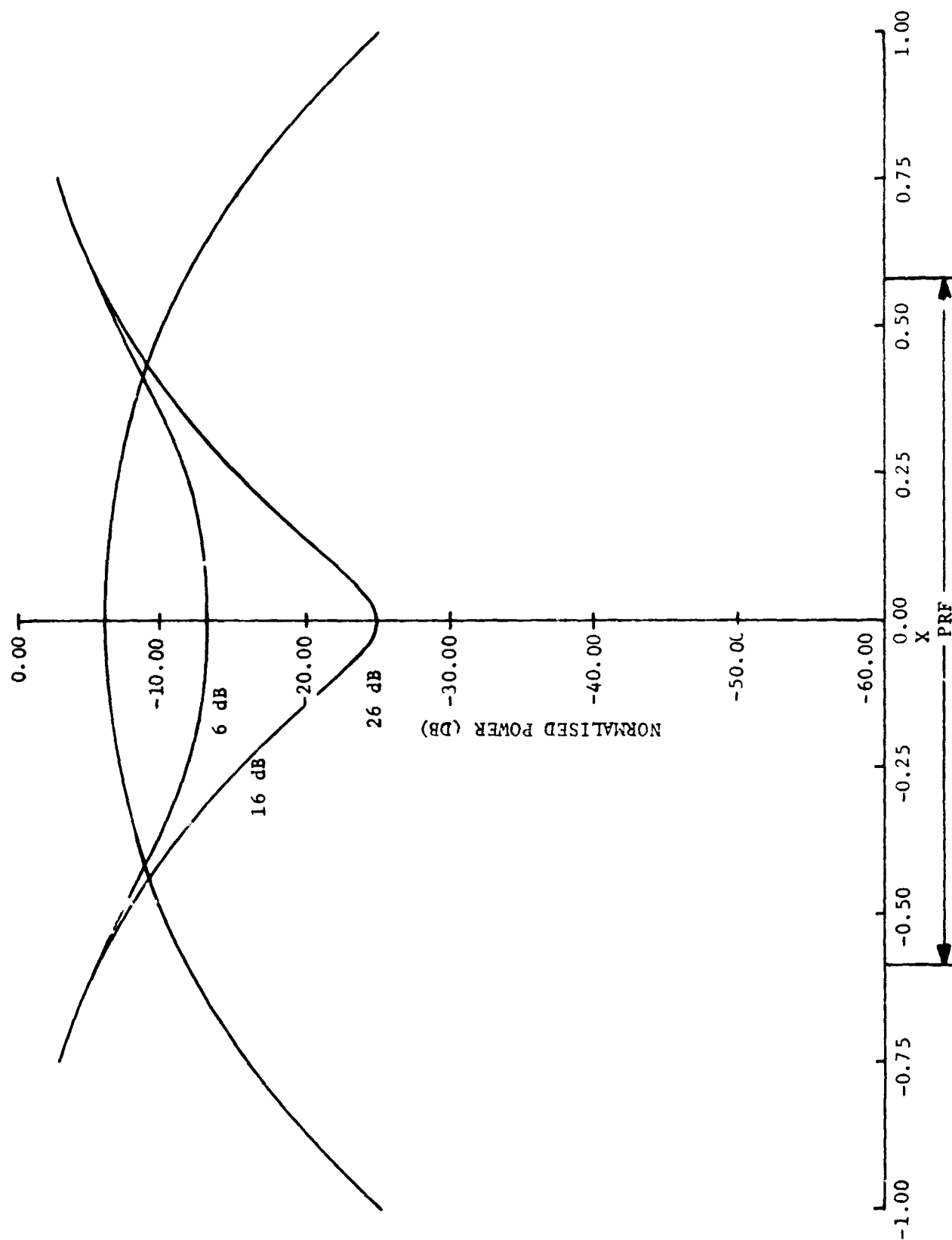
Figure IV-37 Azimuth Channel Ambiguities - Cosine Illumination (Far Range)
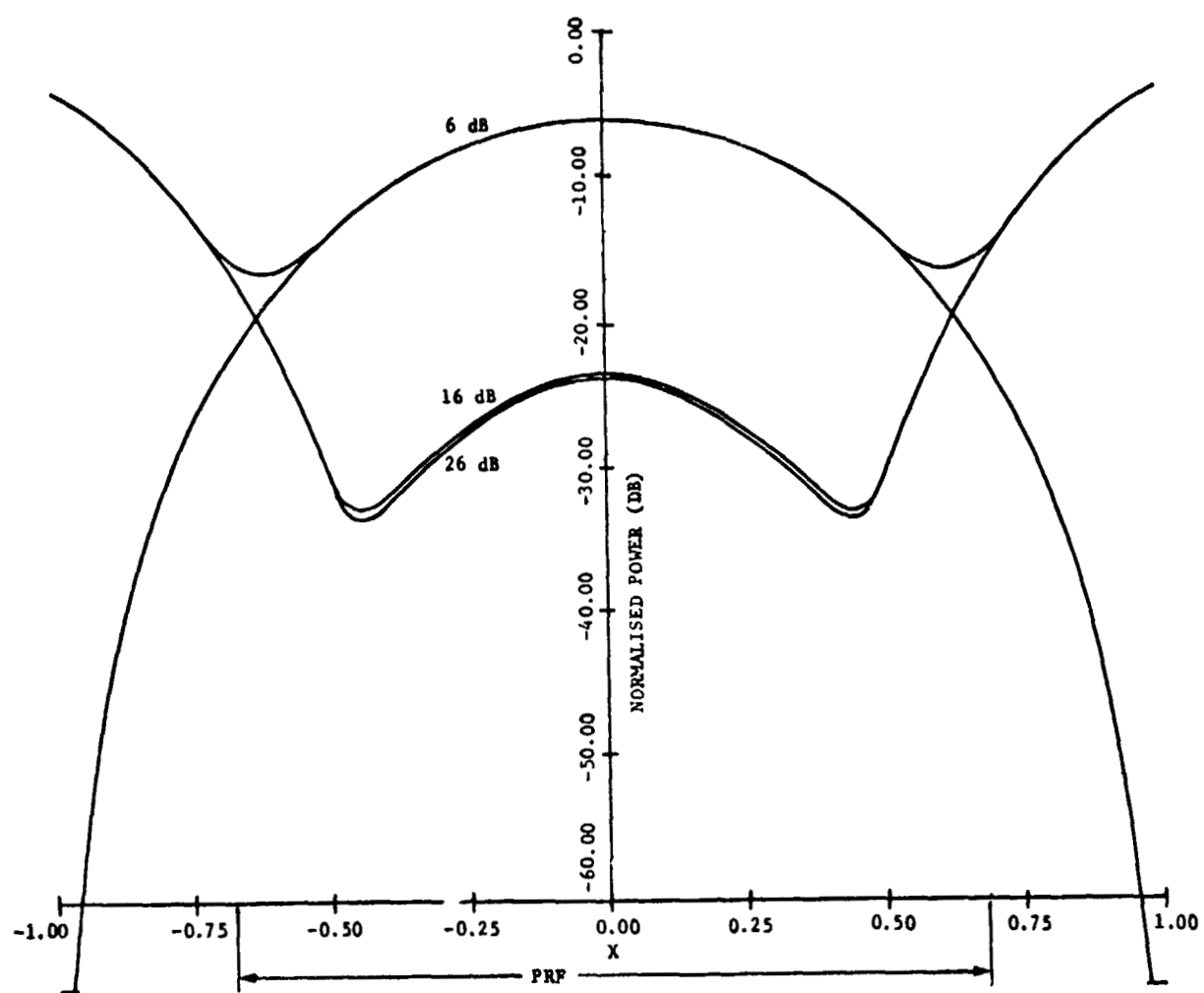
Figure IV-38 Azimuth Channel Ambiguities - Uniform Illumination (Far Range)
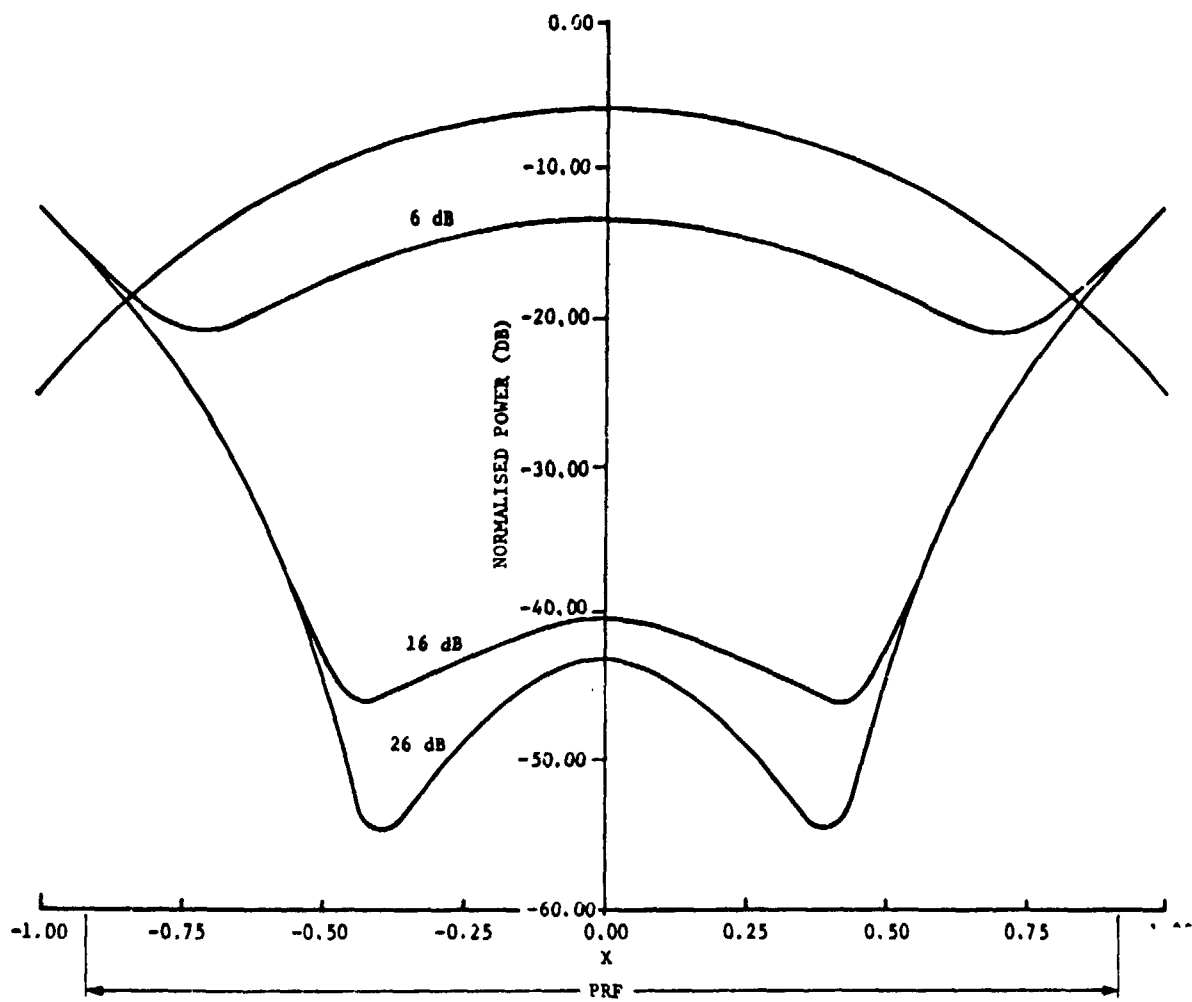
Figure IV-39 Azimuth Channel Ambiguities - Cosine Illumination (Far Range)
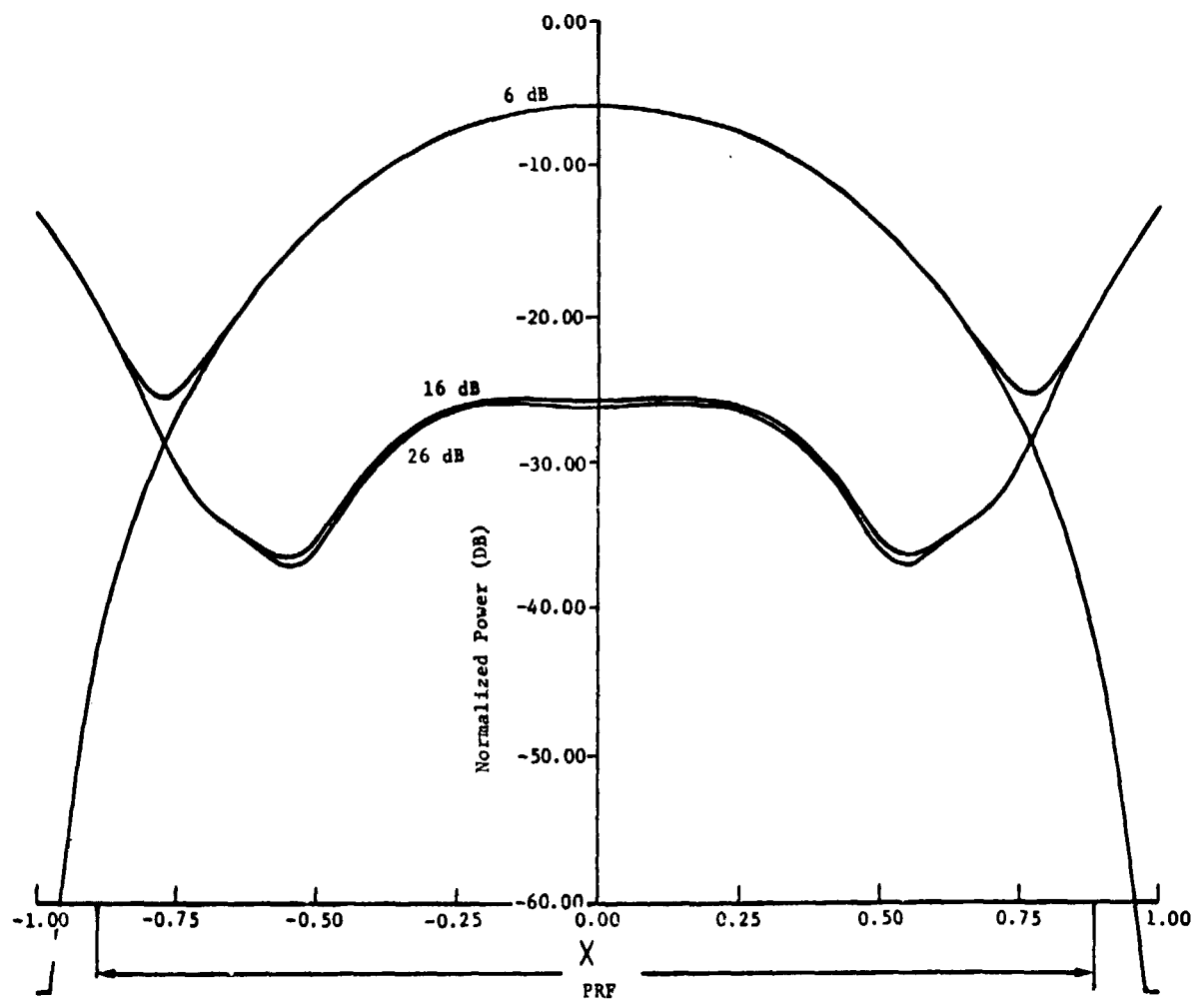
Figure IV-40 Azimuth Channel Ambiguities - Uniform Illumination (Far Range)
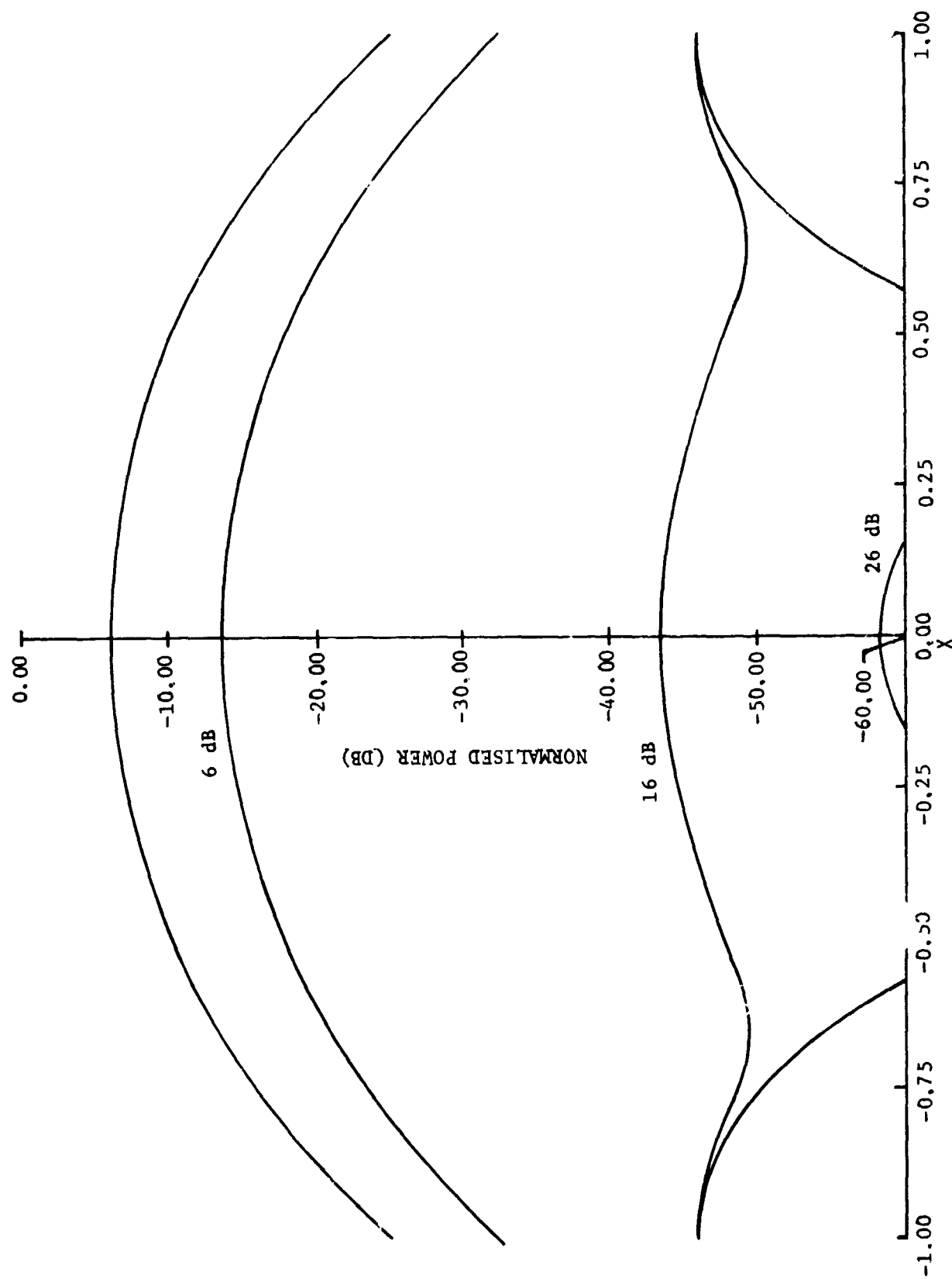
Figure IV-41 Azimuth Channel Ambiguities - Cosine Illumination (Far Range)
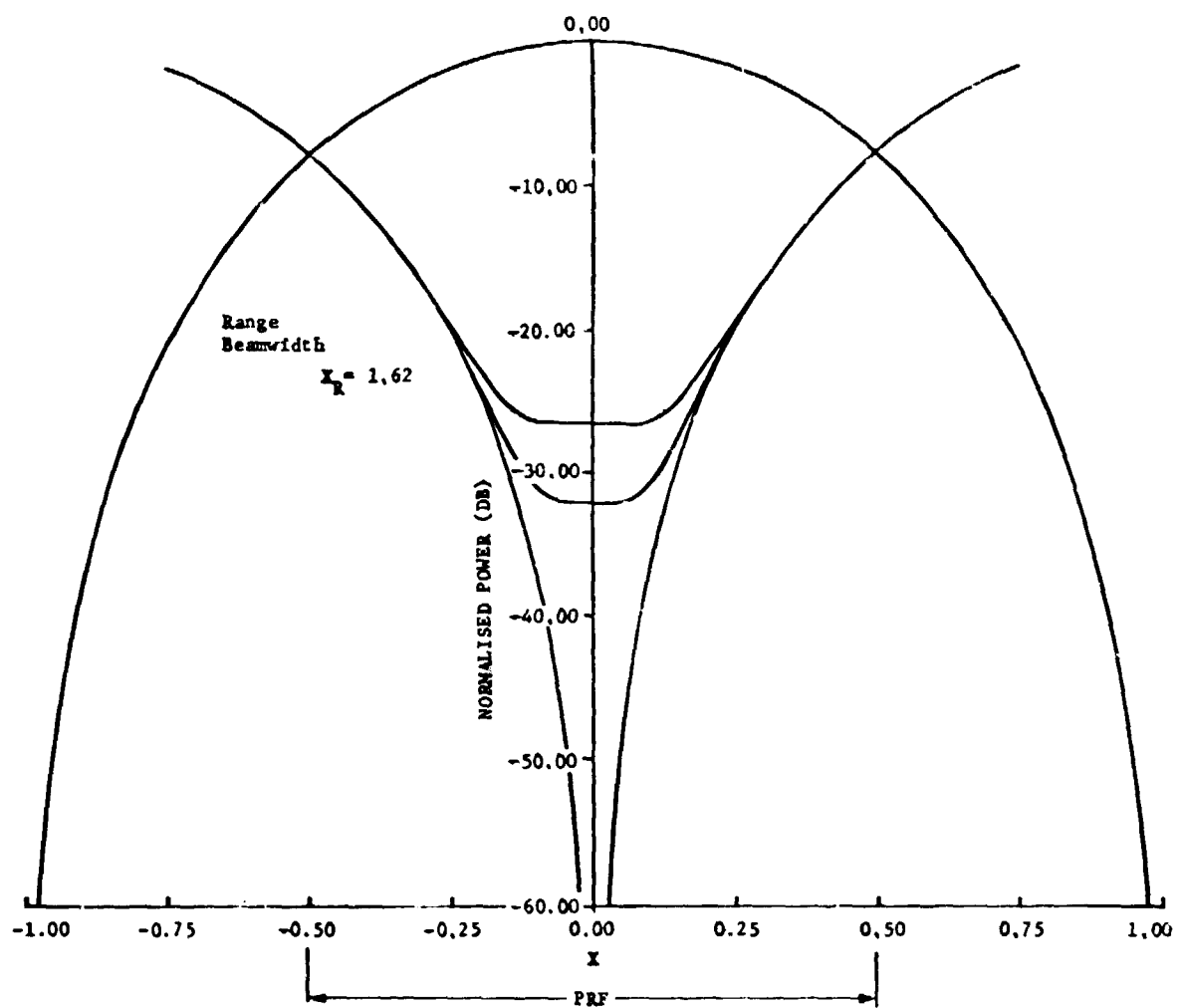
Figure IV-42 Azimuth Channel Ambiguities - Uniform Illumination (Mid-Range)
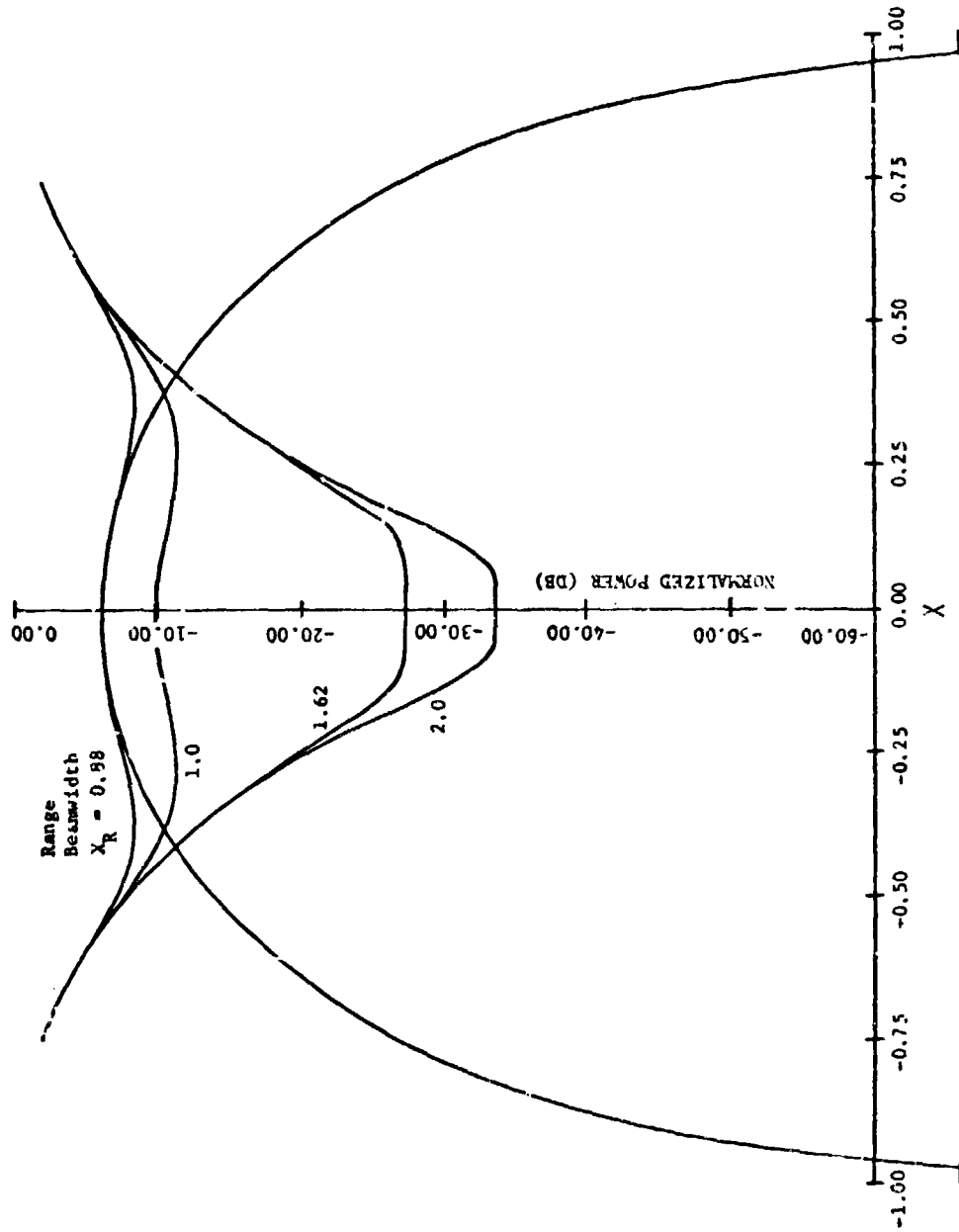
Figure IV-43 Azimuth Channel Ambiguities – Uniform Illumination (Far Range)

Radar System Augmentation

The Venus mapping radar study has concentrated on a single-frequency and single polarization radar which is designed primarily for topography. Radar systems utilizing dual frequency and dual polarization are considered accessory items in this study, which can be added to the baseline system. The estimated cost of the additional equipment is determined as cost above the basic minimum cost baseline systems. The value of these instruments in terms of science return is discussed in the science section of this report. The implementation of these modes is discussed below.

Dual-Polarization Radar - We will assume that the single-mode radar uses a like- or parallel-polarized return. Implementation of a cross-polarized channel requires the addition of a waveguide r. 'e separator or a cross-polarized antenna feed, additional re-...ver, additional presummer, and additional bulk storage capability; i.e., duplication of the receiver and data processing system is shown in Figure IV-44.

An alternate method would be to multiplex the receiver and presummer using alternate PRFs. However, this would double the required transmitter power and limit the PRF to one-half of the single-channel maximum.

Assuming that the receiver and presummer power and weight are small, the primary effect of introducing a cross-polarized channel is the doubling of the required data rate.

Dual-Frequency System - Assume that the normal radar operates at a high frequency (X- or S-band) and that the second frequency is lower (L-band). The high frequency would be used for topographic mapping. The lower frequency would operate at the same resolution and would be used to estimate surface roughness, dielectric constant, etc.
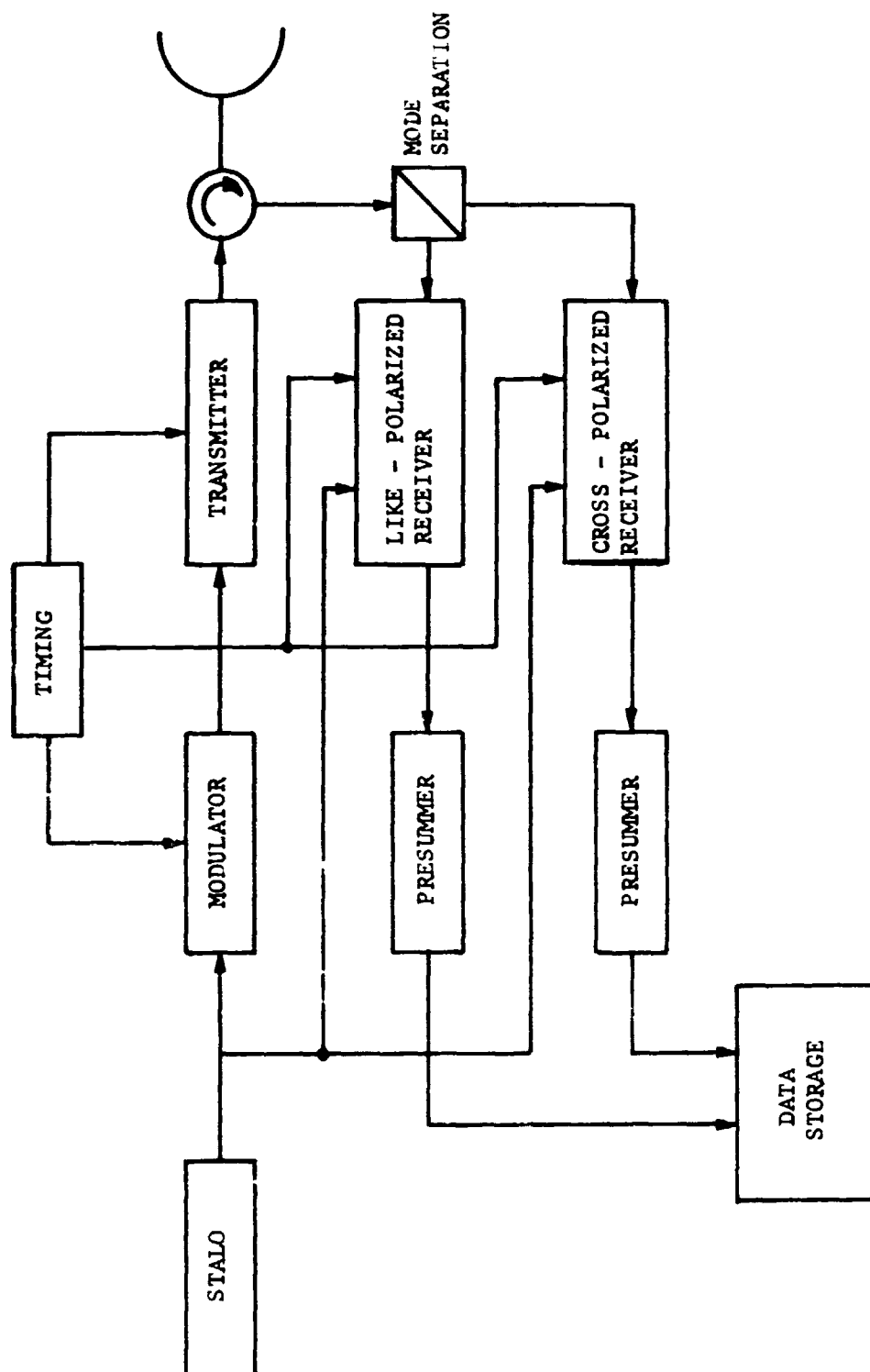
Figure IV-44 Dual Polarized Radar Mapping System

We will assume that an antenna with a common reflector and dual feeds (one for each frequency) is used. Then, assuming the same aperture illumination functions, the longer wavelength channel will have a wider beamwidth. This is more significant in the range dimension since it increases the required unambiguous range interval, thus possibly requiring a lowering of PRF.

In the azimuth channel, the doppler bandwidth is unchanged, but the synthetic aperture length is increased. Thus, azimuth sampling and presumming are not affected by changing the wavelength, but the azimuth processing compression ratio is increased. This latter effect is significant only if on-board processing is used.

Implementation of a dual-frequency system would require the addition of a second Stalo, transmitter, receiver, and processing system. The modulator could be time shared between the two transmitters; however, since the power and weight requirements of the modulator are small, mission reliability would be enhanced by using a separate modulator. Another option is to use a single Stalo and generate the two reference frequencies using a multiple chain. In this case, reliability factors would dictate the actual choice used.

PRF and system timing for the dual-frequency system would be identical with the exception of a fixed delay between the two systems to prevent simultaneous operation of the two transmitters. A simplified block diagram of the dual-frequency system is shown in Figure IV-45.

In summary, the addition of a dual-frequency capability requires duplication of the transmitter, receiver and data processing system. Only the radar timing system and data storage system could reasonably be shared. An additional antenna feed would be required and, if range ambiguities are severe, an increase in the size of the range aperture at the lower frequency would be required.
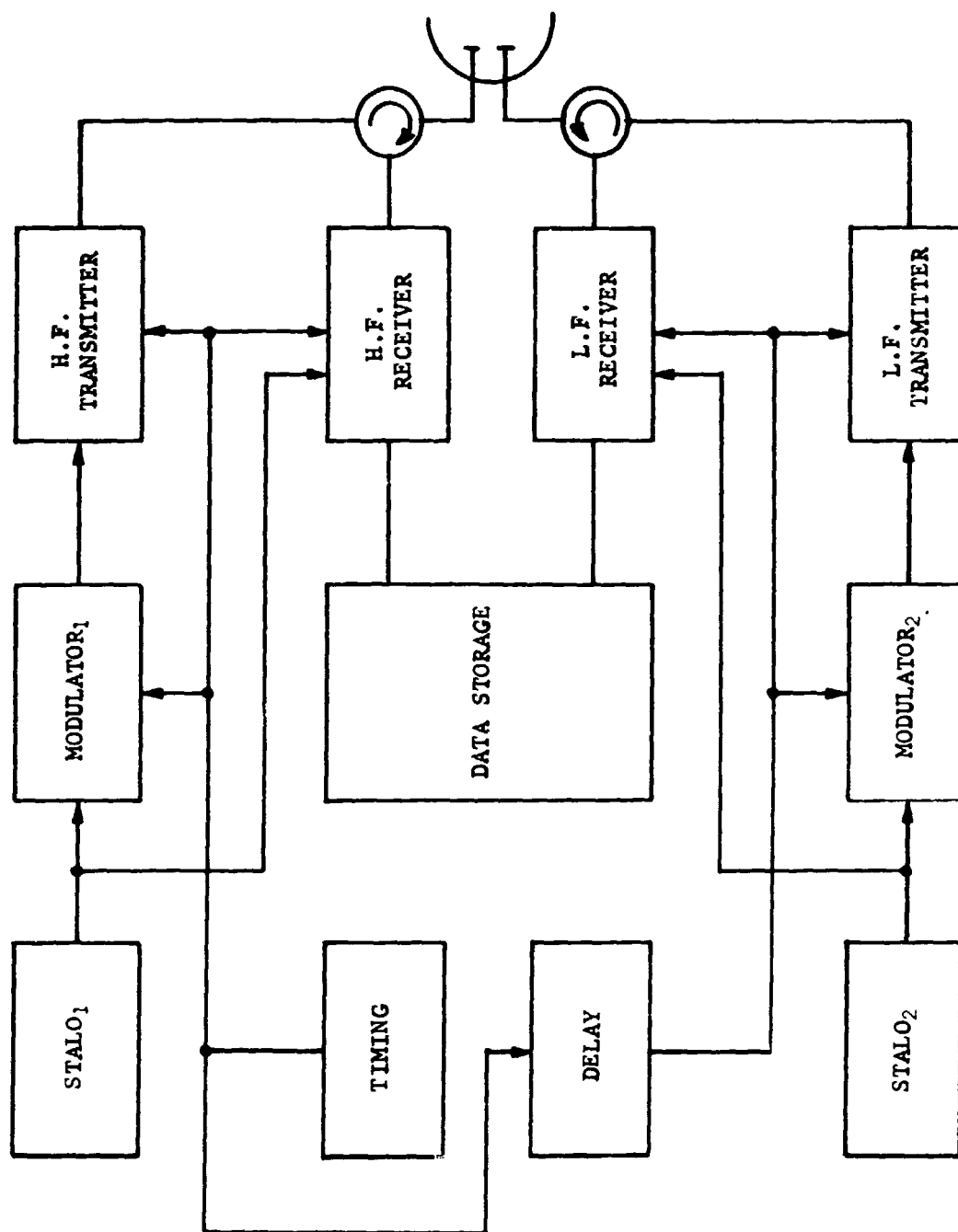
Figure IV-45 Dual Frequency Radar Mapping System

As in the case of a fine-resolution mode discussed in the data
handling discussion, the most serious impact of a dual-frequency
or dual-polarization system appears to be the increased data rate
and data volume if the same mapping area is used. Higher data
rates are available early in the mission when the Earth-Venus
distance is at a minimum. This suggests that the additional power
and weight requirements associated with a dual-mode system would
only be used early in the mission. The limited science return
expected from the additional spacecraft complexity would have to
be weighed against any expected mission limitations caused by
the additional power and weight requirements. For the dual-
polarized system, the major additional power and weight require-
ments reside in the data storage and telemetry system. For the
dual-frequency system, significant additional power and weight
is required for the transmitter as well as the data handling
system. In addition, range ambiguity problems introduced by the
longer wavelength could also have a significant impact on antenna
design and could completely rule out a dual-frequency system.

Reduction of Antenna Size

An antenna size of 1 x 10 meters has been proposed for the
Venus orbiter radar. At a wavelength of 10 cm this would provide
3 db beamwidths of 0.5 degrees and 5 degrees if it is assumed that
the antenna is uniformly illuminated. This section discusses the
possibility of thinning the aperture to reduce weight while pre-
serving the required beamwidths and side lobe levels.

A well known technique in radio astronomy (Ref. IV-15) com-
bines the signals from two elements many wavelengths apart in
such a way that the resultant pattern is the product of the ele-
ment radiation pattern, the interferometer pattern and the pattern
due to the effective distance between the phase center of the
interferometer. The disadvantage of this system is that it

produces high side lobes (about -6 db) but in our case we have a two-way pattern and this should reduce side lobe levels to acceptable values.

Two omnidirectional radiators spaced a distance d gives the radiation pattern

$$f(\theta) = 2 \cos \left(\frac{kd \sin \theta}{2} \right) \qquad \text{(IV-32)}$$

where $k = \frac{2\pi}{\lambda}$, = angle from vertical to plane of radiators.

$$\left.\begin{array}{l} \text{Zeros occur at } \dfrac{\pi d \sin \theta}{\lambda} = \dfrac{\pi}{2}, \dfrac{3\pi}{2}, \ (2N+1) \ \dfrac{\pi}{2} \\[3mm] \text{Maxima occur at } \dfrac{\pi d \sin \theta}{\lambda} = 0, \ \pi, \ \ldots \ N\pi \end{array}\right\} \qquad \text{(IV-33)}$$

If further elements can be placed in positions which produce radiation patterns with minima at the off-axis maxima of the basic interferometer pattern, the product of the patterns will result in suppression of the off-axis lobes. Put

$$f(\theta) = 2 \cos \psi \qquad \text{(IV-34)}$$

where $\psi = \pi d \sin \theta$

then the resultant two-way pattern is given by

$$g(\theta) = 2^N \prod_{K=1}^{N} \cos\left(\frac{\psi}{K}\right) \qquad \text{(IV-35)}$$

where N is an integer.

First consider the case when N=2, i.e.,

$$g(\theta) = 4 \cos \psi \cos \psi/2 \qquad \text{(IV-36)}$$

In order to suppress the far-out side lobes the elements must be directional. Assuming that they are uniformly illuminated we get

$$G(\theta) = 4 \cos \psi \cos \psi/2 \sin^2 \psi_\ell/\psi_\ell^2 \qquad \text{(IV-37)}$$

where $\psi_\ell = \pi \ell \sin \theta$ and ℓ is the element length with all elements having equal length. The configuration of the array is shown in Figure IV-46. Elements 1 and 3 transmit and elements 1 and 2 receive. Figure IV-47 shows the resulting radiation pattern when $\ell = d/4$. This pattern has a grating lobe at $\psi_1 = 38$ ($\theta = 2.24°$ for $d = 50\lambda$). Despite large element sizes this has not been suppressed and the pattern is unacceptable.
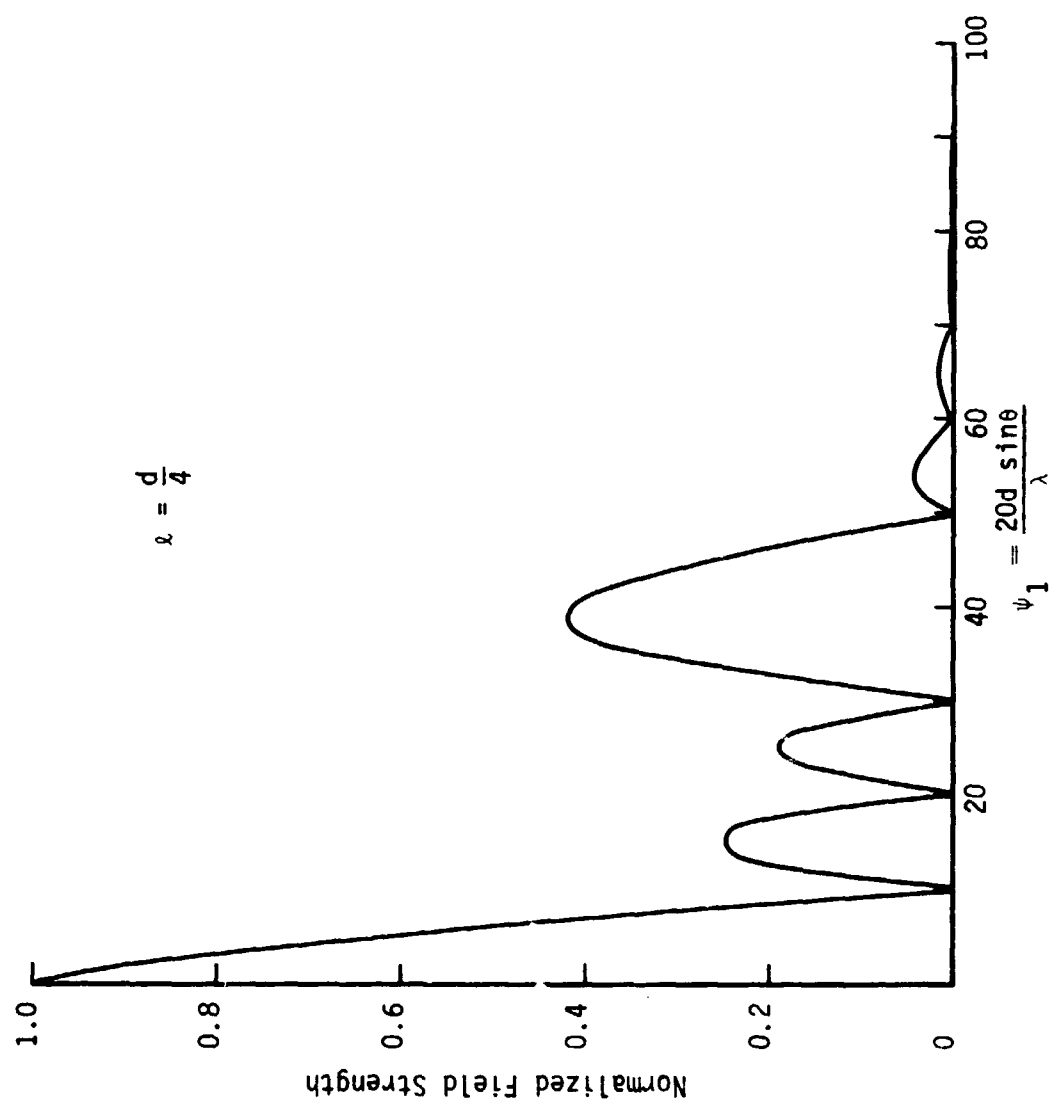
Figure IV-47 Radiation Pattern of 3-Element Array
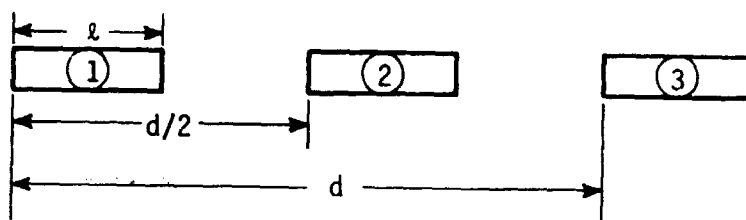
Figure IV-46   Three-Element Array

The next step is to put N=3 in equation (IV-35). The array configuration appropriate to this pattern is shown in Figure IV-48.
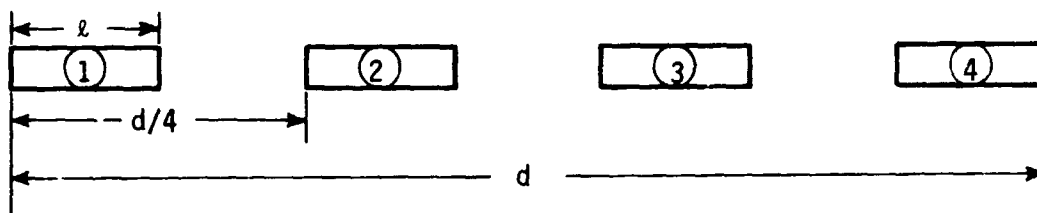
Figure IV-48   Four-Element Array

Elements 1 and 4 transmit and elements 1, 2, 3 and 4 receive. Thus

$$G(\theta) = 8 \cos \psi \cos \psi/2 \cos \psi/4 \sin^2 \psi_\ell/\psi_\ell^2 \qquad \text{(IV-38)}$$

The pattern corresponding to this equation is shown in Figure IV-49 with ℓ = d/5. If we take d=50λ the required beamwidth is obtained. Further reduction in ℓ results in a significant grating lobe at θ = 45 degrees.

The array shown in Figure IV-48 could be designed without much difficulty but would add to the complexity of the system. The array size has been considerably reduced but probably not sufficiently to justify this system as a viable alternative to the single aperture. If h. her side lobes were acceptable the element length could be reduced further but the grating lobe very quickly approaches the size of the main lobe as the length is reduced beyond 0.15d.
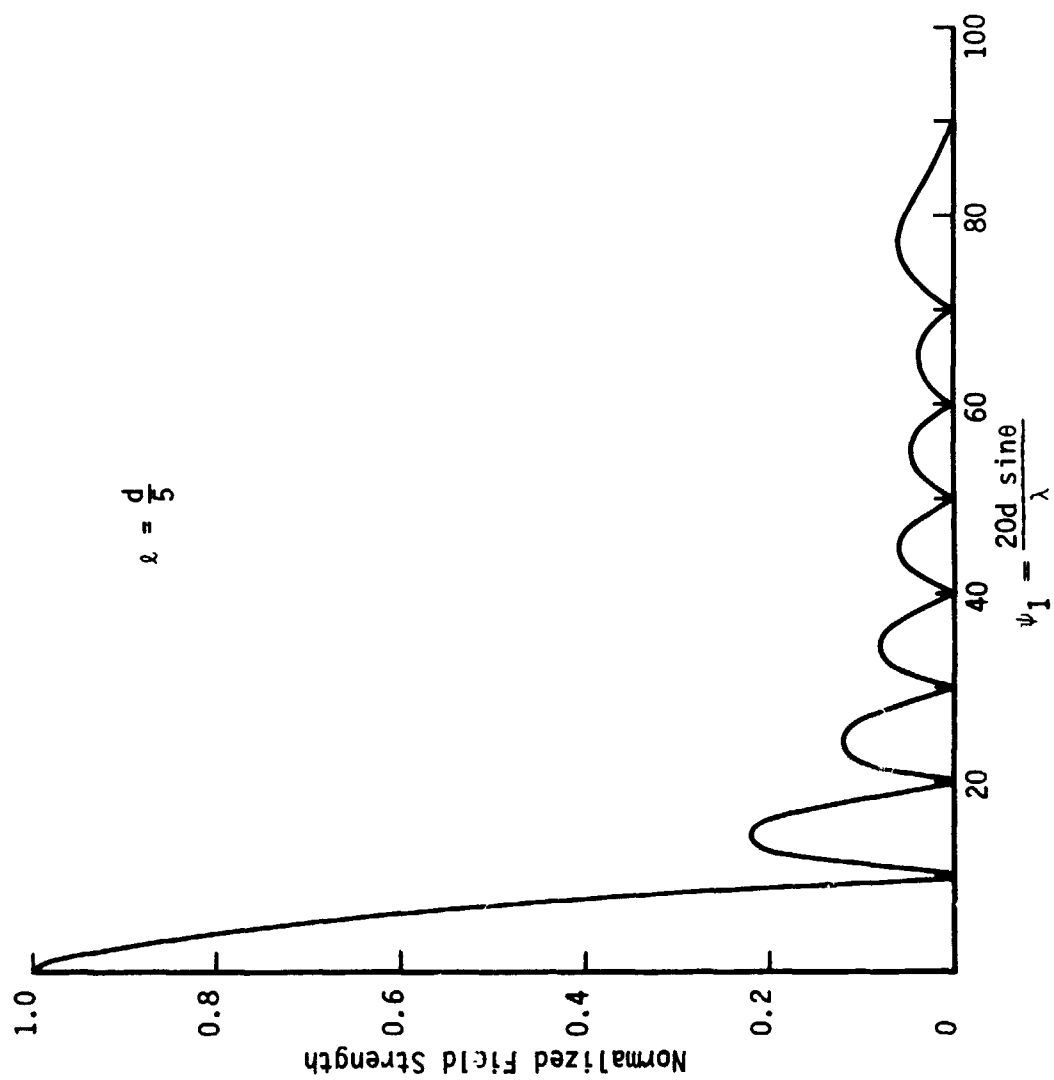
Figure IV-49 Radiation Pattern of 4-Element Array

Range and Azimuth Ambiguity Elimination for Elliptical Orbits

These paragraphs discuss the antenna size, side look angle, and PRF requirements for the elimination of range and azimuth ambiguities for the Venus mapping radar in an elliptical orbit. In our design, we arbitrarily require that the ambiguous clutter return be at least 20 db below the main lobe return in the doppler bandwidth being processed. For simplicity, the design assumes a uniformly illuminated rectangular aperture.

We define antenna beamwidth in terms of the two-way antenna power gain. For a uniformly illuminated rectangular aperture, the 6 db beamwidth is

$$\beta_6 \text{ db} = 0.885 \, \lambda/D \tag{IV- }$$

where   is the wavelength and D is the aperture dimension. Th 16 and 26 db beamwidths are

$$\beta_{16} \text{ db} = 1.356 \, \lambda/D \tag{IV-40}$$

and

$$\beta_{26} \text{ db} = 1.615 \, \lambda/D \tag{IV-41}$$

The illuminated swath width is

$$W = R \text{ csc } \psi \, \beta_r \tag{IV-42}$$

where   R = slant range

ψ = grazing angle

β_r = range beamwidth

The two-way propagation delay is

$$\begin{aligned} \Delta T &= \frac{2W}{C} \cos \psi \\ &= \frac{2R}{C} \text{ ctn } \psi \, \beta_r \end{aligned} \tag{IV-43}$$

where C is the velocity of propagation.

Now, if we require the illuminated swath to be within the 6 db range beamwidth, then from equations (IV-39) and (IV-42) we get a lower beamwidth constraint:

$$\beta_{r_6} \ db \ge \frac{W}{R} \sin \psi \qquad\qquad (IV\text{-}44)$$

or

$$D_r \le 0.885 \frac{R\lambda}{W} \csc \psi \qquad\qquad (IV\text{-}45)$$

To prevent significant range ambiguities, we require the two-way propagation delay over the unambiguous range swath to be less than the PRF interval. In ambiguity spectrum section of this volume it is shown that far-range ambiguities can be kept 20 db below the far-range response if the two-way pattern is 16 db down at the edge of the unambiguous range interval. We then require

$$\frac{1}{PRF} \ge \Delta T_{16} \ db \qquad\qquad (IV\text{-}46)$$

where ΔT_{16} db is the unambiguous range delay. Then from equations (IV-40), (IV-43), and (IV-46) we require

$$\frac{1}{PRF} \ge \frac{2R}{C} \ ctn \ \psi \ \beta_{r_{16} \ db} \qquad\qquad (IV\text{-}47)$$

or

$$D_r \ge 2.71 \frac{R\lambda(PRF)}{C} \ ctn \ \psi \qquad\qquad (IV\text{-}48)$$

Combining equations (IV-44) and (IV-48), we get the range aperture constraint:

$$2.71 \frac{R\lambda(PRF)}{C} \ ctn \ \psi \le D_r \le 0.885 \frac{R\lambda}{W} \csc \psi \qquad\qquad (IV\text{-}49)$$

The theoretical azimuth resolution of a SAR is

$$r_a = D_a/2 \qquad\qquad (IV\text{-}50)$$

Hence, an upper bound on the azimuth aperture is

$$D_a < 2 r_a \qquad\qquad (IV\text{-}51)$$

For the Venus mapper, $D_a > 30$ m; hence, spacecraft limitations will place a more severe upper bound on D_a than given by equation (IV-51). A lower bound on D_a is determined by azimuth sampling ambiguities. The two-sided doppler bandwidth, when the antenna is centered at zero doppler, is

$$B_d = \frac{2V}{\lambda} \beta_a \tag{IV-52}$$

Now only the doppler spectrum near zero is processed. In ambiguity spectrum section it is shown that the ambiguous doppler spectrum at zero doppler can be kept 20 db below the main lobe signal if

$$PRF > B_{d_{6\ db}} = \frac{2V}{\lambda} \beta_{a_{6\ db}} \tag{IV-53}$$

or from equations (IV-39) and (IV-53),

$$D_a > 1.769 \frac{V}{PRF} \tag{IV-54}$$

From equations (IV-48) and (IV-54), we get the PRF constraint:

$$1.769 \frac{V}{D_a} \leq PRF \leq 0.369 \frac{CD_r}{R\lambda} \tan \psi \tag{IV-55}$$

If we use the upper bound on D_r, given by equation (IV-45), the PRF constraint becomes

$$1.76 \frac{V}{D_a} \leq PRF \leq 0.326 \frac{C}{W} \sec \psi \tag{IV-56}$$

if

$$D_r = 0.885 \frac{R\lambda}{W} \csc \psi \tag{IV-57}$$

Using the extreme left and right sides of equation (IV-55) we get the antenna area constraint:

$$A = D_r D_a \geq 4.80 \frac{R\lambda V}{C} \ctn \psi \tag{IV-58}$$

Note that equation (IV-58) is valid only if the range aperture constraint given by equation (IV-45) is satisfied.

If D_a is given by equation (IV-45), then from equation (IV-58), the azimuth aperture constraint is

$$D_a \geq 5.42 \frac{VW}{C} \cos \psi \tag{IV-59}$$

We use the following design strategy for an elliptical orbit.

1) We size the range aperture at perigee for a 30° side look angle.

2) Using the range aperture given by step 1), we size the azimuth aperture at the point at which the radar maps the region nearest the poles at a minimum side look angle of 5°.

3) If ambiguity constraints cannot be satisfied using step 2), a multiple range beamwidth antenna will be used.

Radar mapping parameters are given in Table IV-8, IV-9, and IV-10 for zero doppler azimuth tracking with side look angles of 0 through 30 degrees in five-degree steps.

Hence, for a circular orbit with a 30 degree look angle, the required parameters are

$$\psi = 57.79°$$
$$W = 65 \text{ km}$$
$$R = 467.1 \text{ km}$$
$$V = 7.097 \text{ km/sec}$$

From equation (IV-57), the maximum range aperture is

$$D_r = 0.751 \text{ m} \tag{IV-60}$$

From equation (IV-39), the corresponding 6 db two-way beamwidth is

$$\beta_{r_{6 \text{ db}}} = 6.75 \text{ degrees (118 mrad)} \tag{IV-61}$$

From equation (IV-57), the upper PRF constraint is

$$\text{PRF} \leq 2824 \text{ Hz} \tag{IV-62}$$

Using the upper bound for the PRF, the lower bound on D_a is given by equation (IV-54)

$$D_a \geq 4.45 \text{ m} \tag{IV-63}$$

The corresponding 6 db azimuth beamwidth is

$$\beta_{a_{6 \text{ db}}} = 1.14 \text{ degrees} \tag{IV-64}$$

Then, for a circular orbit, the nominal constraints are

$$D_r < 0.75 \text{ m}$$
$$D_a > 4.5 \text{ m}$$
$$\text{PRF} < 2800 \text{ Hz}$$

Table IV-8 Radar Mapping Parameters for

Zero Doppler Azimuth Pointing

e = 0.0

RADAR MAPPING PARAMETERS FOR ZERO DOPPLER AZIMUTH POINTING

ORBIT ECCENTRICITY = 0.0
SIDE-LOOK ANGLE = 5.0 DEGREES
SWATH WIDTH = 65.0 KM
WAVELENGTH = 10.0 CM

TRUE ANOMALY (DEG)	TIME (HR)	SLANT RANGE (KM)	ORBITAL VELOCITY (KM/S)	DOPPLER ANGLE (DEG)	GRAZING ANGLE (DEG)	LAT (DEG)	LONG (DEG)	RANGE APERTURE (METERS)	PRF (HZ)	AZIMUTH APERTURE (METERS)
0.0	-0.0	401.6	7.097	-0.0	84.7	0.0	-0.3	0.55	16202	0.77
2.0	0.009	401.6	7.097	0.0	84.7	2.0	-0.3	0.55	16203	0.77
4.0	0.018	401.6	7.097	0.0	84.7	4.0	-0.3	0.55	16203	0.77
6.0	0.026	401.6	7.097	0.0	84.7	6.0	-0.3	0.55	16201	0.77
8.0	0.035	401.6	7.097	0.0	84.7	8.0	-0.3	0.55	16202	0.77
10.0	0.044	401.6	7.097	0.0	84.7	10.0	-0.3	0.55	16202	0.77
12.0	0.053	401.6	7.097	0.0	84.7	12.0	-0.3	0.55	16203	0.77
14.0	0.062	401.6	7.097	0.0	84.7	14.0	-0.3	0.55	16201	0.77
16.0	0.070	401.6	7.097	0.0	84.7	16.0	-0.3	0.55	16203	0.77
18.0	0.079	401.6	7.097	0.0	84.7	18.0	-0.3	0.55	16201	0.77
20.0	0.088	401.6	7.097	0.0	84.7	20.0	-0.4	0.55	16201	0.77
22.0	0.097	401.6	7.097	0.0	84.7	22.0	-0.4	0.55	16202	0.77
24.0	0.106	401.6	7.097	0.0	84.7	24.0	-0.4	0.55	16203	0.77
26.0	0.115	401.6	7.097	0.0	84.7	26.0	-0.4	0.55	16202	0.77
28.0	0.123	401.6	7.097	0.0	84.7	28.0	-0.4	0.55	16203	0.77
30.0	0.132	401.6	7.097	0.0	84.7	30.0	-0.4	0.55	16201	0.77
32.0	0.141	401.6	7.097	0.0	84.7	32.0	-0.4	0.55	16202	0.77
34.0	0.150	401.6	7.097	0.0	84.7	34.0	-0.4	0.55	16202	0.77
36.0	0.159	401.6	7.097	0.0	84.7	36.0	-0.4	0.55	16201	0.77
38.0	0.167	401.6	7.097	0.0	84.7	38.0	-0.4	0.55	16203	0.77
40.0	0.176	401.6	7.097	0.0	84.7	40.0	-0.4	0.55	16202	0.77
42.0	0.185	401.6	7.097	0.0	84.7	42.0	-0.4	0.55	16201	0.77
44.0	0.194	401.6	7.097	0.0	84.7	44.0	-0.5	0.55	16202	0.77
46.0	0.203	401.6	7.097	0.0	84.7	46.0	-0.5	0.55	16201	0.77
48.0	0.211	401.6	7.097	0.0	84.7	48.0	-0.5	0.55	16201	0.77
50.0	0.220	401.6	7.097	0.0	84.7	50.0	-0.5	0.55	16202	0.77
52.0	0.229	401.7	7.097	0.0	84.7	52.0	-0.5	0.55	16202	0.77
54.0	0.238	401.6	7.097	0.0	84.7	54.0	-0.6	0.55	16203	0.77
56.0	0.247	401.7	7.097	0.0	84.7	56.0	-0.6	0.55	16202	0.77
58.0	0.256	401.7	7.097	0.0	84.7	58.0	-0.6	0.55	16202	0.77
60.0	0.264	401.7	7.097	0.0	84.7	60.0	-0.7	0.55	16202	0.77
62.0	0.273	401.7	7.097	0.0	84.7	62.0	-0.7	0.55	16202	0.77
64.0	0.282	401.7	7.097	0.0	84.7	64.0	-0.8	0.55	16202	0.77
66.0	0.291	401.7	7.097	0.0	84.7	66.0	-0.8	0.55	16202	0.77
68.0	0.300	401.7	7.097	0.0	84.7	68.0	-0.9	0.55	16201	0.77
70.0	0.308	401.7	7.097	0.0	84.7	70.0	-1.0	0.55	16203	0.77
72.0	0.317	401.7	7.097	0.0	84.7	72.0	-1.1	0.55	16202	0.77
74.0	0.326	401.7	7.097	0.0	84.7	74.0	-1.2	0.55	16202	0.77
76.0	0.335	401.7	7.097	0.0	84.7	76.0	-1.4	0.55	16202	0.77
78.0	0.344	401.7	7.097	0.0	84.7	78.0	-1.6	0.55	16202	0.77
80.0	0.352	401.7	7.097	0.0	84.7	80.0	-1.9	0.55	16203	0.77
82.0	0.361	401.7	7.097	0.0	84.7	82.0	-2.4	0.55	16202	0.77
84.0	0.370	401.7	7.097	0.0	84.7	84.0	-3.2	0.55	16202	0.77
86.0	0.379	401.7	7.097	0.0	84.7	86.0	-4.7	0.55	16201	0.77
88.0	0.388	401.7	7.097	0.0	84.7	88.0	-9.4	0.55	16201	0.77
90.0	0.397	401.7	7.097	0.0	84.7	89.7	-90.0	0.55	16201	0.77

RADAR MAPPING PARAMETERS FOR ZERO DOPPLER AZIMUTH POINTING

ORBIT ECCENTRICITY = 0.0
SITE-LOOK ANGLE = 10.0 DEGREES
SWATH WIDTH = 65.0 KM
WAVELENGTH = 10.0 CM

TRUE ANOMALY (DEG)	TIME (HR)	SLANT RANGE (KM)	URBITAL VELOCITY (KM/S)	DOPPLER ANGLE (DEG)	GRAZING ANGLE (DEG)	LAT (DEG)	LONG (DEG)	RANGE APERTURE (METERS)	PRF (HZ)	AZIMUTH APERTURE (METERS)
0.0	-0.0	406.6	7.097	-0.0	79.3	0.0	-0.7	0.56	8132	1.54
2.0	0.009	406.6	7.097	0.0	79.3	2.0	-0.7	0.55	8132	1.54
4.0	0.018	406.6	7.097	0.0	79.3	4.0	-0.7	0.56	8132	1.54
6.0	0.026	406.6	7.097	0.0	79.3	6.0	-0.7	0.56	8132	1.54
8.0	0.035	406.6	7.097	0.0	79.3	8.0	-0.7	0.56	8132	1.54
10.0	0.044	406.6	7.097	0.0	79.3	10.0	-0.7	0.56	8132	1.54
12.0	0.053	406.6	7.097	0.0	79.3	12.0	-0.7	0.56	8132	1.54
14.0	0.062	406.6	7.097	0.0	79.3	14.0	-0.7	0.56	8132	1.54
16.0	0.070	406.6	7.097	0.0	79.3	16.0	-0.7	0.56	8132	1.54
18.0	0.079	406.6	7.097	0.0	79.3	18.0	-0.7	0.56	8132	1.54
20.0	0.188	406.6	7.097	0.0	79.3	20.0	-0.7	0.56	8132	1.54
22.0	0.097	406.6	7.097	0.0	79.3	22.0	-0.7	0.56	8132	1.54
24.0	0.106	406.6	7.097	0.0	79.3	24.0	-0.7	0.56	8132	1.54
26.0	0.115	406.6	7.097	0.0	79.3	26.0	-0.7	0.55	8132	1.54
28.0	0.123	406.6	7.097	0.0	79.3	28.0	-0.8	0.56	8132	1.54
30.0	0.132	406.6	7.097	0.0	79.3	30.0	-0.8	0.56	8132	1.54
32.0	0.141	406.6	7.097	0.0	79.3	32.0	-0.8	0.56	8132	1.54
34.0	0.150	406.6	7.097	0.0	79.3	34.0	-0.8	0.56	8132	1.54
36.0	0.159	406.6	7.097	0.0	79.3	36.0	-0.8	0.56	8132	1.54
38.0	0.167	406.6	7.097	0.0	79.3	38.0	-0.8	0.56	8132	1.54
40.0	0.176	406.6	7.097	0.0	79.3	40.0	-0.9	0.56	8132	1.54
42.0	0.185	406.6	7.097	0.0	79.3	42.0	-0.9	0.54	8132	1.54
44.0	0.194	406.6	7.097	0.0	79.3	44.0	-0.9	0. .6	8132	1.54
46.0	0.203	406.6	7.097	0.0	79.3	46.0	-1.0	0.56	8132	1.54
48.0	0.211	406.6	7.097	0.0	79.3	48.0	-1.0	0.56	8132	1.54
50.0	0.220	406.6	7.097	0.0	79.3	50.0	-1.0	0.56	8132	1.54
52.0	0.229	406.6	7.097	0.0	79.3	52.0	-1.1	0.56	8132	1.54
54.0	0.238	406.6	7.097	0.0	79.3	54.0	-1.1	0.56	8132	1.54
56.0	0.247	406.6	7.097	0.0	79.3	56.0	-1.2	0.56	8132	1.54
58.0	0.256	406.6	7.097	0.0	79.3	58.0	-1.3	0.56	8132	1.54
60.0	0.264	406.6	7.097	0.0	79.3	60.0	-1.3	0.56	8132	1.54
62.0	0.273	406.6	7.097	0.0	79.3	62.0	-1.4	0.56	8132	1.54
64.0	0.282	406.6	7.097	0.0	79.3	64.0	-1.5	0.56	8132	1.54
66.0	0.291	406.6	7.097	0.0	79.3	66.0	-1.6	0.56	8132	1.54
68.0	0.300	406.6	7.097	0.0	79.3	68.0	-1.8	0.56	8132	1.54
70.0	0.308	405.6	7.097	0.0	79.3	70.0	-2.0	0.56	8132	1.54
72.0	0.317	406.6	7.097	0.0	79.3	72.0	-2.2	0.56	8132	1.54
74.0	0.326	406.6	7.097	0.0	79.3	74.0	-2.4	0.56	8132	1.54
76.0	0.335	406.6	7.097	0.0	79.3	76.0	-2.8	0.56	8132	1.54
78.0	0.344	406.6	7.097	0.0	79.3	78.0	-3.2	0.56	8132	1.54
80.0	0.352	406.6	7.097	0.0	79.3	80.0	-3.8	0.56	8132	1.54
82.0	0.361	406.6	7.097	0.0	79.3	82.0	-4.8	0.56	8132	1.54
84.0	0.370	406.6	7.097	0.0	79.3	84.0	-6.4	0.56	8132	1.54
86.0	0.379	406.7	7.097	0.0	79.3	85.9	-9.5	0.56	8132	1.54
88.0	0.388	406.7	7.097	0.0	79.3	87.9	-18.5	0.56	8132	1.54
90.0	0.397	406.7	7.097	0.0	79.3	89.3	-90.0	0.56	8132	1.54

RADAR MAPPING PARAMETERS FOR ZERO DOPPLER AZIMUTH POINTING

ORBIT ECCENTRICITY = 0.0
SIDE-LOOK ANGLE = 15.0 DEGREES
SWATH WIDTH = 65.0 KM
WAVELENGTH = 10.0 CM

TRUE ANOMALY (DEG)	TIME (HR)	SLANT RANGE (KM)	ORBITAL VELOCITY (KM/S)	DOPPLER ANGLE (DEG)	GRAZING ANGLE (DEG)	LAT (DEG)	LONG (DEG)	RANGE APERTURE (METERS)	PRF (HZ)	AZIMUTH APERTURE (METERS)
0.0	-0.0	415.1	7.097	-0.0	74.0	0.0	-1.0	0.59	5456	2.30
2.0	0.009	415.1	7.097	0.0	74.0	2.0	-1.0	0.59	5456	2.30
4.0	0.018	415.1	7.097	0.0	74.0	4.0	-1.0	0.59	5456	2.30
6.0	0.026	415.1	7.097	0.0	74.0	6.0	-1.0	0.59	5456	2.30
8.0	0.035	415.1	7.097	0.0	74.0	8.0	-1.0	0.59	5456	2.30
10.0	0.044	415.1	7.097	0.0	74.0	10.0	-1.0	0.59	5456	2.30
12.0	0.053	415.1	7.097	0.0	74.0	12.0	-1.0	0.59	5456	2.30
14.0	0.062	415.1	7.097	0.0	74.0	14.0	-1.0	0.59	5456	2.30
16.0	0.070	415.1	7.097	0.0	74.0	16.0	-1.1	0.59	5456	2.30
18.0	0.079	415.1	7.097	0.0	74.3	18.0	-1.1	0.59	5456	2.30
20.0	0.088	415.1	7.097	0.0	74.0	20.0	-1.1	0.59	5456	2.30
22.0	0.097	415.1	7.097	0.0	74.0	22.0	-1.1	0.59	5456	2.30
24.0	0.106	415.1	7.097	0.0	74.0	24.0	-1.1	0.59	5456	2.30
26.0	0.115	415.1	7.097	0.0	74.0	26.0	-1.1	0.59	5456	2.30
28.0	0.123	415.1	7.097	0.0	74.0	28.0	-1.2	0.59	5456	2.30
30.0	0.132	415.1	7.097	0.0	74.0	30.0	-1.2	0.59	5456	2.30
32.0	0.141	415.1	7.097	0.0	74.	32.0	-1.2	0.59	5456	2.30
34.0	0.150	415.1	7.097	0.0	74.0	34.0	-1.2	0.59	5456	2.30
36.0	0.159	415.1	7.097	0.0	74.0	36.0	-1.3	0.59	5456	2.30
38.0	0.167	415.1	7.097	0.0	74.0	38.0	-1.3	0.59	5456	2.30
40.0	0.176	415.1	7.097	0.0	74.0	40.0	-1.3	0.59	5456	2.30
42.0	0.185	415.1	7.097	0.0	74.0	42.0	-1.4	0.59	5456	2.30
44.0	0.194	415.1	7.097	0.0	74.0	44.0	-1.4	0.59	5456	2.30
46.0	0.203	415.1	7.097	0.0	74.0	46.0	-1.5	0.59	5456	2.30
48.0	0.211	415.1	7.097	0.0	74.0	48.0	-1.5	0.59	5456	2.30
50.0	0.220	415.1	7.097	0.0	74.0	50.0	-1.6	0.59	5456	2.30
52.0	0.229	415.1	7.097	0.0	74.0	52.0	-1.7	0.59	5456	2.30
54.0	0.238	415.1	7.097	0.0	74.0	54.0	-1.7	0.59	5456	2.30
56.0	0.247	415.1	7.097	0.0	74.0	56.0	-1.8	0.59	5456	2.30
58.0	0.256	415.1	7.097	0.0	74.0	58.0	-1.9	0.59	5456	2.30
60.0	0.264	415.1	7.097	0.0	74.0	60.0	-2.0	0.59	5456	2.30
62.0	0.273	415.1	7.097	0.0	74.0	62.0	-2.2	0.59	5456	2.30
64.0	0.282	415.1	7.097	0.0	74.0	64.0	-2.3	0.59	5456	2.30
66.0	0.291	415.1	7.097	0.0	74.0	66.0	-2.5	0.59	5456	2.30
68.0	0.300	415.1	7.097	0.0	74.0	68.0	-2.7	0.59	5456	2.30
70.0	0.308	415.1	7.097	0.0	74.0	70.0	-3.0	0.59	5456	2.30
72.0	0.317	415.1	7.097	0.0	74.0	72.0	-3.3	0.59	5456	2.30
74.0	0.326	415.1	7.097	0.0	74.0	74.0	-3.7	0.59	5456	2.30
76.0	0.335	415.1	7.097	0.0	74.0	76.0	-4.2	0.59	5456	2.30
78.0	0.344	415.1	7.097	0.0	74.0	78.0	-4.9	0.59	5456	2.30
80.0	0.352	415.2	7.097	0.0	74.0	79.9	-5.8	0.59	5456	2.30
82.0	0.361	415.2	7.097	0.0	74.0	81.9	-7.3	0.59	5456	2.30
84.0	0.370	415.2	7.097	0.0	74.0	83.9	-9.6	0.59	5456	2.30
86.0	0.379	415.2	7.097	0.0	74.0	85.9	-14.3	0.59	5456	2.30
88.0	0.388	415.2	7.097	0.0	74.0	87.8	-27.0	0.59	5456	2.30
90.0	0.397	415.2	7.097	0.0	74.0	89.0	-90.0	0.59	5456	2.30

RADAR MAPPING PARAMETERS FOR ZERO DOPPLER AZIMUTH POINTING

ORBIT ECCENTRICITY = 0.0
SIDE-LOOK ANGLE = 20.0 DEGREES
SWATH WIDTH = 65.0 KM
WAVELENGTH = 10.0 CM

TRUE ANOMALY (DEG)	TIME (HR)	SLANT RANGE (KM)	ORBITAL VELOCITY (KM/S)	DOPPLER ANGLE (DEG)	GRAZING ANGLE (DEG)	LAT (DEG)	LONG (DEG)	RANGE APERTURE (METERS)	PRF (HZ)	AZIMUTH APERTURE (METERS)
0.0	-0.0	427.6	7.097	-0.0	68.6	0.0	-1.4	0.62	4128	3.04
2.0	0.009	427.6	7.097	0.0	68.6	2.0	-1.4	0.62	4128	3.04
4.0	0.018	427.6	7.097	0.0	68.6	4.0	-1.4	0.62	4128	3.04
6.0	0.026	427.6	7.097	0.0	68.6	6.0	-1.4	0.62	4128	3.04
8.0	0.035	427.5	7.097	0.0	68.6	8.0	-1.4	0.62	4128	3.04
10.0	0.044	427.6	7.097	0.0	68.6	10.0	-1.4	0.62	4128	3.04
12.0	0.053	427.6	7.097	0.0	68.6	12.0	-1.4	0.62	4128	3.04
14.0	0.062	427.6	7.097	0.0	68.6	14.0	-1.4	0.62	4126	3.04
16.0	0.070	427.6	7.097	0.0	68.6	16.0	-1.4	0.62	4128	3.04
18.0	0.079	427.6	7.097	0.0	68.6	18.0	-1.5	0.62	4128	3.04
20.0	0.088	427.6	7.097	0.0	68.6	20.0	-1.5	0.62	4128	3.04
22.0	0.097	427.6	7.097	0.0	68.6	22.0	-1.5	0.62	4128	3.04
24.0	0.106	427.6	7.097	0.0	68.6	24.0	-1.5	0.62	4128	3.04
26.0	0.115	427.6	7.097	0.0	68.6	26.0	-1.5	0.62	4128	3.04
28.0	0.123	427.6	7.097	0.0	68.6	28.0	-1.6	0.62	4128	3.04
30.0	0.132	427.6	7.097	0.0	68.6	30.0	-1.6	0.62	4128	3.04
32.0	0.141	427.6	7.097	0.0	68.6	32.0	-1.6	0.62	4128	3.04
34.0	0.150	427.6	7.097	0.0	68.6	34.0	-1.7	0.62	4128	3.04
36.0	0.159	427.6	7.097	0.0	68.6	36.0	-1.7	0.62	4128	3.04
38.0	0.167	427.6	7.097	0.0	68.6	38.0	-1.8	0.62	4128	3.04
40.0	0.176	427.6	7.097	0.0	68.6	40.0	-1.8	0.62	4128	3.04
42.0	0.185	427.6	7.097	0.0	68.6	42.0	-1.9	0.62	4128	3.04
44.0	0.194	427.6	7.097	0.0	68.6	44.0	-1.9	0.62	4128	3.04
46.0	0.203	427.6	7.097	0.0	68.6	46.0	-2.0	0.62	4128	3.04
48.0	0.211	427.6	7.097	0.0	68.6	48.0	-2.1	0.62	4128	3.04
50.0	0.220	427.6	7.097	0.0	68.6	50.0	-2.2	0.62	4128	3.04
52.0	0.229	427.6	7.097	0.0	68.6	52.0	-2.2	0.62	4128	3.04
54.0	0.238	427.6	7.097	0.0	68.6	54.0	-2.4	0.62	4128	3.04
56.0	0.247	427.6	7.097	0.0	68.6	56.0	-2.5	0.62	4128	3.04
58.0	0.256	427.6	7.097	0.0	68.6	58.0	-2.6	0.62	4128	3.04
60.0	0.264	427.6	7.097	0.0	68.6	60.0	-2.8	0.62	4128	3.04
62.0	0.273	427.6	7.097	0.0	68.6	62.0	-2.9	0.62	4128	3.04
64.0	0.282	427.6	7.097	0.0	68.6	64.0	-3.2	0.62	4128	3.04
66.0	0.291	427.6	7.097	0.0	68.6	66.0	-3.4	0.62	4128	3.04
68.0	0.300	427.6	7.097	0.0	68.6	68.0	-3.7	0.62	4128	3.04
70.0	0.303	427.6	7.097	0.0	68.6	70.0	-4.0	0.62	4128	3.04
72.0	0.317	427.6	7.097	0.0	68.6	71.9	-4.5	0.62	4128	3.04
74.0	0.326	427.6	7.097	0.0	68.6	73.9	-5.0	0.62	4128	3.04
76.0	0.335	427.6	7.097	0.0	68.6	75.9	-5.7	0.62	4128	3.04
78.0	0.344	427.6	7.097	0.0	68.6	77.9	-6.6	0.62	4128	3.04
80.0	0.352	427.6	7.097	0.0	68.6	79.9	-7.9	0.62	4128	3.04
82.0	0.361	427.6	7.097	0.0	68.6	81.9	-9.9	0.62	4128	3.04
84.0	0.370	427.6	7.097	0.0	68.6	83.8	-13.0	0.62	4128	3.04
86.0	0.379	427.6	7.097	0.0	68.6	85.8	-19.1	0.62	4128	3.04
88.0	0.388	427.6	7.097	0.0	68.6	87.6	-34.7	0.62	4128	3.04
90.0	0.397	427.6	7.097	0.0	68.6	88.6	-90.0	0.62	4128	3.04

RADAR MAPPING PARAMETERS FOR ZERO DOPPLER AZIMUTH POINTING

ORBIT ECCENTRICITY = 0.0
SIDE-LOOK ANGLE = 25.0 DEGREES
SWATH WIDTH = 65.0 KM
WAVELENGTH = 10.0 CM

TRUE ANOMALY (DEG)	TIME (HR)	SLANT RANGE (KM)	ORBITAL VELOCITY (KM/S)	DOPPLER ANGLE (DEG)	GRAZING ANGLE (DEG)	LAT (DEG)	LONG (DEG)	RANGE APERTURE (METERS)	PRF (HZ)	AZIMUTH APERTURE (METERS)
0.0	-0.0	444.6	7.097	-0.0	63.2	0.0	-1.8	0.68	3341	3.76
2.0	0.009	444.6	7.097	0.0	63.2	2.0	-1.8	0.68	3341	3.76
4.0	0.018	444.6	7.097	0.0	63.2	4.0	-1.8	0.68	3341	3.76
6.0	0.026	444.6	7.097	0.0	63.2	6.0	-1.8	0.68	3341	3.76
8.0	0.035	444.6	7.097	0.0	63.2	8.0	-1.8	0.68	3341	3.76
10.0	0.044	444.6	7.097	0.0	63.2	10.0	-1.8	0.68	3341	3.76
12.0	0.053	444.6	7.097	0.0	63.2	12.0	-1.8	0.68	3341	3.76
14.0	0.062	444.6	7.097	0.0	63.2	14.0	-1.8	0.68	3341	3.76
16.0	0.070	444.6	7.097	0.0	63.2	16.0	-1.9	0.68	3341	3.76
18.0	0.079	444.6	7.097	0.0	63.2	18.0	-1.9	0.68	3341	3.76
20.0	0.088	444.6	7.097	0.0	63.2	20.0	-1.9	0.68	3341	3.76
22.0	0.097	444.6	7.097	0.0	63.2	22.0	-1.9	0.68	3341	3.76
24.0	0.106	444.6	7.097	0.0	63.2	24.0	-1.9	0.68	3341	3.76
26.0	0.115	444.6	7.097	0.0	63.2	26.0	-2.0	0.68	3341	3.76
28.0	0.123	444.6	7.097	0.0	63.2	28.0	-2.0	0.68	3341	3.76
30.0	0.132	444.6	7.097	0.0	63.2	30.0	-2.1	0.68	3341	3.76
32.0	0.141	444.6	7.097	0.0	63.2	32.0	-2.1	0.68	3341	3.76
34.0	0.150	444.6	7.097	0.0	63.2	34.0	-2.1	0.68	3341	3.76
36.0	0.159	444.6	7.097	0.0	63.2	36.0	-2.2	0.68	3341	3.76
38.0	0.167	444.6	7.097	0.0	63.2	38.0	-2.3	0.68	3341	3.76
40.0	0.176	444.6	7.097	0.0	63.2	40.0	-2.3	0.68	3341	3.76
42.0	0.185	444.6	7.097	0.0	63.2	42.0	-2.4	0.68	3341	3.76
44.0	0.194	444.6	7.097	0.0	63.2	44.0	-2.5	0.68	3341	3.76
46.0	0.203	444.6	7.097	0.0	63.2	46.0	-2.6	0.68	3341	3.76
48.0	0.211	444.6	7.097	0.0	63.2	48.0	-2.7	0.68	3341	3.76
50.0	0.220	444.6	7.097	0.0	63.2	50.0	-2.8	0.68	3341	3.76
52.0	0.229	444.6	7.097	0.0	63.2	52.0	-2.9	0.68	3341	3.76
54.0	0.238	444.6	7.097	0.0	63.2	54.0	-3.0	0.68	3341	3.76
56.0	0.247	444.6	7.097	0.0	63.2	56.0	-3.2	0.68	3341	3.76
58.0	0.256	444.6	7.097	0.0	63.2	58.0	-3.4	0.68	3341	3.76
60.0	0.264	444.6	7.097	0.0	63.2	60.0	-3.6	0.68	3341	3.76
62.0	0.273	444.6	7.097	0.0	63.2	61.9	-3.8	0.68	3341	3.76
64.0	0.282	444.6	7.097	0.0	63.2	63.9	-4.1	0.68	3341	3.76
66.0	0.291	444.6	7.097	0.0	63.2	65.9	-4.4	0.68	3341	3.76
68.0	0.300	444.6	7.097	0.0	63.2	67.9	-4.7	0.68	3341	3.76
70.0	0.308	444.6	7.097	0.0	63.2	69.9	-5.2	0.68	3341	3.76
72.0	0.317	444.6	7.097	0.0	63.2	71.9	-5.7	0.68	3341	3.76
74.0	0.326	444.6	7.097	0.0	63.2	73.9	-6.4	0.68	3341	3.76
76.0	0.335	444.6	7.097	0.0	63.2	75.9	-7.3	0.68	3341	3.76
78.0	0.344	444.6	7.097	0.0	63.2	77.9	-8.5	0.68	3341	3.76
80.0	0.352	444.6	7.097	0.0	63.2	79.8	-10.1	0.68	3341	3.76
82.0	0.361	444.6	7.097	0.0	63.2	81.8	-12.6	0.68	3341	3.76
84.0	0.370	444.6	7.097	0.0	63.2	83.7	-16.6	0.68	3341	3.76
86.0	0.379	444.6	7.097	0.0	63.2	85.6	-24.0	0.68	3341	3.76
88.0	0.388	444.6	7.097	0.0	63.2	87.3	-41.7	0.68	3341	3.76
90.0	0.397	444.6	7.097	0.0	63.2	88.2	-90.0	0.68	3341	3.76

RADAR MAPPING PARAMETERS FOR ZERO DOPPLER AZIMUTH POINTING

ORBIT ECCENTRICITY = 0.0
SIDE-LOOK ANGLE = 30.0 DEGREES
SWATH WIDTH = 65.0 KM
WAVELENGTH = 10.0 CM

TRUE ANOMALY (DEG)	TIME (HR)	SLANT RANGE (KM)	ORBITAL VELOCITY (KM/S)	DOPPLER ANGLE (DEG)	GRAZING ANGLE (DEG)	LAT (DEG)	LONG (DEG)	RANGE APERTURE (METERS)	PRF (HZ)	AZIMUTH APERTURE (METERS)
0.0	-0.0	467.1	7.097	-0.0	57.8	0.0	-2.2	0.75	2824	4.45
2.0	0.009	467.1	7.097	0.0	57.8	2.0	-2.2	0.75	2824	4.45
4.0	0.018	467.1	7.097	0.0	57.8	4.0	-2.2	0.75	2824	4.45
6.0	0.026	467.1	7.097	0.0	57.8	6.0	-2.2	0.75	2824	4.45
8.0	0.035	467.1	7.097	0.0	57.8	8.0	-2.2	0.75	2824	4.45
10.0	0.044	467.1	7.097	0.0	57.8	10.0	-2.2	0.75	2824	4.45
12.0	0.053	467.1	7.097	0.0	57.8	12.0	-2.3	0.75	2824	4.45
14.0	0.062	467.1	7.097	0.0	57.8	14.0	-2.3	0.75	2824	4.45
16.0	0.070	467.1	7.097	0.0	57.8	16.0	-2.3	0.75	2824	4.45
18.0	0.079	467.1	7.097	0.0	57.8	18.0	-2.3	0.75	2824	4.45
20.0	0.088	467.1	7.097	0.0	57.8	20.0	-2.4	0.75	2824	4.45
22.0	0.097	467.1	7.097	0.0	57.8	22.0	-2.4	0.75	2824	4.45
24.0	0.106	467.1	7.097	0.0	57.8	24.0	-2.4	0.75	2824	4.45
26.0	0.115	467.1	7.097	0.0	57.8	26.0	-2.5	0.75	2824	4.45
28.0	0.123	467.1	7.097	0.0	57.8	28.0	-2.5	0.75	2824	4.45
30.0	0.132	467.1	7.097	0.0	57.8	30.0	-2.6	0.75	2824	4.45
32.0	0.141	467.1	7.097	0.0	57.8	32.0	-2.6	0.75	2824	4.45
34.0	0.150	467.1	7.097	0.0	57.0	34.0	-2.7	0.75	2824	4.45
36.0	0.159	467.1	7.097	0.0	57.8	36.0	-2.7	0.75	2824	4.45
38.0	0.167	467.1	7.097	0.0	57.8	38.0	-2.8	0.75	2824	4.45
40.0	0.176	467.1	7.097	0.0	57.8	40.0	-2.9	0.75	2824	4.45
42.0	0.185	467.1	7.097	0.0	57.8	42.0	-3.0	0.75	2824	4.45
44.0	0.194	467.1	7.097	0.0	57.8	44.0	-3.1	0.75	2824	4.45
46.0	0.203	467.1	7.097	0.0	57.9	46.0	-3.2	0.75	2824	4.45
48.0	0.211	467.1	7.097	0.0	57.8	48.0	-3.3	0.75	2824	4.45
50.0	0.220	467.1	7.097	0.0	57.8	49.9	-3.4	0.75	2824	4.45
52.0	0.229	467.1	7.097	0.0	57.8	51.9	-3.6	0.75	2824	4.45
54.0	0.238	467.1	7.097	0.0	57.8	53.9	-3.8	0.75	2824	4.45
56.0	0.247	467.1	7.097	0.0	57.8	55.9	-4.0	0.75	2824	4.45
58.0	0.256	467.1	7.097	0.0	57.8	57.9	-4.2	0.75	2824	4.45
60.0	0.264	467.1	7.097	0.0	57.8	59.9	-4.4	0.75	2824	4.45
62.0	0.273	467.1	7.097	0.0	57.8	61.9	-4.7	0.75	2824	4.45
64.0	0.282	467.1	7.097	0.0	57.8	63.9	-5.0	0.75	2824	4.45
66.0	0.291	467.1	7.097	0.0	57.8	65.9	-5.4	0.75	2824	4.45
68.0	0.300	467.1	7.097	0.0	57.8	67.9	-5.9	0.75	2824	4.45
70.0	0.308	467.1	7.097	0.0	57.8	69.9	-6.4	0.75	2824	4.45
72.0	0.317	467.1	7.097	0.0	57.8	71.9	-7.1	0.75	2824	4.45
74.0	0.326	467.1	7.097	0.0	57.8	73.9	-8.0	0.75	2824	4.45
76.0	0.335	467.1	7.097	0.0	57.8	75.8	-9.1	0.75	2824	4.45
78.0	0.344	467.1	7.097	0.0	57.8	77.8	-10.5	0.75	2824	4.45
80.0	0.352	467.2	7.097	0.0	57.8	79.8	-12.5	0.75	2824	4.45
82.0	0.361	467.2	7.097	0.0	57.8	81.7	-15.5	0.75	2824	4.45
84.0	0.370	467.2	7.097	0.0	57.8	83.6	-20.3	0.75	2824	4.45
86.0	0.379	467.2	7.097	0.0	57.8	85.4	-29.0	0.75	2824	4.45
88.0	0.388	467.2	7.097	0.0	57.8	87.0	-47.9	0.75	2824	4.45
90.0	0.397	467.2	7.097	0.0	57.8	87.8	-90.0	0.75	2824	4.45

Table IV-9 Radar Mapping Parameters for

Zero Doppler Azimuth Pointing

$e = 0.3$

RADAR MAPPING PARAMETERS FOR ZERO DOPPLER AZIMUTH POINTING

ORBIT ECCENTRICITY = 0.3
SIDE-LOOK ANGLE = 5.0 DEGREES
SWATH WIDTH = 44.0 KM
WAVELENGTH = 10.0 CM

TRUE ANOMALY (DEG)	TIME (HR)	SLANT RANGE (KM)	ORBITAL VELOCITY (KM/S)	DOPPLER ANGLE (DEG)	GRAZING ANGLE (DEG)	LAT (DEG)	LONG (DEG)	RANGE APERTURE (METERS)	PRF (HZ)	AZIMUTH APERTURE (METERS)
0.0	-0.0	401.6	8.092	-0.0	84.7	0.0	-0.3	0.81	23935	0.60
2.0	0.008	402.6	8.091	0.5	84.6	2.0	-0.3	0.81	23831	0.60
4.0	0.015	405.3	8.088	0.9	84.6	4.1	-0.3	0.82	23530	0.61
6.0	0.023	410.0	8.084	1.4	84.5	6.1	-0.3	0.83	23049	0.62
8.0	0.031	416.4	8.078	1.8	84.3	8.1	-0.3	0.84	22424	0.64
10.0	0.039	424.8	8.070	2.3	84.1	10.2	-0.4	0.86	21688	0.66
12.0	0.047	435.0	8.060	2.8	83.9	12.2	-0.4	0.88	20881	0.68
14.0	0.054	447.1	8.049	3.2	.6	14.2	-0.4	0.90	20031	0.71
16.0	0.062	461.1	8.036	3.7	83.3	16.3	-0.4	0.93	19164	0.74
18.0	0.070	477.0	8.021	4.1	83.0	18.3	-0.4	0.97	18307	0.78
20.0	0.078	494.8	8.005	4.6	82.7	20.4	-0.4	1.00	17469	0.81
22.0	0.086	514.5	7.986	5.0	82.3	22.4	-0.5	1.04	16662	0.85
24.0	0.094	536.1	7.967	5.5	82.0	24.5	-0.5	1.09	15893	0.89
26.0	0.102	559.8	7.945	5.9	81.6	26.5	-0.5	1.14	15164	0.93
28.0	0.110	585.4	7.922	6.4	81.2	28.6	-0.5	1.19	14477	0.97
30.0	0.118	613.0	7.897	6.8	80.7	30.7	-0.6	1.25	13831	1.01
32.0	0.127	642.7	7.870	7.2	80.3	32.8	-0.6	1.31	13225	1.05
34.0	0.135	674.4	7.842	7.7	79.9	34.8	-0.7	1.38	12658	1.10
36.0	0.143	708.1	7.813	8.1	79.4	36.9	-0.7	1.45	12127	1.14
38.0	0.152	744.0	7.781	8.5	79.0	39.0	-0.8	1.52	11631	1.18
40.0	0.161	782.0	7.748	8.9	78.5	41.1	-0.8	1.60	11166	1.23
42.0	0.169	822.1	7.714	9.3	78.0	43.3	-0.9	1.69	10731	1.27
44.0	0.178	864.5	7.678	9.7	77.6	45.4	-1.0	1.78	10324	1.32
46.0	0.187	909.0	7.641	10.1	77.1	47.5	-1.1	1.87	9942	1.36
48.0	0.196	955.8	7.602	10.5	76.6	49.6	-1.2	1.98	9583	1.40
50.0	0.205	1004.8	7.561	10.9	76.!	51.8	-1.3	2.08	9246	1.45
52.0	0.214	1056.1	7.519	11.3	75.6	53.9	-1.5	2.19	8930	1.49
54.0	0.224	1109.8	7.476	11.7	75.1	56.1	-1.6	2.31	8632	1.53
56.0	0.233	1165.8	7.432	12.0	74.6	58.3	-1.8	2.43	8351	1.57
58.0	0.243	1224.2	7.386	12.4	74.0	60.5	-2.0	2.56	8087	1.62
60.0	0.253	1285.0	7.338	12.7	73.5	62.7	-2.3	2.69	7837	1.66
62.0	0.263	1348.2	7.290	13.1	73.0	64.9	-2.6	2.83	7602	1.70
64.0	0.273	1413.9	7.240	13.4	72.5	67.1	-2.9	2.98	7379	1.74
66.0	0.283	1482.1	7.189	13.7	71.9	69.3	-3.4	3.13	7169	1.77
68.0	0.293	1552.7	7.137	14.0	71.4	71.5	-3.9	3.29	6970	1.81
70.0	0.304	1625.9	7.084	14.3	70.9	73.8	-4.7	3.46	6782	1.85
72.0	0.315	1701.6	7.029	14.6	70.3	76.0	-5.6	3.63	6604	1.86
74.0	0.326	1779.8	6.974	14.9	69.8	78.2	-7.0	3.81	6436	1.92
76.0	0.337	1860.5	6.918	15.2	69.2	80.5	-9.0	4.00	6276	1.95
78.0	0.349	1943.7	6.860	15.4	68.7	82.7	-12.3	4.19	6126	1.98
80.0	0.360	2029.4	6.802	15.7	68.2	84.9	-18.6	4.39	5983	2.01
82.0	0.372	2117.7	6.743	15.9	67.6	87.0	-33.9	4.60	5848	2.04
84.0	0.384	2208.3	6.683	16.1	67.1	88.2	-83.6	4.82	5720	2.07
86.0	0.397	2301.4	6.622	16.3	66.6	87.2	-139.3	5.04	5600	2.09
88.0	0.409	2396.8	6.561	16.5	66.1	85.2	-156.9	5.27	5487	2.12
90.0	0.422	2494.5	6.498	16.7	65.6	82.9	-163.7	5.51	5380	2.14

RADAR MAPPING PARAMETERS FOR ZERO DOPPLER AZIMUTH POINTING

ORBIT ECCENTRICITY =   0.3
SIDE-LOOK ANGLE = 10.0 DEGREES
SWATH WIDTH = 44.0 KM
WAVELENGTH = 10.0 CM

TRUE ANOMALY (DEG)	TIME (HR)	SLANT RANGE (KM)	ORBITAL VELOCITY (KM/S)	DOPPLER ANGLE (DEG)	GRAZING ANGLE (DEG)	LAT (DEG)	LONG (DEG)	RANGE APERTURE (METERS)	PRF (HZ)	AZIMUTH APERTURE (METERS)
0.0	-0.0	406.6	8.092	-0.0	79.3	0.0	-0.7	0.83	12013	1.19
2.0	0.008	407.5	8.091	0.5	79.3	2.0	-0.7	0.83	11999	1.19
4.0	0.015	410.3	8.088	0.9	79.3	4.1	-0.7	0.84	11958	1.20
6.0	0.023	415.0	8.084	1.4	79.2	6.1	-0.7	0.85	11891	1.20
8.0	0.031	421.6	8.078	1.8	79.1	8.1	-0.7	0.86	11797	1.21
10.0	0.039	430.0	8.070	2.3	79.0	10.2	-0.7	0.88	11681	1.22
12.0	0.047	440.4	8.060	2.8	78.9	12.2	-0.7	0.90	11542	1.24
14.0	0.054	452.6	8.049	3.2	78.7	14.2	-0.8	0.93	11385	1.25
16.0	0.062	466.8	8.036	3.7	78.6	16.3	-0.8	0.96	11210	1.27
18.0	0.070	482.9	8.021	4.1	78.4	18.3	-0.8	0.99	11021	1.29
20.0	0.078	500.9	8.005	4.6	78.1	20.4	-0.9	1.03	10820	1.31
22.0	0.086	520.9	7.986	5.0	77.9	22.4	-0.9	1.07	10610	1.33
24.0	0.094	542.9	7.967	5.5	77.6	24.5	-1.0	1.12	10392	1.36
26.0	0.102	566.8	7.945	5.9	77.4	26.5	-1.0	1.17	10169	1.38
28.0	0.110	592.8	7.922	6.4	77.1	28.6	-1.1	1.22	9942	1.41
30.0	0.118	620.7	7.897	6.8	76.8	30.7	-1.2	1.28	9714	1.44
32.0	0.127	650.8	7.870	7.2	76.4	32.8	-1.3	1.35	9486	1.47
34.0	0.135	682.9	7.842	7.7	76.1	34.8	-1.4	1.41	9259	1.50
36.0	0.143	717.1	7.813	8.1	75.7	36.9	-1.5	1.49	9034	1.53
38.0	0.152	753.5	7.781	8.5	75.4	39.0	-1.6	1.57	8811	1.56
40.0	0.161	792.0	7.748	8.9	75.0	41.1	-1.7	1.65	8593	1.60
42.0	0.169	832.7	7.714	9.3	74.6	43.2	-1.9	1.74	8379	1.63
44.0	0.178	875.6	7.678	9.7	74.2	45.4	-2.0	1.83	8170	1.66
46.0	0.187	920.6	7.641	10.1	73.8	47.5	-2.2	1.93	7966	1.70
48.0	0.196	968.2	7.602	10.5	73.4	49.6	-2.4	2.03	7768	1.73
50.0	0.205	1018.0	7.561	10.9	72.9	51.8	-2.7	2.14	7575	1.77
52.0	0.214	1070.1	7.519	11.3	72.5	53.9	-2.9	2.26	7388	1.80
54.0	0.224	1124.5	7.476	11.7	72.0	56.1	-3.2	2.38	7207	1.84
56.0	0.233	1181.3	7.432	12.0	71.6	58.2	-3.6	2.50	7031	1.87
58.0	0.243	1240.6	7.386	12.4	71.1	60.4	-4.0	2.64	6862	1.90
60.0	0.253	1302.3	7.338	12.7	70.6	62.6	-4.5	2.76	6698	1.94
62.0	0.263	1366.6	7.290	13.1	70.1	64.8	-5.2	2.92	6540	1.97
64.0	0.273	1433.3	7.240	13.4	69.6	67.0	-5.9	3.07	6388	2.00
66.0	0.283	1502.5	7.189	13.7	69.1	69.2	-6.8	3.23	6242	2.04
68.0	0.293	1574.3	7.137	14.0	68.6	71.4	-7.9	3.40	6101	2.07
70.0	0.304	1648.7	7.084	14.3	68.1	73.6	-9.4	3.57	5965	2.10
72.0	0.315	1725.6	7.029	14.6	67.6	75.8	-11.3	3.75	5835	2.13
74.0	0.326	1805.2	6.974	14.9	67.1	78.0	-14.0	3.94	5710	2.16
76.0	0.337	1887.3	6.918	15.2	66.6	80.2	-17.8	4.14	5589	2.19
78.0	0.349	1972.0	6.860	15.4	66.0	82.3	-23.9	4.34	5474	2.22
80.0	0.360	2059.3	6.802	15.7	65.5	84.2	-34.4	4.55	5364	2.24
82.0	0.372	2149.1	6.743	15.9	65.0	85.8	-54.0	4.77	5258	2.27
84.0	0.384	2241.5	6.683	16.1	64.5	86.4	-87.4	4.99	5158	2.29
86.0	0.397	2336.3	6.622	16.3	63.9	85.7	-120.3	5.23	5061	2.31
88.0	0.409	2433.6	6.561	16.5	63.4	84.1	-139.4	5.47	4970	2.34
90.0	0.422	2533.3	6.498	16.7	62.9	82.1	-149.6	5.72	4882	2.35

RADAR MAPPING PARAMETERS FOR ZERO DOPPLER AZIMUTH POINTING

ORBIT ECCENTRICITY = 0.3
SIDE-LOOK ANGLE = 15.0 DEGREES
SWATH WIDTH = 44.0 KM
WAVELENGTH = 10.0 CM

TRUE ANOMALY (DEG)	TIME (HR)	SLANT RANGE (KM)	ORBITAL VELOCITY (KM/S)	DOPPLER ANGLE (DEG)	GRAZING ANGLE (DEG)	LAT (DEG)	LONG (DEG)	RANGE APERTURE (METERS)	PRF (HZ)	AZIMUTH APERTURE (METERS)
0.0	-0.0	415.1	8.092	-0.0	74.0	0.0	-1.0	0.87	8060	1.78
2.0	0.008	416.1	8.091	0.5	74.0	2.0	-1.0	0.87	8055	1.78
4.0	0.015	418.9	8.088	0.9	73.9	4.1	-1.0	0.88	8042	1.78
6.0	0.023	423.7	8.084	1.4	73.9	6.1	-1.0	0.89	8019	1.78
8.0	0.031	430.4	8.078	1.8	73.8	8.1	-1.1	0.90	7988	1.79
10.0	0.039	439.1	8.070	2.3	73.8	10.2	-1.1	0.92	7949	1.80
12.0	0.047	449.6	8.060	2.8	73.7	12.2	-1.1	0.94	7901	1.80
14.0	0.054	462.1	8.049	3.2	73.5	14.2	-1.2	0.97	7846	1.81
16.0	0.062	476.6	8.036	3.7	73.4	16.3	-1.2	1.00	7783	1.83
18.0	0.070	493.1	8.021	4.1	73.2	18.3	-1.3	1.04	7714	1.84
20.0	0.078	511.5	8.005	4.6	73.1	20.4	-1.3	1.07	7638	1.85
22.0	0.086	531.9	7.986	5.0	72.9	22.4	-1.4	1.12	7557	1.87
24.0	0.094	554.4	7.967	5.5	72.7	24.5	-1.5	1.17	7470	1.89
26.0	0.102	578.8	7.945	5.9	72.5	26.5	-1.6	1.22	7379	1.90
28.0	0.110	605.4	7.922	6.4	72.2	28.6	-1.7	1.28	7284	1.92
30.0	0.118	634.0	7.897	6.8	72.0	30.7	-1.8	1.34	7185	1.94
32.0	0.127	664.8	7.870	7.2	71.7	32.8	-1.9	1.41	7083	1.97
34.0	0.135	697.6	7.842	7.7	71.4	34.8	-2.1	1.48	6979	1.99
36.0	0.143	732.6	7.813	8.1	71.1	36.9	-2.2	1.56	6872	2.01
38.0	0.152	769.8	7.781	8.5	70.8	39.0	-2.4	1.64	6765	2.03
40.0	0.161	809.2	7.748	8.9	70.5	41.1	-2.6	1.73	6656	2.06
42.0	0.169	850.9	7.714	9.3	70.1	43.2	-2.8	1.82	6546	2.08
44.0	0.178	894.9	7.678	9.7	69.8	45.3	-3.1	1.92	6436	2.11
46.0	0.187	941.1	7.641	10.1	69.4	47.5	-3.4	2.02	6326	2.14
48.0	0.196	989.7	7.602	10.5	69.0	49.6	-3.7	2.13	6216	2.16
50.0	0.205	1040.7	7.561	10.9	68.6	51.7	-4.1	2.25	6107	2.19
52.0	0.214	1094.1	7.519	11.3	68.2	53.9	-4.5	2.37	5999	2.22
54.0	0.224	1149.9	7.476	11.7	67.8	56.0	-5.0	2.50	5892	2.24
56.0	0.233	1208.2	7.432	12.0	67.4	58.2	-5.5	2.63	5786	2.27
58.0	0.243	1269.0	7.386	12.4	67.0	60.4	-6.2	2.77	5682	2.30
60.0	0.253	1332.4	7.338	12.7	66.5	62.5	-6.9	2.92	5579	2.33
62.0	0.263	1398.3	7.290	13.1	66.0	64.7	-7.8	3.08	5478	2.35
64.0	0.273	1466.8	7.240	13.4	65.6	66.9	-9.0	3.24	5379	2.38
66.0	0.283	1538.0	7.189	13.7	65.1	69.0	-10.3	3.41	5282	2.41
68.0	0.293	1611.8	7.137	14.0	64.6	71.2	-12.0	3.59	5187	2.43
70.0	0.304	1688.3	7.084	14.3	64.1	73.4	-14.2	3.77	5094	2.46
72.0	0.315	1767.5	7.029	14.6	63.6	75.5	-17.0	3.97	5004	2.48
74.0	0.326	1849.3	6.974	14.9	63.1	77.6	-20.9	4.17	4916	2.51
76.0	0.337	1933.9	6.918	15.2	62.6	79.6	-26.3	4.38	4830	2.53
78.0	0.349	2021.3	6.860	15.4	62.1	81.5	-34.4	4.60	4746	2.56
80.0	0.360	2111.3	6.802	15.7	61.5	83.1	-46.6	4.83	4666	2.58
82.0	0.372	2204.0	6.743	15.9	61.0	84.2	-65.1	5.07	4587	2.60
84.0	0.384	2299.4	6.683	16.1	60.5	84.6	-88.9	5.31	4511	2.62
86.0	0.397	2397.5	6.622	16.3	59.9	83.9	-111.4	5.57	4438	2.64
88.0	0.409	2498.1	6.561	16.5	59.4	82.5	-127.6	5.83	4368	2.66
90.0	0.422	2601.3	6.498	16.7	58.9	80.8	-138.2	6.11	4300	2.67

RADAR MAPPING PARAMETERS FCR ZERO DOPPLCR AZIMUTH POINTING

ORBIT ECCENTRICITY = 0.3
SICE-LOOK ANGLE = 20.0 DEGREES
SWATH WIDTH = 44.0 KM
WAVELENGTH = 10.0 CM

TRUE ANOMALY (DEG)	TIME (HR)	SLANT RANGE (KM)	ORBITAL VELOCITY (KM/S)	DOPPLER ANGLE (DEG)	GRAZING ANGLE (DEG)	LAT (DEG)	LONG (DEG)	RANGE APERTURE (METERS)	PRF (HZ)	AZIMUTH APERTURE (METERS)
0.0	-0.0	427.6	8.092	-0.0	68.6	0.0	-1.4	0.92	6099	2.35
2.0	0.008	428.5	8.091	0.5	68.6	2.0	-1.4	0.93	6097	2.35
4.0	0.015	431.5	8.088	0.9	68.6	4.1	-1.4	0.93	6090	2.35
6.0	0.023	436.4	8.084	1.4	68.5	6.1	-1.4	0.94	6080	2.35
8.0	0.031	443.4	8.078	1.8	68.5	8.1	-1.5	0.96	6065	2.36
10.0	0.039	452.3	8.070	2.3	68.4	10.2	-1.5	0.98	6045	2.36
12.0	0.047	463.2	8.060	2.8	68.3	12.2	-1.5	1.00	6022	2.37
14.0	0.054	476.1	8.049	3.2	68.2	14.2	-1.6	1.03	5995	2.38
16.0	0.062	491.0	8.036	3.7	68.1	16.3	-1.7	1.06	5964	2.38
18.0	0.070	508.0	8.021	4.1	68.0	18.3	-1.7	1.10	5929	2.39
20.0	0.078	527.0	8.005	4.6	67.8	20.4	-1.8	1.14	5890	2.40
22.0	0.086	548.1	7.986	5.0	67.7	22.4	-1.9	1.19	5849	2.42
24.0	0.094	571.3	7.967	5.5	67.5	24.5	-2.0	1.24	5804	2.43
26.0	0.102	596.5	7.945	5.9	67.3	26.5	-2.1	1.30	5756	2.44
28.0	0.110	623.9	7.922	6.4	67.1	28.6	-2.3	1.36	5706	2.46
30.0	0.118	653.5	7.897	6.8	66.8	30.7	-2.4	1.43	5653	2.47
32.0	0.127	685.3	7.870	7.2	66.6	32.7	-2.6	1.50	5597	2.49
34.0	0.135	719.2	7.842	7.7	66.3	34.8	-2.8	1.58	5540	2.50
36.0	0.143	755.4	7.813	8.1	66.1	36.9	-3.0	1.66	5480	2.52
38.0	0.152	793.9	7.781	8.5	65.8	39.0	-3.3	1.75	5419	2.54
40.0	0.161	834.6	7.748	8.9	65.5	41.1	-3.6	1.84	5356	2.56
42.0	0.169	877.7	7.714	9.3	65.2	43.2	-3.9	1.94	5292	2.58
44.0	0.178	923.2	7.678	9.7	64.8	45.3	-4.2	2.05	5227	2.60
46.0	0.187	971.1	7.641	10.1	64.5	47.4	-4.6	2.16	5161	2.62
48.0	0.196	1021.4	7.602	10.5	64.1	49.6	-5.0	2.28	5094	2.64
50.0	0.205	1074.2	7.561	10.9	63.7	51.7	-5.5	2.41	5026	2.66
52.0	0.214	1129.6	7.519	11.3	63.4	53.8	-6.1	2.54	4959	2.68
54.0	0.224	1187.5	7.476	11.7	63.0	56.0	-6.8	2.68	4890	2.70
56.0	0.233	1248.0	7.432	12.0	62.5	58.1	-7.5	2.83	4822	2.73
58.0	0.243	1311.1	7.386	12.4	62.1	60.2	-8.4	2.98	4754	2.75
60.0	0.253	1376.9	7.338	12.7	61.7	62.4	-9.5	3.14	4686	2.77
62.0	0.263	1445.4	7.290	13.1	61.2	64.5	-10.7	3.32	4618	2.79
64.0	0.273	1516.7	7.240	13.4	60.7	66.7	-12.2	3.49	4551	2.81
66.0	0.283	1590.7	7.189	13.7	60.3	66.8	-14.0	3.68	4485	2.84
68.0	0.293	1667.6	7.137	14.0	59.8	70.9	-16.3	3.88	4419	2.86
70.0	0.304	1747.3	7.084	14.3	59.3	73.0	-19.2	4.09	4353	2.88
72.0	0.315	1829.9	7.029	14.6	58.8	75.0	-22.9	4.30	4289	2.90
74.0	0.326	1915.4	6.974	14.9	58.2	77.0	-27.8	4.53	4225	2.92
76.0	0.337	2003.8	6.918	15.2	57.7	78.8	-34.4	4.76	4163	2.94
78.0	0.349	2095.2	6.860	15.4	57.2	80.4	-43.5	5.01	4102	2.96
80.0	0.360	2189.5	6.802	15.7	56.6	81.7	-56.0	5.27	4042	2.98
82.0	0.372	2286.7	6.743	15.9	56.1	82.5	-72.0	5.54	3983	2.99
84.0	0.384	2386.8	6.683	16.1	55.5	82.5	-89.9	5.82	3925	3.01
86.0	0.397	2489.8	6.622	16.3	54.9	81.9	-106.6	6.12	3869	3.03
88.0	0.409	2595.7	6.561	16.5	54.3	80.6	-119.8	6.42	3814	3.04
90.0	0.422	2704.5	6.498	16.7	53.8	79.0	-129.5	6.74	3761	3.06

RADAR MAPPING PARAMETERS FOR ZERO DOPPLER AZIMUTH POINTING

ORBIT ECCENTRICITY = 0.3
SIDE-LOOK ANGLE = 25.0 DEGREES
SWATH WIDTH = 44.0 KM
WAVELENGTH = 10.0 CM

TRUE ANOMALY (DEG)	TIME (HR)	SLANT RANGE (KM)	ORBITAL VELOCITY (KM/S)	DOPPLER ANGLE (DEG)	GRAZING ANGLE (DEG)	LAT (DEG)	LONG (DEG)	RANGE APERTURE (METERS)	PRF (HZ)	AZIMUTH APERTURE (METERS)
0.0	-0.0	444.6	8.092	-0.0	63.2	0.	1.8	1.00	4936	2.90
2.0	0.008	445.6	8.091	0.5	63.2	2.0	1.8	1.00	4935	2.90
4.0	0.015	448.7	8.088	0.9	63.2	4.1	-1.8	1.01	4931	2.90
6.0	0.023	453.8	8.084	1.4	63.2	6.1	-1.8	1.02	4924	2.90
8.0	0.031	461.0	8.078	1.8	63.1	8.1	-1.9	1.04	4915	2.91
10.0	0.039	470.3	8.070	2.3	63.0	10.2	-1.9	1.06	4904	2.91
12.0	0.047	481.7	8.060	2.8	62.9	12.2	-2.0	1.09	4890	2.92
14.0	0.054	495.1	8.049	3.2	62.8	14.2	-2.0	1.12	4873	2.92
16.0	0.062	510.7	8.036	3.7	62.7	16.3	-2.1	1.16	4854	2.93
18.0	0.070	528.4	8.021	4.1	62.6	18.3	-2.2	1.20	4833	2.94
20.0	0.078	548.2	8.005	4.6	62.5	20.4	-2.3	1.24	4810	2.94
22.0	0.086	570.2	7.986	5.0	62.3	22.4	-2.5	1.29	4784	2.95
24.0	0.094	594.4	7.967	5.5	62.1	24.5	-2.6	1.35	4756	2.96
26.0	0.102	620.8	7.945	5.9	61.9	26.5	-2.8	1.41	4727	2.97
28.0	0.110	649.4	7.922	6.4	61.7	28.6	-2.9	1.48	4695	2.98
30.0	0.118	680.3	7.897	6.8	61.5	30.7	-3.1	1.56	4661	3.00
32.0	0.127	713.4	7.870	7.2	61.3	32.7	-3.4	1.64	4626	3.01
34.0	0.135	748.9	7.842	7.7	61.0	34.8	-3.6	1.72	4589	3.02
36.0	0.143	786.7	7.813	8.1	60.7	36.9	-3.9	1.81	4551	3.04
38.0	0.152	827.0	7.781	8.5	60.5	39.0	-4.2	1.91	4511	3.05
40.0	0.161	869.6	7.748	8.9	60.2	41.1	-4.5	2.02	4470	3.07
42.0	0.169	914.7	7.714	9.3	59.9	43.2	-5.0	2.13	4428	3.08
44.0	0.178	962.4	7.678	9.7	59.5	45.3	-5.4	2.24	4385	3.10
46.0	0.187	1012.5	7.641	10.1	59.2	47.4	-5.9	2.37	4340	3.11
48.0	0.196	1065.3	7.602	10.5	58.8	49.5	-6.5	2.50	4295	3.13
50.0	0.205	1120.7	7.561	10.9	58.4	51.6	-7.1	2.64	4249	3.15
52.0	0.214	1178.6	7.519	11.3	58.0	53.7	-7.9	2.79	4202	3.16
54.0	0.224	1239.6	7.476	11.7	57.6	55.9	-8.7	2.95	4155	3.18
56.0	0.233	1303.2	7.432	12.0	57.2	58.0	-9.7	3.12	4107	3.20
58.0	0.243	1369.6	7.386	12.4	56.8	60.1	-10.8	3.29	4059	3.22
60.0	0.253	1439.0	7.338	12.7	56.3	62.2	-12.2	3.48	4011	3.24
62.0	0.263	1511.2	7.290	13.1	55.9	64.3	-13.8	3.67	3962	3.25
64.0	0.273	1586.4	7.240	13.4	55.4	66.4	-15.7	3.88	3914	3.27
66.0	0.283	1664.6	7.189	13.7	54.9	68.5	-18.0	4.09	3865	3.29
68.0	0.293	1745.9	7.137	14.0	54.4	70.5	-20.9	4.32	3816	3.31
70.0	0.304	1830.4	7.084	14.3	53.8	72.5	-24.4	4.56	3768	3.33
72.0	0.315	1917.9	7.029	14.6	53.3	74.4	-28.9	4.81	3720	3.34
74.0	0.326	2008.7	6.974	14.9	52.7	76.1	-34.7	5.07	3672	3.36
76.0	0.337	2102.7	6.918	15.2	52.2	77.7	-42.1	5.35	3624	3.38
78.0	0.349	2200.0	6.860	15.4	51.6	79.0	-51.5	5.65	3577	3.39
80.0	0.360	2300.6	6.802	15.7	51.0	80.0	-63.3	5.95	3531	3.41
82.0	0.372	2404.5	6.743	15.9	50.4	80.4	-76.8	6.28	3485	3.42
84.0	0.384	2511.7	6.683	16.1	49.7	80.2	-90.8	6.62	3440	3.44
86.0	0.397	2622.2	6.622	16.3	49.1	79.5	-103.6	6.98	3395	3.45
88.0	0.409	2736.1	6.561	16.5	48.4	78.3	-114.3	7.35	3352	3.46
90.0	0.422	2853.2	6.498	16.7	47.8	76.8	-122.8	7.75	3309	3.47

RADAR MAPPING PARAMETERS FOR .R. DOPPLER AZIMUTH POINTING

ORBIT ECCENTRICITY = 0.3
SIDE-LOOK ANGLE = 30.0 DEGREES
SWATH WIDTH = 44.0 KM
WAVELENGTH = 10.0 CM

TRUE ANOMALY (DEG)	TIME (HR)	SLANT RANGE (KM)	ORBITAL VELOCITY (KM/S)	DOPPLER ANGLE (DEG)	GRAZING ANGLE (DEG)	LAT (DEG)	LONG (DEG)	RANGE APERTURE (METERS)	PRF (HZ)	AZIMUTH APERTURE (METERS)
0.0	-0.0	467.1	8.092	-0.0	57.8	0.0	-2.2	1.11	4172	3.43
2.0	0.008	468.2	8.091	0.5	57.8	2.0	-2.2	1.11	417.	3.43
4.0	0.015	471.4	8.088	0.9	57.8	4.1	-2.2	1.12	416.	3.43
6.0	0.023	476.8	8.084	1.4	57.7	6.1	-2.3	1.13	4164	3.43
8.0	0.031	484.4	8.078	1.8	57.7	8.1	-2.3	1.15	4158	3.44
10.0	0.039	494.2	8.070	2.3	57.6	10.2	-2.4	1.18	4150	3.44
12.0	0.047	506.2	8.060	2.8	57.5	12.2	-2.5	1.21	4140	3.44
14.0	0.054	520.4	8.049	3.2	57.4	14.2	-2.5	1.24	4129	3.45
16.0	0.062	536.8	8.036	3.7	57.3	16.3	-2.6	1.28	4116	3.45
18.0	0.070	555.5	8.021	4.1	57.2	18.3	-2.8	1.33	4101	3.46
20.0	0.078	576.4	8.005	4.6	57.0	20.4	-2.9	1.38	4085	3.47
22.0	0.086	599.6	7.986	5.0	56.8	22.4	-3.1	1.44	4067	3.47
24.0	0.094	625.2	7.967	5.5	56.7	24.5	-3.2	1.50	4047	3.48
26.0	0.102	653.0	7.945	5.9	56.5	26.5	-3.4	1.57	4027	3.49
28.0	0.110	683.3	7.922	6.4	56.3	28.6	-3.7	1.65	4004	3.50
30.0	0.118	715.3	7.897	6.8	56.0	30.6	-3.9	1.74	3981	3.51
32.0	0.127	751.0	7.870	7.2	55.8	32.7	-4.2	1.83	3956	3.52
34.0	0.135	788.5	7.842	7.7	55.5	34.8	-4.5	1.92	3929	3.53
36.0	0.143	828.6	7.813	8.1	55.3	36.9	-4.9	2.03	3902	3.54
38.0	0.152	871.2	7.781	8.5	55.0	38.9	-5.3	2.14	3873	3.55
40.0	0.161	916.4	7.748	8.9	54.6	41.0	-5.7	2.26	3844	3.57
42.0	0.169	964.3	7.714	9.3	54.3	43.1	-6.2	2.39	3813	3.58
44.0	0.178	1014.9	7.678	9.7	54.0	45.2	-6.8	2.52	3781	3.59
46.0	0.187	1068.2	7.641	10.1	53.6	47.3	-7.4	2.67	3749	3.61
48.0	0.196	1124.3	7.602	10.5	53.2	49.4	-8.1	2.82	3715	3.62
50.0	0.205	1183.3	7.561	10.9	52.8	51.5	-8.9	2.98	3681	3.63
52.0	0.214	1245.3	7.519	11.3	52.4	53.6	-9.8	3.16	3646	3.65
54.0	0.224	1310.2	7.476	11.7	52.0	55.7	-10.9	3.34	3611	3.66
56.0	0.233	1378.1	7.432	12.0	51.5	57.8	-12.1	3.54	3575	3.68
58.0	0.243	1449.2	7.386	12.4	51.1	59.9	-13.6	3.75	3539	3.69
60.0	0.253	1523.4	7.338	12.7	50.6	62.0	-15.2	3.96	3502	3.71
62.0	0.263	1600.9	7.290	13.1	50.1	64.0	-17.2	4.20	3465	3.72
64.0	0.273	1681.8	7.240	13.4	49.5	66.0	-19.6	4.44	3427	3.74
66.0	0.283	1766.0	7.189	13.7	49.0	68.0	-22.4	4.70	3389	3.75
68.0	0.293	1853.7	7.137	14.0	48.4	69.9	-25.8	4.98	3352	3.77
70.0	0.304	1944.9	7.084	14.3	47.8	71.7	-30.0	5.27	3314	3.78
72.0	0.315	2039.7	7.029	14.6	47.2	73.4	-35.2	5.58	3276	3.80
74.0	0.326	2138.2	6.974	14.9	46.6	75.0	-41.6	5.91	3238	3.81
76.0	0.337	2240.5	6.918	15.2	46.0	76.3	-49.3	6.26	3200	3.82
78.0	0.349	2346.6	6.860	15.4	45.3	77.2	-58.6	6.64	3162	3.84
80.0	0.360	2456.5	6.802	15.7	44.6	77.8	-69.2	7.03	3125	3.85
82.0	0.372	2570.5	6.743	15.9	43.9	77.9	-80.5	7.45	3087	3.86
84.0	0.384	2688.4	6.683	16.1	43.2	77.5	-91.6	7.90	3050	3.87
86.0	0.397	2810.5	6.622	16.3	42.5	76.7	-101.7	8.37	3014	3.89
88.0	0.409	2936.7	6.561	16.5	41.7	75.5	-110.3	8.88	2978	3.90
90.0	0.422	3067.1	6.498	16.7	40.9	73.9	-117.5	9.42	2942	3.91

Table IV-10 Radar Mapping Parameters for

Zero Doppler Azimuth Pointing

$e = 0.5$

RADAR MAPPING PARAMETERS FOR ZERO DOPPLER AZIMUTH POINTING

ORBIT ECCENTRICITY =   0.5
SIDE-LOOK ANGLE =   5.0 DEGREES
SWATH WIDTH = 36.0 KM
WAVELENGTH = 10.0 CM

TRUE ANOMALY (DEG)	TIME (HR)	SLANT RANGE (KM)	ORBITAL VELOCITY (KM/S)	DOPPLER ANGLE (DEG)	GRAZING ANGLE (DEG)	LAT (DEG)	LONG (DEG)	RANGE APERTURE (METERS)	PRF (HZ)	AZIMUTH APERTURE (METERS)
0.0	-0.0	401.6	8.692	-0.0	84.7	0.0	-0.3	0.99	29254	0.53
2.0	0.007	403.0	8.691	0.7	84.6	2.0	-0.3	0.99	28995	0.53
4.0	0.014	407.0	8.687	1.3	84.5	4.1	-0.3	1.00	28256	0.54
6.0	0.022	413.7	8.681	2.0	84.3	6.1	-0.3	1.02	27138	0.57
8.0	0.029	423.2	8.673	2.7	83.9	8.2	-0.4	1.05	25771	0.60
10.0	0.036	435.4	8.663	3.3	83.6	10.2	-0.4	1.08	24276	0.63
12.0	0.043	450.3	8.650	4.0	83.1	12.3	-0.4	1.11	22755	0.67
14.0	0.051	468.1	8.634	4.7	82.7	14.4	-0.4	1.16	21270	0.72
16.0	0.058	488.6	8.617	5.3	82.1	16.4	-0.4	1.21	19861	0.77
18.0	0.065	512.1	8.597	6.0	81.6	18.5	-0.4	1.27	18551	0.82
20.0	0.073	538.4	8.575	6.6	81.0	20.6	-0.5	1.34	17344	0.87
22.0	0.080	567.8	8.550	7.3	80.4	22.7	-0.5	1.41	16239	0.93
24.0	0.088	600.2	8.523	7.9	79.7	24.8	-0.5	1.50	15232	0.99
26.0	0.096	635.7	8.494	8.6	79.1	26.9	-0.6	1.59	14315	1.05
28.0	0.103	674.4	8.463	9.2	78.4	29.0	-0.6	1.69	13479	1.11
30.0	0.111	716.3	8.429	9.9	77.7	31.2	-0.7	1.80	12716	1.17
32.0	0.119	761.7	8.393	10.5	76.9	33.3	-0.7	1.92	12019	1.24
34.0	0.127	810.5	8.355	11.2	76.2	35.5	-0.8	2.05	11380	1.30
36.0	0.135	862.9	8.315	11.8	75.4	37.7	-0.9	2.19	10793	1.36
38.0	0.144	919.0	8.272	12.5	74.6	39.9	-1.0	2.34	10253	1.43
40.0	0.152	979.0	8.228	13.1	73.8	42.1	-1.1	2.50	9755	1.49
42.0	0.161	1043.0	8.181	13.7	73.0	44.3	-1.2	2.68	9293	1.56
44.0	0.169	1111.0	8.132	14.3	72.1	46.6	-1.3	2.87	8866	1.62
46.0	0.178	1183.4	8.081	14.9	71.3	48.9	-1.4	3.07	8468	1.69
48.0	0.187	1260.3	8.027	15.6	70.4	51.2	-1.6	3.29	8097	1.75
50.0	0.196	1341.9	7.972	16.2	69.5	53.5	-1.8	3.52	7751	1.82
52.0	0.206	1428.4	7.915	16.8	68.5	55.9	-2.0	3.77	7427	1.89
54.0	0.215	1519.9	7.855	17.4	67.6	58.3	-2.3	4.04	7123	1.95
56.0	0.225	1616.9	7.794	17.9	66.6	60.7	-2.6	4.33	6837	2.02
58.0	0.235	1719.4	7.731	18.5	65.6	63.1	-3.0	4.64	6568	2.08
60.0	0.245	1827.9	7.666	19.1	64.5	65.6	-3.5	4.98	6315	2.15
62.0	0.256	1942.6	7.598	19.7	63.4	68.1	-4.1	.34	6076	2.21
64.0	0.267	2063.8	7.529	20.2	62.3	70.7	-4.8	5.73	5849	2.28
66.0	0.278	2192.0	7.458	20.8	61.2	73.3	-5.9	6.15	5635	2.34
68.0	0.289	2327.4	7.386	21.3	60.0	75.9	-7.4	6.60	5432	2.40
70.0	0.301	2470.5	7.311	21.9	58.8	78.6	-9.6	7.10	5239	2.47
72.0	0.313	2621.8	7.235	22.4	57.5	81.2	-13.3	7.64	5056	2.53
74.0	0.325	2781.8	7.157	22.9	56.2	83.9	-20.3	8.23	4882	2.59
76.0	0.338	2951.0	7.078	23.4	54.8	86.4	-38.1	8.87	4717	2.65
78.0	0.351	3130.1	6.997	23.9	53.4	87.6	-91.6	9.58	4559	2.71
80.0	0.364	3319.5	6.914	24.4	51.9	86.1	-140.7	10.36	4409	2.77
82.0	0.378	3520.2	6.830	25.0	50.4	83.3	-156.6	11.22	4266	2.83
84.0	0.392	3732.9	6.744	25.3	48.8	80.3	-163.1	12.18	4129	2.89
86.0	0.407	3958.6	6.657	25.7	47.2	77.2	-166.6	13.26	3998	2.94
88.0	0.423	4198.1	6.568	26.2	45.4	73.9	-168.7	14.48	3874	3.00
90.0	0.439	4452.8	6.479	26.6	43.6	70.5	-170.1	15.86	3755	3.05

RADAR MAPPING PARAMETERS FOR ZERO DOPPLER AZIMUTH POINTING

ORBIT ECCENTRICITY = 0.5
SIDE-LOOK ANGLE = 10.0 DEGREES
SWATH WIDTH = 36.0 KM
WAVELENGTH = 10.0 CM

TRUE ANOMALY (DEG)	TIME (HR)	SLANT RANGE (KM)	ORBITAL VELOCITY (KM/S)	DOPPLER ANGLE (DEG)	GRAZING ANGLE (DEG)	LAT (DEG)	LONG (DEG)	RANGE APERTURE (METERS)	PRF (HZ)	AZIMUTH APERTURE (METERS)
0.0	-0.0	406.6	8.692	-0.0	79.3	0.0	-0.7	1.02	14683	1.05
2.0	0.007	408.0	8.691	0.7	79.3	2.0	-0.7	1.02	14649	1.05
4.0	0.014	412.0	8.687	1.3	79.2	4.1	-0.7	1.03	14548	1.06
6.0	0.022	418.9	8.681	2.0	79.1	6.1	-0.7	1.05	14385	1.07
8.0	0.029	428.4	8.673	2.7	78.9	8.2	-0.7	1.07	14165	1.08
10.0	0.036	440.8	8.663	3.3	78.7	10.2	-0.7	1.10	13895	1.10
12.0	0.043	455.9	8.650	4.0	78.5	12.3	-0.8	1.14	13584	1.13
14.0	0.051	473.9	8.634	4.7	78.2	14.4	-0.8	1.19	13240	1.15
16.0	0.058	494.7	8.617	5.3	77.8	16.4	-0.8	1.24	12871	1.18
18.0	0.065	518.4	8.597	6.0	77.4	18.5	-0.9	1.31	12485	1.22
20.0	0.073	545.1	8.575	6.6	77.0	20.6	-1.0	1.37	12087	1.25
22.0	0.080	574.9	8.550	7.3	76.5	22.7	-1.0	1.45	11686	1.29
24.0	0.088	607.7	8.523	7.9	76.1	24.8	-1.1	1.54	11285	1.34
26.0	0.096	643.6	8.494	8.6	75.5	26.9	-1.2	1.63	10888	1.38
28.0	0.103	682.8	8.463	9.2	75.0	29.0	-1.3	1.74	10498	1.43
30.0	0.111	725.4	8.429	9.9	74.4	31.2	-1.4	1.85	10117	1.47
32.0	0.119	771.3	8.393	10.5	73.8	33.3	-1.5	1.97	9748	1.52
34.0	0.127	820.8	8.355	11.2	73.2	35.5	-1.6	2.11	9390	1.57
36.0	0.135	873.9	8.315	11.8	72.5	37.7	-1.8	2.25	9045	1.63
38.0	0.144	930.8	8.272	12.5	71.8	39.9	-1.9	2.41	8713	1.68
40.0	0.152	991.6	8.228	13.1	71.1	42.1	-2.1	2.58	8395	1.73
42.0	0.161	1056.4	8.181	13.7	70.4	44.3	-2.4	2.76	8089	1.79
44.0	0.169	1125.5	8.132	14.3	69.6	46.6	-2.6	2.95	7796	1.85
46.0	0.178	1198.9	8.081	14.9	68.8	48.9	-2.9	3.16	7516	1.90
48.0	0.187	1276.9	8.027	15.6	68.0	51.2	-3.2	3.36	7247	1.96
50.0	0.196	1359.7	7.972	16.2	67.1	53.5	-3.6	3.63	6991	2.02
52.0	0.206	1447.5	7.915	16.8	66.2	5.8	-4.1	3.89	6745	2.08
54.0	0.215	1540.4	7.855	17.4	65.3	56.2	-4.6	4.17	6510	2.13
56.0	0.225	1638.9	7.794	17.9	64.4	60.6	-5.2	4.47	6285	2.19
58.0	0.235	1743.1	7.731	18.5	63.4	63.1	-6.0	4.79	6070	2.25
60.0	0.245	1853.3	7.666	19.1	62.4	65.5	-7.0	5.14	5864	2.31
62.0	0.256	1969.9	7.598	19.7	61.3	68.0	-8.2	5.52	5667	2.37
64.0	0.267	2093.2	7.529	20.2	60.3	70.5	-9.8	5.92	5479	2.43
66.0	0.278	2223.5	7.458	20.8	59.1	73.1	-11.8	6.36	5298	2.49
68.0	0.289	2361.4	7.386	21.3	58.0	75.6	-14.8	6.84	5124	2.55
70.0	0.301	2507.3	7.311	21.9	56.8	78.1	-19.0	7.37	4958	2.61
72.0	0.313	2661.5	7.235	22.4	55.5	80.6	-25.3	7.93	4799	2.67
74.0	0.325	2824.7	7.157	22.9	54.2	82.9	-37.4	8.56	4647	2.72
76.0	0.338	2997.5	7.078	23.4	52.8	84.7	-58.7	9.24	4500	2.78
78.0	0.351	3180.5	6.997	23.9	51.4	85.2	-92.1	9.99	4360	2.84
80.0	0.364	3374.4	6.915	24.4	50.0	84.0	-122.1	10.83	4225	2.89
82.0	0.378	3580.0	6.830	24.8	48.4	81.9	-135.2	11.76	4095	2.95
84.0	0.392	3798.3	6.744	25.3	46.8	79.0	-148.8	12.80	3971	3.00
86.0	0.407	4030.2	6.657	25.7	45.1	76.0	-154.4	13.97	3852	3.06
88.0	0.423	4277.0	6.568	26.2	43.4	72.8	-158.1	15.31	3738	3.11
90.0	0.439	4537.9	6.479	26.6	41.5	69.4	-160.6	16.84	3628	3.16

RADAR MAPPING PARAMETERS FOR ZERO DOPPLER AZIMUTH POINTING

ORBIT ECCENTRICITY = 0.5
SIDE-LOOK ANGLE = 15.0 DEGREES
SWATH WIDTH = 36.0 KM
WAVELENGTH = 10.0 CM

TRUE ANOMALY (DEG)	TIME (HR)	SLANT RANGE (KM)	ORBITAL VELOCITY (KM/S)	DOPPLER ANGLE (DEG)	GRAZING ANGLE (DEG)	LAT (DEG)	LONG (DEG)	RANGE APERTURE (METERS)	PRF (HZ)	AZIMUTH APERTURE (METERS)
0.0	-0.0	415.1	8.692	-0.0	74.0	0.0	-1.0	1.06	9851	1.56
2.0	0.007	416.5	8.691	0.7	74.0	2.0	-1.0	1.06	9840	1.56
4.0	0.014	420.7	8.687	1.3	73.9	4.1	-1.0	1.08	9809	1.57
6.0	0.022	427.6	8.681	2.0	73.8	6.1	-1.1	1.09	9756	1.57
8.0	0.029	437.4	8.673	2.7	73.7	8.2	-1.1	1.12	9684	1.58
10.0	0.036	450.0	8.663	3.3	73.5	10.2	-1.1	1.15	9593	1.60
12.0	0.043	465.5	8.650	4.0	73.3	12.3	-1.2	1.19	9485	1.61
14.0	0.051	483.8	8.634	4.7	73.1	14.4	-1.2	1.24	9361	1.63
16.0	0.058	505.1	8.617	5.3	72.9	16.4	-1.3	1.30	9222	1.65
18.0	0.065	529.4	8.597	6.0	72.6	18.5	-1.4	1.36	9072	1.68
20.0	0.073	556.7	8.575	6.6	72.2	20.6	-1.4	1.44	8910	1.70
22.0	0.080	587.0	8.550	7.3	71.9	22.7	-1.5	1.52	8739	1.73
24.0	0.088	620.6	8.523	7.9	71.5	24.8	-1.7	1.61	8561	1.76
26.0	0.096	657.3	8.494	8.6	71.1	26.9	-1.8	1.71	8378	1.79
28.0	0.103	697.4	8.463	9.2	70.6	29.0	-1.9	1.82	8189	1.83
30.0	0.111	740.9	8.429	9.9	70.1	31.1	-2.1	1.94	7998	1.86
32.0	0.119	787.9	8.393	10.5	69.6	33.3	-2.3	2.07	7805	1.90
34.0	0.127	838.5	8.355	11.2	69.1	35.5	-2.5	2.21	7611	1.94
36.0	0.135	892.9	8.315	11.8	68.5	37.6	-2.7	2.36	7417	1.98
38.0	0.144	951.1	8.272	12.5	67.9	39.8	-3.0	2.52	7224	2.03
40.0	0.152	1013.3	8.228	13.1	67.3	42.1	-3.3	2.70	7032	2.07
42.0	0.161	1079.7	8.181	13.7	66.6	44.3	-3.6	2.89	6843	2.11
44.0	0.169	1150.5	8.132	14.3	65.9	46.5	-4.0	3.10	6657	2.16
46.0	0.178	1225.7	8.081	14.9	65.2	48.8	-4.4	3.32	6473	2.21
48.0	0.187	1305.6	8.027	15.6	64.4	51.1	-4.9	3.56	6293	2.26
50.0	0.196	1390.5	7.972	16.2	63.6	53.4	-5.5	3.81	6117	2.31
52.0	0.206	1480.5	7.915	16.8	62.8	55.8	-6.2	4.09	5945	2.36
54.0	0.215	1576.0	7.855	17.4	61.9	58.1	-7.0	4.39	5776	2.41
56.0	0.225	1677.0	7.794	17.9	61.0	60.5	-8.0	4.71	5612	2.46
58.0	0.235	1784.1	7.731	18.5	60.1	62.9	-9.2	5.06	5452	2.51
60.0	0.245	1897.4	7.666	19.1	59.1	65.4	-10.6	5.43	5296	2.56
62.0	0.256	2017.4	7.598	19.7	58.1	67.8	-12.5	5.84	5145	2.61
64.0	0.267	2144.4	7.529	20.2	57.0	70.2	-14.8	6.28	4997	2.67
66.0	0.278	2278.8	7.458	20.8	55.9	72.7	-17.9	6.76	4854	2.72
68.0	0.289	2421.1	7.386	21.3	54.8	75.1	-22.1	7.28	4715	2.77
70.0	0.301	2571.7	7.311	21.9	53.6	77.4	-28.1	7.85	4580	2.82
72.0	0.313	2731.2	7.235	22.4	52.3	79.6	-37.0	8.48	4450	2.88
74.0	0.325	2900.3	7.157	22.9	51.0	81.4	-50.4	9.16	4323	2.93
76.0	0.338	3079.6	7.078	23.4	49.7	82.6	-69.7	9.93	4200	2.98
78.0	0.351	3269.5	6.997	23.9	48.2	82.6	-92.9	10.77	4081	3.03
80.0	0.364	3471.8	6.914	24.4	46.7	81.5	-113.5	11.71	3966	3.08
82.0	0.378	3686.6	6.830	24.8	45.2	79.5	-128.1	12.77	3854	3.13
84.0	0.392	3915.2	6.744	25.3	43.5	76.9	-137.8	13.98	3747	3.18
86.0	0.407	4159.1	6.657	25.7	41.7	74.0	-144.2	15.35	3642	3.23
88.0	0.423	4419.6	6.568	26.2	39.9	70.8	-148.6	16.94	3542	3.28
90.0	0.439	4698.6	6.479	26.6	37.9	67.5	-151.8	18.79	3445	3.33

RADAR MAPPING PARAMETERS FOR ZERO DOPPLER AZIMUTH POINTING

ORBIT ECCENTRICITY = 0.5
SIDE-LOOK ANGLE = 20.0 DEGREES
SWATH WIDTH = 36.0 KM
WAVELENGTH = 10.0 CM

TRUE ANOMALY (DEG)	TIME (HR)	SLANT RANGE (KM)	ORBITAL VELOCITY (KM/S)	DOPPLER ANGLE (DEG)	GRAZING ANGLE (DEG)	LAT (DEG)	LONG (DEG)	RANGE APERTURE (METERS)	PRF (HZ)	AZIMUTH APERTURE (METERS)
0.0	-0.0	427.6	8.692	-0.0	68.6	0.0	-1.4	1.13	7455	2.06
2.0	0.007	429.0	8.691	0.7	68.6	2.0	-1.4	1.13	7450	2.06
4.0	0.014	433.3	8.687	1.3	68.6	4.1	-1.4	1.14	7435	2.07
6.0	0.022	440.5	8.681	2.0	68.5	6.1	-1.4	1.16	7411	2.07
8.0	0.029	450.6	8.673	2.7	68.4	8.2	-1.5	1.19	7377	2.08
10.0	0.036	463.6	8.663	3.3	68.2	10.2	-1.5	1.23	7335	2.09
12.0	0.043	479.5	8.650	4.0	68.1	12.3	-1.6	1.27	7283	2.10
14.0	0.051	498.4	8.634	4.7	67.9	14.4	-1.7	1.32	7224	2.11
16.0	0.058	520.4	8.617	5.3	67.7	16.4	-1.8	1.38	7156	2.13
18.0	0.065	545.4	8.597	6.0	67.4	18.5	-1.9	1.45	7081	2.15
20.0	0.073	573.6	8.575	6.6	67.1	20.6	-2.0	1.53	6999	2.17
22.0	0.080	604.9	8.550	7.3	66.8	22.7	-2.1	1.62	6911	2.19
24.0	0.088	639.5	8.523	7.9	66.5	24.8	-2.3	1.71	6817	2.21
26.0	0.096	677.5	8.494	8.6	66.1	26.9	-2.4	1.82	6719	2.24
28.0	0.103	718.9	8.463	9.2	65.7	29.0	-2.6	1.94	6615	2.26
30.0	0.111	763.8	8.429	9.9	65.3	31.1	-2.9	2.07	6508	2.29
32.0	0.119	812.3	8.393	10.5	64.9	33.3	-3.1	2.20	6397	2.32
34.0	0.127	864.6	8.355	11.2	64.4	35.5	-3.4	2.36	6283	2.35
36.0	0.135	920.8	8.315	11.8	63.8	37.6	-3.7	2.52	6167	2.38
38.0	0.144	981.0	8.272	12.5	63.3	39.8	-4.1	2.70	6049	2.42
40.0	0.152	1045.4	8.228	13.1	62.7	42.0	-4.5	2.89	5930	2.45
42.0	0.161	1114.1	8.181	13.7	62.1	44.3	-4.9	3.10	5809	2.49
44.0	0.169	1187.4	8.132	14.3	61.5	46.5	-5.4	3.32	5688	2.53
46.0	0.178	1265.3	8.081	14.9	60.8	48.8	-6.0	3.56	5566	2.57
48.0	0.187	1348.2	8.027	15.6	60.1	51.0	-6.7	3.82	5445	2.61
50.0	0.196	1436.3	7.972	16.2	59.3	53.4	-7.5	4.10	5324	2.65
52.0	0.206	1529.8	7.915	16.8	58.5	55.7	-8.5	4.41	5203	2.69
54.0	0.215	1628.9	7.855	17.4	57.7	58.0	-9.6	4.74	5084	2.73
56.0	0.225	1734.0	7.794	17.9	56.8	60.4	-10.9	5.09	4965	2.78
58.0	0.235	1845.5	7.731	18.5	55.9	62.7	-12.5	5.48	4848	2.82
60.0	0.245	1963.6	7.666	19.1	54.9	65.1	-14.5	5.89	4732	2.87
62.0	0.256	2088.8	7.598	19.7	53.9	67.5	-17.0	6.35	4618	2.91
64.0	0.267	2221.5	7.529	20.2	52.9	69.8	-20.1	6.84	4505	2.96
66.0	0.278	2362.1	7.458	20.8	51.8	72.1	-24.2	7.39	4394	3.00
68.0	0.289	2511.3	7.386	21.3	50.6	74.3	-29.6	7.98	4285	3.05
70.0	0.301	2669.5	7.311	21.9	49.4	76.4	-36.9	8.64	4179	3.09
72.0	0.313	2837.5	7.235	22.4	48.1	78.2	-46.9	9.36	4074	3.14
74.0	0.325	3015.9	7.157	22.9	46.8	79.5	-60.2	10.16	3971	3.19
76.0	0.338	3205.7	7.078	23.4	45.4	80.1	-76.6	11.06	3871	3.23
78.0	0.351	3407.7	6.997	23.9	43.9	79.7	-93.9	12.07	3772	3.28
80.0	0.364	3623.0	6.914	24.4	42.3	78.5	-109.1	13.22	3676	3.33
82.0	0.378	3853.1	6.830	24.8	40.7	76.5	-121.0	14.53	3583	3.37
84.0	0.392	4099.3	6.744	25.3	38.9	74.0	-129.6	16.05	3491	3.42
86.0	0.407	4363.7	6.657	25.7	37.0	71.2	-135.9	17.82	3402	3.46
88.0	0.423	4648.4	6.568	26.2	34.9	68.0	-140.5	19.94	3316	3.50
90.0	0.439	4956.6	6.479	26.6	32.7	64.5	-143.9	22.52	3231	3.55

RADAR MAPPING PARAMETERS FOR ZERO DOPPLER AZIMUTH POINTING

ORBIT ECCENTRICITY = 0.5
SIDE-LOOK ANGLE = 25.0 DEGREES
SWATH WIDTH = 36.0 KM
WAVELENGTH = 10.0 CM

TRUE ANOMALY (DEG)	TIME (HR)	SLANT RANGE (KM)	ORBITAL VELOCITY (KM/S)	DOPPLER ANGLE (DEG)	GRAZING ANGLE (DEG)	LAT (DEG)	LONG (DEG)	RANGE APERTURE (METERS)	PRF (HZ)	AZIMUTH APERTURE (METERS)
0.0	-0.0	444.6	8.692	-0.0	63.2	0.0	-1.8	1.22	6033	2.55
2.0	0.007	446.1	8.691	0.7	63.2	2.0	-1.8	1.23	6030	2.55
4.0	0.014	450.5	8.687	1.3	63.2	4.1	-1.8	1.24	6022	2.55
6.0	0.022	458.0	8.681	2.0	63.1	6.1	-1.8	1.26	6008	2.56
8.0	0.029	468.5	8.673	2.7	63.0	8.2	-1.9	1.29	5989	2.56
10.0	0.036	482.1	8.663	3.3	62.9	10.2	-2.0	1.33	5964	2.57
12.0	0.043	498.7	8.650	4.0	62.7	12.3	-2.0	1.38	5935	2.58
14.0	0.051	518.4	8.634	4.7	62.6	14.4	-2.1	1.44	5900	2.59
16.0	0.058	541.3	8.617	5.3	62.4	16.4	-2.3	1.50	5860	2.60
18.0	0.065	567.4	8.597	6.0	62.1	18.5	-2.4	1.58	5816	2.61
20.0	0.073	596.7	8.575	6.6	61.9	20.6	-2.5	1.66	5767	2.63
22.0	0.080	629.4	8.550	7.3	61.6	22.7	-2.7	1.76	5715	2.65
24.0	0.088	665.5	8.523	7.9	61.3	24.8	-2.9	1.86	5658	2.66
26.0	0.096	705.1	8.494	8.6	60.9	26.9	-3.1	1.98	5597	2.68
28.0	0.103	748.3	8.463	9.2	60.6	29.0	-3.4	2.11	5533	2.71
30.0	0.111	795.3	8.429	9.9	60.2	31.1	-3.7	2.25	5465	2.73
32.0	0.119	846.0	8.393	10.5	59.7	33.3	-4.0	2.41	5394	2.75
34.0	0.127	900.7	8.355	11.2	59.3	35.4	-4.4	2.57	5321	2.78
36.0	0.135	959.4	8.315	11.8	58.8	37.6	-4.8	2.76	5245	2.80
38.0	0.144	1022.4	8.272	12.5	58.3	39.8	-5.2	2.95	5167	2.83
40.0	0.152	1089.9	8.228	13.1	57.7	42.0	-5.8	3.17	5088	2.86
42.0	0.161	1161.9	8.181	13.7	57.1	44.2	-6.3	3.40	5006	2.89
44.0	0.169	1238.7	8.132	14.3	56.5	46.4	-7.0	3.65	4923	2.92
46.0	0.178	1320.5	8.081	14.9	55.8	48.7	-7.8	3.92	4838	2.95
48.0	0.187	1407.6	8.027	15.6	55.1	51.0	-8.7	4.22	4753	2.99
50.0	0.196	1500.2	7.972	16.2	54.4	53.2	-9.7	4.53	4667	3.02
52.0	0.206	1598.7	7.915	16.8	53.6	55.5	-11.0	4.88	4580	3.06
54.0	0.215	1703.2	7.855	17.4	52.8	57.8	-12.4	5.26	4492	3.09
56.0	0.225	1814.2	7.794	17.9	51.9	60.1	-14.1	5.66	4405	3.13
58.0	0.235	1932.1	7.731	18.5	51.0	62.4	-16.2	6.11	4317	3.17
60.0	0.245	2057.3	7.666	19.1	50.0	64.7	-18.7	6.60	4230	3.21
62.0	0.256	2190.2	7.598	19.7	49.0	67.0	-21.8	7.13	4142	3.24
64.0	0.267	2331.3	7.529	20.2	47.9	69.2	-25.8	7.72	4056	3.28
66.0	0.278	2481.4	7.458	20.8	46.8	71.3	-30.7	8.37	3969	3.32
68.0	0.289	2641.0	7.386	21.3	45.6	73.2	-37.1	9.08	3883	3.36
70.0	0.301	2810.6	7.311	21.9	44.3	75.0	-45.3	9.89	3799	3.40
72.0	0.313	2991.8	7.235	22.4	43.0	76.3	-55.7	10.78	3714	3.45
74.0	0.325	3184.9	7.157	22.9	41.5	77.1	-68.1	11.80	3631	3.49
76.0	0.338	3391.3	7.078	23.4	40.0	77.1	-81.7	12.96	3549	3.53
78.0	0.351	3612.5	6.997	23.9	38.4	76.4	-95.1	14.29	3468	3.57
80.0	0.364	3849.9	6.914	24.4	36.7	74.9	-106.8	15.84	3389	3.61
82.0	0.378	4105.8	6.830	24.8	34.8	72.8	-116.3	17.67	3310	3.65
84.0	0.392	4382.7	6.744	25.3	32.8	70.2	-123.7	19.88	3233	3.69
86.0	0.407	4684.2	6.657	25.7	30.6	67.2	-129.4	22.60	3158	3.73
88.0	0.423	5015.0	6.568	26.2	28.2	63.7	-133.7	26.08	3084	3.77
90.0	0.439	5381.9	6.479	26.6	25.5	59.9	-137.0	30.71	3011	3.81

RADAR MAPPING PARAMETERS FOR ZERO DOPPLER AZIMUTH POINTING

ORBIT ECCENTRICITY = 0.5
SIDE-LOOK ANGLE = 30.0 DEGREES
SWATH WIDTH = 36.0 KM
WAVELENGTH = 10.0 CM

TRUE ANOMALY (DEG)	TIME (HR)	SLANT RANGE (KM)	ORBITAL VELOCITY (KM/S)	DOPPLER ANGLE (DEG)	GRAZING ANGLE (DEG)	LAT (DEG)	LONG (DEG)	RANGE APERTURE (METERS)	PRF (HZ)	AZIMUTH APERTURE (METERS)
0.0	-0.0	467.1	8.692	-0.0	57.8	0.0	-2.2	1.36	5099	3.02
2.0	0.007	468.7	8.691	0.7	57.8	2.0	-2.2	1.36	5097	3.02
4.0	0.014	473.4	8.587	1.3	57.7	4.1	-2.2	1.36	5092	3.02
6.0	0.022	481.3	8.681	2.0	57.7	6.1	-2.3	1.40	5083	3.02
8.0	0.029	492.3	8.673	2.7	57.6	8.2	-2.4	1.43	5070	3.03
10.0	0.036	506.4	8.663	3.3	57.5	10.2	-2.4	1.46	5054	3.03
12.0	0.043	524.1	8.650	4.0	57.3	12.3	-2.5	1.53	5034	3.04
14.0	0.051	544.9	8.634	4.7	57.2	14.3	-2.7	1.59	5011	3.05
16.0	0.058	569.0	8.617	5.3	57.0	16.4	-2.8	1.67	4985	3.06
18.0	0.065	596.5	8.597	6.0	56.7	18.5	-3.0	1.75	4956	3.07
20.0	0.073	627.5	8.575	6.6	56.5	20.6	-3.2	1.85	4923	3.08
22.0	0.080	662.0	8.550	7.3	56.2	22.7	-3.4	1.96	4887	3.09
24.0	0.088	700.2	8.523	7.9	55.9	24.8	-3.6	2.08	4848	3.11
26.0	0.096	742.0	8.494	8.6	55.6	26.9	-3.9	2.21	4807	3.13
28.0	0.103	787.7	8.463	9.2	55.2	29.0	-4.2	2.36	4763	3.14
30.0	0.111	837.3	8.429	9.9	54.8	31.1	-4.6	2.52	4716	3.16
32.0	0.119	891.0	8.393	10.5	54.4	33.2	-5.0	2.69	4667	3.18
34.0	0.127	948.9	8.355	11.2	53.9	35.4	-5.4	2.88	4615	3.20
36.0	0.135	1011.2	8.315	11.8	53.4	37.6	-6.0	3.09	4562	3.22
38.0	0.144	1078.1	8.272	12.5	52.9	39.7	-6.5	3.32	4506	3.25
40.0	0.152	1149.7	8.228	13.1	52.3	41.9	-7.2	3.57	4449	3.27
42.0	0.161	1226.3	8.181	13.7	51.7	44.1	-7.9	3.84	4390	3.30
44.0	0.169	1308.1	8.132	14.3	51.1	46.4	-8.3	4.13	4329	3.32
46.0	0.178	1395.4	8.081	14.9	50.4	48.6	-9.8	4.45	4267	3.35
48.0	0.187	1488.4	8.027	15.6	49.7	50.8	-10.9	4.79	4203	3.38
50.0	0.196	1587.5	7.972	16.2	49.0	53.1	-12.2	5.17	4139	3.41
52.0	0.206	1693.0	7.915	16.8	48.1	55.3	-13.8	5.58	4073	3.44
54.0	0.215	1805.3	7.855	17.4	47.3	57.6	-15.6	6.04	4007	3.47
56.0	0.225	1924.9	7.794	17.9	46.4	59.8	-17.7	6.53	3940	3.50
58.0	0.235	2052.1	7.731	18.5	45.4	62.0	-20.3	7.08	3872	3.53
60.0	0.245	2187.6	7.666	19.1	44.4	64.2	-23.4	7.68	3804	3.56
62.0	0.256	2332.0	7.598	19.7	43.3	66.3	-27.2	8.35	3735	3.60
64.0	0.267	2486.0	7.529	20.2	42.2	68.3	-31.9	9.10	3667	3.63
66.0	0.278	2650.4	7.458	20.8	40.9	70.1	-37.7	9.94	3598	3.67
68.0	0.289	2826.1	7.386	21.3	39.6	71.7	-44.9	10.89	3529	3.70
70.0	0.301	3014.3	7.311	21.9	38.2	73.0	-53.5	11.97	3460	3.74
72.0	0.313	3216.1	7.235	22.4	36.7	73.8	-63.6	13.21	3392	3.77
74.0	0.325	3433.4	7.157	22.9	35.1	74.0	-74.7	14.66	3324	3.81
76.0	0.338	3668.0	7.078	23.4	33.4	73.5	-86.0	16.37	3256	3.84
78.0	0.351	3922.4	6.997	23.9	31.5	72.3	-96.6	19.43	3189	3.88
80.0	0.364	4200.0	6.914	24.4	29.5	70.4	-105.8	20.97	3122	3.92
82.0	0.378	4505.3	6.830	24.8	27.2	67.9	-113.4	24.21	3056	3.95
84.0	0.392	4845.1	6.744	25.3	24.7	64.8	-119.5	28.53	2991	3.99
86.0	0.407	5229.8	6.657	25.7	21.7	61.1	-124.3	34.68	2926	4.02
88.0	0.423	5678.5	6.568	26.2	18.3	56.7	-128.1	44.44	2863	4.06
90.0	0.439	6234.2	6.479	26.6	13.9	51.3	-130.9	63.70	2800	4.09

For a 0.3 eccentricity orbit with a 30 degree look angle, the parameters at periapsis are

ψ = 57.79 degrees

W = 44 km

R = 467.1 km

V = 8.092 km/sec

Then at periapsis

$D_r \leq 1.11$ m

and

$\beta_{r_{6\,db}}$ > 4.57 degrees (79.5 mrad)   (IV-65)

The PRF constraint is

PRF < 4180 Hz   (IV-66)

and the azimuth aperture constraint is

$D_a \geq 3.42$ m   (IV-67)

Using a fixed 30 degree side look angle, the poles are mapped at 82 degrees true anomaly with parameters

ψ = 43.92 degrees

R = 2570.5 km

V = 6.743 km/sec

Now using the maximum value of D_r determined at periapsis, the PRF constraint at 82 degrees true anomaly is given by equation (IV-55)

$$PRF < \frac{C}{2.71} \frac{D_r}{R\lambda} \tan \psi = 460 \text{ Hz}$$ (IV-68)

Using the upper bound or PRF, the lower bound on D_a given by equation (IV-54)

$$D_a \geq 1.769 \frac{V}{PRF} = 25.9 \text{ m}$$ (IV-69)

This is obviously too large.

Let us now assume a variable range beamwidth and side look angle of 5 degrees when mapping the poles. From Table IV-9, the poles are mapped at 84 degrees true anomaly with parameters

$\psi = 67.12$ degrees

$R = 2208.3$ km

$V = 6.683$ km/sec

Then, the maximum range aperture is given by equation (IV-45)

$$D_r < 4.82 \text{ m} \qquad \text{(IV-70)}$$

The corresponding 6 db range beamwidth is

$$\beta_{r_{6 \text{ db}}} = 1.05 \text{ degrees (18.3 db)} \qquad \text{(IV-71)}$$

The PRF constraint is

$$\text{PRF} < 5670 \text{ Hz} \qquad \text{(IV-72)}$$

The azimuth aperture constraint is

$$D_a \geq 2.08 \text{ m} \qquad \text{(IV-73)}$$

Therefore, by using an antenna with effective range aperture variable from 1.0 to 4.8 meters and azimuth apertures greater than 3.4 m, the ambiguity requirements can be met by using a variable side look angle of 30 to 5 degrees. Of course other combinations could be used and still give reasonable antenna dimensions.

For a 0.5 eccentricity orbit with a 30 degree side look angle, the parameters at periapsis are

$\psi = 57.79$ degrees

$W = 36$ km

$R = 467.1$ km

$V = 8.692$ km/sec

Then at periapsis

$$D_r \leq 1.35 \text{ m} \qquad \text{(IV-74)}$$

The corresponding 6 db beamwidth is

$$\beta_{i_{6 \text{ db}}} = 3.75 \text{ degrees} \qquad \text{(IV-75)}$$

The PRF constraint is

$$\text{PRF} < 5070 \text{ Hz} \qquad \text{(IV-76)}$$

and the azimuth aperture constraint is

$$D_a \geq 3.03 \text{ m} \qquad \text{(IV-77)}$$

As in the case of the 0.3 eccentricity orbit, in order to map the poles, it will be necessary to decrease the range beamwidth and decrease the side look angle. For a 5 degree side look angle, the pole area is mapped at 78 degrees true anomaly with parameters

$$\psi = 53.4 \text{ degrees}$$
$$R = 3130.0 \text{ km}$$
$$V = 6.997 \text{ km/sec}$$

Then,

$$D_r \leq 9.57 \text{ m} \qquad\qquad\qquad (\text{IV-78})$$

and

$$\beta_{r_{6 \text{ db}}} = 0.53 \text{ degrees} \qquad\qquad\qquad (\text{IV-79})$$

The corresponding PRF constraint is

$$\text{PRF} < 4560 \text{ Hz} \qquad\qquad\qquad (\text{IV-80})$$

and azimuth aperture constraint is

$$D_a > 2.73 \text{ m} \qquad\qquad\qquad (\text{IV-81})$$

In this case, the range aperture is excessive and the azimuth aperture is small. However, the range aperture can be decreased if the azimuth aperture is increased in the same proportion. In fact, by decreasing the range aperture to 5 m and increasing the azimuth aperture to 5.2 m, the required PRF is reduced to approximately 2500 Hz.

These results show that range and azimuth ambiguity constraints can be met with a reasonably sized antenna if variable range beamwidth, side look angle, and PRF are used. Of the three parameters, variable range beamwidth is the major parameter which is used to eliminate range ambiguities.

These results yield minimum antenna dimensions for uniform aperture illuminations. If a weighted illumination pattern is used, approximately a 20 percent increase in aperture size will be required. These results also assume that the antenna is stably centered on zero doppler with an accuracy of approximately 10 per-

cent of the azimuth beamwidth. This tolerance is required if the
PRF corresponds to the 6 db azimuth doppler bandwidth. If this
pointing tolerance cannot be held, it will be necessary to in-
crease the azimuth aperture by about 50 percent in order to per-
mit sampling (at the same PRF) at the 16 db doppler bandwidth.

Range and Azimuth Aperture Dimensions for Elliptical Orbits

Tables IV-11 and IV-12 show orbital parameters and antenna
aperture dimensions for orbit eccentricities of 0.3 and 0.5 and
side look angles of 5 to 30 degrees in 5-degree steps. A rec-
tangular illumination is assumed. Aperture dimensions and PRF
are obtained from the following equations in a previous section.

From equation (IV-45), the maximum range aperture dimension
is

$$D_{r_{max}} = 0.885 \frac{R\lambda}{W} \csc \psi \text{ meters} \qquad (IV-82)$$

from equation (IV-56), the maximum PRF is

$$PRF_{max} = 0.326 \frac{C}{W} \sec \psi \text{ Hz} \qquad (IV-83)$$

and from equation (IV-57), the minimum azimuth aperture is

$$D_{a_{min}} = 1.769 \frac{V}{PRF} \text{ meters} \qquad (IV-84)$$

In all cases, the range aperture and PRF can be reduced and the
azimuth aperture increased by the same factor, i.e., for any
$K > 1$.

$$D_r = D_{r_{max}} / K \qquad (IV-85)$$

$$PRF = PRF_{max} / K \qquad (IV-86)$$

and

$$D_a = K D_{a_{min}} \qquad (IV-87)$$

providing that, in equation (IV-41),

$$D_a < 2 r_a \qquad (IV-88)$$

where r_a is the desired azimuth resolution.

Tables IV-11 and IV-12 also give maximum effective range aperture as a function of orbital true anomaly for varying side look angles. These tables can be used to determine the required programmed side look angle and range beamwidth as a function of true anomaly which results in a practical antenna size.

Attitude Control and Radar System Stability

In the range direction, the primary attitude control constraint is uniform illumination of the range swath. In the receiver, the temporal location of the range swath is determined by the range gate. This must correspond to the look angle of the antenna pattern. Antenna pointing errors will result in a decreased amplitude of the return, causing the image intensity to fall off at one dge. Angular rates are of no consequence.

From the section which discusses range and azimuth dimensions for elliptical orbits, the required range beamwidth varies from a minimum of 6.75 degrees for the circular orbit to 0.53 degrees for mapping the polar regions of 0.5 eccentricity orbit. Therefore, a pointing accuracy of ± 0.25 degrees would be adequate for low altitude mapping but marginal for high altitude mapping over a narrow swath. In the latter case, pointing errors could cause a significant increase in ambiguous range returns.

In the along-track or doppler direction, the antenna must remain aligned so that the generated doppler spectrum is within the processor passband. If D_a = 10 m, the azimuth bandwidth is 10 mrad or 0.53 degrees. The required beamwidth for 100 m resolution is 0.5 mrad or 0.03 degrees. Then a pointing accuracy of ± 0.25 degrees will keep the azimuth data within the processor passband. For 30 m resolution, the required processing angle is 1.7 mrad or 0.10 degrees. This requires a pointing accuracy of ± 0.22 degrees. As in the range channel, angular pointing errors

Table .V-11 Radar Mapping Parameters for

Zero Doppler Azimuth Pointing

$e = 0.3$

RADAR MAPPING PARAMETERS FOR ZERO DOPPLER AZIMUTH POINTING

ORBIT ECCENTRICITY = 0.3
SIDE-LOOK ANGLE = 5.0 DEGREES
SWATH WIDTH = 44.0 KM
WAVELENGTH = 10.0 CM

TRUE ANOMALY (DEG)	TIME (HR)	SLANT RANGE (KM)	ORBITAL VELOCITY (KM/S)	DOPPLER ANGLE (DEG)	GRAZING ANGLE (DEG)	LAT (DEG)	LONG (DEG)	RANGE APERTURE (METERS)	PRF (HZ)	AZIMUTH APERTURE (METERS)
0.0	-0.0	401.6	8.092	-0.0	84.7	0.0	-0.3	0.81	23935	0.60
2.0	0.008	402.6	8.091	0.5	84.6	2.0	-0.3	0.81	23831	0.60
4.0	0.015	405.3	8.068	0.9	84.6	4.1	-0.3	0.82	23530	0.61
6.0	0.023	410.0	8.084	1.4	84.5	6.1	-0.3	0.83	23049	0.62
8.0	0.031	416.4	8.078	1.8	84.3	8.1	-0.3	0.84	22424	0.64
10.0	0.039	424.8	8.070	2.3	84.1	10.2	-0.4	0.86	21688	0.66
12.0	0.047	435.0	8.060	2.8	83.9	12.2	-0.4	0.88	20881	0.68
14.0	0.054	447.1	8.049	3.2	83.6	14.2	-0.4	0.90	20031	0.71
16.0	0.062	461.1	8.036	3.7	83.3	16.3	-0.4	0.93	19164	0.74
18.0	0.070	477.0	8.021	4.1	83.0	18.3	-0.4	0.97	18307	0.78
20.0	0.078	494.8	8.005	4.6	82.7	20.4	-0.4	1.00	17469	0.81
22.0	0.086	514.5	7.986	5.0	82.3	22.4	-0.5	1.04	16662	0.85
24.0	0.094	536.1	7.967	5.5	82.0	24.5	-0.5	1.09	15893	0.89
26.0	0.102	559.8	7.945	5.9	81.6	26.5	-0.5	1.14	151 4	0.93
28.0	0.110	585.4	7.922	6.	81.2	28.6	-0.5	1.19	14477	0.97
30.0	0.118	613.0	7.897	6.8	80.7	30.7	-0.6	1.25	13831	1.01
32.0	0.127	642.7	7.870	7.2	80.3	32.8	-0.6	1.31	13225	1.05
34.0	0.135	674.4	7.842	7.7	79.9	34.8	-0.7	1.38	12658	1.10
36.0	0.143	708.1	7.813	8.1	79.4	36.9	-0.7	1.45	12127	1.14
38.0	0.152	744.0	7.781	8.5	79.0	39.0	-0.8	1.52	11631	1.18
40.0	0.161	782.0	7.748	8.9	78.5	41.1	-0.8	1.60	11166	1.23
42.0	0.169	822.1	7.714	9.3	78.0	43.3	-0.9	1.69	10731	1.27
44.0	0.178	864.5	7.678	9.7	77.6	45.4	-1.0	1.78	10324	1.32
46.0	0.187	909.0	7.641	10.1	77.1	47.5	-1.1	1.87	9942	1.36
48.0	0.196	955.8	7.602	10.5	76.6	49.6	-1.2	1.98	9583	1.40
50.0	0.205	1004.8	7.561	10.9	76.1	51.8	-1.3	2.08	9246	1.45
52.0	0.214	1056.1	7.519	11.3	75.6	53.9	-1.5	2.19	8930	1.49
54.0	0.224	1109.8	7.476	11.7	75.1	56.1	-1.6	2.31	8632	1.53
56.0	0.233	1165.8	7.432	12.0	74.6	58.3	-1.8	2.43	8351	1.57
58.0	0.243	1224.2	7.386	12.4	74.0	60.5	-2.0	2.56	8087	1.62
60.0	0.253	1285.0	7.338	12.7	73.5	62.7	-2.3	2.69	7837	1.66
62.0	0.263	1348.2	7.290	13.1	73.0	64.9	-2.6	2.83	7602	1.70
64.0	0.273	1413.9	7.240	13.4	72.5	67.1	-2.9	2.98	7379	1.74
66.0	0.283	1482.1	7.189	13.7	71.9	69.3	-3.4	3.13	7169	1.77
68.0	0.293	1552.7	7.137	14.0	71.4	71.5	-3.9	3.29	6970	1.81
70.0	0.304	1625.9	7.084	14.3	70.9	73.8	-4.7	3.46	6782	1.85
72.0	0.315	1701.6	7.029	14.6	70.3	76.0	-5.6	3.63	6604	1.88
74.0	0.326	1779.8	6.974	14.9	69.8	78.2	-7.0	3.81	6436	1.92
76.0	0.337	1860.5	6.918	15.2	69.2	80.5	-9.0	4.00	6276	1.95
78.0	0.349	1943.7	6.860	15.4	68.7	82.7	-12.3	4.19	6125	1.98
80.0	0.360	2029.4	6.802	15.7	68.2	84.9	-18.6	4.39	5983	2.01
82.0	0.372	2117.7	6.743	15.9	67.6	87.0	-33.9	4.60	5848	2.04
84.0	0.384	2208.3	6.683	16.1	67.1	86.2	-83.6	4.82	5720	2.07
86.0	0.397	2301.4	6.622	16.3	66.6	87.2	-139.3	5.04	5600	2.09
88.0	0.409	2396.8	6.561	16.5	66.1	85.2	-156.9	5.27	5487	2.12
90.0	0.422	2494.5	6.498	16.7	65.6	82.9	-163.7	5.51	5380	2.14

RADAR MAPPING PARAMETERS FOR ZERO DOPPLER AZIMUTH POINTING

ORBIT ECCENTRICITY = 0.3
SIDE-LOOK ANGLE = 10.0 DEGREES
SWATH WIDTH = 44.0 KM
WAVELENGTH = 10.0 CM

TRUE ANOMALY (DEG)	TIME (HR)	SLANT RANGE (KM)	ORBITAL VELOCITY (KM/S)	DOPPLER ANGLE (DEG)	GRAZING ANGLE (DEG)	LAT (DEG)	LONG (DEG)	RANGE APERTURE (METERS)	PRF (HZ)	AZIMUTH APERTURE (METERS)
0.0	-0.0	406.6	8.092	-0.0	79.3	0.0	-0.7	0.83	12013	1.19
2.0	0.008	407.5	8.091	0.5	79.3	2.0	-0.7	0.83	11999	1.19
4.0	0.015	410.3	8.088	0.9	79.3	4.1	-0.7	0.84	11958	1.20
6.0	0.023	415.0	8.084	1.4	79.2	6.1	-0.7	0.85	11891	1.20
8.0	0.031	421.6	8.078	1.8	79.1	8.1	-0.7	0.86	11797	1.21
10.0	0.039	430.0	8.070	2.3	79.0	10.2	-0.7	0.88	11681	1.22
12.0	0.047	440.4	8.060	2.8	78.9	12.2	-0.7	0.90	11542	1.24
14.0	0.054	452.6	8.049	3.2	78.7	14.2	-0.8	0.93	11385	1.25
16.0	0.062	466.8	8.036	3.7	78.6	16.3	-0.8	0.96	11210	1.27
18.0	0.070	482.9	8.021	4.1	78.4	18.3	-0.8	0.99	11021	1.29
20.0	0.078	500.9	8.005	4.6	78.1	20.4	-0.9	1.03	10820	1.31
22.0	0.086	520.9	7.986	5.0	77.9	22.4	-0.9	1.07	10610	1.33
24.0	0.094	542.9	7.967	5.5	77.6	24.5	-1.0	1.12	10392	1.36
26.0	0.102	566.8	7.945	5.9	77.4	26.5	-1.0	1.17	10169	1.38
28.0	0.110	592.8	7.922	6.4	77.1	28.6	-1.1	1.22	9942	1.41
30.0	0.118	620.7	7.897	6.8	76.8	30.7	-1.2	1.28	9714	1.44
32.0	0.127	650.8	7.870	7.2	76.4	32.8	-1.3	1.35	9486	1.47
34.0	0.135	682.9	7.842	7.7	76.1	34.8	-1.4	1.41	9259	1.50
36.0	0.143	717.1	7.813	8.1	75.7	36.9	-1.5	1.49	9034	1.53
38.0	0.152	753.5	7.781	8.5	75.4	39.0	-1.6	1.57	8811	1.56
40.0	0.161	792.0	7.748	8.9	75.0	41.1	-1.7	1.65	8593	1.60
42.0	0.169	832.7	7.714	9.3	74.6	43.2	-1.9	1.74	8379	1.63
44.0	0.178	875.6	7.678	9.7	74.2	45.4	-2.0	1.83	8170	1.66
46.0	0.187	920.8	7.641	10.1	73.8	47.5	-2.2	1.93	7966	1.70
48.0	0.196	968.2	7.602	10.5	73.4	49.6	-2.4	2.03	7768	1.73
50.0	0.205	1018.0	7.561	10.9	72.9	51.8	-2.7	2.14	7575	1.77
52.0	0.214	1070.1	7.519	11.3	72.5	53.9	-2.9	2.26	7388	1.80
54.0	0.223	1124.5	7.476	11.7	72.0	56.1	-3.2	2.38	7207	1.84
56.0	0.233	1181.3	7.432	12.0	71.6	58.2	-3.6	2.50	7031	1.87
58.0	0.243	1240.6	7.386	12.4	71.1	60.4	-4.0	2.64	6862	1.90
60.0	0.253	1302.3	7.338	12.7	70.6	62.6	-4.5	2.78	6698	1.94
62.0	0.263	1366.6	7.290	13.1	70.1	64.8	-5.2	2.92	6540	1.97
64.0	0.273	1433.3	7.240	13.4	69.6	67.0	-5.9	3.07	6388	2.00
66.0	0.283	1502.5	7.189	13.7	69.1	69.2	-6.8	3.23	6242	2.04
68.0	0.293	1574.3	7.137	14.0	68.6	71.4	-7.9	3.40	6101	2.07
70.0	0.304	1648.7	7.084	14.3	68.1	73.6	-9.4	3.57	5965	2.10
72.0	0.315	1725.6	7.029	14.6	67.6	75.8	-11.3	3.75	5835	2.13
74.0	0.326	1805.2	6.974	14.9	67.1	78.0	-14.0	3.94	5710	2.16
76.0	0.337	1887.3	6.918	15.2	66.6	80.2	-17.8	4.14	5589	2.19
78.0	0.349	1972.0	6.860	15.4	66.0	82.3	-23.9	4.34	5474	2.22
80.0	0.360	2059.3	6.802	15.7	65.5	84.2	-34.4	4.55	5364	2.24
82.0	0.372	2149.1	6.743	15.9	65.0	85.8	-54.0	4.77	5258	2.27
84.0	0.384	2241.5	6.683	16.1	64.5	86.4	-87.4	4.99	5158	2.29
86.0	0.397	2336.3	6.622	16.3	63.9	85.7	-120.3	5.23	5061	2.31
88.0	0.409	2433.6	6.561	16.5	63.4	84.1	-139.4	5.47	4970	2.34
90.0	0.422	2533.3	6.498	16.7	62.9	82.1	-149.6	5.72	4882	2.35

PADAR MAPPING PARAMETERS FOR ZERO DUPPLER AZIMUTH POINTING

ORBIT ECCENTRICITY = 0.3
SIDE-LOOK ANGLE = 15.0 DEGREES
SWATH WIDTH = 44.0 KM
WAVELENGTH = 10.0 CM

TRUE ANOMALY (DEG)	TIME (HR)	SLANT RANGE (KM)	ORBITAL VELOCITY (KM/S)	DOPPLER ANGLE (DEG)	GRAZING ANGLE (DEG)	LAT (DEG)	LONG (DEG)	RANGE APERTURE (METERS)	PRF (HZ)	AZIMUTH APERTURE (METERS)
0.0	-0.0	415.1	8.092	-0.0	74.0	0.0	-1.0	0.87	8060	1.78
2.0	0.008	416.1	8.091	0.5	74.0	2.0	-1.0	0.87	8055	1.78
4.0	0.015	418.9	8.088	0.9	73.9	4.1	-1.0	0.88	8042	1.78
6.0	0.023	423.7	8.084	1.4	73.9	6.1	-1.0	0.89	8019	1.78
8.0	0.031	430.4	8.078	1.8	73.8	8.1	-1.1	0.90	7988	1.79
10.0	0.039	439.1	8.070	2.3	73.8	10.2	-1.1	0.92	7949	1.80
12.0	0.047	449.6	8.060	2.8	73.7	12.2	-1.1	0.94	7901	1.80
14.0	0.054	462.1	8.049	3.2	73.5	14.2	-1.2	0.97	7846	1.81
16.0	0.062	476.6	8.036	3.7	73.4	16.3	-1.2	1.00	7733	1.83
18.0	0.070	493.1	8.021	4.1	73.2	18.3	-1.3	1.04	7714	1.84
20.0	0.078	511.5	8.005	4.6	73.1	20.4	-1.3	1.07	7638	1.85
22.0	0.086	531.9	7.986	5.0	72.9	22.4	-1.4	1.12	7557	1.87
24.0	0.094	554.4	7.967	5.5	72.7	24.5	-1.5	1.17	7470	1.89
26.0	0.102	578.8	7.945	5.9	72.5	26.5	-1.6	1.22	7379	1.90
28.0	0.110	605.4	7.922	6.4	72.2	28.6	-1.7	1.28	7284	1.92
30.0	0.118	634.0	7.897	6.8	72.0	30.7	-1.8	1.34	7185	1.94
32.0	0.127	664.8	7.870	7.2	71.7	32.8	-1.9	1.41	7083	1.97
34.0	0.135	697.6	7.842	7.7	71.4	34.8	-2.1	1.48	6979	1.99
36.0	0.143	732.6	7.813	8.1	71.1	36.9	-2.2	1.56	6872	2.01
38.0	0.152	769.8	7.781	8.5	70.8	39.0	-2.4	1.64	6765	2.03
40.0	0.161	809.2	7.748	8.9	70.5	41.1	-2.6	1.73	6656	2.06
42.0	0.169	850.9	7.714	9.3	70.1	43.2	-2.8	1.82	6546	2.08
44.0	0.178	894.9	7.678	9.7	69.8	45.3	-3.1	1.92	6436	2.11
46.0	0.187	941.1	7.641	10.1	69.4	47.5	-3.4	2.02	6326	2.14
48.0	0.196	989.7	7.602	10.5	69.0	49.6	-3.7	2.13	6216	2.16
50.0	0.205	1040.7	7.561	10.9	68.6	51.7	-4.1	2.25	6107	2.19
52.0	0.214	1094.1	7.519	11.3	68.2	53.9	-4.5	2.37	5999	2.22
54.0	0.224	1149.9	7.476	11.7	67.8	56.0	-5.0	2.50	5892	2.24
56.0	0.233	1208.2	7.432	12.0	67.4	58.2	-5.5	2.63	5786	2.27
58.0	0.243	1269.0	7.386	12.4	67.0	60.4	-6.2	2.77	5682	2.30
60.0	0.253	1332.3	7.338	12.7	66.5	62.5	-6.9	2.92	5579	2.33
62.0	0.263	1398.3	7.290	13.1	66.0	64.7	-7.8	3.08	5478	2.35
64.0	0.273	1466.8	7.240	13.4	65.6	66.9	-9.0	3.24	5379	2.38
66.0	0.283	1538.0	7.189	13.7	65.1	69.0	-10.3	3.41	5282	2.41
68.0	0.293	1611.8	7.137	14.0	64.6	71.2	-12.0	3.59	5187	2.43
70.0	0.304	1688.3	7.084	14.3	64.1	73.4	-14.2	3.77	5094	2.46
72.0	0.315	1767.5	7.029	14.6	63.6	75.5	-17.0	3.97	5004	2.48
74.0	0.326	1849.3	6.974	14.9	63.1	77.6	-20.9	4.17	4916	2.51
76.0	0.337	1933.9	6.918	15.2	62.6	79.6	-26.3	4.38	4830	2.53
78.0	0.349	2021.3	6.860	15.4	62.1	81.5	-34.4	4.60	4746	2.56
80.0	0.360	2111.3	6.802	15.7	61.5	83.1	-46.0	4.83	4666	2.58
82.0	0.372	2204.0	6.743	15.9	61.0	84.2	-65.1	5.07	4587	2.60
84.0	0.384	2299.4	6.683	16.1	60.5	84.6	-88.9	5.31	4511	2.62
86.0	0.397	2397.5	6.622	16.3	59.9	83.9	-111.4	5.57	4438	2.64
88.0	0.409	2498.1	6.561	16.5	59.4	82.5	-127.6	5.83	4368	2.66
90.0	0.422	2601.3	6.498	16.7	58.9	80.8	-138.2	6.11	4300	2.67

RADAR MAPPING PARAMETERS FOR ZERO DOPPLER AZIMUTH POINTING

ORBIT ECCENTRICITY = 0.3
SIDE-LOOK ANGLE = 20.0 DEGREES
SWATH WIDTH = 44.0 KM
WAVELENGTH = 10.0 CM

TRUE ANOMALY (DEG)	TIME (HR)	SLANT RANGE (KM)	ORBITAL VELOCITY (KP/S)	DOPPLER ANGLE (DEG)	GRAZING ANGLE (DEG)	LAT (DEG)	LONG (DEG)	RANGE APERTURE (METERS)	PRF (HZ)	AZIMUTH APERTURE (METERS)
0.0	-0.0	427.6	8.092	-0.0	68.6	0.0	-1.4	0.92	6099	2.35
2.0	0.008	428.5	8.091	0.5	68.6	2.0	-1.4	0.93	6097	2.35
4.0	0.015	431.5	8.088	0.9	68.6	4.1	-1.4	0.93	6090	2.35
6.0	0.023	436.4	8.084	1.4	68.5	6.1	-1.4	0.94	6080	2.35
8.0	0.031	443.4	8.078	1.8	68.5	8.1	-1.5	0.96	6065	2.36
10.0	0.039	452.3	8.070	2.3	68.4	10.2	-1.5	0.98	6045	2.36
12.0	0.047	463.2	8.060	2.8	68.3	12.2	-1.5	1.00	6022	2.37
14.0	0.054	476.1	8.049	3.2	68.2	14.2	-1.6	1.03	5995	2.38
16.0	0.062	491.0	8.036	3.7	68.1	16.3	-1.7	1.06	5964	2.38
18.0	0.070	508.0	8.021	4.1	68.0	18.3	-1.7	1.10	5929	2.39
20.0	0.078	527.0	8.005	4.6	67.8	20.4	-1.8	1.14	5890	2.40
22.0	0.086	548.1	7.986	5.0	67.7	22.4	-1.9	1.19	5849	2.42
24.0	0.094	571.3	7.967	5.5	67.5	24.5	-2.0	1.24	5904	2.43
26.0	0.102	596.5	7.945	5.9	67.3	26.5	-2.1	1.30	5756	2.44
28.0	0.110	623.9	7.922	6.4	67.1	28.6	-2.3	1.36	5706	2.46
30.0	0.118	653.5	7.897	6.8	66.8	30.7	-2.4	1.43	5653	2.47
32.0	0.127	685.3	7.870	7.2	66.6	32.7	-2.6	1.50	5597	2.49
34.0	0.135	719.2	7.842	7.7	66.3	34.8	-2.8	1.58	5540	2.50
36.0	0.143	755.4	7.813	8.1	66.1	36.9	-3.0	1.66	5480	2.52
38.0	0.152	793.9	7.781	8.5	65.8	39.0	-3.3	1.75	5419	2.54
40.0	0.161	834.6	7.748	8.9	65.5	41.1	-3.6	1.84	5356	2.56
42.0	0.169	877.7	7.714	9.3	65.2	43.2	-3.9	1.94	5292	2.58
44.0	0.178	923.2	7.678	9.7	64.8	45.3	-4.2	2.05	5227	2.60
46.0	0.187	971.1	7.641	10.1	64.5	47.4	-4.6	2.16	5161	2.62
48.0	0.196	1021.4	7.602	10.5	64.1	49.6	-5.0	2.28	5094	2.64
50.0	0.205	1074.2	7.561	10.9	63.7	51.7	-5.5	2.41	5026	2.66
52.0	0.214	1129.6	7.519	11.3	63.4	53.8	-6.1	2.54	4959	2.68
54.0	0.224	1187.5	7.476	11.7	63.0	56.0	-6.8	2.68	4890	2.70
56.0	0.233	1248.0	7.432	12.0	62.5	58.1	-7.5	2.83	4822	2.73
58.0	0.243	1311.1	7.386	12.4	62.1	60.2	-8.4	2.98	4754	2.75
60.0	0.253	1376.9	7.339	12.7	61.7	62.4	-9.5	3.14	4686	2.77
62.0	0.263	1445.4	7.290	13.1	61.2	64.5	-10.7	3.32	4618	2.79
64.0	0.273	1516.7	7.240	13.4	60.7	65.7	-12.2	3.49	4551	2.81
66.0	0.283	1590.7	7.189	13.7	60.3	66.8	-14.0	3.68	4485	2.84
68.0	0.293	1667.6	7.137	14.0	59.8	70.9	-16.3	3.88	4419	2.86
70.0	0.304	1747.3	7.084	14.3	59.3	73.0	-19.2	4.09	4353	2.88
72.0	0.315	1829.9	7.029	14.6	58.8	75.0	-22.9	4.30	4289	2.90
74.0	0.326	1915.4	6.974	14.9	58.2	77.0	-27.8	4.53	4225	2.92
76.0	0.337	2003.8	6.918	15.2	57.7	78.9	-34.4	4.76	4163	2.94
78.0	0.349	2095.2	6.860	15.4	57.2	80.4	-43.5	5.01	4102	2.96
80.0	0.360	2189.5	6.802	15.7	56.6	81.7	-56.0	5.27	4042	2.98
82.0	0.372	2286.7	6.743	15.9	56.1	82.5	-72.0	5.54	3983	2.99
84.0	0.384	2386.8	6.683	16.1	55.5	82.5	-89.9	5.82	3925	3.01
86.0	0.397	2489.8	6.622	16.3	54.9	81.9	-106.6	6.12	3869	3.03
88.0	0.409	2595.7	6.561	16.5	54.3	80.6	-119.8	6.42	3814	3.04
90.0	0.422	2704.5	6.498	16.7	53.8	79.0	-129.5	6.74	3761	3.06

RADAR MAPPING PARAMETERS FOR ZERO DOPPLER AZIMUTH POINTING

ORBIT ECCENTRICITY = 0.3
SIDE-LOOK ANGLE = 25.0 DEGREES
SWATH WIDTH = 44.0 KM
WAVELENGTH = 10.0 CM

TRUE ANOMALY (DEG)	TIME (HR)	SLANT RANGE (KM)	ORBITAL VELOCITY (KM/S)	DOPPLER ANGLE (DEG)	GRAZING ANGLE (DEG)	LAT (DEG)	LONG (DEG)	RANGE APERTURE (METERS)	PRF (HZ)	AZIMUTH APERTURE (METERS)
0.0	-0.0	444.6	8.092	-0.0	63.2	0.0	-1.8	1.00	4936	2.90
2.0	0.008	445.6	8.091	0.5	63.2	2.0	-1.8	1.00	4935	2.90
4.0	0.015	448.7	8.088	0.9	63.2	4.1	-1.8	1.01	4931	2.90
6.0	0.023	453.8	8.084	1.4	63.2	6.1	-1.8	1.02	4924	2.90
8.0	0.031	461.0	8.078	1.8	63.1	8.1	-1.9	1.04	4915	2.91
10.0	0.039	470.3	8.070	2.3	63.0	10.2	-1.9	1.06	4904	2.91
12.0	0.047	481.7	8.060	2.8	62.9	12.2	-2.0	1.09	4890	2.92
14.0	0.054	495.1	8.049	3.2	62.8	14.2	-2.0	1.12	4873	2.92
16.0	0.062	510.7	8.036	3.7	62.7	16.3	-2.1	1.16	4854	2.93
18.0	0.070	528.4	8.021	4.1	62.6	18.3	-2.2	1.20	4833	2.94
20.0	0.078	548.2	8.005	4.6	62.5	20.4	-2.3	1.24	4810	2.94
22.0	0.086	570.2	7.986	5.0	62.3	22.4	-2.5	1.29	4784	2.95
24.0	0.094	594.4	7.967	5.5	62.1	24.5	-2.6	1.35	4756	2.96
26.0	0.102	620.8	7.945	5.9	61.9	26.5	-2.8	1.41	4727	2.97
28.0	0.110	649.4	7.922	6.4	61.7	28.6	-2.9	1.48	4695	2.98
30.0	0.118	680.3	7.897	6.8	61.5	30.7	-3.1	1.56	4661	3.00
32.0	0.127	713.4	7.870	7.2	61.3	32.7	-3.4	1.64	4626	3.01
34.0	0.135	748.9	7.842	7.7	61.0	34.8	-3.6	1.72	4589	3.02
36.0	0.143	786.7	7.813	8.1	60.7	36.9	-3.9	1.81	4551	3.04
38.0	0.152	827.0	7.781	8.5	60.5	39.0	-4.2	1.91	4511	3.05
40.0	0.161	869.6	7.748	8.9	60.2	41.1	-4.6	2.02	4470	3.07
42.0	0.169	914.7	7.714	9.3	59.9	43.2	-5.0	2.13	4428	3.08
44.0	0.178	962.4	7.678	9.7	59.5	45.3	-5.4	2.24	4385	3.10
46.0	0.187	1012.5	7.641	10.1	59.2	47.4	-5.9	2.37	4340	3.11
48.0	0.196	1065.3	7.602	10.5	58.8	49.5	-6.5	2.50	4295	3.13
50.0	0.205	1120.7	7.561	10.9	58.4	51.6	-7.1	2.64	4249	3.15
52.0	0.214	1178.8	7.519	11.3	58.0	53.7	-7.9	2.79	4202	3.16
54.0	0.224	1239.6	7.476	11.7	57.6	55.9	-8.7	2.95	4155	3.18
56.0	0.233	1303.2	7.432	12.0	57.2	58.0	-9.7	3.12	4107	3.20
58.0	0.243	1369.6	7.386	12.4	56.8	60.1	-10.8	3.29	4059	3.22
60.0	0.253	1439.0	7.338	12.7	56.3	62.2	-12.2	3.48	4011	3.24
62.0	0.263	1511.2	7.290	13.1	55.9	64.3	-13.8	3.67	3962	3.25
64.0	0.273	1586.4	7.240	13.4	55.4	66.4	-15.7	3.88	3914	3.27
66.0	0.283	1664.6	7.189	13.7	54.9	68.5	-18.0	4.09	3865	3.29
68.0	0.293	1745.9	7.137	14.0	54.4	70.5	-20.9	4.32	3816	3.31
70.0	0.304	1830.4	7.084	14.3	53.8	72.5	-24.4	4.56	3768	3.33
72.0	0.315	1917.9	7.029	14.6	53.3	74.4	-28.9	4.81	3720	3.34
74.0	0.326	2008.7	6.974	14.9	52.7	76.1	-34.7	5.07	3672	3.36
76.0	0.337	2102.7	6.918	15.2	52.2	77.7	-42.1	5.35	3624	3.38
78.0	0.349	2200.0	6.860	15.4	51.6	79.0	-51.5	5.65	3577	3.39
80.0	0.360	2300.6	6.802	15.7	51.0	80.0	-63.3	5.95	3531	3.41
82.0	0.372	2404.5	6.743	15.9	50.4	80.4	-76.8	6.28	3485	3.42
84.0	0.384	2511.7	6.683	16.1	49.7	80.2	-90.8	6.62	3440	3.44
86.0	0.397	2622.2	6.622	16.3	49.1	79.5	-103.6	6.98	3395	3.45
88.0	0.409	2736.1	6.561	16.5	48.4	78.3	-114.3	7.35	3352	3.46
90.0	0.422	2853.2	6.498	16.7	47.8	76.8	-122.8	7.75	3309	3.47

RADAR MAPPING PARAMETERS FOR ZERO DOPPLER AZIMUTH POINTING

ORBIT ECCENTRICITY = 0.3
SIDE-LOOK ANGLE = 30.0 DEGREES
SWATH WIDTH = 44.0 KM
WAVELENGTH = 10.0 CM

TRUE ANOMALY (DEG)	TIME (HR)	SLANT RANGE (KM)	ORBITAL VELOCITY (KM/S)	DOPPLER ANGLE (DEG)	GRAZING ANGLE (DEG)	LAT (DEG)	LONG (DEG)	RANGE APERTURE (METERS)	PRF (HZ)	AZIMUTH APERTURE (METERS)
0.0	-0.0	467.1	8.092	-0.0	57.8	0.0	-2.2	1.11	4172	3.43
2.0	0.008	468.2	8.091	0.5	57.8	2.0	-2.2	1.11	4171	3.43
4.0	0.015	471.4	8.088	0.9	57.8	4.1	-2.2	1.12	4168	3.43
6.0	0.023	476.8	8.084	1.4	57.7	6.1	-2.3	1.13	4164	3.43
8.0	0.031	484.4	8.078	1.8	57.7	8.1	-2.3	1.15	4158	3.44
10.0	0.039	494.2	8.070	2.3	57.6	10.2	-2.4	1.18	4150	3.44
12.0	0.047	506.2	8.060	2.8	57.5	12.2	-2.5	1.21	4140	3.44
14.0	0.054	520.4	8.049	3.2	57.4	14.2	-2.5	1.24	4129	3.45
16.0	0.062	536.8	8.036	3.7	57.3	16.3	-2.6	1.28	4116	3.45
18.0	0.070	555.5	8.021	4.1	57.2	18.3	-2.8	1.33	4101	3.46
20.0	0.078	576.4	8.005	4.6	57.0	20.4	-2.9	1.38	4085	3.47
22.0	0.086	599.6	7.986	5.0	56.8	22.4	-3.1	1.44	4067	3.47
24.0	0.094	625.2	7.967	5.5	56.7	24.5	-3.2	1.50	4047	3.48
26.0	0.102	653.0	7.945	5.9	56.5	26.5	-3.4	1.57	4027	3.49
28.0	0.110	683.3	7.922	6.4	56.3	28.6	-3.7	1.65	4004	3.50
30.0	0.118	715.9	7.897	6.8	56.0	30.6	-3.9	1.74	3981	3.51
32.0	0.127	751.0	7.870	7.2	55.8	32.7	-4.2	1.83	3956	3.52
34.0	0.135	788.5	7.842	7.7	55.5	34.8	-4.5	1.92	3929	3.53
36.0	0.143	828.6	7.813	8.1	55.3	36.9	-4.9	2.03	3902	3.54
38.0	0.152	871.2	7.781	8.5	55.0	38.9	-5.3	2.14	3873	3.55
40.0	0.161	916.4	7.748	8.9	54.6	41.0	-5.7	2.26	3844	3.57
42.0	0.169	964.3	7.714	9.3	54.3	43.1	-6.2	2.39	3813	3.58
44.0	0.178	1014.9	7.678	9.7	54.0	45.2	-6.8	2.52	3781	3.59
46.0	0.187	1068.2	7.641	10.1	53.6	47.3	-7.4	2.67	3749	3.61
48.0	0.196	1124.3	7.602	10.5	53.2	49.4	-8.1	2.82	3715	3.62
50.0	0.205	1183.3	7.561	10.9	52.8	51.5	-8.9	2.98	3681	3.63
52.0	0.214	1245.3	7.519	11.3	52.4	53.6	-9.8	3.16	3646	3.65
54.0	0.224	1310.2	7.476	11.7	52.0	55.7	-10.9	3.34	3611	3.66
56.0	0.233	1378.1	7.432	12.0	51.5	57.8	-12.1	3.54	3575	3.68
58.0	0.243	1449.2	7.386	12.4	51.1	59.9	-13.6	3.75	3539	3.69
60.0	0.253	1523.4	7.338	12.7	50.6	62.0	-15.2	3.96	3502	3.71
62.0	0.263	1600.9	7.290	13.1	50.1	64.0	-17.2	4.20	3465	3.72
64.0	0.273	1681.8	7.240	13.4	49.5	66.0	-19.6	4.44	3427	3.74
66.0	0.283	1766.0	7.189	13.7	49.0	68.0	-22.4	4.70	3389	3.75
68.0	0.293	1853.7	7.137	14.0	48.4	69.9	-25.8	4.98	3352	3.77
70.0	0.304	1944.9	7.084	14.3	47.8	71.7	-30.0	5.27	3314	3.78
72.0	0.315	2039.7	7.029	14.6	47.2	73.4	-35.2	5.58	3276	3.80
74.0	0.326	2138.2	6.974	14.9	46.6	75.0	-41.6	5.91	3238	3.81
76.0	0.337	2240.5	6.918	15.2	46.0	76.3	-49.3	6.26	3200	3.82
78.0	0.349	2346.6	6.860	15.4	45.3	77.2	-58.6	6.64	3162	3.84
80.0	0.360	2456.5	6.802	15.7	44.6	77.8	-69.2	7.03	3125	3.85
82.0	0.372	2570.5	6.743	15.9	43.9	77.9	-80.5	7.45	3087	3.86
84.0	0.384	2688.4	6.683	16.1	43.2	77.5	-91.6	7.90	3050	3.87
86.0	0.397	2810.5	6.622	16.3	42.5	76.7	-101.7	8.37	3014	3.89
88.0	0.409	2936.7	6.561	16.5	41.7	75.5	-110.3	8.88	2978	3.90
90.0	0.422	3067.1	6.498	16.7	40.9	73.9	-117.5	9.42	2942	3.91

Table IV-12 Radar Mapping Parameters for

Zero Doppler Azimuth Pointing

e = 0.5

RADAR MAPPING PARAMETERS FOR ZERO DOPPLER AZIMUTH POINTING

ORBIT ECCENTRICITY = 0.5
SIDE-LOOK ANGLE = 5.0 DEGREES
SWATH WIDTH = 36.0 KM
WAVELENGTH = 10.0 CM

TRUE ANOMALY (DEG)	TIME (HR)	SLANT RANGE (KM)	ORBITAL VELOCITY (KM/S)	DOPPLER ANGLE (DEG)	GRAZING ANGLE (DEG)	LAT (DEG)	LONG (DEG)	RANGE APERTURE (METERS)	PRF (HZ)	AZIMUTH APERTURE (METERS)
0.0	-0.0	401.6	8.692	-0.0	84.7	0.0	-0.3	0.99	29254	0.53
2.0	0.007	403.0	8.691	0.7	84.6	2.0	-0.3	0.99	28995	0.53
4.0	0.014	407.0	8.687	1.3	84.5	4.1	-0.3	1.00	28256	0.54
6.0	0.022	413.7	8.681	2.0	84.3	6.1	-0.3	1.02	27138	0.57
8.0	0.029	423.2	8.673	2.7	83.9	8.2	-0.4	1.05	25771	0.60
10.0	0.036	435.4	8.663	3.3	83.6	10.2	-0.4	1.08	24276	0.63
12.0	0.043	450.3	8.650	4.0	83.1	12.3	-0.4	1.11	22755	0.67
14.0	0.051	468.1	8.634	4.7	82.7	14.4	-0.4	1.16	21270	0.72
16.0	0.058	488.6	8.617	5.3	82.1	16.4	-0.4	1.21	19861	0.77
18.0	0.065	512.1	8.597	6.0	81.6	18.5	-0.4	1.27	18551	0.82
20.0	0.073	538.4	8.575	6.6	81.0	20.6	-0.5	1.34	17344	0.87
22.0	0.080	567.6	8.550	7.3	80.4	22.7	-0.5	1.41	16239	0.93
24.0	0.088	600.2	8.523	7.9	79.7	24.8	-0.5	1.50	15232	0.99
26.0	0.096	635.7	8.494	8.6	79.1	26.9	-0.6	1.59	14315	1.05
28.0	0.103	674.4	8.463	9.2	78.4	29.0	-0.6	1.69	13479	1.11
30.0	0.111	716.3	8.429	9.9	77.7	31.2	-0.7	1.80	12716	1.17
32.0	0.119	761.7	8.393	10.5	76.9	33.3	-0.7	1.92	12019	1.24
34.0	0.127	810.5	8.355	11.2	76.2	35.5	-0.8	2.05	11380	1.30
36.0	0.135	862.9	8.315	11.8	75.4	37.7	-0.9	2.19	10793	1.36
38.0	0.144	919.0	8.272	12.5	74.6	39.9	-1.0	2.34	10253	1.43
40.0	0.152	979.0	8.228	13.1	73.8	42.1	-1.1	2.50	9755	1.49
42.0	0.161	1043.0	8.181	13.7	73.0	44.3	-1.2	2.68	9293	1.56
44.0	0.169	1111.0	8.132	14.3	72.1	46.6	-1.3	2.87	8866	1.62
46.0	0.178	1183.4	8.081	14.9	71.3	48.9	-1.4	3.07	8468	1.69
48.0	0.187	1260.3	8.027	15.6	70.4	51.2	-1.6	3.29	8097	1.75
50.0	0.196	1341.9	7.972	16.2	69.5	53.5	-1.8	3.52	7751	1.82
52.0	0.206	1428.4	7.915	16.8	68.5	55.9	-2.0	3.77	7427	1.89
54.0	0.215	1519.9	7.855	17.4	67.6	58.3	-2.3	4.04	7123	1.95
56.0	0.225	1616.9	7.794	17.9	66.6	60.7	-2.6	4.33	6837	2.02
58.0	0.235	1719.4	7.731	18.5	65.6	63.1	-3.0	4.64	6568	2.08
60.0	0.245	1827.9	7.666	19.1	64.5	65.6	-3.5	4.98	6315	2.15
62.0	0.256	1942.6	7.598	19.7	63.4	68.1	-4.1	5.34	6076	2.21
64.0	0.267	2063.8	7.529	20.2	62.3	70.7	-4.8	5.73	5849	2.28
66.0	0.278	2192.0	7.458	20.8	61.2	73.3	-5.9	6.15	5635	2.34
68.0	0.289	2327.4	7.386	21.3	60.0	75.9	-7.4	6.60	5432	2.40
70.0	0.301	2470.5	7.311	21.9	58.8	78.6	-9.6	7.10	5239	2.47
72.0	0.313	2621.8	7.235	22.4	57.5	81.2	-13.3	7.64	5056	2.53
74.0	0.325	2781.8	7.157	22.9	56.2	83.9	-20.3	8.23	4882	2.59
76.0	0.338	2951.0	7.078	23.4	54.8	86.4	-38.1	8.87	4717	2.65
78.0	0.351	3130.1	6.997	23.9	53.4	87.6	-91.6	9.56	4559	2.71
80.0	0.364	3319.5	6.914	24.4	51.9	86.1	-140.7	10.36	4409	2.77
82.0	0.376	3520.2	6.830	24.8	50.4	83.3	-156.0	11.22	4266	2.83
84.0	0.392	3732.9	6.744	25.3	48.8	80.3	-163.1	12.18	4129	2.89
86.0	0.407	3958.6	6.657	25.7	47.2	77.2	-166.6	13.26	3998	2.94
88.0	0.423	4198.1	6.568	26.2	45.4	73.9	-168.7	14.48	3874	3.00
90.0	0.439	4452.8	6.479	26.6	43.6	70.5	-170.1	15.86	3755	3.05

RADAR MAPPING PARAMETERS FOR ZERO DOPPLER AZIMUTH POINTING

ORBIT ECCENTRICITY = 0.5
SIDE-LOOK ANGLE = 10.0 DEGREES
SWATH WIDTH = 36.0 KM
WAVELENGTH = 10.0 CM

TRUE ANOMALY (DEG)	TIME (HR)	SLANT RANGE (KM)	ORBITAL VELOCITY (KM/S)	DOPPLER ANGLE (DEG)	GRAZING ANGLE (DEG)	LAT (DEG)	LONG (DEG)	RANGE APERTURE (METERS)	PRF (HZ)	AZIMUTH APERTURE (METERS)
0.0	-0.0	406.6	8.692	-0.0	79.3	0.0	-0.7	1.02	14683	1.05
2.0	0.007	408.0	8.691	0.7	79.3	2.0	-0.7	1.02	14649	1.05
4.0	0.014	412.0	8.687	1.3	79.2	4.1	-0.7	1.03	14548	1.06
6.0	0.022	418.9	8.681	2.0	79.1	6.1	-0.7	1.05	14385	1.07
8.0	0.029	428.4	8.673	2.7	78.9	8.2	-0.7	1.07	14165	1.08
10.0	0.036	440.8	8.663	3.3	78.7	10.2	-0.7	1.10	13895	1.10
12.0	0.043	455.9	8.650	4.0	78.5	12.3	-0.8	1.14	13584	1.13
14.0	0.051	473.9	8.634	4.7	78.2	14.4	-0.8	1.19	13240	1.15
16.0	0.058	494.7	8.617	5.3	77.8	16.4	-0.8	1.24	12871	1.18
18.0	0.065	518.4	8.597	6.0	77.4	18.5	-0.9	1.31	12485	1.22
20.0	0.073	545.1	8.575	6.6	77.0	20.6	-1.0	1.37	12087	1.25
22.0	0.080	574.9	8.550	7.3	76.5	22.7	-1.0	1.45	11686	1.29
24.0	0.088	607.7	8.523	7.9	76.1	24.8	-1.1	1.54	11285	1.34
26.0	0.096	643.6	8.494	8.6	75.5	26.9	-1.2	1.63	10888	1.38
28.0	0.103	682.8	8.463	9.2	75.0	29.0	-1.3	1.74	10498	1.43
30.0	0.111	725.4	8.429	9.9	74.4	31.2	-1.4	1.85	10117	1.47
32.0	0.119	771.3	8.393	10.5	73.8	33.3	-1.5	1.97	9748	1.52
34.0	0.127	820.8	8.355	11.2	73.2	35.5	-1.6	2.11	9390	1.57
36.0	0.135	873.9	8.315	11.8	72.5	37.7	-1.8	2.25	9045	1.63
38.0	0.144	930.8	8.272	12.5	71.8	39.9	-1.9	2.41	8713	1.68
40.0	0.152	991.6	8.228	13.1	71.1	42.1	-2.1	2.58	8395	1.73
42.0	0.161	1056.4	8.181	13.7	70.4	44.3	-2.4	2.76	8069	1.79
44.0	0.169	1125.5	8.132	14.3	69.6	46.6	-2.5	2.95	7796	1.85
46.0	0.178	1198.9	8.081	14.9	68.8	48.9	-2.9	3.16	7516	1.90
48.0	0.187	1276.9	8.027	15.6	68.0	51.2	-3.2	3.38	7247	1.96
50.0	0.196	1359.7	7.972	16.2	67.1	53.5	-3.6	3.63	6991	2.02
52.0	0.206	1447.5	7.915	16.5	66.2	55.8	-4.1	3.89	6745	2.08
54.0	0.215	1540.4	7.855	17.4	65.3	58.2	-4.6	4.17	6510	2.13
56.0	0.225	1638.9	7.794	17.9	64.4	60.6	-5.2	4.47	6285	2.19
58.0	0.235	1743.1	7.731	18.5	63.4	63.1	-6.0	4.79	6070	2.25
60.0	0.245	1853.3	7.666	19.1	62.4	65.5	-7.0	5.14	5864	2.31
62.0	0.256	1969.9	7.598	19.7	61.3	68.0	-8.2	5.52	5667	2.37
64.0	0.267	2093.2	7.529	20.2	60.3	70.5	-9.8	5.92	5479	2.43
66.0	0.278	2223.5	7.458	20.8	59.1	73.1	-11.8	6.36	5298	2.49
68.0	0.289	2361.4	7.386	21.3	58.0	75.6	-14.8	6.84	5124	2.55
70.0	0.301	2507.3	7.311	21.9	56.8	78.1	-19.0	7.37	4958	2.61
72.0	0.313	2661.5	7.235	22.4	55.5	80.6	-25.8	7.93	4799	2.67
74.0	0.325	2824.7	7.157	22.9	54.2	82.9	-37.4	8.56	4647	2.72
76.0	0.338	2997.5	7.078	23.4	52.8	84.7	-58.7	9.24	4500	2.78
78.0	0.351	3180.5	6.997	23.9	51.4	85.2	-92.1	9.99	4360	2.84
80.0	0.364	3374.4	6.914	24.4	50.0	84.0	-122.1	10.83	4225	2.89
82.0	0.378	3580.0	6.830	24.8	48.4	81.8	-139.3	11.76	4095	2.95
84.0	0.392	3798.3	6.744	25.3	46.8	79.0	-148.8	12.80	3971	3.00
86.0	0.407	4030.2	6.657	25.7	45.1	76.0	-154.4	13.97	3852	3.06
88.0	0.423	4277.0	6.568	26.2	43.4	72.8	-158.1	15.31	3738	3.11
90.0	0.439	4539.9	6.479	26.6	41.5	69.4	-160.6	16.84	3628	3.16

RADAR MAPPING PARAMETERS FOR ZERO DOPPLER AZIMUTH POINTING

ORBIT ECCENTRICITY = 0.5
SIDE-LOOK ANGLE = 15.0 DEGREES
SWATH WIDTH = 36.0 KM
WAVELENGTH = 10.0 CM

TRUE ANOMALY (DEG)	TIME (HR)	SLANT RANGE (KM)	ORBITAL VELOCITY (KM/S)	DOPPLER ANGLE (DEG)	GRAZING ANGLE (DEG)	LAT (DEG)	LONG (DEG)	RANGE APERTURE (METERS)	PRF (HZ)	AZIMUTH APERTURE (METERS)
0.0	-0.0	415.1	8.692	-0.0	74.0	0.0	-1.0	1.06	9851	1.56
2.0	0.007	416.5	8.691	0.7	74.0	2.0	-1.0	1.06	9840	1.56
4.0	0.014	420.7	8.687	1.3	73.9	4.1	-1.0	1.08	9809	1.57
6.0	0.022	427.6	8.681	2.0	73.8	6.1	-1.1	1.09	9756	1.57
8.0	0.029	437.4	8.673	2.7	73.7	8.2	-1.1	1.12	9684	1.58
10.0	0.036	450.0	8.663	3.3	73.5	10.2	-1.1	1.15	9593	1.60
12.0	0.043	465.5	8.650	4.0	73.3	12.3	-1.2	1.19	9485	1.61
14.0	0.051	483.8	8.634	4.7	73.1	14.4	-1.2	1.24	9361	1.63
16.0	0.058	505.1	8.617	5.3	72.9	16.4	-1.3	1.30	9222	1.65
18.0	0.065	529.4	8.597	6.0	72.6	18.5	-1.4	1.36	9072	1.68
20.0	0.073	556.7	8.575	6.6	72.2	20.6	-1.4	1.44	8910	1.70
22.0	0.080	587.0	8.550	7.3	71.9	22.7	-1.5	1.52	8739	1.73
24.0	0.088	620.6	8.523	7.9	71.5	24.8	-1.7	1.61	8561	1.76
26.0	0.096	657.3	8.494	8.6	71.1	26.9	-1.8	1.71	8378	1.79
28.0	0.103	697.4	8.463	9.2	70.6	29.0	-1.9	1.82	8189	1.83
30.0	0.111	740.9	8.429	9.9	70.1	31.1	-2.1	1.94	7998	1.86
32.0	0.119	787.9	8.393	10.5	69.6	33.3	-2.3	2.07	7805	1.90
34.0	0.127	838.5	8.355	11.2	69.1	35.5	-2.5	2.21	7611	1.94
36.0	0.135	892.9	8.315	11.8	68.5	37.6	-2.7	2.36	7417	1.98
38.0	0.144	951.1	8.272	12.5	67.9	39.8	-3.0	2.52	7224	2.03
40.0	0.152	1013.3	8.228	13.1	67.3	42.1	-3.3	2.70	7032	2.07
42.0	0.161	1079.7	8.181	13.7	66.6	44.3	-3.6	2.89	6843	2.11
44.0	0.169	1150.5	8.132	14.3	65.9	46.5	-4.0	3.10	6657	2.16
46.0	0.178	1225.7	8.081	14.9	65.2	48.8	-4.4	3.32	6473	2.21
48.0	0.187	1305.6	8.027	15.6	64.4	51.1	-4.9	3.56	6293	2.26
50.0	0.196	1390.5	7.972	16.2	63.6	53.4	-5.5	3.81	6117	2.31
52.0	0.206	1480.5	7.915	16.8	62.8	55.8	-6.2	4.09	5945	2.36
54.0	0.215	1576.0	7.855	17.4	61.9	58.1	-7.0	4.39	5776	2.41
56.0	0.225	1677.0	7.794	17.9	61.0	60.5	-8.0	4.71	5612	2.46
58.0	0.235	1784.1	7.731	18.5	60.1	62.9	-9.2	5.06	5452	2.51
60.0	0.245	1897.4	7.666	19.1	59.1	65.4	-10.6	5.43	5296	2.56
62.0	0.256	2017.4	7.598	19.7	58.1	67.8	-12.5	5.84	5145	2.61
64.0	0.267	2144.4	7.529	20.2	57.0	70.2	-14.8	6.28	4997	2.67
66.0	0.278	2278.8	7.458	20.8	55.9	72.7	-17.9	6.76	4854	2.72
68.0	0.289	2421.1	7.386	21.3	54.8	75.1	-22.1	7.28	4715	2.77
70.0	0.301	2571.7	7.311	21.9	53.6	77.4	-28.1	7.85	4580	2.82
72.0	0.313	2731.2	7.235	22.4	52.3	79.6	-37.0	8.48	4450	2.88
74.0	0.325	2900.3	7.157	22.9	51.0	81.4	-50.4	9.16	4323	2.93
76.0	0.338	3079.6	7.078	23.4	49.7	82.6	-69.7	9.93	4200	2.98
78.0	0.351	3269.8	6.997	23.9	48.2	82.6	-92.9	10.77	4081	3.03
80.0	0.364	3471.8	6.914	24.4	46.7	81.5	-113.5	11.71	3966	3.08
82.0	0.378	3686.6	6.830	24.8	45.2	79.5	-128.1	12.77	3854	3.13
84.0	0.392	3915.2	6.744	25.3	43.5	76.9	-137.8	13.98	3747	3.18
86.0	0.407	4159.1	6.657	25.7	41.7	74.0	-144.2	15.35	3642	3.23
88.0	0.423	4419.6	6.568	26.2	39.9	70.8	-148.6	16.94	3542	3.28
90.0	0.439	4698.6	6.479	26.6	37.9	67.5	-151.8	18.79	3445	3.33

RADAR MAPPING PARAMETERS FOR ZERO DOPPLER AZIMUTH POINTING

ORBIT ECCENTRICITY = 0.5
SIDE-LOOK ANGLE = 20.0 DEGREES
SWATH WIDTH = 36.0 KM
WAVELENGTH = 10.0 CM

TRUE ANOMALY (DEG)	TIME (HR)	SLANT RANGE (KM)	ORBITAL VELOCITY (KM/S)	DOPPLER ANGLE (DEG)	GRAZING ANGLE (DEG)	LAT (DEG)	LONG (DEG)	RANGE APERTURE (METERS)	PRF (HZ)	AZIMUTH APERTURE (METERS)
0.0	-0.0	427.6	8.692	-0.0	68.6	0.0	-1.4	1.13	7455	2.06
2.0	0.007	429.0	8.691	0.7	68.6	2.0	-1.4	1.13	7450	2.06
4.0	0.014	433.3	8.687	1.3	68.6	4.1	-1.4	1.14	7435	2.07
6.0	0.022	440.5	8.681	2.0	68.5	6.1	-1.4	1.16	7411	2.07
8.0	0.029	450.6	8.673	2.7	68.4	8.2	-1.5	1.19	7377	2.08
10.0	0.036	463.6	8.663	3.3	68.2	10.2	-1.5	1.23	7335	2.09
12.0	0.043	479.5	8.650	4.0	68.1	12.3	-1.6	1.27	7283	2.10
14.0	0.051	498.4	8.634	4.7	67.9	14.4	-1.7	1.32	7224	2.11
16.0	0.058	520.4	8.617	5.3	67.7	16.4	-1.8	1.38	7156	2.13
18.0	0.065	545.4	8.597	6.0	67.4	18.5	-1.9	1.45	7081	2.15
20.0	0.073	573.6	8.575	6.6	67.1	20.6	-2.0	1.53	6999	2.17
22.0	0.080	604.9	8.550	7.3	66.8	22.7	-2.1	1.62	6911	2.19
24.0	0.088	639.5	8.523	7.9	66.5	24.8	-2.3	1.71	6817	2.21
26.0	0.096	677.5	8.494	8.6	66.1	26.9	-2.4	1.82	6719	2.24
28.0	0.103	718.9	8.463	9.2	65.7	29.0	-2.6	1.94	6615	2.26
30.0	0.111	763.8	8.429	9.9	65.3	31.1	-2.9	2.07	6508	2.29
32.0	0.119	812.3	8.393	10.5	64.9	33.3	-3.1	2.20	6397	2.32
34.0	0.127	864.6	8.355	11.2	64.4	35.5	-3.4	2.36	6283	2.35
36.0	0.135	920.8	8.315	11.8	63.8	37.6	-3.7	2.52	6167	2.38
38.0	0.144	981.0	8.272	12.5	63.3	39.8	-4.1	2.70	6049	2.42
40.0	0.152	1045.4	8.228	13.1	62.7	42.0	-4.5	2.89	5930	2.45
42.0	0.161	1114.1	8.181	13.7	62.1	44.3	-4.9	3.10	5809	2.49
44.0	0.169	1187.4	8.132	14.3	61.5	46.5	-5.4	3.32	5688	2.53
46.0	0.178	1265.3	8.081	14.9	60.6	48.8	-6.0	3.56	5566	2.57
48.0	0.187	1348.2	8.027	15.6	60.1	51.0	-6.7	3.82	5445	2.61
50.0	0.196	1436.3	7.972	16.2	59.3	53.4	-7.5	4.10	5324	2.65
52.0	0.206	1529.8	7.915	16.8	58.5	55.7	-8.5	4.41	5203	2.69
54.0	0.215	1628.9	7.855	17.4	57.7	58.0	-9.6	4.74	5084	2.73
56.0	0.225	1734.0	7.794	17.9	56.8	60.4	-10.9	5.09	4965	2.78
58.0	0.235	1845.5	7.731	18.5	55.9	62.7	-12.5	5.48	4848	2.82
60.0	0.245	1963.6	7.666	19.1	54.9	65.1	-14.5	5.89	4732	2.87
62.0	0.256	2088.8	7.598	19.7	53.9	67.5	-17.0	6.35	4618	2.91
64.0	0.267	2221.5	7.529	20.2	52.9	69.8	-20.1	6.84	4505	2.96
66.0	0.278	2362.1	7.458	20.8	51.8	72.1	-24.2	7.39	4394	3.00
68.0	0.289	2511.3	7.386	21.3	50.6	74.3	-29.6	7.98	4285	3.05
70.0	0.301	2669.5	7.311	21.9	49.4	76.4	-36.9	8.64	4179	3.09
72.0	0.313	2837.5	7.235	22.4	48.1	78.2	-46.9	9.36	4074	3.14
74.0	0.325	3015.9	7.157	22.9	46.8	79.5	-60.2	10.16	3971	3.19
76.0	0.338	3205.7	7.078	23.4	45.4	80.1	-76.6	11.06	3871	3.23
78.0	0.351	3407.7	6.997	23.9	43.9	79.7	-93.9	12.07	3772	3.28
80.0	0.364	3623.0	6.914	24.4	42.3	78.5	-109.1	13.22	3676	3.33
82.0	0.378	3853.1	6.830	24.8	40.7	76.5	-121.0	14.53	3583	3.37
84.0	0.392	4099.3	6.744	25.3	38.9	74.0	-129.6	16.05	3491	3.42
86.0	0.407	4363.7	6.657	25.7	37.0	71.2	-135.9	17.82	3402	3.46
88.0	0.423	4648.4	6.568	26.2	34.9	68.0	-140.5	19.94	3316	3.50
90.0	0.439	4956.6	6.479	26.6	32.7	64.5	-143.9	22.52	3231	3.55

RADAR MAPPING PARAMETERS FOR ZERO DOPPLER AZIMUTH POINTING

ORBIT ECCENTRICITY = 0.5
SIDE-LOOK ANGLE = 25.0 DEGREES
SWATH WIDTH = 36.0 KM
WAVELENGTH = 10.0 CM

TRUE ANOMALY (DEG)	TIME (HR)	SLANT RANGE (KM)	ORBITAL VELOCITY (KM/S)	DOPPLER ANGLE (DEG)	GRAZING ANGLE (DEG)	LAT (DEG)	LONG (DEG)	RANGE APERTURE (METERS)	PRF (HZ)	AZIMUTH APERTURE (METERS)
0.0	-0.0	444.6	8.692	-0.0	63.2	0.0	-1.8	1.22	6033	2.55
2.0	0.007	446.1	8.691	0.7	63.2	2.0	-1.8	1.23	6030	2.55
4.0	0.014	450.5	8.687	1.3	63.2	4.1	-1.8	1.24	6022	2.55
6.0	0.022	458.0	8.681	2.0	63.1	6.1	-1.8	1.26	6008	2.56
8.0	0.029	468.5	8.673	2.7	63.0	8.2	-1.9	1.29	5989	2.56
10.0	0.036	482.1	8.663	3.3	62.9	10.2	-2.0	1.33	5964	2.57
12.0	0.043	498.7	8.650	4.0	62.7	12.3	-2.0	1.38	5935	2.58
14.0	0.051	516.4	8.634	4.7	62.6	14.4	-2.1	1.44	5900	2.59
16.0	0.058	541.3	8.617	5.3	62.4	16.4	-2.3	1.50	5860	2.60
18.0	0.065	567.4	8.597	6.0	62.1	18.5	-2.4	1.58	5816	2.61
20.0	0.073	596.7	8.575	6.6	61.9	20.6	-2.5	1.66	5767	2.63
22.0	0.080	629.4	8.550	7.3	61.6	22.7	-2.7	1.76	5715	2.65
24.0	0.088	665.5	8.523	7.9	61.3	24.8	-2.9	1.86	5658	2.66
26.0	0.096	705.1	8.494	8.6	60.9	26.9	-3.1	1.98	5597	2.68
28.0	0.103	748.3	8.463	9.2	60.6	29.0	-3.4	2.11	5533	2.71
30.0	0.111	795.3	8.429	9.9	60.2	31.1	-3.7	2.25	5465	2.73
32.0	0.119	846.0	8.393	10.5	59.7	33.3	-4.0	2.41	5394	2.75
34.0	0.127	900.7	8.355	11.2	59.3	35.4	-4.4	2.57	5321	2.78
36.0	0.135	959.4	8.315	11.8	58.8	37.6	-4.8	2.76	5245	2.80
38.0	0.144	1022.4	8.272	12.5	58.3	39.8	-5.2	2.95	5167	2.83
40.0	0.152	1089.9	8.228	13.1	57.7	42.0	-5.8	3.17	5088	2.86
42.0	0.161	1161.9	8.181	13.7	57.1	44.2	-6.3	3.40	5006	2.89
44.0	0.169	1238.7	8.132	14.3	56.5	46.4	-7.0	3.65	4923	2.92
46.0	0.178	1320.5	8.081	14.9	55.8	48.7	-7.8	3.92	4838	2.95
48.0	0.187	1407.6	8.027	15.6	55.1	51.0	-8.7	4.22	4753	2.99
50.0	0.196	1500.2	7.972	16.2	54.4	53.2	-9.7	4.53	4667	3.02
52.0	0.206	1598.7	7.915	16.8	53.6	55.5	-11.0	4.88	4580	3.06
54.0	0.215	1703.2	7.855	17.4	52.8	57.8	-12.4	5.26	4492	3.09
56.0	0.225	1814.2	7.794	17.9	51.9	60.1	-14.1	5.66	4405	3.13
58.0	0.235	1932.1	7.731	18.5	51.0	62.4	-16.2	6.11	4317	3.17
60.0	0.245	2057.3	7.666	19.1	50.0	64.7	-18.7	6.60	4230	3.21
62.0	0.256	2190.2	7.598	19.7	49.0	67.0	-21.8	7.13	4142	3.24
64.0	0.267	2331.3	7.529	20.2	47.9	69.2	-25.8	7.72	4056	3.28
66.0	0.278	2481.4	7.458	20.8	46.8	71.3	-30.7	8.37	3969	3.32
68.0	0.289	2641.0	7.386	21.3	45.6	73.2	-37.1	9.08	3883	3.36
70.0	0.301	2810.8	7.311	21.9	44.3	75.0	-45.3	9.89	3799	3.40
72.0	0.313	2991.8	7.235	22.4	43.0	76.3	-55.7	10.78	3714	3.45
74.0	0.325	3184.9	7.157	22.9	41.5	77.1	-68.1	11.80	3631	3.49
76.0	0.338	3391.3	7.078	23.4	40.0	77.1	-81.7	12.96	3549	3.53
78.0	0.351	3612.5	6.997	23.9	38.4	76.4	-95.1	14.29	3468	3.57
80.0	0.364	3849.9	6.914	24.4	36.7	74.9	-106.8	15.84	3389	3.61
82.0	0.378	4105.8	6.830	24.8	34.8	72.8	-116.3	17.67	3310	3.65
84.0	0.392	4382.7	6.744	25.3	32.8	70.2	-123.7	19.88	3233	3.69
86.0	0.407	4684.2	6.657	25.7	30.6	67.2	-129.4	22.60	3158	3.73
88.0	0.423	5015.0	6.568	26.2	28.2	63.7	-133.7	26.08	3084	3.77
90.0	0.439	5381.9	6.479	26.6	25.5	59.9	-137.0	30.71	3011	3.81

RADAR MAPPING PARAMETERS FOR ZERO DOPPLER AZIMUTH POINTING

ORBIT ECCENTRICITY = 0.5
SIDE-LOOK ANGLE = 30.0 DEGREES
SWATH WIDTH = 36.0 KM
WAVELENGTH = 10.0 CM

TRUE ANOMALY (DEG)	TIME (HR)	SLANT RANGE (KM)	ORBITAL VELOCITY (KM/S)	DOPPLER ANGLE (DEG)	GRAZING ANGLE (DEG)	LAT (DEG)	LONG (DEG)	RANGE APERTURE (METERS)	PRF (HZ)	AZIMUTH APERTURE (METERS)
0.0	-0.0	467.	8.692	-0.0	57.8	0.0	-2.2	1.36	5099	3.02
2.0	0.007	468.7	8.691	0.7	57.8	2.0	-2.2	1.36	5097	3.02
4.0	0.014	473.4	8.687	1.3	57.7	4.1	-2.2	1.38	5092	3.02
6.0	0.022	481.3	8.681	2.0	57.7	6.1	-2.3	1.40	5083	3.02
8.0	0.029	492.3	8.673	2.7	57.6	8.2	-2.4	1.43	5070	3.03
10.0	0.036	506.6	8.663	3.3	57.5	10.2	-2.4	1.48	5054	3.03
12.0	0.043	524.1	8.650	4.0	57.3	12.3	-2.5	1.53	5034	3.04
14.0	0.051	544.9	8.634	4.7	57.2	14.3	-2.7	1.59	5011	3.05
16.0	0.058	569.0	8.617	5.3	57.0	16.4	-2.8	1.67	4985	3.06
18.0	0.065	596.5	8.597	6.0	56.7	18.5	-3.0	1.75	4956	3.07
20.0	0.073	627.5	8.575	6.6	56.5	20.6	-3.2	1.85	4923	3.08
22.0	0.080	662.0	8.550	7.3	56.2	22.7	-3.4	1.96	4887	3.09
24.0	0.088	700.2	8.523	7.9	55.9	24.8	-3.6	2.08	4848	3.11
26.0	0.096	742.0	8.494	8.6	55.6	26.9	-3.9	2.21	4807	3.13
28.0	0.103	787.7	8.463	9.2	55.2	29.0	-4.2	2.36	4763	3.14
30.0	0.111	837.3	8.429	9.9	54.8	31.1	-4.6	2.52	4716	3.16
32.0	0.119	891.0	8.393	10.5	54.4	33.2	-5.0	2.69	4667	3.18
34.0	0.127	948.9	8.355	11.2	53.9	35.4	-5.4	2.88	4615	3.20
36.0	0.135	1011.2	8.315	11.8	53.4	37.6	-6.0	3.09	4562	3.22
38.0	0.144	1078.1	8.272	12.5	52.9	39.7	-6.5	3.32	4506	3.25
40.0	0.152	1149.7	8.228	13.1	52.3	41.9	-7.2	3.57	4449	3.27
42.0	0.161	1226.3	8.181	13.7	51.7	44.1	-7.9	3.84	4390	3.30
44.0	0.169	1308.1	8.132	14.3	51.1	46.4	-8.8	4.13	4329	3.32
46.0	0.178	1395.4	8.081	14.9	50.4	48.6	-9.8	4.45	4267	3.35
48.0	0.187	1488.4	8.027	15.6	49.7	50.6	-10.9	4.79	4203	3.38
50.0	0.196	1587.5	7.972	16.2	49.0	53.1	-12.2	5.17	4139	3.41
52.0	0.206	1693.0	7.915	16.8	48.1	55.3	-13.8	5.58	4073	3.44
54.0	0.215	1805.3	7.855	17.4	47.3	57.6	-15.6	6.04	4007	3.47
56.0	0.225	1924.9	7.794	17.9	46.4	59.8	-17.7	6.53	3940	3.50
58.0	0.235	2052.1	7.731	18.5	45.4	62.0	-20.3	7.08	3872	3.53
60.0	0.245	2187.6	7.666	19.1	44.4	64.2	-23.4	7.68	3804	3.56
62.0	0.256	2332.0	7.598	19.7	43.3	66.3	-27.2	8.35	3735	3.60
64.0	0.267	2486.0	7.529	20.2	42.2	68.3	-31.9	9.10	3667	3.63
66.0	0.278	2650.4	7.450	20.8	40.9	70.1	-37.7	9.94	3598	3.67
68.0	0.289	2826.1	7.386	21.3	39.6	71.7	-44.9	10.89	3529	3.70
70.0	0.301	3014.3	7.311	21.9	38.2	73.0	-53.5	11.97	3460	3.74
72.0	0.313	3216.1	7.235	22.4	36.7	73.8	-63.6	13.21	3392	3.77
74.0	0.325	3433.4	7.157	22.9	35.1	74.0	-74.7	14.66	3324	3.81
76.0	0.338	3668.0	7.078	23.4	33.4	73.5	-86.0	16.37	3256	3.84
78.0	0.351	3922.4	6.997	23.9	31.5	72.3	-96.6	18.43	3189	3.88
80.0	0.364	4200.0	6.914	24.4	29.5	70.4	-105.8	20.97	3122	3.92
82.0	0.378	4505.3	6.830	24.8	27.2	67.9	-113.4	24.21	3056	3.95
84.0	0.392	4845.1	6.744	25.3	24.7	64.8	-119.5	28.53	2991	3.99
86.0	0.407	5229.8	6.657	25.7	21.7	61.1	-124.3	34.68	2926	4.02
88.0	0.423	5678.6	6.568	26.2	18.3	56.7	-128.1	44.44	2863	4.06
90.0	0.439	6234.2	6.479	26.6	13.9	51.3	-130.9	63.70	2800	4.09

affect the amplitude or SNR of the processed image and angular rates are irrelevant.

A critical factor in SAR image processing is azimuth phase error due to motion of the phase center of the antenna parallel to the line of sight, time jitter in azimuth sampling, reference oscillator drift, etc. It is customary to consider a Taylor series expansion of the phase error, i.e.,

$$\phi_\epsilon(t) = \phi_o + \phi_o' t + \tfrac{1}{2}\phi_o'' t^2 + \ldots \qquad \text{(IV-89)}$$

The constant term, ϕ_o, is of no consequence. The linear term, ϕ_o', is equivalent to a doppler shift and will cause an azimuth displacement of the target field, but does not affect resolution. The quadratic term defocuses the image, but does not change position. Higher order terms cause higher order image aberrations. In general, the effects of azimuth phase errors are negligible if their amplitude is less than $\pi/4$ over the required aperture. For the case of 100 m resolution, the synthetic aperture length varies from approximately 200 m at periapsis to 2000 m at the poles. The corresponding synthetic aperture time varies from approximately 30 to 600 msec. During this time, the uncompensated motion of the antenna phase center in the beam direction can vary no more than $\lambda/8$ meters. Assuming a constant velocity, 600 msec synthetic aperture, time and 10 cm wavelength, the maximum "beam velocity error" is 0.02 m/sec. In an orbiting radar, translational velocity errors are insignificant. However, a beam velocity error may be induced by attitude perturbations of the spacecraft. However, this can be minimized by positioning the phase center of the antenna close to the radius vector from the spacecraft, c.g., to the mapping area. In addition, the motion can be sensed by the spacecraft attitude control system and compensated in the radar receiver.

A second source of error is reference oscillator instability. In a SAR system, the azimuth doppler is measured by comparing the phase of the received signal with that of the transmitted signal. The absolute phase of the transmitted signal is irrelevant. If we allow a maximum phase error of $\pi/4$ radians, the reference oscillator phase cannot shift by more than 1/8 cycle over the two-way path length to the target field. Then we require

$$f_c \Delta T < \frac{1}{8}$$ (IV-90)

where f_c is the carrier frequency and ΔT is the time delay corresponding to the two-way path length. Assuming the phase change is due to a frequency drift, the required relative medium term frequency stability is

$$\frac{\Delta f}{f_c} = \frac{1}{8 \Delta T f_c}$$ (IV-91)

$$= \frac{\lambda}{16R}$$

where R is the slant range. At 4000 km, the required short term oscillator stability for $\lambda = 10$ cm is

$$\frac{\Delta f}{f_c} \approx 2.5 \times 10^{-8}$$

A third source of phase error is range and azimuth timing errors. The range gate must be accurate to about $\frac{1}{4}$ of a resolution cell: then the allowable range gate error is

$$\Delta T_{e_{max}} = \frac{r_r}{2c} = \frac{1}{4B}$$ (IV-92)

where r_r is the slant range resolution and B is the range bandwidth. For 50 m slant range resolution, the range bandwidth is 3 MHz and the required range gate stability is approximately 83 nsec. The relative accuracy is

$$\frac{\Delta T_{e_{max}}}{\Delta T} = \frac{1}{4} \frac{r_r}{R} = 0.3 \times 10^{-6}$$ (IV-93)

at 4000 km range.

In the azimuth direction, we will require the azimuth sampling or PRF accuracy to be within 1/8 of a cycle over the processed doppler signal. The total azimuth phase change is the azimuth compression ratio.

$$K_y = \tfrac{1}{2} \frac{R}{r_a^2} \qquad\qquad (IV\text{-}94)$$

Hence, we require a relative accuracy of 1/8 K_y. For 100 m azimuth resolution at 4000 km range and 10 cm avelength, the required azimuth compression ratio is K_y = 20. Hence, a relative azimuth sampling accuracy of approximately 0.5 percent is required.

CONCLUSIONS AND RECOMMENDATIONS

Recommended Design

An orbit with an eccentricity of 0.5 is preferred as noted in the mission analysis section. In this orbit, the spacecraft m st map every orbit using a S-band radar to obtain reasonable swath widths. Wide swath widths require antennas with large azimuth dimensions that are difficult to articulate. Using a 0.5 eccentricity, a 36 km swath width is needed to obtain 20 percent overlap at periapsis.

Either a constant side look angle or a variable side look angle can be used effectively. The advantage of using a variable side look angle is that increased mapping coverage is obtained. The variable side look scheme can be implemented by controlling the antenna along the zero doppler line, but no advantage is gained by using a variable side look angle. Small grazing angles cannot be achieved because the zero doppler direction deviates from the radial direction at the higher latitudes. The upper PRF constraint and power requirements limit the mapping to the lower latitudes when small grazing angles cannot be obtained. In order to imple-

ment a variable side look angle type of scheme, the antenna must generally be pointed in another direction than the zero doppler direction. Two of the more promising ways of implementing a variable side look angle type of scheme, when the antenna is not generally pointed along the zero doppler line is by using an electronic offset clutterlock system or by biasing the antenna to point at a constant squint angle.

Two side look angle alternatives (constant side look angle and variable side look angle) have been discussed to eliminate ambiguities and reduce the power required. A constant side look angle can be used with a dual beamwidth antenna to map about 80 percent (mapping to $\pm 55°$) of the surface. Increased mapping coverage can be obtained by using a variable side look angle type of scheme. This type of scheme uses small grazing angles to eliminate ambiguities and reduce power. The variable side look angle schemes can be implemented by using an electronic offset clutterlock system or by squinting the antenna forward or rearward at a constant angle, so that complete surface mapping can be obtained. The latter scheme is favored because a constant side look angle coupled with a constant squint angle can be used to get variable grazing angles, eliminating one antenna gimbal and obtaining complete surface mapping.

Reflector type antennas will probably be used for the earlier missions, even if a shared antenna configuration (Configuration A Volume II) is selected and/or a constant side look angle with a dual beamwidth antenna (a more complex antenna design) is used. For the later missions, the planar array may be a competitive design in terms of cost and weight; and would add to the radar and antenna subsystem reliability and flexibility.

The power requirements are derived in the next section for clutter type targets. Point target theory of SAR systems does not apply when clutter type targets are mapped.

Discussions of the ambiguity spectrum for a synthetic aperture radar show the ambiguity levels in the far range return are unacceptable using a 6 db criterion. All the 6 db (two-way antenna patterns) cases are unacceptable for the far range beamwidths. Both uniform and cosine aperture illuminations are discussed, where in practice the illumination is some where between these two extremes. For the far range cases, the rapid change in ambiguity levels lead to a zero doppler level of 4 db, where $X_R = 1.62$ probably represents the most satisfactory compromise.

The radar system augmentation discussions show how the mapping radar subsystem can be mechanized to have dual frequency and dual polarization capabilities. The favored method of implementing a dual polarization system is to have the capability part time to save cost. Only an additional feed and electronic switch are needed to receive the cross polarized return. The radar subsystem would be designed in terms of power for the like polarized return. The mapping may be degraded due to being under-powered when operated in the cross-polarization mode. Mapping can be conducted using the cross-polarization system during the mapping overlap periods to determine the planet surface characteristics. Very little additional cost would be needed to get additional information about the surface. This implementation would require the same data rate and data volume capabilities for the data handling and communication subsystems.

The dual frequency could also be a full time and part time capability. Each operating frequency could be commanded by the control computer or by ground command. Many components can be shared by both frequencies to save subsystem development costs. The same data handling capability would be needed when implemented this way.

If a full time system is required, the size and cost of the radar and data management subsystems are doubled, and it is

doubtful whether this additional cost and weight can be justi-
fied in terms of the additional science return. Since similar
data can be obtained from the radar altimeter that operates on a
different frequency than the mapping radar, the preferred system
appears to be a single frequency mapping radar (S-band) with an
existing L-band radar altimeter system.

Concerns

The biggest radar system concern in this study is how to elim-
inate the range ambiguities in elliptical orbits without using an-
tennas that are too large to articulate. A number of solutions
are suggested, but in depth studies should be conducted to develop
these schemes. The scheme that uses a constant side look angle
and operates in a squint mode, is favored, provided a specified
side lobe can be used to control the antenna. This mode is examined
in more detail in Vol. II. The variable side look angle scheme that
is implemented in this way appears to be a good way to eliminate
range ambiguities. Using this type of scheme, the spacecraft can
map the whole planet from elliptical orbit which needs a much
smaller propulsion capability than a circular orbit. Elliptical
orbits can now be used like circular orbits, which simplify the
radar and antenna subsystem designs. The PRF constraints and power
requirements are easy to meet with the VSL angle type of scheme.

The radar subsystem power requirements at low side look angles
in the influence of essentially specular return is a concern and
the power required may have to be increased to guarantee good
mapping. There is some concern whether the radar range equation
derived previously can be used without some modification for the
small side look angles.

Present technology is all that is required to   ign and
develop the radar and antenna subsystems for the   's mapping
mission. The Venus mapping radar can be built today with presently

available components. Advanced technology should only reduce the weight, power, and reliability of the system. Eventually, phased arrays may be competitive in terms of weight and cost and add flexibility to the mapping aperture.

REFERENCES AND· BIBLIOGRAPHY

IV-1   D. W. Holst: *Evaluation of Deployable Parabolic Reflectors.*
        Martin Marietta Research Report R-69-3, April 1969.

IV-2   P. M. Knox and D. W. Holst: *Evaluation of Flexible Rib
        Deployable Parabolic Reflectors.* Martin Marietta Research
        Report, April 1969.

IV-3   *Satellite Unfurlable Antenna Techniques.* Technical Proposal
        Volume I, Martin Marietta Aerospace.

IV-4   *Phased Array Antenna Comparison Studies.* Final Report,
        MCR-69-70, Volume I.

IV-5   A. O. Oliner and G. Knittel: "Phased Array Antennas."
        Proceedings of the 1970 Phased Array Symposium.

IV-6   J. D. Adams: "Capability of a Projected 1975 Airborne Solid
        State Radar." *Microwave Journal,* September, 1971.

IV-7   W. E. Wilson: "Pulsed LSA and Trapatt Sources for Microwave
        Systems." *Microwave Journal,* August, 1971.

IV-8   K. K. N. Chang, et al: "Trapatt Amplifiers for Phased Array
        Radar Systems." *Microwave Journal,* February, 1973.

IV-9   R. T. Davis: "Hybrid Tube-Semiconductor Device for High
        Power Amplification." *Microwaves,* February 1971.

IV-10   H. Sobol and F. Sterezer: "Microwav· Power Sources." *IEEE
        Spectrum,* April, 1972.

IV-11   H. Sobol: "Applications of Integrated Circuit Technology to
        Microwave Frequencies." *Proc. IEEE,* Vol. 59, No. 8, August,
        1971.

IV-12   B. F. C. Cooper and G. A. Wells: "Six-Times Multiplier with
        Two Watts Output at 2700 MHz." *Proc. f the Institution of
        Radio and Electronic Engineers, Australia,* Vol. 30, No. 10,
        October, 1969.

IV-13   J. W. Rush and D. M. Cole: "A Look at Reliability: Tubes
        and Solid State." *Microwave Journal,* October, 1972.

IV-14   H. C. Okean an 1 P. P. Lomb·.rdo: "N· .se Performance of M/W
        and MM-Wave Receivers." *Microwave Journal,* January, 1973.

IV-15 Covington and Broten: "Interferometer for Radio Astronomy." *PTGAP*, July, 1957.

IV-16 C. E. Cook and M. Bernfield: *Radar Signal* . Academic Press, New York, 1967.

IV-17 A. W. Rihaczek: *Principles of High Resolution Radar*. McGraw Hill, New York, 1969.

IV-18 C. W. Sherwin, J. P. Ruina and R. D. Raucliffe: "Some Early Developments in Synthetic Aperture Radar Systems." *IRE Trans. Mil. Electron.*, Vol MIL-6, pp 111-115, April, 1962.

IV-19 L. J. Cutrona, W. E. Virian, E. N. Luth and G. O. Hall: "A High Resolution Radar Combat- .rveillance System." *IRE Trans. Mil. Electron*, Vol MIL-5, pp 127-131, April, 1961.

IV-20 L. J. Cutrona, E. N. Leith, L. J. Porcello, and W. E. Virian: "On the Application of Coherent Optical Processing Techniques to Synthetic Aperture Radar." *Proc. IEEF*, Vol. 54, pp 1026-1032, August, 1966.

IV-21 W. M. Brown: "Synth i Aperture Radar." *IEEE Trans. Aerospace and Electronics Systems*, Vol. AES-3, pp 217-229, March, 1967.

IV-22 R. O. Harger: "An Optimum Design of Ambiguity Function, Antenna Patterns, and Signal for Side Looking Radars." *IEEE Trans. Military Electronics*, Vol. MIL-9, pp 264-278, July-October 1965.

IV-23 A. W. Rihaczek: "Radar Resolution of Moving Targets." *IEEE Trans. Information Theory*, Vol. IT-13, pp 51-56, January, 1967.

IV-24 W. M. Brown and R. J. Fredricks: "Range Doppler Imaging with Motion Through Resolution Cells." *IEEE Trans. Aerospace and Electronic Systems*, Vol. AES-5, pp 98-105, January, 1969.

IV-25 E. J. Kelly and R. P. Wishner: "Matched-Filter Theory for High-Velocity Accelerating Targets." *IEEE Trans. Military Electronics*, Vol. MIL-9, pp 56-59, January, 1965.

IV-26 B. Harris and S. A. Kramer: "Asymptotic Evaluation of the Ambiguity Function of High-Gain FM Matched Filter Solar Systems." *Proc. IEEE*, Vol. 56, pp 2149-2157, December, 1968.

IV-27 H. Urkowitz: "The Effect of Antenna Pattern on the Performance of Dual-Antenna Airborne Moving Target Indicators." *IEEE Trans Aerospace and Naval Electronics*, Vol. ANE-11, pp 218-223, December, 1964.

IV-28 W. M. Brown and J. F. Riordan: "Resolution Limits with Propagation Phase Errors." *IEEE Trans. Aerospace Electronic Systems*, pp 657-662.

IV-29 M. C. Thomson, Jr. and H. B. Janis: "Measurements of Phase Front Distortion on an Elevated Line-of-Sight Path." *IEEE Trans. Aerospace Electronic System*, pp 645-656.

IV-30 W. M. Brown: "Synthetic Aperture Radar." *IEEE Trans. Aerospace Electronic System*, Vol. AES-3, pp-217-229, March, 1967.

IV-31 W. M. Brown and L. J. Porcello: "An Introduction to Synthetic Aperture Radar." *IEEE Spectrum*, Vol. 6, pp 52-62, September, 1969.

IV-32 L. J. Procello: "Turbulence Induced Phase Errors in Synthetic Aperture Radars." *IEEE Trans. Aerospace Electronic Systems*, Vol. 6, pp 636-644.

IV-33 K. G. Schroeder: "Technology Trends in Spacecraft Phased Arrays." *Easeon 70*, pp 113-120.

IV-34 R. J. Richardson, et al: *Phased Array Antenna C ,parison Study*. Vol. I, NASA Report MCR-69-70, Martin Marietta Corp., February, 1969.

IV-35 R. K. Moore and G. C. Thomann: "Imaging Radar for Geoscience Use." *IEEE Trans. on Geoscience Elect.*, Vol GE-9, pp 155-164, July, 1971.

IV-36 R. K. Moore: "Ground Echo." *M. I. Skolnek, Radar Handbook*, McGraw Hill, pp 25-41, 1970.

IV-37 H. C. MacDonald: "Geologic Evaluation of Radar Imagery from Darir. Province, Panama." *Modern Geology*, Vol. I, pp 1-63, 1969.

IV-38 H. C. MacDonald and W. P. Waite: *Optimum Radar Depression Angles for Geological Analysis*. Center of Research, Inc. Report, University of Kansas, Lawrence, Kansas, August, 1970.

IV-39   I. Kaly: "Wavelength Dependence of the Radar Reflectivity of Earth and Moon." *J. Geophys. Res.* Vol. 71, pp 361-366, January 15, 1966.

IV-40   J. W. Rouse, Jr., H. C. MacDonald, and W. P. Waite: "Geoscience Application of Radar Sensors." *IEEE Trans. on Geoscience Elect.*, Vol. GE-7, pp 2-18, January, 1969.

IV-41   W. J. Pierson, B. B. Scheps, and D. S. Simonett: *Some Applications of Radar Return Data to the Study of Terrestrial and Oceanic Phenomena.* Presented at the Goddard Memorial Symposium, AAS, March 18, 1965.

IV-42   D. C. Parker and M. F. Wolff: "Remote Sensing." *International Science and Technology,* No. 43, July, 1965.

IV-43   R. K. Moore and C. S. Williams: "Radar Terrain Return at Near-vertical Incidence." *Proc. IRE,* Vol. 45, pp 228-238, February, 1957.

IV-44   I. Katz: "Radar Reflectivity of the Earth's Surface." *Appl. Phys. Lab. Tech. Digest.* January-February, 1963.

IV-45   A. K. Fung and R. K. Moore: "Effect of Structure Size on Moon and Earth Radar Return at Various Angles." *J. Geophys. Res.,* Vol. 69, pp 1075-1081, March 1964.

IV-47   R. D. Ellermuir, D. S. Simmett, and L. F. Dellwig: "The Use of Multi-parameter Radar Imagery for the Discrimination of Terrain Characteristics." *1967 IEEE International Conn. Rec.,* Vol. 15, pp 127-135, 1967.

IV-48   S. H. Ward, G. R. Jiracek and W. J. Linlor: "Some Factors Affecting Electromagnetic Detection of Lunar Subsurface Water." *IEEE Trans. on Geoscience Elect.,* Vol. GE-7, pp 19-21, January, 1969.

IV-49   E. N. Leith, A. A. Friesem and A. I. Funkhouser: "Optical Simulation of Radar Ambiguities." *IEEE Trans. Aerospace Electronic Systems,* Vol AES-6, pp 832-840, November, 1970.

IV-50   K. R. Richter: *Propagation of Radio Waves Through the Lower Atmosphere of Venus.* NASA TM X-66046, August 1972.

IV-51   F. A. Vandenberg: *Documentation of SLR Geometry and Symbols.* Venus Mapper Technical Note 2, Martin Marietta Aerospace, September 8, 1972.

IV-156

V. Data Handling and
Communications

V. DATA HANDLING AND COMMUNICATIONS

INTRODUCTION AND ASSUMPTIONS

A planetary topographic mapping mission to Venus will retrieve an astounding volume of data. The fundamental scientific tool of this mission is a synthetic aperture side-looking radar (SAR) due to its ability to penetrate the dense cloud layer obscuring Venus in the visible spectrum and the greatly improved controlled azimuth resolution obtainable through coherent doppler processing compared to more conventional real aperture ground mapping radars. However, the coherent doppler processing concept requires additional data base management, data processing and reduction in comparison to the more traditional vidicon television approach to planetary surface study and mapping. That is, the SAR radar is differentiated from TV in that the raw output of the radar is not a TV-like image, but a hologram of the surface which requires special processing to reduce the hologram image to an intensity image.

The objectives of this study are to 1) parametrically quantify the requirements on data handling and communications due to the mission characteristics; 2) from an understanding of the requirements infer subsystem element characteristics and functional allocations; 3) test mission feasibility and technology development requirements by defining alternative subsystem hardware implementations; 4) expose spacecraft subsystem interactions and performance limitations; 5) recommend preferred implementations which show the best potential for the achievement of an economical, cost effective mission implementation which meets or exceeds science objectives. These objectives are presented in the form of a flow chart in Figure V-1. The blocks single out the key data management study interface; the flow of the determination of derived requirements, and major element tradeoffs.
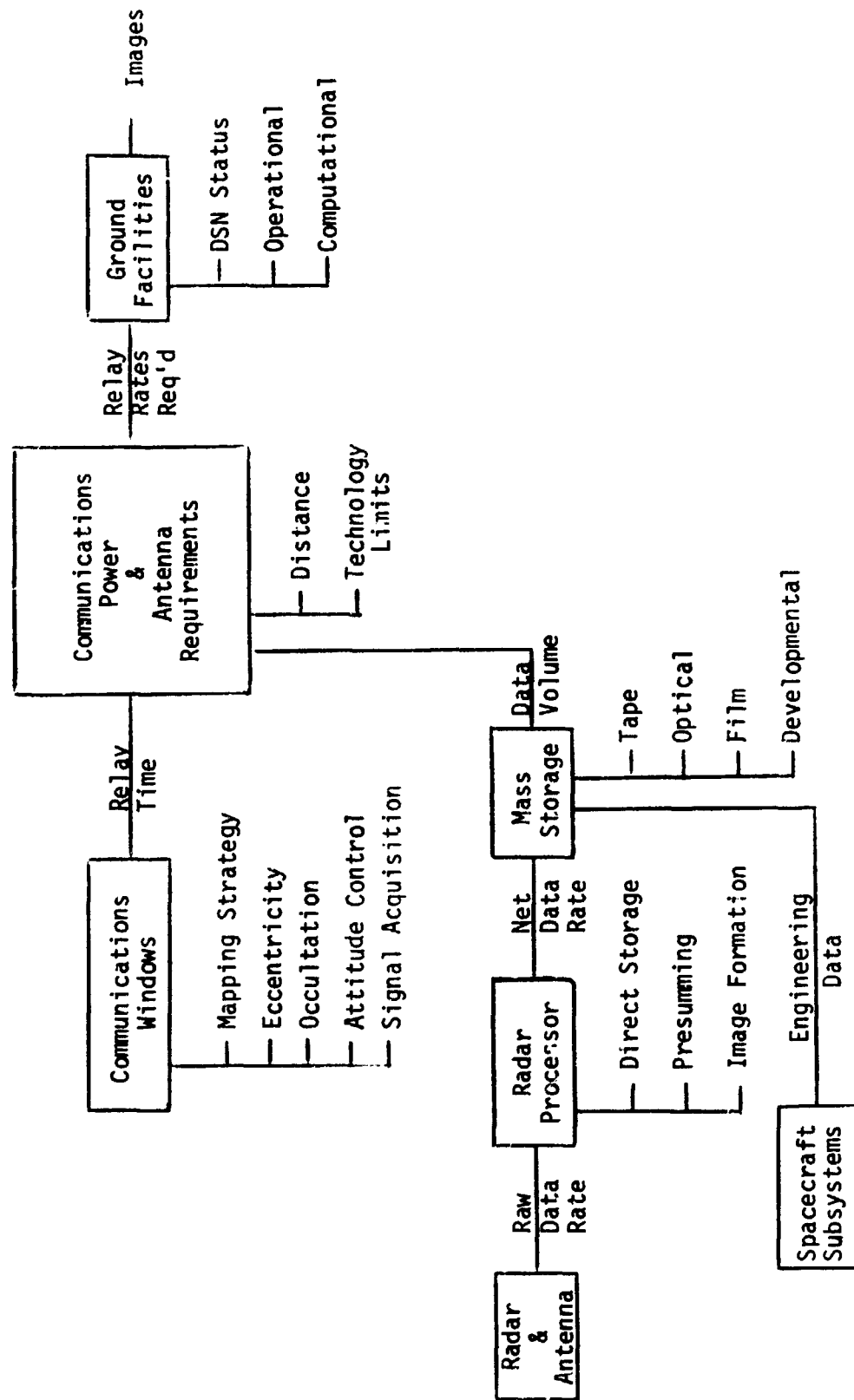
Figure V-1 Data Management Study Interactions and Flow

Table V-1 below exhibits a compendium of mission guidelines, ground rules and assumptions which bounded and directed studies of data handling and communications subsystem elements.

Table V-1 Mission and Study Guidelines and Ground Rules

Science Coverage Objectives

Resolution in Ground Plane: 100 m x 100 m nominal
                              33 m x 33 m telescope selectable

Surface Coverage: ≥90% at nominal resolution

Mission Characteristics

Time Frame: early to mid-1980s.

Duration: 250 day.

Earth-Venus Range: 0.63 to 1.71 AU

Occultation: Earth: periapse and apoapse occultation

              Solar: 3 to 5 days at end of mission with
                      X-band directivity at ground station.

Orbit Availability: circular to 0.5 eccentricity

Mapping Characteristics and Logistics

Mapping Strategy (orbital duty cycle): eccentricity-0.5 : 1:1
                                                   0.3 : 1:2
                                                   0.0 : 1:5

Ground Plane Swath Widths: eccentricity - 0.5 : 36 km
                                            0.3 : 44 km
                                            0.0 : 65 km

Onboard Radar Processing Strategies

Preferred: Onboard presumming/image formation on Earth.

Attractive: Mixed integration image formation onboard,
             final correction on Earth.

Communication Design Basis

Maximum range and peak occultation nearly coincidental.
3 meter antenna referred to Viking capability attitude control.
X-band carrier ≈ 8448 MHz.

Auxiliary Data Acquisition Requirements

Primary Mission: altimeter, receiver AGC, radar antenna
                  gimbals.

Realtime relay of radar data is not possible except under very ideal, limited circumstances, therefore, onboard mass storage is a definite requirement.

The mass storage subsystem stores the processed radar data on a cyclic basis for subsequent relay during Venus-Earth-Venus communications windows. The storage capacity is primarily affected by the required surface swath mapped per cycle, degree of onboard processing, data quantization dynamic range, auxiliary data annotation.

The most significant factor is the degree of onboard radar data processing. The potential resolution of processing all the raw radar data retrieved is significantly in excess of topographic requirements so the simplest radar processor would average the data base to reduce the relay requirement while still meeting resolution requirements (called maximum presumming). Other process.ng candidates include defining the minimum degree of averaging which still meets coverage requirements but does not require an excessive data relay link (minimum presumming) and forming an image on the spacecraft with single (single coherent image) azimuth channel or multiple azimuth channel techniques (mixed integration processing).

The communications link must relay the data volume stored in the mass storage element during available relay time. Dividing data volume by relay time exposes an average data relay rate in bits per second which must be met by the communications subsystem. The study examines communication designs in light of antenna size limits (weight, altitude control pointing and stability), RF power availability (relat to prime power limits, RF amplifier power, efficiency and reliability limits) and the diversity of Earth-Venus slant ranges over the mission duration (0.63 - 1.71 AU) of 250 days.

The average data relay rates are derived by considering both the data volume per mapping cycle and the available communications windows at Venus. These windows (as indicated in Figure V-1) are controlled by times allocated for the mapping strategy, Earth

occultation, and attitude control for high gain antenna orientation
at Venus. Orbit eccentricity affects the allocations. In addi-
tion, the time required for signal acquisition through the Deep
Space Network at Earth also affects the net time available for
data relay from Venus. Required relay rates from Venus as derived
independently from Deep Space Network capability must be put into
perspective by a comparative tradeoff with the current and projected
Deep Space Net characteristics. The Deep Space Net is assumed to
include, as a minimum, three 64 m ground stations with X-band car-
rier reception capability with a current upper data rate capability
of 250 kbps.

Figure V-2 summarizes the previous discussion in terms of a
study objectives flow diagram. This diagram also points the way
to the topical organization of data handling and communication
studies found in Volumes I, II, and III. Volume III is concerned
with parametrically deriving and quantifying performance require-
ments and surveying broad technology bases. Volume II is concerned
with more specific subsystem specifications. That is, based on the
derived requirements and parametric studies of Volume III, candi-
date spacecraft subsystem functional allocations and characteristic
specifications are identified in Volume II. These implementations,
in effect, investigate feasibility by evaluations of technology
limits and subsystem requirement interactions. Included also in
Volume II are system comparisons, technology assessments, and rec-
ommended technology development programs. Volume I is a summary
of salient findings and recommendations of the study.

The following paragraphs present findings of the investigations
of 1) alternative processing modes for planetary synthetic aperture
mapping radar, 2) the factors leading to and definition of required
spacecraft temporary and mass data storage including a survey of
candidate technologies, 3) factors defining required characteris-
tics of a communications subsystem and parametric implementations,

Study Objective Flow
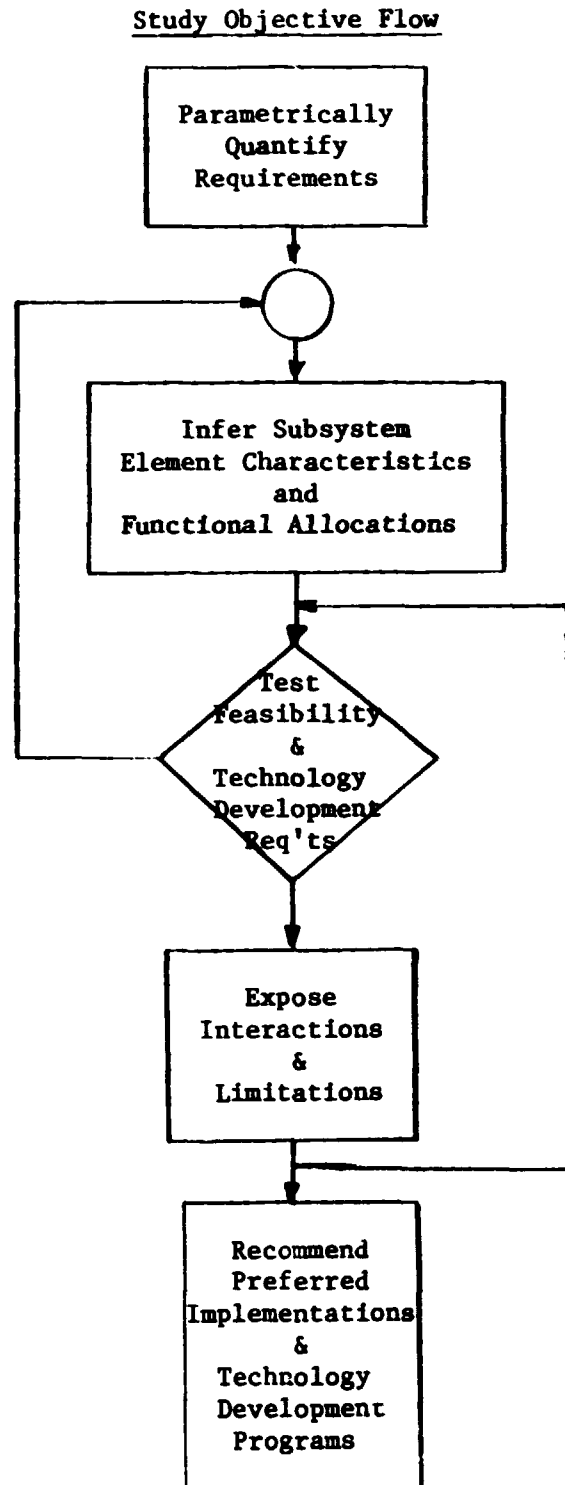
Figure V-2 Data Management Study Objectives Flow

and 4) consideration of impact on and functional requirements of the Deep Space Network.

PARAMETRIC STUDIES

SAR Processing Considerations

Synthetic aperture radar is differentiated from conventional scanned beam radars (and required for planetary mapping) in that its azimuth resolution is not limited by the real antenna beamwidth. Resolution in the radial direction is fundamentally the same for both real and synthetic aperture radar. A comparative summary of potential azimuth resolution for real aperture radar, and several processing options for synthetic aperture radar are found in Table V-2.

Table V-2 Comparative Radar Resolutions

			460 km	3000 km
ρ_a	**Synthetic Aperture Techniques**			
	$\left(\frac{R\lambda}{2}\right)^{\frac{1}{2}}$	Unfocused	152 m	387 m
	$\left(\frac{R\lambda}{2K}\right)^{\frac{1}{2}}$	Partial Focus	100 m $K = 2.3$	100 m $K = 15$
	$D/2$	Full Focus	2 m	2 m
	$\frac{D}{2} \times \frac{1}{F}$	Full Focus – Extended Illumination Time	< 2 m	< 2 m
ρ_a	**Real Aperture**			
	$\frac{R\lambda}{D}$		11.5 km	75 km
ρ_r	$\frac{c\tau_d}{2} \times \frac{1}{C_r} \times \frac{1}{\sin \psi}$		100 m	100 m

A special mode which provides resolutions in excess of ½ the
actual horizontal antenna dimension, often called "spotlight mode"
or "extended illumination time-fully focused mode" is not considered
in this study since its resolution potential is extremely excessive
for a topographic mission. Synthetic aperture radar is different
from conventional scanned beam radar most notably in that its azi-
muth resolution is not limited by the real antenna beamwidth.
Resolution in the radial (range direction) is essentially the same
for radar concepts. A comparative summary of example azimuth reso-
lutions for synthetic and real aperture radar using the same
antenna in Table V-2 exposes the requirement for a SAR in plane-
tary mapping applications. The table includes example resolutions
at slant ranges typical of circular (left column) and eccentric
(0.5) orbits (right hand column) at Venus. The following defini-
tions apply to the table:

R = radar surface slant range

λ = radar wavelength (10 cm preferred reference)

K = processing compression ratio in azimuth

F = extended illumination time factor

D = antenna dimension in azimuth direction (4 meter ref.)

c = speed of light

τ_d = actual transmitted pulse width

C_r = compression ratio in range

ψ = incidence angle at surface

ρ_a = processed azimuth resolution

ρ_r = processed range resolution (in ground range)

The real aperture azimuth resolution for the typical ranges is
seen to be comparable to Earth-based radar and unacceptable in
light of the topographic objectives of this stud; resolution on
the order of 100 meters in the azimuth (and range direction).

Synthetic aperture techniques have been classified according
to the complexity of azimuth signal processing involved as 1) un-
focused, 2) partially focused, 3) fully focused, 4) fully focused
with extended illumination time. All synthetic aperture techniques
provide potential azimuth resolutions considerably in excess of
the real aperture case and comparable to the topographic require-
ments. Resolutions achievable from a fully focused technique with
antennas practical with spacecraft (~4 meters) is greatly in excess
of topographic requirements, therefore a partially focused processor
is necessary here.

To summarize, the data processing for a SAR system consists
essentially of the following three steps:

1) azimuth presumming for bandwidth and data storage
   reduction;

2) range and azimuth correlation for image generation;

3) post-correlation noncoherent integration for image
   variance reduction.

For the Venus mapping mission it is recommended that the first
step be done on the spacecraft, and that the final two steps be
done on Earth. The following paragraphs discuss in some detail
the characteristics of processing in the range channel, azimuth
channel, typical processor implementations for a multi mode pre-
summer and mixed integration processor, characteristic resolutions
versus processor type and complexity, and concludes with a summary
of recommended data handling strategy.

Range Channel - The basic geometry of the range channel re-
lating slant range, ground range, grazing angle, and transmitted
pulse bandwidth is found in Figure V-3.

$$\Delta R_s = \Delta R_g \sin \psi = \frac{c}{2B}$$

$$\Delta R_g = \Delta R_s \csc \psi$$

where ΔR_s = slant range resolution

ΔR_g = ground range resolution

ψ = incidence angle

τ_d = dispersed pulse width

C_r = pulse compression ratio

c = propagation velocity

B = transmitted bandwidth
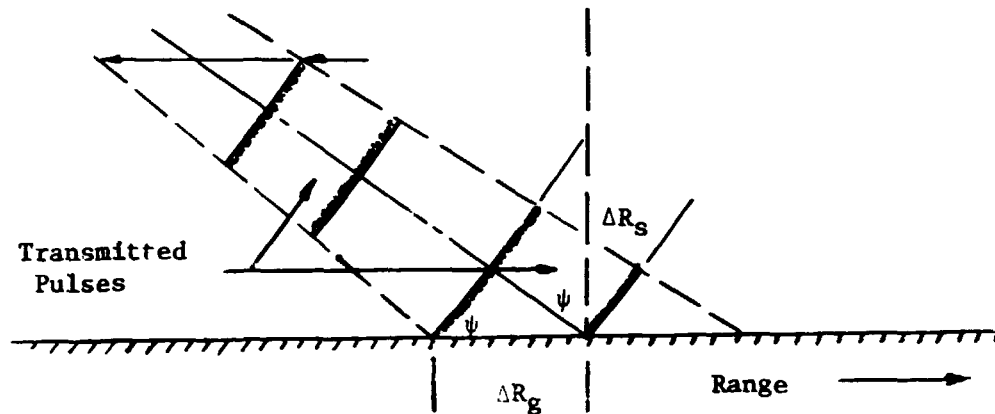
Figure V-3 Ground Range Resolution and Bandwidth

To obtain 100 m ground range resolution the required radar bandwidth is

$$B = \frac{c}{2\rho_r}\ \csc\ \psi\ \text{Hz} \tag{V-1}$$

where   B = bandwidth required

c = velocity of propagation

ρ_r = range resolution

ψ = grazing angle

For 100 m resolution at a 30 degree grazing angle, the required bandwidth is 3 MHz. Improving the resolution to 33 m requires a bandwidth of 10 MHz. Analog or digital pulse coding and pulse compression techniques can be used to increase average transmitted power for a given transmitter peak power limitation. Unless total image processing is done on board the spacecraft the range processing would be done on Earth.

Equation (V-1) also leads to the input data rate of the on-board data processing system in complex words/second; i.e., the real data rate is 2B samples/second. Data rate and volume are addressed in a later paragraph, Data Storage Requirements.

Azimuth Channel - The azimuth resolution of a real-aperture side looking radar system is

$$\rho_a = R \beta_a \qquad\qquad (V-2)$$
$$= R\lambda/d_a$$

where   R = slant range

β_a = azimuth beamwidth

λ = wavelength

d_a = azimuth aperture

By coherently recording the data (i.e., recording both phase and amplitude of the return) the data can be processed to obtain a resolution of

$$\rho_a = \frac{\lambda}{4 \sin \theta_a/2} \qquad\qquad (V-3)$$

where θ_a is the total change in viewing angle measured in the slant range plane. If the antenna is fixed, $\theta_a = \beta_a$ and

$$\rho_a = \frac{\lambda}{4 \sin \beta_a/2} \qquad\qquad (V-4)$$

$$\approx d_a/2$$

which is the usual equation defining azimuth resolution potential of a fully focused SAR. However, for the Venus mapper, d_a will be of the order of 5 meters or less, and the system will be capable of azimuth resolutions finer than the mission requirements. Hence, a partially focused synthetic aperture is sufficient.

Solving equation (V-3) for θ_a as a function of resolution yields:

$$\theta_a = 2 \sin^{-1} \frac{\lambda}{4\rho_a} \qquad\qquad (V-5)$$

$$\approx \frac{\lambda}{2\rho_a}$$

Then for $\lambda = 10$ cm, and 100 m resolution, the required viewing angle is 0.5 mrad. For 33 m resolution, this is increased to 1.5 mrad. If a 5 m azimuth aperture is used, the corresponding azimuth beamwidth is 20 mrad. This is illustrated in Figure V-4 with the processing aperture shown within the real aperture beamwidth.

The instantaneous doppler frequency in the azimuth channel is

$$f_d = \frac{2V}{\lambda} \cos \theta \tag{V-6}$$

where θ is the cone angle between the spacecraft velocity vector and a target point. The total doppler bandwidth is

$$\begin{aligned} B_d &= \frac{2V}{\lambda} \beta_a \\ &\approx \frac{2V}{d_a} \text{ Hz} \end{aligned} \tag{V-7}$$

The required doppler bandwidth is

$$\begin{aligned} B_a &= \frac{2V}{\lambda} \beta_a \\ &\approx \frac{V}{\rho_a} \text{ Hz} \end{aligned} \tag{V-8}$$

where ρ_a is the desired resolution and θ_a is the required processing aperture given by equation (V-5).

The doppler bandwidth, B_d, given by equation (V-7) represents the azimuth data rate of the radar which also determines the minimum PRF, discussed further in Volume III, Section IV.

The previous paragraphs have discussed briefly the ability of doppler processing to define a net azimuth beamwidth controllably smaller than the actual beamwidth of the antenna which is utilized by conventional scanning radars. The following paragraphs present typical azimuth presummer functional diagrams and implementations.

Azimuth Presummer Implementations - The azimuth presummer is a band-pass filter which reduces the azimuth bandwidth to that required for the desired resolution. This permits resampling at a lower rate to reduce data storage and data processing requirements.

Azimuth Resolution:

$$r_a \approx \frac{\lambda}{2\,\theta_a}$$

Azimuth Beamwidth
β_a

Processing
Aperture
θ_a
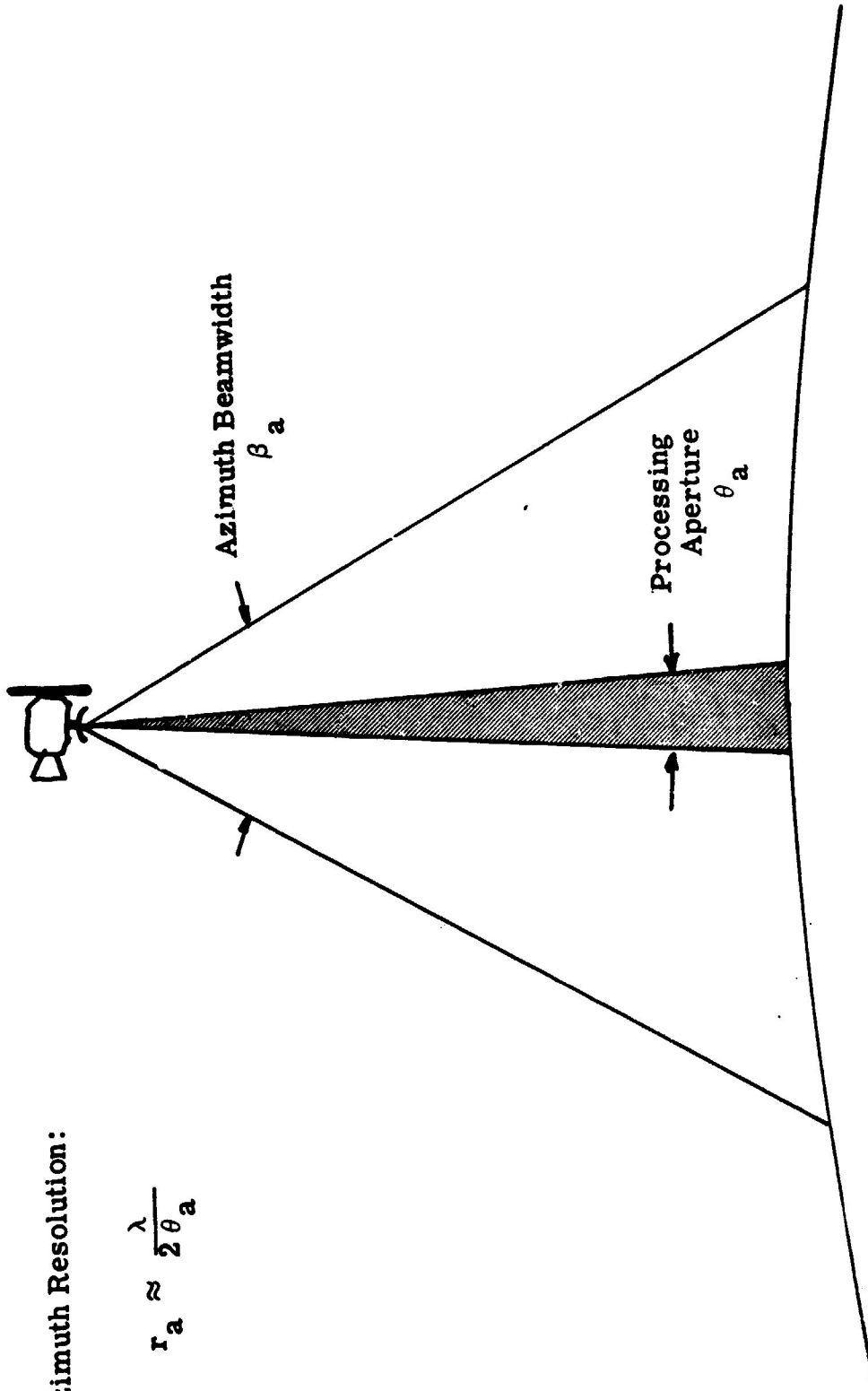
Figure V-4   Single Channel Azimuth Processing

One form of presummer is a finite impulse response transverse filter of length N. This requires N strong elements for each range cell. A conceptual diagram is shown in Figure V-5. However, since the filter output is resampled at a lower rate, PRF/K, a practical configuration requiring less storage can be used. This is shown in Figure V-6. The storage requirements are further developed in the Data Storage Requirements paragraph of this section.

In Figures V-5 and V-6, the sequence $\{s_n\}$ represents the azimuth samples obtained at a fixed range on successive PRFs, and the reference $\{w_n\}$ represents the presummer weighting coefficients. These coefficients correspond to the impulse response of a digital filter which selects the portion of the doppler spectrum to be processed. By changing the center frequency of the band-pass filters, any portion of the azimuth spectrum corresponding to different azimuth look angles within the beam can be selected for processing.

If the required processing angle, θ_a (see Fig. V-4), is appreciably less than the azimuth beamwidth, β_a, then it is possible to simultaneously select several non-overlapping or contiguous portions of the azimuth spectrum to permit multilook or multichannel azimuth processing.

Figure V-7 indicates the corresponding multiple azimuth apertures which can be selected by the bank of presummers shown in Figure V-8, each centered about a portion of the azimuth doppler spectrum corresponding to look angles other than the normal antenna boresight. Normally, the antenna electrical boresight is oriented to the zero doppler. The bank of presummers is essentially a multimode presummer which can be commanded to relay more channels of data when telemetry data rates are favorable or at the expense of areal coverage with a fixed volume mass storage system. Data from the multiple channels can be non-coherently integrated on Earth for image quality (various) improvement.
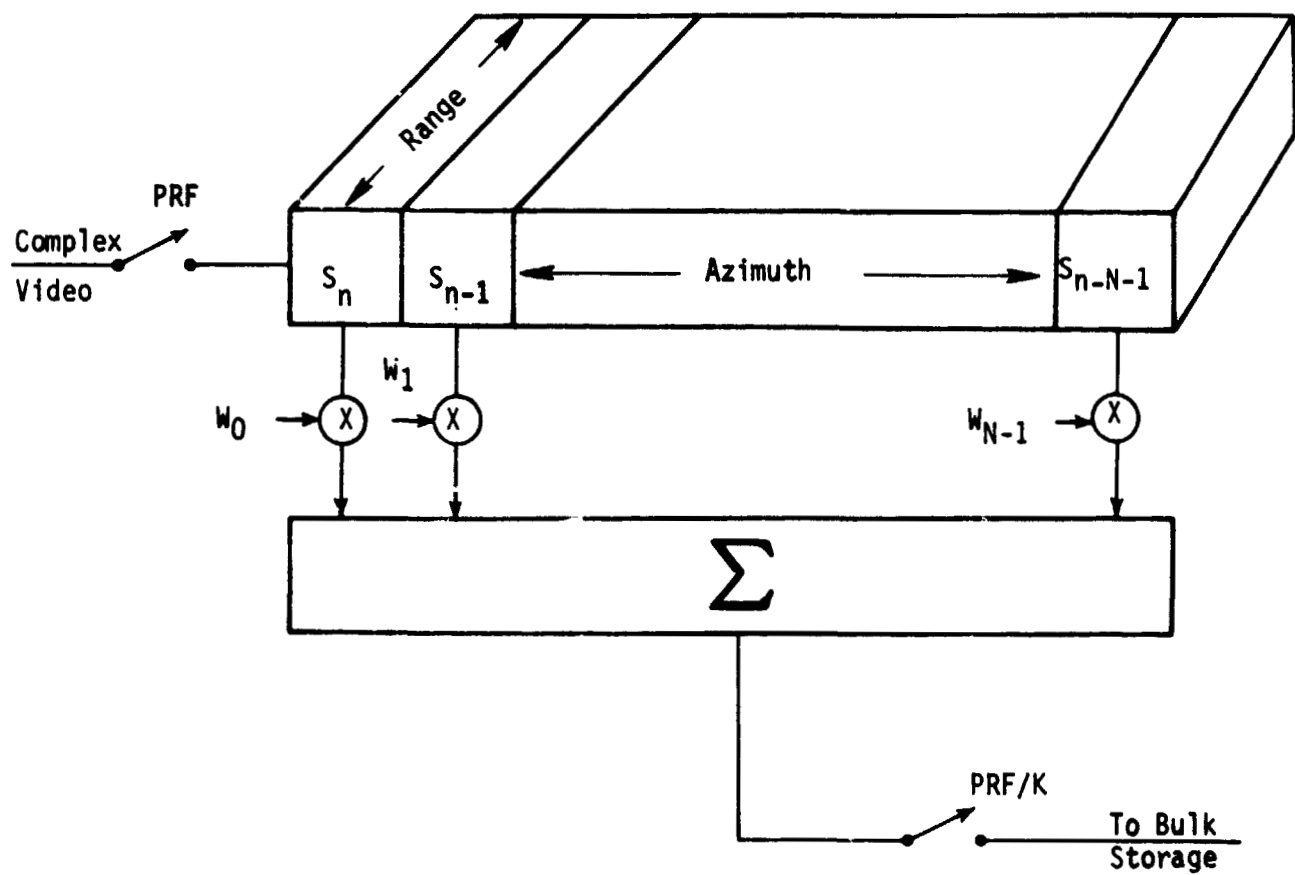
Figure V-5 Azimuth Presummer - Conceptual Diagram
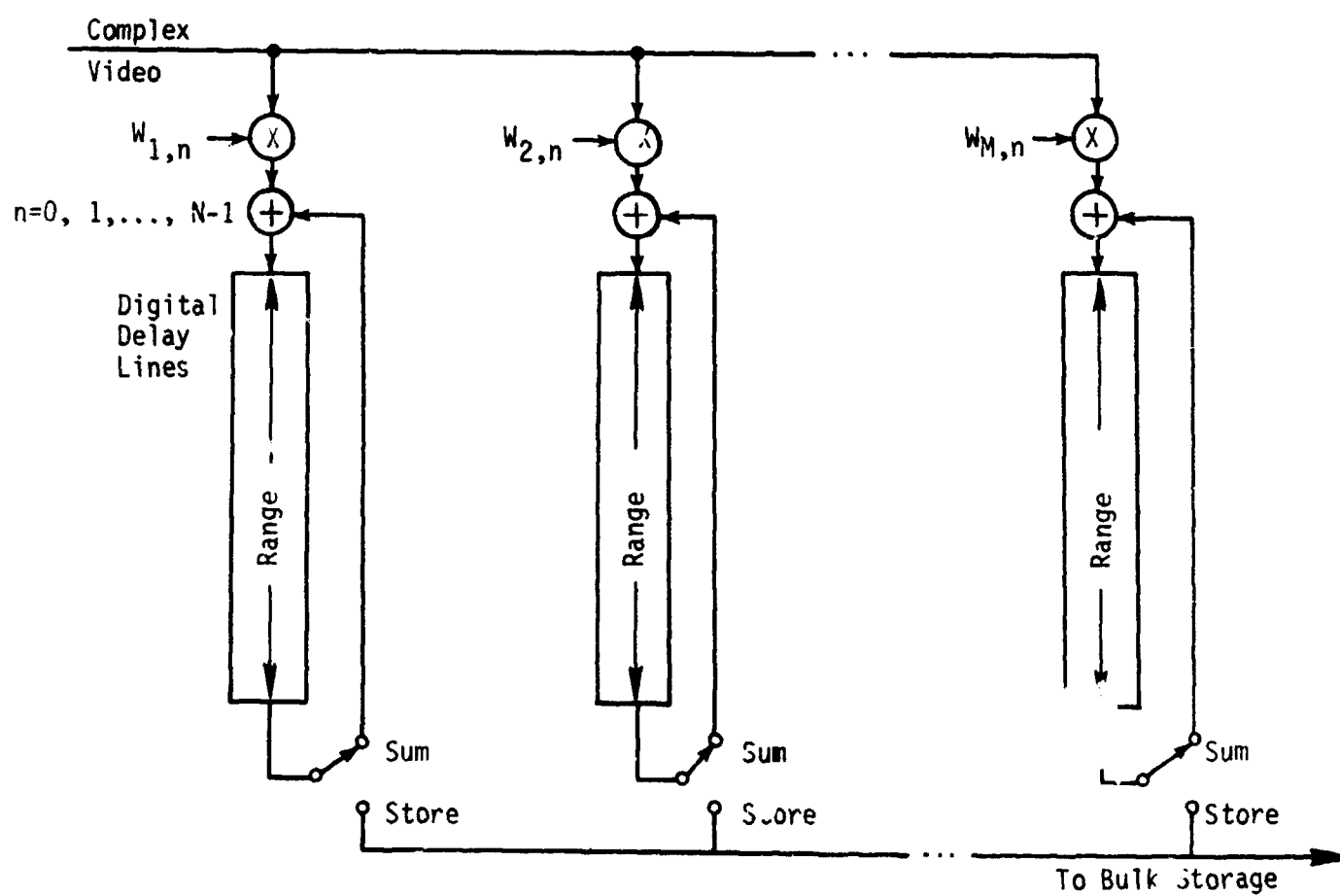
Figure V-6 Azimuth Presummer - Implementation
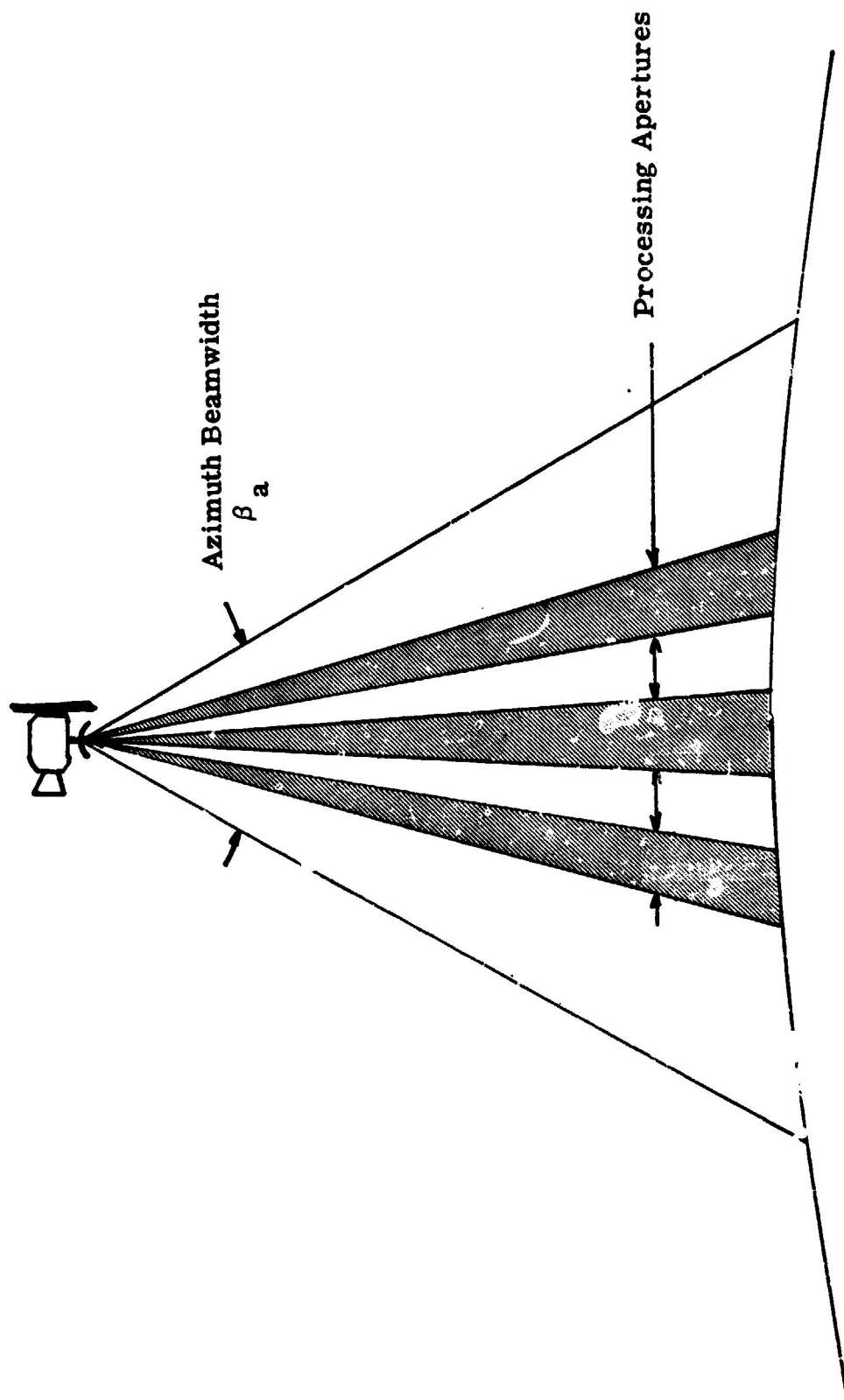
Figure V-7 Multichannel Azimuth Processing
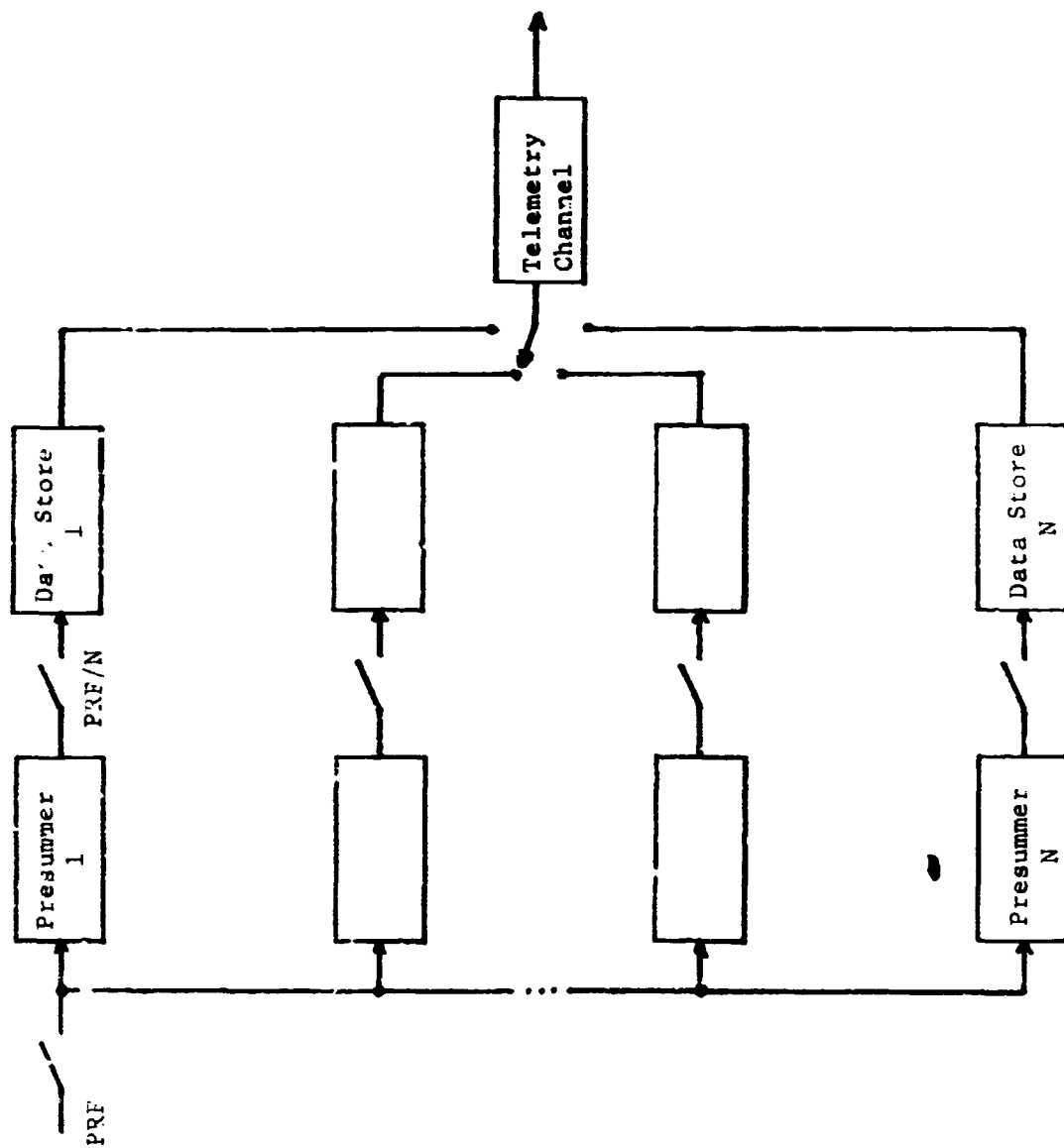
Figure V-8 Multichannel Adaptive Data Handling System

The buffered data rate out of a single presummer is equal to the azimuth bandwidth times the number of range resolution cells:

$$B_p = B_a \frac{W}{\rho_r}$$

$$= \frac{VW}{\rho_a \rho_r} \quad \text{complex samples/second} \qquad \text{(V-9)}$$

where B_p = presummer bandwidth

B_a = azimuth doppler bandwidth

W = swath width

ρ_r = range resolution

ρ_a = azimuth resolution

V = velocity

This must be multiplied by the number of azimuth channels to obtain the total data rate.

The output of the presummer is sent to the range-azimuth correlator for image generation. Corresponding data storage impact is developed in the Data Storage Requirements paragraph in this section.

Azimuth Processing Complexity - A measure of the azimuth processing complexity is the required azimuth compression ratio

$$K = \tfrac{1}{2} \frac{R\lambda}{\rho_a^2} \qquad \text{(V-10)}$$

which is equal to the minimum synthetic aperture divided by the corresponding resolution. It also represents th minimum number of discrete samples required to image the target to the specified resolution. For a fixed wavelength, the required azimuth compression ratio is proportional to range and inversely proportional to the square of the resolution. This is shown in Figure V-9.

If the compression ratio is fixed at the value K, then the azimuth resolution is

$$\rho_a = \sqrt{\frac{R\lambda}{2K}} \qquad \text{(V-11)}$$
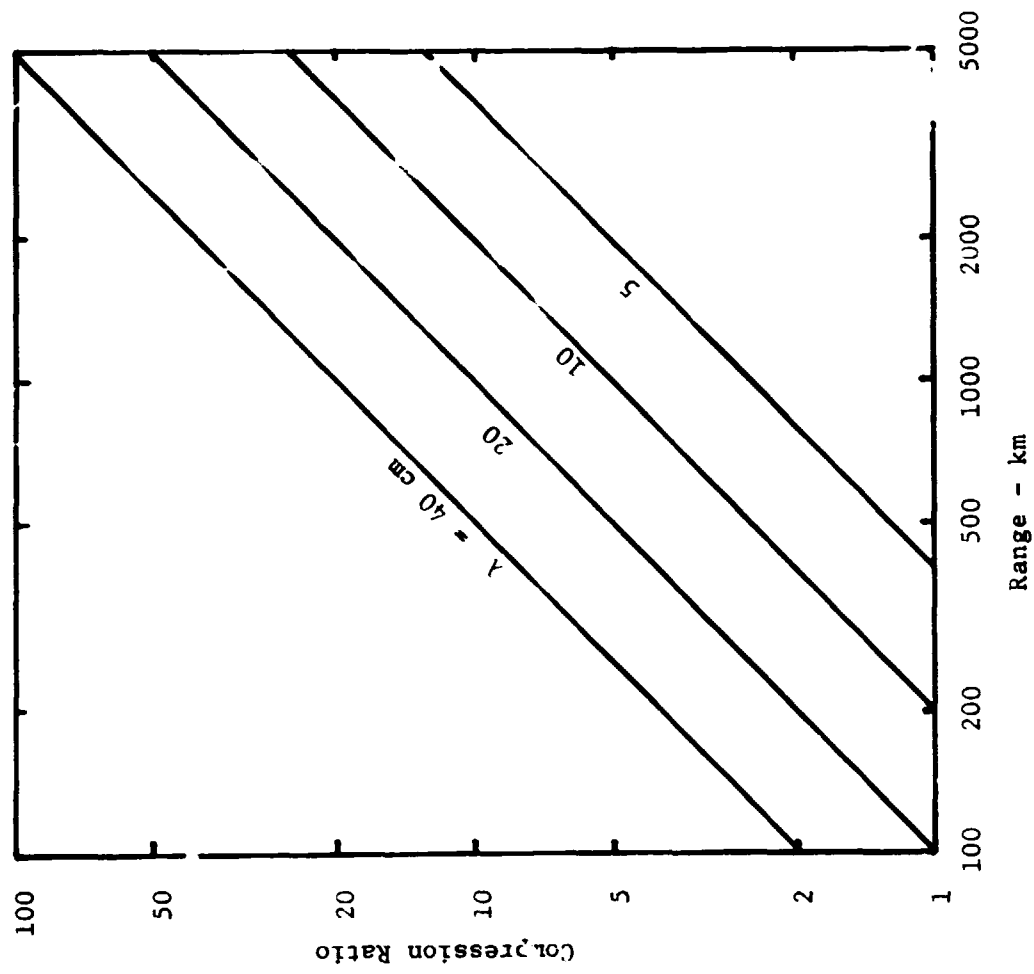
Figure V-9   Required Processor Compression Ratio for 100 Meter Azimuth Resolution

In this case, for a fixed wavelength, the azimuth resolution is
proportional to the square root of range. If K = 1, the processor
is "unfocused", i.e., the azimuth signal is integrated without a
phase correction.

This ratio applies to the resolution in the image. If the
image is formed on Earth, then the only concern is that data taken
from the surface possesses spatial frequency of at least one sample
per resolution element. Subsequent paragraphs will discuss the
impact of fixed and variable compression ratio for the option of
forming an image on the spacecraft.

Figure V-10 indicates the potential azimuth resolution of an
unfocused processor and Figure V-11 indicates the potential azimuth
resolution of a partially focused processor having a fixed com-
pression ratio of 25.

The unfocused processor is identical to the presummer, i.e.,
is simply a band-pass filter, and hence, would be the easiest to
implement on board the spacecraft. However, the best resolution
attainable is 158 m at 500 km slant range with λ = 10 cm. This
does not meet the reference mission requirements of 100 meter
resolution, hence a partially focused processor would be required
with compression ratio varying from 2 to 20 for λ = 10 cm and the
typical slant range variation of 400 to 4200 km in eccentric orbit.
The azimuth processor must be specified for the largest compression
ratio to preserve resolution at maximum distance. This is no prob-
lem for a ground processor, but would have significant impact on a
spacecraft processor. In particular, since a limited area is
mapped at the longer ranges, it may be more cost effective to use
a fixed compression ratio on-board processor specified for approxi-
mately 2000 km slant range, and then accept the small (x $\sqrt{2}$) azi-
muth resolution degradation at long range. Hence, because of the
varying azimuth compression required for constant resolution pro-
cessing in an elliptical orbit, it is recommended that image pro-
cessing be done on Earth.
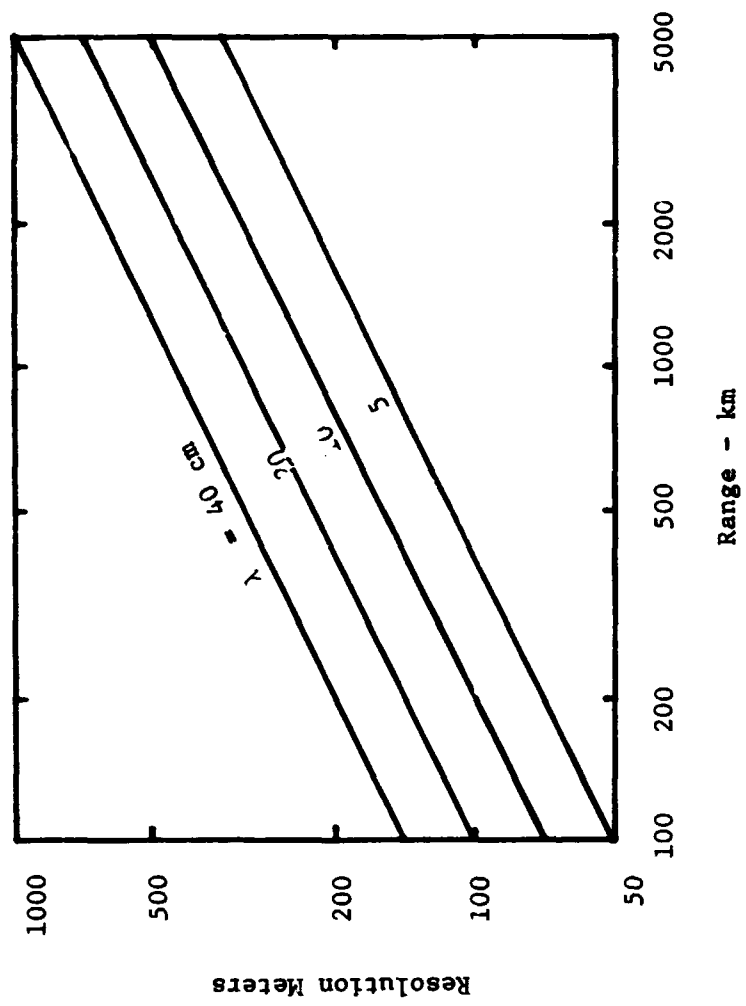
Figure V-10   Resolution for Unfocused Processor - Compression Ratio = 1
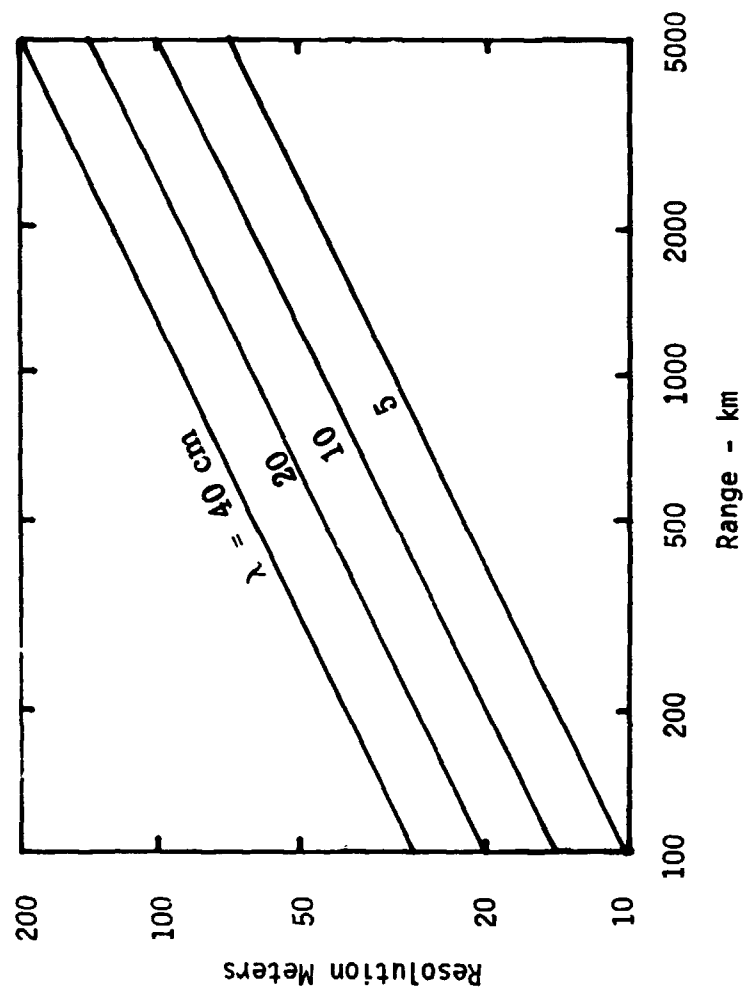
Figure V-11 Resolution for Focused Processor - Compression Ratio = 25

Mixed Integration Processing - The $(\text{mean}^2/\text{variance})$ ratio
of a single coherent image is unity. This is evidenced as image
speckle.

Figure V-12 illustrates one form of a mixed integration azimuth
processor used to reduce image speckle. The data is first pre-
summed to the minimum required bandwidth in N contiguous band-
pass filters. This data can then be resampled at the minimum
rate and stored in separate azimuth memories. The data is then
compressed in azimuth and square-law detected to generate N separ-
ate images. A single target will be imaged successively in each
processor. Hence, theoutputs must be delayed before noncoherent
summation to generate the final image. The $(\text{mean}^2/\text{variance})$ ratio
of the noncoherent sum is $1/\sqrt{N}$

If mixed integration processing is done on Earth, then the
telemetered data volume must be increased by N, the number of
channels added. If the processing is done on the spacecraft,
then the data rate is reduced to that of a single coherent image.
However, in the latter case, the cost (size, power and weight)
of the onboard processor could make this approach unfeasible. Hence,
it 's recommended that mixed integration processing be done on
Earth when the required additional telemetry bandwidth is avail-
able.

In summary, the recommended data processing strategies are given
in the following order of complexity:
1. Telemeter presummed azimuth and unprocessed range data for 100
   X 100 meter resolution.
2. Use additional data link capacity for finer azimuth resolution
   or mixed-integration ground processing.
3. Mixed integration onboard processing with fixed compression ratio.
4. Mixed integration onboard processing with fixed resolution.
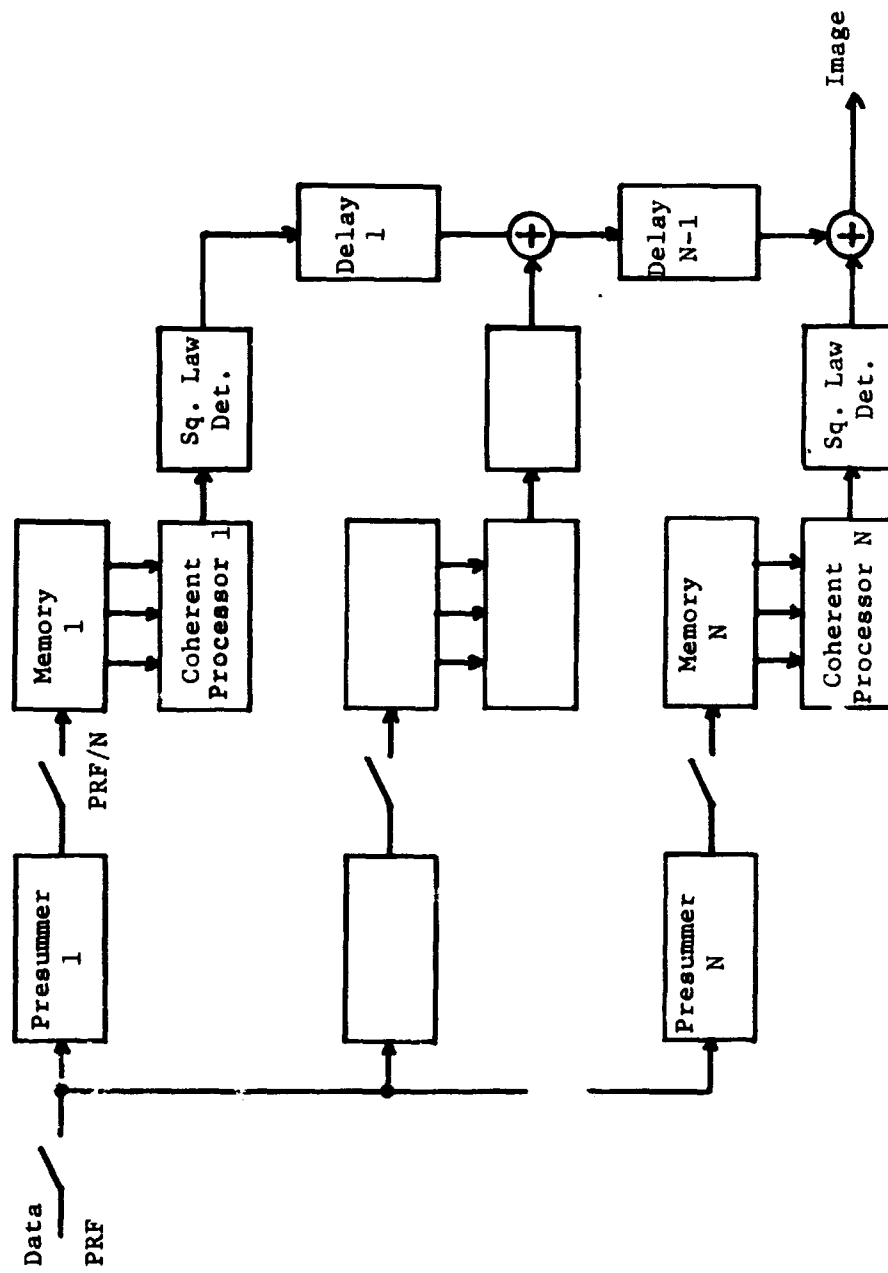
Figure V-12 Mixed-Integration Processor Configuration

Possible spacecraft impact versus processing type are com-
pared in Table V-3 which shows comparative weight and power for
onboard processing options.

Table V-3   Impact to Spacecraft for Onboard Radar Processing

Type	Weight	Power
Presummer (33 m res.)	5 kg	10 w
Presummer (100 m res.)	7 kg	15 w
Single Channel Image (Fixed K, 100 m res.)	20 kg	30 w
Mixed Integration - 4 Channels (100 m res.)	75 kg	125 w

In conclusion, this discussion has indicated that unfocused
processing can provide acceptable resolution for a circular
orbit and that a focused processor with variable compression
ratio is required to maintain a fixed resolution for eccentric
orbit.

Data Storage Requirements - The requirement for data storage
devices on board an orbital radar mapping spacecrfat is a firm
requirement due to the occurrence of Earth occultations, attitude
maneuvers (which misalign high gain antennas), possible mutually
exclusive surface mapping and high rate data relay (due to power
source and configuration limitations) and programming of Deep
Space Network receiving stations.

The storage requirements which will be discussed in this para-
graph will be those related to a) temporary storage used only to
buffer raw data rates (or do processing) and b) mass storage for
the control of conditioned radar data retrieved on a cyclic basis.
The relationship of processing to various synthetic aperture con-
cepts is discussed in the previous paragraph, SAR processing consid-
erations.

The study has shown (See Data Storage Considerations, Vol. III
Section V) that current or presently developmental semiconductor
technology is capable of meeting the temporary storage require-
ments at reasonable system impact, and that magnetic tape mass
storage machines will meet the cyclic bulk storage requirement.
Data flows into the system as indicated in Figure V-13 below.
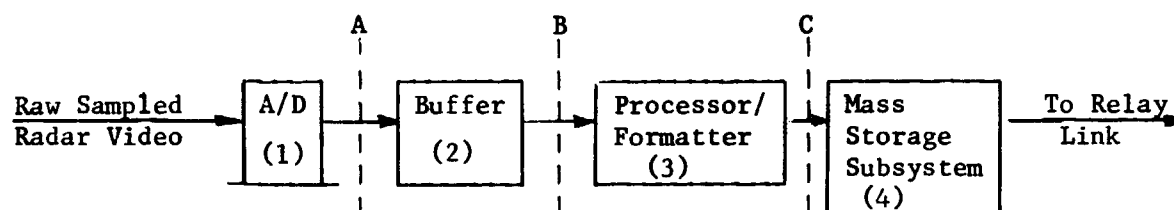
Figure V-13 Radar Data Flow

The data volume required in the mass storage is just the prod-
uct of the average data rate at point C (of Figure V-13) multi-
plied by the time that radar data is being retrieved. The study
has shown that an analog (film) mass storage system is excessive
for this mission (Vol. III, Section V, Data Storage Considerations)
therefore the discussion developed below will proceed in terms of
equivalent digital data rates.

Refer to Figure V-13. The data rate at point C can be related to key radar and orbital characteristics by:

Avg Data Rate at C:

$$\overline{B}_R = \frac{2V\ W\ Kk}{\frac{D_a}{2}}\rho_r = \frac{2V\ W\ Kk}{\rho_a\ \rho_r} \qquad (V-13)$$

Where: 2: minimum of 2 samples per resolution cell (One complex word)

V = velocity in ground plane (m/sec)

W = swath width in ground plane (m), nominal

K = number of bits per sample

k = additional sampling for aperture weighting and control. $(1 \leq k \leq 3)$

ρ_a = azimuth resolution dimension if full compression applied

ρ_r = range resolution dimension after compression

D_a = real antenna horizontal dimension

Equation V-13 is the average data rate after nominal presumming. The burst data rate at point A is related to radar parameters and swath width by:

$$B_B = \frac{W \times \frac{1}{\rho_r} \times N_s \times B_s \times k}{PRF^{-1} - (\Delta T_p + \Delta T_G)} = \frac{W \times \frac{1}{\rho_r} \times N_s \times B_s \times k}{\Delta T_W} \qquad (V-14)$$

Where: W = swath width in ground range

ρ_r = ground range resolution (ml, nominal)

N_s = number of samples per cell

B_s = bits per sample

PRF = pulse repetition frequency (Hz)

$$\Delta T_p = \text{dispersed pulse width (sec)}$$

$$c = \text{speed of light}$$

$$\psi = \text{grazing angle}$$

$$\Delta T_G = \text{PRF}^{-1} - \Delta T_p - \Delta T_W =$$

Interpulse guard time

$$\Delta T_W = \text{Propagation delay over swath}$$

$$= \frac{2W}{c} \cos \psi$$

The initial buffer relieves the impact of ΔT_W and provides the average rate determined by Equation V-13. Now, if all the data retrieved by the SAR were coherently processed, the resultant azimuth resolution would be on the order of $D_a/2$, or 1/2 the real antenna azimuth dimension. Thus, to process all radar data is excessive for the resolutions required by the topographic mapping mission. Thus a 200 meter antenna could meet the 100 m resolution requirement. But since antennas larger than about 10 meters are impractical with a spacecraft, a synthetically generated long antenna must be employed. The simplest processor is just an averaging device with a bandpass filter to limit spatial bandwidth to just that needed to achieve the desired azimuth resolution, and synthetically generated long antenna. The equivalent averaged data rate can be described by:

$$\bar{B}_p = \frac{2V \, W \, K \, k}{\rho_a} = \frac{2V \, W \, K \, k}{\frac{D_a}{2} \times \rho_r \times \frac{}{D_a}} \quad \text{BPS} \quad (\text{V-15})$$

Where: 2: minimum of two samples per resolution element,
            real sampling

        V: Relative velocity, m/sec

        ρ_a = potential azimuth resolution after averaging,
             ground range

        ρ_r = ground range resolution dimension (m)

        D_a = antenna real horizontal dimension (m)

        W = ground plane swath width (m)

        K = bits per sample $(3 \leq K \leq 6)$

        k = additional aperture sampling constant $(1 \leq k \leq 2)$

        $\dfrac{2\rho_a}{D_a}$ = presum number indicates spatial bandwidth reduction

̇ ̇e above equations are for uncompressed radar data that leads
to an image, but is not yet an image.

The equivalent digital data rate if images were formed can
also be related to radar and orbital parameters that data rate for
a single image:

$$\bar{B}_I = \frac{V\,W\,K\,k_a^{\,k}{}_r}{\rho_a\,\rho_r} \qquad \text{BPS} \qquad\qquad (V\text{-}16)$$

Where: $\bar{B}_I$ = average processed image data rate (single
             channel image)

        k_a = azimuth sampling density constant $(1 \leq k_a \leq 2)$

        k_r = range sampling density constant $(1 \leq k_r \leq 2)$

        K = quantization level, $(6 \quad K \quad 9)$

        ρ_a, ρ_r , V, W = defined above

The data rate for image formation by the "mixed integration
processing" approach is (when uncorrelated averaging is accomplished
on Earth):

$$\bar{B}_{MI} = N\,\bar{B}_I \qquad\qquad (V\text{-}17)$$

Where N is the number of azimuth channels added.

If the mixed integration, o. image averaging were accomplished on the spacecraft, the net rate to Earth would be the same as a single channel image, Equation V-16. The mixed integration processing is discussed in further detail in this section.

The data rates presented above are collected in Table V-4.

Table V-4 Derived Data Rates vs Processing Strategy

Rate for Processing Mode (BPS)	Characteristics Data Rate	Comments
Raw Burst Rate	$B_B = \dfrac{W \times \frac{1}{\rho_r} \times N_s \times B_s \times k}{\Delta T_W}$	Directly after ADC, varies with swath
Averaged Raw Rate	$\bar{B}_B = \dfrac{W \times \frac{1}{\rho_r} \times N_s \times B_s \times k}{(PRF^{-1})}$	After initial buffer
Post-presumming Rate	$\bar{B}_P = \dfrac{2 \times V \times W \times B_s \times k}{\rho_a \times \rho_r}$	Con. olled by degree of pre-summing
Single Channel Image	$\bar{B}_I = \dfrac{V \times W \times B_s \times k_a \times k_r}{\rho_a \times \rho_r}$	Final corrections on earth
Mixed Integration Image	$\bar{B}_{MI} = N \times \bar{B}_I$	If mixed integration on S/C, rate $\div$ N

(Varibles defined in previous paragraphs)

The above discussion has presented parametric data rates for the various processing and data acquisition strategies of this study. A key element of each equation is the required swath width which is determined primarily by the planet rotation rate and size, time between mapping cycles, and desired mapping overlap. A reference of about 20% overlap at the equator has been assumed for this study.

Figure V-14 presents parametrically the required swath widths versus orbital eccentricity referred to equatorial overlap. The figure also includes several orbital mapping strategies. A mapping strategy refers to the orbital mapping duty cycle that is a mapping strategy of 1:N implies that the surface is mapped every Nth orbit.

These swath widths are defined (Vol. III, Section V, Introduction and Assumptions) for a reference coverage at the equator, therefore, since the reference orbits are polar, or near polar, the overlap with a fixed swath width will follow an inverse cosine (latitude) function due to the variation in surface velocity at the planet with $\cos(\xi)$.

For the data management/communications study the widths are important because they directly affect the burst data rate, the average raw data rate, and presummer memory capacity. (Presummer memory capacity is also affected by quantization dynamic range and sampling frequency).

The burst data rate is described by:

$$\bar{B}_r = \frac{W \times \frac{1}{\rho_r} \times N_s \times B_s \times k}{\Delta T_W} = \qquad (V-18)$$
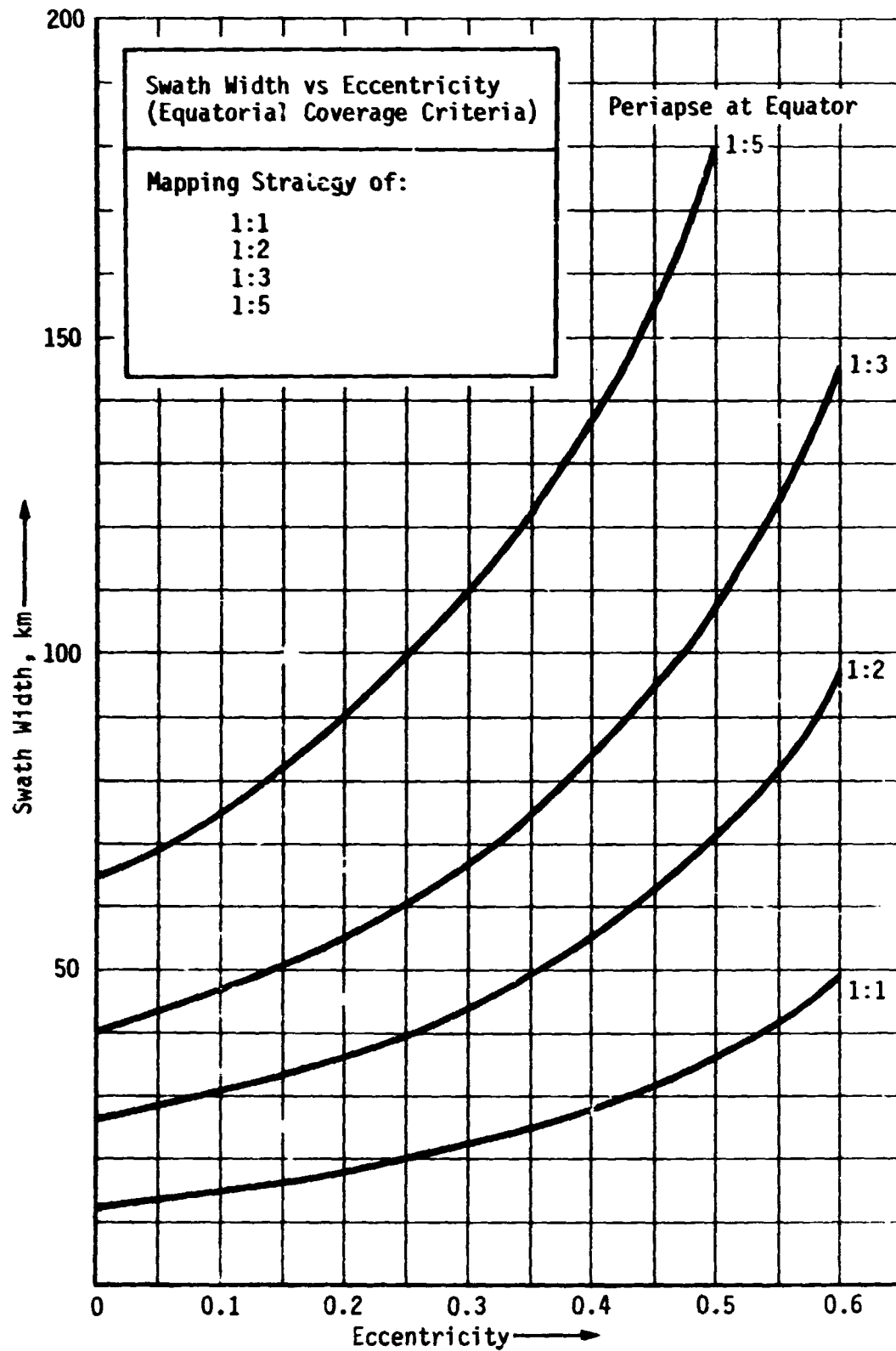
Figure V-14   Swath Width vs Eccentricity

Where: W = swath width ground range (m)

ρ_r = ground resolution, range (m), nominal

N_s = number samples per cell

B_s = bits per sample

k = sampling rate factor 1 k 2

PRF = pulse repetition frequency (Hz)

ΔT_W = Time data received over the illuminated swath =

$\dfrac{2\ W}{c}\ \cos\psi$

c = speed of light

ψ = grazing angle

The dependence on swath width is direct. The burst rate is conditioned to an average rate by the onboard presummer.

Now, when the swath width is designed for a given overlap at planet equator excessive overlap occurs at higher latitudes. Initial data field sizing employed the swath widths presented in Figure V-14. A refinement, then, to better utilize the data channel would be to store a data field based on the equatorial swath width, but actually relay a truncated data field to more closely follow a given (viz 20%) overlap criterion. This concept is diagrammed in Figure V-15 under ideal conditions of constant mapping altitude, (for swath width control with a changing altitude). The effects of illuminated swath width in the ground plane with eccentric orbit is discussed in Vol. III, Section IV. The study has not addressed the additional data base management required for such data averaging. All data would be initially accessed then catalogued with truncated groups of sweep such as those indicated by Figure V-15 in a preferred policy. Alternately, the swath widths processed could be truncated based on altitude with direct storage of a lower quantity of data. It would be necessary to provide data base overlap to assure contiguous equal resolution. An assessment

Legend:
- - - - Raw Swath Projection
——— Truncated Swath Projection

Planetary Disc

Equator

Truncation to Control
Overlap and Reduce Redundancy
of Data Relay
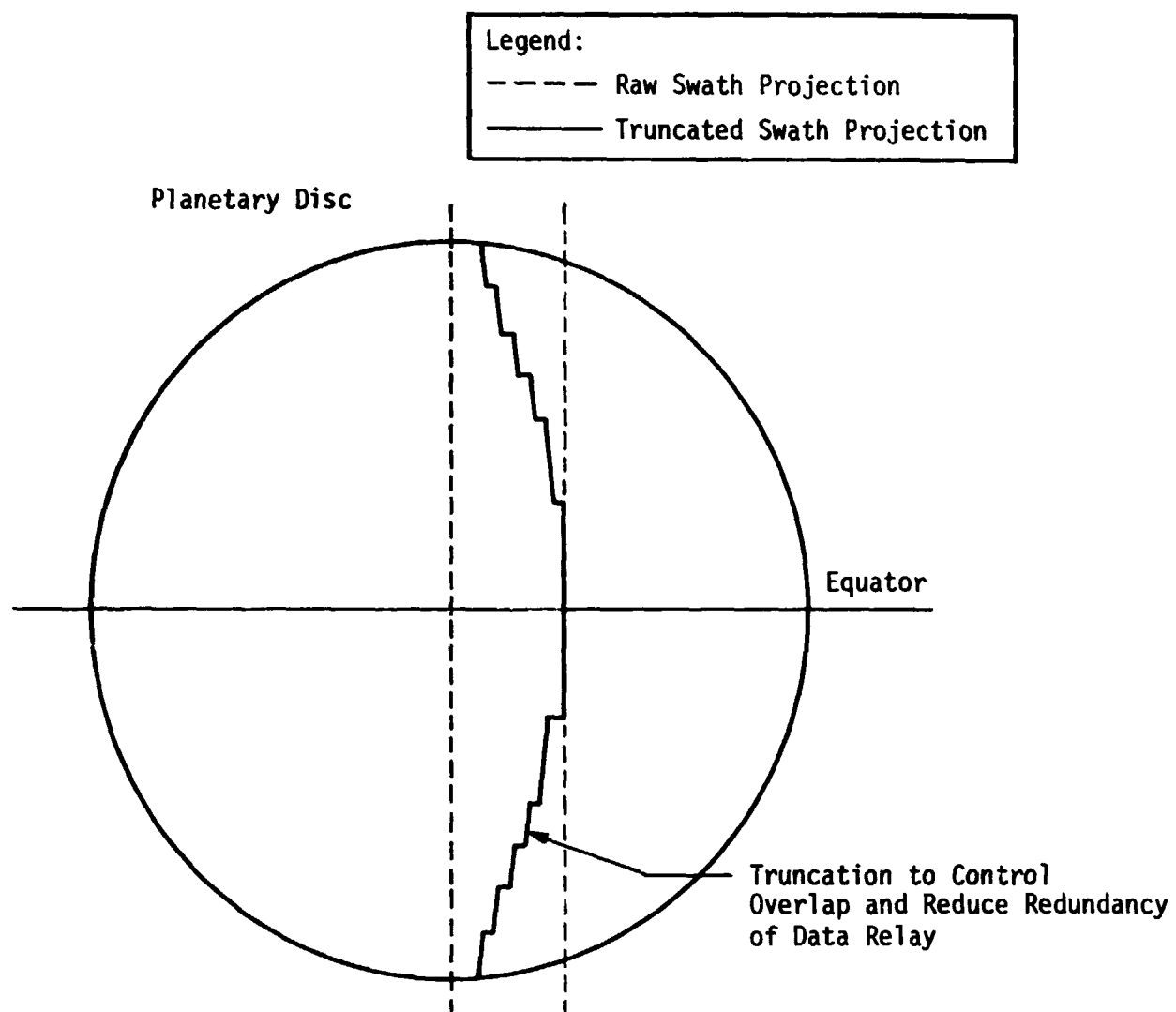
Figure V-15   Idealized Swath with Sampling Truncation to Equalize Overlap

of potential data reduction over the references taken for this study can be shown by deriving an "average" resolution cell rate based on overall planet area, rotation rate, and processing sampling. With the assumption that the entire surface must be sampled the average resolution cell rate is:

$$\text{cells/hour} = \frac{\text{surface area}}{\substack{\text{resolution cell dimensions x} \\ \text{total mission hours}}} \qquad \text{(V-19)}$$

$$= \frac{4\pi R_p^2}{\rho_a \times \rho_r \times 242.6 \times 24}$$

$$= \frac{4\pi \times (6050 \times 10^3 \text{ m})^2}{(100 \text{ m}) \times (100 \text{ m}) \times 242.6 \times 24} =$$

$$= 79 \times 10^5 \text{ cells/hour} \qquad \text{(V-20)}$$

where R_p = planet radius

$\rho_a = \rho_r$ = 100 meter reference resolution

242.6 = nominal Venus year (Earth days)

24 = 24 hours per Earth day.

Then on the basis of a minimum of one complex sample per resolution cell quantized to 4 bits each for amplitude and phase an average data acquisition rate per hour would be:

$$7.9 \times 10^6 \text{ cell/hour} \times 8 \text{ bits/cell} = 63.2 \times 10^6 \text{ bit/hr} \qquad \text{(V-21)}$$

Now if the data volume were averaged over every orbit, then for the reference 0.5 eccentricity orbit of 4.48 hours the data volume would be (on the average)

$$4.48 \text{ hr} \times 63.2 \times 10^6 \text{ bit/hr} = 283 \times 10^6 \text{ bit/orbit} \qquad \text{(V-22)}$$

When compared to a typical design (Section V, Vol. II) for the .5 eccentricity orbit (mapping every orbit) the potential for an average data relay reduction can be determined:

$$\frac{\text{reference rate}}{\text{average rate}} \sim \frac{880 \times 10^6 \text{ bit}}{283 \times 10^6 \text{ bit}} = 3.1 \qquad \text{(V-23)}$$

Now, if a nominal 20% overlap were desired in azimuth and an arbitrary 20% overlap in range was assumed, the "excess ratio" of 3.1 would become:

$$0.8 \times 0.8 \times 3.1 = 1.99 \approx 2.0 \qquad (V-24)$$

Thus, "on the average" additional data base management onboard might reduce the required volume of data relayed by nearly a factor of two, not a significant reduction. The tradeoff between the advantage of additional redundant data (nominal design of this study) and a more accurate control of overlap criterion is assessed to be highly subjective so that this study does not pursue this characteristic further. This discussion is included to recognize the potential data rate reduction by swath width variation to control the overlap criterion more closely, but is not recommended for the mission due to the relatively little overall total data base reduction possible.

The discussion following presents factors of the remaining data rate factor, data quantization level.

Analog to Digital Data Conversion

The data rates developed previously all include the number of bits per sample which relates directly to the quantization dynamic range. Data dynamic range follows from the coarseness of the input analog/digital converter (ADC). For an n-bit converter (where maximum voltage is denoted by V_{max}) + $V_{max}/2$ results in all ones and $-V_{max}/2$ to all zeros at the converter output. The minimum voltage of interest, V_{min}, for a given conversion is that signal detectable at the least significant bit of the ADC. Dynamic range is given by:

$$R_{ADC} = \frac{V_{max}}{V_{min}} = 20 \ \log_{10} \frac{2^B}{2} = 20 \ \log_{10} 2^{B-1} \qquad (V-25)$$

Thus the voltage dynamic range of a 4 bit ADC is:

$$20 \ \log_{10} 2^3 = 18.06 \ db \qquad (V-26)$$

Figure V-16 presents parametrically the ADC voltage dynamic range based on the above equation versus number of bits, up to 7. The figure presents voltage dynamic range in terms of:

DR = data rate

n = number of bits

The dynamic range of the data quantization should be correlated to the expected radar video S/N ratios. Nominal designs have provided for a radar S/N of at least 10 db based on the average cross section. Two policies are possible for the ADC; a) a static fixed conversio: for all radar signal levels, or b) data conversion referenced to the actual signal level in the radar receiver. Case b) is preferred and only requires the ADC to be continuously referenced to the receiver automatic gain control. This dynamic reference scheme can allow the 18 db converter voltage dynamic range to follow the entire dynamic range of the radar receiver. The receiver AGC is available as a desired auxiliary science data type.

The quantizer word size of fine resolution digital SAR signal processors is, however, a controversial factor. The discussion following presents a statistical basis for quantizing for minimum distortion and presents brief conclusions regarding possible quantization to a low as one bit. Insufficient results are currently available to confidently recommend one bit quantization for the partially focused Venus mapping application, but further evaluation is recommended for this approach which could drastically reduce data volume required.

Recent experiments have shown that dispersed SAR data quantized to one-bit amplitude resolution can produce imagery only slightly inferior to the best quality imagery obtained from "linear" recorded data. The term "linear" is placed in quotations to emphasize the fact that the radar systems used are not strictly linear, but exhibit varying degrees of RF, IF and recorder saturation.
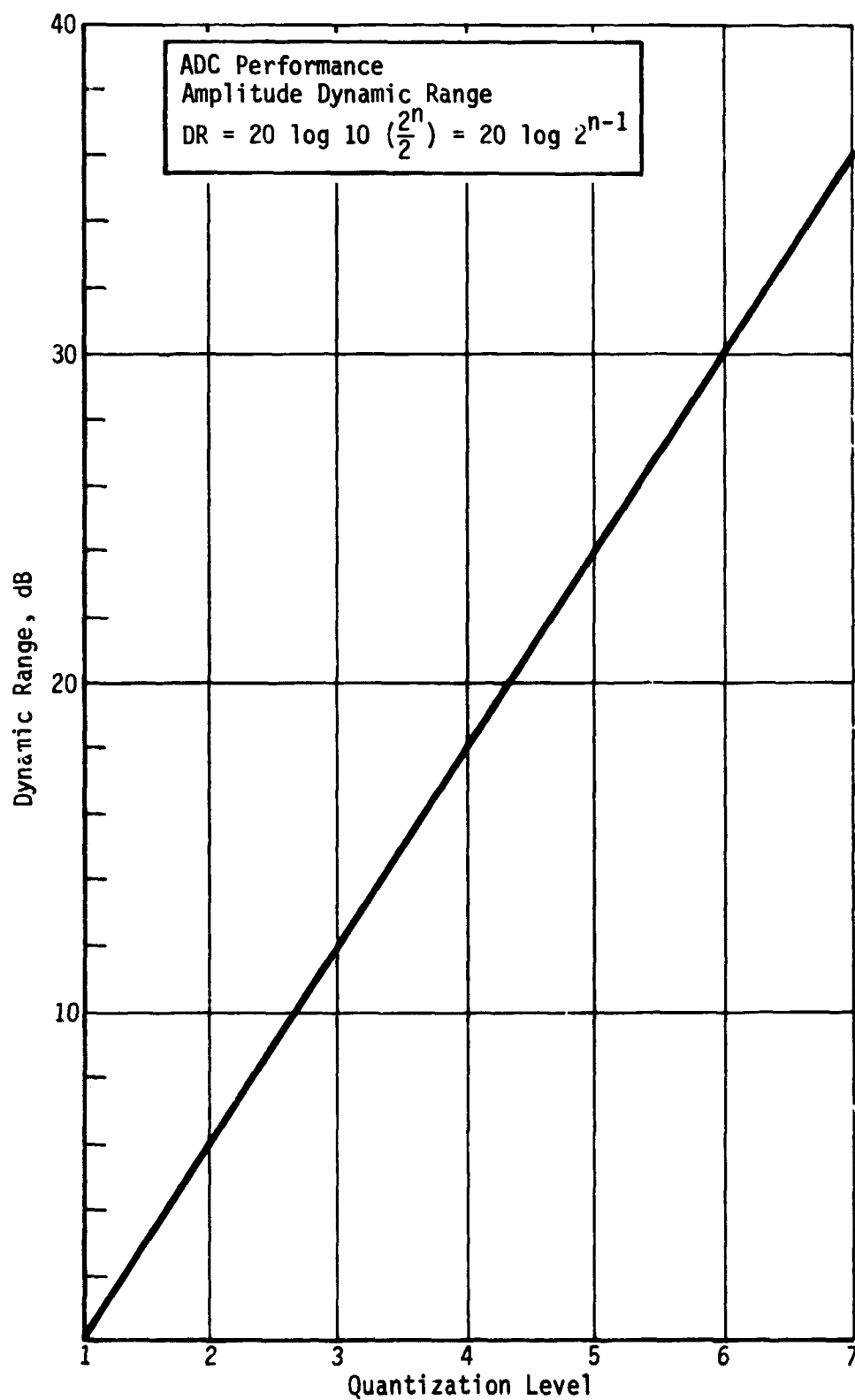
Figure V-16 ADC Dynamic Range vs Quantization Level

ADC Performance
Amplitude Dynamic Range
$DR = 20 \log 10 \left(\frac{2^n}{2}\right) = 20 \log 2^{n-1}$

In particular, the one-bit quantization did not introduce observable false targets due to intermodulation distortion as predicted by analysis of simple high SNR models. In the limited airborne quantization experiment conducted by ERIM (Environmental Research Institute of Michigan) the dominant effect was essentially large signal suppression, or image AGC, for imagery obtained of an agricultural ar.. (ref. V-1). Surprisingly, ground painting (clutter mapping) was ot significantly affected. In the airborne experiment conducted by Goodyear and processed by ERIM, the dominant effect was a 3 to 4 db increase in uniform background noise for imagery obtained over an urban scene and over water. Imagery of a calibrated corner reflector field showed no change in dynamic range of the correlator output.

These results suggest that for large time-bandwidth product signals the actual video signal dynamic range, based on instantaneous r.m.s. signal to r.m.s. clutter plus noise, is close to unity, such that the dominant effect of limiting is signal suppression with respect to the noise.

Consequently, the phase histories of the (point target) signals are undistorted and compress at the processor output. The video limiting does not significantly change the noise structure within the processed signal bandwidth, hence, the noise does not compres. before or after quantization.

Consider the quantizer transfer characteristic and error function shown in Figure V-17 where v represents the input signal, v_q the quantized signal and

$$v_q = v - v_q \tag{V-27}$$

is the error or distortion signal. If the signal, v, is randomly distributed, and a sound measure of the dynamic range of the quantizer or A/D converter is the ratio of signal power to distortion power at the quantizer output. For a quantizer of reasonable size

Output Signal

Equivalent Noise Signal

Equivalent Quantizer Noise Model
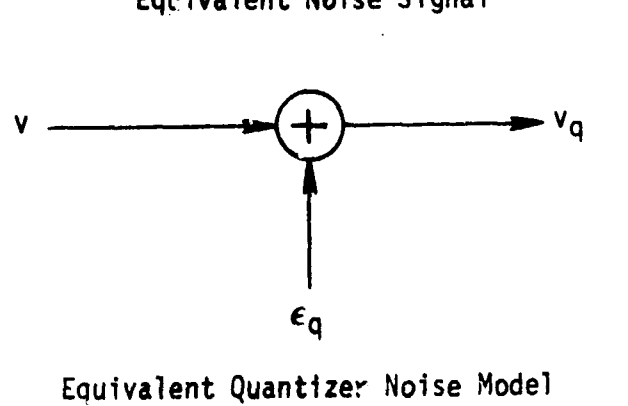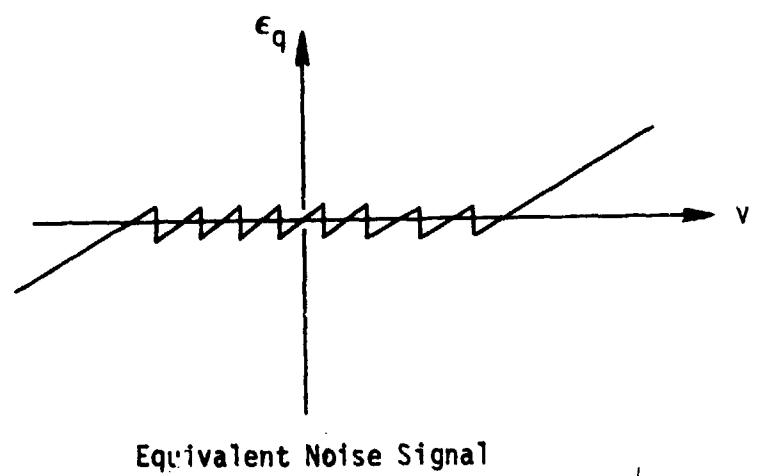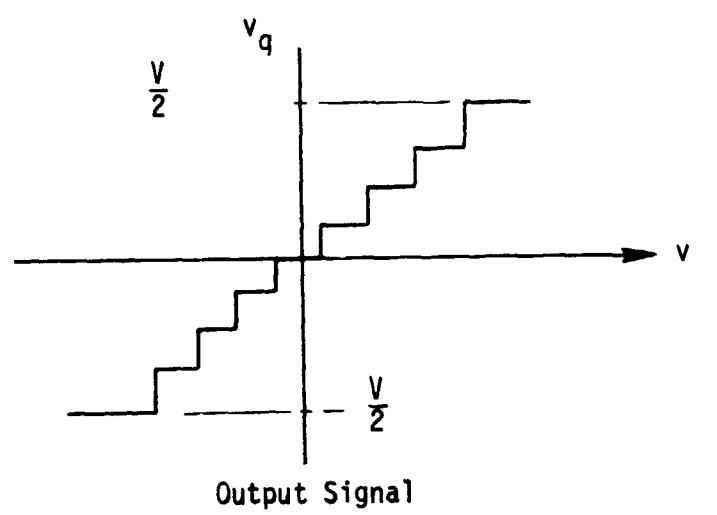
Figure V-17 Quantizer Transfer Functions

(3 bits or more) the distortion or quantization noise is nearly uncorrelated with the input and, hence, acts as an equivalent added noise with variance

$$\sigma_q^2 = \frac{(\Delta v)^2}{12} \tag{V-28}$$

where Δv is the quantization interval. This is shown in Figure V-17.

Let $N = 2^k$ (V-29)

be the number of quantization levels, where k is the number of bits in the quantized word. Then the saturation levels of a symmetric bipolar quantizer are $\pm V/2$ where

$$V = N\Delta v \tag{V-30}$$

is the quantizer range. If the input signal, v, is uniformly distributed over the quantizer range, then the variance of the input is

$$\sigma_v^2 = \frac{V^2}{12} \tag{V-31}$$

and the quantizer dynamic range or SNR is

$$\begin{aligned} SNR_Q &= \sigma_v^2 / \sigma_q^2 \\ &= N^2 \\ &= 6 \ k \ db \end{aligned} \tag{V-32}$$

However, the video signals are not uniformly distributed in amplitude, hence, equation (V-32) has little value in describing the effects of quantization on the signal.

If the video signal has a Gaussian amplitude distribution, then the effects of A/D saturation must be considered. In this case, for a given number of quantization levels, the scale factor (saturation value/r.m.s. signal) can be set to minimize the total distortion. Max (ref. V-2) determines the optimum quantization level for N from 1 through 36. Results for N = 8, 16 and 32 (k = 3, 4, or 5 bits) are shown below.

Scale Factor and Dynamic Range
For Optimum Quantization of Gaussian Signals

k (bits)	Scale Factor (V/2)	Dynamic Range (SNR$_Q$-db)
3	2.35	14.3
4	2.68	19.4
5	2.83	24.6

Let us now relate A/D converter size to video SNR. Let SNR_{IN} be the video SNR defined as the ratio of average uncompressed signal power to average noise plus clutter power. Let SNR_Q be the dynamic range or equivalent SNR of the quantizer. Then if quantizer noise is uncorrelated with the input, the output SNR is given by

$$\frac{1}{SNR_{OUT}} = \frac{1}{SNR_{IN}} + \frac{1}{SNR_Q} \qquad (V-33)$$

From Equation (V-33) we see that the output SNR is ,nated by the lesser of SNR_{IN} and SNR_Q. Hence, from an equivalent noise point-of-view, there is no advantage to setting SNR_Q much greater than SNR_{IN}. In particular, if

$$SNR_Q = SNR_{IN} \qquad (V-34)$$

then

$$SNR_{OUT} = \tfrac{1}{2} SNR_{IN} \qquad (V-35)$$

A reasonable range of SNR_Q is

$$SNR_{IN} \leq SNR_Q \leq 4\ SNR_{IN} \qquad (V-36)$$

We are now, however, faced with the problem of defining input video SNR which is highly target dependent. For example, if the radar is used for terrain mapping of ground clutter, then SNR_{IN} is the ratio of clutter power to receiver noise power. If the radar is mapping a sparse field of point targets, then SNR_{IN} is the ratio of instantaneous uncompressed target signal power to clutter plus receiver noise power. If the radar is mapping a dense field of point targets, then the composite signal will be nearly Gaussian

and SNR_{IN} may be interpreted as the ratio of desired signal power
to clutter plus noise power.

It then makes sense to base the quantizer dynamic range on some
statistical measure of expected input SNR. If the input SNR drops,
then no information is lost. If the input SNR increases due to a
strong target, the A/D converter will saturate. However, the one-
bit quantization experiments indicated that occasional saturation
does not seriously affect image quality; consequently, extending
the dynamic range of the quantizer to accommodate occasional large
targets does not appear to be cost effective.

To summarize, from Table V-5 we note that a 4-bit A/D converter
has a dynamic range of 19.4 db and saturation levels of $\pm 2.68\ \sigma$ for
Gaussian inputs. This should be adequate if the input SNR is less
than 20 db. However, experimentation with coarse quantization of
moderate time-bandwidth product signals like those expected with
the Venus orbiter is recommended to verify this conclusion.

Temporary Storage Requirements, Presummer

A presummer for synthetic aperture radar data is a device which
operates on raw digitized radar data to provide averaged data with
reduced spatial frequency* (and bandwidth) for storage. The pre-
summer requires a temporary storage element since a group of range
bins must be operated on simultaneously to compute the resultant
average value (amplitude, and phase) of the received clutter signal
for storage.

A conceptual diagram of a basic fully expanded azimuth presummer
is presented in Figure V-5.

---

*Spatial frequency is a measure of the distance along the ground
between range sweeps of the side looking radar. In eccentric orbit
a variable PRF is required to maintain a constant spatial increment.

The figure indicates that the complex (amplitude and phase) radar receiver output is sampled and stored in a temporary memory device with subsequent range sweeps next to each other. Corresponding range bins (i.e., cells at the same slant range from the radar) from subsequent sweeps are each multiplied by a weighting factor for spatial side lobe control, summed, and averaged before storage in the onboard mass memory. This process of taking data at a higher rate, and storing it at a lower rate is indicated by an input switch being toggled at the PRF (pulse repetition frequency) and an output switch being toggled at a lower rate, PRF/K where K depends on the amount of averaging or combining done on the raw data. The number of range sweeps needed in order to compute a composite value is related to theory about the spectral distribution of energy reflected from a given surface area, and as a minimum is determined by the ratio $2\rho_a/D_a$, where ρ_a = azimuth resolution and D_a is the antenna dimension in the horizontal direction. Workers (ref. V-3) in the field define a sufficient maximum number of additional sweeps averaged as 3 Np; Np is presum number.

In Figure V-5 the following definitions are used:

N = azimuth presum number, $2\rho_a/D_a$

W_i = weighting factors for side lobe control and spatial filtering

PRF = pulse repetition frequency

K = data rate reduction factor

The purpose of a presummer is to average the raw data, limit frequency and spatial bandwidth, and incorporate weighting to maintain side lobe suppression. Presented in Figure V-18 are parametric data rates which would impinge on a presummer or buffer memory.

Figure V-18 presents the raw data rates versus number of range bins. Number of range bins is computed by:

$$N_{RB} = W \times 1/\rho_r \tag{V-37}$$

where W = swath width in ground range

ρ_r = range resolution in ground range

The number of range bins required for this mission fall between 130 and 720 with a nominal 100 m ground range. Corresponding raw data rates fall between 5-27 Mbps, compatible with current solid state technology). The basis for the parametric curves is complex sampling of amplitude and phase quantized to 4 bits each.

The presummer storage is dictated by swath width, presum number, quantization level, and sampling policy such as complex amplitude and phase. The temporary storage may be described by the equation:

$$S_p = \frac{W}{\rho_r} \times C \times B_s \times N_p \times k \tag{V-38}$$

where S_p = temporary presummer storage, bits

W = swath width on ground, meters

C = samples per cell $C \geq 2$

B_s = bits per sample $2 \leq B_s \leq 6$, 4 nominally

N_p = $2 \rho_a / D_a$, presum number $15 \leq N_p \leq 50$, typically with D_a = 4 meter

k = over sampling factor, $1 \leq k \leq 3$, reference of 1

if a fully expanded presum implementation were used. Recent implementations use iterative integration (integrate-and-dump) methods to reduce storage. This is discussed in a later paragraph.
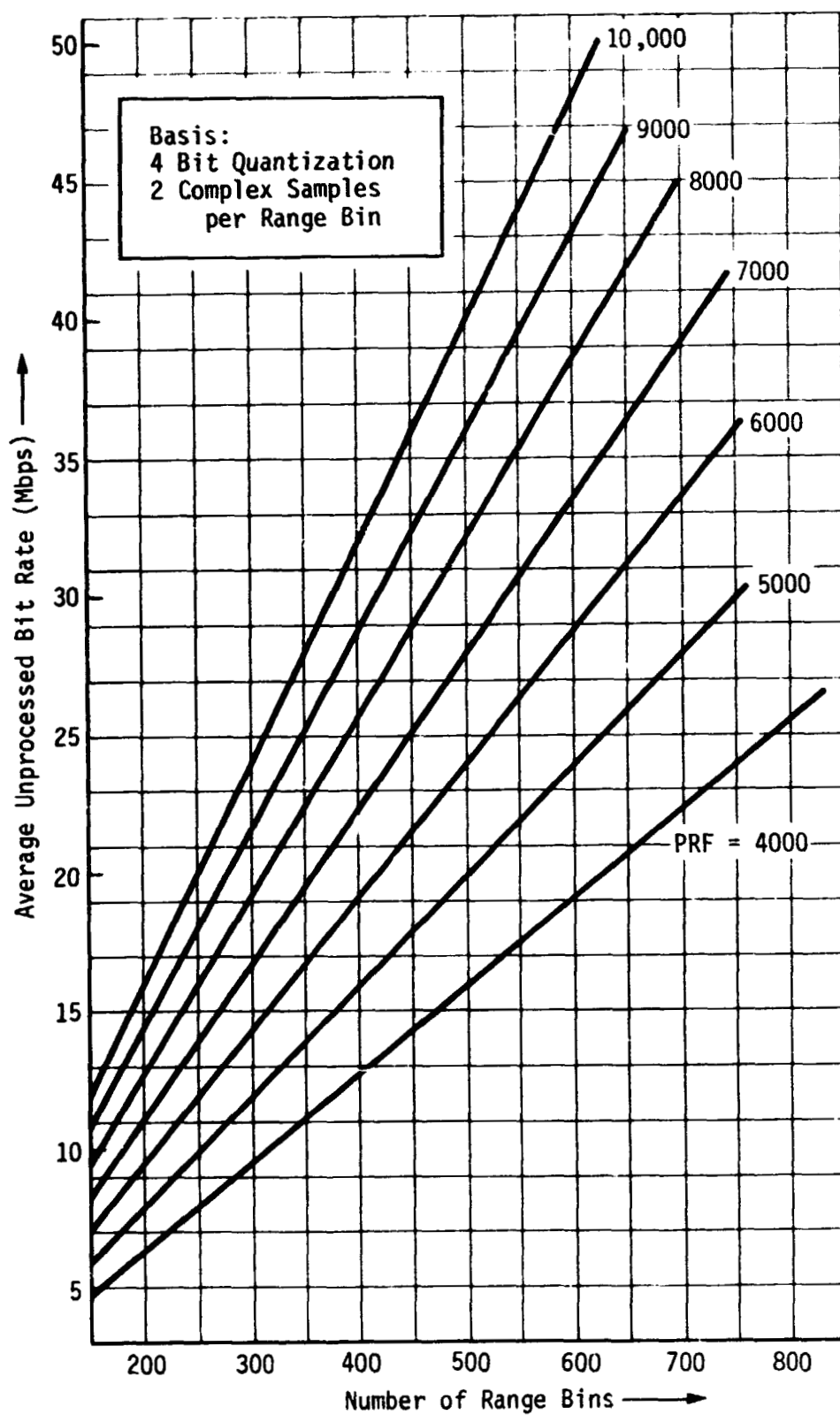
Figure V-18   Average Unprocessed Bit Rates

These requirements can be presented parametrically based on swath width (eccentricity, mapping strategy) and nominal assignments for the other variables. The results of sample parametric analyses are shown in Figures V-19 through V-22. From Equation (V-38) the expanded presummer storage is:

$$S_p = \frac{C \times B_s \times N_p \times k}{\rho_r} \times W \text{ bits} \tag{V-39}$$

$$S_p = \frac{2 \times 4 \times 16 \times 1 \times W}{10^2} \text{ bits} \tag{V-40}$$

$$= 1.6 \text{ W, } Np = 16 \ (\rho_a' = 33 \text{ m, } D_a = 4 \text{ m})$$

$$= 4.0 \text{ W, } Np = 50 \ (\rho_a' = 100 \text{ m, } D_a = 4 \text{ m})$$

Figure V-19 shows storage for 1:1 mapping strategy. Figure V-20 presents storage for 1:2 strategy. Figure V-21 shows the 1:3 strategy. Figure V-22 shows the requirements for the 1:5 mapping strategy.

An alternate implementation, and the recommended concept, of the presummer is conceptually diagrammed in Figure V-6. This technique employs digital delay lines as the storage element. Weighted values are stored in the dynamic shift registers. This technique can result in a lower storage requirement depending on the relative value of the presum number, Np, and the number of range bins per swath. This is the preferred concept, and requires reduced storage relative to the fully expanded presummer discussed previously.
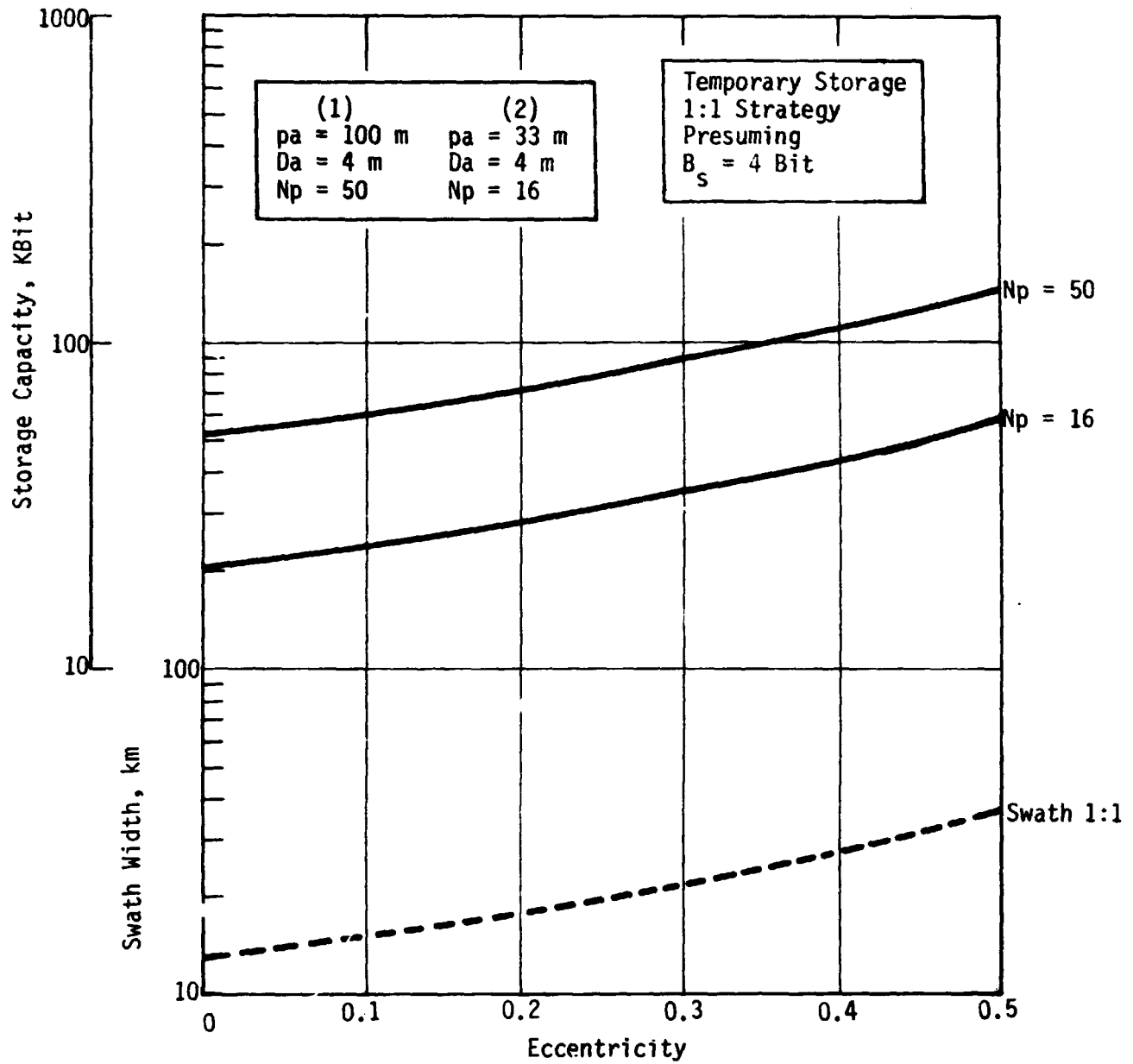
Figure V-19 Temporary Storage -- 1:1 Strategy, Expanded Presummer
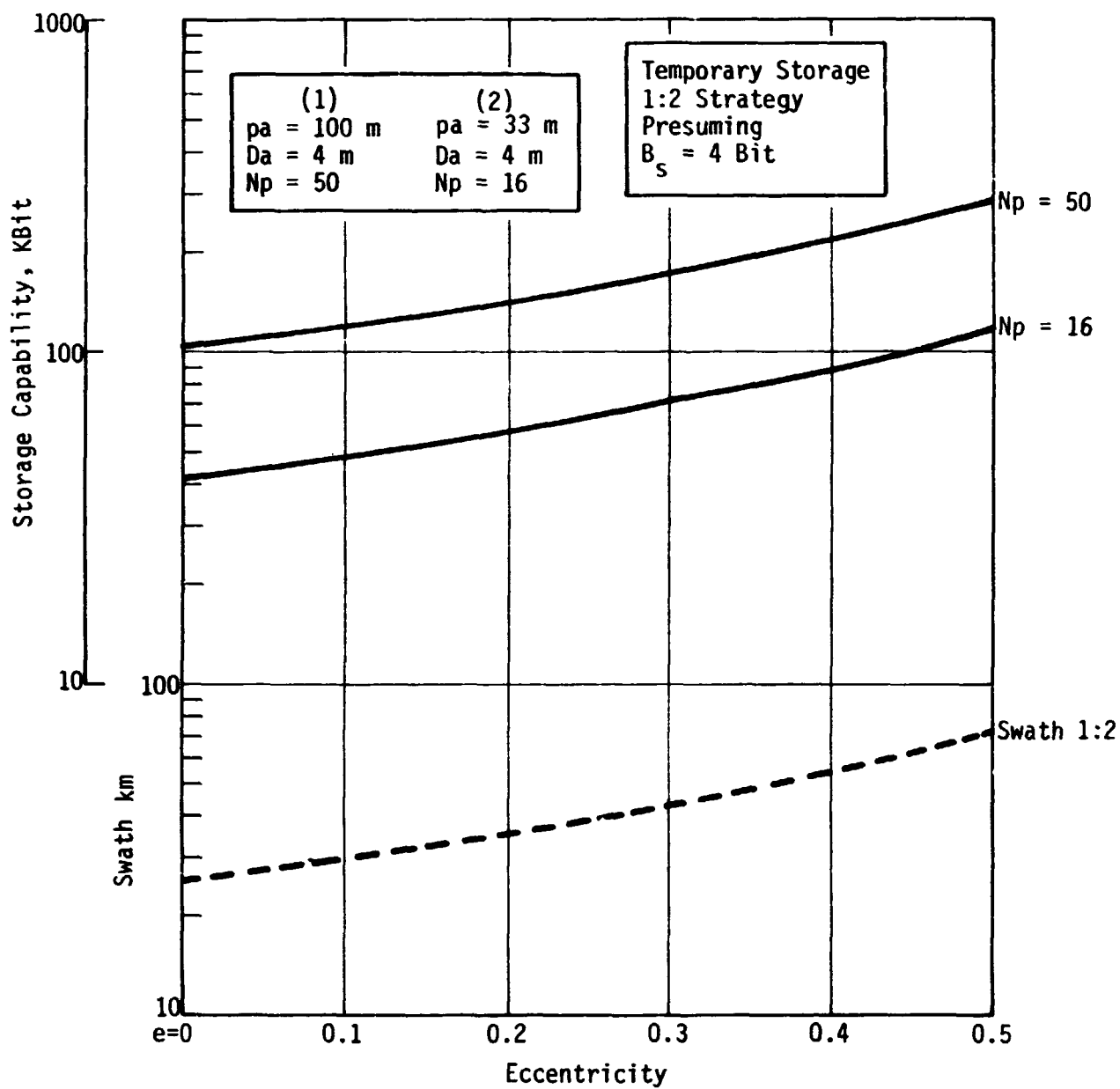
Figure V-20   Temporary STorage -- 1:2 Strategy, Expanded Presummer
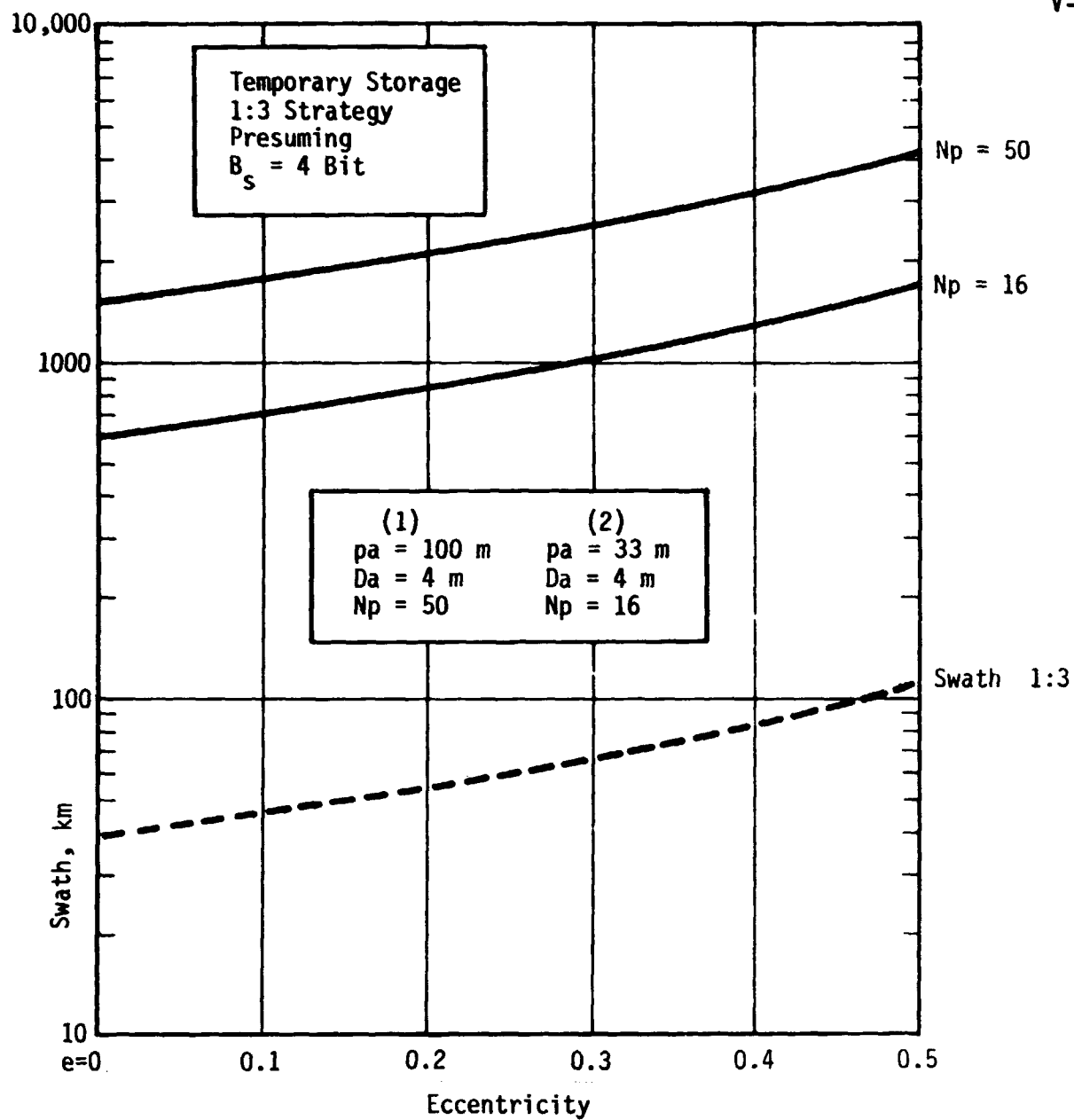
Figure V-21   Temporary Storage -- 1:3 Strategy, Expanded Presummer
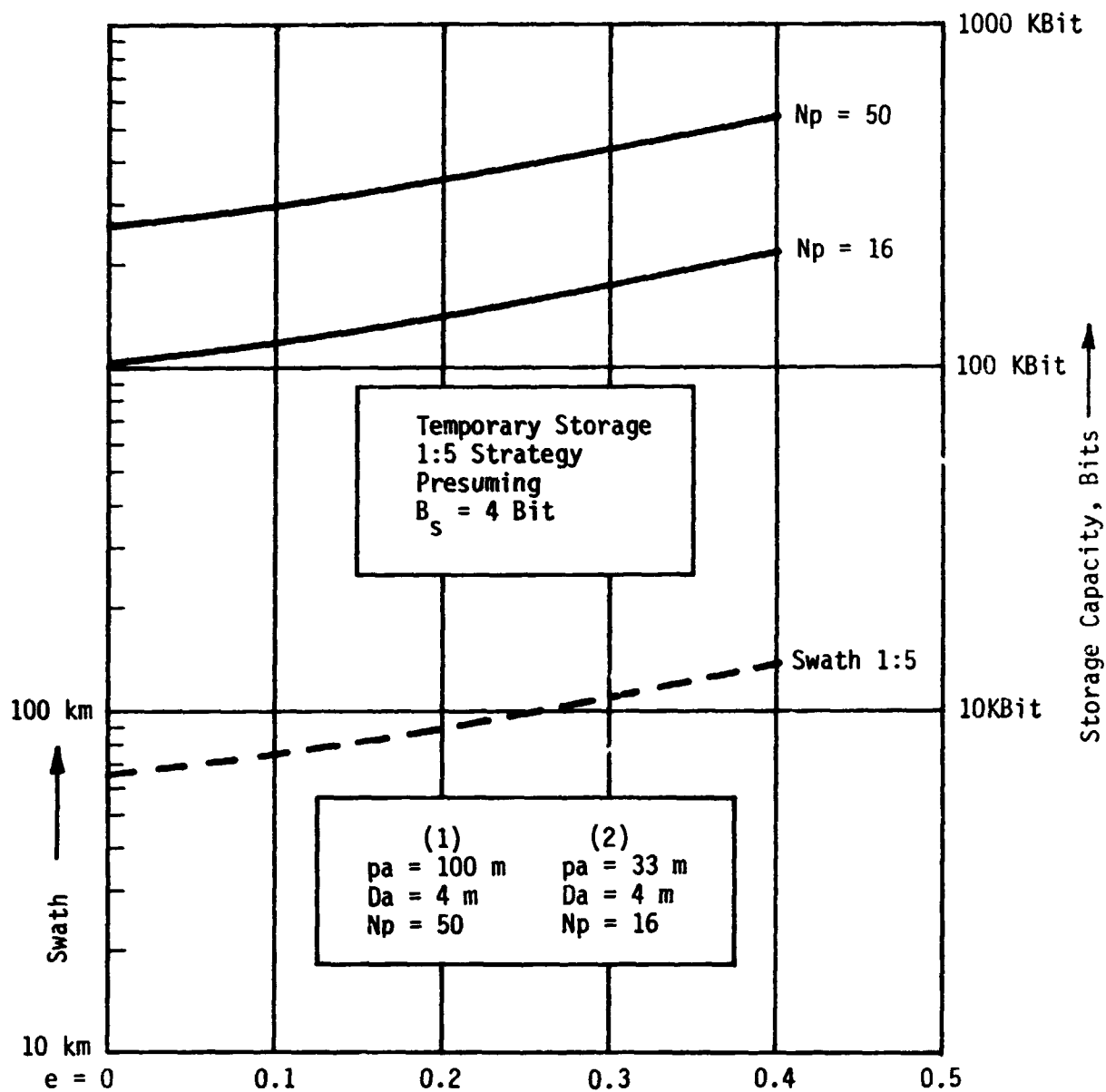
Figure V-22   Temporary Storage -- 1:5 Strategy, Expanded Presummer

This configuration, by storing the weighted values in dynamic shift registers can be implemented with fewer components but somewhat reduces the overall flexibility of data base management possible relative to the complex fully expanded presummer which could provide direct access to all data. The recommended concept is the form usually employed in practice by Earth-based systems. The digital delay lines are accumulators of a composite weighted sum. The memory required for the coefficients, $W_{i,j}$ is nominally determined by:

$$M_c = K \times N \times \frac{W}{\rho_r} \tag{V-41}$$

where   K = oversamplir   factor for side lobe control

   N = number of sweeps averaged

   W = swath width – ground range

   ρ_r = range resolution – ground range

   M_c = memory requirement for coefficients

Mass Storage Derived Requirements

Requirements for onboard mass storage are derived through the product of recorded data rate times mapping time per cycle. Additional storage capacity could be allocated to provide for ground station view window programming, or redundant relay of data.

Data volume per cycle is described by equation (V-42) below for the raw radar data.

$$RDV = \overline{B}_R \times T_m \tag{V-42}$$

where   RDV = required data volume

   $\overline{B}_R$ = average bit rate for a given processing option

   T_m = mapping time (Figs. V-23 and V-24)

Additional data is possible for radar data annotation, and auxiliary science and radar data, and engineering data. These contributions are typically a small percent (i.e. $\leq 5\%$) of the raw radar volume. The range of typical data rates derived from the SAR sub-

system are presented in Table V-4. These rates are further summar-
ized in Figure V-25. This figure is referenced to eccentricity
and mapping strategy since the swath width follows directly from
the choice of orbit and strategy. Figure V-23 shows the time re-
quired for mapping of $\pm 90^{\circ}$ true anomaly which is the goal of mission
designs. However, some practical limiting constraints have imposed
further altitude and true anomaly limits which drop the net mapping
time and coverage as a function of spacecraft configuration, shown
in Fi ure V-24. Configuration A (shared antenna) spacecraft can
map approximately $\pm 55^{\circ}$ true anomaly in an e = 0.5 orbit using the
dual beamwidth antenna concept. The curves of Figures V-26 through
V-29 present parametric requirements for the radar data above.

Example implementations of Vol. II Section V impact the stor-
age with additional data for completeness. Table V-5 summarizes
parametrically possible auxiliary data sources and allocated ranges
of sampling rate and data volume impact. The engineering data is
or can be relayed redundantly over a separate low power engineering
telemetry link.

Presented in Figures V-26 through V-2^ are parametric digital
data storage requirement estimates for the mapping radar data.
These data are plotted versus orbital eccentricity for the various
mapping strategies of 1:1, 1:2, 1:3, 1:5, according to the basic
equation for radar data volume given as equation (V-42). For
example, referring to Figure V-26, with a strategy of mapping every
orbit (1:1) at 0.5 eccentricity the indicated radar volume is 790 x
10^{6} bits for radar data alone. At the same eccentricity mapping
every second orbit (1:2) the indicated data volume is approximately
1550 x 10^{6} bits due to the doubled swath width size. Specific
point designs must impact this volume further with additional re-
quirements of optional auxiliary science data, engineering data,
and annotation. For typical estimates of such impact, see Volume
II Section V, Example Spacecraft Implementations.
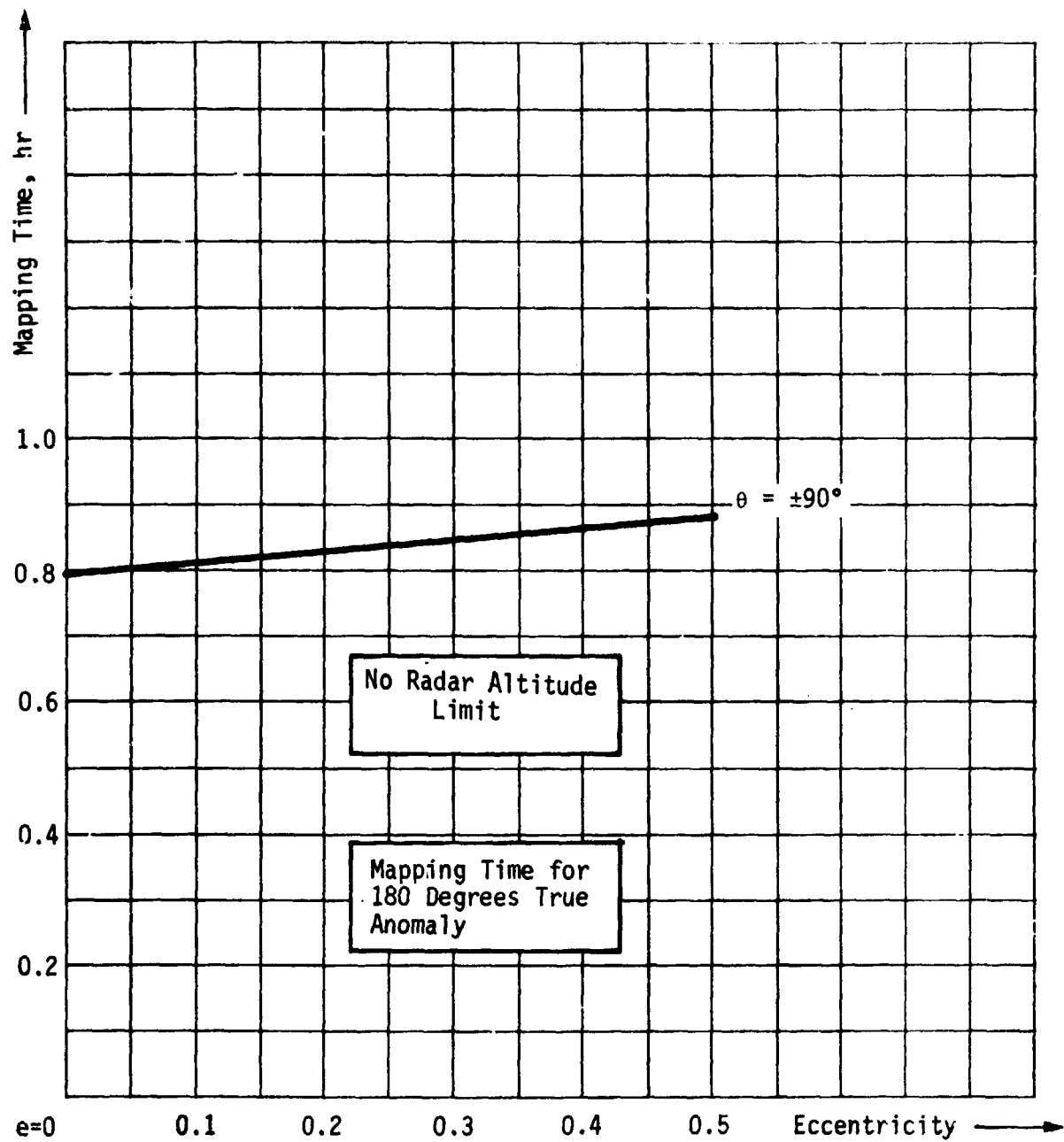
Figure V-23 Mapping Time versus Eccentricity
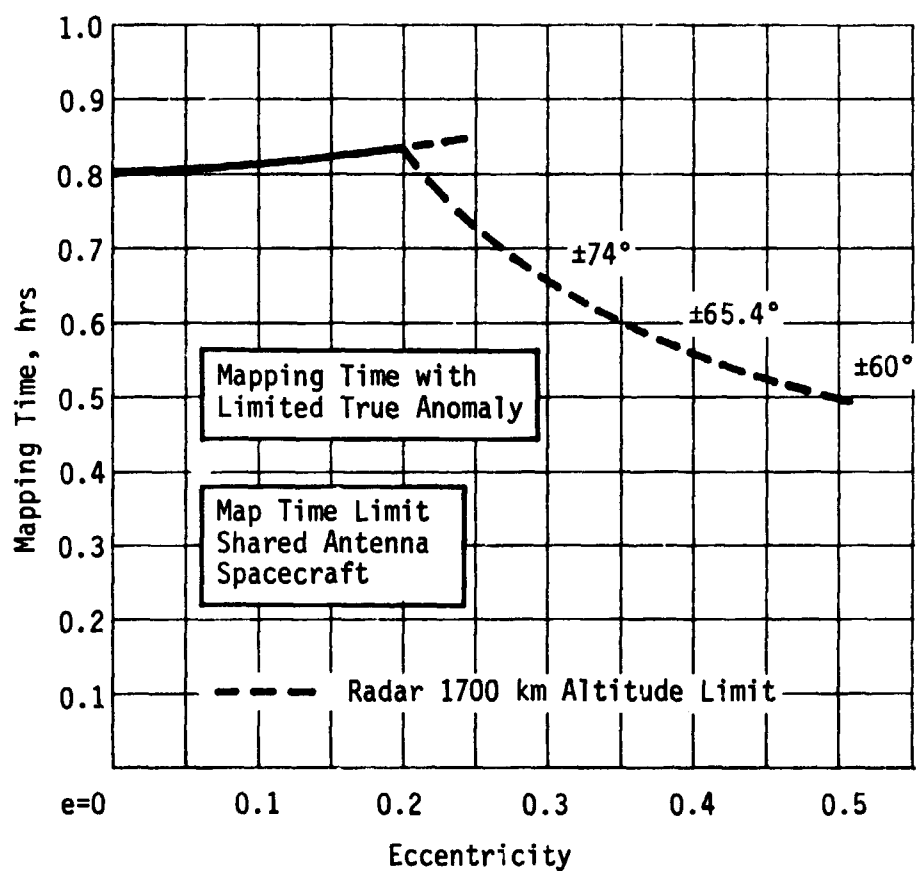
Figure V-24 Mapping Time Limited by Radar Subsystem
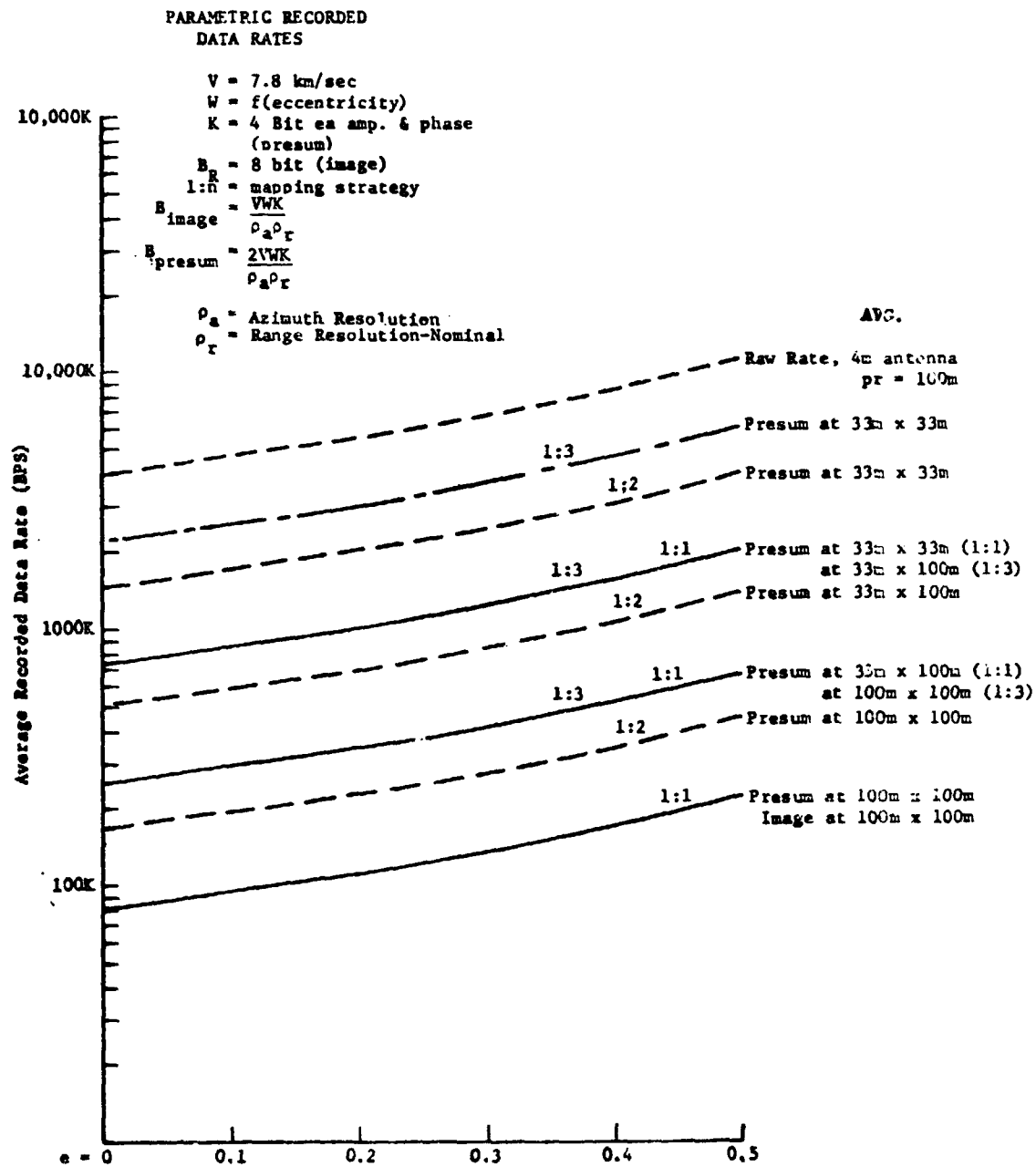
Figure V-25 Parametric Average Recorded Data Rates vs Eccentricity

Table V-5 Potential Auxiliary Data Sources & Characteristics

ITEM	Reference Average Data Rate	Utilization: % of Orbit	Typical Data Volume/Orbit
(1) Altimeter	$\dfrac{6 \text{ Bit}}{100\text{msec}} = 60$ BPS → $\dfrac{6 \text{ Bit}}{30\text{msec}} = 180$ BPS	25 %	0.225×10^6 Bit → 0.675×10^6 Bit
(2) Receiver Automatic Gain Control	$\dfrac{6 \text{ Bit}}{30\text{msec}} = 200$ BPS	25%	0.750×10^6 Bit
(3) Engineering Data	1 KBPS	100%	16.2×10^6 Bit @ 4.4 hr/orbit
(4) Dual Polarization Receiver Data (Not Time Shared)	400 KBPS	During Mapping 20% - 25%	1200×10^6 Bit @ 3×10^3 sec/mapping time
(5) Dual Frequency (Not Time Shared)	400 KBPS	During Mapping 20% - 50%	1200×10^6 Bit @ 3×10^3 sec/mapping time
(6) Radar Antenna Gimbals (2 DOF)	$\dfrac{10 \text{ Bit}}{30\text{msec}} \times 2 = 670$ BPS	During map + margin @ 1 hr nominal	2.5×10^6 Bit
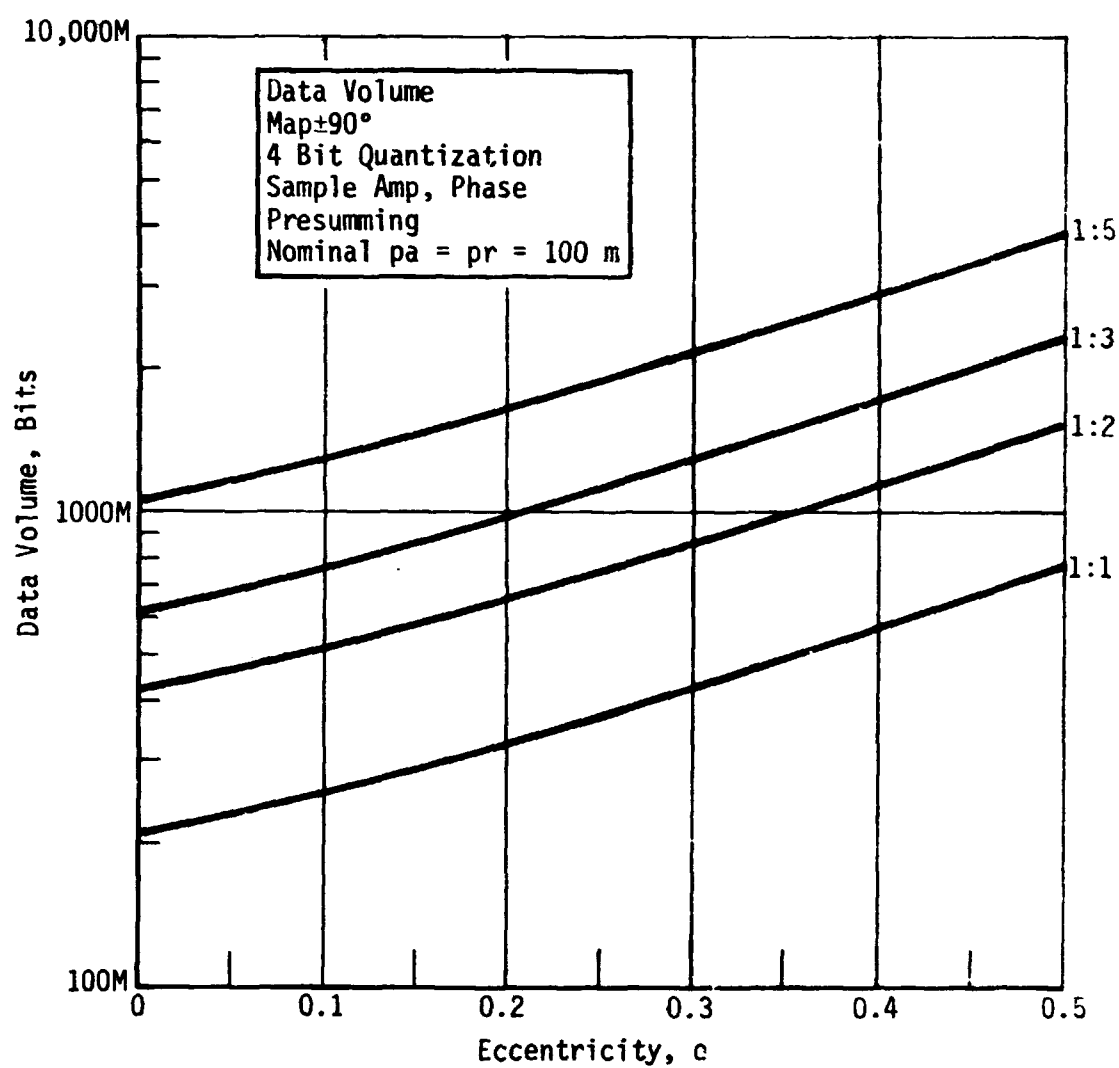
Figure V-26   Radar Data Volume -- Maximum Azimuth Presumming

Figure V-26 summarizes these data volume parametrics for the processing choice of maximum presumming (nominal $\rho_a = \rho_r = 100$ m). Figure V-27 summarizes these data volume parametrics for the option of averaging data to maintain $\rho_a = 33$ meter ($\rho_r = 100$ m), called minimum presumming. This mode would provide 33 meter azimuth resolution which could be averaged on Earth to the 100 meter resolution to match the nominal range resolution dimension. Figure V-28 shows the radar data volume for the option of forming an image from a single azimuth channel quantized to 8 bits per resolution cell (single coherent image). Figure V-29 shows the data volume in storage for a radar forming an image from several azimuth channels. The solid lines indicate the data volume for an image from a single channel. The dotted lines are required volume if the mixed integration is accomplished on Earth using nine azimuth channels of relayed data. If the mixed integration were accomplished on the spacecraft, the data volume for relay is indicated by the solid lines.

The following paragraphs document a number of trade studies based on parametric requirements which were identified for the mission. These trades surveyed both analog (i.e., film) recording systems and digital recording media. A synopsis of the survey is presented in Table V-6. For the Venus mapping mission none of the analog techniques appear desirable due to their lack of reuse, environmental control and lifetime of developers, and the auxiliary readout systems requirements. It is excessive to carry sufficient storage media on the spacecraft to handle the radar data for the entire mission. If the film cassette could be returned to Earth, then the highest storage density of the analog film technique would be an advantage.

The following paragraphs discuss briefly the attributes of the storage technologies surveyed and present assessments as the applicability to the Venus mission. These paragraphs initially discuss
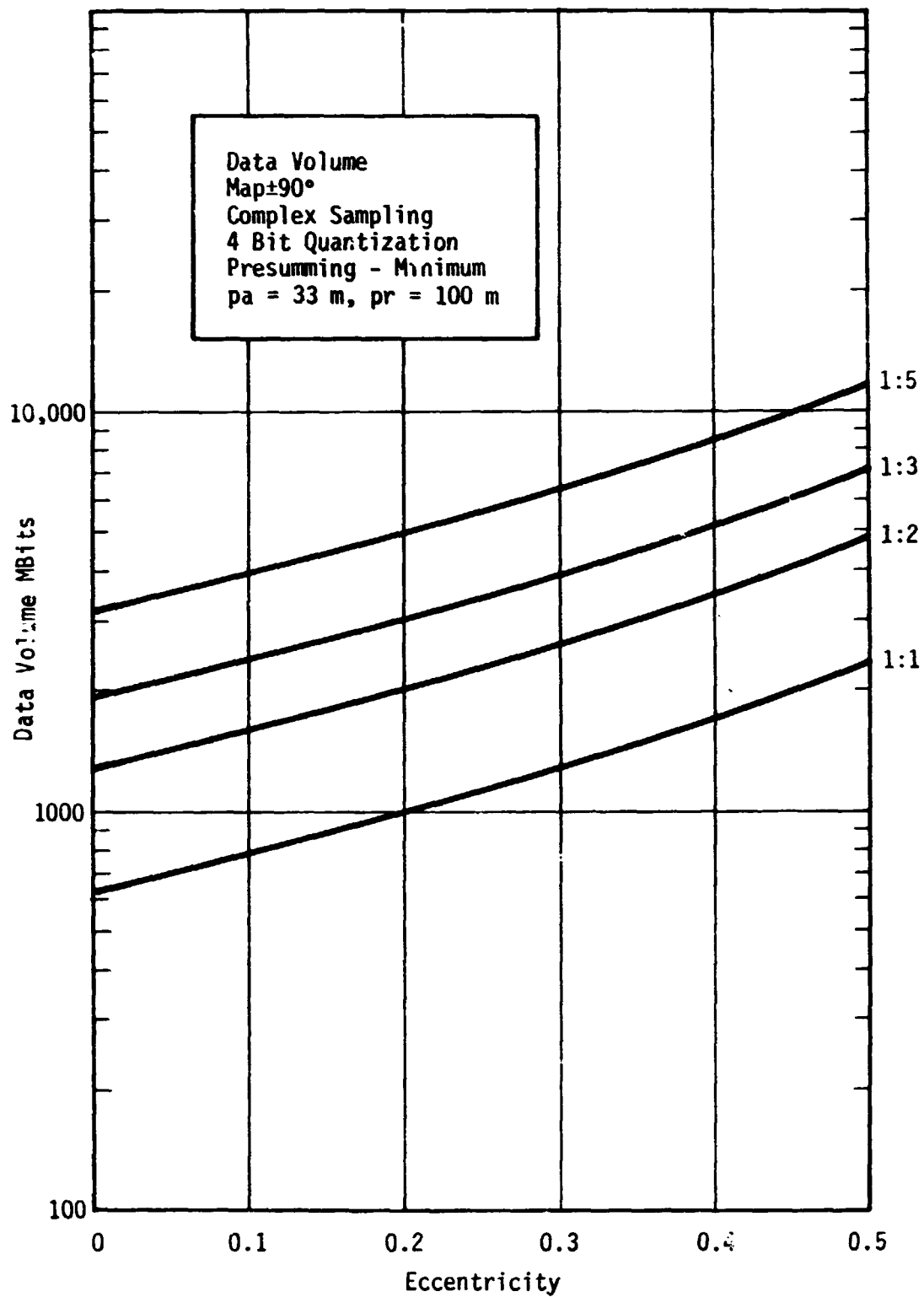
Figure V-27   Radar Data Volume -- Minimum Azimuth Presumming
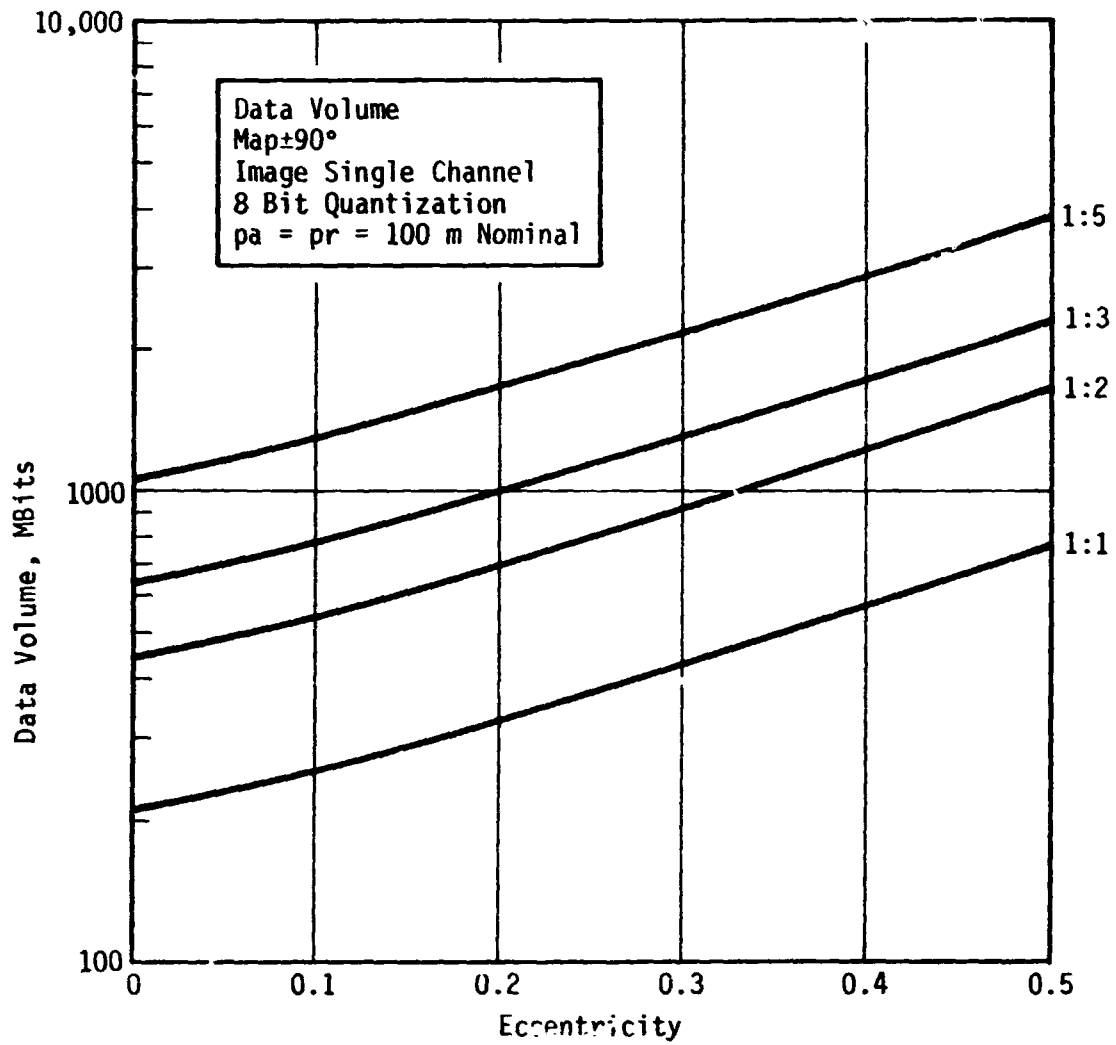
Figure V-28 Radar Data Volume -- Single Channel Image
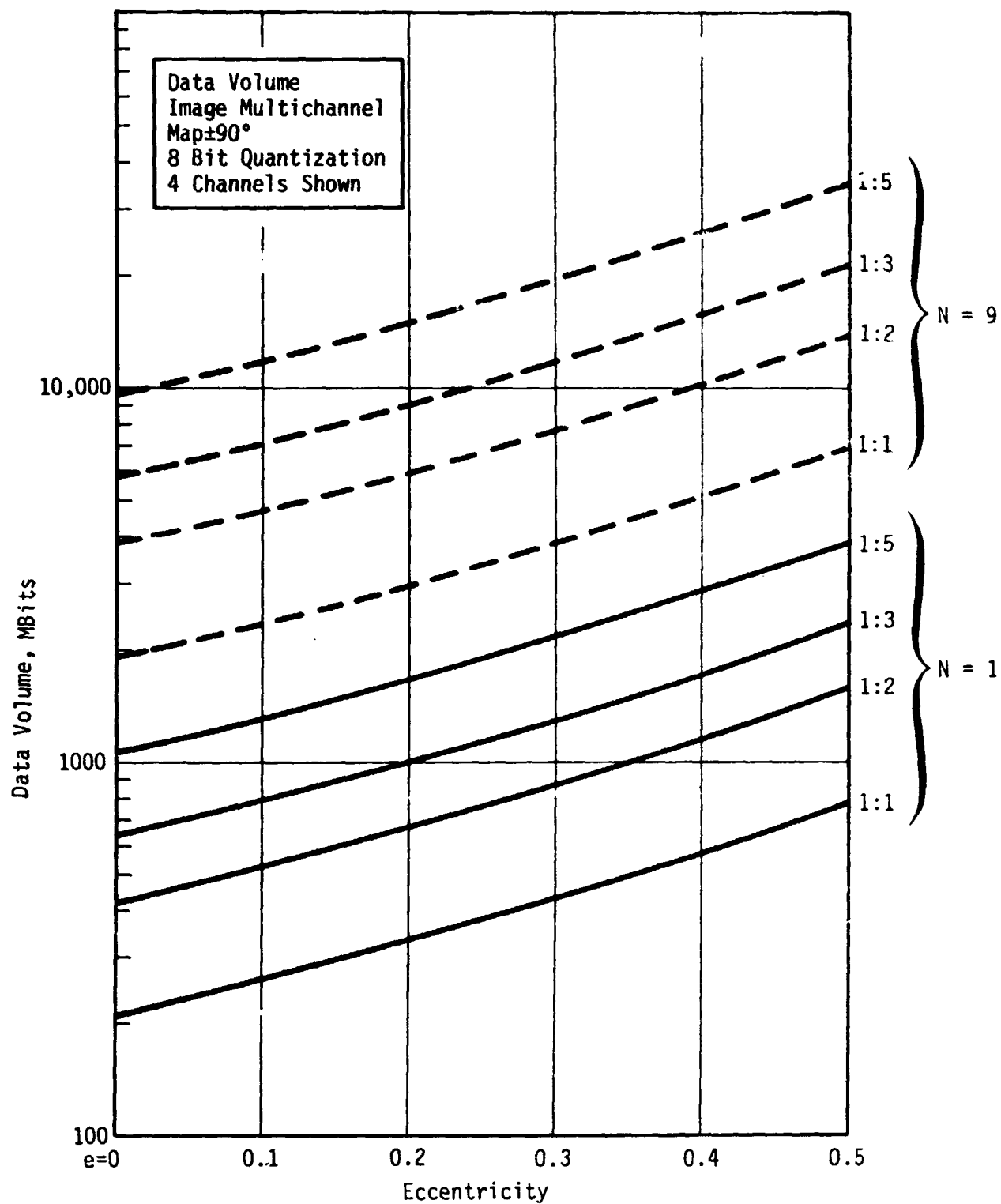
Figure V-29 Radar Data Volume -- Multichannel Image

Table V-6   Data Storage Survey Synopsis

Technology	Space Qualified Systems Now	Space Qualifiable by 1980	Reusable	Long Life in Space	MBit/mm³	Representative Maximum Capabilities in Bits	Weight Relative to Mag Tape	Power Relative to Mag Tape
Silver halide emulsion film	Yes	Yes	No	Marginal	5.2	10^{20}	Higher	Higher
Non-silver (Diazo) emul. film	No	No	No	No	7.0	10^{15}	Higher	Higher
Organic dye emulsion film	No	No	No	No	13	10^{30}	Higher	Higher
Dielectric film/tape	Yes-Lab	Yes	Yes	Yes	.14	10^{12}	Similar	Lower
Thermoplastics	No	Yes	Yes	Yes	7.0	10^{20}	Higher	Higher
Charge coupled devices	No	Yes	Yes	Yes	.01	10^{6}	Lower	Lower
Photo plastic film	No	?	No	?	5.	10^{18}	Higher	Higher
Magnetic tape	Yes	Yes	Yes	Yes	.057	10^{11}	Similar	Similar
Magnetic plated wire	Yes	Yes	Yes	Yes	.02	10^{7}	Lower	Similar
Magnetic core	Yes	Yes	Yes	Yes	10^{-7}	10^{6}	Similar	Similar
Magnetic bubble	No	Yes	Yes	Yes	.1	10^{15}	Lower	Lower
Magnetic disc	No	Yes	Yes	Yes	.005	10^{9}	Lower	Higher
Magnetic deposited closed flux	No	Yes	Yes	Yes	.0001	10^{6}	Similar	Lower
Magneto-optic	No	Yes	Yes	Yes	2	10^{13}	Higher	Higher
Electro-optic	No	Yes	Yes	Yes	1	10^{12}	Higher	Higher
LSI bipolar	Yes	Yes	Yes	Yes	3×10^{-4}	10^{6}	Lower	Higher
LSI MOS, MOSFET, CMOS	Yes	Yes	Yes	Yes	7×10^{-4}	10^{8}	Lower	Similar
Electrostatic tape	Yes	Yes	Yes	Yes	.15	10^{11}	Similar	Similar
Electrostatic tubes	Yes	Yes	Yes	Yes	.01	10^{7}	Lower	Higher
Charge coupled devices	No	Yes	Yes	Yes	.01	10^{6}	Lower	Lower
Surface wave effect	No	Yes	Yes	Yes	.01	10^{6}	Lower	Lower
Thermoplastic tape	No	Yes	Yes	Yes	.1	10^{7}	Higher	Similar

analog storage systems relative to the need to provide storage for the entire mission, introduces representative space type digital machines, then surveys a wide range of storage technologies such as magnetic core, magnetic bubble, electro deposited closed flux magnetic memories, plated wire memories, semi-conductor memories, optical arrays, electro-optic photo sensitive planar memories, magneto-optic memories, photochromics, amorphous semi-conductors.

The survey may be summarized in several key points:

1) The digital magnetic tape recorders which have (or will soon have) been identified and qualified for space will meet the capacity and bandwidth requirements of the Venus mapping mission. The question of long life reliability cannot be answered by this study but our initial assessment is that a qualification program could establish their adequacy. In particular, the Viking Orbiter, ERTS, or EREP technology is directly applicable. The Viking Orbiter is sufficient for most cases mapping to 100 meter resolution.

2) The analog mass memory (film) is excessive for this mission due to the characteristics that it is not reusable, is very temperature sensitive (ref. recent SKYLAB film thermal contamination), lifetime of automatic developers is questionable and multiple systems must be carried for film readout. Both tape recorders and film systems suffer from the electromechanical reliability question. It is recognized that the storage density is the highest with good film systems.

3) Of the many new mass memory technologies currently under development, the magnetic bubble technology offers the greatest potential for space program weight, power, reliability, and capacity benefit.

4) Solid state technology is fully adequate for temporary data storage, processing and management.

Analog Mass Memory Technology - Film System

Film technologies include such approaches as: a) emulsion type-silver halide, free radical organic dyes; b) electrostatic type-dielectric tape; c) thermo plastic type; d) dry process diazo base emulsion. In addition, for this application, a film system must be automatically developed and readout on the spacecraft. If the film is not reusable, the resident capacity must provide for data retrieval over the entire 240 day mission; for a reusable type, a design must provide for approximately 700 to 3700 cycles depending on choice of mapping strategy or approximately 600 recording hours over the year. Further, the modulation transfer function (MTF), a measure of spatial resolution on the film, must be sufficient to compactly store the data from mapping passes in the bounds of available film widths. Key environmental criteria include thermal, radiation, and overall shelf life considerations.

It has been noted that with a film system data could be read out at controlled (variable) resolution, and data from previous orbits would be available for redundant transmission, etc. Due to the continuous mapping requirement and data link constraints, however, the availability of past mapping data may be questionable.

Photographic Exposure of a Silver Halide Emulsion Film - Commonly, this technique images data displayed on a cathode ray tube (CRT) into a silver-halide emulsion deposited on a film. For the Venus application, the film would be developed by a wet, or semi-wet chemical process. Later the film is read out by a scanner and photo pickup device for relay to Earth. Such a technique was used on the Ranger and Lunar Orbiter programs. (The traditional side looking radar application retrieves the exposed film for development on Earth.)

The automatic development process of silver-halide film is based on the diffusion transfer technique in which the chemical reactions occur in a rigidly controlled environment by bringing

the exposed film in contact with a second film in contact with a
second film containing the development chemicals. The positive
print is produced on the second film and later read out optically.

The film system concept employed on the lunar orbiter program
is presented briefly below.

A system was used in the Lunar Orbiter program which opti-
cally stored video images for later transmission to Earth. The
system weighed 68 kg (one hundred fifty pounds) including the
weight of two cameras. Figure V-30 shows a schematic of the
system. In our case, the image presented to the storage system
would be generated from a camera. After exposure, the film moves
forward to a storage or buffer area between the image generator
and processor. In the processor the film is chemically developed
by the Eastman Kodak "Bimat" process. The negative film is stored
on a take-up reel until the electronic readout process begins. A
film scanner, in which a flying spot of light and suitable optical
elements are linked with a photomultiplier pickup, is the heart of
the readout equipment. Figure V-31 illustrates the readout process
and individual elements involved.

The scanning lens moves the spot of light in a regular pattern
across a small segment of the developed film covering the 61 cm
(24 inch) width of the image on the negative with 17,000 horizontal
scans of the beam, each one-tenth of an inch long. A complete scan
across the film takes 23 seconds. The film then advances 0.25 cm
(one-tenth of an inch) and the scanning lens traverses over the
next segment in the opposite direction.

By this process, the Lunar Orbiter requires 43 minutes to scan
the 29.5 cm (11.6 inches) of film which corresponds to a single
exposure by the two lenses.

As the spot of light passes through the image on the negative
it is modulated by the density of the image exposure.
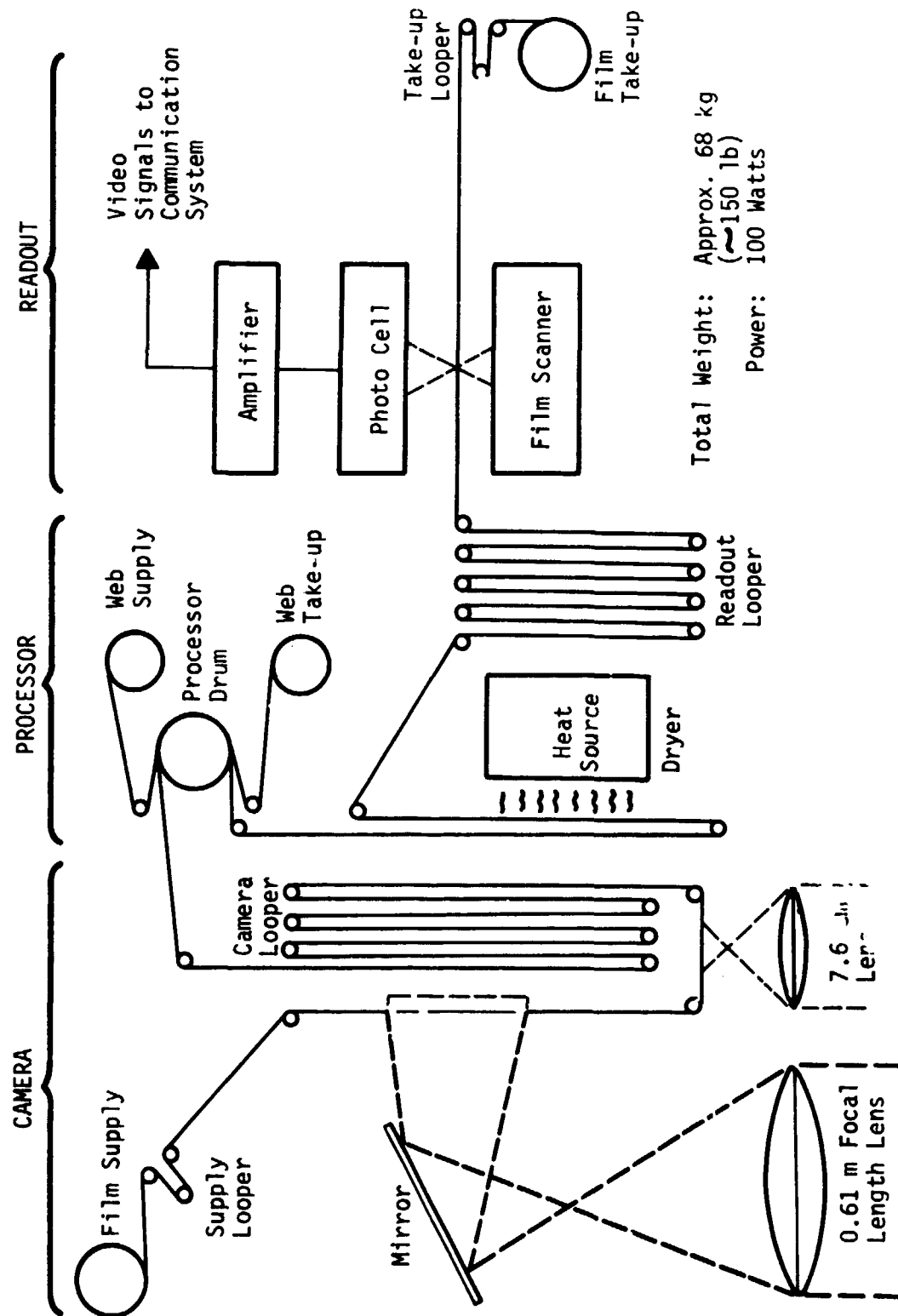
Figure V-33 Typical Film Data Storage System
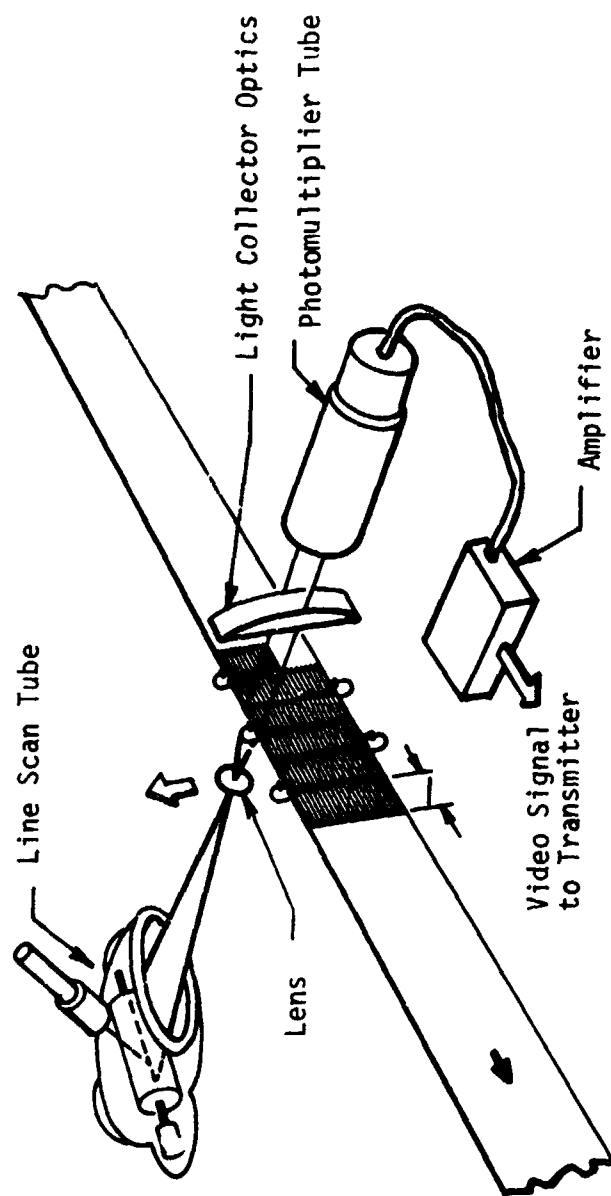
Figure V-31 Example Film Readout System

After passing through the film the light is sensed by a photo-multiplier tube which generates an electronic signal proportional to the intensity of the transmitted light. The signal is amplified, timing and synchronization pulses are added, and the result is fed into the communications link as the Lunar Orbiter's composite video signal for transmission to Earth.

Several factors of this system become very significant with respect to the Venus application. First, this system was designed to readout video images taking the equivalent of a stepped-raster scan in the azimuth direction of a SLAR film. Since in no case do the equivalent of 17,000 range lines exist for the Venus case, the readout process would have to be modified on both the range and azimuth direction. The 0.25 cm (1/10 inch) registration in the azimuth direction is too great for the synthetic aperture radar case a light of the requirement to store the entire mission data in the film system.

Consider the case that a 3.05 m antenna is used and the maximum synthetic aperture length were 60 m (corresponding to a zoom mode azimuth resolution of 30 meters) with a circular orbit, 1:5 strategy, PRF of 4000, map time per orbit of 0.8 hours. The film length for a single mapping pass is derived below. The principal advantage of a silver-halide film system is the ability to store "unprocessed" or minimally presummed data for later relay at variable resolutions. Then the film length per pass is:

$$4000 \text{ sweep/sec} \times 0.8 \text{ hr} \times 3.6 \times 10^3 \text{ sec/hr} \times 70 \text{ mm/17,000 sweep}$$
$$= 47.4 \text{ m/pass} \tag{V-43}$$

for the mission:

$$700 \text{ mapping passes} \times 47.4 \text{ m/pass} = 33,200 \text{ m/mission or}$$
$$100,000 \text{ ft of film.} \tag{V-44}$$

By comparison, 214 m (700 ft) of film in a cassette for the Apollo 17 sounder experiment weighed approximately 6.8 kg (15 lbs). The trend apparent from such studies is that the film system when

impacted with storage data for the entire mission becomes un-
necessarily complicated and heavy for this application. Definitely
an advancement in technology over the lunar orbiter system is
required.

Along with the required volume to store data for the entire
mission is the need for an extremely well controlled environment
since the emulsion film is very sensitive to temperature, radiation,
and vibration. Single use film developed by wet or semi-wet processes
is assessed to be prohibitive due to the requirement to store un-
processed data for the entire mission.

Apollo 17 Optical Recorder - The optical recorder of Apollo 17
recorded SLAR type data for approximately 10 hours of mapping onto
70 mm film in a cassette which was manually retrieved by the astro-
naut. This recorder consisted of a cathode ray tube to display the
radar video from each range sweep to the film which was driven at
a rigidly controlled speed related to orbital velocity. Film speed
was 5 mm/sec using a panatonix X film. Also recorded on the film
were a time code and dynamic range calibration reference. The
cassette weight was approximately 6.8 kg (15 lb); total system
weight was 58.3 kg (115 lb) using 100 watt average power. The film
was, of course, not reusable, and was developed in ground facilities.

By way of example, the reference performance of this recorder
could be extrapolated to the Venus mapping mission to further ap-
preciate the impact of storing data for the entire mission. This
comparison shows that it is also excessive to consider storing only
partial data for the entire mission.

With film speed of 5 mm/sec and a PRF of 400 for the Apollo
mission, the film was advanced about 5 mm/sec x sec/400 sweep or
12.5×10^{-3} mm/sweep, which would be equivalent to a density of
approximately (line pair/12.5×10^{-3}) mm = 0.798×10^3 or 100 lp/mm

As an example, assume a MTF of 100 lp/mm and the following
mission characteristics:

$$PRF = 2V/D_a \quad \text{where } V = 8 \times 10^3 \text{ m/sec}, \ D_a = 3 \text{ m} \quad (V-45)$$

$$PRF = 2 \times 8 \times 10^3/\text{m/sec}/3\text{m} = 5.33 \times 10^3 \text{ sweep/sec} \quad (V-46)$$

at 0.8 hr/mapping pass and 720 passes the total map time is:

$$0.8 \text{ hr/pass} \times 720 \text{ passes} \times 3.6 \times 10^3 \text{ sec/hr} = 2080 \times$$
$$10^3 \text{ sec} \quad (V-47)$$

Finally to estimate a total film length:

$$2080 \times 10^3 \text{ sec/mission} \times 5.33 \times 10^3 \text{ sweep/sec} \times$$
$$12.5 \times 10^3 \text{ mm/sweep} = 1.38 \times 10^6 \text{ mm/mission} \quad (V-48)$$

Total film length to record all data at 100 lp/mm:

$$\text{Total film: } 138 \times 10^3 \text{ meter.} \quad (V-49)$$

To record at 500 line pair/mm (an upper limit)

$$\text{Total film: } 7 \times 10^3 \text{ meter.}$$

Based on the weight of the Apollo 17 film cassette which included 213 m (700 feet) at 6.8 kg (15 lb), the weight of an equivalent cassette of 7000 m of film would be 6.8 × 7000/213 = 240 kg (525 lb).

Regardless of the scale factors, etc, employed, initial analysis concludes that non-reusable film which will store data from an entire mission will be relatively heavy.

Alternative Optical Storage Techniques - The paragraphs below identify several alternate demonstrated optical/film recording techniques which have been used in space (Apollo 17) and the laboratory (Wright-Patterson Air Force Base - Flight Dynamics Laboratory).

Representative of advanced film type recording devices is the multichannel laser film recorder (after Synergetics Corp.). Such devices are commercially available to record digital, analog and PCM signals on 8 mm microfilm. When such a system records digital data several undesirable factors related to analog film recorders are overcome; i.e., nonlinear film and modulator $\cos^2$ transfer functions, film stretch, and cross talk from adjacent channels due to diffraction effects.

The Synergetics PDR-5 is a 36-track laser film recorder capable of recording digital, analog and PCM signals on 8 mm wide microfilm. The system consists of excellent components (laser, multi-channel, modulator, diode array) and provides a long-overdu capability of multi-channel recording at high packing densities.

The PDR-5 is configured to record digital data as this mode circumvents several problems inherent in any analog film recorder. These include nonlinear film and modulator $\cos^2$ transfer functions, film stretch and cross talk from adjacent channels due to diffraction effects. These problems are present in all film recorders and must be dealt with if the machine is used to produce input film to an optical Fourier processor.

The machine is similar in operation to a magnetic tape recorder. Referring to Figure V-32, a sensitized tape is transported at a uniform rate in front of the recording transducer where data is written on the tape. Playback duplicates this process except that data is read off at the transducer. The significant difference is the sensitive tape which is film and the recording transducer which modulates a light beam.

The film transport utilizes a high inertia capstan-pinch roller drive for low wow and flutter and supply and takeup reels tensioned by torque motors. The electro-optic transducer consists of a continuous gas laser, cylindrical optics to form the beam to the desired shape, a 36 channel electro-optic modulator and a 36-channel solid state photodetector. The output from the laser is a circular beam of light approximately 0.8 mm in diameter at the $1/e^2$ intersity points. The beam of light passes through an optical assembly, which reshapes the beam into an elliptical cross section that is less than 2.5 cm (one inch) wide by 0.025 cm (0.01 inch) thick. This elliptical cross section beam is incident on an array of 36 modulator cells is reshaped so that at the surface of the record the beam is approximately 0.64 cm (0.24 inch) in width across the film and approximately 0.2 mm (0.0002 inch) in thickness, measured longitudinally to the film.
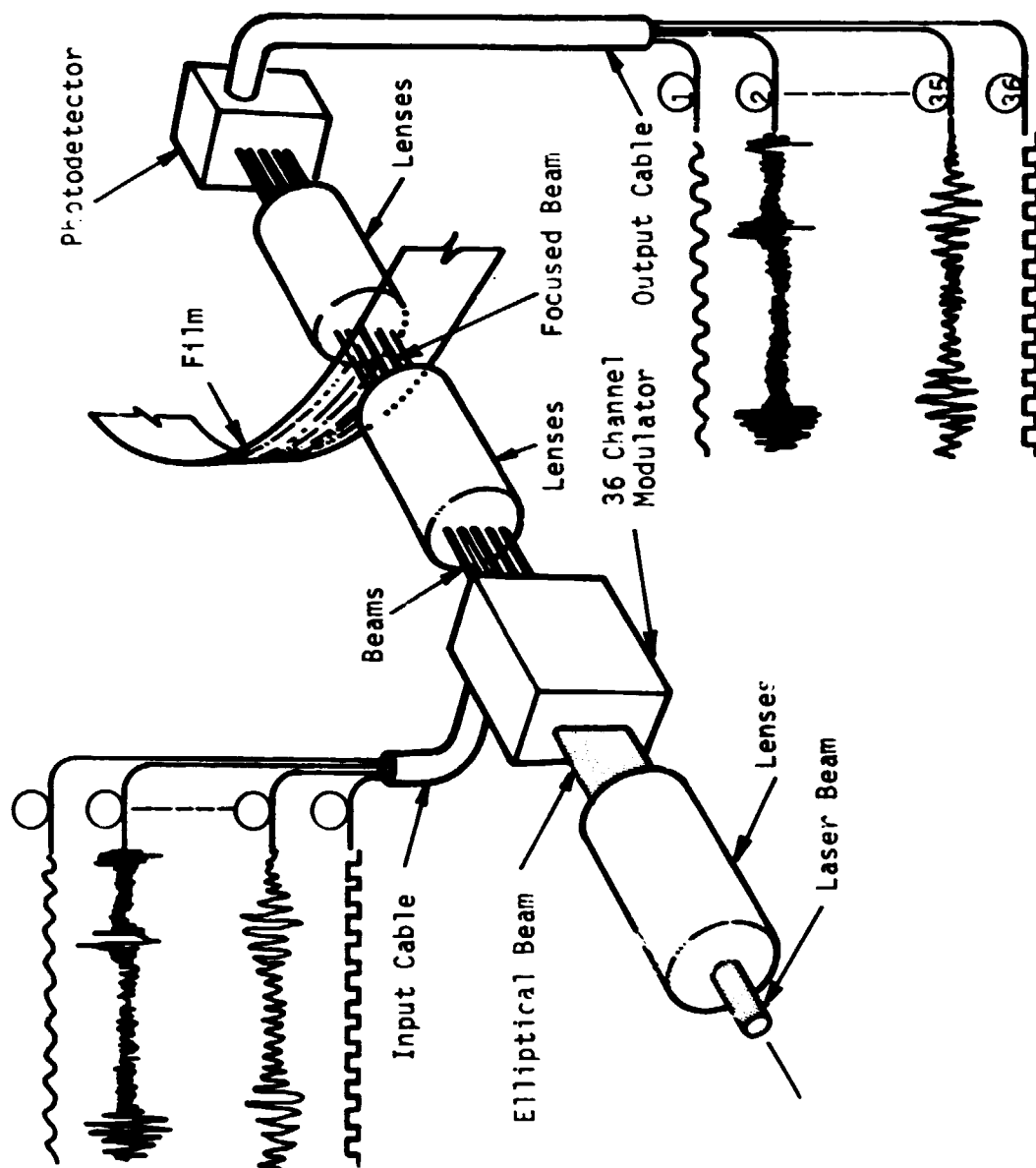
Figure V-32 36-Channel Laser Recorder Schematic

The film used is 8 mm microfilm (Agfa 8E75) and is developed by conventional processes.

Advance Technology Film Systems - A number of advance technology film system approaches were surveyed for potential application to the Venus radar mapping mission. These are presented in the following paragraphs. These include free radical dye films, thermo plastics, and nonsilver dry process emulsion.

Free radical dye films have been investigated for Earth application for use with the duplication of aerial negatives, direct electron beam racording or for miscellaneous photographic applications.

Higher resolution than silver-halide film is inherently possible with this film, i.e., in excess of 750 line pair/mm. The development process is dry and involves irradiating the latent image with uniform illumination within the absorptive bandwidth of the lateral dye image (which is outside the initial spectral sensitivity region). The images are fixed by heating the film to about $120^{\circ}C$ for three minutes.

However, shelf life of prepared film is only a few days at room temperature or several weeks if refrigerated. The dry processing is a great benefit if film lifetimes could be extended to 2-3 years. This film technology is currently not available for a space application.

It has been shown that an optical image can be recorded in special plastic tape which is sensitive to incident photons. The incident light causes minute physical deformations on the surface of the tape. However, in order to sense the deformations Schieren optical systems must be employed. Thermo plastic film sensitivity is approximately equal to that of free radical organic films and the theoretical resolution of thermo plastic film is higher than the silver halide emulsion films i.e., 750 line pair/mm).

Thermo plastics have received much development attention recently, but with little attention toward space application. There are many potential advantages such as high sensitivity comparable to high resolution photographic emulsions. Additionally, thermo plastics are grainless with resolution potentially of 2000-3000 lp/mm. Information storage life is long. Information can be read out nondestructively indefinitely.

Thermo plastics have been shown to be erasable but current record times are in the millisecond realm and erase time on the order of one second. Further, the heat erasure is not always complete. Laboratory development tests have shown in some cases that a high cycle life is possible (up to 10,000) under rigidly controlled conditions.

Thermo plastics are assessed as probably not applicable to the Venus radar mapping mission. Further discussion is included in the paragraph on optical memory techniques.

An advanced technology system has been demonstrated in the laboratory (after Laser-Comp Information Systems, Inc., East Haven, Conn.) which uses a novel non-silver, dry process film. The film is composed of a diazo recording medium embedded in a unique polymeric matrix. With this process the diazo molecules are broken down by the blue or green light from an argon laser. Breakdown of the diazo molecules liberates free nitrogen (N_2) gas, and when the polymeric matrix is heated the free gas expands and forms bubbles in the softened polymer. The bubbles (micron dimension) in the polymer backscatter light being transmitted through the film and the written image can be projected. Development is accomplished either by heating the film after exposure or by the input beam itself if power is sufficient. Thus exposures and development can occur simultaneously.

For the SLAR application a laser beam could be modulated with the radar video and deflected over the film to record the data. The data could be read out with an electron beam scanning device such as a flying spot scanner.

This film is also not reusable and would therefore require enough film to record the entire mission. No data is available for suitability to space qualification.

Novel Technology or Devices - Several technologies were found which seem to fall in a gray area of classification somewhere between a film and a tape. The advantage of the dielectric film (tape) is that the "emulsion" or dielectric/conductive lazer is reusable while offering high data storage densities. Discussion following presents the apparent status of the dielectric tape technology. Development studies sponsored by NASA-GSFC, JPL, WPAFB, CBS Laboratories, RCA, indicate that this technique can be reusable without degradation for up to two years and is insensitive to temperature and radiation.

Dielectric tape is fundamentally concerned with recording an image (or analog data) on a special composite laminated tape which stores an image in the form of charge patterns. The image is read-out by flooding individual small areas on the film with electrons and recording how many it takes to restore the charge in that particular area to neutral potential.

The film is composed of a thin metallic layer evaporated onto a base of milar which is folded at the edges to prevent contact at the center of the tape when the tape is rolled. The evaporated layer is covered by a photoconductor which serves to convert photons incident to charge pattern on the insulator layer. Finally, the photo conductor is covered with a transparent insulating layer of polystyrene.

The film (tape) can be erased and reused. To prepare the film an electron flood beam saturates the film to a uniform charge potential. To record, both light from the object plane and the electron flood beam are used. The film may be exposed from the front or back (by a CRT for the radar application). Simultaneously with exposure of the image the tape is flooded with the electron beam to allow secondary electrons to be produced in the thin metallic tape layer. Due to the varying conductivity of the photo conductive layer the insulating layer is charged in accord with the optical image. For readout an electron beam scans the film with a small spot; the amount of charge from the beam required to neutralize a spot on the film corresponds to the image intensity at that point. By raster scanning strips on the film, the radar signal film could be read out to an auxiliary recorder or data link, or processor.

A versatile SLAR processor could be envisioned which would employ a traditional CRT to display the result of each range sweep to a dielectric film camera which would record the data in the usual sweep by sweep for later processing or read out to a data link.

Alternately, noncoherent image integration could be accomplished on an image storage tube which is read out and stored by a dielectric film camera. Since this could be done on a map cycle basis the amount of tape required would not be excessive. In addition, the possibility of storing data from several mapping cycles for redundant relay to Earth is available.

Both slit-type and frame type cameras have been demonstrated. Read out could also be nondestructive. Packing density is inherently high with the limiting factors being lens resolution and read-out beam control instead of the tape. An example comparison is shown in Table V-7.

Table V-7 Dielectric Tape Camera Comparison

Parameter	Manufacturer	
	RCA	Westinghouse
Sensitivity	0.003 to 0.1 fc-sec 10, 2 grey scale stops	0.008 fc-sec 8, 2 grey scale stops
Resolution	90 line pairs/mm	75 line pairs/mm
Storage time for an image	No discernable degradation after 4 mo. After 10 readouts amplitude down to 40%.	No degradation after 41 hours.
Operating Lifetime	5000 hours possible	Same.
Electronic Shuttering	Possible	Possible
Radiation Resistance	Very good.	Very good.
Weight	Space qualified camera - 37.5 kg (panoramic) High Resolution Lab Model - 68 kg (ex	
Power Record	Space qual. 25 watt Laboratory Hi Res 100 watt	
Playback	Space qual. 30 watt Hi Res. Lab. 300 watt	

The dielectric tape concept has been further reduced to prac-
tice in the form of the "electrichon" storage tube or "electrichon
electrostatic tape recorder." (Ref. Westinghouse Corp.) The
electrichon tube could be envisioned as recording SLAR data by
allowing SLAR analog data to modulate a focused electron beam which
scans across an "endless loop" tape which effectively replaces the
target of the conventional vidicon tube. The "electrechon" is a
signal storage tube. The storage surface is in the form of endless
loop tape for electrostatic storage of information written by a
focused electron beam. Readout is accomplished by an electron beam.
A "harmonic drive" provides smooth rotary motion to the capstan
through a flexing thin metal wall which forms a vacuum-tight seal.
After standard vacuum tube outgassing and processing, a tape loop
was run at speeds varying from 0.254 cm/sec to 9.62 cm/sec (0.1 to
3 inches/second) for over 150 miles without mechanical degradation.
Various TV pictures and test patterns were stored and read at stan-
dard rates and bandwidth. Electrechons have been built in the 3-
inch diameter format that have an image orthicon electron gun used
to perform all three functions: erase/prime, write, and read. Also,
a 4.5 inch Electrechon tape signal storage tube has been built with
two coaxial image orthicon electron guns, one for each of the writ-
ing and reading functions, and a line beam electron source for
erase/prime action. Thus all three functions may occur simultaneous-
ly. Storage tapes about 300 mm long, 35 mm wide (25 mm useful width),
and 150 mm long, 70 mm wide (60 mm useful width) have been used with
these tubes. A nuclear reactor has been used to irradiate several
samples of storage tape with neutrons and gamma rays. Signals were
stored and read from the samples as they had been previously.
There was no evidence of damage to the storage surface or to stor-
age properties.

The "Cinechon" storage camera tube uses an endless loop tape for electrostatic storage of the photoelectrons from a photocathode retina. This tube converts an optical image into a photoelectron charge pattern which is electron optically focused and stored as an electrostatic charge pattern on a very thin dielectric grille on an endless loop of metal tape. The tape drive is by means of a harmonic drive reduction gear. Single pictures may be recorded with the tape being moved between exposures, or a panoramic exposure may be made with the tape motion being synchronized with the training of the camera in azimuth. Exposure time can be controlled by a mechanical shutter in the optical system or by an electronic shutter within the photoelectron image section. The photographic speed index may be raised at the option of the operator by a factor up to 30 or more by an electronic process of electrostatic latent image development after exposure. Reading is accomplished by a high resolution, scanned electron beam in the same manner as in an image orthicon television camera. The electrical video signal output is suitable for display on a high resolution kinescope, or for telemetry, or permanent magnetic recording, over a wide range of video bandwidths. The pictures may be erased electronically so that the electrostatic storage tape is reusable. Only electrical energy is consumed during the entire exposures, developing, reading, and erasing cycle. It has been estimated that life expectancy of the camera tubes is on the order of 15×10^3 hours. Tube life is gun dependent not tape dependent. Even though read and erase can be accomplished with one gun, two guns are preferred.

Magnetic Memory Technologies - Digital Mass Memory Systems

Mass memories employing magnetic tape can also be an analog memory such as a video tape recorder or analog type scientific recorders. This discussion will focus on the current and projected digital types which have evolved as the fundamental element to support the digital communication requirements and performance benefits of current space programs. The magnetic techniques which will be discussed include magnetic tape, core, bubble, plated wire, and electrodeposited closed flux.

Magnetic Tape Techniques - Magnetic tape memories have been a standard for space applications and have evolved in capacity to those of the Earth Resource Technology and Earth Resources Experiment Programs, on the order of 3×10^{10} bits. Lower capacity systems $(1.3 \times 10^9$ bits) for the Viking '75 Orbiter and Lander $(4 \times 10^8$ bits). have been developed. Earlier Mariners had capacities on the order of 1.8×10^8 bits. In addition to capacity, however, the parameters of recording bandwidth, cycle life, bit error rates, weight, power, etc. must be evaluated.

The magnetic tape system could be envisioned to store the data from one to several mapping cycles, depending on the data processing options considered. Storing data over several mapping cycles would allow an extra degree of redundancy in recording at a penalty to the communications system; increased data rate. This feature could be incorporated during the initial mission phases when the closer Earth-Venus distance would allow the higher data rate at no power penalty.

The performance of the Mariner '71 recording system is indicative of possible reliability available with space type magnetic tape recorders. Magnetic tape storage systems currently identified for space use do not exceed 50,000 Mbit total reusable capacity which is very adequate for the radar mapping mission.

Table V-8 summarizes a number of competitive large storage
capacity magnetic tape recorder technologies.

Magnetic Core Memories - Magnetic core memories are based on
an array of ferrite toroidal cores which are each traversed by a
set of two orthogonal wires. Usually a third wire interconnects
all core in a related address block. By passing controlled currents
through the orthogonal wires (one at a time) one can change the
direction of the magnetization of the core thus storing or retriev-
ing a digital data bit. Some memories eliminate the third wire.
Core memories have found many applications in the space environ-
ments but storage capacities would limit them only to a temporary
storage device. Capacities for core memories rarely exceed 10^6
bits; an example of a space qualified core memory is found with the
Viking '75 soft lander (0.200 Mbit capacity). By comparison to
other Mars storage candidates core memories are very reliable but
heavy and power consuming.

Magnetic Bubble Memories - The developmental magnetic bubble
memory technique represents a major breakthrough in high capacity
low power mass memory technology. This technique, if developed
completely, will most certainly be a major contender for the mass
memory on a Venus radar mapper spacecraft. Potential densities
could be the order of 0.1 Mbit/mm^3 ($\sim$ 100 Mbit/in^3) according to
some references. It has also been noted that the power to perform
10^{12} binary operations a second in magnetic bubble devices could be
as low as 0.04 watt, compared to 10 watts for semiconductor switches.
Current research is examining both discrete arrays of magnetized
bubble guideways and amorphous substrates.

A magnetic bubble domain memory consists of a magnetic bubble
source and host crystal (e.g., magnetic oxide or the ferrite),
conducting lattices formed by micro etching techniques to route the
bubble domains, a modulating field to manage the bubble domains,
and sensing conductors. The presence of a magnetic field in a

Table V-8 Magnetic Tape Recorder Characteristic Summary

Type	Wt (kg)	Power (W)	Rates	Capacity (M bits)	ER	Cycle Lifetime
Viking Orbiter	20.5	48	2.2 Mbps/16.2 kbps	1,280	10^{-4}	3000
Viking Lander	6.8	10	4 - 16 kbps	40	10^{-4}	3000
ERTC-VTR	33.6	88	15 Mbps	30,000	10^{-4}	4000
EREP*	91.0	23/260	1 Mbps/channel 28 Mbps total	40,000	10^{-6}	3000
New RCA	45.5	100	345 Mbits total 3 Mbits/track	50,000	10^{-6}	4000
Advanced	15.9	40	5 Mbps/track 35 Mbps	50,000	10^{-6}	4000

* Exclusive of tapes for Earth return.

region as small as 0.1 cm - 0.005 cm (0.04 - 2 x 10^{-3} inches) in a diameter represents a binary digit. The conductor guideways are deposited using thin film techniques directly on thin slices of the orthoferrite bubble domain source and host.

Reference V-4 notes several characteristics of magnetic bubble domain techniques which limit storage densities and controllability; a) with orthoferrite substrates the diameter of the smallest bubble is about equal to the slice thickness; b) domain diameters can range from 2 mils (terbium ferrite) to 0.04 mil magnetoplumbite; c) domains move across a plate in the direction of reduced bias; d) a single bubble can move over its diameter in less than 100 nanoseconds allowing typical transfer rates of about 3 Mbps; e) domains have no mass; f) domains can be split with both parts assuming the size of the original domain; this process (called replication) can be repeated an unlimited number of times; g) usable spatial storage locations should be separated by three domain diameters.

This technology, although currently available in laboratory models only, is being advanced by several private organizations. As a minimum the following companies are known to be pursuing the bubble technology: Bell Labs, IBM, Honeywell, Hewlett-Packard, Monsanto, RCA, Singer, Texas Instruments, Univac, plus many foreign companies and universities. This technique of magnetic recording is already envisioned to replace the workhorse magnetic tape systems of today's spacecraft.

Electrodeposited Closed Flux Magnetic Memories - By electrodeposition micro circuit techniques magnetic digital storage tech nology has been greatly advanced. Recent examples of micro circuitry and photographic etching techniques have produced bit densities on the order of 0.04 Mbit/cm^2 (0.25 Mbit per square inch) in a memory plane which can be as thin as several mils. Such packing would provide for volumetric densities on the order of 0.061 Mbit/cm^3 (1.-1.5 Mbit per cubic inch).

These microcircuit memories are directly applicable to po-
tential onboard processing temporary storage implementations.
Advantages of the magnetic memory remain since individual storage
areas retain the presence of a bit by holding magnetization. Power
is required for reading, writing, and peripheral control.

Plated Wire Memories - A plated wire memory is composed of
orthogonal wires with a magnetic coating plated on all the wires
parallel to one of the orthogonal wires in the basic framework.
The memory digits are formed at the intersections of the plated
wires and the non-plated orthogonal wires. A plated wire memory
is inherently nondestructive on readout.

Relative to the space application, the capacities are less than
ten megabit and would apply only to a temporary lower capacity
storage device.

Semiconductor Memory Technologies

High density semiconductor photographically etched semiconductor
memories are completely applicable to the radar processor temporary
storage requirement. Metallic oxide semiconductor LSI memories are
available which consume as little as 1μ watt per bit to maintain
storage, and tenths of milliwatts per bit to manipulate data. Dy-
namic MOS memories achieve the highest densities. LSI bipolar im-
plementations are also applicable. Bipolar memories are less de-
sirable due to their radiation sensitivity. Typical capacities of
this technology approach several megabits of random access storage.
The high reliability at relatively low weight make this technique
desirable for long life space missions.

Optical Memory Techniques

A wide array of implementation techniques fall within the classification of optical memories: laser addressed optical substrates, holographic thermoplastics, electron-optic photo sensitive materials magneto-optic substrates, photo chromics, and amorphous semiconductor. Storage is either direct bit or holographic in most optical memories.

Inherent storage densities of optical memories are extremely high limited primarily by diffraction of optics or by the beam control for read and write electron or laser beams. A number of alternate approaches to realizing planar memory arrays are currently in development laboratories.

Electro-optic Photo Sensitive Planar Memories - Recently an optical memory of 10^{13} bit capacity (Ref. Laser Computer Corp., Anaheim, Calif.) was developed and is currently under test. This system is stated to be random access, with a read/write/erase cycle of 40 n sec, bit error rate less than 10^{-9}. Storage is by direct bit recording on a doped lithium niobate substrate at a density of approximately 10^7 bits/mm^2. Recording is accomplished by one 2.5 W argon ion laser and read out by a second laser at a different wavelength on the opposite side of the memory plane.

The same corporation has proposed development of memories in excess of 10^{13} bits, approaching 10^{20} bits.

The system requires a relatively large volume for the radar mapping application since the memory plane is approximately 1.3 m^2. Read and write lasers and optics are in addition to these representative dimensions.

Magneto-optic Materials - Magneto-optic materials offer potential implementation advantage of indefinite storage, being read and write cycle life, high resolution in thin films, and the possibility of writing and erasing with the same beam. One of the best magneto optic materials is manganese bismuth. To

produce good holograms requires more peak power and repetition
rates than exists currently in laser technology to achieve data rates
competitive with other systems technologies. Direct bit storage
requires less power and remains feasible and development work is
currently underway on an optical disk memory (reference Honeywell
Corporation).

With this concept bits are stored linearly along a series of
concentric tracks in a medium of manganese bismuth which is mag-
netized to saturation in a direction normal to the surface. Re-
cording is by a laser beam focused to a spot of several microns in
diameter which heats the medium under the spot so that after cool-
ing the magnetization direction has reversed. Reauout can be accom-
plished by allowing a similar low intensity laser beam to be re-
flected or refracted by the spot on the medium and observing the
rotation of the polarization of the laser light. Erasure is by uni-
formly heating the spot so that it will remagnetize in the original
direction or by an electromagnet. This technology has not been
reduced to reliable practice currently, but will probably be avail-
able for a 1980 time frame mission and could offer great advantage
in memory density and reliability.

Photo Chromics - Photochromics of the color center type exhibit
potentially high resolution ($\sim$ 1000 line pairs/mm) and can be opti-
cally erased, but are relatively insensitive (high write energies)
exhibit thermal decay of information over time, and demonstrate
fatigue after several read/write cycles. A different wavelength
must be used for reading and writing if readout is nondestructive.
Studies have shown an inherently high dynamic range possible with
photochromics, but little development work has been sponsored.

Recent developments of photodichroic substances, however, show
desirable advantages for optical memories. These materials are
under study in an optical read/write memory research effort at the
University of Illinois Science Laboratory. Photodichroics polarize

in response to incident polarized light and the response is reversible by a second optical technique and thus allows the determination of the presence of a bit by subsequently illuminating a spot in the memory plane with a reference polarized light and monitoring if transmission was blocked or not. Some photodichroics must be very cold to operate ($K \ Cl_2$) while others work at room temperature (Na^F).

Currently this technique is in advance development stages and s<ems to offer no particular advantage to the radar mapping application.

Amorphous Semiconductors - An amorphous semiconductor memory material responds to laser light by changing from an amorphous glassy state which is transparent to a crystalline state that is opaque. The crystalline state exhibits a sharp change in optical transmission and reflection. The change can be reversed by reexposure to laser light at a different intensity. Advance studies have shown that storage life is indefinite and write times as short as 100 n sec. The memory would be planar with laser read/write/ erase control. Advanced development work (re: IBM Corporation) is currently underway.

Telecommunications Requirements

The telecommunications requirements originate with the required average data relay rates which must be met to accomplish the mission. With this requirement in focus, parametric analyses proceed in light of all the other factors which influence or limit telecommunications performance. The approach for this study has been to analyze derived requirements in sufficient depth so that resultant communication designs can avoid excessive system impact.

Following derivation of parametric requirements, current and projected communications technology is discussed in light of the Venus mission objectives. Discussion in the following paragraphs

include the derived data rate requirements, communications windows, parametric link performance, system interactions, imposed limitations, and technology projections. Signal acquisition at Earth is discussed in a later paragraph.

Data Relay Rate Versus Processing Approaches - The goal of communications design is that it must provide the capability to relay all necessary science data for the entire mission duration. Required data rate, then, is the strongest derived requirement.

The major factors affecting communications windows are mapping strategy and time, Earth and solar occultation, attitude maneuver time, propagation delay (Earth-Venus), and high rate signal acquisition times. The required relay rate is determined by dividing a nominal data volume (per relay cycle) by the range of available relay time. The relay time is the communication window. Data volume for the radar is presented parametrically in the paragraph entitled Data Storage Considerations. Communications windows at Venus are developed in this paragraph.

Presented in Figures V-33 through V-36 are the parametric required data relay rates compared by spacecraft configuration, mapping strategy, eccentricity, attitude control concept, and Earth occultation. A pair of rate requirements is shown for each mapping strategy which bounds the rates over periods of no Earth occultation and peak Earth occultation. These derived data rate requirements are the core of parametric system implementations discussed in later paragraphs. Example point design implementations are presented in Section V Volume II. The following discussion will state general findings and conclusions possible from the parametric data.

Practical Deep Space Net current (~ 250 Kbps) and projected (~ 2500 Kbps) receiving data rates are shown all required relay rate plots. Reviewed in light of Earth occultation impact on derived data rate requirements, the parametric benefit of multi-
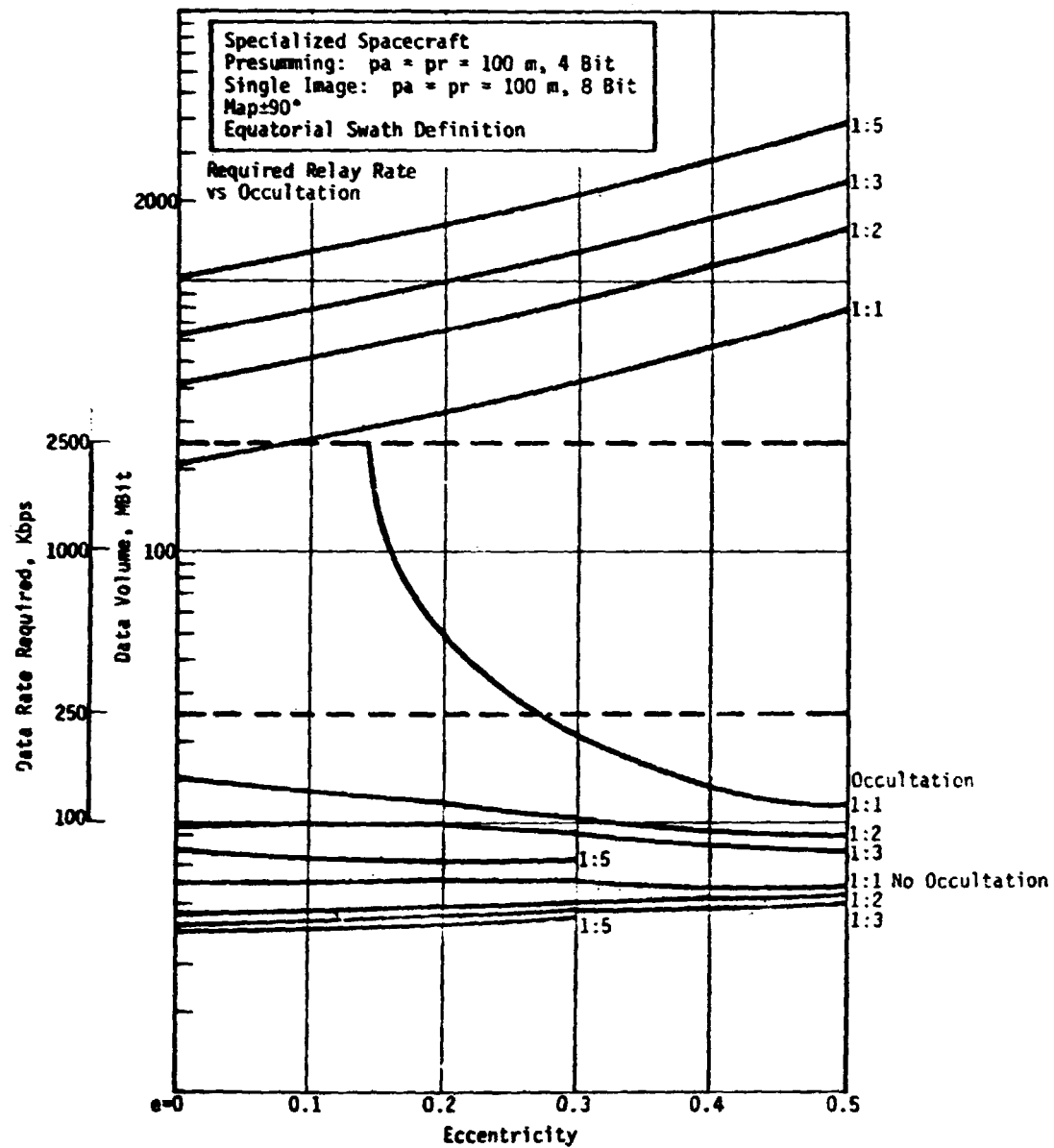
Figure V-33 Required Relay Rate -- Maximum Presumming or
Single Channel Image, Configuration C

V-92
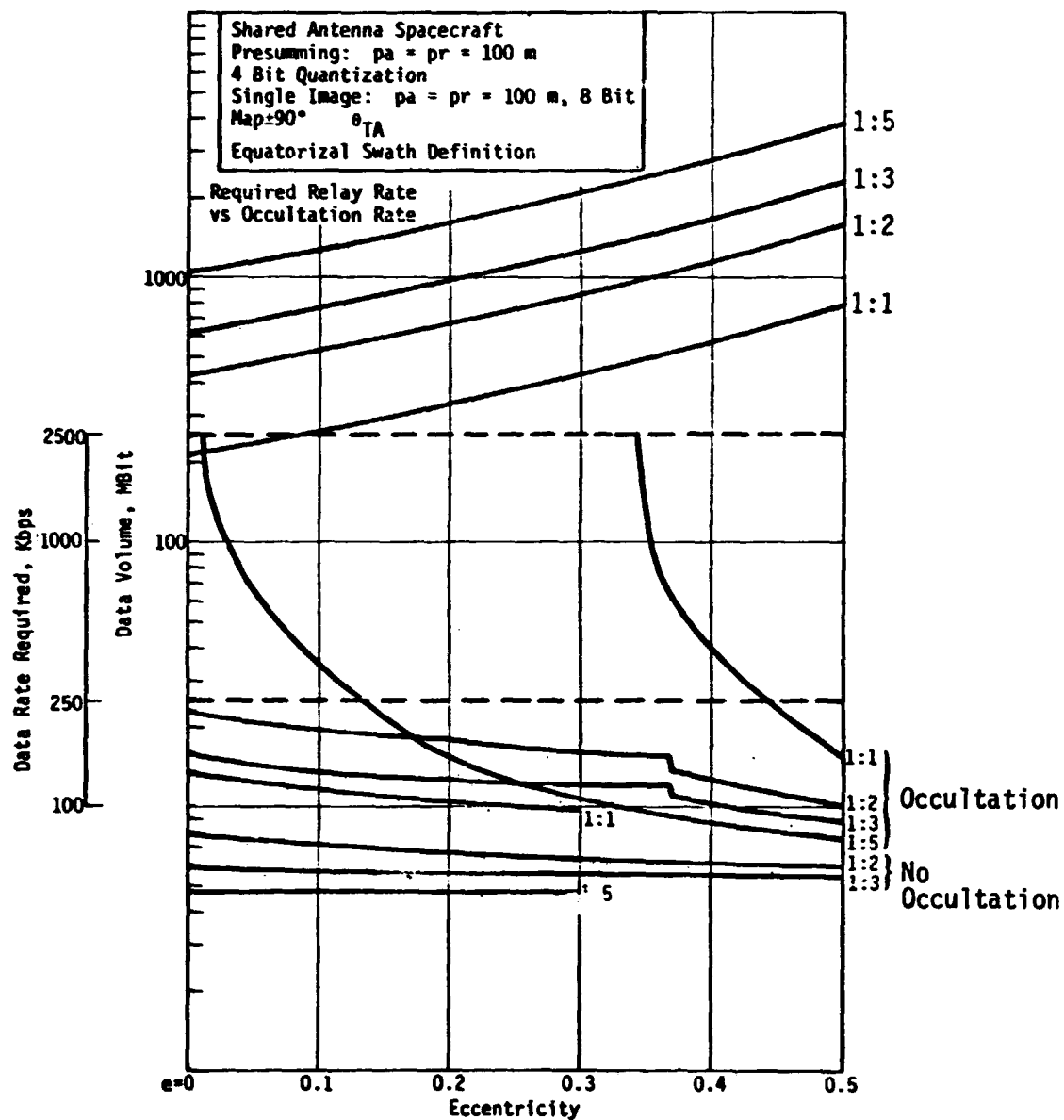
Figure V-34 Required Relay Rate -- Maximum Presumming or
Single Image, Configuration A
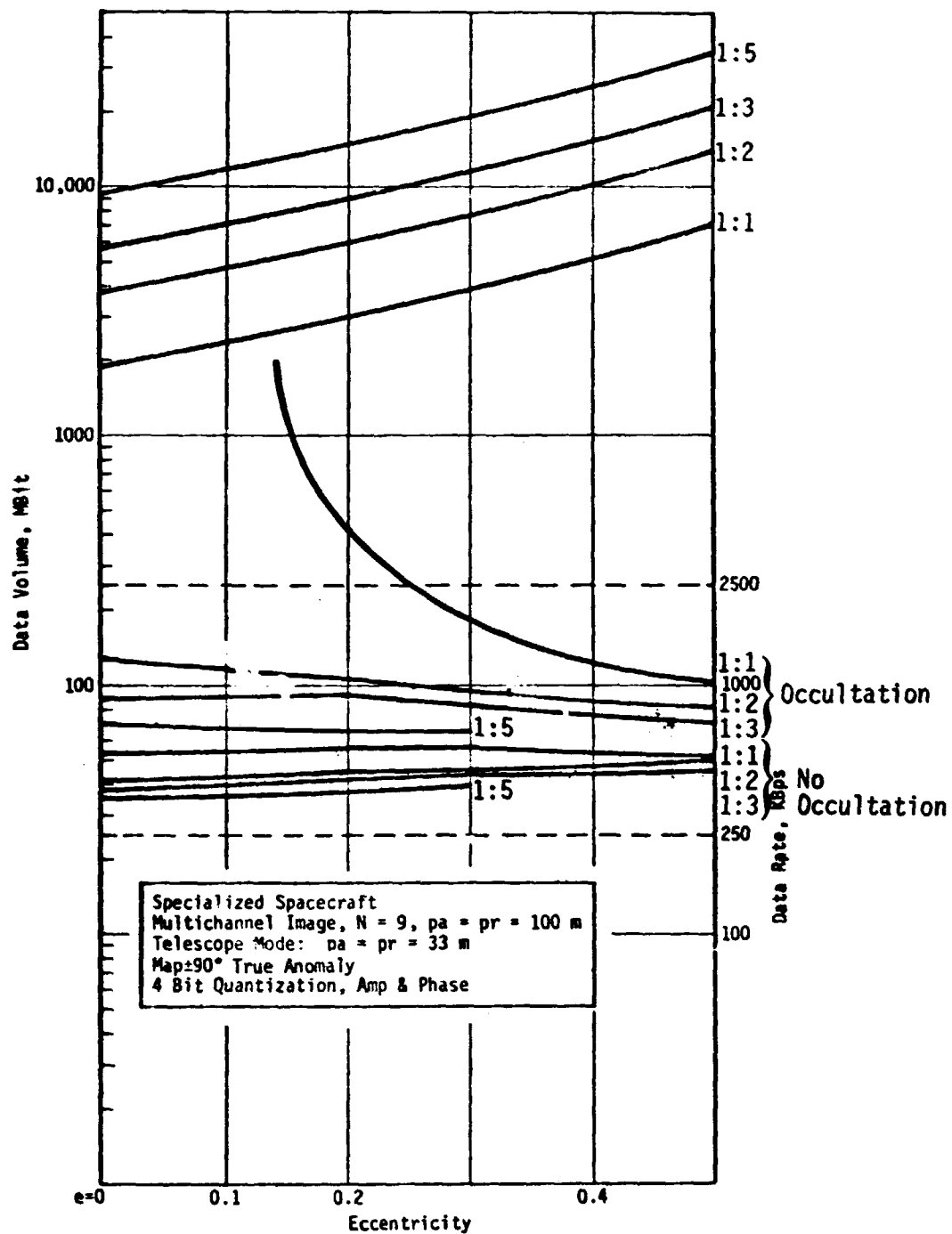
Figure V-35 Multichannel Telescope Rates -- Configuration C
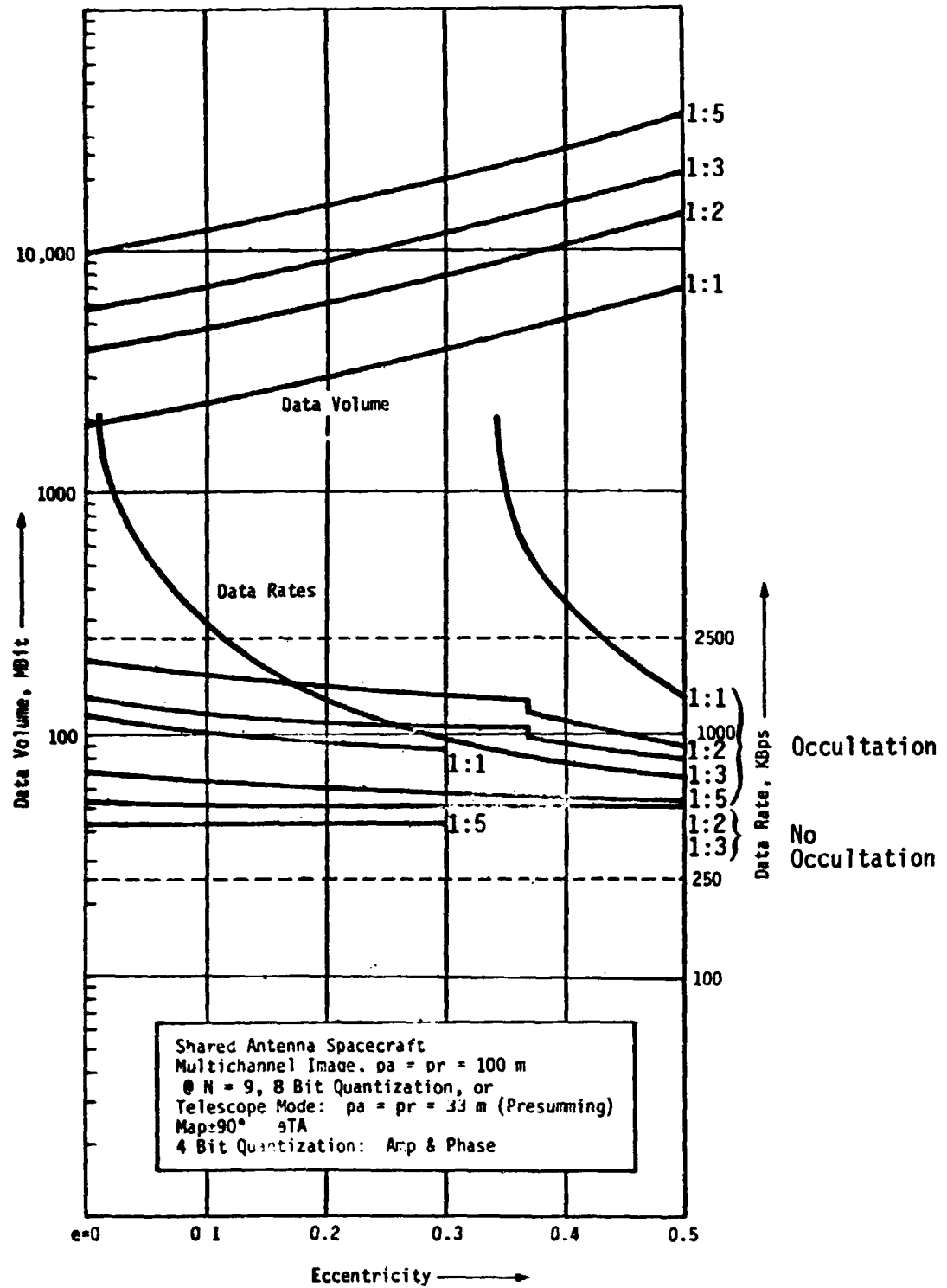
Figure V-36 Multichannel Telescope Rates -- Configuration A

orbit mapping cycles is outstanding; to relay the same average
data rate during occultation with the shared antenna configuration
spacecraft is impractical with a single orbit mapping strategy,
except at highest eccentricity. For multiple orbit mapping strate-
gies required data rate varies within a factor of 5 over all
eccentricities and both classes of spacecraft type.

The lowest average data rates and corresponding spacecraft
radio frequency subsystem magnitude are graphically demonstrated
for the longest time between mapping (multiple orbits) and higher
eccentricities in all figures.

Figures V-35 and V-36 present parametric requirements for more
ambitious approaches or mission enhancement items: a) relay at
continuous high resolution data which has been presummed, or b)
relay of channels of imagery allowing uncorrelated image addition
on Earth. Nine channels of uncorrelated summing is shown because
the image statistic improvement by this approach is equivalent to
the uncorrelated averaging of presummed data taken at 3 times the
resolution in both the range and azimuth direction.

Significantly the corresponding mass storage increase due to
the additional data is still compatible with magnetic tape distance
storage technology. The required relay rates, however, are all
within the realm of the next generation Deep Space Network under
the same higher eccentricity or multiple orbit mapping strategies
as summarized for the case of relaying the planetary 100 meter
range and azimuth resolution.

Communications Window at Venus - The communications window from
Venus is a salient characteristic which allows the determination of
required data relay rate bounds. Above paragraphs discussed the
range of required with and without peak earth occultation. Figure
V-1 of the introduction singles out the salient contributors to
the communications window: a) the mapping strategy (i.e. number
of orbits per mapping cycle); b) orbit eccentricity, c) earth

occultation; d) attitude control/orientation time; e) signal
acquisition by the Deep Space Network. The following paragraphs
will discuss parametrically the assumptions and timeline contri-
butions of the factors leading to a communications window deter-
mination.

Communications at maximum power (data rate) are assumed to be
mutually exclusive except for a strategy of signal acquisition
which was attributable to some implementations of Configuration
C (see Section V, Vol. II). This approach serves to avoid an
unnecessary high peak power demand requirement on the power
subsystem. The special case mentioned utilizes a lower power
communications mode only available with Configuration C, to
maintain a minimal coherent signal lock-up time at the ground
station.

Earth occultation effect was included in the timeline analysis
for communications. The reference occultation for example designs
(see Vol. II, Section V) was peak occultation, but the required
relay rate contours of this section can be used to determine a
power based on no occultation (at maximum range) by proportioning
the required data relay shown in the parametric required data
rates (Figures V-33 through V-36).

The effect of earth occultation is most significant at e = 0
and least significant at e = 0.5 as graphically shown by Figure V-37.
Nominal designs have provided for peak occultation to test subsystem
feasibility. With eccentric orbits the reduced actual occultation
duration is translated to additional design margins of the reference
designs. Required data rates were determined for both occultation
and no occultation. The Earth-Venus range is superimposed on the
occultation contours to emphasize the near coincidence of maximum
range and peak occultation.
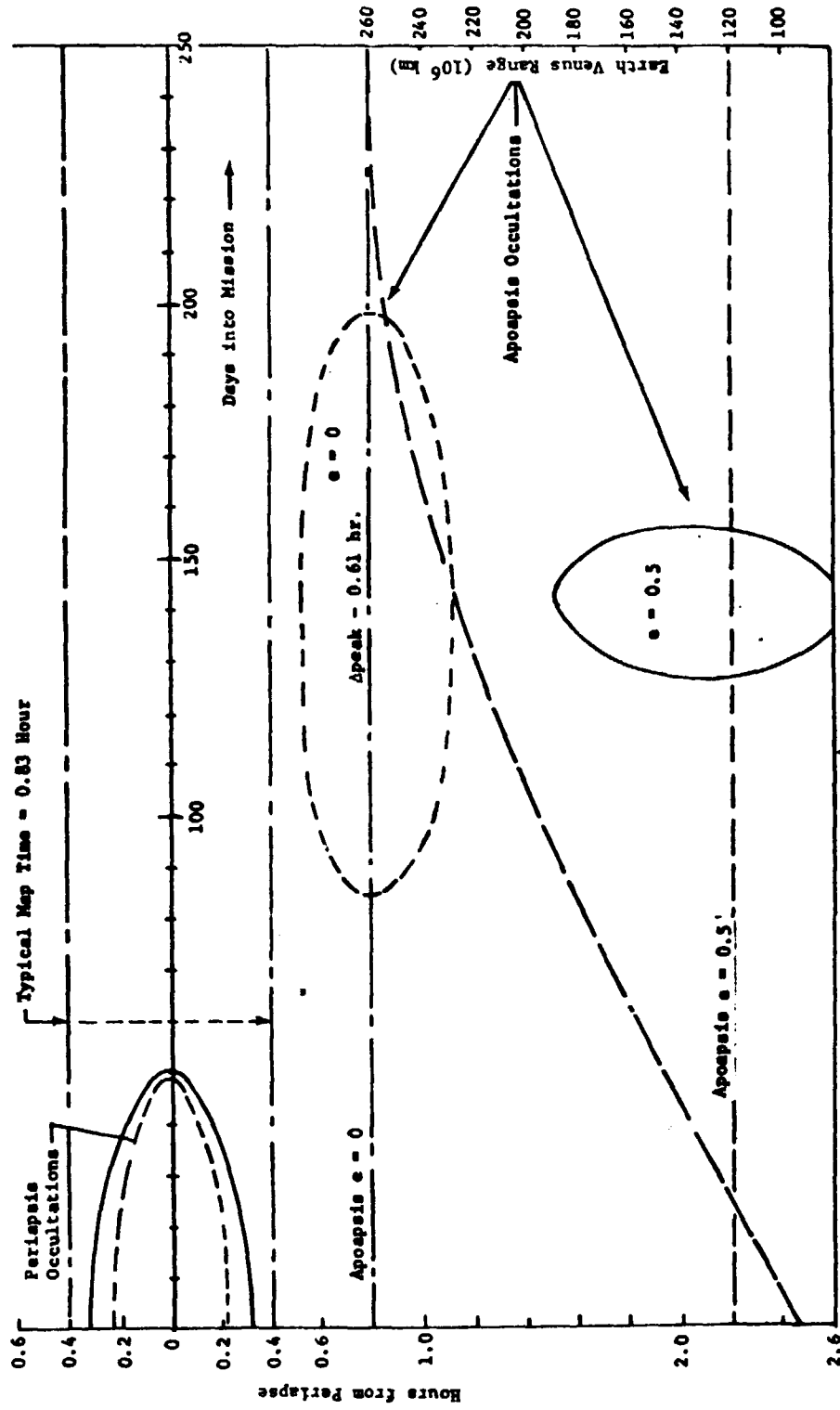
Figure V-37 Earth Occultation Variation with Eccentricity Extremes

The occultation histories change slightly for eccentric orbits when periapsis is shifted from positive latitude through zero to negative latitude, but the change in peak occultation overall is < 10% for the range of periapsis locations considered. The table V - 9 below, further summarizes the significance of the occultation considerations which shows the percent of total mission orbits experiencing some occultation.

Table V-9 Summary of Earth Occultation vs Eccentricity

Orbital Location	Eccentricity Ranges		
	0	0.2	0.5
Apoapsis	46%	29%	11%
Periapsis	20%	26%	21%
Apoapsis + Periapsis	66%	55%	32%
None	34%	45%	68%

For single orbit mapping cycles the earth occultation occurring near orbit apoapsis is the factor to consider since occultation at periapsis would not interfere under a policy of mutually exclusive mapping and data relay (mappers occurs only around periapsis). For multi-orbit mapping cycles with data relay through subsequent orbits, the periapsis occultation is also significant, but again the impact to an eccentric orbit is less than that for a circular orbit.

The contribution to timeline due to attitude control and point-ing is spacecraft configuration dependent. The times allocated to antenna or spacecraft attitude slewing are summarized in Table V-10. These values are deducted from the communications window once per mapping cycle. The primary advantage of a fully articulated (i.e. radar antenna, communication antenna, solar panels) spacecraft con-figuration becomes explicit; the impact to the communications time-line by the altitude control and pointing requirement is removed.

Table V-10 Attitude Control Timeline Impact vs Configuration

Spacecraft Configuration	Communication Time Lost To Attitude Control (Hr)	Comment
A	0.3	Slew antenna.
B	0.9	Slew spacecraft.
C	0	Communication antenna continuously Earth oriented.
A=Shared Antenna; B=Dedicated Antenna; C=Specialized Spacecraft		

Composite communications windows compared by generic space-craft configurations are shown in Figures V-38 and V-39. The communication windows for Configuration B follow directly from Figure V-39 by subtracting an additional 0.i hr for additional attitude maneuver/control slew times at an obvious penalty to re-quired relay rate. Figure V-38 indicates the benefit in communications time per cycle available using a communications antenna which is continuously earth oriented. These curves include for lower eccentricities (<0.3) the option of completing signal acqui-sition sequences into the mapping phase. This would employ a power level that does not excessively impact the power subsystem and was shown feasible. The effect of these derived communications windows on necessary average data relay rate was presented in the Data Relay Rate versus Processing Approaches paragraph in this section.

Communications Implementations - Two very significant communi-cations parameters are the required data bandwidth (rate) and mission operating ranges. A complete understanding of communi-cations subsystem impact will define the effects of mission Earth-Venus ranges, transmitter power, antenna dimensions and type, operating frequency, data modulation scheme, ground station antenna, ground support baseband equipment characteristics, system losses and typical operating efficiencies.

V-100
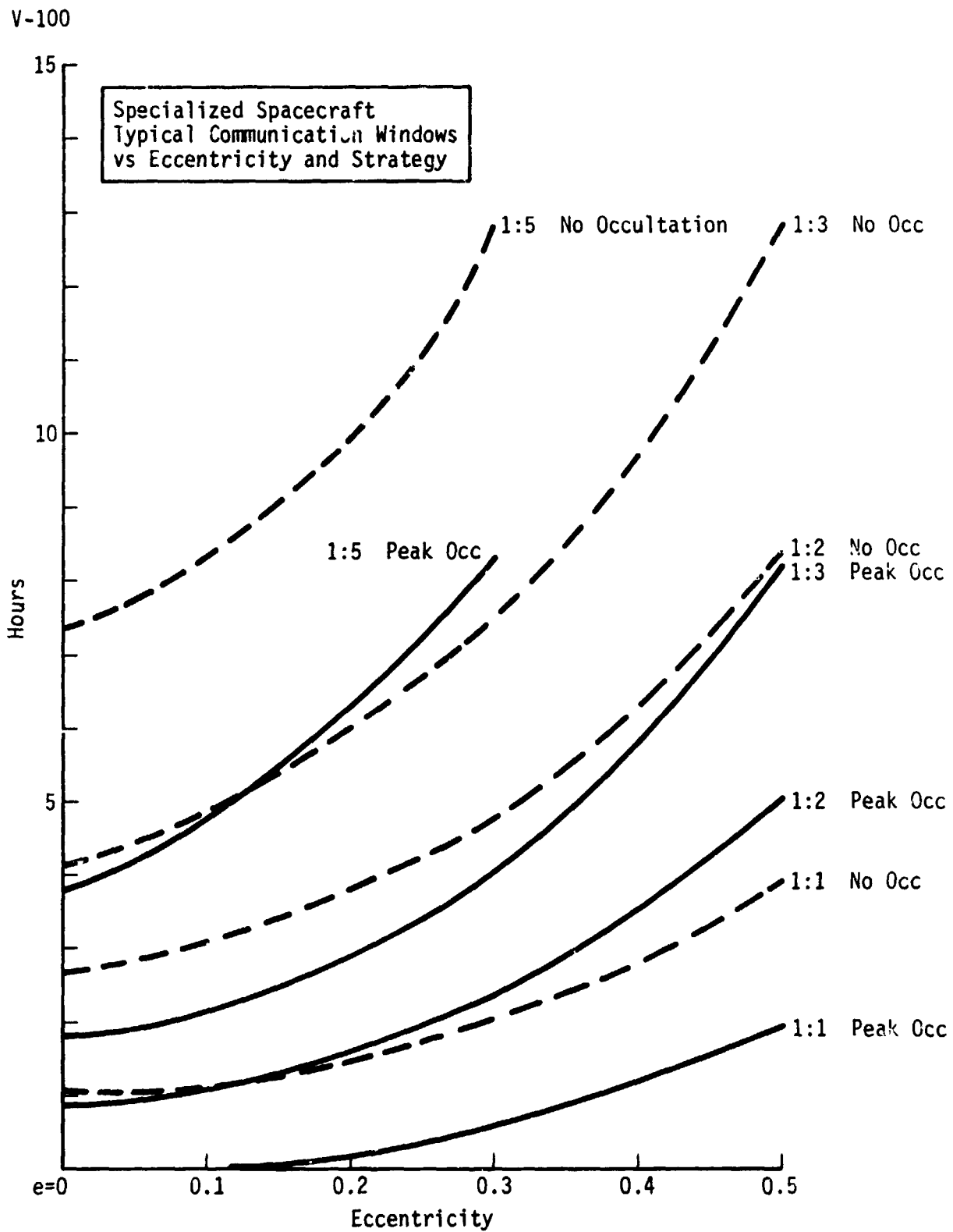
Figure V-38 Venus Communication Windows -- Configuration C
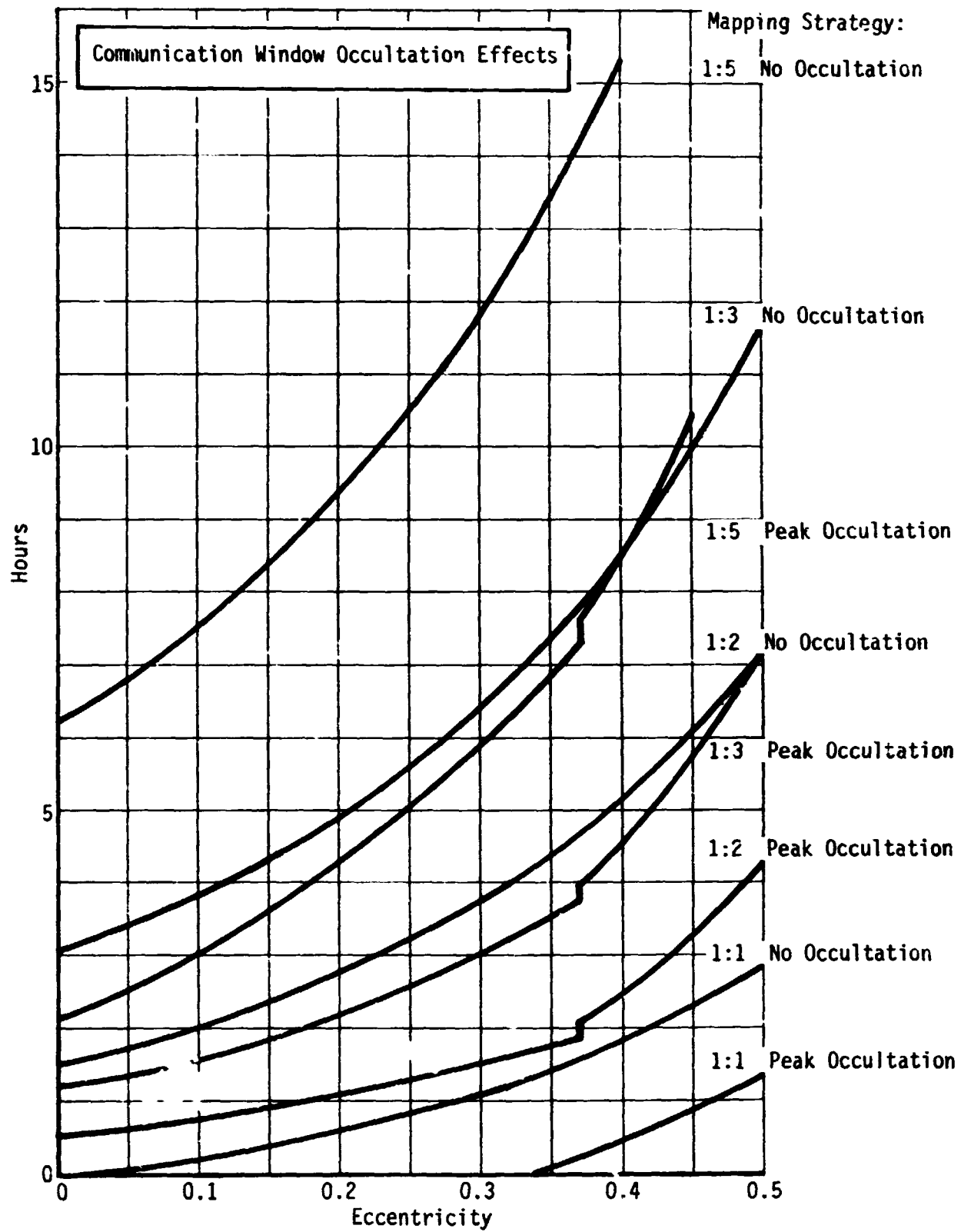
Figure V-39   Venus Communication Windows -- Configuration A

The basis for communications parametric studies is found in
Table V-11 where the reference values of a "nominal" relay link
utilizing X-band (i.e., 8448 mHz) and the 64 meter Deep Space
Network are documented. Parametric implementations have employed
the data resulting from including pointing loss at the spacecraft
and ground station, uncoded data, and maximum mission range of
1.71 AU (Earth-Venus). Discussion in the Communications Enhance-
ment Tradeoff with Channel Encoding paragraph of this section pre-
sents performance enhancement available by employing data channel
coding and other alternative design approaches. The inclusion of
100 watts at X-band as a reference maximum power is considered to
be a current maximum based on a compound TWTA system composed of
50 watt units. This is a current feasibility reference assessment
only and does not necessarily draw directly on a particular space
program. Contact with recognized space qualified TWTAs resulted
in the assessment that high powers could be proven by a qualifi-
cation program for Earth-based electronic countermeasures (ECM)
type X-band tubes.

Several forms of the basic equation describing communications
performance is shown below:

$$S/N = \frac{PG_t}{4\pi R^2} \times A_r \times \frac{1}{KTFB} \times \frac{1}{L_{sys}} \times L_m \times T_h \times M \qquad (V-50)$$

$$= \frac{PG_t}{4\pi R^2} \times \frac{G_r \lambda^2}{4} \times \frac{1}{KTFB} \times \frac{1}{L_{sys}} \times L_m \times T_h \times M \qquad (V-51)$$

$$= \frac{PG_t G_r}{\left(\frac{4\pi R}{\lambda}\right)^2} \times \frac{1}{KTFB} \times \frac{L_m}{L_{sys}} \times T_h \times M \qquad (V-52)$$

Table V-11 Telecommunication Reference Performance Values

			Adverse Allowance (db)
1.	Total transmitter power - 100W @ X-band, dbm	+ 50	0.0
2.	Circuit loss (db)	- 1.6	0.1
3.	Spacecraft antenna gain @ 8448 MHz - 2m (db)	+ 42.28	1.5
4.	Pointing loss (db)	- 3.0	0.0
5.	Space loss $(4\pi R/\lambda)^2$ @ 1 AU=149.6 x 10^6 km (db)	-274.45	0.2
6.	Polarization loss	- 0.10	0.1
7.	DSIF antenna gain (64 m @ 8448 MHz) (db)	+ 72.35	1.0
8.	DSIF loss (inc. atmosphere) (db)	- 3.0	1.0
9.	Net transmission loss	-282.15	3.9
10.	Total received power (dbm)	-117.52	3.9
11.	Receiver noise spectral density-37°K (dbm/Hz)	-182.70	0.2
12.	Carrier modulation loss (1.12 rad) (db)	- 6.86	0.1
13.	Received carrier power	-124.38	3.9
14.	Carrier loop bandwidth noise $(2B_{LO}=12Hz)$(db)	+ 19.8	
15.	Threshold SNR (db)	+ 10.0	
16.	Threshold carrier power (dbm)	-161.9'	4.2
17.	Margin @ 1. AU	+ 37.52	(+33.32)
18.	Data modulation loss (1.12 rad) (db)	- 1.02	0.1
19.	Received data power (dbm)	-118.54	4.0
20.	Threshold SNR p(bit) error .5x10^{-3} PSK (db)	+ 7.3	
21.	Desired margin + misc. loss allowance (db)		4.0
22.	Threshold data power (dbm)	-171.40	4.0
23.	Remaining data rate bandwidth @ 1 AU (db) (includes S/C pointing loss & DSIF loss)	+ 52.86	

Data Rates:			
	@ 0.63 AU arrival	486 KBPS	1944 KBPS
	@ 1.0 AU (arrival + 80 days)	193	772
	@ 1.59 AU (arrival + 160 days)	76.3	305.2
	@ 1.71 AU (arrival + 240 days)	66.	264

$$PG_t = \frac{(\frac{S}{N}) \times (\frac{4\pi R}{\lambda})^2 \times KTF \times \frac{L_{sys}}{L_m} \times T_h \times M}{G_r} \times B \qquad \text{(V-53)}$$

$$= \frac{(\frac{S}{N}) \times (\frac{4\pi R}{\lambda})^2 \times KTF \times \frac{L_{sys}}{L_m} \times T_h \times M}{G_t G_r} \times B \qquad \text{(V-54)}$$

$$\frac{P}{B} = \frac{(\frac{S}{N}) \times (\frac{4\pi R}{\lambda})^2 \times KTF \times \frac{L_{sys}}{L_m} \times T_h \times M}{G_t G_r} \times T_h \times M \qquad \text{(V=55)}$$

Equations V-50 - V-52 single out the S/N requirement which is re-
lated to bit error performance. Equations V-53 - V-55 relates
satellite ERP to data bandwidth.

Where P = average spacecraft transmitter power

G_t = transmitters antenna boresight gain

G_r = receiving antenna boresight gain

R = slant range (spacecraft to Earth)

A_r = effective area of receiving aperture, $G = 4\pi A_e/\lambda^2$

λ = carrier wavelength, (3.56 cm @ 8448 MHz)

K = Bolt   constant, 1.38×10^{-23}

T = receiving system noise temperature (K^o)

L_m = ratio of modulation side band power to carrier power

L_{sys} = composite system losses typically includes antenna
pointing losses, transmitter circuit loss, polari-
zation losses, recording and detection losses

$(\frac{S}{N})$ = required bit (Eb/No) signal to noise level for a
given probability of error

T_h = link threshold ratios where applicable

M = desired performance margin

Data rates at alternate power levels can be inferred by taking
the ratio below with no other changes:

$$B_N = P'_{RF}/P_{REF} \times B_{REF}$$

where B_N = new data rate

P'_{RF} = new RF power value

P_{REF} = RF reference power, 100 watt @ X-band

B_{REF} = reference data rates from Table V-12

Generally, the required effective radiated power (product of space-craft transmitter power and antenna gain) can be inferred for the reference ranges according to the equation and table below in db values:

$$ERP(db) = B_d(db) + B_R(db) \qquad (V-56)$$

where   ERP = effective radiated power (db)

B_d = data rate (BPS)(db)

D_R = multiplier value from Table V-12 below

Table V-12 D_R Values for ERP Interference

Earth-Venus Range (AU)	D_R (db)
0.63	5.37
1.0	9.42
1.59	13.62
1.71	14.08

Collected in Table V-13 are several representative antenna sizes, characteristics, and reference data rates which result. The antenna sizes shown resulted from radar and communications parametric implementations. The data rates were derived based on Table V-11 and employing the differences in antenna gains and stated reference distances different from the basic range of I.A.U. The alternate distances shown correspond to convenient points in the mission: arrival, arrival + 80 days, arrival + 160 days, arrival + 240 days.

Table V-13 Reference Data Rates with Alternate Antennas

	Gain (db)	HPBW (mrad)(1)	Reference Data Rates (KBPS)(2)			
			0.63 AU	1.00 AU	1.59 AU	1.71 AU
1.77 m Parabola	41.22	20.1	382	151.5	39.8	51.8
2.0 m Parabola	42.28	17.8	486	193	76.3	66
3.0 m Parabola	45.74	10.9	1080	428	169	146.5
3.55 m Parabola	47.19	10.1	1505	597	236	202
4.0 m Parabola	48.28	8.9	1945	772	305	264
4.6 m Parabola	49.49	7.75	2560	1016	402	347
6 m Parabola	51.78	5.93	4330	1720	680	588
.6 m x 3.5 m Array	38.93	59.3 x 10.1	225	89.2	35.3	30.5
1.2 m x 3.5 m Array	41.94	29.6 x 10.1	450	178.5	70.5	61.0
.85 m x 3.05 m Array	41.57	42 x 11.7	413	164	64.8	56.1
1.75 m x 3.05 m Array	44.57	20.4 x 11.7	825	327	129.2	111.5
1 m x 4 m Array	43.5	35.6 x 8.9	644	256	101	87.3
2.9 m x 4.57 m Array	48.52	12.3 x 7.8	2020	810	321	278
3.5 x 3.66 m Array	48.36	10 x 9.75	1965	780	309	267

(1) θ HP = λ/D, λ = .0356 meter

(2) Coherent, uncoded data, S/N = 7.3 db reference

Communications Antenna Considerations - The requirement for
communications at X-band imposes more restrictive pointing require-
ments than experienced by the Vikin Orbiter mission. The combined
spacecraft must orient the communications antenna to within its
half-power beamwidth over the time required for high data rate
relay. The basis for this study is to assume a spacecraft which
is inertially oriented and which has on board computational capa-
bility sufficient to orient an antenna toward earth. This capa-
bility is found with the basic Viking Orbiter, but this paragraph
will discuss the pointing requirements of the Venus mapping rela-
tive to the present Viking Orbiter capability of approximately
12.6 mrad (0.72 degree).

Figure V-42 summarizes the antenna (parabolic) half-power
beamwidth versus antenna diameter for typical high focal length to
diameter ratios (i.e. ≥0.4). The solid line demonstrates the half-
power beamwidth for $\lambda = 0.0356$ m and an aperture distribution typi-
cal of such antennas. This illumination is not fully uniform ($\theta_{HP} = $
0.89 λ/D, even more restrictive), but represents typical aperture
tapers employed in practice. The dotted line shows the effect of
an alternate aperture distribution which could be employed to
broaden the beamwidth at the expense of loss in gain. These dis-
tributions would nearly encompass reasonable candidates.

It is seen that the present Viking Orbiter capability just
meets the requirement for the 3 meter antenna, and that the 4
meter antenna cannot be oriented properly with the present Viking
Orbiter.

Attitude control analyses (Vol. III, Section VI) have determined
that the requirement of the 3 meter antenna can be met with small
improvements to the current Viking Orbiter. Therefore, this size
will be used as a reference size. The 4 meter antenna can be
oriented by providing additional precision (such as an auxiliary
control moment gyro subsystem) to most elements of the attitude
control subsystem.
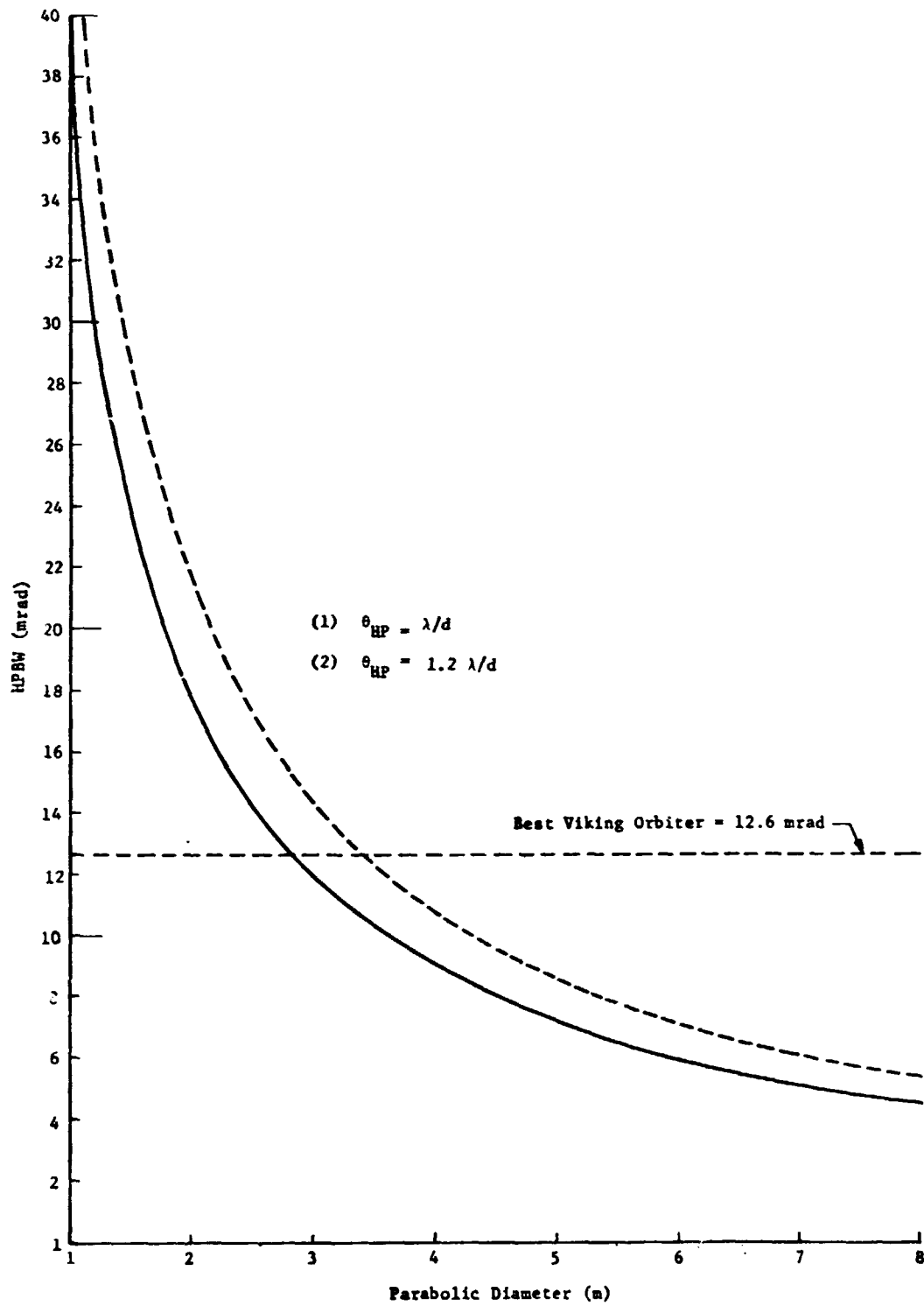
Figure V-40 Communications Antenna Pointing Requirements

This discussion exposes the most critical subsystem interaction of the communication subsystem: antenna orientation through the attitude control subsystem. The great performance flexibility available with larger antennas (≈ 4 meter) are presented as performance enhancement options and are discussed in Volume II, Section V.

The antenna would probably be furlable which is not considered a problem based on available technology reports. The thermal effect on surface integrity is a consideration, certainly, but is not considered significant. Nominal communications link analyses have incorporated losses which account for such degradations from nominal performance.

The articulation control primary sensor would require an absolute shaft encoder or more precise feedback potentiometer for sizes in excess of 3 meters (relative to the Viking Orbiter).

Effective Radiated Power Considerations - Parametrically defined effective radiated power (ERP) is most directly derived from required relay rate, antenna availability, and transmitter power. ERP is usually defined as the product of transmitter radio frequency power and antenna maximum gain. In light of a spacecraft system study, it is convenient to relate the ERP requirement to derived data bandwidth (i.e., required relay rate). Thus the effects of data encoding, improved transmitter efficiency, and alternate antennas can be readily identified. Accordingly, this paragraph will present parametric ERP requirements relative to the required data bandwidth of radar data only for the various mission strategies. The data presented examines Configuration C for the reference mapping strategies of mapping 1:1 (every orbit) and e = 0.5, 1:2 (every second orbit) and e = 0.3, and 1:5 (every fifth orbit) and e = 0. More specific example implementations of both Configuration C and A spacecraft are found in Section V, Volume II of this report. The derived powers are found in Figures V-41 through V-43.

V-110
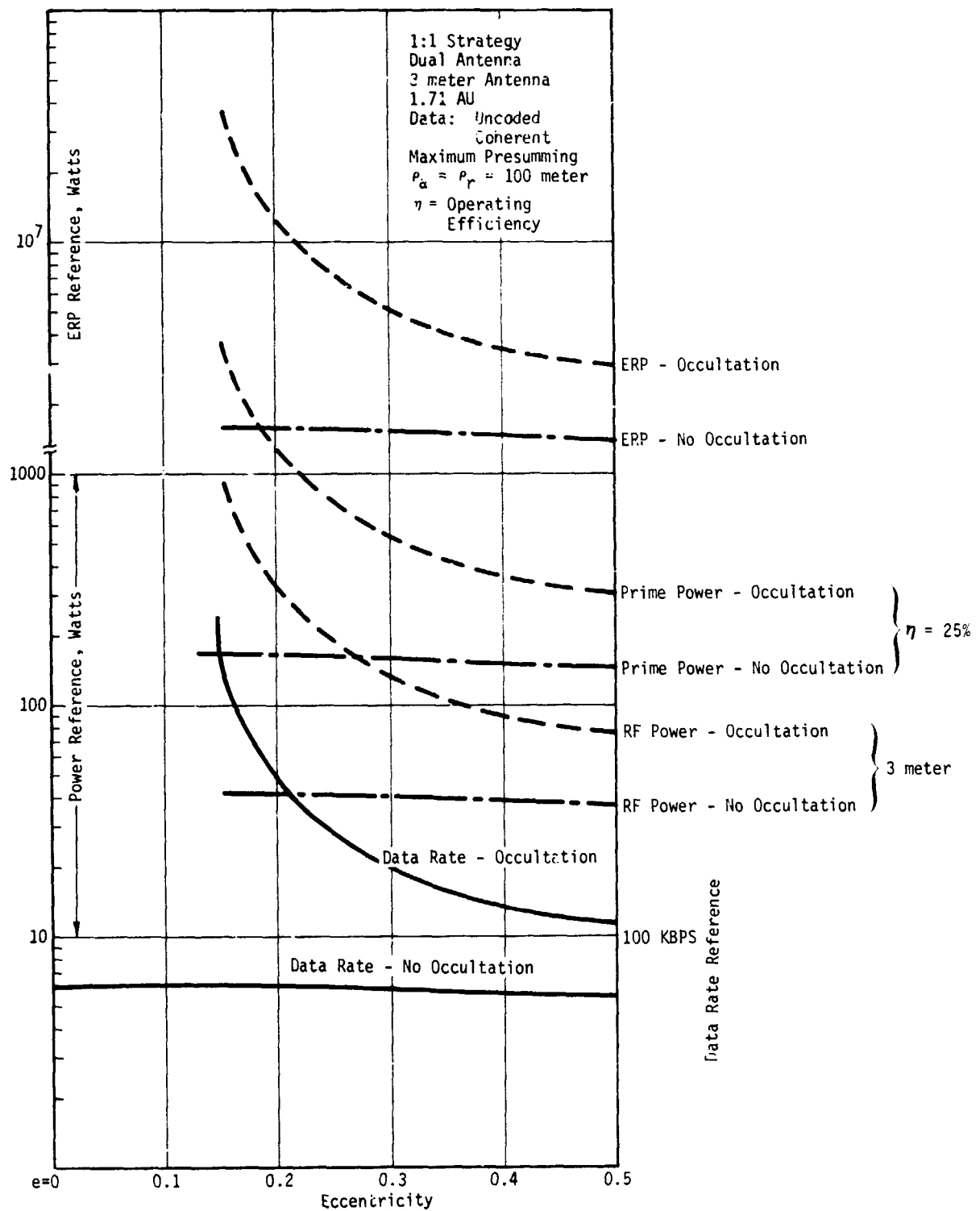
Figure V-41   T/M Power Requirements vs Eccentricity -- Configuration C 1:1
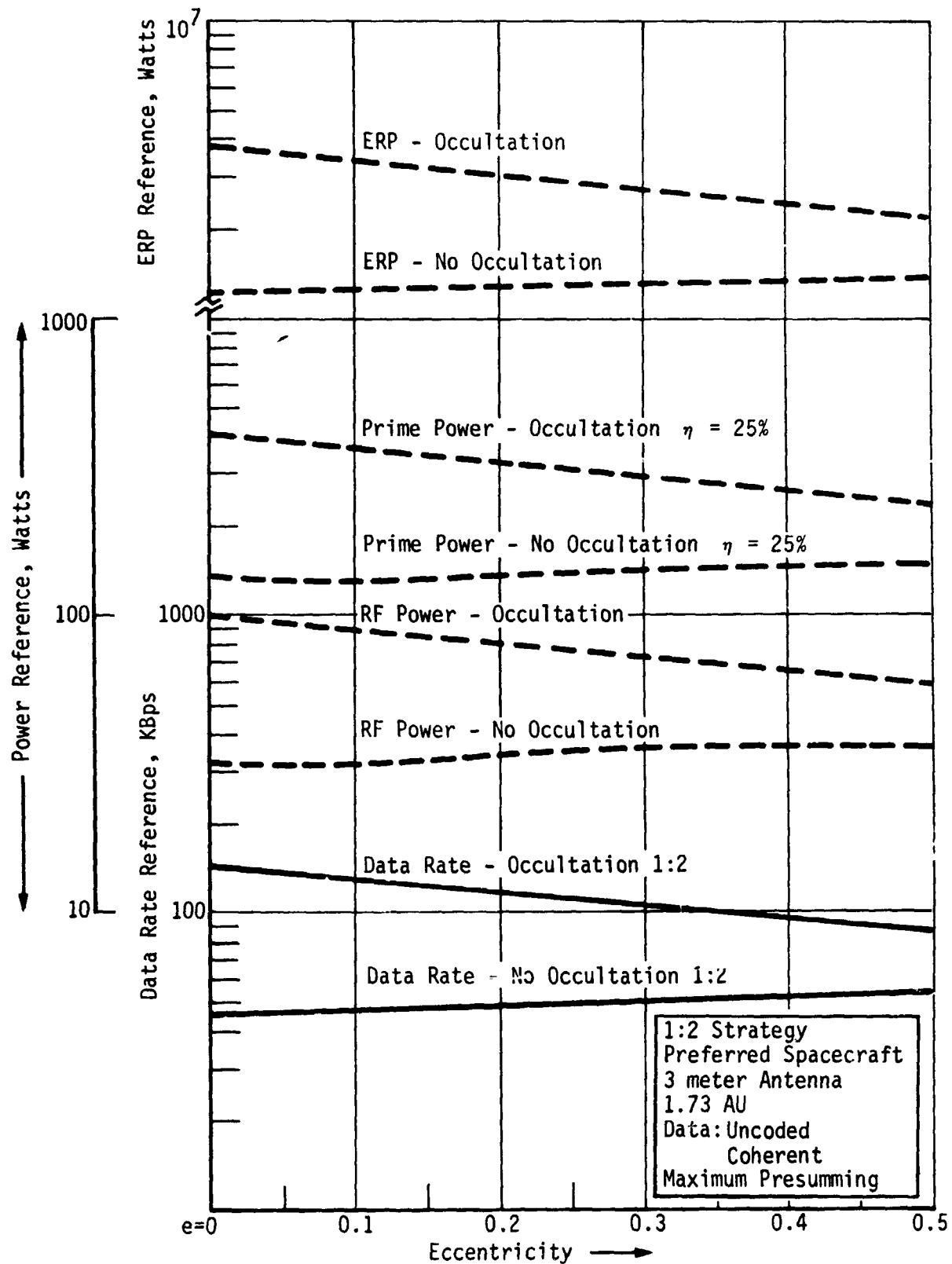
Figure V-42 T/M Power Requirements vs Eccentricity -- Configuration C 1:2
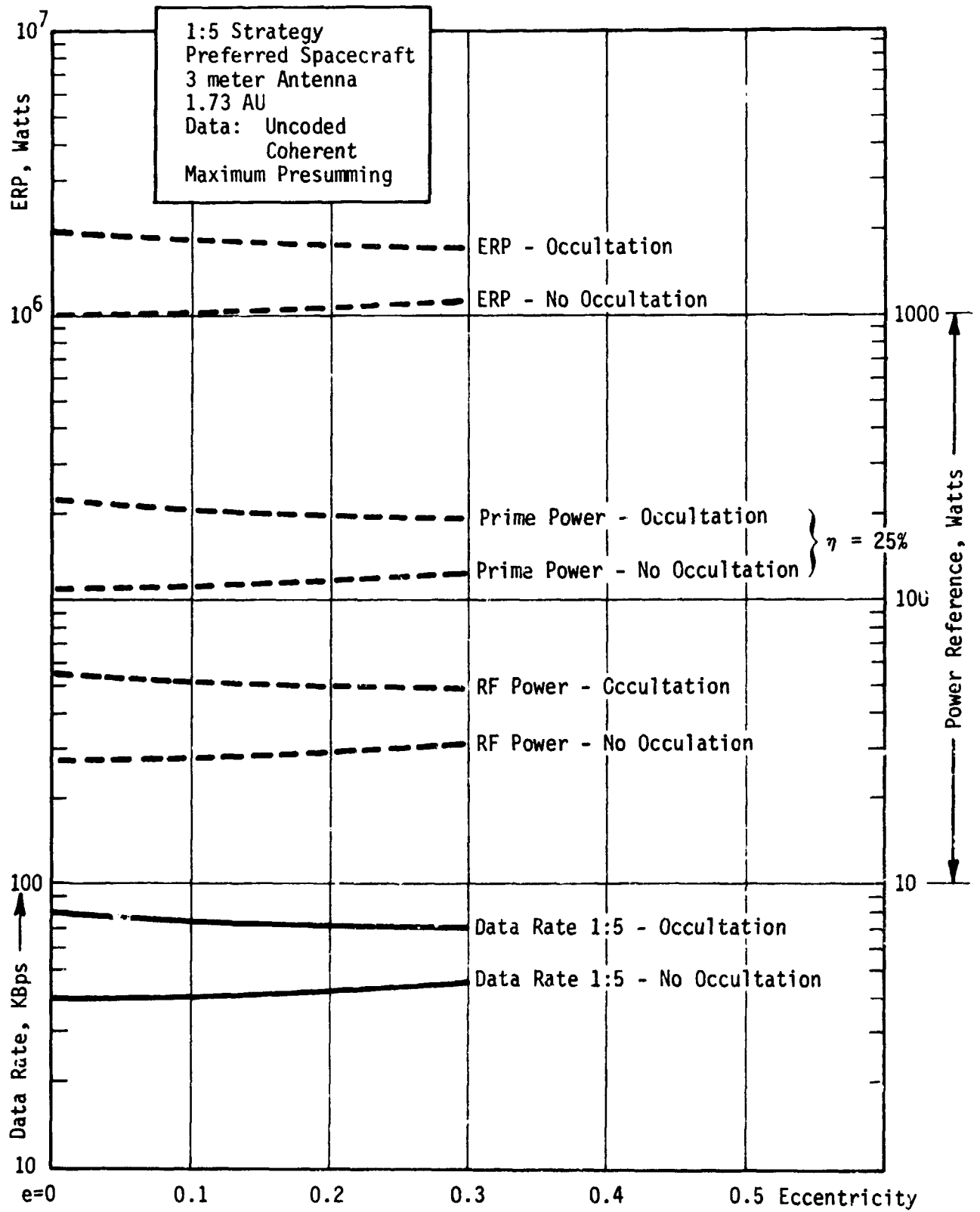
Figure V-43 T/M Power Requirements vs Eccentricity -- Configuration C 1:5

Figure V-41, for example, shows that Configuration C in an
orbit of 0.5 eccentricity mapping every orbit over 180 degrees
true anomaly would require approximately 80 watts of X-band power
to relay uncoded coherent data at 100 meter resolution at mission
end under peak occultation geometry with a 3 meter antenna. For the
same maximum distance, if the mission were designed to ignore the
occultation period the derived average power for radar data would
be approximately 37 watts for the same data. Further, for example,
if it were desired to incorporate communications enhancement feature
such as convolutional coding the channel symbol rate would double
(rate $\frac{1}{2}$, convolutional code), but the spacecraft transmitter power
would drop to approximately $\frac{1}{2}$ of the original reference value.
Comparisons between Configuration C and A are possible through the
example designs of Volume II, Section v, example spacecraft
implementations.

Communications Enhancement Tradeoffs with Channel Encoding -
Channel encoding is attractive because it offers the capability to
reduce required spacecraft transmitter power at little penalty to
the spacecraft for an encoder. The complexity is added to the
ground station where generally it would imply a lower cost impact
than to a spacecraft. This discussion will not treat in detail
the multitude of encoding and decoding strategies identified by
the many contributions to the technology but will expose typical
spacecraft advantages possible with encoding. This potential
relaxed power requirements on the spacecraft communications
TWTAs is significant due to technology limits on TWTA power at
X-band and the communication antenna size limitation ($\sim$3 meter
for Viking Orbiter class ACS).

The comparisons of this paragraph are made on the basis of un-
coded, coherent detection, a representative block code, and a typi-
cal convolutional code applicable to space communications. Data
detection is based on threshold decoding for the block code, soft
decision Viterbi and sequential decoding for the convolutional
code. The study is not intended to select a "best" code but
simply demonstrate representative performance benefits with
channel encoding.

Several characteristics of an encoded channel must be considered
in light of total system interactions. First, the inclusion of
encoding adds redundant, additional bits to the communications link.
That is, the data stream carries information bits plus coding bits
at a net increase in the required bandwidth of the receiving sta-
tion. This increased data stream rate is called the symbol rate
since for coded data several code bits are relayed with each in-
formation bit, the greater the benefit to transmitter power, and
the greater the decoding problem.

Second, since the derived data rates for the Venus mapper mission
are relatively high (60-250 KBPS (and higher)) there is an implied
lower limit on coding rate (i.e., upper limit on symbol rate) deter-
mined by the DSN capability. For example, for a coding rate equal
to ½ the symbol rate is twice the information rate. Note that for
the block code used with Mariners, the (3 o) code, the coding
rate is 6/32 ÷ .187. This implies a symbol bit rate of 534 KBPS
for 100 KBPS required information rate. This is in excess of
apparent present DSN upper symbol rate reception limits and within
the next generation DSN capability. Although it is not excluded,
this type code even with its good performance potential uld
overburden the DSN significantly for typical radar mapper data
rates. In light of the derived high data rates of the Venus radar
mission example codes are kept to a short constraint length and
coding rate around ½, arbitrarily. The short constraint length

codes generally also imply the simplest decoding computation re-
quirement, or the lesser impact on DSN data handling complexity.

The trends demonstrated by Figure V-44 can be summarized as
follows. At the 10^{-3} probability of error level the example block
code would allow a power reduction of 1.58 (1.9 db), and 2.4
(2.8 db) for the K=7 rate $\frac{1}{2}$ convolutional code. Now, lower coding
rate, longer frame length block codes approach the performance of
the higher coding rate convolutional codes, but the symbol rates
would be higher. The best convolutional decoding strategy is
sequential as shown by the figure but it is the most complex and
limited decoder with present technology.

Table V-14 below summarizes a relative assessment of the
coding tradeoffs.

Table V-14 Coding Comparison Assessment Matrix

Detection Scheme	Spacecraft Power Gain	Detection, Decoding Complexity	Channel Symbol Rate Impact	Risk
Uncoded	Reference	Reference	Least	Least
Block Coded	Modest	Minimal	Worst	Minimal
Convolutional - Viterbi Decoding	Good	Moderate	Moderate	Moderate
Convolutional - Sequential Decoding	Best	Unknown, Highest	Moderate	Most

The recommended approach for maximum benefit is a code such
as the convolutional code with either Viterbi or sequential de-
coding. It is noted that previous work sponsored by JPL address-
ing a multiple mission sequential convolutional decoder would be
particularly applicable to this mission. A recommended maximum
data rate for the advanced engineering model were on the order of
121 kd. for a rate $\frac{1}{2}$, short constraint length convolutional code.
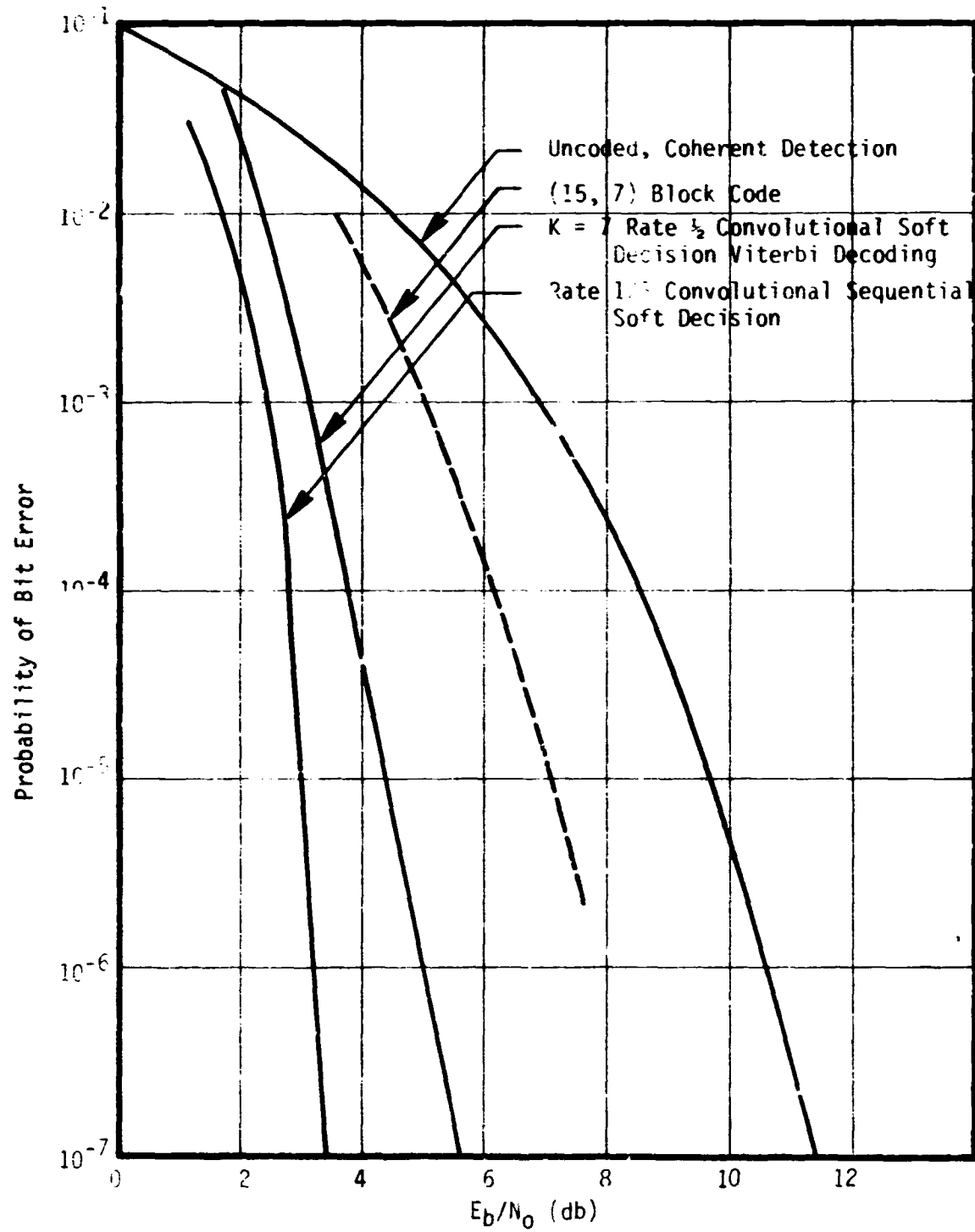
Figure V-44 Coding Gain Comparison

These codes should provide the best performance enhancement at high coding efficiency (high code rates). As a minimum block code should be employed with as high a code rate as practical. High code rates are required due to the already high data rate requirements for the typical mission.

Deep Space Network Considerations - The three ground stations of the Deep Space Network (DSN) employing the 64 m. articulated antennas will be required to support a radar mapping mission to Venus. Those 64 m stations currently existing (Goldstone, Canberra, Madrid) would further require an X-band (≈ 8448 MHz) carrier reception capability. The study has demonstrated that a very effective mission could be performed with the current station maximum data rate capability (~ 250 KBPS) and that the mission science return would be considerably enhanced by employing data rates within projected (Mark IV) next generation DSN bandwidth capability (~ 2500 KBPS). This paragraph will summarize investigations that addressed a) current and projected DSN status; b) on line computation and operational support; c) off line computation and support; d) Earth and Venus communication view window phasing.

The salient characteristics of the DSN implied by the requirements of the Venus radar mapping mission are summarized in Table V-15. The table compares the key requirements interacting with the DSN with expected DSN capability.

Those features which should be incorporated to realize the full science potential of the Venus radar mapping mission are:

1)   provision of X-band carrier reception and demodulation;

2)   provision of wide band (to 2500 KHz) data baseband;

3)   provision of high data rate convolutional decoding to match the 100-250 KBPS typical required data rates from Venus;

Table V-15 DSN Capability and Venus Radar Mapping Requirements

	Characteristic	Deep Space Network		Venus Radar Mapping
		Current	Projected	Typical Requirement
1.	Downlink Carrier Frequency	S-Band	S/X-Band	X-Band
2.	Uplink Carrier Frequency	S-Band	S-Band	S-Band
3.	64 m Locations	Goldstone (1) Canberra (1) Madrid (1)	Goldstone (2) Canberra (1) Madrid (1)	Goldstone (1) Canberra (1) Three Stations Madrid (1)
4.	Data Demodulation & Rate	Uncoded (to 250 KBPS) Block Coded (250 KSPS) Convolutional, Sequential Decoding to 4 KSPS	(to 2500 KBPS) (to 2500 KSPS) 16 KBPS, Sequential Decoding	Uncoded coherent to 2500 KBPS Block coding undesirable Undesirable if convolutional available. Convolutional preferred with short constraint length to 2500 KSPS. Rate 1/2 or 1/3, Viterbi decoding.
5.	Online Computation	Block decoding to 32 KSPS Convolutional, sequential decoding to 2 KBPS	Block decoding to 250 KSPS 16 KBPS	Significant computation if convolutional coding used, or for quick-look at radar data
6.	Offline Computation	JPL Image Processing Laboratory	Same	SAR data compression capability. Digital or optical.
7.	Data Station Data Relay	Commercial Satellite (up to 6 MHz band-width)	Unknown	Relay up to 10^{11} bits daily to a central facility for prompt reduction.
8.	Operational	24 hr continuous coverage for either 120 or 240 days.	Same	Continuous Venus observation for 120 or 240 days.
9.	Data Stream Recording	Predetection-Digital Postdetection-Digital Analog Tape Recording	Same- Increased Bandwidth Same as above	Potentially store up to 2×10^{11} bits/day for 120 or 240 days.

4) provision of increased and wide bandwidth ground station, on-site data recording capability;

5) provision of a wide band intra-station data relay system;

6) creation of a dedicated synthetic aperture radar data reduction facility.

It is our assessment that the performance of an effective mission is possible with just the incorporation of the X-band carrier reception capability at data rates (uncoded data) up to the current 250 KBPS limit and matching on-site recording. Final data reduction could be accomplished at distributed subcontractor sites.

Data reduction for the preferred mission approach of telemetering averaged radar data from the spacecraft would employ image formation (focusing, compression) on the Earth.

Further study is necessary to determine whether the most effective SAR data reduction i. by optical or digital implementations. Initial assessments based on the swath widths and resolution typical to this mission (viz 13 km < swath width $\leq$ 100 km, $\rho_r = \rho_a =$ 100 m) indicate that digital data compression is feasible. This would imply dedicated processing equipment due to the volume of data involved. The Jet Propulsion Laboratory's Image Processing Laboratory should be further examined for application to this mission as well as established SAR data reduction sites within DOD and private industry (re: U.S. Army Map Service, Environmental Research Institute of Michigan, et al).

On line data reduction is mainly concerned with the demodulation of the data stream from the carrier and decoding encoded data.

Based on the typical data rates derived for the Venus radar mapping mission, uncoded data could be accommodated by current equipment operating at full capacity but coded data would require updated or new baseband equipment.

On line processing could include "quick-look" processing of a segment of data relayed during a mapping cycle. This could be accomplished digitally with the image being displayed on a cathode ray tube (CRT). Such capability would permit strategy modification based on actual findings and performance integrity monitoring.

The bulk of data processing for the mission would occur on a non-real time, off line basis; this is the full reconstruction of the radar images. In addition to computing the spatial frequency transform of the raw data received over the telemetry link, all the various corrections and image rectification is also accomplished at this phase.

A list of the corrections and rectification activities required for the reduction of radar images following the basic focusing and frequency transform processing are:

1) slant-range/ground-range conversion

2) planet curvature correction

3) dynamic range normalization

4) aspect ratio correspondance: correction for scale differences in range and azimuth

5) correction to true orthographic correspondance

6) correction for orbital relative velocity (doppler) effects

7) distortion corrections for time base nonlinearities.

Several of these (2, 3, 5, 7) are common to the traditional planet surface sensing by TV imagery. The others are unique to side looking radar requiring a dedicated processing facility. Further study would determine the applicability of the SAR map analysis facilities already existing for such groups at the U. S. Army Map Service and U. S. Geological Survey, and others which could be determined.

The correspondence of Deep Space Network ground station view windows to Venus to orbital communication windows in Venus orbit were examined to determine the need for ground station operational programming to avoid loss of data due to timeline phasing.

This simulation capability permits the propagation of orbital time lines throughout the entire 250 day mission on an orbit by orbit basis to determine timeline correspondence. The simulation was used to provide a histogram of communications coverage versus sample mapping strategies of: a) map every orbit at $e = 0.5$, b) map every second orbit at $e = 0.3$, and c) map every fifth orbit at $e = 0$, using typical orbital timelines during periods of peak Earth occultation.

Typical results of this simulation are summarized in Figure V-45 where the "total hours for communications" is the summation of the total potential time for communications from Venus (under assumptions of maximum earth occultation; worst case). This establishes the higher eccentricities as exhibiting the most time for data relay. This is due to the fact that the higher eccentricity orbits are occulted from earth the least. The total hours of joint viewing by Venusian and Earth antennas are catalogued in hours and distributed among the three ground stations jointly, and in pairs in the figure. The availability of joint ground station tracking is significant in that redundant reception of data is achieved and the opportunity for long baseline interferometric orbital tracking is possible for a large amount of this time. There is no simultaneous viewing by Madrid and Canberra stations due to their relative location on Earth. The hours labeled "lost" signify the extent of time that no station was in view of the spacecraft during its nominal geometric opportunity to communicate. This would be avoided in the mission by proper ground station programing or possible redundant relay of the data during the short periods of the mission experiencing this characteristic. In this simulation the effect is slightly exaggerated due to the utilization of peak earth occultation timeline characteristics but is characteristic.
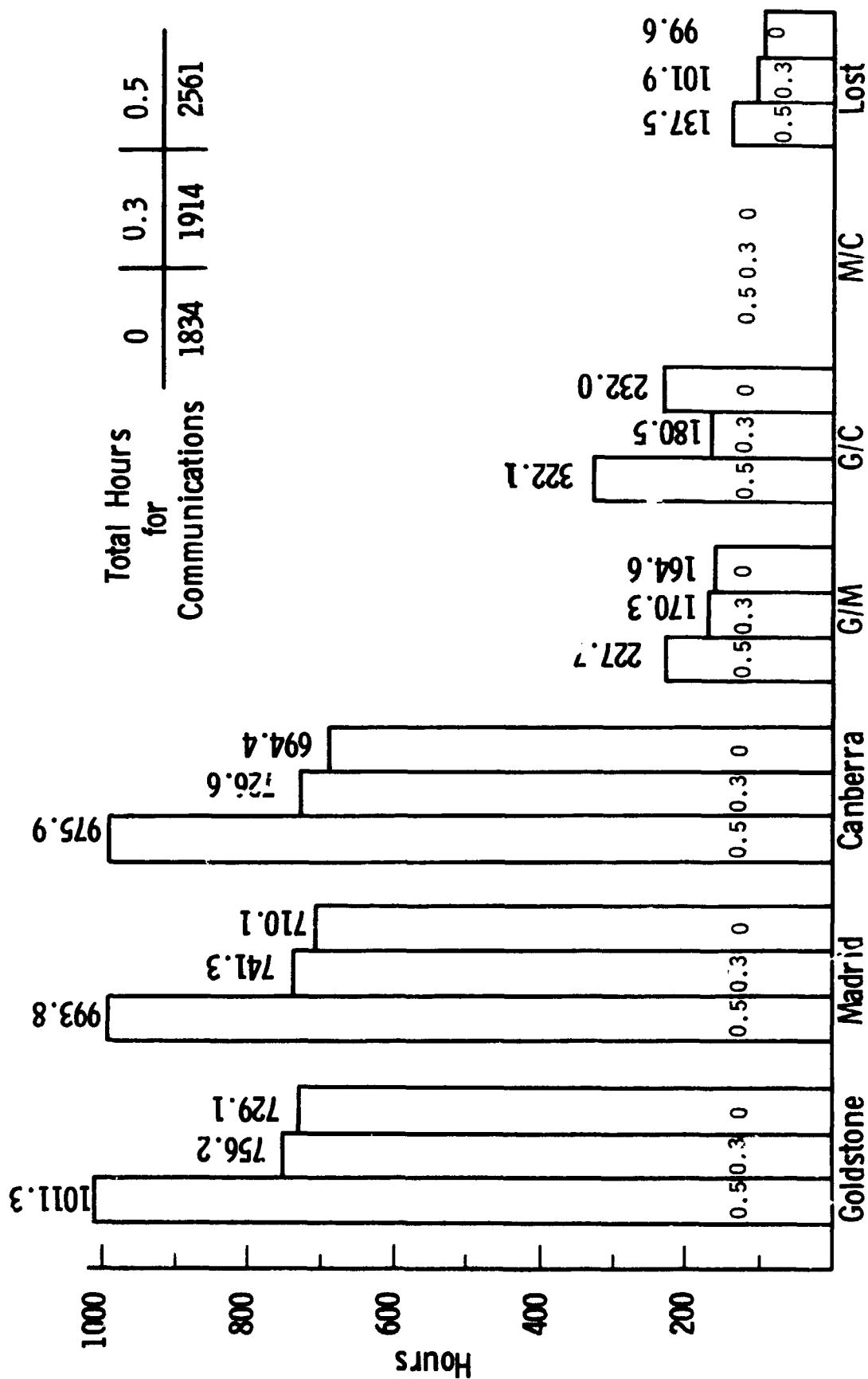
Figure V-45 Deep Space Network - Ground Station Compatibility vs Map Strategy

Signal Acquisition at Earth - The telecommunications link must be designed with sufficient margin at mission end to assure that coherent signal acquisition is a minimum problem. Nominal lockup time of 0.1 hr plus the two-way propagation delay at 1.71 AU or maximum Earth-Venus range was assumed for this study. The 250 day mission experiences Earth-Venus ranges from 0.63 to 1.71 AU for nearly all launch opportunities.

Although most of the required average data or symbol rates of the Venus mapper mission are above precedents set by past deep space mission, the acquisition time allocations are substantiated by extrapolations of the following excerpts from the Deep Space Network Applications Manual (JPL 810-5, Rev. C). The reference Figures V-46 and V-48 are shown for block coded and uncoded data since there currently is not a precedent within the DSN for convolutional decoding at data rates in excess of two kilobits per second. Advanced technology studies by Jet Propulsion Laboratory and others have established the feasibility of convolutional coding with Viterbi decoding at high data rates using short constraint length codes, soft decision logic, etc.

Figure V-46 presents current published DSN telemetry equipment capability (viz. symbol synchronization assembly, SSA) with uncoded data. Significant lowering of lock-up time is achievable as shown with the wide data bandwidth characteristic of the Venus mapper mission. Figure V-47 shows acquisition times typical to the (32, 6) block code of Mariner application.

Presented in Figure V-48 are composite signal acquisition times for sequential decoding of convolutional coded data. The subcarrier demodulation assembly does not impact the acquisition time for the Venus mapper mission as indicated by Figures V-40 through V-42.
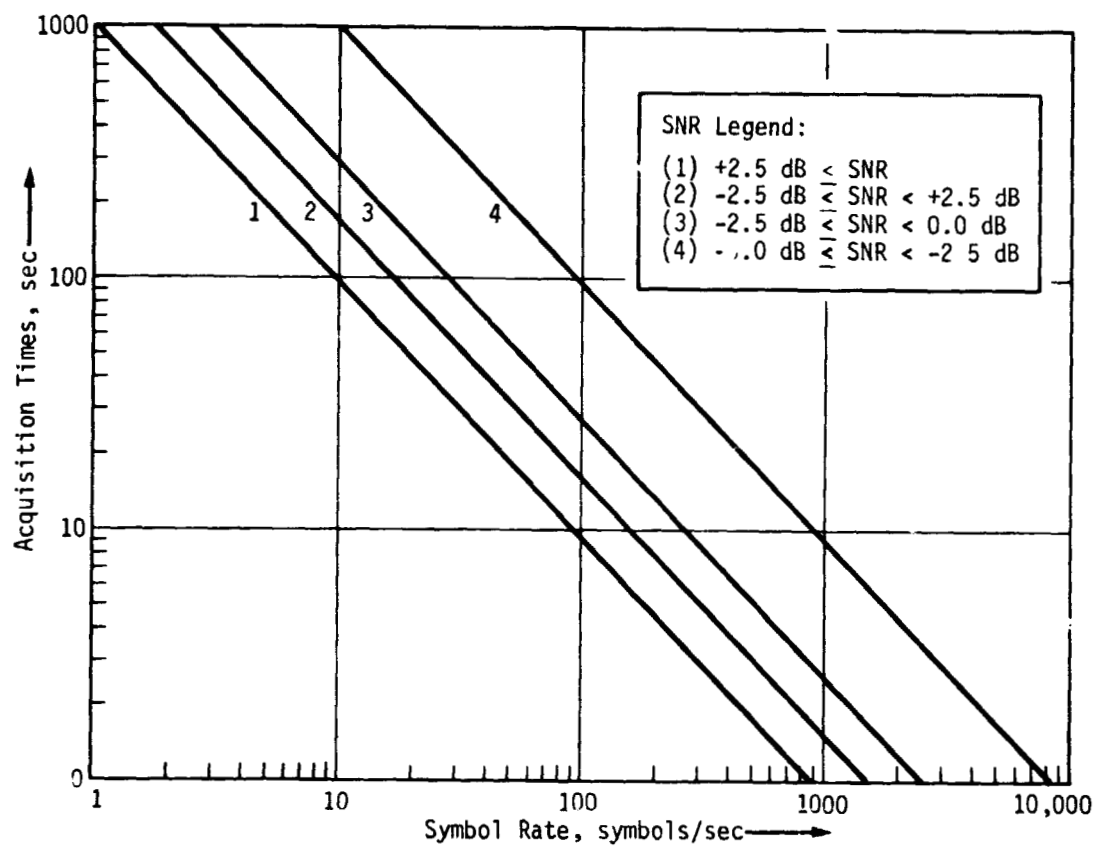
Figure V-46 Acquisition Times (0.99 Probability) for SSA on Uncoded Data
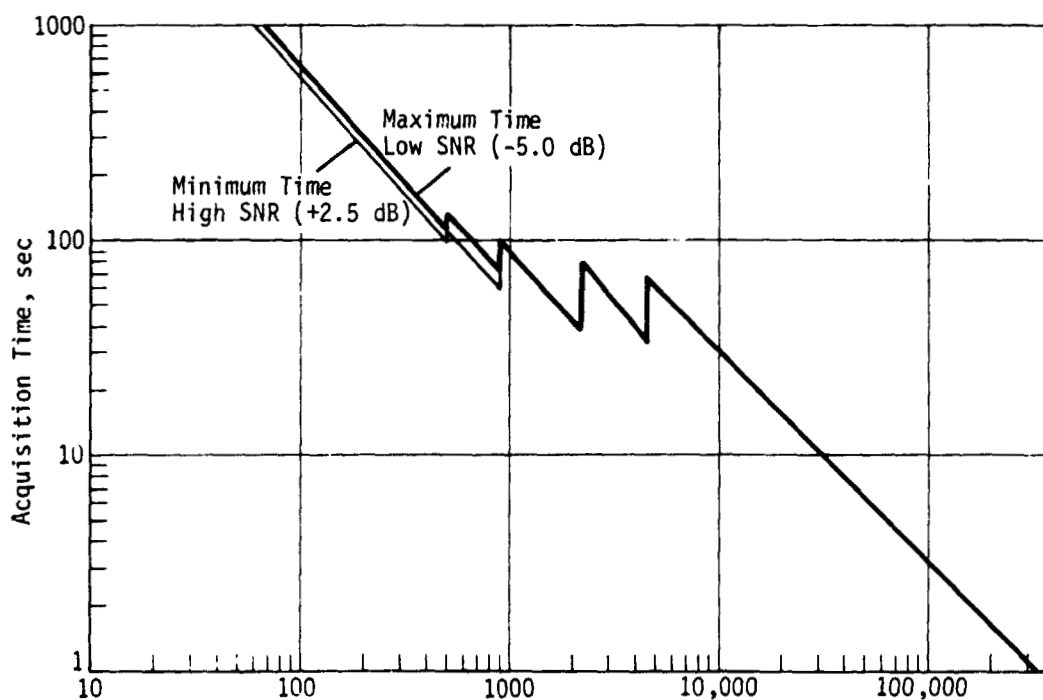
Figure V-47 Composite SSA and BDA Acquisition for (32, 6) Block Code Data
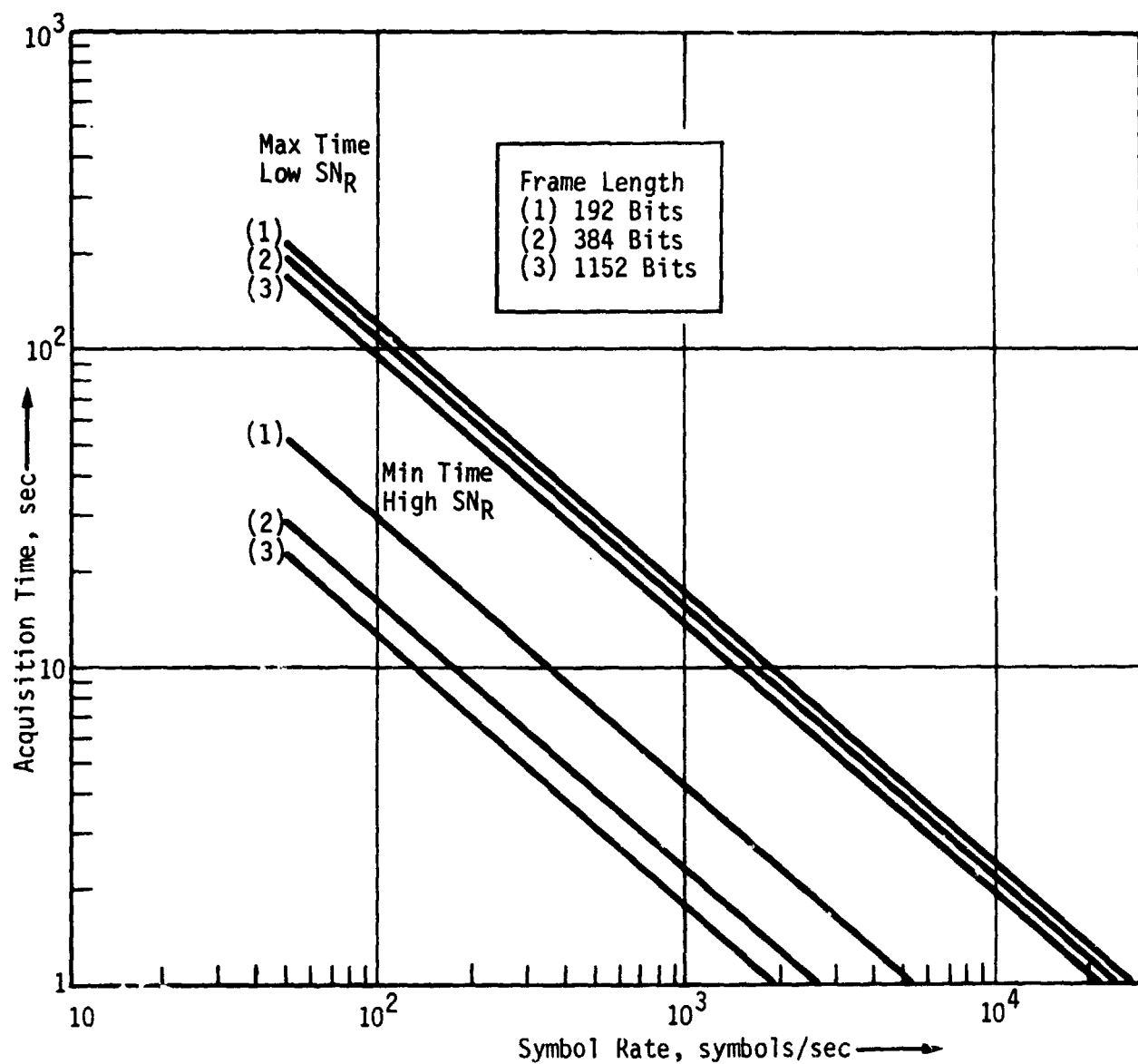
Figure V-50 Composite SSA and DDA Acquisition on Convolutional Data (Sequential Decoding)

CONCLUSIONS AND RECOMMENDATIONS

Derived requirements established parametrically, several con-
clusive observations and collected recommendations can be made.
Foremost, there are many approaches to the mission which appear
entirely feasible for data management and communications. These
approaches employ subsystem characteristics which have been
assessed to be reasonable and effective and are developed in
Volume II Section V.

The recommended radar data processing is a multimode presummer
for azimuth (doppler) data, and direct sampling of range channel
data. The multimode presummer provides the best image quality and
resolution with the least impact to the data link and spacecraft
cost and complexity. Recommended resolution in azimuth is nominally
100 meters, with 33 meters selectable. This is achieved simply by
doing less averaging of azimuth data and relaying more data to Earth
for later processing. Recommended range resolution is a nominal
100 meter (ground range) with 33 meter selectable. This is pos-
sible without major impact to spacecraft design. A presummer is
well matched to technology and is not a concern. It is recommend-
ed that further study and development of a mixed integration pro-
cessor for a spacecraft be done. In current technology, this is
thought to be a risky item 'ut deserves further study be.   its
potential image quality is best unless all raw data were relayed
from the spacecraft, which is impossible.

The required data rate to Earth should be maintained below
approximately 250 KBPS so that sufficient margin at the DSN is
available for relay of higher resolution data without exceeding the
projected upper data rate limit ($\sim$2500 KBPS). If the increased
data rates are not available to the DSN, then mission strategies
should maintain bit or symbol rates to the current 250 KBPS value.
The Configuration C spacecraft can maintain required data rates for

100 meter resolution data well below 250 kbps except at lower
(< 0.25) eccentricities when mapping every orbit, and is recom-
mended. The configuration A spacecraft generally required higher
data rates and is not recommended.

An X-band communications frequency is required for nominal
100 meter or better resolution data to maintain feasible RF power
and good mission flexibility within the limits on antenna size
which are determined by attitude pointing precision. In addition,
for approaches employing minimal changes to the Viking Orbiter
attitude control concept, a coded data channel is recommended to
assure that RF power can be met with current TWTA technology. The
most desirable code is a high rate efficient code such as con-
volutional code of short constraint length. Overall, the com-
munication link for the relay of 100 meter data throughout a
typal mission is not a concern if X-band is available. The
TWT with power in excess of ~40 watts has not been space quali-
fied but appears available through a qualification program.

Mass storage should be reusable and able to tolerate the ther-
mal, radiation, and long life characteristics without excessive
impact to weight and complexity. Already existing or identified
digital magnetic tape systems appear to fully meet such criteria.
In particular the recorder system of the Viking Orbiter ($\approx$1300
Mbits) meets the typical required capacity of from 1000 to 3000
Mbits. Film (analog) systems are excessive for this mission even
through their storage capacity is the highest since they are not
reusable. The automatic film develop rs are complex and have a
relatively short life and the film 's quite sensitive to thermal
and radiation deviation. Both mass memory approaches experience
the electromechanical drive reliability questions. A likely
replacement for the digital magnetic tape technology is the
developmental magnetic bubble system and should be monitored
for application to this mission.

If a single antenna spacecraft is used there is a concern that the antenna possess sufficient bandwidth and efficiency for communications at X-band. For the recommended configuration, the concern with the communication antenna is the attitude control precision which determin the upper limit on antenna size and corresponding minimum beamwidth. The recommended 3 meter antenna can be oriented with relatively minor improvements to the Viking Orbiter basic system, however. The orientation of antennas of ~3.5 m or larger require significant additional precision over the Viking Orbiter possibly including active radio frequency interferometric devices.

Therefore, the data rate through the communications link is a key design characteristic, and ultimately, a major factor limiting final image resolution and quality, but is not a concern for most approaches retrieving 100 meter resolution data with the recommended Configuration C spacecraft.

REFERENCES AND BIBLIOGRAPHY

V-1   R. W. Bayma and B. T. Larrowe: "Synthetic Aperture Radar
      Imagery from Hard-Limited and One-Bit Quantized Video Signals
      (U)." *Proceedings of the Eighteenth Annual Tri-Service
      Radar Symposium,* 1972 (SECRET).

V-2   *Satellite Imaging Radar Signal Processor.* Martin Marietta
      Report TR-48512-1 (IRAD), December 1972.

V-3   M. Skolnik: *Introduction to Radar Systems.* McGraw Hill, 1962.

V-4   H. R. Karp: "Magnetic Bubbles -- Technology." *Electronics,*
      1 September 1972.

V-5   D. B. MacLeod: "Magnetic Discs for Video Recording." *J.
      of the SIMPTE,* Vol. 80, April 1971.

V-6   H. Howard: "Memories -- Survey." *EDN Magazine,* April 1969.

V-7   J. E. Cervi: *Trip Report on Survey of Film Imagery Conversion
      to Digital Data.* Martin Marietta Corporation IDC, 8 September
      1969.

V-8   Editor: "Laser Recording System Uses Non-silver Dry Process
      Film." *Electro-optical Systems Design,* December 1972.

V-9   E. Stepke, OCR: "Scanning for the Future." *Electro-optical
      Systems Design,* December 1972.

V-10 G. W. Stroke: "Optical Computing." *IEEE Spectrum,* December
      1972.

V-11 E. T. Stepke: "Optical Memories ...." *Electro-optical
      Systems Design,* October 1972.

V-12 *Experiments Application for Post Skylab Mission Study, Vol.
      III.* Martin Marietta Aerospace, MSC-03155.

V-13 *Viking Orbiter Systems Document, Addendum 2.* Jet Propulsion
      Laboratory, JPL 611-2.

V-14 O. N. Tufte, D. Chen: "Optical Techniques for Data Storage."
      IEEE Spectrum, February 1973.

V-15 Dr. D. Hankins: *Optical Data Processing Study.* TRW Systems
      Group, Technical Report AFFDL-TR-70-76, July 1970.

V-16 R. T. Schappell, et al: *Improved Guidance Hardware Study for the Scout Launch Vehicle, Final Report.* Martin Marietta Aerospace, February 1972.

V-17 *Parametric Analysis of Microwave and Laser Systems for Communications and Tracking, Vol. III.* Hughes Aircraft Company, Culver City, Calif., February 1971.

V-18 Gerald Lapidus: "The Domain of Magnetic Bubbles." *IEEE Spectrum,* September 1972.

V-19 *Deep Space Network Systems Document.* JPL 810-5 Rev. C, Jet Propulsion Laboratory, Pasadena, California.

V-20 J. R. Odenwalder, et al: *Hybrid Coding System Study Final Report.* Linkabit Corporation, San Diego, Calif., September 1972.

V-21 Dr. Denis Hankins: *Optical Data Processing Study Report.* AFFDL-TR-70-76, TRW Systems Group, Redondo Beach, Calif., July 1970.

V-22 R. E. Oliver, et al: *Furlable Spacecraft Antenna Development Second Interim Report.* Technical Memorandum 33-606, Jet Propulsion Laboratory, Pasadena, California, March 1973.

V-23 D. R. Lumb, et al: *Performance of Several ... Codes ... Threshold Decoding.* NASA TND-4402, Ames Research Center, Moffett Field, Calif., March 1968.

V-24 J. Benton, et al: *Latest Advances in Space TWTs.* Hughes Aircraft Company, Torrence, Calif., April 1970.

V-25 J. R. Hall: *Private Communication.* Telecommunications Branch, Jet Propulsion Laboratory, Pasadena, Calif., April 1973.

V-26 B. Corner: *High Power X-Band TWTAs.* Private Communications and Company literature, Watkins-Johnson Company.

V-27 L. Mohrfield: *High Power TWTA for Space.* Private Communications and literature, Hughes Aircraft Company.

V-28 Golomb, et al: *Digital Communications with Space Applications.* Prentice Hall, Inc., 1964.

V-29 R. O. Harger: *Synthetic Aperture Radar Systems--Theory and Design*. Academic Press, 1970.

V-30 W. R. Wilson, J. C. Fleming: *Reusable Image Storage Systems Final Report*. Martin Marietta Corporation document T-71-48803-003, December 1971.

V-31 J. Max: "Quantizing for Minimum Distortion." *IEEE Trans*, IT-6, pp 7-12 (1960).

V-32 Editor: "Computers: Minis and Memories . . . . Topics." *Electronic Design News*, March 15, 1972.

V-33 R. W. Stafford: *Mass Storage Considerations*. Venus Mapper Technical Note 52, Martin Marietta Aerospace, April 1973.

V-34 R. W. Stafford: *Reference Orbital Timelines...Communications*. Venus Mapper Technical Note 39, Martin Marietta Aerospace, March 1973.

V-35 R. W. Lewis: *Mixed Integration Processing*. Venus Mapper Technical Note 33, Environmental Research Institute of Michigan.

V-36 R. W. Stafford: *Data Rates and Volumes to Earth*. Venus Mapper Technical Note 13, Martin Marietta Aerospace, October 1971.

V-37 R. W. Stafford: *Earth Relay Communication Opportunity--Sample Mission*. Venus Mapper Technical Note 11, Martin Marietta Aerospace, October 1972.

V-38 R. W. Larson: *Image Quality Improvement by Non-coherent Integration*. Venus Mapper Technical Note 25, Environmental Research Institute of Michigan, January 1973.

V-39 R. W. Lewis: *Elliptical Orbit Mapping Parameters*. Venus Mapper Technical Note 45, Environmental Research Institute of Michigan.

V-40 R. W. Bayma: *Clutterlock*. Venus Mapper Technical Note 46, Environmental Research Institute of Michigan, May 1973.

V-41 R. W. Bayma: *Range and Azimuth Ambiguity Elimination for Elliptical Orbits*. Venus Mapper Technical Note 63, Environmental Research Institute of Michigan, June 1973.

VI. Spacecraft Systems

VI. SPACECRAFT SYSTEMS

INTRODUCTION AND ASSUMPTIONS

The basic objective of the spacecraft systems parametric studies is to define the major subsystem interactions and constraints rather than to optimize spacecraft designs for a specific set of mission requirements. An ancillary objective of each of the individual subsystem studies is to utilize existing spacecraft components wherever possible in order to minimize total program costs. Wherever appropriate during the course of the study extensive use is made of previous studies such as the SSD preliminary feasibility study and the JPL radar system study.

At the beginning of the parametric study effort, a series of ground rules was mutually agreed upon by the MMC study team and by the SSD. These ground rules are summarized in Table VI-1. Also, as preliminary results of the study began to develop, a series of study generated ground rules evolved. These ground rules are shown in Table VI-2.

Table VI-1 SSD Study Directed Ground Rules

o Previous SSD and JPL study data to be used as basic reference data.

o Mission in mid to late 1980's.

o Mission science requirements have first priority.

o Viking/Mariner class spacecraft is basic design consideration with advanced spacecraft concepts considered where appropriate.

o Low cost missions to be prime consideration.

o Consider existing and new technology as appropriate.

o Coverage and resolution (minimum).

80% of surface at 1 km resolution.

20% of surface at 100 m resolution.

Table VI-2 MMC Derived Study Ground Rules

o   Titan III/Centaur basic launch vehicle.

o   Shuttle launch vehicle performance to be compared with Titan III/Centaur and evaluated.

o   Minimally modified Viking Orbiter to be baseline spacecraft design.

o   Orbital eccentricities between 0.20 and 0.50 considered.

STUDY APPROACH

The Venus radar mapping mission is one of the more complex unmanned planetary missions that has been consi ered to date. The large array of mission modes and system options available for consideration produce a very large number of potential mission/system approaches that are worthy of investigation. This requires that the study approach be designed to provide early definition of the many potential mission/system approaches and a means for consistent screening and evaluation of alternates to arrive at the most promising concepts for further detailed analysis.

The overall study plan is shown in Figure VI-1. The general approach in performing the study is to first establish a nominal baseline mission profile that is relatively simple but that still embodies all of the essential mission sequences. This approach allows us to test parametrically the sensitivity of the critical parameters; such as orbital eccentricity, radar frequency, coverage and resolution, power, thermal control, mission risk, and systems cost and complexity, to the various mission options that are available to us. Analyses are then made of the individual elements of the mission design to preliminarily identify a range of design requirements that would be evaluated in the subsystem trade studies. In configuring
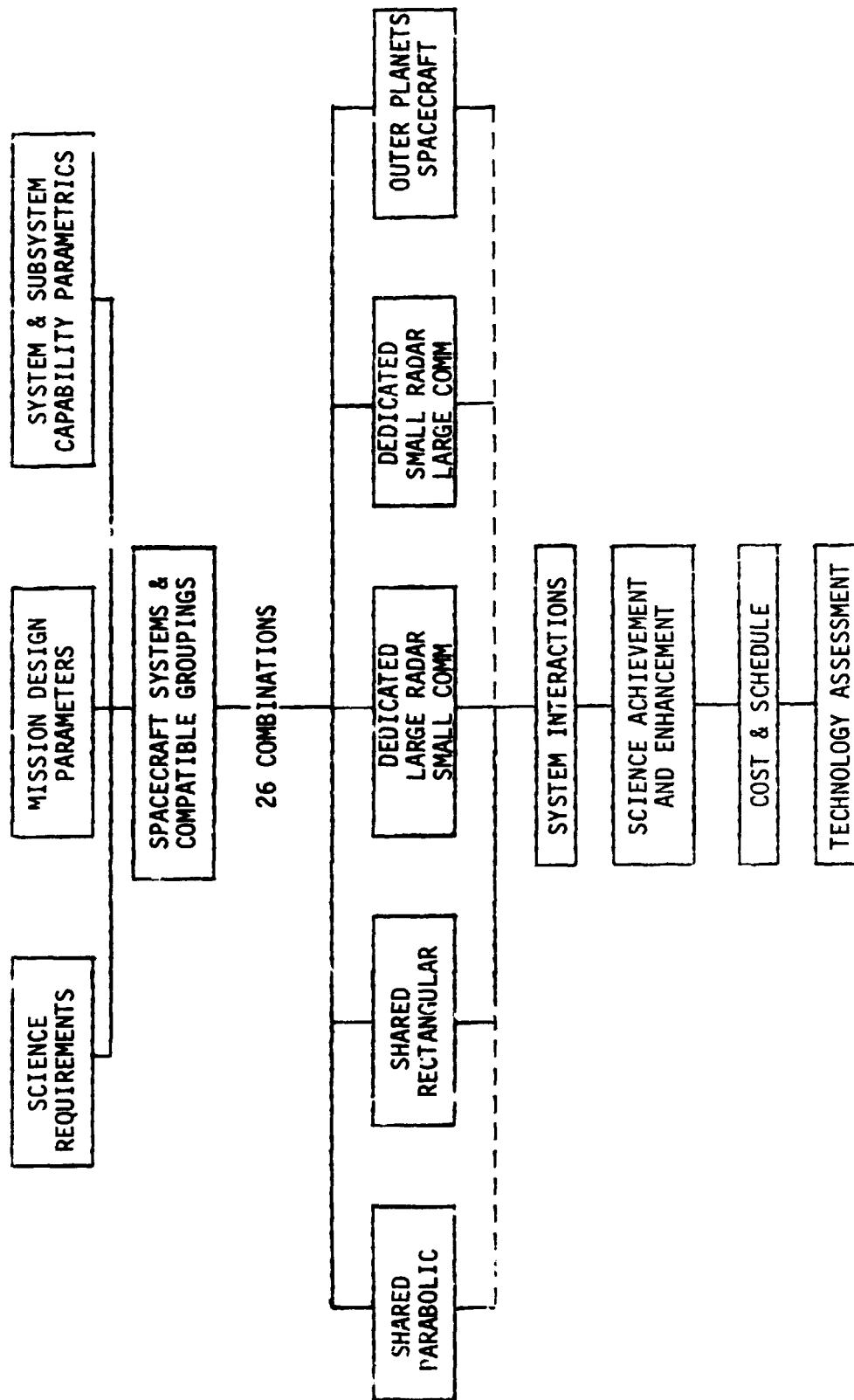
Figure VI-1   Study Flow

the individual subsystems, the approach used is to employ existing
qualified systems and hardware from programs already in being or
in the planning stage, wherever feasible, and the Viking systems in
particular. Completion of the individual subsystem parametric anal-
yses, allows a spacecraft configuration to be developed which allows
spacecraft integration problems to be identified and solved.

In all, twenty-six combinations of frequency, mapping strategy,
eccentricity and antenna design have been considered with various
spacecraft concepts and these fall into the five categories shown
in Figure VI-1. As discussed more fully in Section VII, the shared
parabolic, dedicated concept with the large communications antenna,
and the outer planets spacecraft were de-emphasized. The remaining
two concepts have been carried through the study and expanded as re-
quired to develop an acceptable mission.

This section summarizes the parametric trade studies that were
conducted in the propulsion, power, thermal control, and attitude
control subsystem areas. Spacecraft design trade studies are dis-
cussed in Section VII.

PARAMETRIC STUDIES

Propulsion Parametric Studies

The propulsion options that have been considered for use in
satisfying the Venus orbit insertion and fixed excess delta V re-
quirements are shown in Table VI-3. The first three options are
existing systems, the fourth is a combination of existing systems
and is in the development stage.

The rationale for selecting the first three options of Table
VI-3 is the potential program cost savings that could be achieved
by using flight qualified existing propulsion systems. An ancil-
lary consideration is the fact that preliminary studies have indi-
cated that the vehicle payload requirements are such that the greater

capability of the advanced high energy system, such as the space storable system are not required.

Table VI-3 Propulsion System Trade Studies

```
o   Basic Viking Orbiter propulsion system

o   Stretched Viking Orbiter

        Two tank/two engine

        Four tank/two engine

o   LM Ascent Propulsion System

o   LM Ascent Engine with Viking Orbiter Propulsion System

        Two tank configuration

        Four tank configuration

o   Space Storable Propellant with Viking Orbiter Pro-
    pulsion System
```

The baseline mission assumed for the parametric studies is the 1983 Type I trajectory, combined with Venus orbital eccentricities between 0.2 and 0.5

In addition to the orbit insertion delta velocity requirements an additional fixed excess delta velocity requirement of 250 mps is used. For study purposes this fixed excess velocity requirement has been allocated as shown in Table VI-4.

Table VI-4 Fixed Excess ΔV Allocation

Midcourse Corrections	20 mps
Finite Burn Losses	100 mps
Navigation Uncertainties	100 mps
Orbital Trims	30 mps
Total	250 mps

The 100 mps value for the finite burn losses is an estimated value. Additional studies conducted during the second phase of the study indicated that finite burn losses could be as large as 400 mps, depending upon the magnitude of certain spacecraft parameters, such as initial weight, thrust/weight ratio and number of engines. Results of these studies are presented in Section III of this volume.

Table VI-5 summarizes the equations that have been used for determining the inert propulsion weight of each of the propulsion systems that are being studied. These inert weights are expressed as a function of propellant requirements.

Table VI-5 Propulsion System Inert Weights

Propulsion System	Propellant Inert Weight (kg) $(XK_1) + (XK_2)$ (Propellant)	Specific Impulse (sec)
Viking Orbiter		
Two Tank/Two Engine	54 kg + 0.129 (Propellant)	286
Four Tank/Two Engine	102 kg + 0.117 (Propellant)	286
LM Ascent	132 kg + 0.174 (Propellant)	310.5
Modified LM Ascent		
Two Tank	130 kg + 0.129 (Propellant)	310.5
Four Tank	201 kg + 0.117 (Propellant)	310.5
Space Storable	57 kg + 0.145 (Propellant)	383

The final actual in orbit weight is a function of the total delta velocity, propellant inert constants, and the desired useful weight in orbit and is calculated by the following equation:

$$W_{orbital} = \left(W_{useful} + XK_1\right) / \left(1.0 + XK_2 \cdot e^{\frac{\Delta V}{gI_{sp}}}\right) \qquad \text{(VI-1)}$$

where: XK_1 is the constant in the propellant inert equation of Table VI-5.

XK_2 is the propellant inert equation of Table VI-5

W_{useful} is the desired useful weight in orbit.

ΔV is the total ΔV required for the mission.

g is the Earth's gravity value (9.78×10^{-3} km/sec^2)

I_{sp} is the specific impulse of the engine (sec)

The initial spacecraft weight, with its propellant is determined by the following equation:

$$W_{initial} = W_{orbital} \times e^{\frac{\Delta V}{gI_{sp}}}$$

(VI-2)

The spacecraft propellant requirements are then simply the difference between the initial spacecraft weight determined by equation (2) and the actual spacecraft weight in orbit calculated from equation (1).

Stretched versions of the basic Viking Orbiter propulsion systems have been studied up to growths of 50 percent. Growth requirements greater than 50 percent necessitate four tank configurations. This arrangement is required in order to maintain acceptable center of gravity locations in the launch configuration and to avoid encroaching into the launch vehicle dynamic envelope. Two 1330 nt thrust engines are used in order to allow a fixed attitude burn and not to exceed the allowable engine burn time. Figure VI-2 presents the propellant requirements as a percentage of change to the Viking Orbiter propulsion system for eccentricities between 0.2 and 0.5. Three constant useful spacecraft weights in orbit were considered (800 kg, 900 kg, and 1000 kg). Also shown are the propellant requirements if the maximum useful spacecraft weight is placed into orbit (limited by the TIIIE/Centaur's capability of injecting 3113 kg spacecraft). As shown in Figure VI-2 the propellant inert weight shifts when the 50 percent increase limit
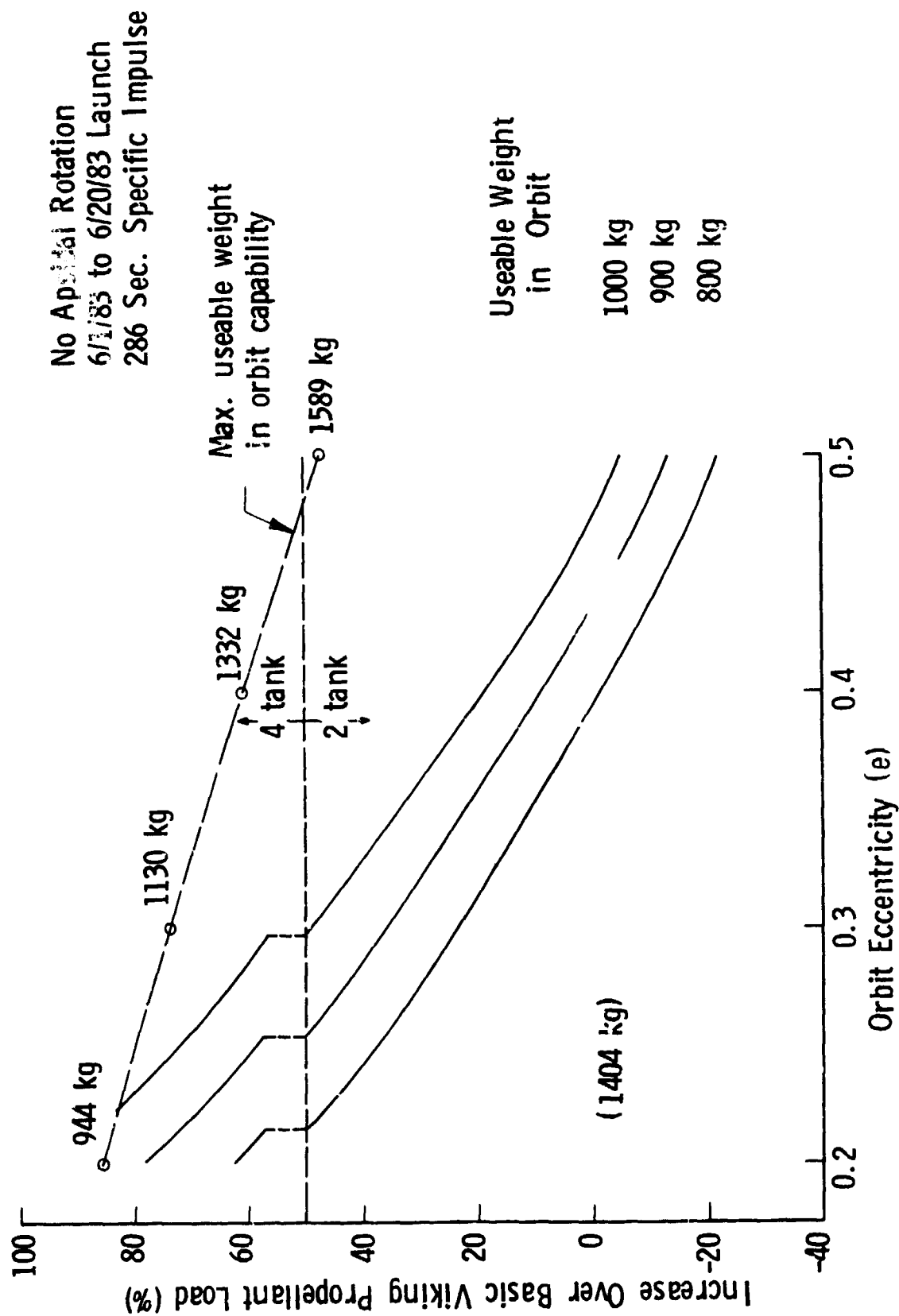
Figure VI-2 Viking Orbiter Propulsion System

(tw. tank) is reached. At this point the additional propellant
inert weight of the four tank configuration yields a discontinuity
in the propellant required curves since additional propellant is
required just to carry the additional propellant inert weights.

Studies were also conducted using the LM ascent propulsion sys-
tem. Since this system is a man-rated system it is the heaviest
system for equivalent propellant requirements of all the consider-
ed systems. For this reason this concept has been eliminated from
further study consideration.

In an attempt to reduce the excessive inert weight associated
with the LM ascent propulsion system a hybrid system comprised of
the LM ascent engine (having a thrust level of 15550 Nt and an I_{sp}
of 310.5) and Viking Orbiter type tanks was considered. Although
some increase in performance is obtained this concept has been
eliminated from consideration in view of the difficult packaging
problems presented by the relatively large size of the LM ascent
engine.

A final system utilizing space storable propellants is consider-
ed. The application of a high energy space storable propulsion sys-
tem results in increased vehicle performance which surpasses that of
the earth storable propellant systems that have been examined. The
earth storable propellant systems that were studied are character-
ized by high bulk densities, (1200 kg/cm^3) and low specific impulse
(280 sec.). The space storables, on the other hand, are character-
ized by moderately high specific impulse, (383 sec) and high bulk
densities (1280 kg/cm^3).

Investigations by JPL conducted over the last several years have
revealed several promising space storable propellant propulsion sys-
tems. The combinations that were considered are shown in Table VI-6.

VI-1J

Table VI-6   Candidate Space Storable Propellant Combinations

o   Fluorine/Hydrazine (F_2/N_2H_4)

o   Oxygen Difluoride/Diborane (CF_2/B_2H_6)

o   Flox/Monomethylhydrazine $(FLOX/CN_2H_6)$

o   Flox/Methane $(FLOX/CH_4)$

o   Flox/Light Hydro Carbons (Ethane, Ethylene & Propane)

Of these propellants, fluorine/hydrazine was chosen by JPL for
further in depth system study because of its inherent superior sys-
tem performance, operational flexibility, and state of system devel-
opment.   The fluorine/hydrazine propulsion system that JPL is cur-
rently developing for use on unmanned planetary spacecraft in the
post 1977 time period is a pressure fed system.   The engine is a
dual mode concept operating in the full thrust (2670 Nt, 383 sec I_{sp})
bipropellant mode for large maneuvers, such as orbit insertion or
plane changes and in the low thrust (665 Nt, 235 sec I_{sp}) monopro-
pellant mode for midcourse maneuvers or orbit trims.   Figure VI-3
presents a schematic of the F_2/N_2H_4 propulsion system that JPL is
presently studying.

Figures VI-4 through VI-6 present the propellant requirements
as a percentage of change to the Viking Orbiter propulsion system
for eccentricities between 0.2 and 0.5, for the LM ascent propulsion
system, modified LM propulsion system and the space storable con-
cept respectively.

The results of the propulsion parametric studies indicate that
two of the four options studied have potential application for the
Venus Radar Mapper spacecraft.   These are: the stretched Viking

VI-11
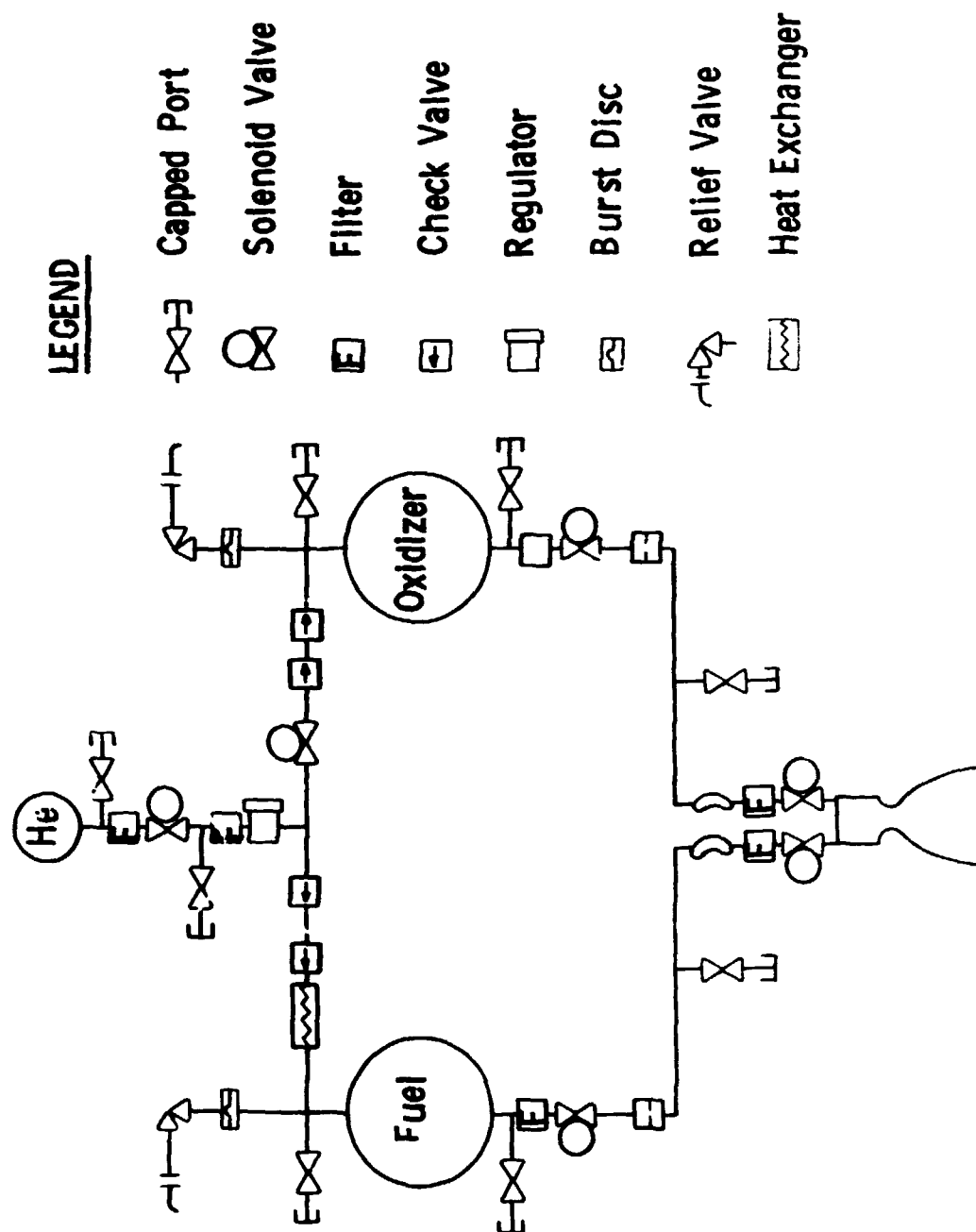
Figure VI-3 Schematic Diagram of F_2/N_2H_4 Orbiter Propulsion System

LEGEND

Capped Port
Solenoid Valve
Filter
Check Valve
Regulator
Burst Disc
Relief Valve
Heat Exchanger
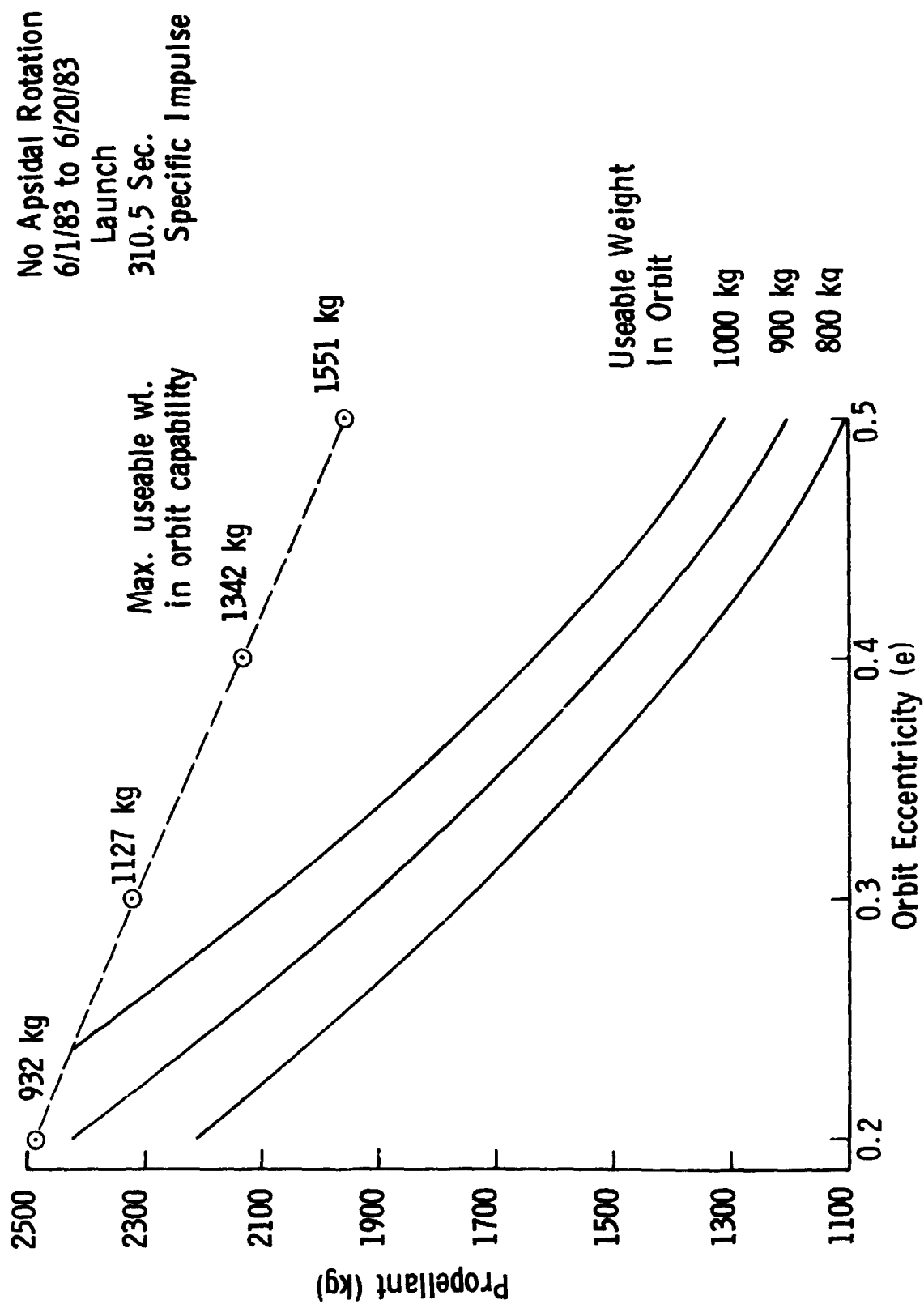
Figure VI-4 LM Ascent Propulsion System
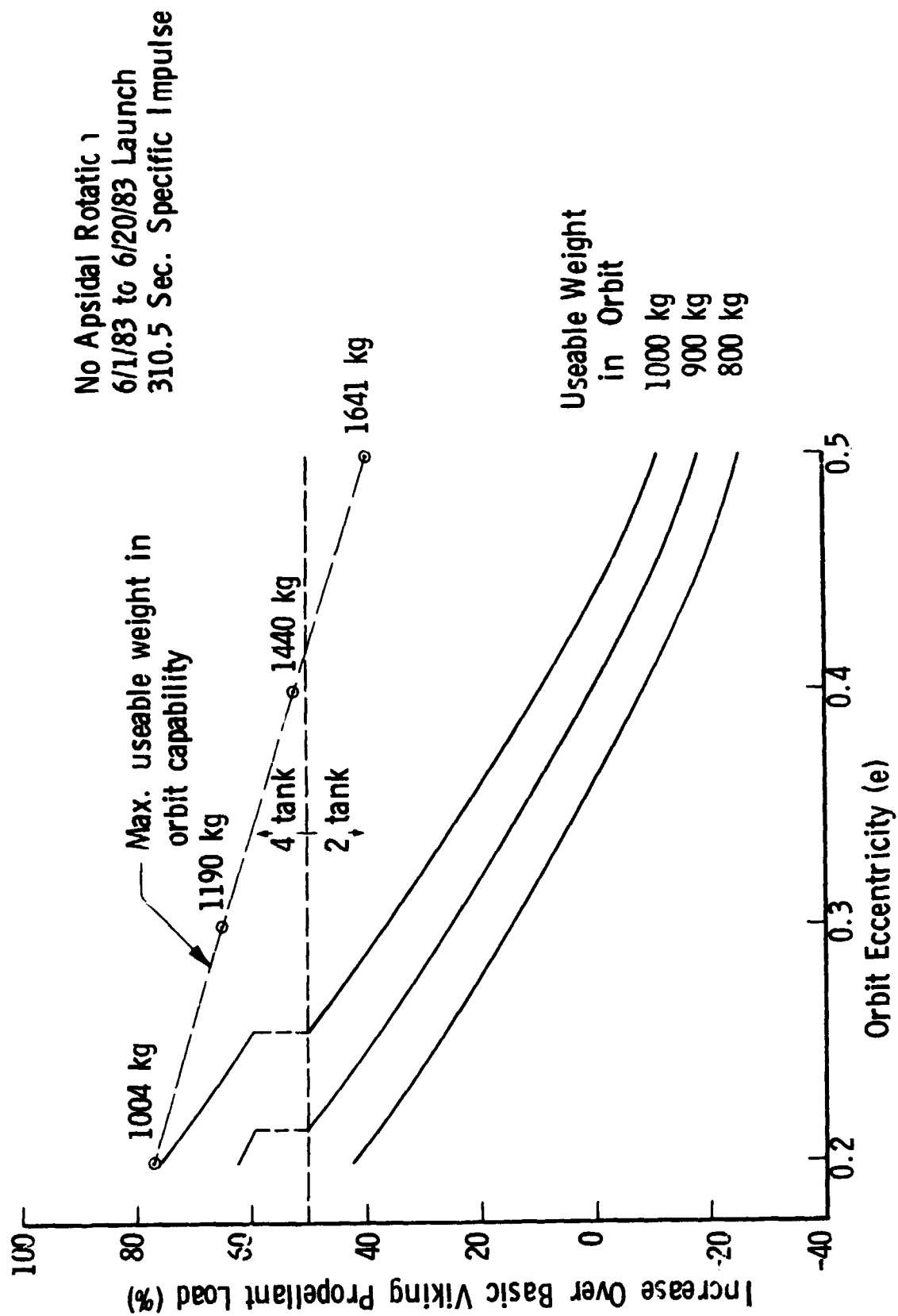
Figure VI-5 LM Ascent Engine with Viking Orbiter Tank

No Apsidal Rotation
6/1/83 to 6/20/83
Launch
383 Sec. Specific
Impulse

Max. useable wt.
in orbit capability

2000 kg

1802 kg

1613 kg

1428 kg

Useable Weight
in Orbit

1000 kg
900 kg

800 kg

Orbit Eccentricity (e)

Propellant (kg)

0.2   0.3   0.4   0.5

700   900   1100   1300   1500   1700   1900   2100
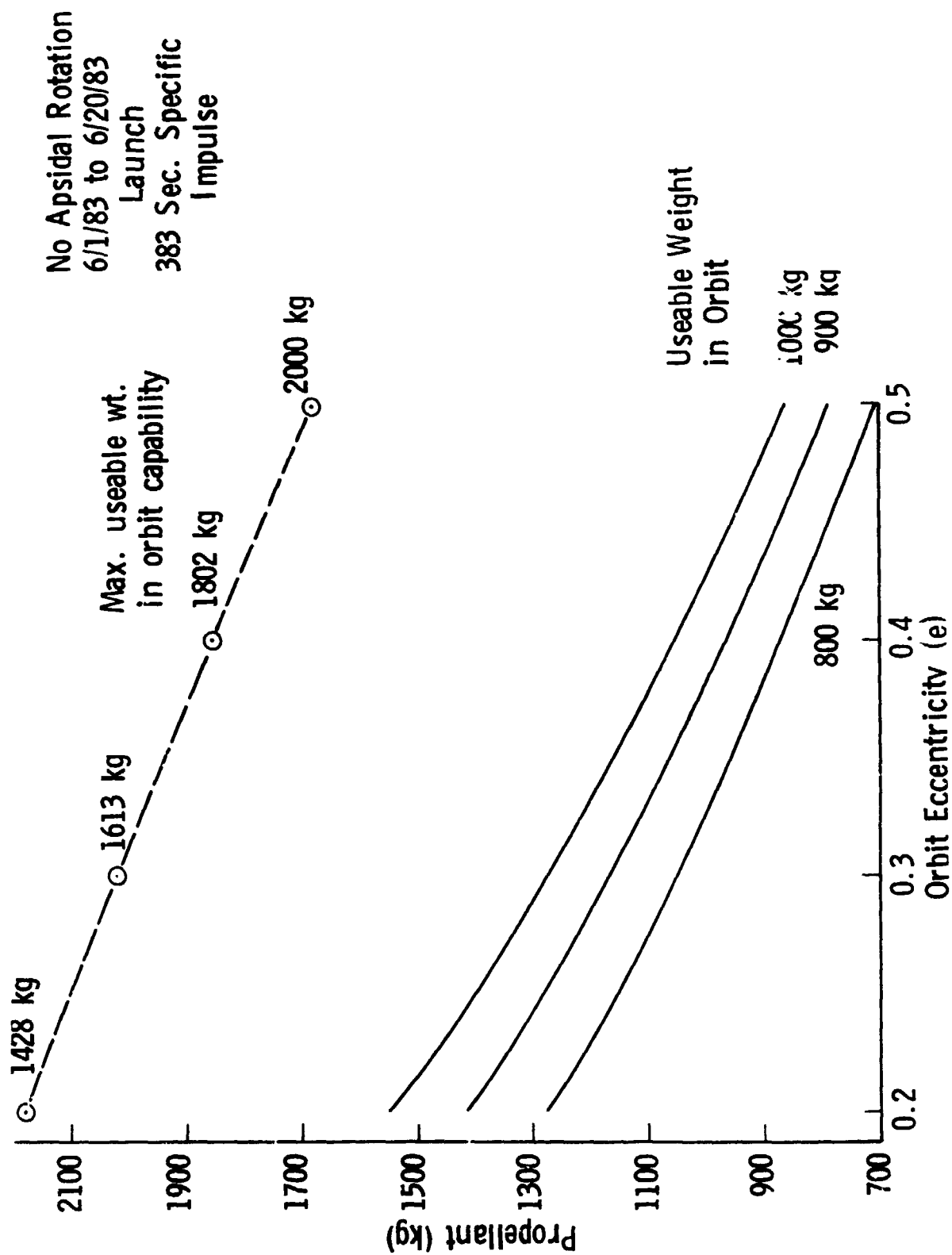
Orbiter concept and the space storage system. These selections are made on the basis of minimum system inert mass, superior system performance capabilities and minimum program costs.

The stretched Viking Orbiter concept has its most effective application when orbital eccentricities between 0.35 and 0.50 are required. The lower value of eccentricity (0.35) has been defined by an allowable Viking Orbiter propellant growth of approximately 10 percent. JPL in several recent studies (Refs. VI-1 and VI-2) examined the applicability of "stretching" the present Viking Orbiter propulsion system to accommodate a future Viking mission. The results of this study indicated that growths up to and including 10 percent could be accommodated with only a minimum modification to the present propulsion system. Growths from 10 to approximately 40 percent require more extensive detail design revisions but are still entirely feasible. Therefore, for purposes of this parametric study it war assumed that growths of 10 percent would define the lower limit of orbital eccentricity that would be considered as applicable for a stretched Viking Orbiter propulsion system that required minimum modifications. For the maximum stretched orbiter (approximately 30%) concept the allowable orbital eccentricity can be assumed to be approximately 0.30. For orbital eccentricities between 0.35 and 0.20, the parametric studies indicated that use of the space storable propellant concept was the most desirable approach.

Power Subsystem

Preliminary evaluation of the Venus radar mapper requirements indicated that the power level to be supplied would be less than 1 kw and in most configurations studied around 600 watts. Figure VI-7 summarizes the classical operating regions of available power systems in terms of power output and mission duration. Based upon the mission duration and the power levels cited, only two types of systems need be considered as prime source candidates. These are solar cells and radioisotope thermoelectric generators (RTGs).
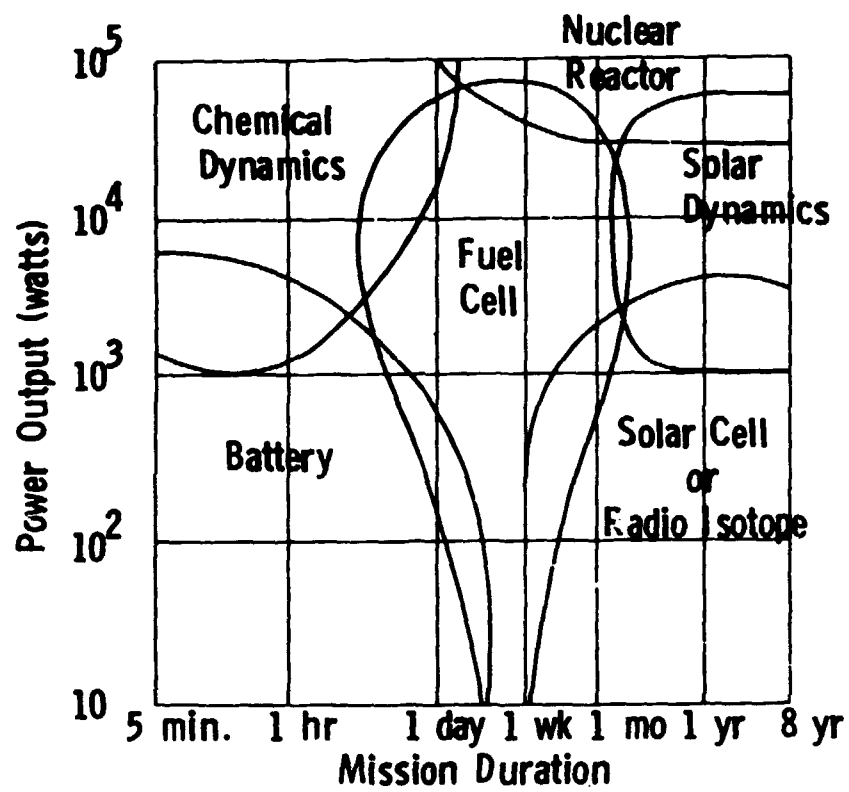
Figure VI-7 Candidate Power Sources

Solar cells can be mounted on either rigid or flexible arrays
arranged to fold-out or roll-out. Both types were considered. The
rigid arrays utilizing Mariner technology produce specific outputs
near Earth of around 22 watts/kg. Arrays employing flexible sub-
strates yield specific outputs of approximately 48 to 66 watts/kg.

Several cell and cover-glass concepts were evaluated. Fused
silica coverglasses equipped with a standard blue interference
filter and front surface antireflective coating have been selected
because at the Venus distance from the Sun their performance com-
pares favorably with other filter types, as shown in reference VI-3.

In the decade elapsing before the Venus radar mapping mission
some improvement in solar cell efficiency may be expected. The
effect of this is demonstrated in Figure VI-8, where outputs of
solar cells of three different efficiencies is shown. Efficien-
cies shown are those obtained under standard conditions with sunlight
intensity at 1 AU and the solar cell at $28^{o}C$. Power outputs shown
are based upon equilibrium temperatures which will be attained
by oriented panels at corresponding AU distances. Output varies
from 141 watts/m^2 at 0.7 AU for the Mariner class panel up to a
theoretical maximum of 223 watts/cm^2.

RTGs evaluated ranged from the state-of-the-art SNAP-19 yield-
ing a specific output of 2.2 watts/kg, to the advanced multi-hundred
watt concepts with specific power ranging from 3.98 to 4.48 watts/
kg. Characteristics of three advanced thermoelectric generators
are tabulated in Table VI-7.

Both nickel-cadmium and silver cadmium batteries were consider-
ed as candidates for supplying power during solar occultations. Life
cycle data for the two types is displayed in Figure VI-9. The en-
ergy density of silver cadmium batteries is twice (10 Wh/kg) that
of nickel cadmium batteries (5 Wh/kg). It would appear that the
silver cadmium battery would be the logical contender for this
application since only 500 cycles of use are involved. However,
there has not been enough space experience with the design of cell
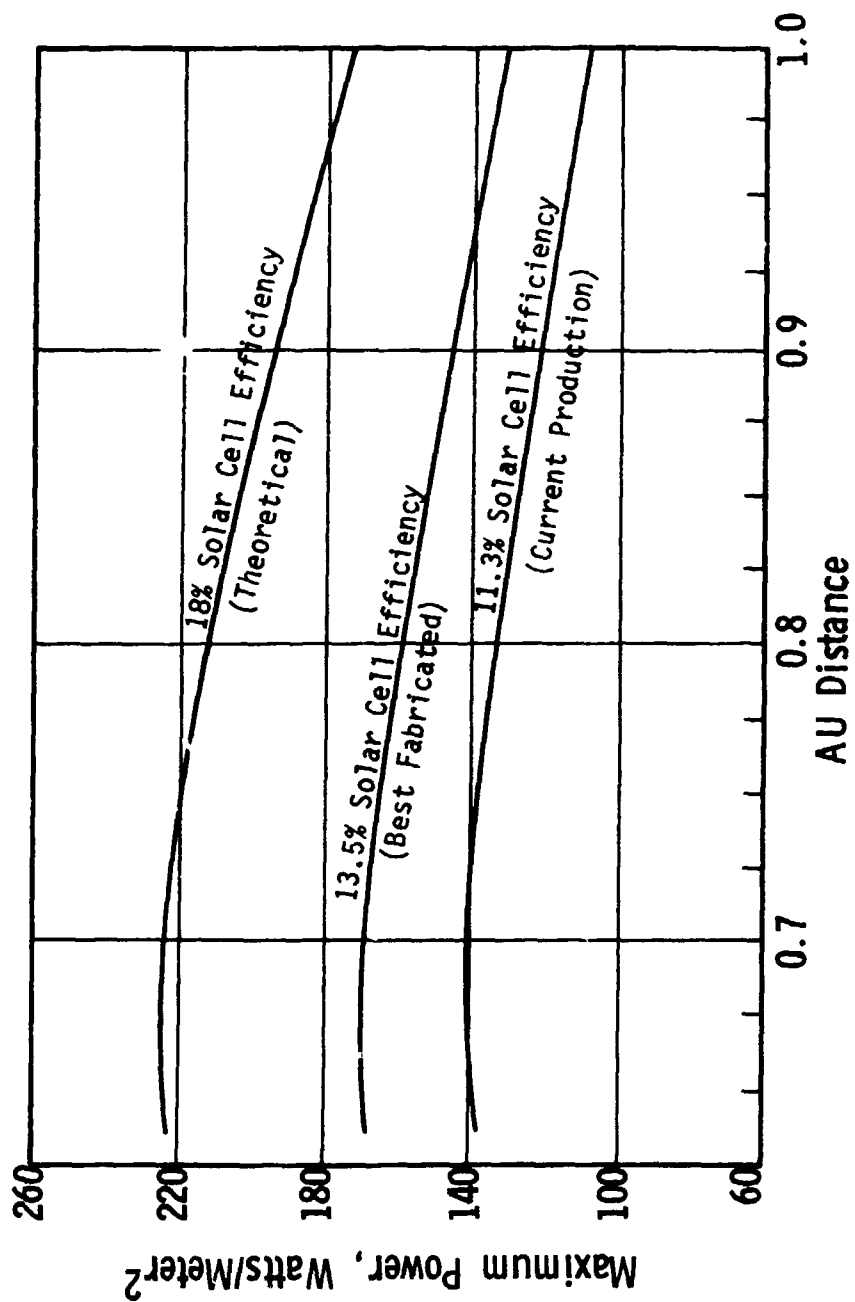
Figure VI-8 Solar Array Specific Output versus AU Distance
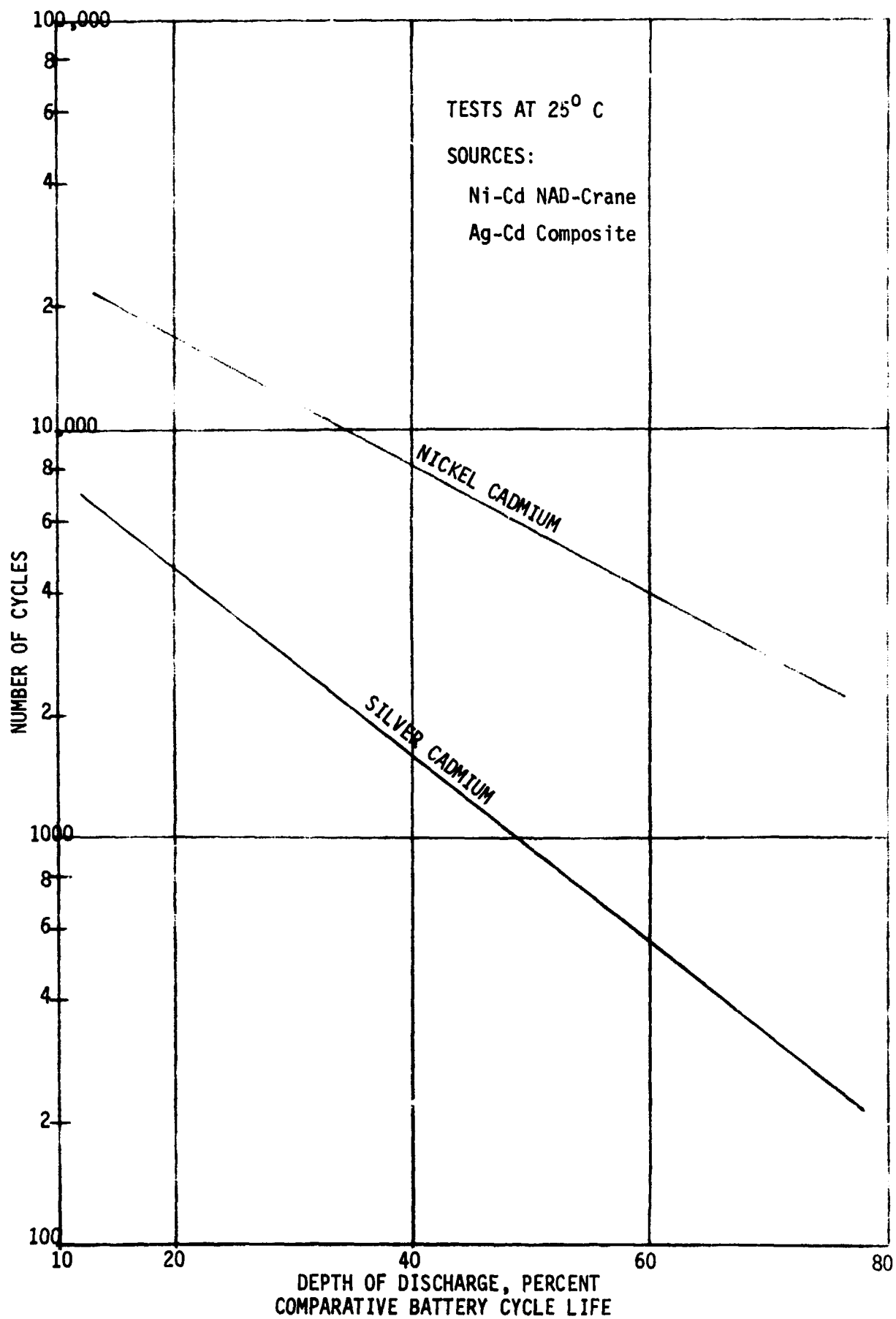
Figure VI-9 Comparative Battery Cycle Life

VI-20

to give sufficient confidence for its selection. Unlike the
nickel-cadmium system, the silver-cadmium cell will tolerate
only limited amounts of overcharge. Problems in cell divergence
when used in a battery are far more severe than those encountered
in the nickel-cadmium system because of the lack of tolerance of
overcharge and from the unpredictability of placement in the charge
cycle of the transition between lower and upper voltage plateaus.
Advanced batteries utilizing metal gas concepts were also examined.
Current development contracts may yield designs which can be con-
sidered for application at a later date.

Table VI-7 Advanced Thermoelectric Generators

Item	Multi-hundred Watt (General Electric)	Advanced Transit (Gulf General Atomic)	Isotopes Inc. (Teledyne)
Power (watts)	150.00	150.00	15C.00
Efficiency (%)	6.48	5.50	6.30
Weight (kg)			
Si Ge Stage	19.30		
2 N/TAGS Stage		12.10	
Heat Source	18.40	20.40	
Total	37.70	33.50	34.40
Specific Power (w/kg)	3.98	4.48	4.40

In making the selection of a system its integration with the
vehicle becomes of importance. Listed in Table VI-8 is a quali-
tative comparison between the solar array and RTG systems. In
addition to these, mounting more than three RTGs on the baseline
spacecraft would be difficult from a structural point of view.
Seven units would be necessary to carry peak loads if batteries were
not used. Mass comparisons of the two systems made on the basis
of carrying a continuous load of 600 watts, with peaks of 950 watts,

for the 0.5 eccentricity reference orbit are shown in Figure VI-10.
The figure shows that the solar array system is lighter for the
duration of mission considered. The increase in mass with mission
is due to allowances for solar cell degradations and battery re-
placement.

The configuration selected for study was obtained by using two
of the four VO-75 subarrays and retaining the two 30-AH-nickel
cadmium batteries. The selection was made on the basis of cost
effectiveness and confidence of performance. Since mass limits
are not reached on the spacecraft it is not necessary to go to
the lighter weight flexible arrays.

Once the type of subsystem has been selected it is then neces-
sary to establish the parametric relationship of its elements. Des-
cribed below is the development of solar cell data for use in sim-
ulation studies.

Table VI-8 Power System Integration Factors

Factor	Solar Array	RTG
Weight	Good	Poor
Volume	Poor	Good
Freedom of Location	Average	Poor
Shielding Required	Good	Poor
Attitude Control Requirement	Poor	Average
Spacecraft Maneuvering	Poor	Average
Prelaunch Handling	Good	Poor
Vulnerability to Environment	Poor	Good
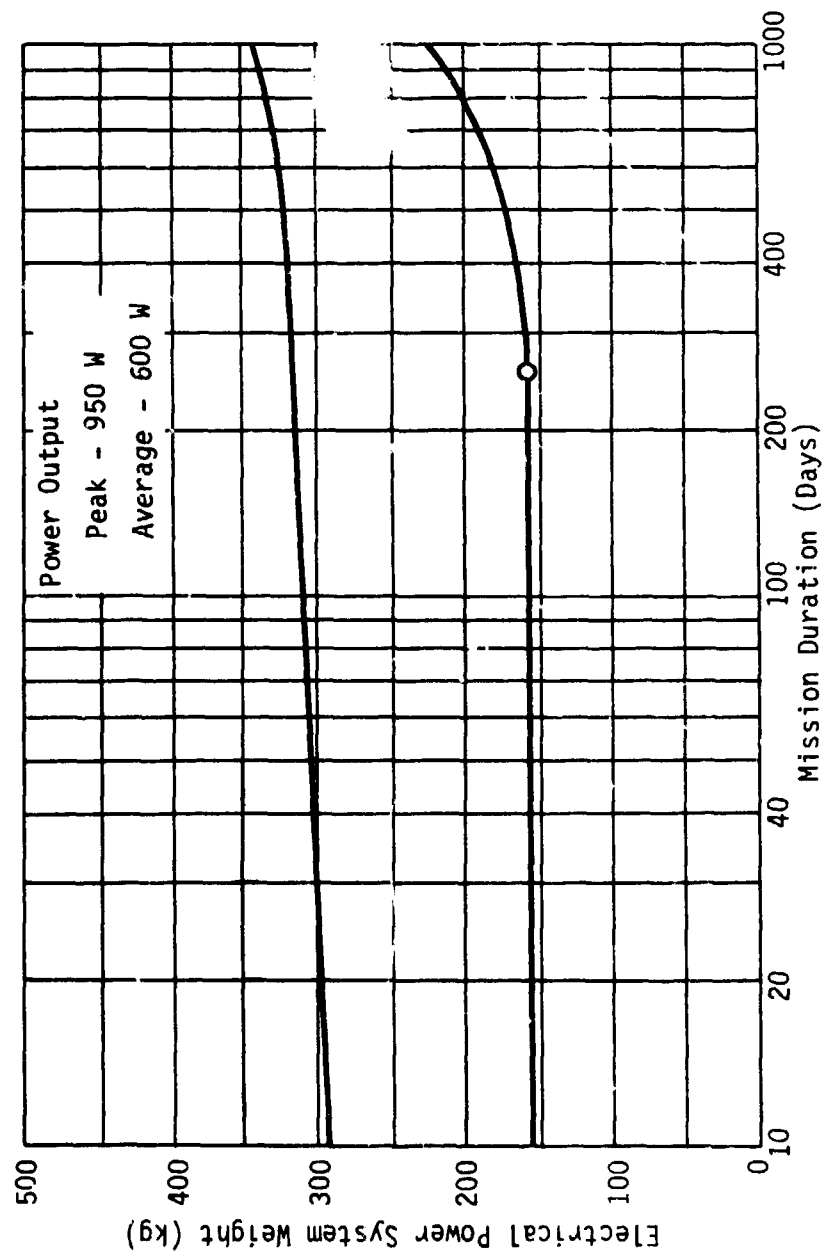
Figure VI-10   Power Subsystem Masses Versus Mission Duration

Parametric presentation of solar cell electrical performance
is necessary to describe the quantitative relationship between
the solar cell output and temperature intensity conditions. Ref-
erence VI-4 describes a program developed at Martin Marietta Aero-
space which takes account of varying short-circuit current and
open-circuit voltage temperature coefficients in predicting
solar cell performance under different light intensities. This
program was used in establishing a reference cell characteristic
for use in power subsystem simulation. Figure VI-11 shows the
steps. Curve A represents the characteristics of a solar seg-
ment of the solar array. It is based upon panel tests in which
account has been taken of the erosion in performance resulting
from the fabrication of the cells into a solar panel. This in-
cludes a reduction in short circuit current from coverslide ap-
plication by 3 percent and a reduction in peak power voltage due
to both interconnection resistance and mismatch of individual cell
performance of 7 percent. Curve B shows the curve modified by the
described computer program and indicates the proportional output
of the cell under a light intensity of 267 mW/cm^2 at a temperature
of 110°C. These are representative of conditions encountered by
a solar array when orbiting Venus. Curve C is the curve which was
used as the reference in power system computer simulation. It
includes allowance for radiation damage and uncertainties associated
with the mission. Radiation damage computed by using the program
in Reference VI-5 amounts to 4.5 percent of the total allowance of
16 percent. Characteristics of a solar cell segment after allow-
ances for degradations are displayed for a range of temperatures in
Figure VI-12.
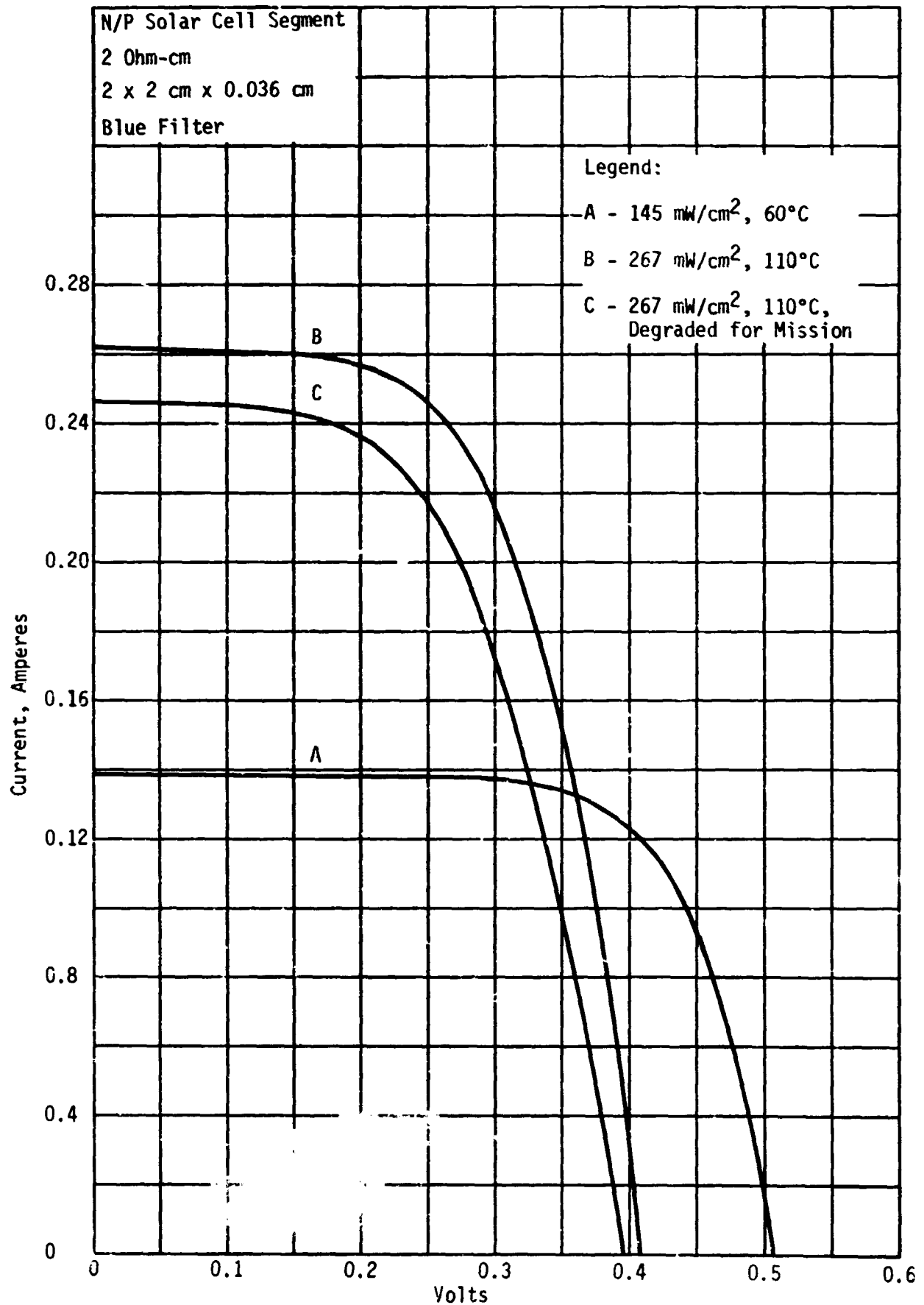
Figure VI-11 Reference Solar Cell Characteristics
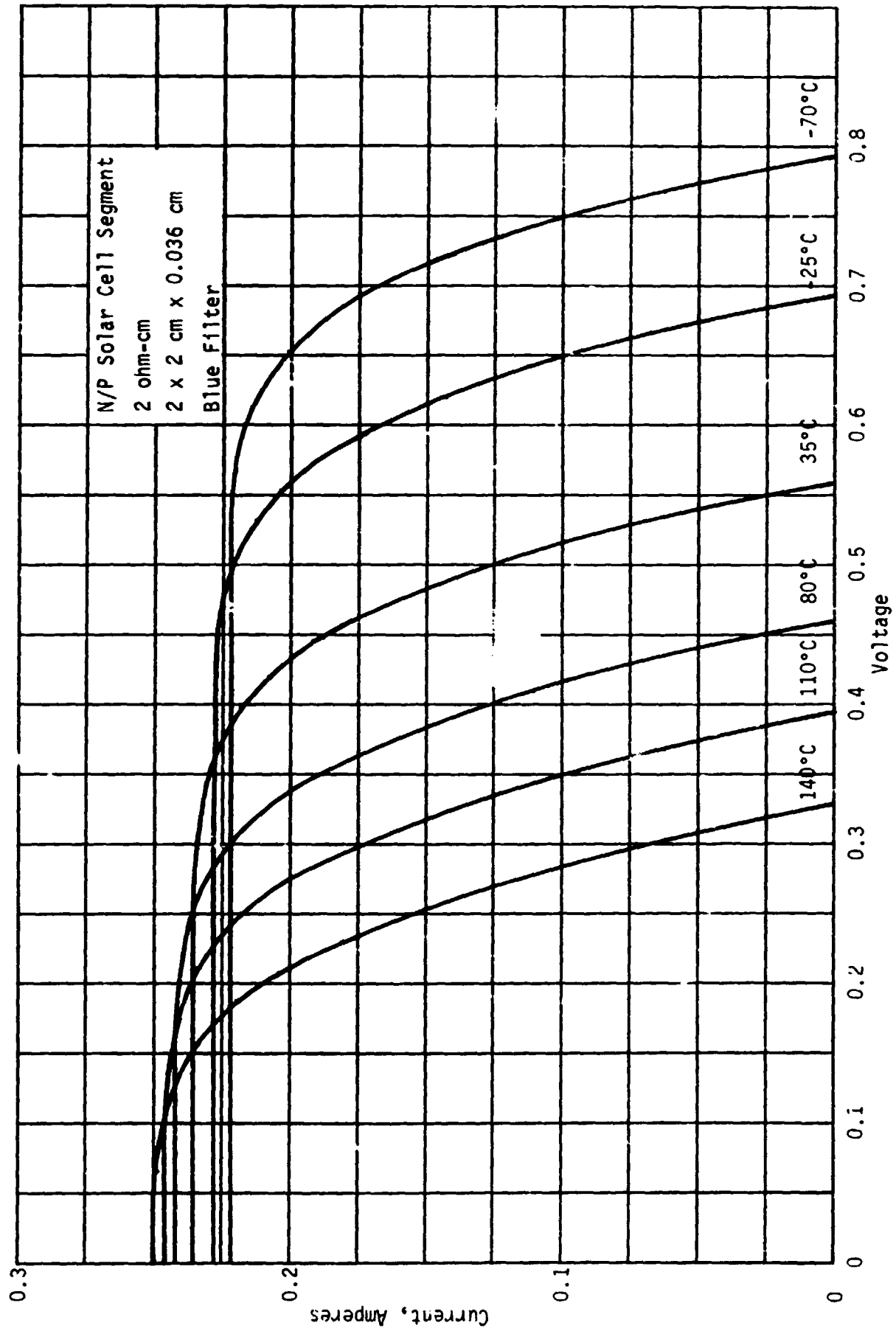
Figure VI-12   Degraded Current-Voltage Characteristics of a Solar Cell Segment

Thermal Control

Introduction - The function of the spacecraft thermal control
subsystem is to maintain equipment temperatures within specified
limits throughout the mission. These limits constitute the success
criteria for the thermal design. The temperatures are controlled
indirectly by controlling the heat flow patterns within the space-
craft, and to the environments, to which the temperature fields are
related by the basic equations of heat transfer. Two significant
characteristics of thermal design should be noted at this point:

First, since virtually all of the spacecraft takes part in the
heat transfer processes determining its temperatures, the thermal
control subsystem as a whole cannot be physically separated, nor
independently tested, from the rest of the spacecraft. Conse-
quently, the minimum thermal effort usually required during the
implementation phases of a program must include an iterative
thermal analysis of the complete spacecraft, supplemented by a
systems-level thermal test program. This holds true, even when
proven concepts, or similarity to previous designs, are resorted
to. Conversely, the relative impact of new technology requirements
on the total cost of the thermal control of advanced spacecraft
is minimized by this integrated character of thermal design.

Second, the impact of thermal design on the final spacecraft
configuration may take one or more of several possible forms
listed below in order of preference:

        a. Addition of thermal control hardware. These ad-
            ditions are said to be "active" if their function-
            ing depends on moving parts or fluids; otherwise
            they are considered "passive". Typical active elements
            include fluid loops, heat pipes, louvers, thermal switches,
            and thermostatically controlled heaters. Passive elements

include insulation, thermal standoffs, coatings and
finishes, and phase change heat sink materials (PCM).
Intuitive reasoning would tend to assign the highest
reliabilities to the passive systems. This is not
necessarily true, however; for example a number of
"passive" coatings have shown to be susceptible to
UV degradation, while active elements such as louvers
and thermostats have proved to be highly reliable in
flight.

b. Impacting the configuration design, in order to in-
prove heat distribution within the "non-thermal-
control" hardware. This may take the form of re-
arranging of electronics, or changes in the external
configuration design.

c. Impacting the equipment design and qualification pro-
gram with the aim to increase their range of permissible
temperature limits. The wider the permissible range,
the less thermal effort is required. (In theory at
least, this reasoning could be extrapolated to "no
thermal control required".)

d. Imposition of constraints on flight maneuvers. The
position and orientation of the spacecraft in orbit
(or space) have major effects on its thermal couplings
to the sun and planets, and on its capability to
reject heat to space (normally assumed a $4^{o}K$ radia-
tion heat sink).

In order to provide a conservative evaluation of feasibility
and technology requirements, an attempt was made in the initial
phases of the study to minimize the thermal impacts of the form
(b), (c), and (d) above. Such an approach also minimizes the

thermal constraints on the iterative design of the primary sub-
system (radar). Alternative approaches are _o t considered
later in the study, after firming up the radar, communications
and power subsystems designs.

Criteria and Guidelines for Thermal Design - The iterative
phase thermal study was based on the following detailed considera-
tions.

Assumptions relating to the thermal characteristics of the
spacecraft:

a. The permissible temperature limits for the equipment
    compartment are comparable to those of Viking, ranging
    from -18° to $49^\circ C$ for electronics (including radar),
    and 10° to $32^\circ C$ for the batteries.

b. The average power dissipation during the orbital phases
    of the mission is in the order of 500 watts, with po-
    tential increase to 600 watts by the end of the study.

c. The radar and communications electronics represent con-
    centrated heat sources both spatially and temporaly.
    Thermally significant peaks of heat dissipation may
    range up to 0.9 KW during mapping, and 0.7 KW during
    high rate relay. It is further assumed that packag-
    ing is on a one-subsystem per bay basis.

Assumptions relating to the environment:

a. The planetary emitted (IR) and reflected (albedo)
    solar radiation of Venus originate at the "cloud
    top" level, assumed to be a spherical surface with
    a radius of 6120 Km. (Compare this with the radar
    surface radius of 6050 Km).

b. Both the IR planetary and the solar reflected radi-
    ation are diffused, obeying Lambert's cosine law.

c. The following flux densities apply at the cloud top
   level:
   Infrared: $C_E = 160.1$ W/m^2, uniformly distributed over
   the sphere.
   Albedo: $C_A = 2760.4$ W/m^2 at the subsolar point
   (≈ 0.76 x solar constant near Venus), and varies
   as the cosine of the zenith angle away from the sub-
   solar point.

d. The solar constant near Venus is $C_S = 2667.9$ W/m^2,
   corresponding to a mean distance from the sun of
   0.723 AU (Astronomical Units). The solar rays are
   assumed to be collimated (parallel), except when
   otherwise not ;d.

e. The outer space provides a radiation heat sink with
   an effective blackbody temperature of $4^\circ K$.

Initial aim at design flexibility. As pointed out earlier,
it is a goal of the sample configuration thermal design to mini-
mize the configuration constraints on the primary subsystem de-
sign iterations. This may not result in an optimum approach,
however, it provides the basis for establishing the feasibility
of thermal design, and for ramifications into alternate designs.

State-of-the-art considerations. Projections of state-of-
the-art are notoriously difficult to make, since they must be
based on subjective evaluation of future developments that are
usually beyond the control of any sing.e individual or organi-
zation. A relatively "safe" prediction of the state-of-the-art
for the late 1980's and early 1990's can be made, however, by
considering those concepts currently under development (including
flight-development). Thermal control elements in this category
are heat pipes, phase-change materials, and specular louvers.

Thermal Design of the Sample Configurations - A thermal control
concept that fits all of the criteria listed above consists of
a single radiator, coupled to the internal heat sources by a heat
pipe system. The radiator represents the spacecraft/environment
thermal interface through which all of the internal heat is re-
jected, the rest of the equipment compartment being isolated from
the environment by the use of high-performance (multilayer) in-
sulation. The heat pipe system provides an effective means of
distributing the internal heat from the concentrated sources
throughout the thermal mass of the equipment compartment, there-
by minimizing temperature gradients and fluctuations, as well as
providing an efficient means of thermal coupling between the
equipment and the radiator. The single radiator concept per-
mits maximum flexibility with regard to location and orientation
of the radiator, hence minimum constraints on overall configura-
tion design.

Since the heat pipe is a near-isothermal device, as a first
approximation, the radiator design temperatures may be equated
with the desired equipment temperatures, which provides for a
considerable simplification in the analysis. The conceptual
design problem is reduced, then, to determining the required
thermophysical properties, size, location and orientation
of the radiator, consistent with total heat rejection requirements,
and with the configuration constraints of the radar, communications,
and power subsystems. These will be discussed in the subsequent
paragraphs.

The preliminary design of the radiator may be accomplished
in three somewhat overlapping steps, viz. (a) conversion of the
equipment compartment temperature limits into radiator tempera-
ture requirements; (b) conversion of the radiator temperature

requirements into heat emission criteria; and (c) satisfying
the heat emission criteria by heat balance considerations.
Step (a) is very simple to accomplish in the case of the sample
thermal design, since the heat pipe system provides a thermal
coupling with practically no thermal gradients between equip-
ment and the radiator. Consequently, the radiacor is subject
to the same temperature limitations as the inside of the com-
partment, the average "design" temperature selected for this
study being $21^{\circ}C$ ($294^{\circ}K$), the mean temperature of the batteries.

The relation between the emissive power of the radiator
surface and its temperature (Step (b)) is provided by Stefan-
Boltzmann's Law, according to:

$$q_{em} = \varepsilon \sigma T_R^4 \tag{VI-3}$$

where q_{em} = radiant energy emitted per unit surface area in
$Kcal/m^2$ - hr,

ε = effective emissivity of the surface, dimensionless

σ = the Stefan-Boltzmann constant = 4.88×10^{-8} Kcal/
m^2 - hr - K^4

T_R = absolute radiator temperature, K

The emissivity is a material property in the case of simple
surfaces, but it is also a function of geometry in the case of
more complex surfaces, such as provided by louvers. (In the latter
case, the effective emissivity is "controlled" by the position
of the blades).

In Step (c), q_{em} is related to internal and external heat
loads according to the heat balance equation:

$$q_{em} = Q_{int}/A_R + \alpha (I_S + I_A + I_{is}) + \varepsilon (I_E + I_{ie}) \tag{VI-4}$$

where Q_{int} = total internal heat load, watts

A_R = area of radiator, m^2

α = absorbtivity of the radiator surface in the solar wavelength

I = incident radiation (or irradiance) on the radiator surface, W/m^2

and the subscripts stand for: S = direct solar; A = albedo; E = planetary-emitted (IR); is = induced-solar origin; and ie = induced IR. The "induced" heat loads are those due to reflection or emission by spacecraft appendages (or other external surfaces) "seen" by the radiator.

For a given q_{em}, a minimum radiator size would be achieved in the absence of external heat loads. In this case, according to equations (VI-3 and VI-4)

$$(A_R)_{min} = Q_{int} / \epsilon \sigma T_R^4$$

which gives for Q_{int} = 500 W, ϵ = 0.7, and T_R = 294 K, an

$$(A_R)_{min} = 1.68 \ m^2$$

In the case of the VRM mission this ideal situation cannot be realized, and the required radiator area will be larger than $(A_R)_{min}$; the latter, however, will serve as a reference basis for evaluating the effectiveness of the design.

In order to minimize the effect of external heat loads on the radiator, a combination of three approaches has been used (a) the selection of a low α/ϵ ratio surface for the radiator; (the state-of-the-art value for the second surface mirrors (SSM) is α/ϵ = 0.1/0.7;) (b) the elimination of the "induced" radiation effects by proper location and orientation of the radiator on the spacecraft; and (c) by minimizing the total incident radiation from the sun and Venus by imposing further constraints on the location and orientation of the radiator.

The first approach is straight-forward; the second proved
to be well within the constraints of conf⁴·guration design. The
third is discussed in more detail below, in relation to parametric
variation of orbital parameters and the associated radiator area
requirements.

Each of the three remaining incident radiation terms in
Equation (IV-4) may be expressed as the product of a source constant
C. and a radiation view factor F, according to:

$$I_S = C_S F_S; \quad I_A = C_A F_A ; \quad \text{and } I_E = C_E F_E \tag{VI-5}$$

The source constants have already been defined in Criteria and
Guidelines for Thermal Design; the view factors are functions of
position and orientation of the radiator in orbit. Referring to
Figure VI-13 for the definitions of radiation geometry, these
functions may be formally written:

$$F_S = F_S (\beta) = \cos \beta \tag{VI-6a}$$

$$F_A = F_A (\gamma , \delta , \nu , R) \tag{VI-6b}$$

$$F_E = F_E (\gamma , R) \tag{VI-6c}$$

The explicit terms of Equations (VI-6b) and (VI-6c) (omitted here
for brevity) generally require numerical solutions. Such solutions
have been tabulated in the literature (Ref. VI-6) for a number
of geometries, and these have been used in the present study.
From these data, and the equations (VI-6), the instantaneous
incident fluxes can be determined. Further insight into the
thermal aspects of orbital flight may be obtained by using
integral forms of the above view factors, based on a thermal
analogy to Kepler's Second Law developed during the course of
the study, and outlined in the ᴧollowing. In the analogy,
the true anomaly Θ and its time-derivative $\dot{\Theta}$ are preserved, but
the position radius R is replaced by a thermal radius defined as
$RF^{\frac{1}{2}}$, or, in non-dimensionalized form: $\phi = rF^{\frac{1}{2}}$, where $r = R/R_o$.
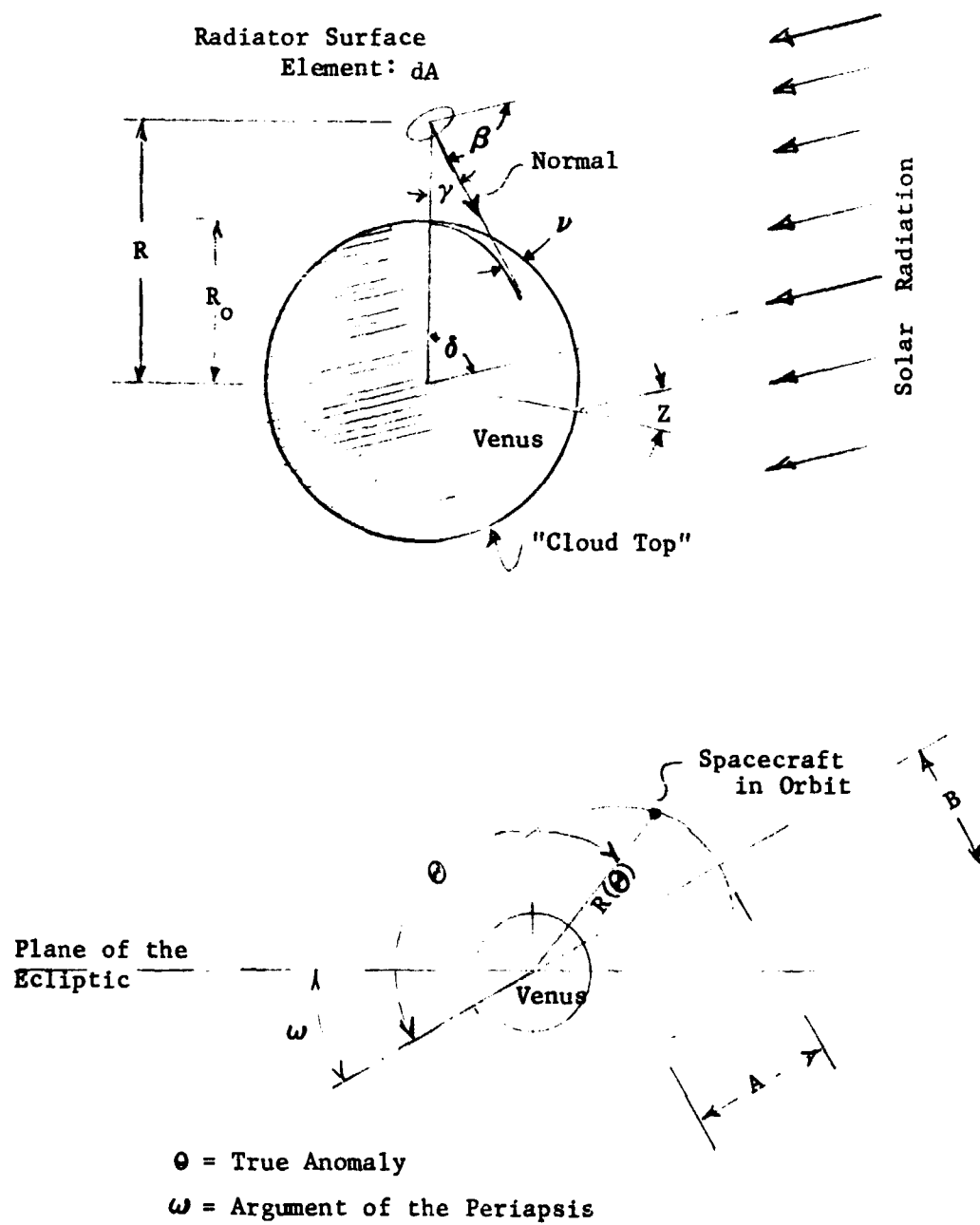
Figure VI-13 Radiation Geometry

In orbital mechanics, the area swept by R is proportional to
the time-integral of angular momentum, hence to time, when the
latter is constant, such as in a Keplerian orbit. The area
swept by the thermal radius is proportional to the time-integral
of the flux I, hence with time, when the latter is constant. (In
this case the "orbit" described by the thermal radius is an ellipse).
For the important special class of proble:s where the incident
flux varies as the inverse-square of distance from the source
(e.g., solar system), the thermal radius is a constant, and the
"orbit" described by it is a cricle (when the mechanical orbit
is an ellipse) or an arc of a circle (when the mechanical orbit is
a parabola or hyperbola); and the(cumulative) total incident
radiation on the orbiting body is proportional to the true anomaly.

An advanatage of the analogy-method is that it provides a
bas.s for the geometrical representation of the thermal aspects
of orbital flight in the form of polar diagrams. To facilitate
the construction of such diagrams, there have been developed
a set of diagrams showing the thermal radius as a function of
the position radius, r, and of orientation, for flat surface
elements in orbit. Specific results pertaining to the Sample
Configuration studies are summarized below.

The orbital-average incident flux originating from the planet
(i.e., I_A and/or I_E) is given by the equation of the form:

$$\overline{I} = \frac{C}{\pi \, ab} \; 1/2 \int_0^{2\pi} \phi^2 \, d\theta \tag{VI-7a}$$

$$= \frac{C}{\pi \, r_p^2} \cdot \frac{(1-e)^2}{\sqrt{1-e^2}} \; 1/2 \int_0^{2\pi} \phi^2 \, d\theta \tag{VI-7b}$$

where $\bar{I}$ = orbital-average incident flux, $a = A/R_o$, $b = B/R_o$,
A = semi-major axis of orbit, B = semi-minor axis of orbit, $r_p =$
R_p/R_o, R_p = periapsis (position) radius, e = eccentricity, and
C, ϕ , and θ are as defined before. Our study has indicated that the
integral on the right-hand side of Equation (VI-5) does not change
significantly when the eccentricity is varied, hence to a first
approximation, $\bar{I}$ is proportional to $Y = (1-e)^2/ (1-e^2)^{\frac{1}{2}}$. For the
three eccentricities considered:

e = 0.0   0.3   0.5

Y = 1.0   0.513   0.288

The net effect on required radiator area is considerably smaller,
however, than the above numbers would indicate. For example, for
the ase of no direct solar impingement on the radiator, A_R is
inversely proportional to $\left(q_{em} - \alpha\ \bar{I}_A - \epsilon\ \bar{I}_E \right)$ in accordance with
Equation (VI-4), and the net effect on the Shared Antenna Concept
is as follows:

e =   0.0   0.3   0.5

A_R= $1.8m^2$ $1.9m^2$ $2.1m^2$

On Figure VI-14 are shown two superimposed polar diagrams of ab-
sorbed environmental radiation for two radiator orientations: paral-
lel and perpendicular to the eclipt'c, respectively. The diagrams
are drawn for the worst-case situations of the Shared Antenna Con-
cept, an eccentricity of 0.5, and for no direct solar impingement.
It is shown that case "B" (radiator perpendicular to ecliptic)
is the preferred configuration, although the environmental heat
loads are relatively small (10.8 and 15.0 W/m^2) as compared to
the internal heat load (over 200 W/m^2).

Shared vs Dedicated Antenna Concepts - Polar diagrams
of environmental heat loads (absorbed radiation per unit radiator
area) for the Shared and Dedicated Antenna Concepts are shown

NOTE: Area swept by thermal radius φ represents heat absorbed from environment.

"A" : RADIATOR PARALLEL TO ECLIPTIC
$q_{abs} = 15$ w/m^2

"B" : RADIATOR PERPENDICULAR TO ECLIPTIC
$q_{abs} = 10.8$ w/m^2
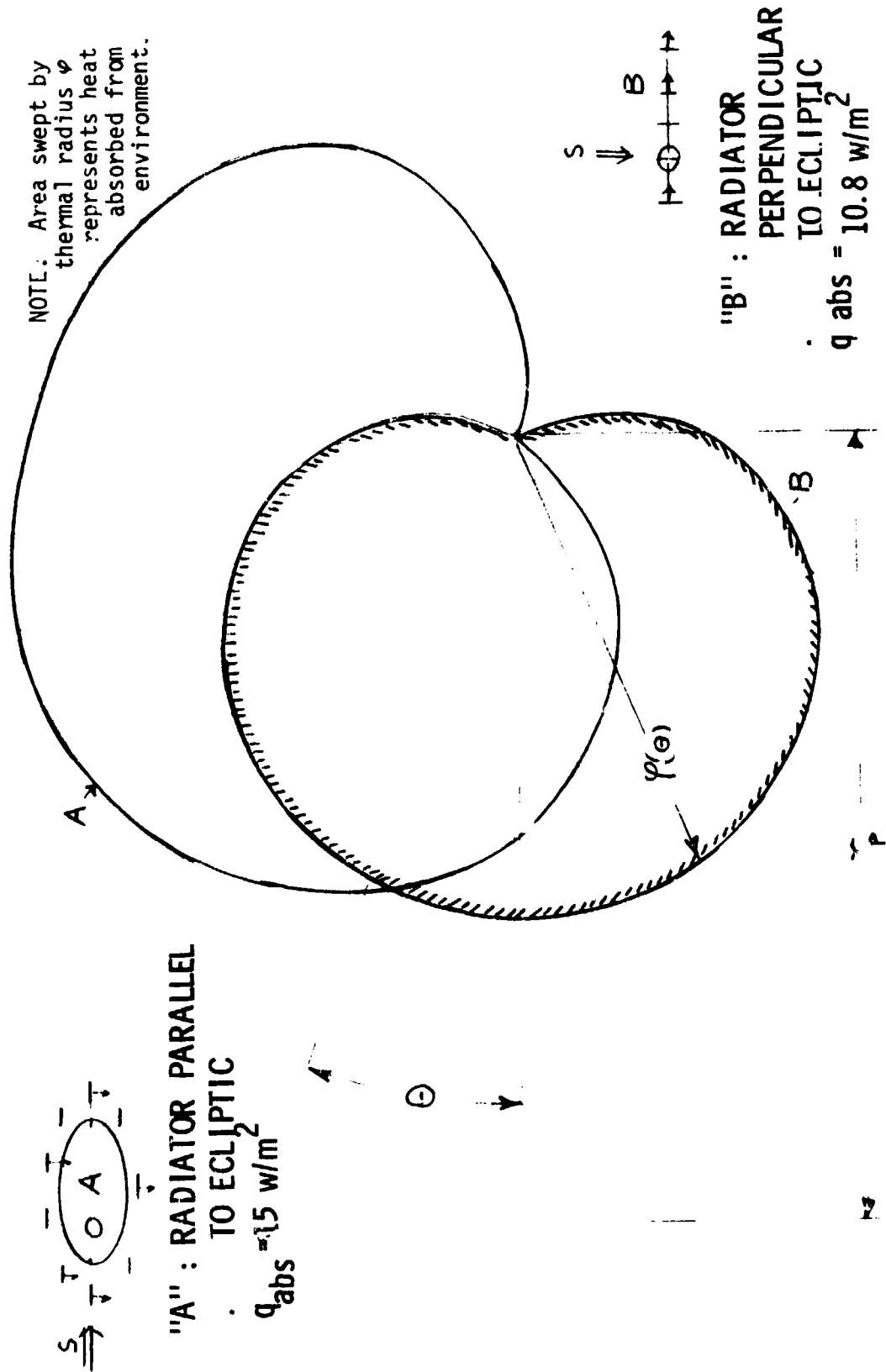
Figure VI-14 Comparison of Two Radiator Orientations - Shared Antenna Concept

by the shaded areas on Figures VI-15 and VI-16 respectively. The
area of the ellipse--with a thermal radius ρ --on both diagrams rep-
resents the emissive power of the radiator, i.e., q_{em}. The diagrams
represent worst-case environmental conditions for the mission, the
Dedicated Antenna Concept being characterized by partial exposure
of the radiator to direct solar radiation during the mapping phases
of the mission. It may be concluded that:

The single-radiator concept provides a highly flexible thermal
design for the VRM spacecraft, with the thermal control elements
conceptually within present state-of-the-art, but with some hard-
ware development and qualification required.

The effect of environmental heat loads are minimized, and the
required radiator size is determined essentially by internal heat
dissipation requirements, with the proposed concept.

The Shared-Antenna concept is the thermally preferred configura-
tion.

Attitude Control Parametric Studies

Introduction - General goals of the ACS parametric design
studies for the Venus Mapper Mission are: (1) to meet radar imaging,
communication, attitude and attitude rate pointing requirements;
and (2) to be compatible with the spacecraft design in terms of
ACS size, weight and power. Spacecraft and antenna maneuver
times, based on mission requirements, must be met. An additional
objective is to determine applicability of the Viking Orbiter
cold gas - Sun/Canopus ACS. If this system is applicable, the
objective is to define the required modifications. Any long-
life hardware problems will be identified.

A trade study was performed between momentum exchange systems
and mass expulsion systems. The momentum exchange systems are
Reaction Wheels (RW) and Control Moment Gyros (CMCs). The mass

NOTE: Area swept by thermal radius φ represents heat absorbed from environment.
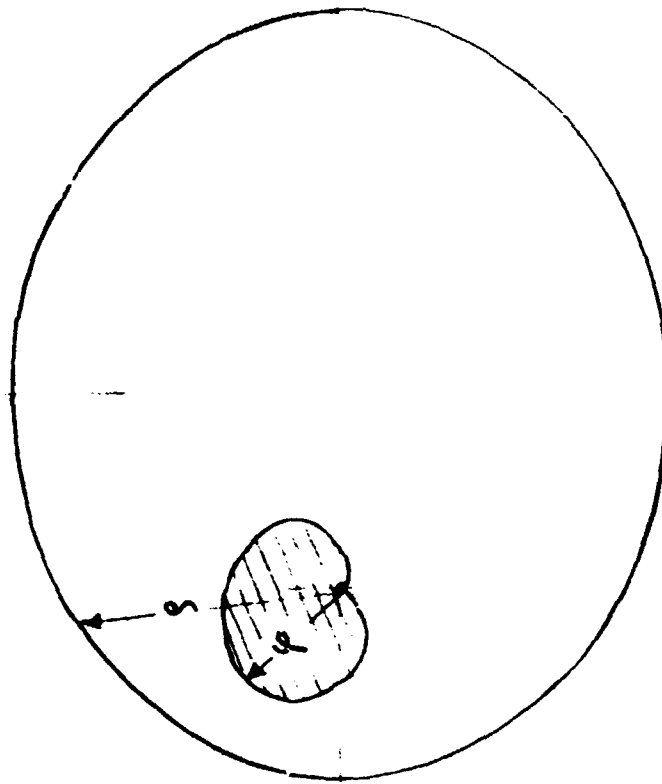
q_{em} = 298 w/m^2

q_{abs} = 14.8 w/m^2

q_{net} = 283.2 w/m^2

Q_{int} = 500 w

Min. Radiator Area:

A_R = 500/283 = 1.8 m^2

Figure VI-15   Radiator Performance - Shared Antenna Concept

VI-40

NOTE: Area swept by thermal radius φ represents heat absorbed from environment.
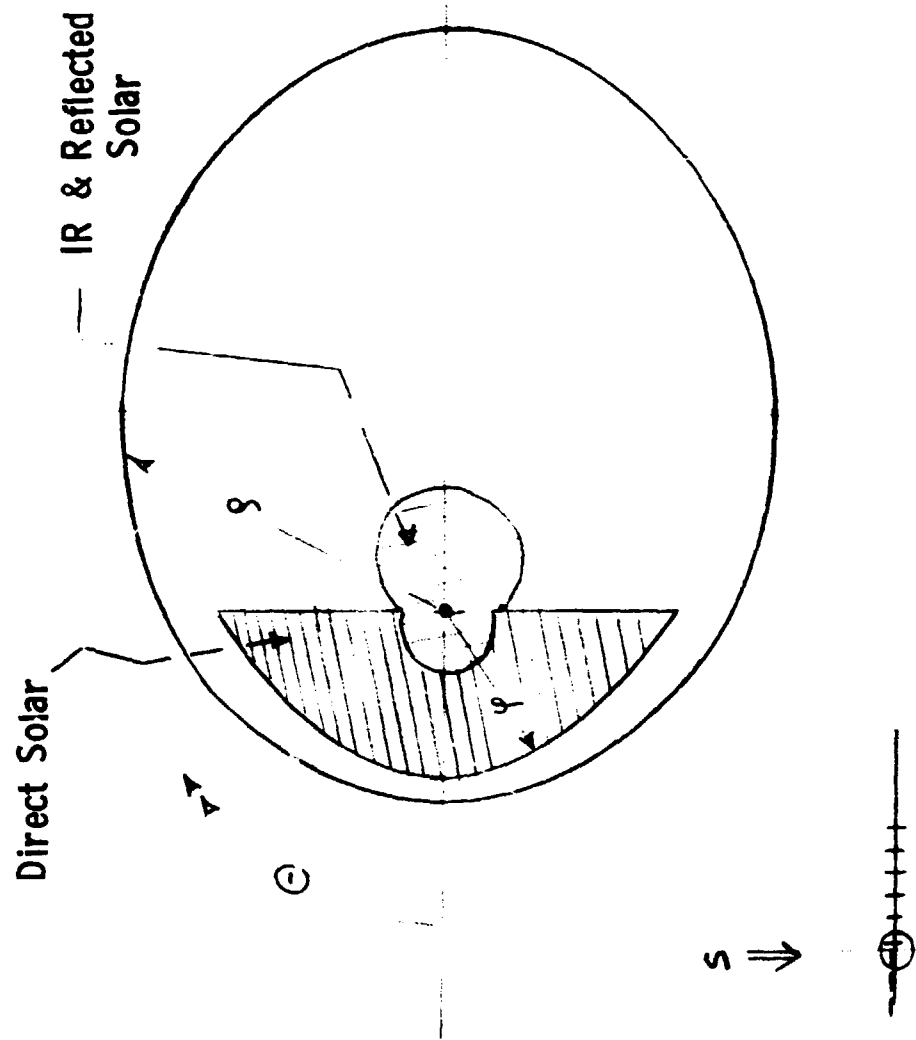
$q_{em} = 298 \ w/m^2$

$q_{abs} = 53 \ w/m^2$

$q_{net} = 245 \ w/m^2$

$Q_{int} = 500 \ w$

Min. Radiator Area:

$A_R = 500/245 = 2.1 \ m^2$

Figure VI-16 Radiator Performance - Dedicated Antenna Concept

expulsion systems which were studied are nitrogen cold gas (GN_2) and a hydrazine/plenum dual propellant system. The trade studies involved a sizing analysis to determine the weight, dimensions, and electrical power requirements of possible ACS, as well as identifying any lifetime problems.

Trade studies that considered momentum exchange systems were done only for Configurations A (shared) and B (dedicated). This was sufficient to reach a conclusion. Momentum exchange systems that were considered are: 1) four skewed single gimbal CMGs; 2) five skewed single gimbal CMGs; 3) four skewed reaction wheels; and 4) two double-gimballed reaction wheels. These momentum exchange systems are compared to mass expulsion systems on Configuration A and Configuration B. Mass expulsion systems on Configuration A are: 1) a GN_2 system with yaw thrusters on the solar panels (yaw moment arm of 0.61 m); 2) a GN_2 with yaw thrusters on a boom (moment arms of 4.8 m); 3) a GN_2 system with yaw thrusters on the spacecraft (yaw moment arm of 1.25 m); and 4) a hydrazine/plenum dual propellant system.

Mass expulsion systems on configuration B are a GN_2 system and a hydrazine/plenum dual propellant system.

The following is a list of mission requirements and some ground rules that are used in the ACS tradeoff studies.

- o Viking Orbiter '75 spacecraft serves as a baseline. This baseline provides a three-axis stabilized spacecraft with a Sun/Canopus celestial reference system and an Inertial Reference Unit (IRU).
- o The "half-gas" ACS philosophy is adpated (except as noted) where a redundancy factor on propellant is 3.0.
- o The momentum exchange systems are sized to allow for one complete wheel failure.

o   For Configuration A, the shared antenna is moved between
    Earth and Venus every 5th orbit for e = 0, every 2nd orbit
    for e = 0.3, and every orbit for e = 0.5. The solar panels
    always point to the sun. The antenna is maneuvered in
    pitch and yaw simultaneously with the antenna pitch rate
    being 0.5 deg/sec and the antenna yaw rate being 0.75
    deg/sec.

o   The Configuration B must maneuver between mapping and re-
    charging phases. The communication antenna is articulated.
    Worst case manuevering for each mapping phase assumes a
    pitch up of 90°, roll of 135°, and after recharging, a
    de-roll of 135°, and a pitch down 90°. This maneuver
    must be performed in 0.9 hour per phase to meet communi-
    cations requirements. This translates into a spacecraft
    maneuver rate of 0.417 deg/sec in pitch and roll, taking
    into account time for transients to damp.

o   Spacecraft command turns for all attitude maneuvers, except
    for the mapping and charging maneuvering of Configuration
    B, are 0.18 deg/sec.

o   Booster separation rate and rates induced by spacecraft
    main engine shutdown are 1 deg/sec RSS total ($\sqrt{3}/3$ deg/sec
    in each axis).

o   When on celestial reference, attitude deadband is $\pm$ 4.4
    x 10^{-3} rad in yaw, pitch, and roll. When occulated, gyro
    reference is used with an attitude deadband of $\pm$ 3.0 x 10^{-3}
    rad in yaw and pitch and $\pm$ 1.5 x 10^{-3} rad in roll. When
    occulted from the Sun, yaw, pitch, and roll are on gyros.
    When occulted from Canopus, roll is on gyros, yaw and pitch
    remain on Sun reference. These deadbands are based on
    VO'75 specifications and therefore should be attainable.

o   Main engine burn time is assumed to be 40 seconds for
    midcourse corrections. One gimballed engine is assumed
    to be used for midcourse corrections, thus the ACS supplies
    roll control. Main engine burn time is assumed to be
    800 seconds for orbit insertion. Three engines are used
    for orbit insertion with only the center engine gimballed:
    roll control is supplied by the ACS.

o   The ACS is also assumed to provide a vernier ΔV of 0.16 m/
    sec following main engine shutdowns.

o   Minimum on-time for the GN_2 or plenum ACS thrusters is
    0.020 seconds.

The following timeline is part of the mission requirements and
ground rules that are used in the ACS tradeoff and sizing studies.

1. Booster separation, reduce tip-off rates with ACS.

2. Two Sun and Canopus acquisition attitude maneuvers. Maximum
    allowed time due to batteries is approximately 30 minutes.
    (This time constraint is easily met).

    a. At booster separation.

    b. Due to some other cause.

3. Two midcourse correction maneuvers.

    a. Attitude maneuver to thrusting attitude and maneuver
        back to celestial attitude in roll-pitch sequence.

    b. Fire one main engine, reduce spacecraft rate transients
        due to main engine shutdown. Worst case one engine burn
        time is 40 sec: assume roll control is provided by the
        ACS during this time. Assume rate reduction same as
        booster tip-off rates (1 deg/sec total).

    c. ACS is used to provide a 0.16 m/sec ΔV vernier correc-
        tion. Roll control is maintained continuously during
        vernier.

4. Limit cycle during cruise. Assume no external torque. Use celestial reference. Transit time is 175 days.

5. Orbit insertion.

    a. Attitude maneuver to thrusting attitude and maneuver back in roll-pitch sequence.

    b. Fire three main engines with only center engine gimballed. Maintain roll control continuously with ACS for 800 sec, reduce rate transients (1 deg/sec total) due to main engine shutdown.

6. Limit cycle in orbit. Time is 250 days. ACS propellant usage is dependent on the ACS deadband which is determined by oc-cultation conditions.

    a. Pitch and yaw time on gyro reference is 5.8×10^6 seconds for $e = 0$ and 4.1×10^6 seconds for $e = 0.5$. Deadband = $\pm 3.0 \times 10^{-3}$ rad.

    b. Pitch and yaw time on celestial reference is 15.7×10^6 seconds for $e = 0$ and 17.4×10^6 seconds for $e = 0.5$ Deadband = $\pm 4.4 \times 10^{-3}$ rad.

    c. Roll time on gyro reference is 11.8×10^6 seconds for $e = 0$ and 8.76×10^6 seconds for $e = 0.5$. Deadband = $\pm 1.5 \times 10^{-3}$ rad.

    d. Roll time on celestial reference is 9.76×10^6 seconds for $e = 0$ and 12.74×10^6 seconds for $e = 0.5$. Deadband = $\pm 4.4 \times 10^{-3}$ rad.

7. Two orbital trim burns, $e = 0.5$ only. This is the same as 3. except that this is for $e = 0.5$ only and $e = 0.5$ orbital mass properties are used.

8. Antenna meneuvering. For Configuration A only.

9. Spacecraft maneuvering in orbit. For Configuration B only.

For purposes of discussion, the ACS is arranged into the following block diagram:

```
┌─          ┐        ┌─              ┐       ┌─            ┐
│ SENSORS _ │        │ ON-BOARD      │       │ SPACECRAFT  │
│           │        │ COMPUTER      │       │             │
│           │        │ ACS           │       │             │
│           │        │ CONTROL       │       │             │
│ ...       │        │ EFFECTOR      │       │             │
└─          ┘        └─              ┘       └─            ┘
```
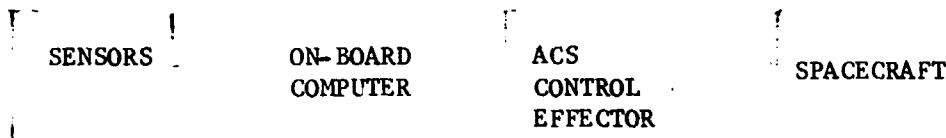
For the mass expulsion systems the control effector sizing includes propellant, tankage and support structure, nozzles, valves, pressure regulators, plumbing, and reactors or catalysts. For momentum exchange systems, the control effector sizing includes wheels, housings, support structure, drive motors, gimbal actuators, and drive and control electronics.

The mass properties that are used for Configurations A and B ACS sizing analysis are given in Table VI-9. Inputs that are used for the momentum exchange sizing analysis are:

o Torque required to maneuver = $\pm$ 0.122 newton-meter.

o Peak external torque due to gravity gradient, aerodynamic and solar pressure effects = 1.556×10^{-4} newton-meters.

o Peak momentum required = $\pm$ 13.8 n-m-sec. This momentum value excludes all high-rate transients due to booster separation and main engine shutdown because mass expulsion is used to damp these transients. This momentum value is based on Configuration B maneuvering between mapping and charging phases. (Peak momentum for antenna maneuvering for Configuration A is $\pm$ 0.374 n-m-sec; therefore, the sized CMG system can easily accommodate disturbances due to antenna articulation).

o These torque and momentum requirements were assumed symmetric in pitch, yaw and roll.

Table VI-9 Mass Properties Used for Configurations A and B
ACS Sizing Tradeoff Analysis

Mission Portion	e = 0.3				e = 0.5			
	Weight (kg)	Inertia n-m-sec^2			Weight (kg)	Inertia n-m-sec^2		
		I_x Yaw	I_y Pitch	I_z Roll		I_x Yaw	I_y Pitch	I_z Roll
Booster separation to prior to orbit insertion, antenna stowed.	3230	2460	3575	2360	2270	1310	2180	2000
Orbit insertion to end of mission, antenna extended.	1165	1310	1900	1780	1055	1020	1540	1700

Use of candidate momentum exchange systems assumes availability of a digital computer to mechanize the control laws, and use of a GN_2 ACS for all rate reductions and Sun Canopus acquisition. The remainder of the mission will use the momentum exchange system with the GN_2 system for desaturation and vernier ΔVs and perhaps as a backup. This allows the wheels to be spun-up after the boost phase to avoid the extreme environmental problems associated with boost.

The CMGs were sized according to the design philosophy contained in Reference VI-8 and Reference VI-9 which involves a scaling law derived assuming a stress-limited design.

No lifetime problems (425 days) are identified for the mass expulsion systems or for the momentum exchange systems. No technology development requirements are identified for either system.

Discussion of Results - Results of the ACS sizing analysis
tradeoff study between mass expulsion systems and momentum ex-
change systems are given in Tables VI-10 through VI-21.

Table VI-10 compares control effector size, weight, and power
for momentum exchange systems. The reaction wheel systems are not
candidates because of the high power requirement. Peak power re-
quirements are summarized in Table VI-14. On the basis of size,
weight, and power, Table VI-10 shows that 4 or 5 skewed simple
gimbal CMGs are an acceptable ACS.

For Configuration A, Table VI-11 shows that a GN_2 ACS is accep-
table if the yaw moment arm is sufficiently long. When the yaw
moment arm is as short as 0.61 m (yaw thrusters mounted on the cor-
ners of the solar panel tips), a GN_2 ACS is unacceptable on the
basis that the total system weight is greater than 10% of the
spacecraft in orbit. Table VI-11 shows that a hydrazine dual
propellant system is acceptable from a weight standpoint even when
the yaw moment arm is 0.61 m.

Table VI-12 shows that both the GN_2 and hydrazine ACS are too heavy
for Configuration B. The total system weights given in Table VI-12
are largely independent of the yaw moment arm because maneuvering
for Configuration B is done in pitch and roll. Most of the

Table VI-10 - Momentum Exchange System Size, Weight, and Power
Configuration A or B, e = 0.3 or 0.5

	4 Skewed Simple Gimbal CMGs	5 Skewed Simple Gimbal CMGs	4 Skewed Reaction Wheels	2 Double Gimballed Reaction Wheels	Nitrogen Cold Gas System for Separation and Desaturation for Each Momentum Exchange System
Control Effector Size	• d = 0.4 m • Volume of CMG system = 0.0152 m³ • Volume of N₂ system = 0.058 m³ • Total volume = 0.07 m³	• d = 0.5 m • Volume of CMG system = 0.03 m³ • Volume of N₂ system = 0.058 m³ • Total volume = 0.09 m³	• d = 0.8 m • Volume of CMG system = 0.12 m³ • Volume of N₂ system = 0.058 m³ • Total volume = 0.18 m³	• d = 0.6 m • Volume of CMG system = 0.22 m³ • Volume of N₂ system = 0.058 m³ • Total volume = 0.28 m³	• d = 0.38 m • Volume per tank = 0.029 m³ • Total volume = 0.058 m³ • Pressure per tank = 2.21 E7 n/m²
Total System Weight	• CMG system = 19 kg • N₂ system = 40 kg • Total weight = 59 kg • Sensors, etc. = 45 kg • Total system weight = 104 kg	• CMG system = 18 kg • N₂ system = 40 kg • Total weight = 58 kg • Sensors, etc. = 45 kg • Total system weight = 103 kg	• CMG system = 29 kg • N₂ system = 40 kg • Total weight = 69 kg • Sensors, etc. = 45 kg • Total system weight = 114 kg	• CMG system = 17 kg • N₂ system = 40 kg • Total weight = 57 kg • Sensors, etc. = 45 kg • Total system weight = 102 kg	• 40 kg including 14 kg of N₂
Control Effector Input Electrical Power	• At separation (N₂) & main engine shutdown - Peak of 20 watts for 25 sec. - Average of 10 watts for 130 sec. • During command turns (CMGs) - Peak of 22 watts for 115 sec. - Average of 15 watts for 345 sec. • During vernier ΔV burns (N₂) - Peak of 20 watts for fractions of second. - 8 watts for 1000 sec.	• At separation (N₂) - Peak of 20 watts for 25 sec. - Average of 10 watts for 130 sec. • During command turns (CMGs) - Peak of 14 watts for 115 sec. - Average of 10 watts for 345 sec. • During vernier ΔV burns (N₂) - Peak of 20 watts for fractions of second. - 9 watts for 1000 sec.	• At separation (N₂) - Peak of 20 watts for 25 sec. - Average of 10 watts for 130 seconds. • During command turns (RWs) - Peak of 498 watts for 115 seconds. - Average of 321 watts for 345 seconds. • During vernier ΔV burns (N₂) - Peak of 20 watts for fractions of second. - 8 watts for 1000 sec.	• At separation (N₂) - Peak of 20 watts for 25 sec. - Average of 10 watts for 130 seconds. • During command turns (RWs) - Peak of 206 watts for 115 seconds. - Average of 192 watts for 345 seconds. • During vernier ΔV burns (N₂) - Peak of 20 watts for fractions of second. - 8 watts for 1000 sec.	• At separation (N₂) - Peak of 20 watts for 25 sec. - Average of 10 watts for 130 seconds. • During vernier ΔV burns (N₂) - Peak of 20 watts for fractions of second. - 8 watts for 1000 sec.

Table VI-11 Mass Expulsion System Size, Weight, and Power for Configuration A

	Nitrogen Cold Gas (GN$_2$) with Yaw Thrusters on Solar Panels (ℓ = 0.61 m)	Nitrogen Cold Gas (GN$_2$) with Yaw Thrusters on Boom (ℓ = 4.6 m)	Hydrazine (N$_2$H$_4$) Dual Propellant System (ℓ = 0.61 m)	GN$_2$ with Yaw Thrusters on Body (ℓ = 1.25 m)
Control Effector Size	• d = 0.6 m (e=0.3 or 0.5) • Volume per tank = 0.113 m^3 • Total volume = 0.226 m^3	• d = 0.4 m (e=0.3 or 0.5) • Volume per tank = 0.033 m^3 • Total volume = 0.066 m^3	e = .3 or .5 N$_2$H$_4$ Plenum N$_2$H$_4$ Plenum • d$_1$ = 0.38 m, d$_2$ = 0.184 m • Volume/N$_2$H$_4$ tank=0.0280 m^3 • Volume/Plenum tank=0.0033 m^3 • Total volume = 0.062 m^3	• d=0.49m(e=0.3 or 0.5) • Volume/tank = 0.06 m^3 • Total volume=0.12 m^3
Total System Weight	• e = 0.3, 189 kg • e = 0.5, 195 kg	• e = 0.3 or 0.5, 107 kg	• e = 0.3, 91 kg • e = 0.5, 92 kg	• e = 0.3, 134 kg • e = 0.5, 136 kg

Control Effector Input Electrical Power	• Peak of 20 watts for 25 sec @ separation
	• Average of 10 watts for 130 sec @ separation
	• Vernier ΔV burns
	  - 20 watts for fractions of second
	  - 8 watts for 1000 sec.
	• Maneuvers or command turns (including antenna articulation)
	  - 20 watts for fractions of second
	  - 8 watts for 25 sec or 5 watts for 75 sec
		• Same as GN$_2$ system with ℓ = 0.61 m	• Same as GN$_2$ system with ℓ = 0.61 m	• Same as GN$_2$ system with ℓ = 0.61 m

Table VI-12 Mass Expulsion System Size, Weight, and Power for Configuration B
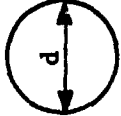
	Nitrogen Cold Gas (N_2) (ℓ = 0.61 m)	Hydrazine (N_2H_4) Dual Propellant System (ℓ = 0.61 m)
Control Effector Size	 ● d = 0.97 m, e = 0.3 ● volume per tank = 0.475 m^3 ● total volume = 0.950 m^3 ― ― ― ― ― ● d = 0.99 m, e = 0.5 ● volume per tank = 0.51 m^3 ● total volume = 1.02 m^3	 ● d_1 = 0.58 m (e = 0.3 or 0.5) ● d_2 = 0.184 m ● volume per N_2H_4 tank = 0.101 m^3 ● volume per plenum tank = 0.0033 m^3 ● total volume = 0.208 m^3
Total System Weight	● e = 0.3, 690 kg ● e = 0.5, 742 kg	● e = 0.3, 175 kg ● e = 0.5, 181 kg
Control Effector Input Electrical Power	Same as configuration A plus ● During vehicle maneuvering in orbit - 20 watts for fractions of second - 8 watts for 10 sec. - 5 watts for 16 sec.	Same as N_2 System.

Table VI-13 Control Effector Weight Summary for Momentum Exchange Systems for Configurations A or B

	4 Skewed Simple Gimbal CMGs	5 Skewed Simple Gimbal CMGs	4 Skewed Reaction Wheels	2 Double Gimballed Reaction Wheels
Momentum envelope geometric shape factor for redundancy	1.67	0.59	1.11	3.
Peak momentum requirement per wheel (n-m-sec)	23.	8.1	15.2	41.4
Radius of each wheel (m)	0.1	0.1	0.2	0.2
Form factor, h	0.6	0.6	0.6	0.6
Equivalent tip velocity for stress Limited design using steel, $\sqrt{\sigma/\rho}$ (m/sec)	500.	500.	300.	300.
Total wheel mass, steel (kg)	3.1	1.4	1.7	2.3
Total housing mass, aluminum (kg)	5.5	6.9	16.0	14.0
Total support structure mass, aluminum (kg)	2.5	3.1	5.0	1.2
Total drive motor mass (kg)	1.0 $\left(\frac{.2 \text{ kg}}{\text{motor}}\right)$	1.0 $\left(\frac{.2 \text{ kg}}{\text{motor}}\right)$	2.4 $\left(\frac{.6 \text{ kg}}{\text{motor}}\right)$	1.2 $\left(\frac{.6 \text{ kg}}{\text{motor}}\right)$
Total gimbal actuator mass, (kg) (.4 ~g/actuator)	2.0	2.0	---	2.0
Total mass for drive and control electronics (kg)	4.0	4.0	4.0	3.0
Total Mass (kg)	19.	18.	29.	23.7

Table VI-14 Summary of Peak Control Effector Input Electrical Power Requirements for
Momentum Exchange Systems for Configurations A or B

	4 Skewed Simple Gimbal CMGs	5 Skewed Simple Gimbal CMGs	4 Skewed Reaction Wheels	2 Double Gimballed Reaction Wheels
Rotor Friction (watts)	22.	14.	8.	12.
Rotor Reaction (watts)	Not Applicable	Not Applicable	490.	274.
Gimbal Friction (watts)	0.8×10^{-4}	1.0×10^{-4}	Not Applicable	2.0×10^{-4}
Gimbal Actuator Work (watts)	2.2 E-3	2.0×10^{-3}	Not Applicable	12.0×10^{-3}
Total (watts)	22.	14.	498.	286.

Table VI-15   Summary of Miscellaneous Data Defining the Momentum Exchange Systems
for Configurations A or B

	4 Skewed Simple Gimbal CMGs	5 Skewed Simple Gimbal CMGs	4 Skewed Reaction Wheels	2 Double Gimballed Reaction Wheels
Saturation Speed of Each Wheel (rps)	3350.	3350.	1125.	1125.
Maximum Gimbal Deflection per Wheel (rad)	Unlimited	Unlimited	N/A	0.522
Maximum Gimbal Deflection Rate per Wheel (rps)	0.0016	0.005	N/A	0.009
Power Factor Due to Skewing	Negligible	Negligible	1.69	Negligible
Wheel Inertia Ratio, μ	0.9	0.9	0.8	0.8
Rotor Friction Torque per Wheel (n·m)	8.1 E-4	2.8 E-4	8.4 E-3	5.8 E-3
Efficiency of Drive Motors and Electronics	0.7	0.7	0.5	0.5

Table VI-16 Configuration A: Total System Weight Using Nitrogen Cold Gas Mass Expulsion System With Yaw Thrusters on Solar Panels (ℓ = .61 m)

	e = .3	e = .5
Yaw Impulse Requirement	8616. n-sec	9350. n-sec
Pitch and Roll Impulse Requirement	2258.	2093.
Total Impulse Requirement	10874. n-sec	11443. n-sec
GN$_2$ Propellant Weight (for both half-gas systems including factor of 3.0 for thruster failed-on at liftoff. Note: I_{sp} = 655. n-sec/kg)	50. kg	52.5 kg
Ullage or Allowance of 10%	5.	5.
Both Tanks plus Support Structure (tankage factor of 1.5 using a pressure of 2.21 E7 n/m^2)	83.	86.
Leakage Thrust (0.379 n-sec/day for 425 days)	0.3	0.3
Nozzles, Valves, Pressure Regulators and Plumbing	5.7	5.7
Total Torque Source Weight	144. kg	150. kg
Sensors (IRU, Sun/Canopus, etc.), Gimbal Actuators (main engine TVC and antenna), Flight Control Computer, Articulation Control Computer	45.	45.
System Total Weight	189. kg	195. kg

Table VI-17 Configuration A: Total System Weight Using Nitrogen Cold Gas Mass Expulsion System With Yaw Thrusters on Spacecraft (ℓ = 1.25 m)

	e = 0.3	e = 0.5
Yaw Impulse Requirement	4268. n-sec	4629. n-sec
Pitch and Roll Impulse Requirement	2258. n-sec	2093. n-sec
Total Impulse Requirement	6526. n-sec	6722. n-sec
GN_2 Propellant Weight (for both half-gas systems including factor of 3.0 for thruster failed-on at liftoff. Note: I_{sp} = 655. n-sec/kg)	30. kg	30.8 kg
Ullage or Allowance of 10%	3.	3.
Both Tanks plus Support Structure (tankage factor of 1.5 using a pressure of 2.21 E7 n/m^2)	49.5	51.
Leakage Thrust, Nozzles, Valves, Pressure Regulators and Plumbing	6.0	6.0
Total Torque Source Weight	89. kg	91. kg
Sensors (IRU, Sun/Canopus, etc.), Gimbal Actuators (main engine TVC and antenna), Flight Control Computer, Articulation Control Computer	45.	45.
System Total Weight	134. kg	136. kg

Table VI-18 Configuration A: Total System Weight Using Nitrogen Cold Gas Mass Expulsion System With Yaw Thrusters on Boom (ℓ = 4.8 m)

	e = 0.3	e = 0.5
Yaw Impulse Requirement	1447. n-sec	1540. n-sec
Pitch and Roll Impulse Requirement	2258.	2093.
Total Impulse Requirement	3705. n-sec	3633. n-sec
GN₂ Propellant Weight (for both half-gas systems including factor of 3.0 for thruster failed-on at liftoff Note: I_{sp} = 655. n-sec/kg)	17. kg	17. kg
Ullage or Allowance of 10%	2.	2.
Both Tanks plus Support Structure (tankage factor of 1.5 using a pressure of 2.21 E7 n/m²)	29.	29.
Leakage Thrust, Nozzles, Valves, Pressure Regulators, Plumbing, Booms and Outrigger (8.0 kg)	14.	14.
Total Torque Source Weight	62. kg	62. kg
Sensors (IRU, Sun/Canopus, etc.), Gimbal Actuators (main engine TVC and antenna), Flight Control Computer, Articulation Control Computer	45.	45.
System Total Weight	107. kg	107. kg

Table VI-19 Configuration A: Total System Weight Using Hydrazine/Plenum Dual Propellant Mass Expulsion System With Yaw Thrusters on Solar Panels (ℓ = 0.61 m)

	e = 0.3	e = 0.5
Impulse Requirement for Maneuvers	4257. n-sec	4826. n-sec
Impulse Requirement for Steady State Control	6617. n-sec	6617. n-sec
Hydrazine Propellant Weight for Maneuvers (for both half-gas systems including factor of 3.0 and using I_{sp} = 1770. n-sec/kg)	7. kg	8. kg
Hydrazine Propellant Weight for Plenum System Used for Steady-State Control (for both half-gas systems including factor of 3.0 and using I_{sp} = 1080. n-sec/kg)	18.	18.
Ullage or Allowance of 10%	3.	3.
Both Hydrazine Tanks and Support Structure (tankage factor of 0.2 using a blowdown system where pressure varies from 0.276 E7 to 0.138 E7 n/m^2 and using a tank size of 2 parts tank to 1 part hydrazine)	6.	6.
Leakage Thrust, Nozzles, Valves, Pressure Regulators, Plumbing, Reactor (catalyst) and Both Plenum Tanks (0.0173 E7 n/m^2)	12.	12.
Total Torque Source Weight	46. kg	47. kg
Sensors, Actuators, and Computers	45.	45.
System Total Weight	91. kg	92. kg

Table VI-20 Configuration B: Total System Weight Using Nitrogen Cold Gas Mass Expulsion System With Yaw Thrusters on Solar Panels (ℓ = 0.61 m)

	e = 0.3	e = 0.5
Yaw Impulse Requirement	494. n-sec	558. n-sec
Pitch and Roll Impulse Requirement	51122.	54347.
Total Impulse Requirement	51616. n-sec	54905. n-sec
GN_2 Propellant Weight (for both half-gas systems including factor of 3.0 for thruster failed-on at liftoff. Note: I_{sp} = 655. n-sec/kg)	235. kg	251. kg
Ullage or Allowance of 10%	24.	25.
Both Tanks plus Support Structure (tankage factor of 1.5 using a pressure of 2.21 E7 n/m^2)	380.	415.
Leakage Thrust (.379 n-sec/day for 425 days)	0.5	0.3
Nozzles, Valves, Pressure Regulators and Plumbing	5.7	5.7
Total Torque Source Weight	545. kg	697. kg
Sensors (IRU, Sun/Canopus, etc.), Gimbal Actuators (main engine TVC and antenna), Flight Control Computer, guidance control Computer	45.	45.
System Total Weight	690. kg	742. kg

Table VI-21 Configuration B: Total System Weight Using Hydrazine/Plenum Dual Propellant Mass Expulsion System With Yaw Thrusters on Solar Panels ($\ell = 0.61$ m)

	e = 0.3	e = 0.5
Impulse Requirement for Maneuvers	50561. n-sec	53850. n-sec
Impulse Requirement for Steady State Control	1055. n-sec	1055. n-sec
Hydrazine Propellant Weight for Maneuvers (for both half-gas systems including factor of 3.0 and using I_{sp} = 1770. n-sec/kg)	86. kg	91. kg
Hydrazine Propellant Weight for Plenum System Used for Steady-State Control (for both half-gas systems including factor of 3.0 and using I_{sp} = 1080. n-sec/kg)	3.	3.
Ullage or Allowance of 10%	9.	9.
Both Hydrazine Tanks and Support Structure (tankage factor of 0.2 using a blowdown system where pressure varies from 0.276 E7 to 0.138 E7 n/m^2 and using a tank size of 2 parts tank to 1 part hydrazine)	20.	21.
Leakage Thrust, Nozzles, Valves, Pressure Regulators, Plumbing, Reactor (catalyst) and Both Plenum Tanks (0.0173 E7 n/m^2)	12.	12.
Total Torque Source Weight	130. kg	136. kg
Sensors, Actuators, and Computers	45.	45.
System Total Weight	175. kg	181. kg

ACS propellant usage is due to spacecraft maneuvering between mapping and charging attitudes. This leaves a CMG ACS as the best candidate for Configuration B.

Table VI-13 shows that from weight considerations the reaction wheel systems are not competitive with 4 or 5 skewed simple gimbal CMGs.

Tables VI-13, 14, and 15 give details on the data that were used to compile Table VI-10. Tables VI-16, 17, 18, 19, 20, and 21 give details on the data there were used to compile Tables VI-11 and 12.

In summary, Configuration B requires a 4 or 5 skewed simple gimbal CMG ACS, and a GN_2 ACS is acceptable for Configuration A provided that a sufficiently long yaw moment arm is used.

Time Constraints on ACS Performance - Performance of the Venus mapper ACS is constrained by time in two cases. One case is that the batteries can only be "off the Sun" for a certain amount of time. For purposes of ACS consideration, this time is conservatively taken as one hour. (The worst case Sun occultation time in Venus orbit, e = 0.5, is approximately 1.1 hour). As a baseline goal, the spacecraft will be required to complete all maneuvers in transit or in orbit rapidly enough so that the solar panels are not pointed away from the Sun for more than 1 hour. The worst case maneuver time equals 3481 seconds and it occurs when one main engine is assumed to provide orbit insertion. The burn time can be as high as 2200 sec. The total time for this maneuver also includes time to maneuver to thrusting orientation through 110 deg, time to maneuver to orbital orientation through 110 deg, and time to damp maneuver transients. For another example, the total worst case time required to damp booster separation rates, acquire the Sun through a 180 deg acquisition maneuver, and to damp maneuver transients is 1059 seconds. Therefore, ACS maneuver performance is expected to meet battery time constraints.

The other time constraint is that the time required for antenna positioning must be kept to a minimum. Time spent for antenna positioning is subtracted from the time available for communication with Earth and this in turn affects RF subsystem power requirements. This time constraint affects Configurations A and B. For Configuration A, the antenna must be slewed from the mapping orientation to the communicating orientation. A high slew rate causes correspondingly high ACS propellant usage, unless a CMG system is used. A slow slew rate may not leave enough time for data transmission to Earth. A similar situation exists for Configuration B, but here the entire spacecraft is being slewed instead of just the antenna.

For Configuration A, 0.1 hour total is allowed to position the antenna over and back between mapping and communication. Antenna angular range is ± 90 deg in pitch and ± 135 deg in yaw. Pitch rate is 0.5 deg/sec and yaw rate is 0.75 deg/sec. Thus 0.1 hr. is needed to move the antenna full range. No time is left for damping of spacecraft attitude transients when antenna motion is stopped; however, the antenna usually will not need to travel full range. Also, if necessary, the slew rate can be increased to save time. The present VO '75 gimbal rate can reach 1.0 deg/sec.

For Configuration B, maneuver time over and back between mapping and solar charging is 0.9 hr total including time to damp transients. This requires a maneuver rate of 0.417 deg/sec. To perform this maneuvering for Configuration B, a cold gas system would be too heavy and therefore a CMG momentum exchange system is required.

Antenna Articulation Control Subsystem - This subsection
discusses the interrelation between antenna pointing require-
ments, the ACS, and the antenna articulation control subsystem.
VO'75 Lander specification defines high-gain antenna (HGA) point-
ing control accuracy as the 99th percentile of the total pointing
error for the HGA electrical boresight with respect to the
spacecraft-Earth vector. The HGA pointing control accuracy
requirement is interpreted as one which may not be exceeded
at any time in the mission due to limit cycle motion. VO'75
Lander specification tabulates approximate values of contributions
relative to the interface accuracy requirement for groups of
"3σ value" error sources. The resulting 99th percentile HGA
pointing control accuracy while on celestial reference is 0.70
degree, when an in-flight calibration procedure is used.

When the spacecraft is on inertial reference, the following
3σ error values are used to estimate the HGA pointing control
accuracy.

Table VI-22   Pointing Errors From VO'75 Specifications

Error Source Name	In-Flight Calibrated 3 Value
Gyro & Integrator Drift Rate Uncertainty	0.15°/hr
Accuracy of In-Flight Calibration of Gyro and Integrator Drift	0.065°/hr
Residual In-Flight Calibration Error	0.70 deg

If an occultation time of one hour per orbit is assumed, the HGA pointing control accuracy from Table VI-22 is $(0.15)^2 +$ $(0.065)^2 + (0.70)^{2 \; \frac{1}{2}} = 0.72$ deg. (The VO'75 requirement for HGA pointing control accuracy is 2.5 degrees when the spacecraft is not on celestial reference.)

For the case of the Venus mapper spacecraft, the baseline 3 meter antenna requires a pointing accuracy of 11.9 mrad (0.67 deg). A 4 meter antenna requires a pointing accuracy of 9 mrad (0.515 deg). Therefore, the VO '75 spacecraft essentially meets the Venus mapper baseline requirements on antenna pointing.

Major pointing error sources for the VO '75 spacecraft must be identified before recommendations to improve pointing accuracy can be made. According to reference 10, the major contributors to the HGA pointing control error when on celestial reference and assuming in-flight calibration is the limit cycle deadband, 61.4%; antenna azimuth and elevation gimbal mechanical and electrical null offsets, 9.5%; gimbal actuator resolution error, 11.1%; gimbal actuator feedback pot calibration error, 7.5%; and residual in-flight calibration error, 10.4%. The percentages are in relative percent of the mission requirement for VO '75 which is 0.70 deg. When on IRU reference, a major contributor to the HGA pointing control error is gyro drift.

Based on the preceding percentages, antenna accuracy can be improved by narrowing the ACS deadband and by improving the accuracy of the antenna gimbal servo. Gyros with a lower drift rate can improve the antenna pointing accuracy when on IRU reference. Table VI-23 compares candidate modifications of the VO'75 ACS which would improve the HGA pointing accuracy. A technique not mentioned previously, appearing in Table VI-23, is RF interferometering. This technique is an adaptation of the Pioneer-Jupiter

application. An improved antenna gimbal servo is still required. An immediate and inexpensive way to improve HGA pointing is to reduce the deadband slightly and improve the servo accuracy. This will assure that 3 meter pointing requirements will be met and possibly 4 meter antenna pointing requirements can be met. This approach should be traded off with CMGs and with the RF interferometering technique in future studies.

An example of how the antenna pointing servo can be improved is as follows. The VO '75 antenna control system uses digital control signals, stepper motors, and a feedback potentiometer, all of which may be sources for improving the servo accuracy. Ten bits of actuator position information is used to command the VO '75 antenna over a 204.6 degree range. This is equivalent to a 0.2 degree command step size. There is room here for improvement in accuracy if a register size greater than 10 bits is used for the command signal.

Table VI-23 VO-75 ACS Modifications Comparisons to Improve HGA Pointing Accuracy

VO'75 ACS Modification	Impact	HGA Pointing Accuracy Improvement
Reduce Deadband	ACS propellant usage increases inversely to deadband width. Reduction of ACS thrust to lower propellant usage impacts ACS performance.	Proportional to deadband decrease.
Improve Antenna Gimbal Servo Accuracy	Requires hardware modifications on servo.	Proportional to servo accuracy improvement. Probably can obtain another 0.1 deg accuracy.
Incorporate CMGs	May need better antenna gimbal servos, Sun sensors, and star tracker.	Spacecraft pointing accuracies in arc-min or arc-sec can be obtained.
RF Interferometering	Requires a control loop around the antenna servo. Will need hardware modifications on antenna servo to improve accuracy.	Antenna pointing accuracies of 4 milliradians can be achieved.

Conclusions and Recommendations

In conclusion then, Configuration A (shared antenna configuration) utilizes the present Viking orbiter cold gas attitude control system with some increase in the amount of gaseous nitrogen onboard. The yaw thrusters are moved to the orbiter bus body and the Canopus tracker has been relocated.

Configuration B employs the exiting Viking Orbiter '75 nitrogen cold gas system for vernier delta velocity, booster separation rate reduction, and for CMG desaturation. In addition a 5 skewed simple gimbal CMG system has been incorporated. As in Configuration A, the yaw thrusters have been relocated to the orbiter body and the Canopus tracker has relocated to provide an unobstructed field-of-view.

Mass Properties Estimating Procedures

This section covers the mass properties estimates and parametric data developed for this study. One ground rule of tnis study is to utilize Viking Orbiter (VO) '75 hardware to a maximum. As discussed in Volume II, the Orbiter bus structure and much of its equipment is retained. Whenever possible mass estimates of new equipment is based upon VO '75 components. Thus providing estimates based upon proven, current design conepts for which detail mass data is available.

Propulsion. - Three types of propulsion systems have been studied: versions of the VO '75, high performance Earth storable (310 I_{sp}) system, and space storable systems.

VO '75 versions considered one to four engines and both existing (off-loaded) and stretched tankage. Mass properties data were developed for these variations for all propulsion-dependent hardware, including structure and thermal, pyrotechnics, cabling and engine activators, and are shown in Table VI-24. Data from this table gives the following approximate propulsion sizing equations:

1 Engine $M_{PROP} = 71.35 + 0.133 \, M_p$

2 Engine $M_{PROP} = 101.35 + 0.135 \, M_p$

3 Engine $M_{PROP} = 108.77 + 0.137 \, M_p$

4 Engine $M_{PROP} = 138.32 + 0.140 \, M_p$

VI-68

Table VI-24 Propulsion Dependent Mass, VO'75 Tankage (kilograms)

	1 Engine VO'75 (1 Engine Gimballed)	2 Engines (2 Engines Gimballed)	3 Engines (1 Engine Gimballed)	4 Engines (2 Engines Gimballed)
Fixed Mass				
Structure & Thermal				
Engine Mount	4.94	7.85	9.52	12.70
Thermal Attach	0.54	0.54	0.54	0.54
Thermal Switch	1.95	2.86	3.63	4.54
Pyrotechnics	0.23	0.45	0.77	0.77
Engine Actuator	2.49	4.99	2.49	4.99
Propulsion				
Engine	8.48	16.96	25.45	33.93
Isolation Assembly	11.34	22.68	11.34	22.68
Pyrotechnic Isol.	-----	-----	8.89	8.89
Pressurization Control	15.15	15.15	15.15	15.15
Piping & Misc.	-----	.91	1.36	1.81
Tankage Fixed Wt.	3.08	3.08	3.08	3.08
Total	48.20	75.47	82.22	109.08
Contingency 10%	4.82	7.55	8.22	10.91
Trapped Propellant	18.33	18.33	18.33	18.33
	71.35	101.35	108.77	138.32
Variable Mass				
Structure & Thermal				
Thermal Blanket	8.75	8.75	8.75	8.75
Tank Support	11.88	11.88	11.88	11.88
Pressure Tank Support	2.81	2.81	2.81	2.81
Cabling	3.36	6.21	9.07	11.93
Propulsion				
Pressure Tank	37.19	37.19	37.19	37.19
Pressure Gas	4.22	4.22	4.22	4.22
Fuel Tank	50.71	50.71	50.71	50.71
Oxidizer Tank	50.71	50.71	50.71	50.71
Total	169.63	172.48	175.34	178.20
Contingency 10%	16.96	17.25	17.53	17.82
Total	186.59	189.73	192.87	196.02
Variable Factor	0.1328	0.1351	0.1373	0.1396

NOTE: VO'75 Propellant Capacity
Usable   1404.8
Trapped   18.3
Total   1423.1

Most of the data in Table VI-24 came directly from basic Viking
Orbiter data. However, several assumptions are made relative to the
addition of engines. One is that for the two engine configuration
both engines will be gimballed, for three engines only one engine
will be gimballed, and for four engines two of the four will be
gimballed. The other assumption is that isolation valves for gim-
balled engine will each have its own pair of valves identical to
VO '75 units and pyro valve isolation assemblies will be used for
each pair of fixed engines which require activation only for orbit
insertion.

A mass estimate for this pyro valve assembly, based upon the
VO '75 components is shown in Table VI-25

Table VI-25 Pyro Valve Isolation Assembly Mass Estimate

Pyro Valves, 3 @ 0.39 (per VO'75)	1.17
Filter (capacity increased over VO'75)	1.01
Low Pressure Transducer (per VO'75)	0.20
Service Valve, 2 @ 0.08 (per VO'75)	0.16
Total Components	2.54
Structure Piping, etc. . . (per VO'75)	1.90
Total Assembly	4.44
Ordnance Required, 3 @ 0.09	0.27
Total Assembly including Ordnance	4.71

Additional items associated with the number of engines are
cabling and engine mounts. For this study the mass of cabling
is increased directly as the number of engines. The engine moun-
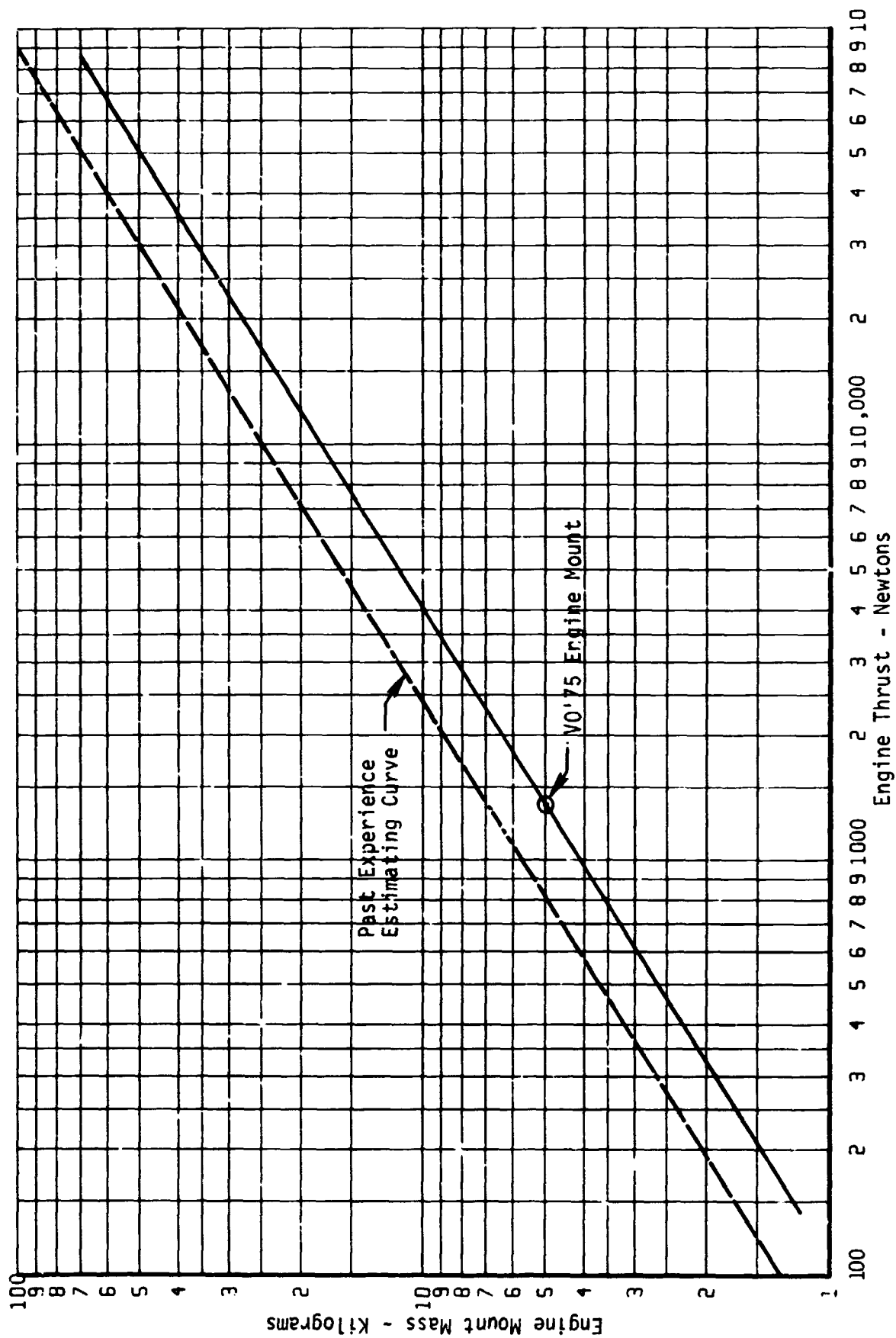mass is taken from the curve, Figure VI-17.

Figure VI-17 Engine Mount Mass Estimating Curve

In addition to the approximate sizing factors shown, detail factors for growth tank versions are developed using geometry of the VO'75 tanks and other emperical parameters. The detail estimating technique and factors are summarized in Table VI-26.

Table VI-26 Detail Tank Stretch Mass Estimating

Baseline VO'75 Reference Size	
Usable Propellant	1404.8 kg
Tank Diameter	0.914 m
Tank Length	1.372 m
Straight Section Length	0.457 m

Tank Stretch

$$M_{P\Delta} = M_P - 1404.8$$

Tank Stretch Meters $\Delta L = M_{P\Delta}/35.88$

New Tank Length $L = \Delta L + 1.372$

Stretch Ratio $R = L/1.372$

Mass Factors

M_B - Thermal Blanket = 8.75 R

M_C - Cabling = M_{ci} R

Where M_{ci} is mass of cabling for particular number of engines in Table VI-24

M_T - Propellant Tanks = 83.42 + 1.268 L + 18R

M_G - Pressure Shell and gas = 0.0298 M_p

M_{TS} - Propellant Tank Support (from Fig. VI-18 using $M_p + M_T$)

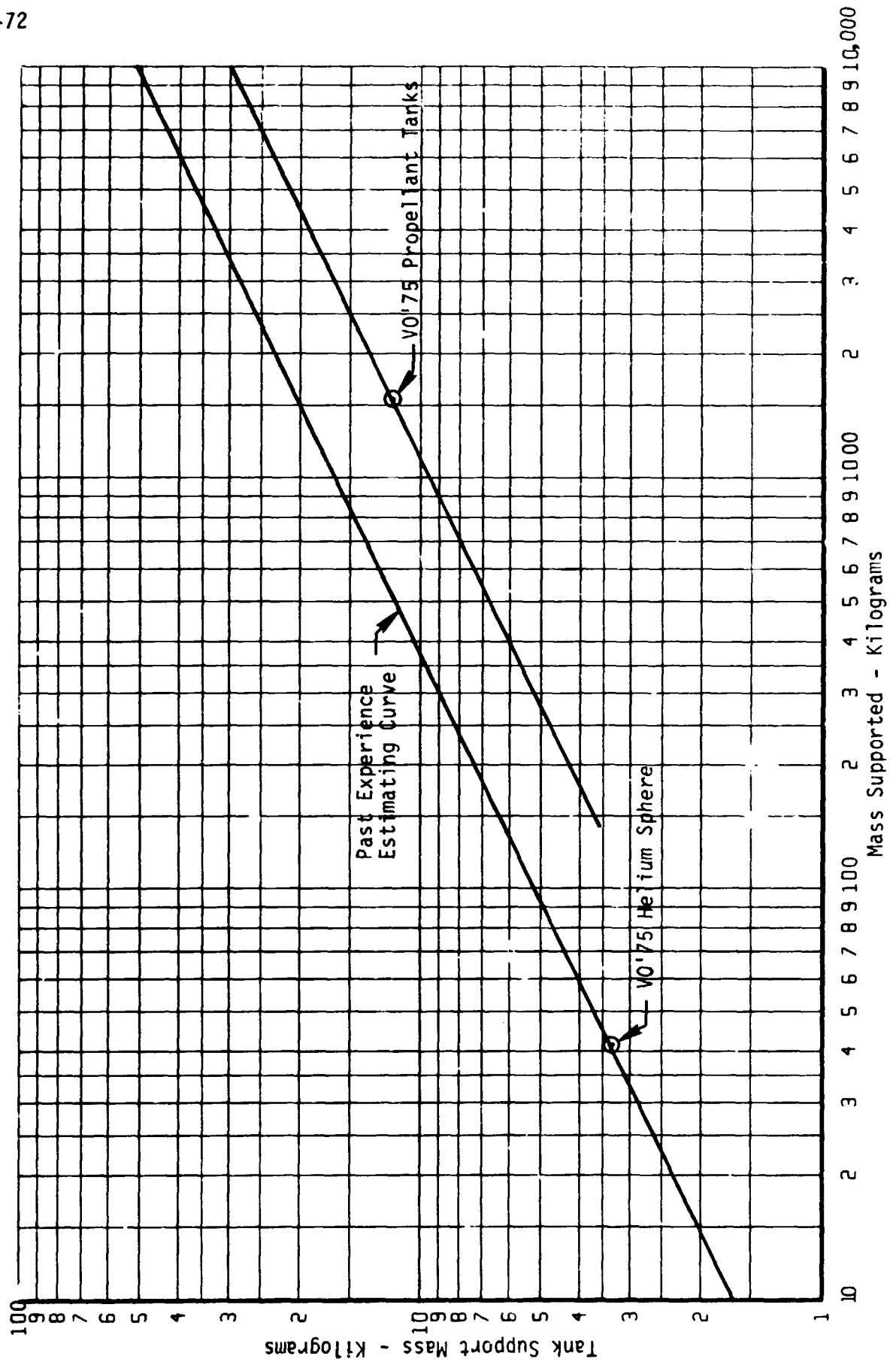M_{PS} - Pressure Tank Support (from Fig. VI-18 using W_G)

Figure VI-18   Tank Support Mass Estimating Curve

The high performance Earth storable (310 I_{sp}) system was considered only to the extent of developing an approximate sizing equation. The system is an Earth storable design using nitrogen tetroxide and hydrazine. Tankage used was the same as VO'75 so it was only necessary to develop a new fixed weight. This was developed as follows.

Engine (4448.2 newtons thrust)	19.50
Engine Mount	10.88
Isolation Assemblies (increased flow)	13.61
Engine Actuators	5.44
Thermal	2.81
Pressure Control	15.15
Contingency 10%	6.74
Trapped Propellant	18.32
Total Fixed	92.45

This gives the following approximate sizing equation

$$M_{PROP} = 92.44 + .133\ M_p$$

The space storable propulsion system considered for this study uses fluorine(F_2) and hydrazine (N_2H_4) with a nominal I_{sp} of 3677.5 newton sec/kg and two 2668.9 newton thrust engines. The oxidizer tank is fabricated of aluminum and the fuel tank of titanium.

To be able to develop propulsion system mass data for various size systems the point design masses were estimated and divided into fixed and variable items. Table VI-28 gives this division of all of the propulsion dependent items on the spacecraft. Also shown are the variation relationships for each variable item. The following approximate sizing equation comes from data in Table VI-27.

$$M_{PROP} = 123.77 + 0.134\ M_p$$

Table VI-27 Space Storable Specific Sizing Factors

Item	Mass (kilograms)			Variation Factor
	Total	Fixed	Variable	
Structure & Thermal				
Tank Support	13.61		13.61	$M_p + M_T$ (curve Fig. III-2)
Press. Tank Support	9.07		9.07	$M_p + M_T$ (curve Fig. III-2)
Eng. Mount	12.25	12.25		
Blanket & Shield	7.98		7.98	$D/1.16$
Oxidizer Tank Foam	5.44		5.44	$D^2/1.16^2$
Blanket Attachment	0.54	0.54		
Pyrotechnics	0.45	0.45		
Cabling	6.39	1.36	5.03	$(2 \times D + 0.18)/2.49$
Attitude Control System	5.44	5.44		
Propulsion				
Pressure Gas	10.97		10.97	$M_p/1807.6$ (incl. trapped)
Pressure Tanks	85.05		85.05	$M_p/1807.6$ (incl. trapped)
Pressure Control	18.14	18.14		
Fuel Tank	25.81	2.72	23.09	$M_p/1807.6$ (incl. trapped)
Oxidizer Tank	44.18	2.72	41.46	$M_p/1807.6$ (incl. trapped)
Propellant Management	15.87		15.87	$M_p/1807.6$ (incl. trapped)
Isolation Assy	12.25	12.25		
Piping	0.91	0.91		
Engines	37.19	37.19		
Total	311.54	93.93	217.57	
Contingency	31.15	9.40	21.75	
	342.69	103.37	239.32	D = Diameter in Meters
Trapped	20.40	20.40		
TOTAL	363.09	123.77	239.32	

RTG Power System Study - In order to study an RTG alternate
power system, a computer run (CBK) for a configuration of interest
with VO'75 tankage was modified to develop mass properties of an
RTG configuration. The average power requirement for this con-
figuration is 490 watts. This assumes one of the two VO'75
batteries is retained to handle peak power demand. To provide a
one RTG out capability the following options are available: three
250 watt RTGs, four 165 watt RTGs, five 125 watt RTGs. Currently
development is under way on a 150 watt RTG with a mass of 31.75 kg.
This unit could probably be modified to satisfy the four RTG case
or used directly for the five RTG case. However, installation of
four or five RTGs on a VO'75 bus, considering thermal and mounting
location difficulties, appeared undesirable.

Because RTGs in this size range are in the development
stage the three 250 watt RTG configuration was assumed. Past
experience has shown that RTG mass varies directly with wattage.
Therefore a 250 watt RTG mass is estimated to be 60 kg. With three
RTGs the spacecraft will be heavier than the solar panel version
and an estimated 106.6 kg of additional propellant would be re-
quired. This increase will still fit in the VO'75 tankage. The
comparison of mass properties shown in Table VI-28 were used to
check attitude control sizing. That check indicated no net change
to the attitude control system.

Thermal Control - The thermal control systems for Venus Or-
bital Mappers vary for each configuration. However, they all con-
sisted of the following elements:

Table VI-28 Venus Orbiter Mapper Mass Properties
Comparison Solar Cell vs RTG Electrical System

	Mass	c. g. cm			Moment of Inertia kg m^2		
	kg	X	Y	Z	K_x	K_y	K_z
Solar Cell Configuration							
Liftoff	2023.5	4.6	0.9	-38.2	1196.1	2107.7	1842.3
Pre-Insertion	2002.4	4.6	0.9	-37.8	1190.7	2098.3	1835.5
In Orbit (Antenna Extended)	1005.6	.7	-8.5	- 6.1	1189.3	1556.4	1853.1
In Orbit (Antenna Retracted)	1005.6	.7	1.8	- 6.1	861.5	1556.4	1526.6
Burn Out	1002.4	.6	1.9	- 5.4	860.2	1553.7	1525.3
RTG Configuration							
Liftoff	2236.3	6.2	4.5	-38.2	1345.1	1742.9	1572.7
Pre-Insertion	2213.1	6.2	4.6	-37.9	1339.7	1742.0	1565.9
In Orbit (Antenna Extended)	1114.6	3.8	-0.2	- 6.3	1319.4	1148.7	1568.6
In Orbit (Antenna Stowed)	1114.6	3.8	9.1	- 6.3	975.3	1148.7	1224.6
Burn Out	1110.8	3.8	9.1	- 6.1	972.6	1146.0	1227.3

Louvers used on 3 bays

    VO'75 mass = 0.816 kg each

Heat pipes: mass per meter for heat pipes was developed as follows:

Aluminum tube 1/2 in. x 0.035	0.0911 kg/m
Attachment (aluminized epoxy)	0.0678
Freon and wick	0.0286
Total	0.1875 kg/m

Total estimate with and without separate radiator follows:

	With Radiator	Without Radiator
Heat Pipes in Bus 10.7 m x 0.1875	2.0 kg	2.0 kg
Fittings and Lead to Radiator	0.27	0.73
Helium Compensator		0.45
Total	2.27 kg	3.18 kg

Mass per square meter for radiators using heat pipes as the transfer medium is developed as follows assuming 0.15 meter spacing between pipes.

Aluminum Plate (0.060)	4.20 kg/m^2
Second Surface Mirrors (OSRs)	0.83
Heat Pipes	1.22
Back Side Insulation	0.68
Misc. Framing and Fittings	0.88
Total	7.81 kg/m^2

Miscellaneous Items are estimated on a mass per square meter basis.

Second Surface Mirrors (OSRs)	0.83 kg/m^2
Insulation	0.68 kg/m^2

VI-78

Communications and Data Handling - Mass estimates for the com-
munications TWTA are based on the curve (Figure VI-19) of mass
vs average output power, and assumes redundant TWTAs, power supply,
and other necessary electronic components.

Two elements of data handling gear are added to all configur-
ations; an A to D converter and a video processor. Mass estimates are
based upon mass of cased units (adequate for the requirements) mod-
ified to uncased configurations for insertion into the VO'75 bus:

A to D converter   5.67 kg
Video processor   7.03 kg

Antenna Items- Mass estimates for the various antennas and
antenna mount and drive systems come from data on similar elements
from VO'75 and other sources.

Two types of dish and hub designs are used. A rigid dish is
used for antennas up to 3.66 meters diameter. All larger dishes
and all Configuration C dishes are furlable mesh type. Mass esti-
mates for rigid dishes are based upon the emperical equation
$M_D = 0.32 + 2.7 A^{0.75}$ developed from analyses of a number of
antennas. In this equation A = dish area in square meters and
M_D includes approximately 0.45 kg of hub mass. The mass of furlable
antennas are estimated on the basis of 0.39 kg per square meter
antenna area plus 8.16 kg for unfurling mechanism.

Antenna feed weight was estimated based upon the particular
antenna as follows:

Share Antenna   1.81 kg
Dedicated Radar Antenna   1.81 kg
Tower Mounted Radar Antenna   1.36 kg
Communications Antenna   3m   1.36 kg
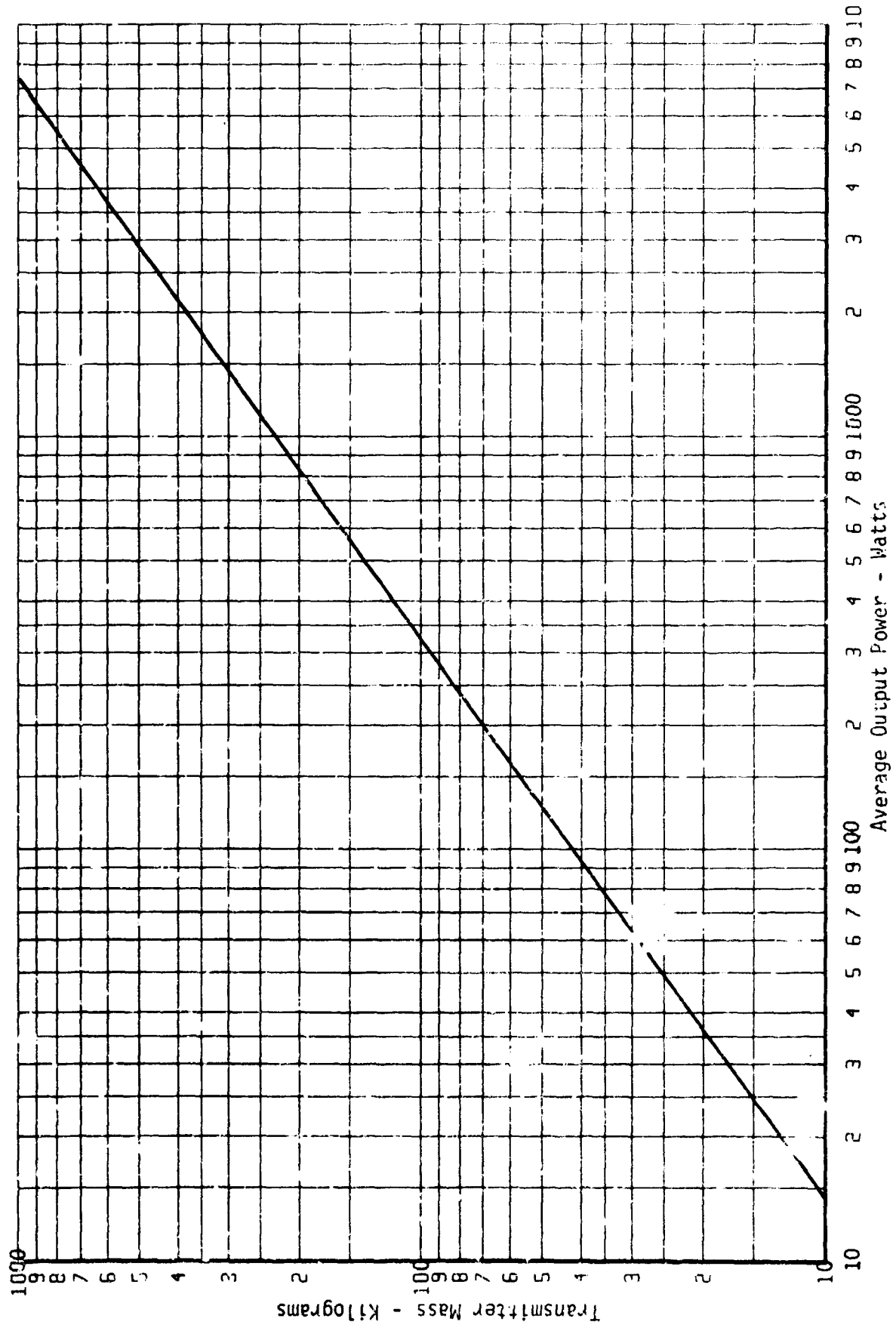Communications Antenna   4m   1.59 kg

Figure VI-19   Communications Transmitter Electronics Mass Estimating Curve

There are three basic antenna support and drive mechanisms used for mass estimating purposes. These are categorized as deployment booms, fixed support, and center tower. The following mass estimates for these designs are derived from VO'75 high gain antenna.

The deployment boom consists of:

Upper Gimbal		3.22 kg
Housing	2.22	
Articulation Drive	0.73	
Waveguide Swivel	0.27	
Boom		5.12
Structure $0.95\left(\dfrac{1.52}{0.76}\right)^{1.6}$	2.86	
Waveguide $1.13\left(\dfrac{1.52}{0.76}\right)$	2.26	
Lower Drive		2.
Housing	1.13	
Articulation Drive	1.54	
Waveguide Swivel	0.27	
Lower Drive Support		
Long Support		4.08
(Drive point 0.61 m from Bus A configuration)		
Short Support		2.04
(Drive point 0.1 m from Bus all but A configuration)		
Launch Latch		3.22
Mechanism (per VO'75)	0.95	
Truss Support	2.27	
Total with Long Support		18.58 kg
Total with Short Support		16.54 kg

The fixed antenna support required for the dedicated radar antenna is estimated at 1.81 kg.

Some radar antenna concepts considered mount to a central tower on the centerline of the Orbiter bus. The antenna short dimension determines the height of this tower. Mass estimates for these towers for representative tower heights are summarized below:

Overall Tower Height (meter)	0.89	1.57	1.88
Upper Drive (mass kg) (Articulation .73, waveguide .27 kg)	2.49	2.49	2.49
Lower Drive (mass kg) (Articulation 1.54 kg, waveguide .27 kg)	3.40	3.40	3.40
Upper Mast	2.73	5.12	6.21
Structure 2.0		3.58	4.31
Waveguide .73		1.54	1.90
Lower Mast(Waveguide 2.5)	3.17	3.17	3.17
TOTAL	11.79	14.18	15.27

Radar Electronics - Radar electronics mass estimates utilize JPL travelling wave tube estimating equations. These equations are given in Table VI-29

Table VI-29 Radar Electronics Weight Estimate Equations

$$TWT = 0.55 \ (\lambda/0.3)^{0.4}(P)^{0.6}$$

$$\text{High Voltage Power Supply} = 4.55 + 0.455 \ (P/0.4)^{0.5} \ (\lambda/0.3)^{-0.28}$$

$$\text{Modulator} = A \text{ Constant} = 3.18 \text{ kg}$$

$$\text{Energy Storage Capacitor} = 34.5/PRF \ (P/0.4) \ (\lambda/0.3)^{-0.57}$$

$$\text{Filament Current Supply} = \text{Constant} = 1.36 \text{ kg}$$

$$\text{Clutter lock and Beam Splitter} = \text{Constant} = 1.5 \text{ kg}$$

$$\text{Receiver} = \text{Constant} = 1.18 \text{ kg}$$

$$\text{Miscellaneous} = 3\% \text{ of above}$$

Where: λ = wavelength = 0.1 for this study

P = average power = watts

PRF = pulse repetition frequency -

Radar Altimeter - The Viking Lander radar altimeter was
assumed for mass estimating purposes, with the addition of co-ax
interconnect between the electronics and the antenna as follows:

Radar Electronics	4.58 kg
Antenna	0.59
Co-ax Cable	0.73
Total	5.90 kg

Attitude Control System - The attitude control system can be
considered in two parts; the sensing and computing system and
the maneuvering system. For this study mass of the sensing
and computing system is assumed identical to the VO'75 except
that for configurations where a 1.36 kg rotation device will be
required on the Canopus sensor. Sensing and computing elements
mass are contained in the weight of the stripped bus.

Early studies considered two types of mass expulsion maneuver
systems; cold gas and dual mode hydrazine thruster/plenum, and
two types of momentum exchange systems; control moment gyros and
reaction wheels. Two of these were eliminated based upon approximate
mass estimates and other considerations. Therefore, detail mass
estimating data was developed for only the cold gas N_2 system and
the 3 gyro CMG system.

Table VI-30 gives a typical mass estimate of an N_2 maneuver
system. The momentum exchange system using control moment gyros
appears optimum for configurations which have greater maneuver
requirement. An N_2 gas system is used for gyro desaturation.
A typical momentum exchange system mass estimate is given in
Table VI-31.

Table VI-30 Attitude Control Maneuver System
Mass Expulsion Type
Typical Estimate Calculation

Gas Required from Calculations		4.14 kg
Sample Mass Calculation - kg		
Times Factor of 2	8.28	
Ullage and Leakage 5%	.41	
Total Gas		8.69
Gas Spheres 8.69 x 1.23		10.69
Sphere Supports (in bus)		
Pressure Module 2 @ 2.653		5.31
Nozzles		
On + X 6 @ 0.193 = 1.16		
On - X 6 @ 0.193 = 1.16		
On + Y 4 @ 0.193 = 0.77		
On - Y 4 @ 0.193 = 0.77		
(1.5 kg in stripped orbiter)		
Piping		2.37
On X Axis 2 @ 0.73 = 1.46		
On Y Axis 2 @ 0.45 = 0.91		
(1.36 kg in stripped orbiter)		
TOTAL SYSTEM		30.92

Table VI-31 Attitude Control Maneuver System Energy Exchange Type

	Mass (kg)
Control Moment Gyros, 5 @ 2.55	
(from Figure VI-20, `^.5 n-m-sec)	12.75
CMG Electronics	10.00
Gyro Desaturation System	
Total Gas Provided	14.00
Spheres, 14 x 1.23	17.22
High Pressure Modules	5.31
Nozzles, 12 @ .193	2.32
Piping, 2 @ .73	
(1.5 kg nozzles and 1.36 kg piping	
in stripped orbiter)	1.46
TOTAL SYSTEM	63.06

Total Vehicle Estimates - The first step of a total vehicle estimate is to develop a non-propulsion dependent mass. When this has been achieved the propulsion dependent mass and required propulsion is estimated using approximate sizing equations and required delta V for the first iteration, and detail stretch or sizing factors for later iterations. This is a tedious iteration process and will not be shown in this report. However, all of the mass data required to perform the iteration are shown in this section and the delta V data is given in Section III. When propellant required is less than VO'75 capacity (1404.8 kg usable) the full VO'75 tankage is used.
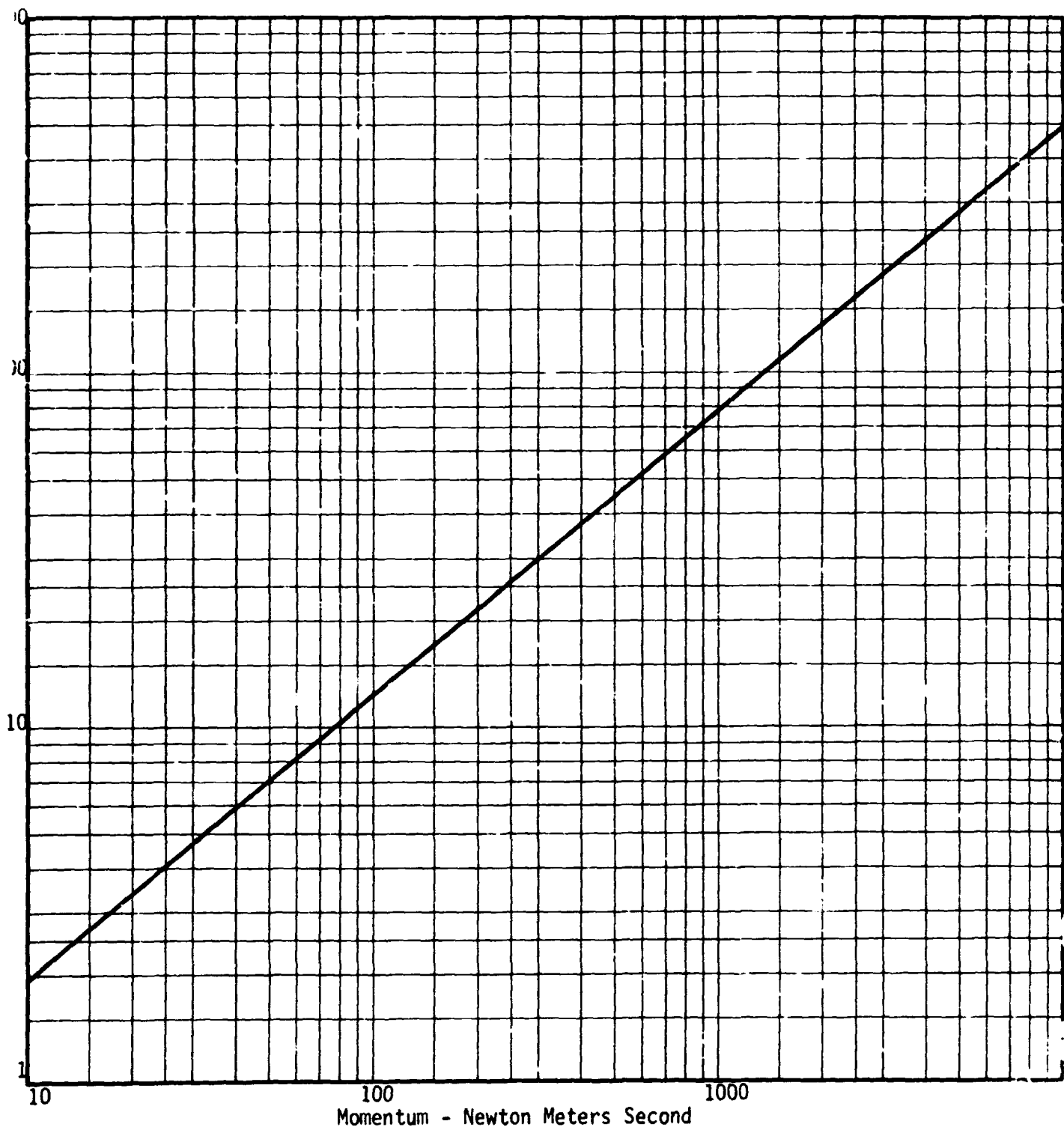
Figure VI-20   Control Moment Gyro Mass Estimating Curve

Propellant mass calculations are based on nominal I_{sp} of
2856.7 N-sec/kg for VO'75 propulsion systems and 3677.5 N-sec/kg
for space storable propulsion systems when operating as a bi-
propellant. A nominal I_{sp} of 2255.5 N-sec/kg is used for space
storable systems operating in the monopropellant mode. Two
percent of the nominal usable propellant is assumed as reserve.
This reserve is part of the propellant value shown in Table
VI-27 (Vol. II) and is assumed unburned in the burn out condi-
tions of Table VI-28 (Vol. II). Propellant calculations are
made for three mission phases, midcourse, orbit insertion and
orbit trim. For midcourse the space storable system operates in
a monopropellant mode, and the VO'75 system is operated on only
gimballed engines. Full power from all systems is required for
orbit insertion. Orbit trim is assumed necessary for e 'n the
e = 0.5 orbits and again only gimballed engines are used.

REFERENCES AND BIBLIOGRAPHY

VI-1   J. F. Stocky: *Extrapolations Based on VO'75 Propulsion Subsystem Mass and Performance,* Additional Data. JPL VO75-72-333, May 17, 1972.

VI-2   J. F. Stocky: *Propulsion Subsystem Extrapolated Performance Data for Future Viking Missions.* JPL VO75-72-379, June 9, 1972.

VI-3   R. G. Ross, Jr., R. K. Yasui, W. Jawctski, L. Wen, E. L. Cleveland: *Measured Performance of Silicon Solar Cell Assemblies Designed for Use at High Solar Intensities.* JPL Technical Memorandum 33-473.

VI-4   F. A. Blake: *A Computer Program to Obtain Solar Panel Performance Between 0.3 and 3.8 Suns Intensity.* Martin Marietta Corporation, T 70-48824-008.

VI-5   *The Revised Solar Array Synthesis Computer Program.* Prepared by RCA Corporation for Goddard Space Flight Center under Contract No. NAS5-11669, February 1, 1970.

VI-6   J. A. Stevenson, J. C. Grafton: *Radiation Heat Transfer Analysis for Space Vehicles.* Aeronautical Systems Division Technical Report 61-119 Part I, December 1961.

VI-7   H. Posnansky: *Momentum Exchange Technology Manual.* Martin Marietta Aerospace, Denver Division Report No. T-71-48842-002, December, 1971.

VI-8   H. Posnansky: *CMG Control Laws for Precision Attitude Control.* Martin Marietta Aerospace, Denver Division Report No. R-72-48677-001, December, 1971.

VII. Preliminary Evaluation of Compatible Groupings

VII. PRELIMINARY EVALUATION OF COMPATIBLE GROUPINGS

INTRODUCTION

The choice of an appropriate mission and system design for an
orbital radar mapper of Venus is based on a combination of many
systems compromises. There are strong interactions between the
mapping strategies selected; such as frequency, coverage and reso-
lution on the one hand, and the mission design parameters of orbical
eccentricity and periapsis altitude on the other. The final choices
of these mission design parameters in turn affect the selection of
subsystem alternatives for the radar antenna, power, attitude con-
trol, data handling, communications and propulsion. It is for these
reasons then, that the early part of the study addressed itself to
the parametric evaluation of the various mission and system tradeoffs
in order to define boundary conditions and limiting designs. The
basic system and mission parametric data that have been generated
are integrated into compatible mission and system groupings. Alto-
gether, twenty-six combinations of radar system frequencies, map-
ping strategies, orbital eccentricities and antenna designs are con-
sidered. These twenty-six compatible groupings are configured into
five spacecraft categories. Four of the five spacecraft concepts
utilize the basic Viking Orbiter configuration, while the fifth
concept employs an outer planets spacecraft configuration.

The four concepts which utilize the basic Viking Orbiter config-
uration have been developed to assess the system impact of various
combinations of radar and communications subsystems. The four con-
cepts evaluated are: a shared parabolic antenna design, a shared
rectangular antenna, an articulated radar antenna combined with a
fixed communication antenna, and a fixed radar antenna combined
with an articulated communications antenna. The shared parabolic

antenna concept necessitates that the radar system be limited to L-band frequencies in order to meet PRF and coverage constraints. Since the use of L-band is not optimum from a science standpoint this concept has been de-emphasized from further study. The articulated radar antenna concept with a fixed communications antenna yielded packaging and attitude pointing problems which eliminates it as a viable study concept.

The outer planets spacecraft concept has been studied to evaluate the systems impact of using RTGs as the primary spacecraft power source. This concept also has been de-emphasized from further study because of the weight and environmental problems associated with the use of RTGs as well as the attendant problems derived from the requirements for an earth-fixed attitude and the necessity of developing an entirely new spacecraft.

The remaining two spacecraft concepts; the shared rectangular antenna and the fixed radar antenna with an articulated communications antenna, are carried through the study and expanded as required to develop an acceptable mission. The impact of eccentricity, data processing level and frequency were defined for these concepts. The costs of adding dual frequency, dual polarization, multiple viewing angles, and fine resolution mode were also assessed.

SPACECRAFT STUDY CONFIGURATIONS

Five major categories of spacecraft designs have been identified during the systems and mission parametric phase of the study. The basic goal of each of these alternative spacecraft designs is: "How do we maximize the spacecraft's payload capability, while at the same time minimize the spacecraft's total weight?" The incentive, of course, is the potential program cost savings that may be achieved while still delivering adequate payloads to satisfy the basic mission

requirements. In keeping with this philosophy then, the designs to be studied are selected on the basis of adequate payload capability, existing systems utilization, minimum modifications required to be made to existing payload delivery systems (Viking/Mariner and Outer Planets classes of spacecraft), and the flexibility of payload usage (i.e., identification of increased system complexity for adding mission versatility and increasing science enhancement).

Table VII-1 presents the five basic design options that have been identified during the systems and mission parametric study. Each of the design options presented meet all study objectives and guidelines, and are all capable of accommodating the range of mission parameters described in Section III.

Table VII-1 Spacecraft Options Considered

A. A single articulated parabolic antenna that is shared between the mapping and communication subsystems.

B. A single articulated rectangular antenna that is shared between the mapping and communication subsystems.

C. A fixed radar antenna with an articulated communications antenna.

D. A fixed communications antenna with an articulated radar antenna.

E. An outer planets type vehicle with a fixed communications antenna and an articulated radar antenna.

Referring to the five basic design options A through E identified in Table VII-1, Option A, the shared parabolic antenna concept forces the radar system to L-band frequencies in order to meet PRF and coverage constraints. The use of L-band frequency is not entirely desirable from a science standpoint therefore this design option is not carried forward into the detailed configurational studies. Option D, yielded relatively complex packaging and pointing problems and thus it too is not evaluated in detail. Option E which was generated to reflect the possible use of an outer planets type of

vehicle with RTGs as a power source has been de-emphasized because
of the weight and environmental problems associated with RTGs, as
well as pointing problems derived from the requirement for an Earth-
fixed attitude. The remaining two options; Options B and C, are
carried through the detailed spacecraft integration studies and are
described in detail in the following sections.

Many subsystem implementation alternatives have been evaluated
for the two options examined, each of which satisfied the mission
options that were developed during the parametric evaluation phase
of the study. Each of these implementation alternatives have been
evaluated to some degree to assess their impact on the total space-
craft integration problem. However, to prepare configurational lay-
outs of each of these possible alternatives would obviously have
been prohibitive. Thus, the approach has been to utilize the recom-
mended subsystem configurations that result from the individual sub-
system parametric studies and to integrate them into an overall
spacecraft configuration. The resulting configurational layouts
then, should be considered as representative of a spacecraft that
would satisfy the two general classes of options considered, viz,
the shared and dedicated antenna options.

Shared Antenna Configuration

The shared antenna spacecraft configuration is shown in Figure
VII-1. The configuration shown is sized for an e = 0.5. It con-
sists of the basic Viking Orbiter structure, both the octagonally
shaped bus and propulsion modul and the adapter truss which attaches
the orbiter to the Titan III/Centaur launch vehicle. Outriggers are
attached at the short side of the bus to provide support for two
solar panels at their hinge line. The solar arrays have a total cell
mounting area of 7.6 m^2 and generate 870 W of gross power in Venus
orbit. A symmetrically cut parabolic antenna, 3.05 meters by 1.75
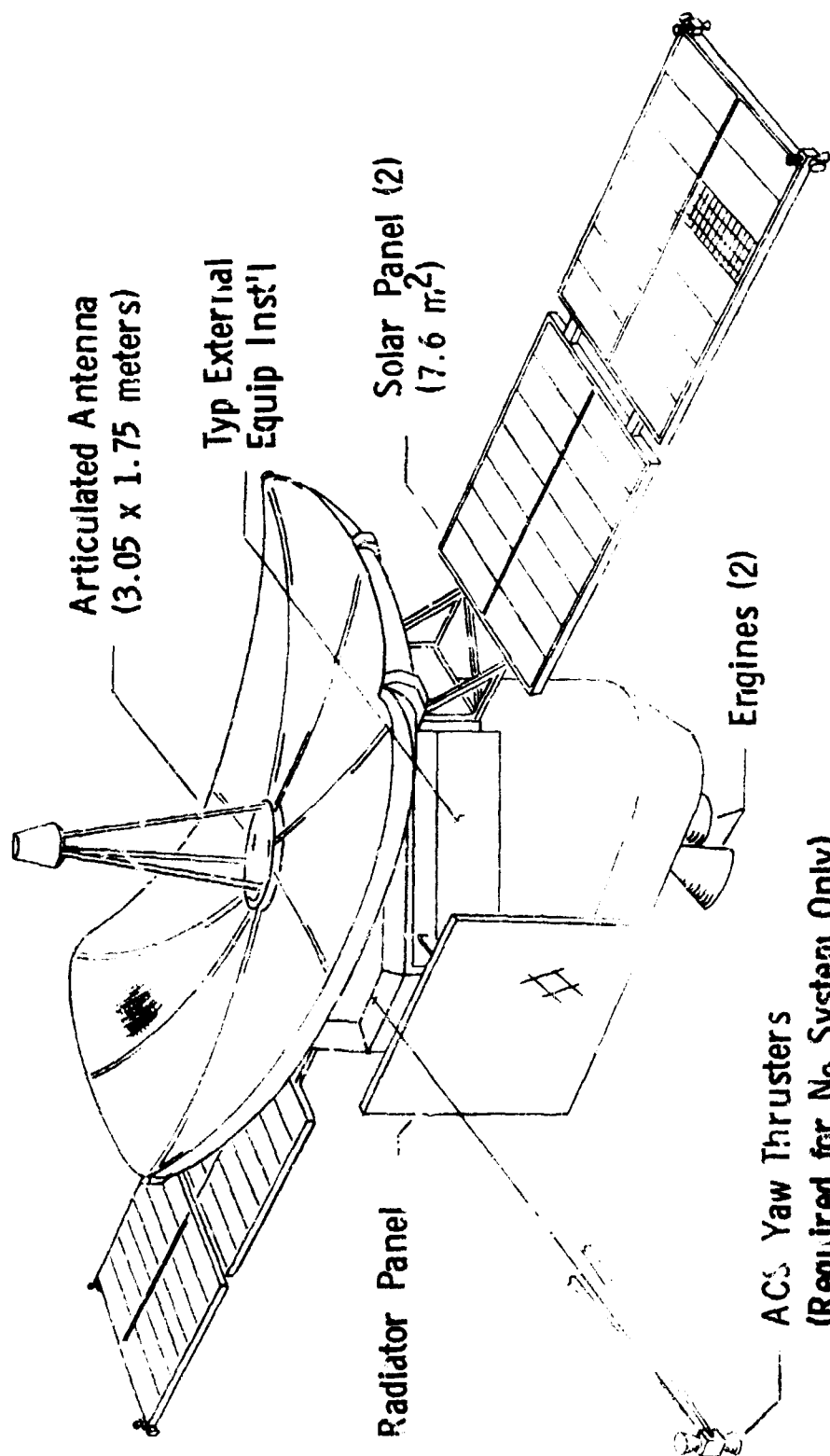meters, is attached to the basic orbiter bus at the same attachment

Articulated Antenna
(3.05 x 1.75 meters)

Typ External
Equip Inst'l

Solar Panel (2)
(7.6 m^2)

Engines (2)

Radiator Panel

ACS Yaw Thrusters
(Required for N_2 System Only)

Figure VII-1 Spacecraft Configuration – Shared Antenna

points as the present Viking '75 Lander is mounted. The primary
propulsion system is the basic Viking Orbiter system with two 1330
nt (300 lbf) thrust engines instead of the single one used in Viking
'75.

The solar array assembly consists of a fixed two panel array
located 180° apart and mounted to the short side of the orbiter bus
by means of outriggers. Cable harnesses and attitude control plumb-
ing are routed on the outriggers to the solar panels. The cell sur-
face is a single skin on transverse corrugations supported on beams.
The panels are folded down and their tips are supported by the space-
craft adapter during launch. A damper assembly is provided at this
tiedown to attenuate vibration response of the panels. Nickel cad-
mium batteries are used as a secondary source of power during periods
of Sun occultation.

The 3.05 meter by 1.75 meter symmetrically cut parabolic shared
antenna is mounted on the upper surface of the Viking orbiter bus
by means of an antenna boom arrangement with a biaxial rotation
joint. Care has been taken to preclude shading of the solar array
and obstruction of optical sensor fields of view by any pointing
position of the antenna. This antenna is used for both mapping and
communications and is articulated with two degrees of freedom.
S-band frequencies are used for mapping purposes while X-band is
employed for data transmission to Earth.

Three-axis attitude control of the vehicle is provided by a
hydrazine/plenum type of system employing four clusters of three
thrusters each mounted on the tip of each solar panel. Yaw thrus-
ters are located on the orbiter bus. Total impulse requirements
are approximately 13560 n-secs. Four systems were initially examined
for a shared antenna configuration. These were: a nitrogen cold
gas with yaw thrusters on a boom, and CMGs combined with a nitrogen
cold gas system. The nitrogen cold gas system weight was found to

be prohibitive (224 kg) therefore it was eliminated from further consideration. The remaining three systems were competitive from a weight standpoint. The hydrazine plenum system was selected as the recommended ACS system since it is an operational system and needs only to be flight qualified. The propellant for the ACS system is housed in spherical bottles located within the octagon shaped bus structure.

Celestial sensors comprised of a Canopus sensor, cruise and acquisition Sun sensors, Sun gate, and a stray light sensor, are mounted on the appropriate sides of the bus and solar panels to meet the required fields of view of the instruments.

The inertia' reference units consisting of gyros, inertial sensors and electronic controls are also mounted within the orbiter bus structure.

The primary propulsion system is the basic Viking orbiter system. It consists of two cylindrical propellant tanks which are attached by a network of trusses. These trusses structurally integrate the propulsion tankage and provide the primary load path and attachment interface between the assembled propulsion module and the bus structure assembly. For this spacecraft configuration and an orbital eccentricity of 0.5 the propellant requirement is approximately 245 kg less than is required for the basic Viking '75 mission. The pressurant tank assembly consists of a single spherical tank containing helium for pressurizing the propellant tank and is located in the upper portion of the propulsion module assembly between the two propellant tanks. The engine support structure attaches to the propellant tanks and locates the two engines on the spacecraft Z axis. Two engines instead of one (used for the Viking '75 mission) are required for the Venus Mapping Mission in order to reduce the orbit insertion burn duration. Later finite burn loss studies discussed in Volume II require three engines.

Electronic assemblies are housed within the eight-sided bus structure assembly. Compartments are approximately .51 meters and 1.4 meters in width. Twelve standard size bays are provided for electronic assemblies and four smaller bays, centrally located on each long side, are equipped with structural closures and mounting provisions for interfacing mechanical equipment. Where possible the black boxes required to support the radar and communications subsystems would be installed in these equipment compartments in space now occupied by Viking Orbiter components that are not required for this mission. Provisions have been made, however, to also house this equipment external to the basic octagon orbiter bus if required.

The thermal control design approach employs the "enclosure concept" whereby the equipment compartment is partially isolated from the thermal environment by the use of multilayer insulation, and partially coupled to it by a radiator. The surface of the radiator is highly reflective in the solar wavelength (0.25 to 0.75 microns), in order to minimize the effects of the external environment, which is "hot" in the solar wavelength only. Radiator surface area requirements are approximately 1.8 m. The principal thermal transients encountered in orbit are due to the relatively high peak-to-average internally generated power during the mapping and relay phases. An internal heat pipe is used to "isothermalize" the compartment, thus making the entire thermal mass of the compartment effective in smoothing out these internal temperature transients.

The weight of the shared antenna concept is summarized in Table VII-2 at the subsystem level. Useful weight in orbit which is defined as the total spacecraft weight sans propulsion inerts and propellants is approximately 960 kg. Total injected weight is 2460 kg.

Table VII-2 Shared Antenna Concept Weight Statement

	Wt (kg)
Structure, Mech. Devices, Thermal Control	260.0
Radar and Antenna	52.0
Communications	40.0
Processor/Recorder	18.7
Command Receiver/Mod/Demod	13.7
Attitude Control/Command Computer	95.0
Attitude Control Propellant	32.0
Cabling	52.9
Power	322.0
Pyrotechnics	5.5
Contingency	69.0
Spacecraft Weight (usable weight in orbit)	960.8
Propulsion Inerts	219.0
Propellant	1280.0
Injected Weight	2459.8

Dedicated Antenna Configuration

The dedicated antenna spacecraft configuration is presented in Figure VII-2. This concept also uses a modified Viking oribter as the basic structural configuration. Two antennas are used, a two (2) meter parabolic communication antenna which is articulated with two degrees of freedom and a fixed symmetrically cut parabolic radar antenna. The mapping phase of the mission is accomplished by
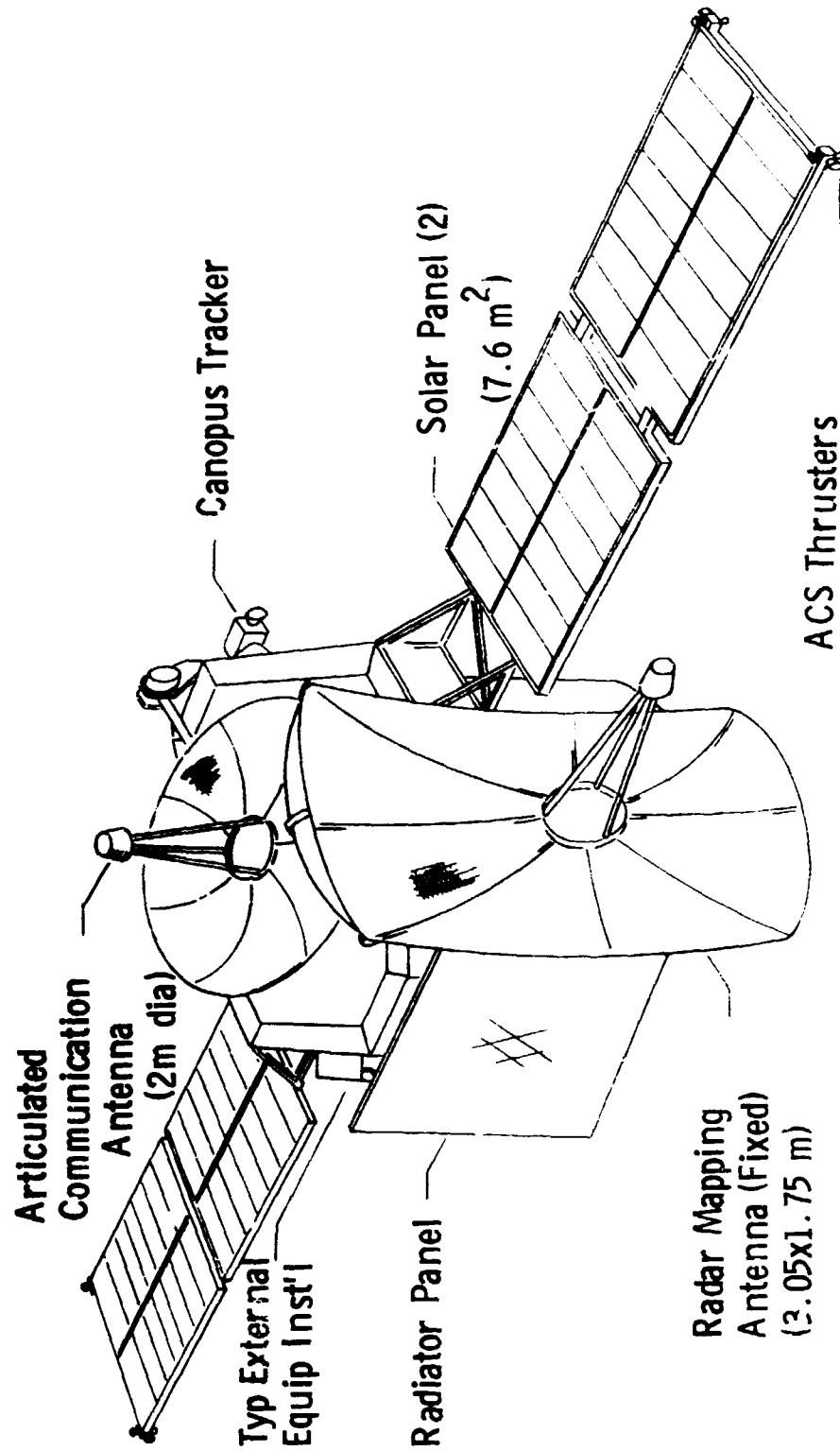
Articulated
Communication
Antenna
(2m dia)

Canopus Tracker

Solar Panel (2)
(7.6 m^2)

ACS Thrusters

Typ External
Equip Inst'l

Radiator Panel

Radar Mapping
Antenna (Fixed)
(3.05x1.75 m)

Figure VII-2 Spacecraft Configuration - Dedicated Antennas

VII-11

pointing the spacecraft. The solar arrays are identical to those utilized for the shared array concept.

The power subsystem consists of the solar array assembly, nickel-cadmium batteries, power conditioning and regulation equipment and power distribution assembly. An additional complem 't of batteries are required compared to the shared antenna concept due to the fact that when the spacecraft is pointed toward the planet during the mapping phase of the mission the solar array is off the Sun line requiring additional battery usage.

The radar antenna is a 3.05 meter by 1.75 meter symmetrically cut parabolic and is mounted on one of the short sides of the eight-sided bus structure. Location of this antenna is such to preclude possible shading of the solar array. S-band frequencies are used for mapping purposes.

The communications antenna is a two (2) meter parabolic antenna mounted on the upper surface of the Viking orbiter bus in the same fashion as the shared antenna configuration. This antenna is articulated with two degrees of freedom. X-band is used for data transmission to Earth.

Unlike the shared antenna concept, three-axis attitude control is provided by a combination of control moment gyros (CMGs) and GN_2. Three systems were studied for possible application; these were, a nitrogen cold gas system, hydrazine/plenum and CMGs and nitrogen cold gas. The system weights for these concepts were: 551 kg, 211 kg and 109 kg, respectively. Although the selected system is probably the most complex of the systems studied, it was recommended because of its very substantial weight advantage over the other systems. Pitch and roll control is provided by four clusters of three thrusters each mounted on the tip of each solar panel. Yaw thrusters are located on the orbiter bus. Vehicle maneuvering is performed in pitch and roll to take advantage of

the larger moment arms. Total impulse requirements are 39840 n-secs, or approximately three times larger than the requirements for the shared antenna concept. This is because the total vehicle must be maneuvered between the mapping and communication phases rather than just moving the antenna as was the case in the shared antenna version.

Celestial sensors, comprised of a Canopus sensor, cruise and acquisition Sun sensors, Sun gate, and a stray light sensor, are mounted on the appropriate sides of the bus and solar panels to meet the required fields of view of the instruments and to eliminate interference from the solar panels. Propellant for the ACS system is housed in spherical bottles located within the bus structure. The inertial reference units consisting of gyros, inertial sensors and electronic controls are also mounted within the orbiter bus structure.

As in the shared antenna concept the primary propulsion system is the basic Viking orbiter system with two 1330 nt (300 lbf) thrust engines. Again the propellant requirement is less than is required for the basic Viking '75 mission, approximately 1165 kg.

The spacecraft electronic assemblies are contained within the eight-sided bus structure. An initial study indicated that adequate volume was available within the present orbiter equipment compartments to house the additional radar and communications components. Provisions have been made, however, to also house this equipment external to the basic bus if required.

The thermal control subsystem utilizes the same radiator concept as the shared antenna configuration except that the orientation of the Sun in relation to the spacecraft does not remain constant during the mission, therefore, a larger (2.1 m^2) radiator surface is required.

The weight of the dedicated antenna concept is summarized in Table VII-3 at the subsystem level. Useful weight of the spacecraft in Venus orbit (e = 0.5) is approximately 963 kg. Total injected weight is 2468 kg.

Table VII-3 Dedicated Antenna Concept Weight Statement

	Wt (kg)
Structure, Mech. Devices, Thermal Control	270.0
Radar and Antenna	48.0
Communications and Antenna	50.0
Processor/Recorder	20.0
Command Receiver/Mod/Demod	13.7
Attitude Control/Command Computer	95.0
Attitude Control Propellant	14.0
Cabling	52.5
Power	324.0
Pyrotechnics	5.5
Contingency	70.0
Spacecraft Weight (usable wt in orbit)	962.7
Propulsion Inerts	220.0
Propellant	1285.0
Injected Weight	2467.7

VIII. Conclusions and Concerns

VIII. CONCLUSIONS AND CONCERNS

INTRODUCTION

The principal conclusions drawn from the parametric studies are summarized in this section.

These studies have demonstrated the feasibility of using a minimally modified Viking Orbiter to accomplish a radar mapping mission to the planet Venus in the mid-1980 time period. For the baseline mission chosen, a Titan III/Centaur launch vehicle has the capability to deliver the spacecraft into an orbit about Venus which allows total planet mapping coverage at 100 meter resolution. Mariner and Mars Viking hardware and technology were found to be adequate to meet all of the spacecraft systems and subsystems requirements with the exception of the radar and certain elements of the communication subsystems. Even these elements do not require advanced technology applications since present state-of-the-art components exist to implement the designs recommended for the mapping mission.

In summary then, no high-risk technology problems were identified in the various subsystem mechanizations that were examined. During the course of the study, however, several technology requirement areas were identified. Supporting Research and Technology (SRT) work performed in these areas would be beneficial in building confidence in mission flexibility, reducing possible development risk, and in reducing overall spacecraft inert weight. These studies are described in detail in Volume II.

SUBSYSTEM CONCLUSIONS AND CONCERNS

The important conclusions and recommendations that have
evolved from the individual subsystem parametric trade studies
are summarized in Table VIII-1.

Table VIII-1 Principal Spacecraft Design Conclusions

Feature	Option Selected	Selection Criterion or Rationale
Radar and Antenna Subsystem		
Antenna	Articulated Reflector	o Reduce Cost and Weight o Minimizes Sensor Requirements o Minimizes Shadowing of the Solar Panels o Fits well within Packaging Constraint o Minimizes ACS Requirements
Frequency	S-band (10 cm)	o Uses State-of-the-Art Components o Satisfies Mapping Requirements o Reasonable Antenna Sizes o Reasonable Power Requirements o Maximum Topographical Data with Acceptable Atmosphere Attention
Single Frequency Single Polarization		o Simple and Cost Effective Design o Meets Topographical Objectives
Radar Altimeter		o Required for Stereo Image Rectification
Communication & Data Handling		
Antenna	Articulated Reflector	o Lowest Cost and Weight o Minimizes Shadowing of Solar Panels o Fits Packaging Constraints o Minimizes ACS Requirements

(continued)

VIII-4

Table VIII-1 Principal Spacecraft Design Conclusions (continued)

Feature	Option Selected	Selection Criterion or Rationale
Communication & Data Handling (conc.)		
Frequency	3m, X-band, 100 watts	o Technology Limit on TWTA's o Power is Minimized o Antenna Pointing Capabilities Restrict Antenna Size
Data Storage	Digital Tape	o Reliability Considerations o Low Weight o Mission Requirements do not Require Analog Capabilities o Reusable Feature
Processor	Presuming	o Best Image Quality at same Data Rate
Propulsion		
Multiple Engines	2-3, 1330nt VO Engines	o Minimum Cost o Allows Fixed Attitude Burn o Reduces Total Burn Time
Propulsion Module ($\epsilon = 0.30$ to $\epsilon = 0.50$)	Stretched VO Propulsion Module	o Minimizes Cost and Development Risk o Stretched Tanks Capable of Handling Orbital Eccentricities of 0.30 to 0.50 o Minimum Inert Weight
Propulsion Module ($\epsilon = 0.30$ to $\epsilon = 0.00$)	Space Storable Propellant in Combination with VO Propulsion Module	o Required for Orbital Eccentricities between 0.30 to 0.00 o Superior System Performance Capabilities o Extensive Development Work Accomplished

Table VIII-1 Principal Spacecraft Design Conclusions (continued)

Feature	Option Selected	Selection Criterion or Rationale
Power		
Solar Array Configuration	Two Paddles (1/2 of VO '75)	o Minimum Cost o Low Development Risk o Versatile, Fits Launch Vehicle Envelope
Battery Complement	NiCd, VO '75	o Low Cost o Existing off-the-shelf from VO '75
Thermal Control		
Radiator and Multi-layer Insulation	Integrated Radiator Concept	o Concepts are in Advanced Development Stage o Temperature Controlled Heat Pipe Meets Mission Requirements
Attitude Control		
Mass Expulsion	Cold Gas VO '75 System	o Minimum Cost o Low Development Risk
Momentum Exchange	CMG's & GN$_2$ VO '75 System	o Required for Dedicated Antenna Design Concepts o Pointing Mode Requirement o Avoids Excessive Weight Penalty of all Cold Gas System

Table VIII-1 Principal Spacecraft Design Conclusions (concluded)

Feature	Option Selected	Selection Criterion or Rationale
Spacecraft Design		
Vehicle Orientation	3-Axis Controlled	o Freedom of Orientation of Thrust, Solar Panels and Antennas
Center Body	VO '75 Bus, Modified	o Minimum Cost o Low Development Risk o Fits Antenna, Solar Panel Arrangements Well o Minimum Packaging Problems o Minimizes Integration Problems
Mission Design		
Orbital Eccentricity	0.50	o Requires Simplified, Cost Effective Insertion Stages
Periapsis Altitude	400 km	o Minimum for Required Insertion Accuracy
Orbit Orientation	Polar	o Provides Total Surface Coverage o Provides Viewing of Both Poles